

NASA Contractor Report 185249

Cryogenic On-Orbit Liquid Depot Storage, Acquisition, and Transfer Satellite(COLD-SAT)

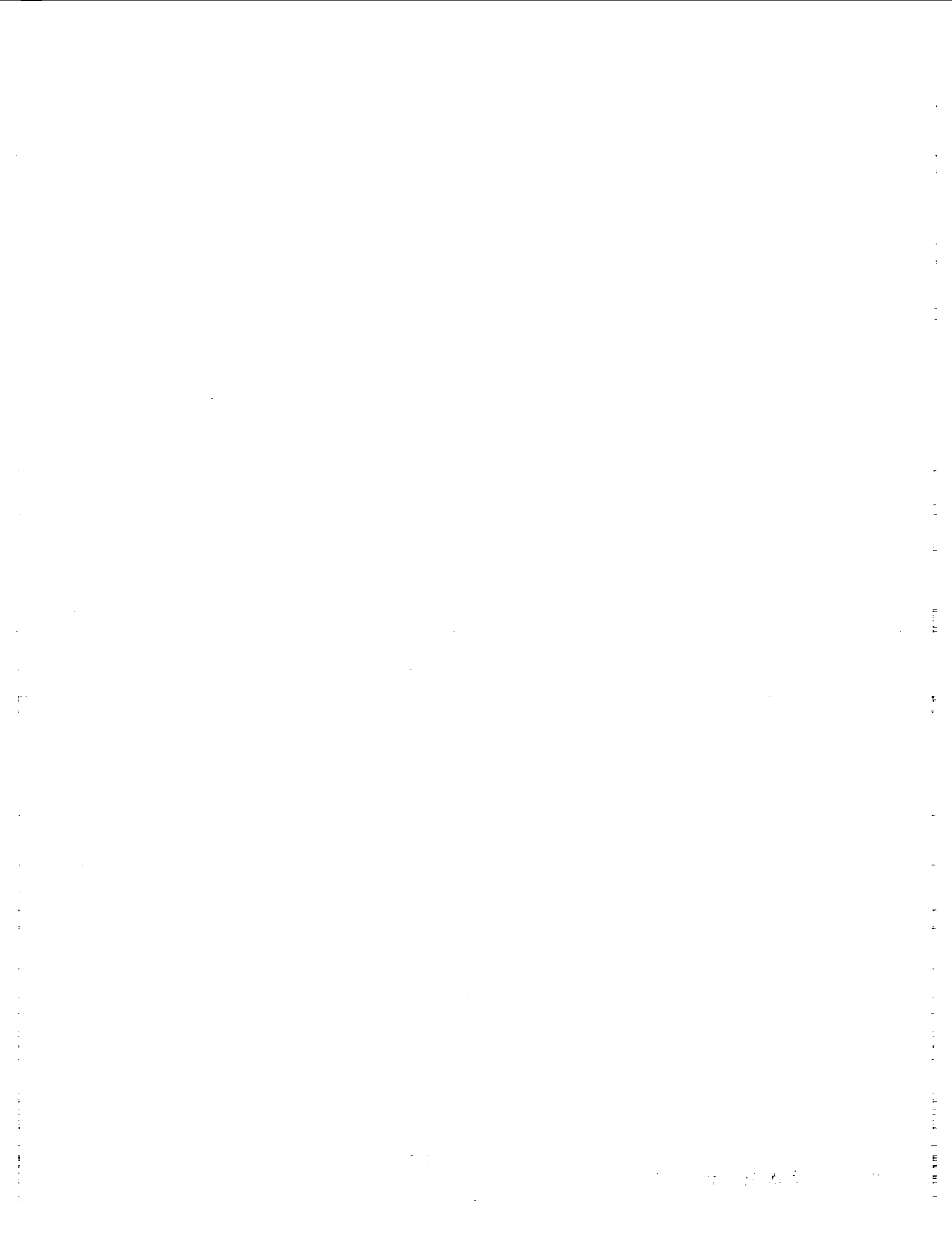
Feasibility Study Final Report

John R. Schuster and Edwin J. Russ
General Dynamics Space Systems Division
and
Joseph P. Wachter
Ford Aerospace Space Systems Division

July 1990

Prepared for
Lewis Research Center
Under Contract NAS3-25062

NASA
National Aeronautics and
Space Administration



FOREWORD

This report was prepared by General Dynamics Space Systems Division (GDSS) and its subcontractor Ford Aerospace Corporation Space Systems Division (FAC) for the NASA Lewis Research Center (LeRC) under Contract NAS3-25062. The report documents results of a twenty-four month technical effort carried out from March 1988 through February 1990.

Three NASA/LeRC Project Managers directed the effort. In reverse chronological order they are Daniel M. Vento, Erich W. Kroeger, and Albert G. Powers. The GDSS/FAC study team acknowledges the important contributions made by these gentlemen.

The following GDSS personnel contributed to this report:

John R. Schuster	Study Manager
Michael J. Gruszczynski	Deputy Manager
Franklin O. Bennett	Thermodynamics
Charles A. Davis	Avionics
Gerald S. Davis	Operations
Steve D. Douthat	Fluid Systems
James A. Feinn	Thermodynamics
Warren J. Hauschild	Safety
Glen T. Hied	Reliability
Scott C. Honkonen	Thermodynamics
Greg V. Mehle	Structures
Luis R. Pena	Systems Engineering
Joe R. Pietrzyk	Thermodynamics
Clifford B. Phillips	Test Planning
Edwin J. Russ	Thermodynamics Lead
Leroy Siden	Design
Grant E. Williams	Thermal Control

The following FAC personnel contributed to this report:

Joseph P. Wachter	Study Manager
Chris Frank	Electrical Power Systems
Grant Gould	Mission Analysis
Mike Hollars	Attitude Control
Ying-Yan Kuo	Thermal Control
John Legg	Reliability
Leonard Losik	Telemetry, Command & Data Handling
Bruce Minners	Configurations & Structures
Dave Pidgeon	Telemetry, Command & Data Handling
Carlos Renowitzky	Configurations
Lee Rotlisberger	Electrical Power Systems
Rebecca Royer	Propulsion
Bill Schatz	Propulsion
John Schierholtz	Configurations & Structures



TABLE OF CONTENTS

1. SUMMARY	1-1
1.1 BACKGROUND	1-1
1.2 EXPERIMENT SUMMARY	1-1
1.2.1 Pressure Control	1-1
1.2.2 Tank Chill-down	1-2
1.2.3 Tank No-vent Fill	1-2
1.2.4 Liquid Acquisition Device Fill/Refill	1-3
1.2.5 Tanker Tank Thermal Performance	1-3
1.2.6 Tank Pressurization	1-3
1.2.7 Low-g Settling and Outflow	1-3
1.2.8 Liquid Acquisition Device Performance	1-3
1.2.9 Transfer Line Chill-down	1-4
1.2.10 Outflow Subcooling	1-4
1.2.11 Low-Gravity Vented Fill	1-4
1.2.12 Fluid Dumping	1-4
1.2.13 Advanced Instrumentation	1-4
1.3 SPACECRAFT DESIGN SUMMARY	1-4
1.4 MISSION SUMMARY	1-8
2. INTRODUCTION	2-1
2.1 OBJECTIVES AND SCOPE	2-1
2.2 REQUIREMENTS, GUIDELINES AND ASSUMPTIONS	2-6
3. EXPERIMENT DESCRIPTIONS AND REQUIREMENTS	3-1
3.1 EXPERIMENT GOALS	3-2
3.2 CLASS I EXPERIMENTS	3-2
3.2.1 Pressure Control	3-2
3.2.2 Tank Chillover	3-10
3.2.3 No-Vent Fill	3-14
3.2.4 LAD Fill/Refill Experiment	3-18
3.3 CLASS II EXPERIMENTS	3-20
3.3.1 Tanker Thermal Performance	3-20
3.3.2 Tank Pressurization	3-21
3.3.3 Low-G Settling and Outflow	3-23
3.3.4 LAD Performance	3-24
3.3.5 Line Chillover	3-27
3.3.6 Outflow Subcooling	3-29
3.3.7 Low-Gravity Vented Fill	3-31
3.3.8 Fluid Dumping	3-33

PRECEDING PAGE BLANK NOT FILMED

TABLE OF CONTENTS (Cont.)

4. MISSION DESCRIPTION	4-1
4.1 MISSION REQUIREMENTS	4-1
4.2 LAUNCH VEHICLE PERFORMANCE	4-1
4.3 PAYLOAD FAIRING	4-1
4.4 PAYLOAD MASS AND CENTER OF GRAVITY ENVELOPE	4-1
4.5 ORBIT ANALYSIS	4-4
4.5.1 Baseline Orbit	4-4
4.5.2 Orbit Perturbations	4-5
4.5.3 Orbital Environment	4-5
5. EXPERIMENT MODULE DESIGN	5-1
5.1 EXPERIMENT SUBSYSTEM OVERVIEW	5-1
5.2 FLUID SYSTEM SCHEMATIC AND OPERATION	5-4
5.2.1 Thermal Control	5-4
5.2.2 Tank Pressure Control	5-4
5.2.3 Fluid Transfer	5-7
5.2.4 Tanking	5-8
5.3 OVERALL MODULE ARRANGEMENT AND MASS PROPERTIES	5-8
5.4 SUPPLY TANK (TANK 1)	5-13
5.4.1 Supply Tank General Arrangement and Internal Components	5-13
5.4.2 Tank 1 Insulation Features	5-13
5.4.3 Tank 1 Aft Bulkhead Equipment Installation	5-23
5.4.4 Tank 1 Valve Module on Aft Bulkhead	5-23
5.4.5 Tank 1 Vent System on Forward Bulkhead	5-23
5.4.6 Tank 1 Heat Exchanger Module	5-23
5.5 TANK 2	5-29
5.5.1 Tank 2 General Arrangement	5-29
5.5.2 Tank 2 Internal Components	5-29
5.5.3 Tank 2 Insulation Features	5-32
5.5.4 Bulkhead Equipment and Installation	5-38
5.6 TANK 3	5-41
5.6.1 Tank 3 General Arrangement and Internal Components	5-41
5.6.2 Tank 3 Insulation	5-41
5.6.3 Tank 3 Bulkhead Fittings and TVS Heat Exchanger	5-44
5.6.4 Tank 3 Valve Module	5-44

TABLE OF CONTENTS (Cont.)

5.7 FLUID LINES AND FLUID COMPONENT MODULES	5-49
5.7.1 LH ₂ Fill, Drain, and Ground Vent Arrangement	5-49
5.7.2 LH ₂ Transfer Circuit Plumbing	5-49
5.7.3 Vent and Pressurization Plumbing	5-52
5.8 EXPERIMENT MODULE STRUCTURE GENERAL FEATURES	5-52
5.8.1 Experiment Module Outer Structure	5-55
5.8.2 Outer Structure Vent Arrangement	5-55
5.9 FLUID SYSTEM COMPONENTS	5-55
5.9.1 Thermodynamic Vent Systems	5-55
5.9.2 Transfer and Pressurization Pumps	5-60
5.9.3 Autogenous Pressurization System	5-62
5.9.4 Outflow Subcooler	5-65
5.9.5 Stored Gas Pressurization System	5-65
5.9.6 Valves and Regulators	5-67
5.10 INSTRUMENTATION, POWER AND CONTROL	5-72
5.10.1 Instrumentation Summary	5-72
5.10.2 Experiment Power Requirements	5-75
5.10.3 Experiment Control Concept	5-78
5.11 EXPERIMENT COMPONENTS AND DEVELOPMENT STATUS	5-78
6. EXPERIMENT MODULE SUPPORTING ANALYSES	6-1
6.1 FLUID SYSTEM PRESSURE DROP	6-1
6.1.1 Results and Implications	6-1
6.1.2 Analysis Technique	6-2
6.2 MEASUREMENT ACCURACY REQUIREMENTS	6-2
6.2.1 Instrument Accuracy	6-2
6.2.2 Uncertainty Analysis for Pressure Control Experiments	6-4
6.2.3 Tank Chill and No-Vent Fill Uncertainty Analysis	6-7
6.3 PRESSURE CONTROL	6-7
6.3.1 Thermal Stratification	6-7
6.3.2 Passive TVS	6-16
6.3.3 Supply Tank Mixing	6-23
6.3.4 Active TVS	6-26
6.4 PRESSURIZATION AND TRANSFER	6-27
6.4.1 Analytical Methods	6-29
6.4.2 Effect of System Parameters on Pressurant Requirements	6-31
6.4.3 Boiloff Requirements for Thermal Conditioning	6-36
6.4.4 Energy Requirements for Pumped and Pressurized Transfers	6-37
6.4.5 Summary of GH ₂ Pressurant Requirements for the Class II Pressurization Experiment	6-39

TABLE OF CONTENTS (Cont.)

6.5 TANK MLI VENTING	6-40
6.6 THERMAL PERFORMANCE	6-41
6.6.1 Space Heating and External Temperatures	6-41
6.6.2 Earth -To-Orbit Performance	6-42
6.6.3 On-Orbit Tank Heating	6-45
6.6.4 Spacecraft Bus / Experiment Module Thermal Exchange	6-49
6.7 MICROMETEOROID/DEBRIS SHIELDING	6-51
6.8 STRUCTURAL REQUIREMENTS	6-53
6.8.1 Analysis of External Structure	6-54
6.8.2 Experiment Module Pressure Vessel Design	6-54
6.8.3 Experiment Module Tank Support Struts	6-56
6.8.4 Experiment Module Separation System	6-56
7. SPACECRAFT BUS DESIGN	7-1
7.1 DESIGN FEATURES AND HERITAGE	7-1
7.1.1 Overall Arrangement	7-1
7.1.2 Equipment Layout	7-1
7.1.3 Mass Properties	7-5
7.1.4 System Heritage	7-5
7.2 TELEMETRY, COMMAND AND DATA HANDLING	7-7
7.2.1 Telemetry, Command and Data Handling Requirements	7-7
7.2.2 Telemetry, Command and Data Handling Description	7-9
7.2.3 Telemetry, Command and Data Handling Performance	7-13
7.3 ATTITUDE DETERMINATION AND CONTROL	7-16
7.3.1 Requirements	7-16
7.3.2 Description	7-16
7.3.3 Performance Analysis	7-19
7.4 PROPULSION	7-21
7.4.1 Requirements	7-21
7.4.2 Description	7-23
7.4.3 Performance Analysis	7-25
7.5 THERMAL CONTROL	7-29
7.5.1 Thermal Control Requirements	7-29
7.5.2 Thermal Control System Description	7-29
7.5.3 Thermal Analysis Results	7-29
7.6 ELECTRIC POWER	7-32
7.6.1 System Requirements	7-32
7.6.2 System Description	7-32
7.6.3 Electric Power System Analysis Results	7-34

TABLE OF CONTENTS (Cont.)

8. INTERFACES	8-1
8.1 BUS-TO-EXPERIMENT MODULE	8-1
8.1.1 Fluid and Mechanical Interfaces	8-1
8.1.2 Instrumentation, Power and Control	8-1
8.2 SPACECRAFT-TO-ATLAS LAUNCH VEHICLE	8-3
8.2.1 Fluid and Mechanical Interfaces	8-3
8.2.2 Flight Termination System.	8-7
8.3 LAUNCH COMPLEX INTERFACES	8-7
8.3.1 Fluid Interfaces	8-7
8.3.2 Telemetry, Power, and Control	8-9
8.3.3 Ground Support Equipment Interfaces	8-13
9. OPERATIONS	9-1
9.1 MANUFACTURE	9-1
9.1.1 Buildup and Integration	9-1
9.1.2 Transport	9-4
9.2 LAUNCH PAD MODIFICATIONS	9-5
9.3 GROUND OPERATIONS AND LAUNCH PREPARATION	9-7
9.4 LAUNCH COUNTDOWN	9-8
9.4.1 Tanking	9-8
9.4.2 Venting	9-8
9.4.3 Thermal Control/Purge	9-11
9.5 ASCENT/TRANSFER ORBIT	9-13
9.6 ON-ORBIT OPERATIONS	9-13
9.6.1 Deployment and Checkout	9-13
9.6.2 Spacecraft Bus Operations	9-14
9.6.3 Experiment Operations	9-15
10. SAFETY	10-1
10.1 LAUNCH VEHICLE AND COLD-SAT GROUND SUPPORT	10-1
10.2 HAZARDS	10-1
10.2.1 On-Orbit Environment	10-1
10.2.2 Tanks	10-1
10.2.3 Bus Subsystems	10-2
10.2.4 Ordnance Subsystems	10-2

TABLE OF CONTENTS (Cont.)

11. RELIABILITY	11-1
11.1 SPACECRAFT RELIABILITY	11-1
11.2 BUS MODULE RELIABILITY	11-2
11.3 EXPERIMENT MODULE RELIABILITY	11-3
12. PROJECT PLANNING	12-1
12.1 TECHNOLOGICAL RISKS	12-1
12.1.1 Experiment Module	12-1
12.1.2 Spacecraft Bus	12-1
12.2 FACILITIES	12-5
12.2.1 Test Facilities	12-5
12.2.2 Spacecraft Processing and Checkout	12-6
12.3 TESTING	12-6
12.4 SCHEDULE	12-6
13. REFERENCES	13-1
A. EXPERIMENT MODULE ADDITIONAL DESIGN DETAILS	A-1
A.1 SUMMARY OF EXPERIMENT MODULE GENERAL ARRANGEMENT STUDIES	A-1
A.2 DETAILED MASS BREAKDOWN FOR TANKS 1,2 AND 3, AND THE OUTER STRUCTURE	A-3
A.3 TANK 3 ASSEMBLY, NOZZLE AND VENT DETAILS	A-3
A.3.1 Tank 3 Assembly	A-3
A.3.2 Tank 3 Internal Nozzle Details	A-3
A.3.3 Tank 3 Vent Arrangement	A-16
A.4 DETAILS OF THE FLUID COMPONENT MODULES	A-16
A.4.1 Tank 1 Pump Module	A-16
A.4.2 Pressurization Control Module	A-16
A.4.3 Tank 1 Evaporator Module	A-16
A.4.4 Junction Module	A-21
A.5 EXPERIMENT MODULE ALTERNATIVE LIGHTWEIGHT STRUCTURE DESIGN USING GRAPHITE EPOXY	A-21
B. LIST OF FLUID SYSTEM COMPONENTS IN THE FLUID SYSTEM DIAGRAM	B-1

TABLE OF CONTENTS (Cont.)

C. INSTRUMENTATION AND CONTROL LISTS AND DIAGRAMS	C-1
D. TANK FLUID MOTION AND HEAT TRANSFER CONSIDERATIONS	D-1
D.1 BACKGROUND ACCELERATION DISTRIBUTION	D-1
D.2 CHILLDOWN MODEL IMPROVEMENTS	D-5
D.2.1 Conduction Heat Transfer Limit	D-5
D.2.2 Large Turbulent Eddy Decay Model	D-7
D.2.3 Tank Chillardown Results	D-9
D.3 TANGENTIAL FLOW	D-11
D.3.1 Velocity Profile Following a Charge	D-11
D.3.2 Decay of Laminar Tangential Flow	D-14
D.3.3 Decay of Turbulent Tangential Flow	D-17
E. DETAILED EXPERIMENT SEQUENCES	E-1
F. ADDITIONAL SCHEDULE INFORMATION	F-1
F.1 TEST SCHEDULE	F-1
F.2 LAUNCH VEHICLE SCHEDULE	F-1



LIST OF FIGURES

<u>Figure</u>	<u>Title</u>	<u>Page</u>
1-1	On-orbit Spacecraft Configuration	1-6
2-1	Some Future Space Transportation System Elements Utilizing Cryogens	2-2
2-2	COLD-SAT Spacecraft Configured for Atlas Launch	2-5
2-3	COLD-SAT Team Responsibilities	2-6
3-1	Tank Pressure Profile expected during TVS, Constant Pressure Experiments	3-9
3-2	Pressure Profile expected in Tank 1 during Thermal Stratification and Passive TVS Thermal Conditioning Experiments	3-9
3-3	Tank Pressure Profile expected during Thermal Stratification, Mixer Destratification, and Active TVS Thermal Conditioning Experiments	3-10
3-4	Typical GDNVF Tank Chillover Results	3-12
3-5	Typical GDNVF Pressure Rise Results for No-Vent Fill Process	3-15
3-6	The Effect of Subcooling and Initial Bubble Radius on Bubble Collapse Time for Liquid Hydrogen in a Low-G Environment	3-18
3-7	Effect of Mass Outflow Rate on the Residual Volume in Low-G	3-23
4-1	Atlas Parking Orbit Ascent Payload Capability to Circular Orbit	4-2
4-2	COLD-SAT Configuration within the Atlas I Payload Fairing	4-3
4-3	Atlas I Payload Mass/Center of Gravity Envelope	4-4
4-4	Eclipse Duration for an Initial Orbit Right Ascension of Zero Degrees	4-6
4-5	Beta Angle for an Initial Orbit Right Ascension of Zero Degrees	4-7
4-6	Tracking Station and TDRSS Visibility	4-7
4-7	Typical Daily Tracking Station Contacts	4-8
4-8	Accelerations Induced by Atmospheric Drag	4-8
4-9	COLD-SAT Orbital Lifetime from an Initial Circular Orbit	4-9
4-10	COLD-SAT Altitude Increase due to Experiment Thrusting	4-9
4-11	Distribution of Atomic Oxygen	4-10
4-12	Distribution of Orbital Debris	4-10
4-13	Annual Radiation Dose	4-11
5-1	COLD-SAT Fluid System Schematic	5-5
5-2	Overall Spacecraft Arrangement and Mass Properties	5-9
5-3	Systems Hardware Details	5-12
5-4	Tank 1 General Arrangement	5-14
5-5	Tank 1 TVS/Mixer Assembly Installation	5-15
5-6	Tank 1 Insulation	5-16
5-7	Tank 1 Insulation/Typical Penetrations	5-18
5-8	Tank 1 Vapor-Cooled Shield	5-19
5-9	Tank 1 Ground Purge Enclosure	5-20
5-10	Tank 1 Ground Purge Enclosure	5-22
5-11	Tank 1 Aft Bulkhead Equipment Installation	5-24
5-12	Tank 1 Valve Module/Aft Bulkhead	5-25
5-13	Tank 1 Vent System/Forward Bulkhead	5-26
5-14	Tank 1 Vent Valve Module	5-27
5-15	Tank 1 Heat Exchanger Module	5-28
5-16	Tank 2 General Arrangement	5-30

LIST OF FIGURES (CONT)

<u>Figure</u>	<u>Title</u>	<u>Page</u>
5-17	Tank 2 Spray Fill and Instrumentation Tree	5-31
5-18	Tank 2 Wall Heat Exchanger and TVS	5-33
5-19	Tank 2 Liquid Acquisition Device/LAD	5-34
5-20	Tank 2 Liquid Acquisition Device/Additional Details	5-35
5-21	Tank 2 Insulation	5-36
5-22	Tank 2 Insulation and Typical Blanket Construction	5-37
5-23	Tank 2 System Equipment Installation/Aft Bulkhead	5-39
5-24	Tank 2 Vent and Pressurization Installation	5-40
5-25	Tank 3 General Arrangement	5-42
5-26	Tank 3 Insulation	5-43
5-27	Aft Bulkhead Penetrations and Accessories	5-45
5-28	Tank 3 Forward Bulkhead Penetration and Accessories	5-46
5-29	Tank 3 Wall Heat Exchanger/TVS	5-47
5-30	Tank 3 Valve Module	5-48
5-31	LH2 Fill, Drain, and Ground Vent Arrangement	5-50
5-32	LH2 Transfer Circuit Plumbing	5-51
5-33	Vent and Pressurization Plumbing	5-53
5-34	Outer Structure/All Aluminum/Baseline/General Features	5-54
5-35	Outer Structure/All Aluminum/Baseline	5-56
5-36	Outer Structure/All Aluminum/Baseline	5-57
5-37	Outer Structure Vent Arrangement	5-58
5-38	Maximum Efficiency versus Specific Speed for Various Pump Types (References 5-2 and 5-3)	5-61
5-39	Cross Section of Helical Evaporator	5-64
5-40	Forced Convection Boiling Heat Transfer Coefficients	5-64
5-41	Hydrogen Gas Storage Bottles	5-66
5-42	Helium Gas Storage Bottle	5-68
5-43	Valcor's Floating Seal Gate Valve Concept	5-70
5-44	Consolidated's Poppet Valve Concept	5-71
5-45	Instrumentation Block Diagram	5-73
5-46	Power Distribution Block Diagram	5-77
5-47	Experiment Control Subsystem Block Diagram	5-79
6-1	Configuration of Tank with Heaters	6-8
6-2	Heat Flux Variation for Low Values of the Parameter hL/K	6-9
6-3	Heater Coverage Required on the Tank Wall Outer Surface to obtain 20 Percent Heat Flux Variation on the Inner Surface	6-10
6-4	Heat Flux Distributions on the Tank Wall Inner Surface	6-11
6-5	Isotherms in the Tank Wall	6-11
6-6	Transient Behavior of the Heat Flux Through Tank Wall	6-12
6-7	Relationship between Wall Heat Flux and Wall Temperature	6-13
6-8	Heat Flux to Initiate Nucleate Boiling on a Heated Wall	6-14
6-9	Magnitude of the Fluid Velocity in a Buoyancy-Driven Flow Near the Heated Wall	6-17
6-10	Maximum Pressure Rise Times	6-17
6-11	Steady State Boiloff	6-18
6-12	Time for Each Pressure Reduction Test	6-19
6-13	Boiloff Amount for Each Pressure Reduction Test	6-21
6-14	TVS Tube Lengths	6-22
6-15	Jet Diameter Effects on Axial Jet Mixer	6-24

LIST OF FIGURES (CONT)

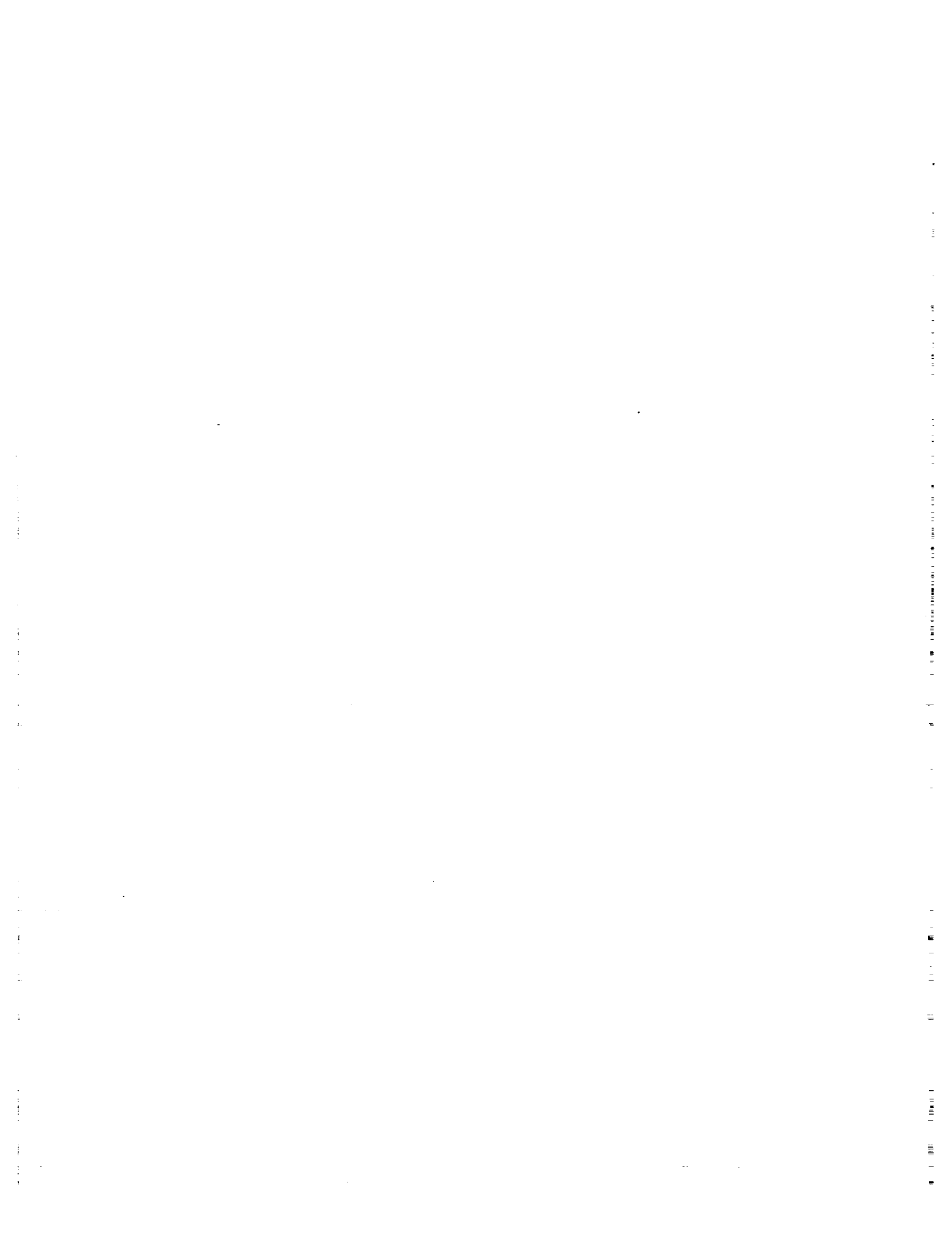
<u>Figure</u>	<u>Title</u>	<u>Page</u>
6-16	Acceleration Level Effect on Axial Jet Mixer	6-25
6-17	Mixing Time Using Axial Jet Mixer	6-25
6-18	Active TVS Test Duration	6-28
6-19	Mass Boiloff to Perform Active TVS Tests	6-28
6-20	TNKTHRM Model of Pressurization Using Stored Gas or Liquid Supply	6-30
6-21	Effect of Pressurant Temperature on Pressurant Requirements	6-31
6-22	Effect of G-level on Ramp Pressurant Requirements	6-34
6-23	Effect of Ramp Time and Fill Level on Cold Gaseous Hydrogen Ramp and Pressurant Mass Requirements (Pump-assisted Transfer)	6-35
6-24	Effect of Ramp Time and Fill Level on Gaseous Hydrogen Ramp and Pressurant Mass Requirements (Pressurized Transfer)	6-35
6-25	Conditioning Mass Requirements	6-36
6-26	Effect of Ramp Time and Fill Level on Average Evaporator Power (Pump-assisted Transfer)	6-38
6-27	Effect of Ramp Time and Fill Level on Average Evaporator Power (Pressurized Transfer)	6-38
6-28	Effect of Fill Level on Total Energy Requirements for Pump-assisted and Pressurized Transfers	6-39
6-29	Pressure Profiles for Nitrogen under Micrometeoroid Shield and Helium within MLI	6-41
6-30	Average Surface Temperature Profile for Maximum Heating Orbit (Beta = 52)	6-42
6-31	Average Surface Temperature Profile for Minimum Heating Orbit (Beta = 0)	6-43
6-32	Schematic of Prelaunch-To-Orbit Thermal Model	6-44
6-33	Supply Tank Heating Profile from Prelaunch through Ascent	6-44
6-34	Receiver Tank Insulation Performance Summary	6-46
6-35	Schematic of Fluid Penetration Thermal Model	6-48
6-36	Schematic of Interface Heating Model	6-50
6-37	Summary of Interface Heat Flow Parametric Analysis	6-50
6-38	Effect of Penetration Resistance on Shield Mass	6-52
6-39	Effect of Mission Duration on Shield Mass and Thickness	6-52
6-40	Effect of Mission Duration on Shield Skin Thickness	6-53
6-41	Experiment Module External Structure Design Drivers and V-Band Clamp Loads	6-54
6-42	External Structure Cross-Section Geometry	6-55
6-43	Experiment Tank Wall Thicknesses	6-55
6-44	Experiment Tank Support Strut Dimensions	6-56
7-1	COLD-SAT Deployed Configuration Showing Antennae Field-of View	7-2
7-2	COLD-SAT Spacecraft Bus Exploded View	7-3
7-3	COLD-SAT Equipment Layout	7-4
7-4	Telemetry Command and Data Handling Configuration	7-8
7-5	DCU Functional Architecture	7-10
7-6	Command Message Format	7-11
7-7	Attitude Determination and Control System Equipment Layout	7-17
7-8	Attitude Determination and Control System Schematic	7-18
7-9	Round Robin Thrust Scheme	7-20
7-10	Propulsion System Schematic	7-24

LIST OF FIGURES (CONT)

<u>Figure</u>	<u>Title</u>	<u>Page</u>
7-11	Thruster Study to Produce the Required Experiment Accelerations	7-26
7-12	Six Thruster Configuration Firing Sequences	7-26
7-13	Thermal Control Requirements	7-30
7-14	Electrical Power System Block Diagram	7-32
8-1	Summary of Interfaces Between the Spacecraft Bus and the Experiment	8-2
8-2	Experiment Module / Spacecraft Bus Instrumentation Interface	8-3
8-3	Experiment Module / Spacecraft Bus Power Interface	8-3
8-4	Experiment Module / Spacecraft Bus Control Interface	8-4
8-5	Interfaces Between the Spacecraft and the Atlas I Launch Vehicle	8-5
8-6	Spacecraft "V" Band Clamp Separation System	8-6
8-7	COLD-SAT Ground and Ascent Vent System Arrangement	8-8
8-8	Launch Facility Fluid Interfaces	8-10
8-9	Titan/Centaur Umbilical Panel Installed on COLD-SAT Outer Structure	8-11
8-10	COLD-SAT Ground Umbilical Arrangement Using Existing Titan/Centaur Panel	8-12
9-1	Spacecraft Assembly Process	9-2
9-2	Experiment Module-to-Bus Attachment Sequence	9-3
9-3	Preparation of Spacecraft for Transport	9-4
9-4	Launch Complex COLD-SAT Umbilical Arrangement	9-6
9-5	Typical Umbilical Interface Locations for Atlas II	9-7
9-6	Summary Launch Countdown Timeline	9-9
9-7	COLD-SAT Tanking Timeline	9-9
9-8	COLD-SAT/Centaur Vent Interface Schematic	9-10
9-9	Schematic Representation of Insulation Purge Sequence	9-12
9-10	Typical 24 Hour Operations Cycle	9-16
12-1	COLD-SAT Phase C/D Master Schedule	12-9
A-1	Summary of General Arrangement Configurations	A-2
A-2	Tank 3 Assembly	A-14
A-3	Tank 3 Internal Nozzle Details	A-15
A-4	Tank 3 Vent Arrangement	A-17
A-5	Tank 1 Pump Module	A-18
A-6	Pressurization Control Module	A-19
A-7	Tank 1 Evaporator Module	A-20
A-8	Junction Module	A-22
A-9	Overall Features of the Graphite Epoxy and Aluminum Outer Structure	A-23
A-10	Details of the Graphite/Epoxy Outer Structure Interface	A-24
A-11	Details of the Structural Joints of the Graphite/Epoxy Outer Structure	A-25
C-1	Accelerometer Measurements	C-2
C-2	Command Status Measurement	C-2
C-3	Current Measurement	C-3
C-4	Flow Measurements	C-3
C-5	Liquid vapor Sensor Measurement	C-3
C-6	Pressure Measurement	C-4
C-7	Temperature Measurement	C-4
C-8	Voltage Measurements	C-4

LIST OF FIGURES (CONT)

<u>Figure</u>	<u>Title</u>	<u>Page</u>
D-1	Background Axial Acceleration Distribution	D-2
D-2	Background Radial Acceleration Distribution	D-3
D-3	Magnitude and Direction of Background Acceleration Vector	D-4
D-4	Heat Transfer Regimes During the Charge-Hold-Vent Cycle	D-6
D-5	Free Convection Heat Transfer Predicted Using Empirical Correlation	D-7
D-6	Effect of Nozzle Configuration on Flow Pattern in Tank	D-8
D-7	Model Improvements Implemented Into GDNVF	D-10
D-8	Chilldown Time Sensitivity to Model Constant	D-12
D-9	Acceleration Level Effects on the Chilldown Time	D-12
D-10	Initial Velocity Profiles	D-13
D-11	Laminar Flow, Tangential Velocity Decay	D-15
D-12	Laminar Flow, Angular Velocity Decay	D-16
D-13	Laminar Flow, Convection Coefficient Decay	D-17
D-14	Turbulent Flow, Tangential Velocity Decay	D-20
D-15	Turbulent Flow, Angular Velocity Decay	D-21
D-16	Comparison of Laminar and Turbulent Near-Wall Velocity Profiles	D-22
D-17	Comparison of Nusselt Number Decay for Laminar and Turbulent Tangential Flow Cases	D-23
D18	Comparison of Heat Transfer Results	D-23
F-1	COLD-SAT Phase C/D Test Schedule	F-2
F-2	Launch Vehicle Schedule	F-3



LIST OF TABLES

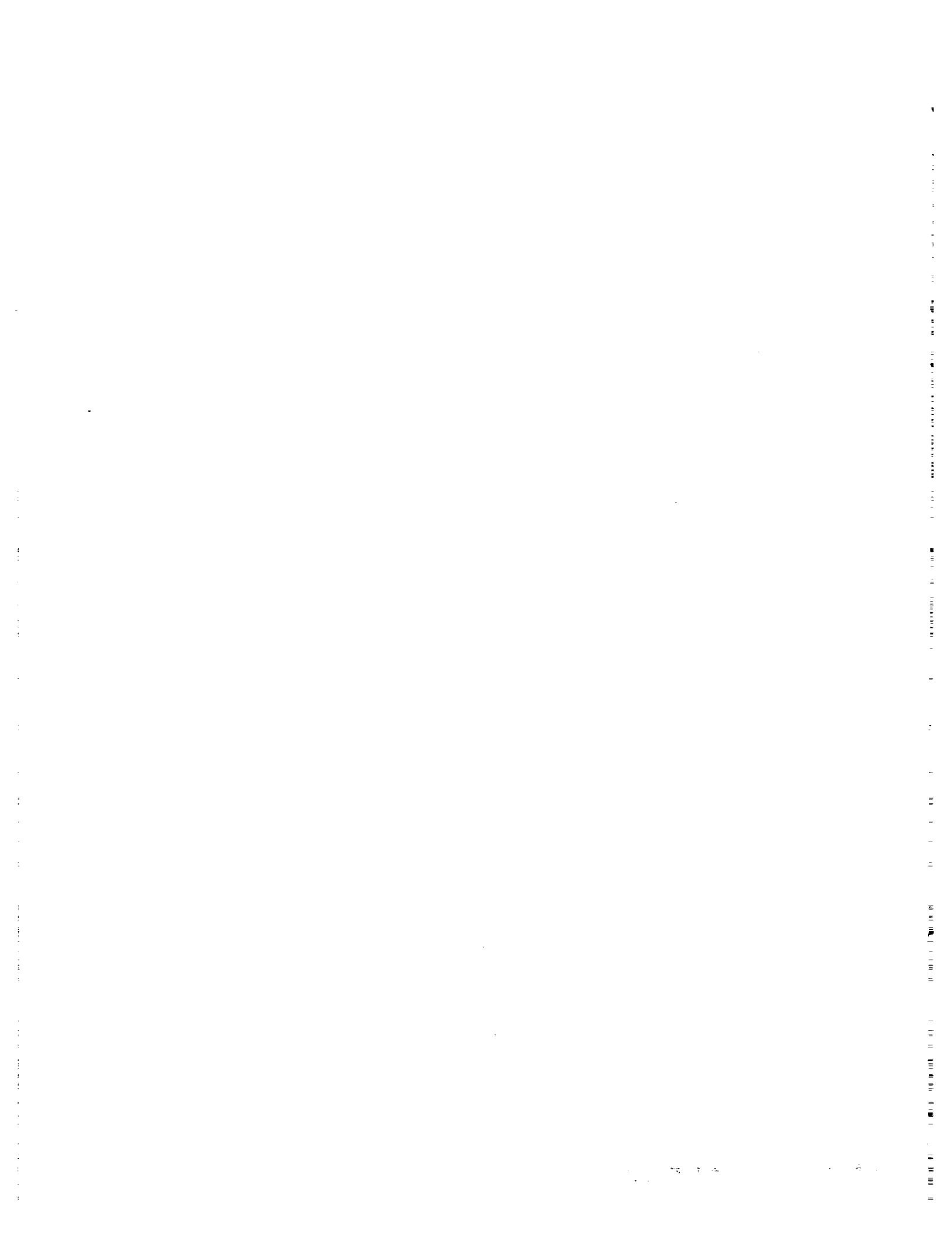
<u>Table</u>	<u>Title</u>	<u>Page</u>
1-1	List of COLD-SAT Experiments and Application	1-2
1-2	COLD-SAT Mass Summary	1-7
1-3	Propellant Budget	1-7
2-1	Cryogenic Fluid Management Technology Needs	2-3
2-2	In-Space Experimentation Needs	2-4
2-3	Summary of Requirements for the COLD-SAT Study	2-7
2-4	Summary of Guidelines and Assumptions for the COLD-SAT Study	2-8
3-1	List of COLD-SAT Experiment by Class	3-1
3-2	Tests for Tank Pressure Control	3-5
3-3	Tests for the Tank Chilldown Experiment	3-13
3-4	Tests for the No-Vent Fill Experiment	3-17
3-5	Tests for the LAD Fill and Refill Experiment	3-19
3-6	Tests for the Experiment on the Pressurization of Cryogenic Tankage in Low-G Experiment	3-22
3-7	Tests for the Low-Gravity Settling and Outflow Experiment	3-25
3-8	Tests for the LAD Performance Experiment	3-26
3-9	Tests for the Transfer Line Chilldown Experiment	3-28
3-10	Tests for the Class II Outflow Subcooling Experiment	3-30
3-11	Tests for the Low-G Vented Fill Experiment	3-32
3-12	Tests for the Fluid Dumping Experiment	3-34
4-1	Orbit Parameters and Characteristics	4-6
5-1	COLD-SAT Experiment Tank Configurations and Experiments Supported	5-3
5-2	Experiment Module Mass Properties	5-11
5-3	COLD-SAT Pump Requirements	5-60
5-4	Development Pump Specifications	5-61
5-5	Summary of Fluid Component Types being used on COLD-SAT	5-69
5-6	COLD-SAT Measurement Requirements	5-73
5-7	Experiment Equipment Power Requirements	5-76
5-8	Experiment Commands	5-79
5-9	Development Status Assessment - Avionics Category	5-80
5-10	Development Status Assessment - Mechanical Category	5-81
5-11	Preliminary Flowmeter Requirements	5-83
5-12	Recommended Flowmeters	5-84
6-1	Liquid Transfer Pressure Drop Summary	6-1
6-2	Nozzle Requirements and Characteristics	6-3
6-3	Measurement Accuracy Expressed as a Percent of Instrument Range	6-3
6-4	Free Convection Coefficient Uncertainties	6-5
6-5	Liquid Transfer Sensitivity to Temperature Uncertainty	6-7
6-6	Residence Time of Fluid in Wall-Mounted TVS Heat-Exchanger	6-20
6-7	Pressure Drop Through Wall-Mounted TVS Tube	6-24
6-8	Energy Requirements for Pumped and Pressurized Transfers	6-37
6-9	Summary of the Pressurant Mass Requirements	6-40
6-10	Orbital Average Temperature Summary	6-43
6-11	Structural Penetration Heat Flow Summary	6-47

LIST OF TABLES (CONT)

<u>Table</u>	<u>Title</u>	<u>Page</u>
6-12	Electrical Lead Thermal Analysis Parameters	6-47
6-13	Electrical Penetration Heat Flow Summary	6-47
6-14	Summary of Heat Flow into Filled Tanks through Fluid Penetrations	6-48
6-15	Total On-Orbit Heat Flow to Experiment Tanks	6-49
6-16	Atlas Launch Vehicle Payload Acceleration Factors	6-53
7-1	Spacecraft Bus Mass Properties	7-6
7-2	TC&DH Telemetry and Command Word Requirement	7-7
7-3	Command Message Modes	7-11
7-4	TC&DH Subsystem Performance	7-14
7-5	Forward Command Link Performance	7-14
7-6	Normal Mode Telemetry Format	7-15
7-7	Return Telemetry Link Performance	7-15
7-8	Representative Background Accelerations	7-22
7-9	COLD-SAT Environmental Disturbance Torques	7-22
7-10	Propellant Budget	7-27
7-11	Class I Experiment Propulsive Requirements	7-28
7-12	Class II Experiment Propulsive Requirements	7-28
7-13	Bus Subsystem/Element Heat Loads For The Task III Design	7-31
7-14	Bus Temperature Predictions For The Task III Design	7-31
7-15	Spacecraft Overall Power Budget	7-35
7-16	Spacecraft Bus Component Power Budget	7-35
8-1	COLD-SAT Launch Facility Fluid Interface Summary	8-7
9-1	SLC-36B LH2 Capacity and Requirements Summary	9-5
9-2	Sequence of Events for the Ground Purge Conditioning	9-11
9-3	Attitude Acquisition/Deployment Timeline	9-14
9-4	Roll Maneuver Timeline	9-15
9-5	Incomplete Experiments in the Shift-Scheduled Plan	9-17
10-1	Preliminary Hazard Analysis	10-3
10-2	Procedures Which Control Hazards	10-4
10-3	Major Safety Restrictions Imposed By Safety Policies	10-4
11-1	COLD-SAT Reliability Goals for Class I Experiments	11-1
11-2	Spacecraft Bus Module Reliability Assessment Summary	11-2
11-3	Experiment Module Reliability Assessment Summary	11-3
12-1	Development Categories and Technological Risk Factors for Experiment Module Mechanical Components	12-2
12-2	Development Categories and Technological Risk Factors for Experiment Module Avionics Components	12-2
12-3	Spacecraft Bus Component Risk and Heritage Assessment	12-3
12-4	Test Facilities	12-5
12-5	Spacecraft Processing and Checkout Facilities	12-7
12-6	Major Tests Required	12-8
A-1	Tank 1 Mass Breakdown	A-4
A-2	Tank 2 Mass Breakdown	A-7
A-3	Tank 3 Mass Breakdown	A-9

LIST OF TABLES (CONT)

<u>Table</u>	<u>Title</u>	<u>Page</u>
A-4	Aluminum Outer Structure Mass Breakdown	A-11
A-5	Graphite/Epoxy Outer Structure Mass Breakdown	A-13
B-1	Experiment Module Fluid System Components	B-2
C-1	COLD-SAT Experiment Measurement Requirements	C-5
C-2	COLD-SAT Experiment Commands	C-24
D-1	Decay of the Heat Transfer Coefficient Associated with Large Turbulent Eddies	D-9
E-1	Experiment Sequence Based on Continual Staffing of SOCC	E-2
E-2	Experiment Sequence Based on NASA Plan for Staffing of SOCC	E-6



LIST OF ACRONYMS

Acronym	Definition
ACS	Attitude Control System
ADCS	Attitude Determination and Control System
AOCS	Attitude & Orbital Control System
AWG	American Wire Gage
BBC	Battery Charge Converter
BCC	Battery Charge Converter
BECO	Booster Engine Cutoff
BOL	Beginning of Life
BPJ	Booster Pod Jettison
BPSK	Binary Phase-Shift Keying
BSFR	Back Surface Field/Reflector
BSR	Back Surface Reflector
BTS	Blockhouse Test Set
CFTO	Cryogenic Fluids Technology Office
CG	Center of Gravity
COLD-SAT	Cryogenic On-Orbit Liquid Depot Storage, Acquisition and Transfer Satellite
CPU	Central Processing Unit
CRES	Corrosion-Resistant Steel
DAK	Double Aluminized Kapton
DC	Direct Current
DCU	Digital Concentrator Unit
DIRA	Digital Integrating Rate Assembly
ECU	Experiment Control Unit
EED	Electro-Explosive Device
EMI	Electro-Magnetic Interference
EOL	End of Life
EPS	Electrical Power System
ERD	Experiment Requirements Document
ETR	Eastern Test Range
FAC	Ford Aerospace Corporation
GDNVF	General Dynamics No-Vent Fill Program
GDSS	General Dynamics Space Systems Division
GH ₂	Gaseous Hydrogen
GHe	Gaseous Helium
GN ₂	Gaseous Nitrogen
GSE	Ground Support Equipment
GSTDN	Ground Spaceflight Tracking and Data Network
HPF	Hazardous Processing Facility
ISDS	Independent Separation Destruct System
J-T	Joule-Thomson
KBPS	Kilobits per Second
KSC	Kennedy Space Center
L/D	Length-to-Diameter Ratio
LAD	Liquid Acquisition Device
LeRC	Lewis Research Center
LH ₂	Liquid Hydrogen
LO ₂	Liquid Oxygen

LIST OF ACRONYMS (CONT.)

Acronym	Definition
MDF	Mild Detonating Fuse
MDU	Master Data Unit
MECO	Main Engine Cutoff
MES	Main Engine Start
MESA	Miniature Electrostatic Accelerator
MLI	Multi-Layer Insulation
MMS	Micrometeoroid/Debris Shield
NASA	National Aeronautics and Space Administration
ONB	Onset of Nucleate Boiling
PCM	Pulse Code Modulated
PCU	Power Control Unit
PPO	Polyphenylene Oxide
QPSK	Quaternary Phase-Shift Keying
RAM	Random Access Memory
RF	Radio Frequency
ROM	Read Only Memory
SADA	Solar Array Drive Assembly
SCE	Spacecraft Control Electronics
SECO	Sustainer Engine Cutoff
SLC-36	Space Launch Complex 36
SMA	S-band Multi-access
SOC	Science Operations Center
SOCC	Spacecraft Operations & Control Center
SPS	Samples per Second
SSU	Sequential Shunt Unit
STDN	Space Tracking Data Network
TC&DH	Telemetry Command and Data Handling
TDRS	Tracking Data Relay Satellite
TDRSS	Tracking Data Relay Satellite System
TT&C	Telemetry, Tracking, and Control
TVS	Thermodynamic Vent System
UPS	Uninterruptable Power Supply
VCS	Vapor Cooled Shield

LIST OF SYMBOLS

LATIN

A	Area	m^2
B	Tank wall thickness	m
c_p	Specific heat	J/kg-K
C_f	Friction coefficient	Dimensionless
d	Diameter	m
	Flow diameter	m
D	Diameter	m
D_h	Hydraulic diameter	m
D_p	Diameter of helix	m
f	Friction factor	Dimensionless
g	Gravitational acceleration	m/s^2
g_c	Dimensional constant	$kg\cdot m/N\cdot s^2$
g_o	Gravitational acceleration on earth	m/s^2
G	Mass velocity	$kg/m^2\cdot s$
Gr	Grashof number	Dimensionless
h	Heat transfer coefficient	$W/m^2\cdot K$
h_{fg}	Heat of vaporization	J/kg
H	Head rise	m
k	Thermal conductivity	$W/m\cdot K$
$k(T)$	Temperature dependent thermal conductivity	$W/m\cdot K$
K	Empirical constant used in large eddy model	Dimensionless
	Pressure Loss Coefficient	Dimensionless
L	Length	m
	Length scale or tank wall heater spacing	m
	Dimensionless mixing length	Dimensionless
L_e	Equivalent pipe diameter lengths	Dimensionless
m	Mass	kg
\dot{m}	Mass flow rate	kg/s
M	Thermal mass	kg
n_s	Pump specific speed	Dimensionless
N	Flux of micrometeoroid or debris particles	Number/ m^2/s
Nu	Nusselt Number	Dimensionless
OD	Outer diameter	m
P	Pressure	Pa
P_o	Probability of not receiving an impact at a specific flux level of a specific particle size or larger	Dimensionless
Pr	Prandtl Number	Dimensionless

LIST OF SYMBOLS (CONT.)

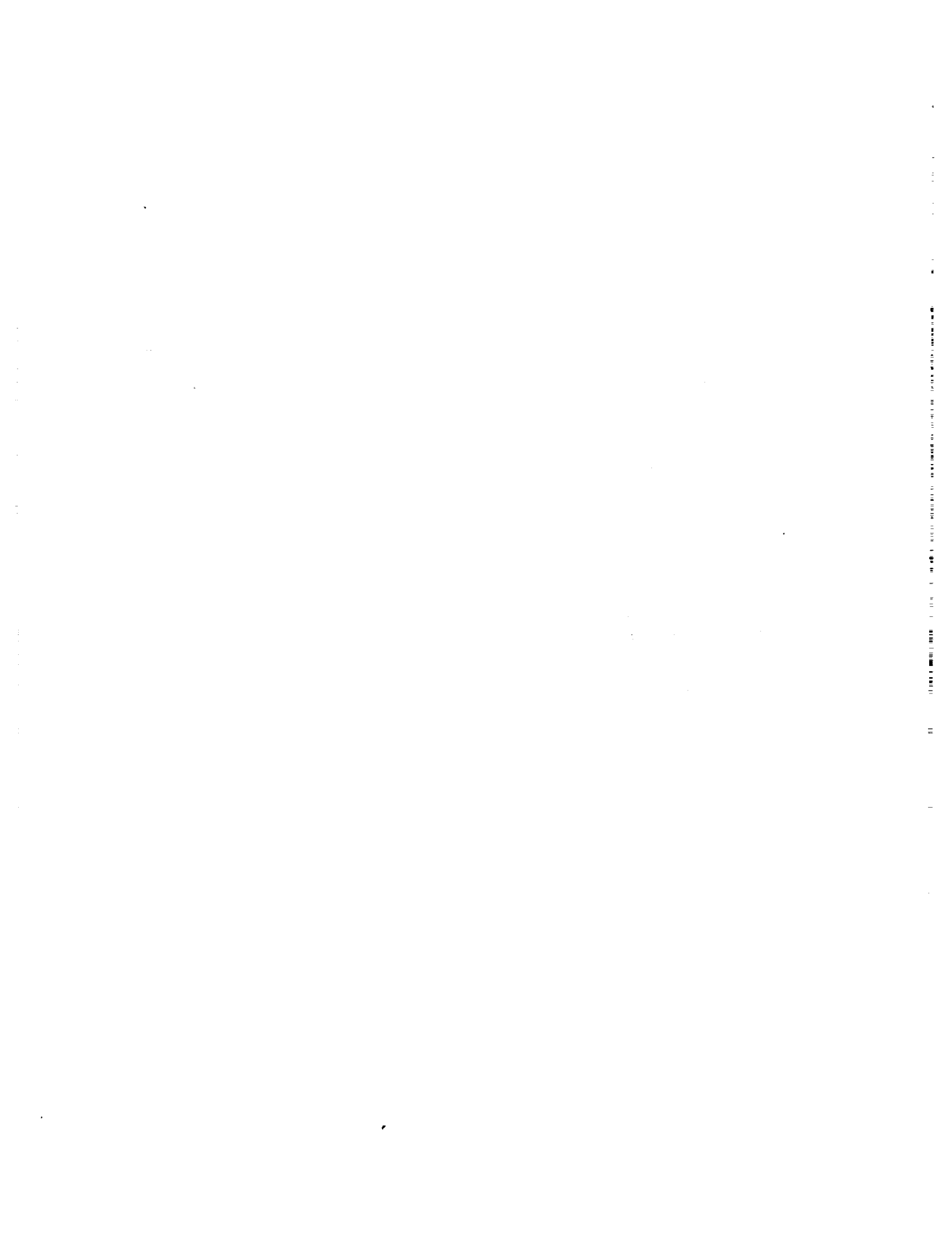
q	Heat flux	W/m ²
q''	Heat flux	W/m ²
q'' _H	Heater heat flux	W/m ²
Q	Volumetric flowrate	m ³ /s
	Heat flow	W
r	Radial distance	m
R	Radial distance	m
	Dimensionless radial distance	Dimensionless
Re	Reynolds Number	Dimensionless
S	Micrometeoroid/debris shield inner wall thickness	m
St	Stanton Number	Dimensionless
t	Time	s
T	Temperature	K
	Dimensionless time	Dimensionless
u	Specific internal energy	J/kg
	Velocity	m/s
U	Dimensionless velocity	Dimensionless
	Convection velocity or axial velocity	m/s
	Overall heat transfer coefficient	W/m ² -K
v	Specific Volume	m ³ /kg
V	Velocity	m/s
	Transverse velocity	m/s
	Volume	m ³
W	Dimensionless angular velocity	Dimensionless
	Tank wall heater width	m
x	Flow direction coordinate or axial coordinate along spacecraft	m
	Fluid quality	Dimensionless
X	Lockhart-Martinelli correlation factor	Dimensionless
y	Transverse coordinate or distance from wall	m
<u>GREEK</u>		
β	Thermal expansion coefficient	1/K
δ	Length scale	m
Δ	Change in the quantity	
ε	Dissipation rate	m ² /s ³
	Emittance	Dimensionless

LIST OF SYMBOLS (CONT.)

μ	Absolute viscosity	N-s/m ²
ν	Kinematic viscosity	m ² /s
ρ	Density	kg/m ³
σ	Surface tension Stefan Boltzmann constant	N/m W/m ² K
τ	Shear stress Perforation grade	N/m ² Dimensionless
ω	Angular velocity	radians/s

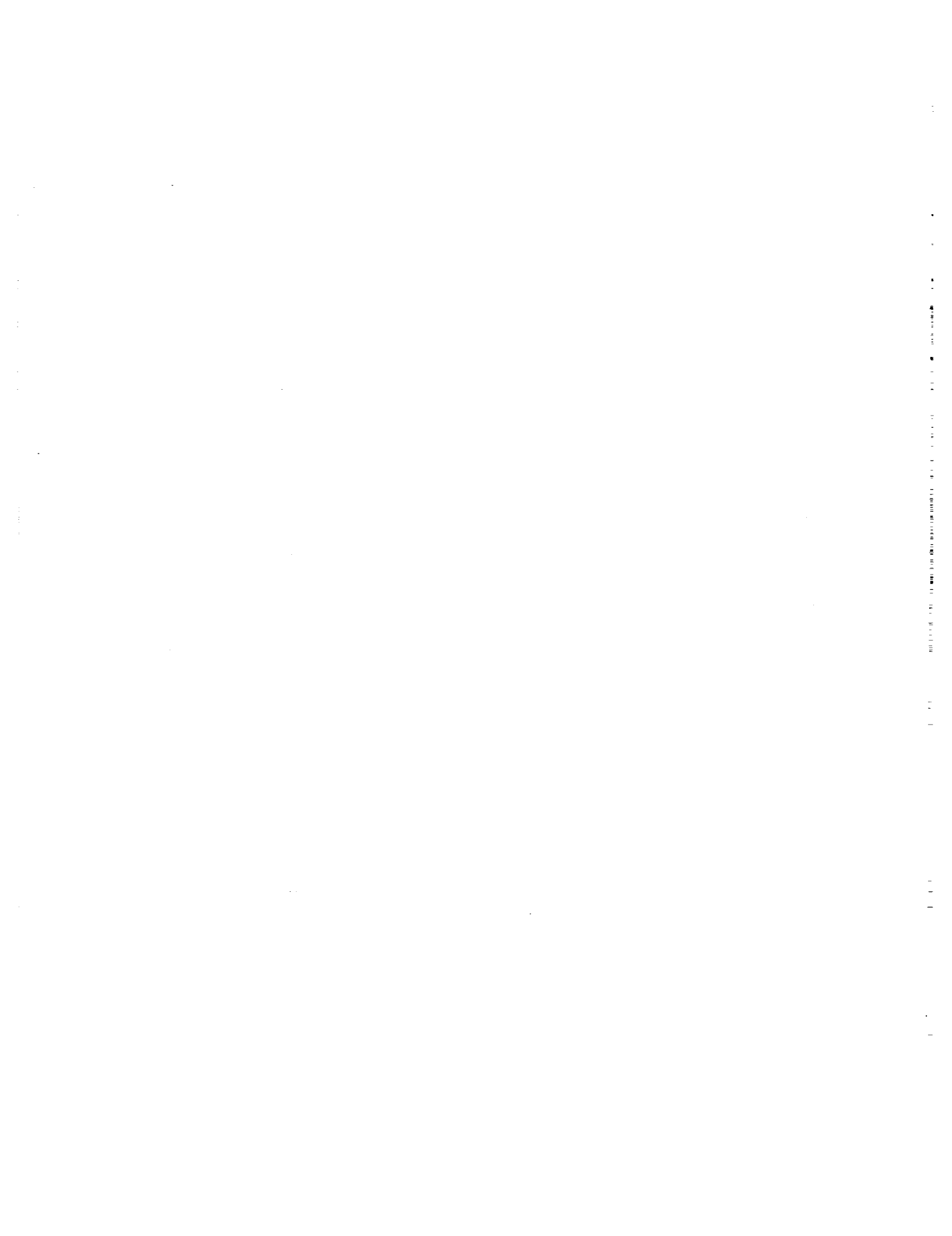
SUBSCRIPTS

10	To the base ten
463	Altitude of 463 km
1297	Altitude of 1297 km
abs	Absorbed
avg	Average
c	Corrected for helix
eff	Effective value
f	Saturated liquid
g	Saturated vapor
i	Inner
l	Liquid
lm	Log-mean
max	Maximum
min	Minimum
o	Outer or initial
p	Particle
s	Shield
sat	Saturation
t	Tube
turb	Turbulent value
v	Vapor
w	Wall



CONVERSION FACTORS

<u>QUANTITY</u>	<u>METRIC QUANTITY</u>	<u>ENGLISH EQUIVALENT</u>
Acceleration	1 m/s ²	3.281 ft/sec ²
Angular momentum	1 N•m•s	8.545x10 ⁴ lb _m •ft ² /h
Area	1 m ²	10.76 ft ²
Diffusion coefficient	1 m ² /s	3.875x10 ⁴ ft ² /h
Dynamic viscosity	1 Pa•s	2419 lb _m /ft•h
Energy	1 J	9.479x10 ⁻⁴ Btu
	1 J	2.778x10 ⁻⁴ W•h
Force	1 N	0.2248 lb _f
Heat transfer rate	1 W	3.412 Btu/h
Heat flux	1 W/m ²	0.3171 Btu/h•ft ²
Heat transfer coefficient	1 W/m ² •K	0.1761 Btu/h•ft ² •°R
Kinematic viscosity and diffusivity	1 m ² /s	3.875x10 ⁴ ft ² /h
Latent heat, enthalpy and internal energy	1 J/kg	4.300x10 ⁻⁴ Btu/lb _m
Length	1 m	3.281 ft
	1 mm	0.03937 in
	1 km	0.5396 NM
Mass	1 kg	2.205 lb _m
Mass density	1 kg/m ³	0.06243 lb _m /ft ³
Mass flowrate	1 kg/s	7937 lb _m /h
Mass flux	1 kg/m ² •s	737.4 lb _m /ft ² •h
Mass moment	1 cm•kg	0.8681 in•lb _m
Mass transfer coefficient	1 m/s	1.181x10 ⁴ ft/h
Pressure and stress	Pa	0.02089 lb _f /ft ²
	Pa	1.450x10 ⁻⁴ lb _f /in ²
Specific heat	1 J/kg•K	2.389x10 ⁻⁴ Btu/lb _m •°R
Specific impulse	1 N•s/kg	0.1020 lb _f •sec/lb _m
Temperature	K	0.5556 °R
Temperature difference	K	1.800 R°
Thermal conductivity	1 W/m•K	0.5778 Btu/h•ft•°R
Volume	1 m ³	35.31 ft ³
Volume flowrate	1 m ³ /s	1.271x10 ⁵ ft ³ /h



1
SUMMARY

1.1 BACKGROUND

The United States is entering an era of expanded space activity that will involve space-based operations to carry out and support new space transportation missions. A key aspect of these missions is their dependence on high energy, cryogenic propellants. Long-lived space systems that depend on the use of subcritical cryogenics present low-gravity fluid management challenges as well as special storage and utilization problems due to the low fluid temperatures. Cryogenic fluid management is clearly a critical development area for these future space missions. In-space testing will be required to verify much of the technology needed for future space missions. Much of the testing will address systems-level behavior and control during representative operations under low-gravity conditions.

In recognition of these technology needs, the NASA Lewis Research Center has funded feasibility studies of COLD-SAT (Cryogenic On-Orbit Liquid Depot Storage, Acquisition, and Transfer Satellite), a free-flying orbital experiment to be launched by an expendable launch vehicle (ELV) in 1997. The objectives of the feasibility studies included the following: creation of a set of detailed requirements for Class I (mission enabling) and Class II (mission enhancing) cryogenic fluid management experiments; conceptual design of an ELV-launched orbital spacecraft for carrying out the experiments; preparation of preliminary plans for the COLD-SAT project; and, project cost estimates.

1.2 EXPERIMENT SUMMARY

The general experiments which are being performed on COLD-SAT are listed in Table 1-1. The Class I experiments are those considered to be "enabling" and were given priority in our study. Our system was designed to achieve at least a 92 percent probability of success in completing these experiments. For the design in this report the estimated probability of success is 95 percent. The Class II experiments are considered to be "enhancing" and were given lower priority, in order to minimize the resources for their implementation. The major space transportation systems which would benefit from the technology being addressed by COLD-SAT include Space Transfer Vehicles (STVs), Orbital Fuels Depots, Propellant Resupply Tanker, and Space Station Freedom. The applicability of the COLD-SAT experiments to these is indicated in the table.

The following paragraphs contain brief descriptions of all of the experiments, including a brief statement of the problem, the objective of the experiment, and the major parameters of interest. In all cases, in addition to the objectives stated, a common objective is that data be obtained to correlate with ground test data and models being used to predict the various phenomena.

1.2.1 Pressure Control

Cryogenic fluids are not "storable", either on the ground or in space. A net heat inflow to the storage tank causes the fluid to warm and the pressure to rise, making venting necessary. Settled venting is the pressure control technique used on the Centaur upper stage, and it is a possible technique for some applications. However, cryogenic tanks will most likely be required on platforms which will not allow the artificially imposed acceleration necessary for settling. Thus, an alternative approach is required.

Table 1-1. List of COLD-SAT Experiments and Application

Experiments	Application			
	STV	Space-based Depot	Resupply Tanker	Space Station
Class I Experiments				
Tank Pressure Control	X	X	X	X
Tank Chill-Down	X	X		X
Tank No-vent Fill	X	X		X
LAD Fill/Refill	X	X		X
Class II Experiments				
Tanker Thermal Performance			X	
Pressurization	X	X	X	X
Low-G Settling and Outflow	X	X	X	
LAD Performance	X	X	X	X
Transfer Line Chill-down	X	X		X
Outflow Subcooling		X	X	X
Low-G Vented Fill	X	X		
Fluid Dumping	X	X	X	X
Advanced Instrumentation	X	X	X	X

The most promising approach for pressure control in low-g is the thermodynamic vent system (TVS). Besides maintaining tank pressure, it can also be designed to subcool the liquid in the tank. However, there are a number of alternative TVS designs and essentially no data on their performance, nor the severity of the tank thermal stratification and pressure control problem. The objectives of this experiment are to 1) investigate stratification and pressure rise in tanks subjected to various heating rates, and 2) evaluate tank pressure control techniques using active and passive TVS concepts. The major elements of these concepts include mixers, internal wall-mounted heat exchangers, external wall-mounted heat exchangers, compact heat exchangers, and Joule-Thomson throttling devices.

1.2.2 Tank Chill-down

Transfer of cryogenic fluids from one tank to another in space will be an essential feature of future space transportation systems. Since the cost of transporting material from the ground to LEO is high, it is essential that losses due to chill-down of receiver tanks be minimized. This experiment will evaluate the "charge/hold/vent" tank chill-down procedure in low gravity, including an evaluation of the effects of tank shape, tank mass, nozzle orientation and flowrate, mass injection profile, and staged venting on the injected mass required and on the time to accomplish the chill-down.

1.2.3 Tank No-vent Fill

Following the chilling of the receiver tank, the tank must be filled with liquid. It is paramount that this process be performed to minimize the loss of stored liquid cryogen. A procedure termed "no-vent fill" has been proposed to minimize the liquid losses that could occur in a low-g environment. It is similar to the tank chill-down procedure in that nozzles are used to inject the liquid into the tank and promote mixing and collapse of the existing vapor. This procedure has yet to be demonstrated in space. The objective of the experiment is to determine the effects of nozzle orientation, nozzle flowrates, g level, and tank fill level on the no-vent fill process. The fill level goal is at least 95 percent.

1.2.4 Liquid Acquisition Device Fill/Refill

A passive, channel-type, total communication liquid acquisition device (LAD) is an ideal system for use with a space-based cryogenic depot. Such systems have been used extensively in space, but only with storable fluids. These devices are notoriously difficult to fill in one-g, and it is anticipated that the problems could be magnified in low gravity, where the liquid could more readily wet the screen surface before trapped vapor is ejected. Two different LAD configurations will be evaluated. The objectives include determination of the effects of filling rate, LAD configuration, LAD venting through the TVS, LAD initial temperature, and tank pressurant species on the ability to fill the LAD and collapse the bubbles within.

1.2.5 Tanker Tank Thermal Performance

The supply tank insulation system will have features characteristic of both Earth-to-orbit resupply tankers and on-orbit depots. It will have a helium-purged multi-layer (MLI) insulation system to prevent cryopumping of condensable gases on the ground and a vapor-cooled shield (VCS) for absorbing more of the tank heat leak when on orbit. A major question concerning the MLI, which is quite thick (76 mm), is whether the escape of gas during ascent may adversely affect the subsequent insulation performance. The structural and thermal performance of the system will be evaluated during the ascent phase and after space equilibrium conditions are achieved. The time required to achieve space equilibrium conditions, and the measurement of the space thermal performance over an extended period of time will be investigated.

1.2.6 Tank Pressurization

Pressurant collapse due to cooling and condensation in cryogenic tanks on the ground or when undergoing acceleration has been quantified. However, these conditions are substantially different from those for long cryogenic tank transfers in low-gravity. The objective of the experiment is to determine the amount of pressurants required for the LH₂ transfer process under varying conditions of pressurant flow, g-level, tank fill-level, pressurant temperature, and tank pressure. Data will be taken to compare the performance of an autogenous hydrogen pressurization system, a stored gaseous hydrogen pressurization system, and a stored gaseous helium pressurization system.

1.2.7 Low-g Settling and Outflow

An alternative to the use of a total communication liquid acquisition device is the process of applying a low acceleration level to settle and outflow liquid from one tank to another. This experiment will determine settling times under controlled low-gravity conditions and determine residuals at vapor pull-through for various g-levels and outflow rates. Settling under the influence of pulsed thrusting will also be tested.

1.2.8 Liquid Acquisition Device Performance

Screened channel-type liquid acquisition devices are commonly used with storable liquids in zero-gravity. New problems surface when the fluid is cryogenic and the screens are subject to premature dryout and breakdown. The performance of a LAD will be investigated under normal and adverse operating conditions. As with many of the Class II experiments, these will be integrated with the Class I transfer tests. Objectives are to evaluate the effects of a tank hot spot, g-level, and flowrate on the ability of channel-type LADs to transfer vapor-free liquid from tanks.

1.2.9 Transfer Line Chill-down

Another aspect of minimizing liquid loss in space is the optimization of transfer system chill-down. The phenomena associated with fluid flow and heat transfer inside a pipe are known to be gravity dependent, and this experiment will quantify those effects. Two different transfer lines will be tested in conjunction with other COLD-SAT transfers. The objective is to determine the flowrate, the time, and the liquid quantity required for transfer line chill-down. Both continuous and intermittent flow of the chill-down liquid will be tested. The venting of the line chill-down fluid through a tank to accomplish some degree of tank chilling will also be tested.

1.2.10 Outflow Subcooling

The subcooling of liquids in space will be required in conjunction with liquid transfers. One approach is to subcool the outflow from the supply tank as it passes through the transfer plumbing and to the receiver tank. For this purpose, a subcooling heat exchanger, cooled by throttled fluid from the supply tank, can be used. The fluid passing through the cold side of the heat exchanger is vaporized before it exits the unit, subcooling the main transfer flow of liquid. The objective of this experiment is to evaluate the effectiveness of a compact heat exchanger in subcooling tank outflow, and the use of intermittent flow of the cold side fluid in controlling the capacity of the subcooler.

1.2.11 Low-Gravity Vented Fill

This experiment will investigate the type of filling process used in one-g, but at a very low acceleration level. The objective is to determine the effect of g-level, inflow rate and initial tank temperature on the ability to fill the tank without ingesting liquid into the vent. Tests will be conducted on one tank with a LAD, and one without a LAD.

1.2.12 Fluid Dumping

Operational scenarios are expected in which it could be necessary to dump cryogenic fluid from a tank in space, whether under emergency or planned conditions. Under such conditions freeze-up of the tank or lines could inhibit the operation. This experiment will focus on the evaluation of liquid dumping effectiveness and tank freeze-up in the two receiver tanks. Line freeze-up, which can be tested on the ground and is less gravity dependent, will also be tested in conjunction with other transfers. The rate of dumping, tank pressurization parameters, and heater power will be determined.

1.2.13 Advanced Instrumentation

This experiment has not been defined since the instrumentation is still in the process of development. Candidates for test include a compression mass gage, a two-phase flowmeter, and other more advanced instruments. These may include leak detectors, velocimeters, liquid orientation detectors, and fiber optic/video visualization systems.

1.3 SPACECRAFT DESIGN SUMMARY

The philosophy employed for the design of the COLD-SAT spacecraft has been to physically separate the experiment and bus systems to the extent possible to facilitate design, production,

checkout and assembly. Great emphasis has been placed on keeping the interfaces between the bus and experiment simple, adhering to experiment performance goals in the bus design, using flight-proven bus components to minimize development risk, and designing for high reliability. The selection of the launch vehicle is a major factor in the design of the spacecraft and the capability of the experiment. After studying the capabilities and cost of U.S. launchers and the experiment features they could accommodate, the Atlas I was chosen, along with the 4.2 m diameter, 64.4 m³ payload fairing option. This combination provides ample lift and volumetric capacity, and the Atlas I allows the use of existing liquid hydrogen handling facilities and procedures, trained personnel at the launch pad, and the use of an experiment liquid hydrogen supply tank without a heavy, costly vacuum jacket. Ground and ascent venting of the supply tank is accomplished through connection to the Centaur existing flight vent system.

With the Atlas I, launch pad fluid supply modifications are limited to extending GN₂, GHe and LH₂ supply lines higher up the tower and using a retractable boom and umbilical to service the COLD-SAT spacecraft through an experiment-mounted disconnect panel accessed through a spring-loaded door in the payload fairing. A COLD-SAT purge control module would be mounted on the boom and the Centaur tanking control panel in the blockhouse would be supplemented with a panel to control COLD-SAT tanking.

The COLD-SAT spacecraft, illustrated in Figure 1-1, is composed of two main modules, the experiment module and the spacecraft bus module. The experiment module consists of structure, the three insulated experiment tanks, instrumentation sensors, pumps, valves and associated plumbing. The experiment tanks consist of a 5.38 m³ ellipsoidal supply tank, a 1.27 m³ cylindrical receiver tank, and a 0.62 m³ spherical receiver tank. The experiment structure is of aluminum honeycomb, and encloses the experiment module to provide micrometeoroid/debris protection as well as support the tanks and other components. Some experiment equipment, including the stored helium and hydrogen gas pressurant tanks and all of the experiment support electronics is mounted within the bus module. The bus module consists of the bus structure and attitude control, propulsion, electrical power, telemetry and data handling, spacecraft control electronics, and thermal control hardware. The cut-away view of the vehicle shows it in its operational configuration with the solar arrays, high gain S-band antenna and omni-directional S-band antenna deployed. The solar arrays are canted at a 26 degree angle to the Y-axis to keep the solar vector as close to the normal of the solar array as possible, thus permitting the use of a single-axis solar array drive. The earth sensors mounted on the +X and -X ends of the vehicle have conical shields to protect their optics from thruster plume contamination.

The bus structure is a design adapted from Ford Aerospace's typical bus construction for a three-axis stabilized spacecraft. To efficiently package the experiment module, reduce weight and lower the center of gravity of the vehicle, it was necessary to select a new structure based on previously flown designs. The main load structure of the bus is the central cylinder which was enlarged to contain one of the experiment tanks and its insulation system. The bus enclosure is an aluminum honeycomb panel box supported by shear webs off the central cylinder. The experiment module is bolted to the +X end of the cylinder and a launch vehicle separation clamp is attached to the -X end. The propellant tanks, helium and hydrogen pressurant tanks, and the internal experiment tank are supported off the cylinder by struts.

A mass summary for the spacecraft is given in Table 1-2 and a propellant budget is given in Table 1-3. A 20 percent mass contingency was maintained to allow for design uncertainties and future modifications. The total liftoff mass for the spacecraft, including contingencies, is 3455 kg, and added to the payload adapter and separation system is well within the capability of the Atlas I launch vehicle (4750 kg capacity to 1300 km).

Under the control of the Spacecraft Control Electronics (SCE), the spacecraft bus can function autonomously for up to 28 days without ground commands. Since real-time control of the

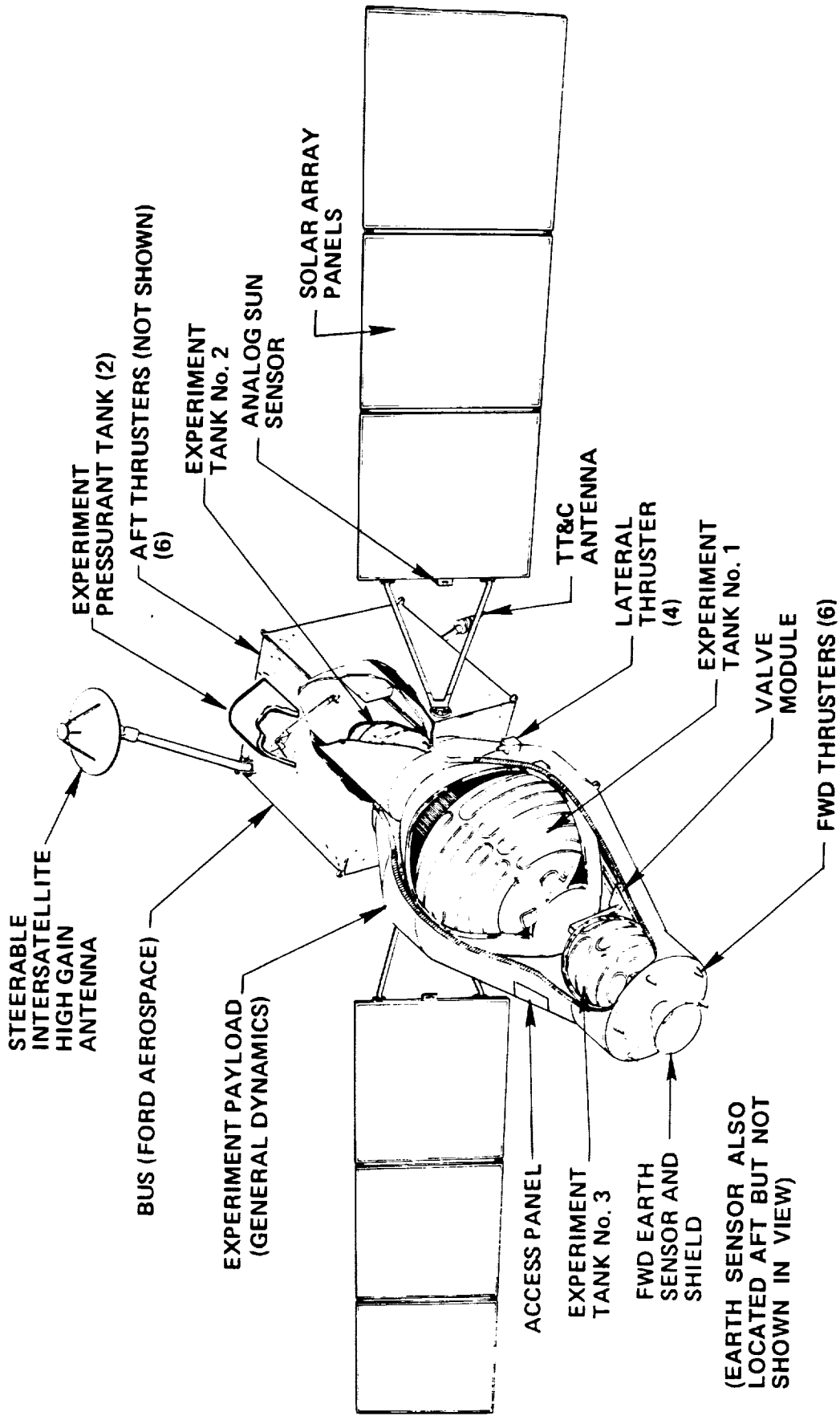


Figure 1-1. On-orbit Spacecraft Configuration

Table 1-2. COLD-SAT Mass Summary

<u>Experiment Module</u>	1199.4 kg	<u>Spacecraft Bus</u>	784.4 kg
Primary Structure	290.0	Structure	218.2
Fairings & Supports	111.0	Mech. Integration	22.7
Tank 1	109.9	Elect. Power	141.9
Tank 2	33.3	Solar Arrays	118.9
Tank 3	16.1	Elect. Integration	31.8
Fluid Systems	376.4	Propulsion	68.5
Thermal Control	106.9	T C & D H	86.0
Instr. & Control	56.8	Attitude Control	76.1
Electrical	99.0	Thermal Control	20.3
	Spacecraft Dry Mass	1983.8	
	Liquid Hydrogen	364.5	
	Hydrazine Propellant	530.5	
	20% Mass Contingency	575.8	
	<u>Payload Adapter & Clamp</u>	<u>72.0</u>	
	Total Payload Mass	3526.6 kg	

Table 1-3. Propellant Budget

EVENT	PROPELLANT (kg) ISP = 2157.7 $\frac{\text{N-sec}}{\text{Kg}}$
Initial Attitude Acquisition	6.80
Drag Makeup	NONE*
Reaction-Wheel Unloading	27.22
Experimental Maneuvers	
- Class I	292.35
- Class II	66.89
<u>Unallocated Contingency</u>	<u>22.68</u>
Subtotal	415.94
Residual/Holdup	6.80
Total Propellant (Hydrazine)	422.74
Pressurant (Helium)	1.81
Launch Tankage Capacity (90%) (4 hydrazine propellant tanks)	530.5
Excess Capacity Available	105.95

* Thrusting for experiments totally negates need for drag makeup

experiment from the ground is not possible due to communications limitations, the SCE will control the experiment with limited autonomy for periods up to a few orbits. The SCE provides telemetry processing, command, and control for all of the subsystems. The processor analyzes the data from the attitude control system sensors and generates the necessary signals to maintain attitude for all mission phases, including pointing the spacecraft +X axis along the velocity vector for the experiments, positioning the solar arrays and high gain antenna, and maintaining attitude during thrusting maneuvers. Additionally, the SCE autonomously controls battery charge and discharge management, maintains thermal control by operating heaters, performs data acquisition and management for both the bus and the experiment, and tracks center of mass changes due to propellant consumption.

COLD-SAT communications provides telemetry command and ranging functions to facilitate data downlink, tracking, and ground control. The primary communications link to the ground is through the TDRSS S-Band Multiple Access Service using the COLD-SAT high gain steerable antenna. Experiment and bus telemetry data will be sequentially sampled by the SCE, formatted, and stored in solid state memory for later downlink. Telemetry data is transmitted through TDRSS at 38 kbps during a 10 minutes per orbit TDRS contact time (available capacity on the S-Band MA link is 50 kbps). Command data is uplinked at 1 kbps simultaneously during downlink operations for efficient use of the TDRS contact time. The uplink data capability includes functional commands and replacement software code for either the attitude control system or the experiment. Contingency communications is provided by a half-omni antenna diametrically positioned relative to the high gain antenna for a low rate data link either through the TDRSS or directly to a STDN ground station.

The three-axis stabilization attitude control system uses conical Earth sensors, analog and digital sun sensors, and gyros as sensors. Thrusters, reaction wheels, and magnetic torquers are used as actuators. The SCE provides processing of the sensor data, actuator control, automatic momentum dumping, thruster selection during maneuvers, processing and storage of commands, maintenance of ephemeris data, and the processing of attitude control information required by other subsystems. Three orthogonal magnetic torquers dump excess reaction wheel momentum, avoiding the use of thrusters which would disturb the experiments.

Onboard propulsion is required to provide a wide range of linear acceleration for certain experiments and to provide backup attitude control actuation. Both +X and -X thrusters were used for experiment thrusting so that different internal equipment could be used at each end of the experiment tanks, increasing the flexibility of the experiment design. Each of the thrusters has 0.53 Newton thrust. For each test an appropriate number of thrusters will be used to produce nominal accelerations of either 20, 50, or 100 μg for continuous periods up to 46.5 hours.

1.4 MISSION SUMMARY

COLD-SAT is designed for a one year operational lifetime but the liquid hydrogen is expected to be expended through experiment usage and storage losses within six months. Orbital analysis was based on an expected launch from Kennedy Space Center in 1998 using an Atlas I expendable launch vehicle. The Atlas I will use a two-burn boost sequence to place COLD-SAT into a 1300 km circular orbit at 28.5 degree inclination. The altitude was chosen to provide a 500 year orbital lifetime and to fit within a current minimum in the orbital debris environment. Also, at this altitude the drag accelerations and the atomic oxygen concentrations are negligible. The orbital period is 111.5 minutes with a maximum eclipse duration of 35.2 minutes.

Shortly before launch the spacecraft is placed on internal battery power and a variety of internal equipment is activated including the Spacecraft Control Electronics (SCE), command receivers, selected sensors, gyros, and reaction wheels. After liftoff, telemetry is unavailable from the spacecraft. The launch base will keep the control center team apprised of progress via the voice network. Upon separation of the spacecraft from the upper stage of the Atlas I, the TC&DH omni

antenna and the high gain antenna will be pyrotechnically released. Commanding will then commence from a STDN ground station via the omni antenna. The high gain antenna gimbal mechanism will be enabled, allowing the antenna to track TDRS.

At separation, COLD-SAT will have an initial roll rate of 2 Hertz. Pitch and yaw will be negligible unless tip-off rates are encountered. The attitude control system will be activated and checked. Then the propulsion system will be vented, thruster operation verified, and the vehicle despun. The spacecraft will be commanded to a stable control mode for solar array deployment. After solar array deployment, the Earth acquisition mode will be commanded, the solar arrays slewed to acquire the sun and placed in their sun tracking mode. These operations will be done during the first three orbits. Next, on-orbit checkout of the spacecraft bus and the experiment will be done for several orbits. After the checkout is completed, normal operations and experimental testing can begin.

The spacecraft will fly with the long axis (X-axis) of the vehicle coincident with the orbital velocity vector. The Y-axis will be normal to the orbital plane which will allow the solar arrays to track the sun. Since the solar arrays have only a one degree-of-freedom drive and are canted to the body of the spacecraft, they will require a 180 deg. roll or pitch maneuver about once a month. This will keep the solar vector to within 26 deg. of the normal to the plane of the arrays and limit the loss in efficiency due to off-normal operation. No drag make-up thruster firings are required, but thrusters will be used as a backup for reaction wheel momentum dumping. Normally, reaction wheel desaturation will be done using the three-axis magnetic torquer array.

During normal orbital operations communications will be through the TDRS system (TDRSS) using the high gain antenna. The contact time has been limited for link sizing purposes to ten minutes per orbit to minimize potential TDRSS scheduling problems. The orbital altitude is sufficient to be above the zone of exclusion where the Earth blocks the line-of-sight between both Tracking Data Relay Satellites however, during a portion of the orbit the high gain antenna is blocked by the spacecraft. This occurs during predictable portions of the orbit and normal TDRSS contacts will be scheduled accordingly. Since the omni antenna is on the opposite side of the vehicle from the high gain antenna, during these periods it would still be possible to send commands to COLD-SAT, if necessary. Backup command communications will be through the three remaining STDN ground stations using the omni antenna. On any given orbit, from zero to three of the STDN ground stations may be in a position to communicate with the spacecraft. However, as many as six consecutive orbits (11.2 hours) may pass without a STDN ground station being visible. An on-board bubble memory storage device can store up to eight hours of telemetry data in the event that the TDRS link is not available.

On-orbit ground operations consist of monitoring spacecraft telemetry data for health and safety, collecting stored experiment data via approximately seven minute (of the ten minute contact period) data dumps per orbit, and sending commands to the spacecraft as needed. Real-time telemetry will be monitored for approximately 10 minutes per orbit. During the contact, experiment data will be dumped from the recorder. Hard copies of all major display pages will be made at each contact. Primary telemetry parameters will be monitored. Any unexpected changes or alarms will be responded to according to the contingency procedures developed for the mission.

The Spacecraft Control Electronics (SCE) will control and monitor the experiment since real-time control of the experiment is not possible because continuous communications contact is not maintained with the spacecraft. A test or conditioning sequence can be initiated either with a real-time or a time-tagged command. Stored command sequences used to control each test will be resident onboard in the experiment Application Program Software. A test is initiated by identifying the appropriate stored sequence to be used and passing the desired parameters to be used in the sequence. Experiment test sequences are reprogrammable so that new or modified sequences can be substituted for the stored sequences if necessary.

The tests will be done in the order specified by experiment procedures. This procedure is developed based on the priority of the individual tests, the current status of the thermodynamic state of each tank, pretest conditioning requirements, the efficiency of performing the next test operation, allowance for bus housekeeping maneuvers, and ground personnel scheduling constraints.

The experiment requires extended periods of continuous thruster firings to provide acceleration environments greater than the background accelerations imposed by the spacecraft environment. These thruster firings will be in either the +X or -X directions depending on the specific test. Providing thrust in both of these directions allows different internal hardware to be used at each end of the experiment tanks to increase the variety of tests that can be performed. Over the lifetime of the mission, these firings would raise the altitude of the orbit. There are no plans to correct the change in altitude since none of the effects appear to impact the mission. Since the majority of the firings are in the +X direction, it will be necessary to occasionally rotate the vehicle so that experiment thrusting will be in the opposite direction, thus limiting the total increase in altitude.

Before initiating an experiment, the control system will be reconfigured in one of two ways. First, for no-thrust experiments, which require very low acceleration fields, the spacecraft will be configured to minimize all torque effects. This is accomplished by decreasing control loop gains, and enabling magnetic torquers to provide wheel unloading. Second, for experiments requiring higher accelerations, thrusters will be enabled. The thruster combinations used for a particular acceleration level will be alternated during the firing to perform continual wheel unloading to prevent wheel saturation.

When the supply of liquid hydrogen has been depleted, testing will be terminated and the spacecraft will be shut down. The orbit was selected to provide a minimum of 500 years orbital lifetime so no end of life maneuvers will be required unless it is desired to burn any remaining propellant.

2 INTRODUCTION

The United States is entering an era of expanded space activity that will involve space-based operations to carry out and support new space transportation missions, as indicated in Figure 2-1. These missions, along with their earliest forecasted dates, include the Space Station Freedom (1998), Orbital Fuels Depot (2004), Space Transfer Vehicle (STV) (initial 1999, space-based 2005), Resupply Tanker (2004), and, in the longer term, such human exploration missions as lunar base (2007) and piloted Mars expeditions (2010-2020). The missions are technically challenging, and will require strong, sustained technology development efforts.

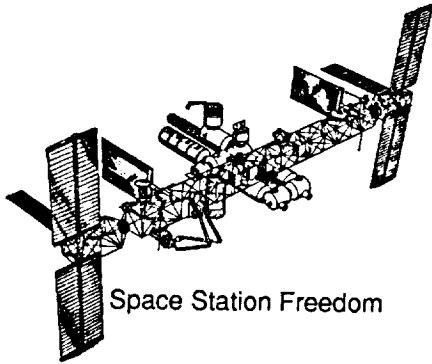
A key aspect of these missions is their dependence on high energy, cryogenic propellants. Long-lived space systems that depend on the use of subcritical cryogenics present low-gravity fluid management challenges as well as special storage and utilization problems due to low fluid temperature. Fluid management needs were recently addressed in a NASA-sponsored workshop devoted to requirements for in-space testing (Reference 2-1). Table 2-1 lists future missions along with cryogenic fluid management technology categories where enabling or enhancing data will be needed. Enabling technology is that which must be made available in order to perform the mission. Enhancing technology isn't essential, but it could provide substantial mission benefits in the areas of performance, cost, risk and schedule. Cryogenic fluid management is clearly a critical development area for these future space missions.

Testing objectives are given in Table 2-2 for the cryogenic fluid management technology categories. System developers, whether in government or industry, are faced with needs for an engineering data base, validated performance models, and brassboards or prototypes that have had certain key features demonstrated in the appropriate environments and at the appropriate systems level. In-space testing will be required to verify much of the technology needed for future space missions. Much of the testing will address systems-level behavior and control during representative operations under low-gravity conditions.

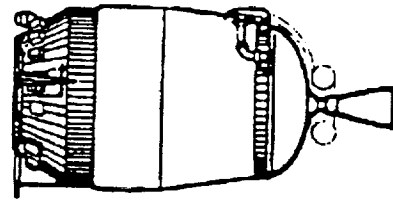
In recognition of these technology needs, the NASA Lewis Research Center has conducted ground-based research while planning a cryogenic flight experiment. The Cryogenic Fluid Management Flight Experiment (CFMFE) was to be a subcritical liquid hydrogen experiment performed in the cargo bay of the Space Shuttle Orbiter. Plans for it were discontinued after reassessment of payload safety criteria following the *Challenger* accident. Lewis Research Center has continued its investigations, funding feasibility studies of COLD-SAT (Cryogenic On-Orbit Liquid Depot Storage, Acquisition, and Transfer Satellite), a free-flying orbital experiment (Figure 2-2) to be launched by an expendable launch vehicle (ELV) in 1997. This report presents results from the Feasibility Study performed by General Dynamics Space Systems Division and its subcontractor Ford Aerospace Corporation Space Systems Division.

2.1 OBJECTIVES AND SCOPE

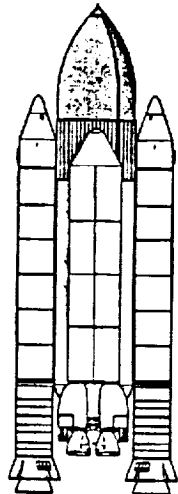
The objectives of the Feasibility Study included the following: creation of a set of detailed requirements for Class I (mission enabling) and Class II (mission enhancing) cryogenic fluid management experiments; conceptual design of an ELV-launched orbital spacecraft for carrying out the experiments; preparation of preliminary plans for the COLD-SAT project; and, project cost estimates. Figure 2-3 illustrates the COLD-SAT team responsibilities. General Dynamics led the study, including the project planning and documentation efforts, which were supported by Ford Aerospace. Ford Aerospace was responsible for the spacecraft bus and launch vehicle integration. General Dynamics was responsible for the experiment and the ground segment. Interfaces between the experiment and bus were treated jointly, as was launch vehicle evaluation. Southwest Research Institute provided consultation on low-gravity fluid mechanics. The work was performed over the



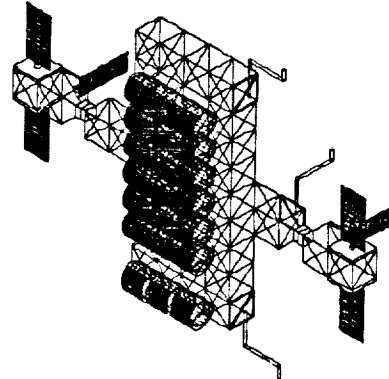
Space Station Freedom



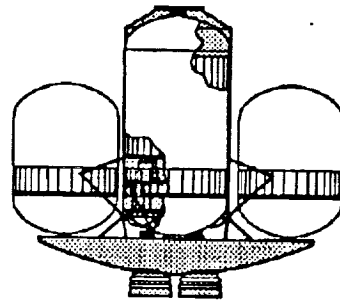
Initial Space Transfer Vehicle



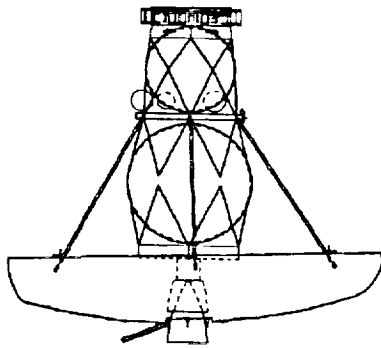
Shuttle C Resupply Tanker



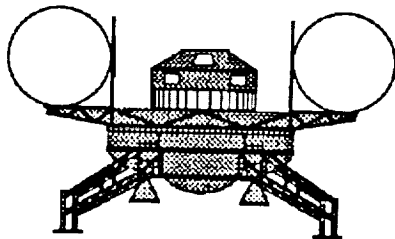
Orbital Fuels Depot



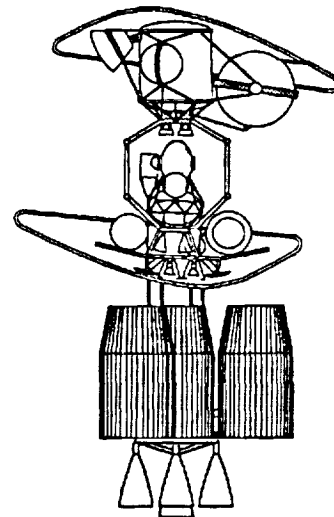
Lunar Transfer Vehicle



LEO-to-GEO STV



Lunar Excursion Vehicle



MTV/TMIS

Figure 2-1. Some Future Space Transportation System Elements Utilizing Cryogenics

Table 2-1. Cryogenic Fluid Management Technology Needs

Technology Category	Mission Criticality					
	Interim STV	Space-based STV	Orbital Depot	Resupply Tanker	Lunar Base	Mars Expedition
Liquid storage						
• Thermal control systems		Enhance	Enhance		Enhance	Enable
– Degradation of material	Enable	Enable	Enable	Enhance	Enable	Enable
– Effect of launch environment on thick MLI	Enhance			Enhance		
– Combined foam/MLI sys			Enhance		Enhance	Enhance
– Para/ortho conversion			Enhance		Enhance	Enable
– Multiple/coupled VCS						
• Pressure control systems						
– TVS performance	Enhance	Enhance	Enable	Enhance		Enable
– Fluid mixing for stratification control	Enhance	Enhance	Enable	Enhance		Enable
– Refrigeration/reliquefaction			Enhance		Enhance	Enable ?
Liquid supply						
• Pressurization system performance						
– Autogenous	Enhance	Enable	Enable	Enhance	Enable	Enable
– Helium	Enable					
– Mech (pumps/compressors)			Enhance	Enhance	Enhance	Enhance
• Fluid acquisition						
– Fine mesh screen LAD performance		Enhance ?	Enable	Enable		Enable
– Fluid settling and outflow under low-g conditions	Enhance	Enhance	Enhance	Enhance		Enhance
– Fluid settling and outflow under impulsive accel	Enhance	Enhance		Enhance		Enhance
– Impact of heat addition on LAD performance		Enhance	Enhance ?	Enhance		Enhance
– Thermal subcooling of liquid outflow			Enhance	Enhance	Enhance	Enhance
Liquid transfer						
• Transfer line chilldown		Enable	Enable	Enhance	Enable	Enable
• Tank chilldown with spray		Enable	Enhance			Enhance
• No-vent fill		Enable	Enable			Enhance
• LAD fill		Enhance ?	Enhance			Enhance
• Low-g vented fill		Enhance	Enhance			Enhance
• Pump assist		Enhance	Enhance	Enhance	Enhance	Enhance
Fluid handling						
• Liquid dynamics/slosh control	Enhance	Enhance	Enhance	Enhance		Enhance
• Fluid dumping and tank inerting		Enable	Enable	Enhance		Enhance
• Earth-to-orbit transport as subcooled liquid or slush	Enhance	Enhance	Enhance	Enhance		Enhance
Advanced instrumentation						
• Quantity gauging	Enhance	Enhance	Enable			Enhance
• Mass flow/quality metering			Enhance		Enhance	Enhance
• Leak detection		Enhance	Enable		Enable	Enable
• Liquid/vapor sensors	Enhance	Enable	Enable	Enhance	Enable	Enable
Tank structures and materials						
• Low thermal conductivity components	Enhance	Enhance	Enhance	Enhance	Enhance	
• Low-pressure tankage	Enhance	Enhance				Enhance
• Composite (lightweight) vacuum jackets	Enhance			Enhance		
• Contamination/degradation of LAD		Enhance ?	Enhance			Enhance

GST0505-1

Table 2-2. In-Space Experimentation Needs

Technology Category	Testing Objective				
	Engineering data base	Performance modeling	Environmental validation	System validation	In-space testing required
Liquid storage				Yes	Yes
• Thermal control systems					
– Degradation of material	Yes		Yes		Yes
– Effect of launch environment on thick MLI	Yes		Yes		
– Combined foam/MLI sys	Yes	Yes	Yes		
– Para/ortho conversion	Yes	Yes			
– Multiple/coupled VCS	Yes	Yes			
• Pressure control systems					
– TVS performance	Yes	Yes	Yes		Yes
– Fluid mixing for stratification control	Yes	Yes	Yes		Yes
– Refrigeration/reliquefaction	Yes	Yes			Yes
Liquid supply				Yes	Yes
• Pressurization system performance					
– Autogenous	Yes	Yes	Yes		Yes
– Helium	Yes	Yes	Yes		Yes
– Mech (pumps/compressors)	Yes	Yes			
• Fluid acquisition					
– Fine mesh screen LAD performance	Yes	Yes	Yes		Yes
– Fluid settling and outflow under low-g conditions	Yes	Yes	Yes		Yes
– Fluid settling and outflow under impulsive accel	Yes	Yes	Yes		Yes
– Impact of heat addition on LAD performance	Yes	Yes			
– Thermal subcooling of liquid outflow	Yes	Yes			
Liquid transfer				Yes	Yes
• Transfer line chilldown	Yes	Yes	Yes		Yes
• Tank chilldown with spray	Yes	Yes	Yes		Yes
• No-vent fill	Yes	Yes	Yes		Yes
• LAD fill	Yes	Yes	Yes		Yes
• Low-g vented fill	Yes	Yes	Yes		Yes
• Pump assist	Yes	Yes			
Fluid handling				Yes	Yes
• Liquid dynamics/slosh control	Yes	Yes	Yes		Yes
• Fluid dumping and tank inerting	Yes	Yes	Yes		Yes
• Earth-to-orbit transport as subcooled liquid or slush	Yes	Yes			
Advanced Instrumentation				Yes	Yes
• Quantity gauging	Yes	Yes	Yes		Yes
• Mass flow/quality metering	Yes	Yes			
• Leak detection	Yes	Yes			
• Liquid/vapor sensors	Yes	Yes			
Tank structures and materials					
• Low thermal conductivity components	Yes	Yes	Yes		
• Low-pressure tankage	Yes		Yes		
• Composite (lightweight) vacuum jackets	Yes	Yes			
• Contamination/degradation of LAD	Yes				

GST0505-2

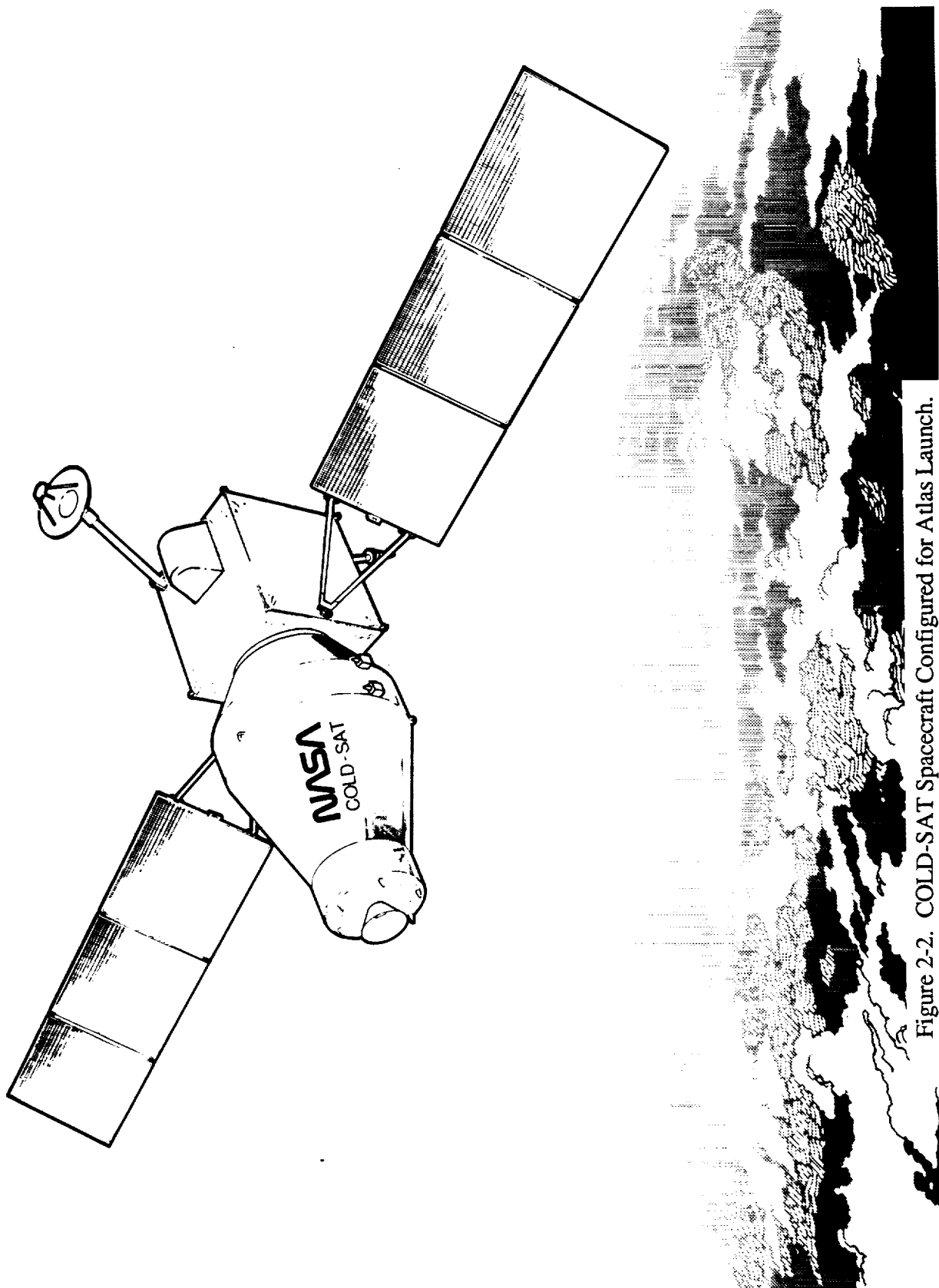


Figure 2-2. COLD-SAT Spacecraft Configured for Atlas Launch.

period from March 1988 through February 1990, and consisted of four tasks: Task I, Program Management; Task II, Initial Concept Development; Task III, Concept Refinement and Preliminary Requirements Definition; and, Task IV, Preliminary Experiment Design.

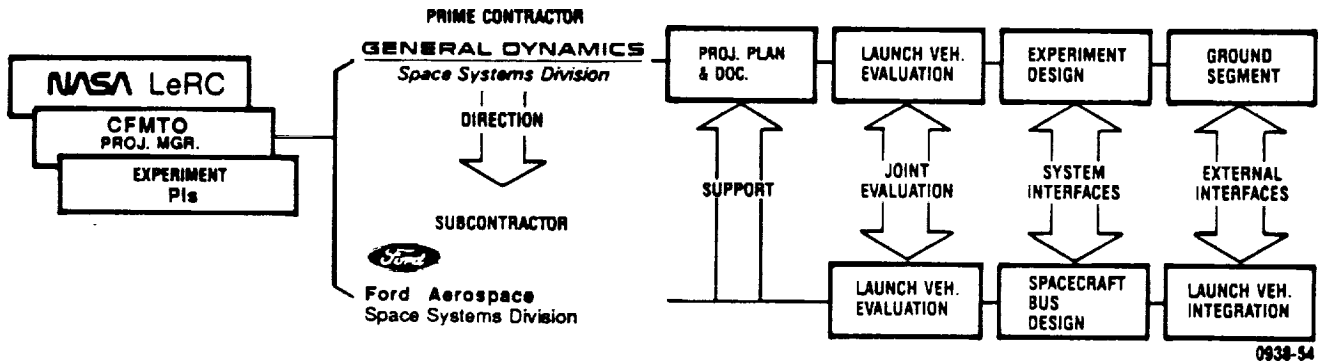


Figure 2-3 COLD-SAT Team Responsibilities

2.2 REQUIREMENTS, GUIDELINES AND ASSUMPTIONS

The eventual requirements, guidelines and assumptions used in our design and definition activities are summarized in Tables 2-3 and 2-4. The major source of the requirements was the contract statement of work and the initial Experiment Requirements Documents received from NASA at the outset of the contract. Subsequently, at technical coordination meetings and during other communications, NASA provided additional requirements, directions and clarifications. After the Conceptual Design Review and the Program Requirements Review, NASA also provided specific directives and requested answers to Review Item Dispositions which in some instances resulted in changes to the guidelines and assumptions being used.

Table 2-4. Summary of Guidelines and Assumptions for the COLD-SAT Study

GUIDELINES AND DIRECTIONS	SOURCE
<ul style="list-style-type: none"> • Use the design goals stipulated in Appendix A of the contract SOW which includes: <ol style="list-style-type: none"> 1. Achieve maximum total technology return for a minimum total system cost. 2. Reliability for proper execution of Class I experiments to be 92 percent or greater. 3. Total estimated time for production of a fully functional, tested spacecraft to be four years or less. 4. Minimize technological risk by using existing hardware and proven designs and approaches. 5. Minimize modifications to the ELV launch facilities. 6. Maximize the use of existing test facilities. • Base micrometeoroid/debris shield design on the elapsed time needed to complete the Class I experiments. • Avoid the use of CRES in the high pressure H2 bottles because of potential embrittlement. • Avoid the use of modulating control valves by using simpler orificed shut-off valves and discrete control levels. • Concentrate chill-down tests in Tank 3, the smallest tank, to conserve LH2. • Perform supply tank passive pressure control tests at only 0.32 w/m2 and background heat fluxes. 	<p>NASA NASA NASA NASA NASA NASA NASA NASA NASA NASA NASA NASA</p>
<p style="text-align: center;">ASSUMPTIONS</p>	<p>SOURCE</p>
<ul style="list-style-type: none"> • Used the Atlas I/Centaur as the launch vehicle. • Used the Atlas I/Centaur launch loads, vibration, pressure profile, etc for the spacecraft design. • Assumed the use of Launch Complex 36 at the Eastern Space and Missile Center. • Use helium-purged MLI on the supply tank instead of a vacuum jacket. • Used a safety factor of 2.0 in the design of the high pressure gaseous bottles. • Assumed an attitude of the spacecraft with its axis continually aligned along the flight path. • Assumed the Saab 1666 mm separation clamp in the design of the spacecraft. • Used a 1300km orbit to achieve a 500 year orbital lifetime. • Used solar cells and batteries for spacecraft power. • Used monopropellant hydrazine for artificially-imposed accelerations. • Single-failure tolerant heating elements used in the design. 	<p>GDSS/NASA GDSS/NASA GDSS/NASA GDSS/NASA GDSS GDSS GDSS GDSS GDSS GDSS GDSS</p>

EXPERIMENT DESCRIPTIONS AND REQUIREMENTS

This section contains summary descriptions of all experiments which are to be conducted, as well as the specific tests being planned for each experiment. The term "experiment" is used in discussing a category of testing such as pressure control. The term test refers to the individual tests being performed during each of the experiments. The experiment module is described in Section 5.0, and employs three tanks, consisting of an oblate spheroid supply tank, a cylindrical receiver tank, and a spherical receiver tank. A sketch of the spacecraft was shown previously in Figure 1-1.

The list of experiments which were considered at the beginning of the Feasibility Study is shown in Table 3-1. The experiments are divided into Class I and Class II categories and correspond to the list given by NASA in the statement of work to the contract. The original experiment numbering has been retained and is shown in the table.

Table 3-1. List of COLD-SAT Experiments by Class

Class I Experiments		Class II Experiments	
Number	Name	Number	Name
I-1&2	Tank Pressure Control	II-1	Tanker Tank Thermal Performance
I-3	Tank Chill-Down	<i>II-2</i>	<i>Depot Tank Thermal Performance</i>
I-4	Tank No-vent Fill	<i>II-3</i>	<i>OTV Tank Thermal Performance</i>
I-5	LAD Fill/Refill	II-4	Pressurization
<i>I-6</i>	<i>Mass Gaging</i>	II-5	Low-G Settling and Outflow
<i>I-7</i>	<i>Slosh Dynamics and Control</i>	II-6	LAD Performance
		II-7	Transfer Line Chill-down
		II-8	Outflow Subcooling
		II-9	Low-G Vented Fill
		II-10	Fluid Dumping
		II-11	Advanced Instrumentation

As stipulated by NASA, the Class I experiments address "enabling" technology, and the GDSS COLD-SAT spacecraft has been designed to provide at least a 92 percent reliability for carrying out these experiments. The Class II experiments are considered to be "enhancing" technology, and were given a lower priority. During the study, some of the Class I and Class II experiments were eliminated for technical and cost reasons. They are shown in the table in italics. They were generally considered lower in priority, or capable of being investigated using platforms other than COLD-SAT. For example, slosh dynamics is planned to be investigated on the Shuttle using a fluid other than LH₂.

All the experiments address important issues of space-based fluid management, and no attempt was made to prioritize the experiments. However, of the Class I experiments that have been retained (non-italicized), the tank chill-down experiment is considered lower in priority. The chill-down experiment is aimed at determining an optimum process, rather than whether the process is feasible, as is the case in some of the pressure control tests. Among the Class II experiments, the tank pressurization experiment is considered to be of high priority. It is recommended that the tank pressurization experiment be included in the Class I category because of the lack of applicable data on the phenomenon of pressurant collapse in low-g, and the importance of the process in space-based operations.

3.1 EXPERIMENT GOALS

The goals of the experiments include answering questions about both optimum and feasible designs and processes for space-based fluid management. The experiments also have the objective of providing data for the construction of analytical models for the characterization of these processes. Comprehensive modelling is necessary to minimize the number of space-based experiments and eliminate the high cost of such testing. Once validated, the models can be used for the design of future space systems. A number of the analytical models which are currently being used are based on 1-g correlations. They are not totally applicable in the micro-g environment, and the COLD-SAT results will be the first check as to the validity of these correlations.

The experiments which are being performed on COLD-SAT are quite comprehensive considering the resources of the spacecraft. For this reason, the specific tests for each experiment were carefully selected. Tests are included of all the important parameters, and yet the number of tests required to survey the parameter ranges has been minimized. The intent was to provide a comprehensive mapping of the characteristics of the processes with a minimum number of data points. In addition to the tests specifically outlined in the following sections, additional data will be acquired on many of the phenomena of interest due to opportunities presented as a result of carrying out the various functions necessary to operate the experiment system.

3.2 CLASS I EXPERIMENTS

3.2.1 Pressure Control

3.2.1.1 Discussion of Experiments. Little is known about the long-term fluid conditions in a well-insulated cryogen storage tank in a micro-g space environment. Techniques to control tank pressure without undue loss of fluid are required. As discussed below, five types of pressure control tests will be conducted; thermal stratification tests, passive TVS constant tank pressure tests, passive TVS pressure reduction tests, mixer destratification tests, and active TVS thermal conditioning tests.

Thermal Stratification Tests

The objective of these tests is to investigate the pressure rise rate and the distribution of thermal energy in a well-insulated tank of LH₂ in low-g. During these tests the TVS and mixer will not be operating. The tank fluid will initially be in thermal equilibrium. Thermal stratification caused by heat leak into the tank can cause pressure rise rates higher than if the fluid remained in thermal equilibrium. Higher pressure rise rates lead to premature venting and greater fluid loss.

The effects of the following parameters will be investigated; tank geometry, heat flux level, acceleration level, and liquid fill level. The degree of thermal stratification is expected to increase as the heat flux level increases because of the low thermal diffusion expected in the tank fluid. Thermal stratification is also expected to increase as the liquid fill level decreases because of the lower heat transfer rates expected in the vapor. The tank pressure rise rate will increase as the heat flux level increases and the liquid fill level decreases.

Thermal diffusion in the tank fluid under quiescent, low-g conditions may be limited by the relatively inefficient processes of free convection and molecular conduction. However, other convective processes may also be significant, e.g., fluid motion due to spacecraft disturbances and fluid motion persistence from earlier mixer operations. These convective processes, if significant, will decrease the rate of thermal stratification in the tank fluid. Thermal stratification tests will be performed at different g-levels to indicate the significance of free convection relative to other convective processes that are less dependent on the acceleration level.

Passive TVS, Constant Tank Pressure Tests

The objective of these tests is to evaluate the ability of a passive wall-mounted TVS heat exchanger to intercept the tank heat leak to prevent thermal stratification in the fluid, and therefore maintain a constant tank pressure with the lowest venting rate. During these tests the mixer will not be operating and the TVS energy removal rate will equal the heat leak rate into the tank. Both continuous and intermittent TVS operation will be evaluated.

Ideally, all of the heat leak into the tank will be conducted along the tank wall to the TVS tube where two-phase forced convection will transfer the energy to the TVS fluid. The micro-g space environment is expected to have little effect on these two heat transfer processes. Depending on the significance of the convective environment on the tank wall inner surface, which is dependent on the acceleration level, a portion of the tank heat leak will likely be convected into the tank fluid. The wall-mounted heat-exchanger design, i.e., tube spacing and routing over the tank wall, will have a large influence on its effectiveness for intercepting the tank heat leak. For the final design, the wall-mounted heat exchanger will be located to intercept the predicted heat flux into the tank, however the precise heat flux distribution is difficult to predict. "Hot spots" on the tank wall, where heat leaks into the fluid, are practically unavoidable. These hot spots will lead to vapor formation, thermal stratification of the tank fluid, and a slow rise in the tank pressure.

Passive TVS, Pressure Reduction Tests

The objective of these tests is to evaluate the ability of a passive TVS to thermally condition the tank fluid and cause a reduction in the tank pressure. During these tests the mixer will not be operating and the TVS energy removal rate will be greater than the tank heat leak, therefore the total energy of the tank fluid will decrease.

As discussed above in the description of the thermal stratification tests, little is known about fluid heat transfer mechanisms in a micro-g environment. Heat leak into the tank will likely cause vapor formation in the saturated fluid adjacent to the wall. Due to the low-g environment and the wettability of cryogenic liquids, the vapor will be pushed away from the wall by liquid moving in to wet the surface. The surfaces of the passive TVS heat exchanger will likely be wetted by liquid, particularly for high tank fill levels. Operation of the passive TVS will probably subcool the surrounding liquid and cause little immediate decrease in the tank pressure, which is dependent on the vapor/liquid interface temperature. Heat transfer within the tank fluid may be limited by the relatively inefficient processes of free convection and molecular conduction. If these are the dominant heat transfer mechanisms, then operating the passive TVS with an energy removal rate greater than the tank heat leak will likely subcool the surrounding liquid, and result in a substantial loss of fluid before any appreciable decrease in the tank pressure occurs. Subcooled liquid surrounding the TVS heat exchanger will decrease its efficiency and may ultimately cause liquid to be vented. However other convective processes may also be significant in a micro-g environment, e.g., fluid motion due to spacecraft disturbances and fluid motion persistence from earlier active TVS operation. If these convective mechanisms are significant, the passive TVS may be successful in reducing thermal stratification and tank pressure.

Mixer Destratification Tests

The objective of these tests is to evaluate the ability of an axial-jet mixer to reduce thermal stratification in the fluid and bring the liquid and vapor phases into thermal equilibrium. The pressure will decrease as a tank of thermally stratified fluid is mixed. Rapid destratification due to ullage disruption by a liquid jet will be investigated. However, mixing adds energy to the tank fluid

and should be minimized. The effectiveness of mixing only the bulk liquid and promoting condensation at the vapor/liquid interface will also be investigated. The following parameters will be evaluated: tank liquid fill level, jet velocity, and acceleration level.

Active TVS Thermal Conditioning Tests

The objective of these tests is to evaluate the ability of a TVS heat exchanger used in conjunction with an axial-jet mixer to thermally condition the tank fluid and cause a reduction in the tank pressure. Both the compact and wall-mounted heat exchangers will be evaluated. The performance of the active TVS is largely dependent on the mixing process.

Heat transfer within the compact heat exchanger will be primarily due to single-phase and two-phase forced convection. These physical processes will be dominated by viscous and inertial effects, and are not expected to be significantly affected by the micro-g space environment. The thermal performance for a wall-mounted heat-exchanger is more difficult to predict. The convective environment on the outer surface of the wall-mounted TVS heat exchanger will be strongly influenced by the mixing process.

Key Parameters and Ultimate Variables

Uncertainty analyses were performed to determine measurement requirements and accuracies. The results of these analyses are summarized in Section 6.2. Key parameters are listed below which affect the pressure control experiments and will be evaluated:

KEY PARAMETERS

1. Liquid fill level;
2. Tank wall heat flux;
3. Acceleration level;
4. Tank geometry;
5. TVS geometry, flowrate, and duty cycle;
6. Mixer flowrate and power.

The time history of the following quantities will be monitored during each test; data sampling rates will be greater than the TVS duty cycle frequency:

ULTIMATE EXPERIMENTAL DATA

1. Tank pressure, to quantify the rate of tank pressure rise or drop;
2. Distributions of temperature and phase in the tank Fluid, to quantify thermal stratification;
3. Heat transfer coefficients on the tank wall;
4. Heat transfer coefficients for the TVS heat exchangers;
5. Temperature distribution along TVS tube and "dry-out" location.

Emphasis will be placed on measuring near-wall temperature gradients at a number of locations, including near a known "hot-spot". The temperature distribution in the vicinity of the liquid/vapor interface will also be measured. The location of this interface changes and is generally unknown, making it difficult to measure. Predictions of its location during the various tests will be made in future work and the instrumentation located accordingly.

3.2.1.2 Summary of Tests. The pressure control tests are discussed below and listed in Table 3-2. For a schematic showing the experiment tanks and the fluid system see Figure 5-1.

Table 3-2. Tests for Tank Pressure Control

(TESTS IN TANKS 2 AND 3 CAN BE PERFORMED SIMULTANEOUSLY WITH TANK 1 TESTS)

TYPE OF TEST	PROCESS DESCRIPTION	FILL FLUID LEVEL (%)	FLUID MASS (kg)	HEAT FLUX (W/m ²)	GND HEAT LEAK TBD	10 ⁻⁶	TBD	TANK PRESSURE (kPa)	HEAT-X MIXER FLOW	EST. TIME (Hours)	COMMENTS ON TESTS
TANK 1: VOL=5.38 m ³ , AREA=15.1 m ² , P _{IVS} =34.5kPa, SAT VAP AT TVS EXIT, ACTIVE=1.20x10 ⁻³ kg/sec, PASSIVE=6.63x10 ⁻⁵ kg/sec											
	PRELAUNCH AND ASCENT	95									GROUND BASED, 1-G REFERENCE DATA POINT
	MIX FLUID	95	361.8	-		BGND	103	103	OFF	0.4	Start tests with tank fluid in thermal equilibrium.
I-1.1	PASSIVE, PRESSURE REDUCTION					BGND	103-138	103-138	OFF	35	First half of TVS test starts with fluid stratified. Second half starts with fluid in thermal equilibrium
	MIXER DESTRAT	95	361.8	1.89		BGND	138-	138-	WALL	20.8	
	PASSIVE TVS	-	-	0.32		BGND	-121	-121	WALL	0.4	
	MIX FLUID	-	-	0.32		BGND	121-	121-	WALL	20.8	
	MIX FLUID	92.3	351.8	0.32		BGND	-103	-103	WALL	0.4	
I-1.2	ACTIVE PRESSURE CONTROL					BGND	103-138	103-138	OFF	34.2	Start tests with tank fluid in thermal equilibrium.
	MIXER DESTRAT	-	-	1.89		BGND	-138	-138	OFF	L/M/H	
	ACTIVE TVS	90	343.2	1.89		BGND	138-103	138-103	COMP	2	
I-1.3	MIX FLUID	65	249.9	-		BGND	103	103	OFF	0.3	Start tests with tank fluid in thermal equilibrium.
	PASSIVE TVS	65	249.9	1.89		BGND	103-	103-	WALL	26.5	
	MIX FLUID	63.3	243.5	1.89		BGND	-103	-103	WALL	0.3	
I-1.4	ACTIVE, LOW Q, PRESS CNTRL					BGND	103-138	103-138	OFF	156.2	Start tests with tank fluid in thermal equilibrium.
	MIXER DESTRAT	-	-	0.32		BGND	-138	-138	OFF	L/M/H	
	ACTIVE TVS	61.6	237.3	0.32		BGND	138-103	138-103	WALL	1.4	
	MIX FLUID	61.6	237.3	-		BGND	103	103	OFF	0.3	
I-1.5	ACTIVE, MED Q, PRESS CNTRL					BGND	103-138	103-138	OFF	51.1	Start tests with tank fluid in thermal equilibrium.
	MIXER DESTRAT	-	-	0.95		BGND	-138	-138	OFF	L/M/H	
	ACTIVE TVS	59.9	231	0.95		BGND	138-103	138-103	WALL	1.4	
I-1.6	ACTIVE, HIGH Q, PRESS CNTRL					BGND	103-138	103-138	OFF	25.1	Start tests with tank fluid in thermal equilibrium.
	MIXER DESTRAT	-	-	1.89		BGND	-138	-138	OFF	L/M/H	
	ACTIVE TVS	58.2	224.7	1.89		BGND	138-103	138-103	COMP	1.5	
	MIX FLUID	40	156.6	-		BGND	103	103	OFF	0.2	
I-1.7	PASSIVE, PRESSURE REDUCTION					BGND	103-138	103-138	OFF	19.5	First half of TVS test starts with fluid stratified. Second half starts with fluid in thermal equilibrium
	MIXER DESTRAT	40	156.6	1.89		BGND	138-	138-	WALL	11.6	
	PASSIVE TVS	-	-	0.32		BGND	-121	-121	WALL	0.2	
	MIX FLUID	-	-	0.32		BGND	121-	121-	WALL	11.6	
	MIX FLUID	38.5	151	0.32		BGND	-103	-103	WALL	0.2	

Table 3-2. Tests for Tank Pressure Control (Cont.)

TYPE OF TEST	PROCESS DESCRIPTION	FILL LEVEL (%)	FLUID MASS (kg)	HEAT FLUX (W/m ²)	GLEVEL x 10 ⁶	TANK PRESSURE (kPa)	HEAT-X	MIXER FLOW	EST. TIME (Hours)	COMMENTS ON TESTS
I-1.8 ACTIVE PRESSURE CONTROL	STRATIFICATION	38.5	151	1.89	BGND	103-138	OFF	OFF	19	
	MIXER/DESTRAT	-	-	1.89	BGND	-138	OFF	L/M/H	A	
	ACTIVE TVS	37.2	146.2	1.89	BGND	138-103	COMP	HIGH	1.1	
I-1.9 ACTIVE, HIGH-G, PRESS CNTL	STRATIFICATION	37.2	146.2	1.89	20	103-138	OFF	OFF	18.7	Do simultaneously with Tank 2 and Tank 3 tests at g/go = 10 ⁻⁴ -5
	MIXER/DESTRAT	-	-	1.89	20	-138	OFF	L/M/H	A	
	ACTIVE TVS	36	141.5	1.89	20	138-103	COMP	HIGH	1.1	
I-1.10 ACTIVE, HIGH-G, PRESS CNTL	STRATIFICATION	36	141.5	1.89	100	103-138	OFF	OFF	18.3	Do simultaneously with Tank 2 and Tank 3 tests at g/go = 10 ⁻⁴ -4
	MIXER/DESTRAT	-	-	1.89	100	-138	OFF	L/M/H	A	
	ACTIVE TVS	34.7	136.9	1.89	100	138-103	COMP	HIGH	1.1	
	MIX FLUID	10	44.7	-	BGND	103	OFF	HIGH	0.1	Start tests with tank fluid in thermal equilibrium.
I-1.11 PASSIVE, CONSTANT PRESSURE	PASSIVE TVS	10	44.7	1.89	BGND	103-	WALL	OFF	11	
	MIX FLUID	9.3	42.0	1.89	BGND	-103	WALL	HIGH	0.1	
I-1.12 ACTIVE PRESSURE CONTROL	STRATIFICATION	9.3	42.0	1.89	BGND	103-138	OFF	OFF	10.8	
	MIXER/DESTRAT	-	-	1.89	BGND	-138	OFF	L/M/H	A	
	ACTIVE TVS	8.6	39.3	1.89	BGND	138-103	COMP	HIGH	0.6	
503.3 Hours 20.971 Days										
TANK 2: CYL., DIA.=1.02 m, LEN.=1.83 m, VOL.=1.28 m ³ , NO MIXER, TVS WITH WALL MOUNTED HX., TVS Flow Rate = 0.408 kg/hr.										
I-1.13 PASSIVE, CONSTANT PRESSURE	PASSIVE TVS	75	68.5	1.58	BGND	103	WALL	NONE	20.7	OPERATE TVS CONTINUOUSLY, LOW FLOW RATE.
		73.1	66.8	1.58	BGND	103			A	
I-1.14 PASSIVE, PRESSURE REDUCTION	STRATIFICATION	75	68.5	1.58	BGND	103-138	OFF	NONE	20.7	OPERATE TVS CONTINUOUSLY, HIGH FLOW RATE.
	PASSIVE TVS	72.7	66.4	1.58	BGND	138-103	WALL	NONE	5.1	
I-1.15 PASSIVE, HIGH-G, CONST PRESS	PASSIVE TVS	75	68.5	1.58	20	103	WALL	NONE	20.7	20% TVS DUTY CYCLE, HIGH FLOWRATE.
		73.1	66.8	1.58	20	103			A	
I-1.16 PASSIVE, HIGH-G, PRESS REDUC	STRATIFICATION	75	68.5	1.58	20	103-138	OFF	NONE	20.7	OPERATE TVS CONTINUOUSLY, HIGH FLOW RATE.
	PASSIVE TVS	72.7	66.4	1.58	20	138-103	WALL	NONE	5.1	
I-1.17 PASSIVE, CONSTANT PRESSURE	PASSIVE TVS	25	24.0	1.58	BGND	103	WALL	NONE	10.7	OPERATE TVS CONTINUOUSLY, LOW FLOW RATE.
		24	23.1	1.58	BGND	103			A	
I-1.18 PASSIVE, PRESSURE REDUCTION	STRATIFICATION	25	24.0	1.58	BGND	103-138	OFF	NONE	10.7	OPERATE TVS CONTINUOUSLY, HIGH FLOW RATE.
	PASSIVE TVS	23.8	22.9	1.58	BGND	138-103	WALL	NONE	2.6	

Table 3-2. Tests for Tank Pressure Control (Cont.)

TYPE OF TEST	PROCESS DESCRIPTION	FILL LEVEL (%)	FLUID MASS (kg)	HEAT FLUX (W/m ²)	GLEVEL x 10 ⁻⁶	TANK PRESSURE (kPa)	HEAT-X	MIXER FLOW	EST. TIME (Hours)	COMMENTS ON TESTS
I-1.19	PASSIVE, HIGH-G, CONST PRESS	25	24.0	1.58	100	103	WALL	NONE	10.7	OPERATE TVS CONTINUOUSLY, LOW FLOW RATE.
	PASSIVE TVS	24	23.1	1.58	100	103			^A	
I-1.20	PASSIVE, HIGH-G, PRESS REDUC	25	24.0	1.58	100	103-138	OFF	NONE	10.7	
	PASSIVE TVS	23.8	22.9	1.58	100	138-103	WALL	NONE	2.6	OPERATE TVS CONTINUOUSLY, HIGH FLOW RATE.
TANK 3: SPHERICAL, DIA.=1.07 M, VOL=0.63 M3, NO MIXER, TVS HX MOUNTED ON TANK WALL OUTER SURFACE. TVS FLOWRATE = 0.23 KG/HR.										
I-1.21	PASSIVE, CONSTANT PRESSURE	75	33.88	1.58	BGND	103	WALL	NONE	17.6	OPERATE TVS CONTINUOUSLY, LOW FLOW RATE.
	PASSIVE TVS	73.1	33.02	1.58	BGND	103			^A	
I-1.22	PASSIVE, PRESSURE REDUCTION	75	33.88	1.58	BGND	103-138	OFF	NONE	17.6	
	PASSIVE TVS	72.6	32.84	1.58	BGND	138-103	WALL	NONE	4.6	OPERATE TVS CONTINUOUSLY, HIGH FLOW RATE.
I-1.23	PASSIVE, HIGH-G, CONST PRESS	75	33.88	1.58	100	103	WALL	NONE	17.6	OPERATE TVS CONTINUOUSLY, LOW FLOW RATE.
	PASSIVE TVS	73.1	33.02	1.58	100	103			^A	
I-1.24	PASSIVE, HIGH-G, PRESS REDUC	75	33.88	1.58	100	103-138	OFF	NONE	17.6	
	PASSIVE TVS	72.6	32.84	1.58	100	138-103	WALL	NONE	4.6	OPERATE TVS CONTINUOUSLY, HIGH FLOW RATE.
I-1.25	PASSIVE, CONSTANT PRESSURE	25	11.88	1.58	BGND	103	WALL	NONE	9.1	OPERATE TVS CONTINUOUSLY, LOW FLOW RATE.
	PASSIVE TVS	23.8	11.34	1.58	BGND	103			^A	
I-1.26	PASSIVE, PRESSURE REDUCTION	25	11.88	1.58	BGND	103-138	OFF	NONE	9.1	
	PASSIVE TVS	23.8	11.34	1.58	BGND	138-103	WALL	NONE	2.4	OPERATE TVS CONTINUOUSLY, HIGH FLOW RATE.
I-1.27	PASSIVE, HIGH-G, CONST PRESS	25	11.88	1.58	20	103	WALL	NONE	9.1	20% TVS DUTY CYCLE, HIGH FLOWRATE.
	PASSIVE TVS	23.8	11.34	1.58	20	103			^A	
I-1.28	PASSIVE, HIGH-G, PRESS REDUC	25	11.88	1.58	20	103-138	OFF	NONE	9.1	
	PASSIVE TVS	23.8	11.34	1.58	20	138-103	WALL	NONE	2.4	OPERATE TVS CONTINUOUSLY, HIGH FLOW RATE.
141 Hours 5.875 Days										
120.8 Hours 5.0333 Days										

Thermal Stratification Tests

With the fluid initially in thermal equilibrium, the tank will be locked-up, and a uniform heat flux applied to the tank wall until the pressure rises 34.5 kPa. Four liquid fill levels will be considered in the supply tank; nominally 95, 65, 40, and 10 percent, and two liquid fill levels in the receiver tanks; 75 and 25 percent. The effect of three different heat flux levels (1.90, 0.95, and 0.32 W/m²) will be investigated in the supply tank. Only the background heat flux level will be used on the receiver tanks. Three acceleration levels will also be evaluated; a background level on the order of 10⁻⁷ g's (see Appendix D), 20x10⁻⁶ g's, and 100x10⁻⁶ g's. Thermal stratification tests will be performed prior to all mixing tests and all active and passive TVS thermal conditioning tests.

Passive TVS, Constant Tank Pressure Tests

The tank fluid will initially be in thermal equilibrium. The supply tank TVS will be operated continuously and the mixer will not be operating. The heater heat rate will be adjusted to equal the TVS energy removal rate. In Tanks 2 and 3, the TVS will operate intermittently. The duty cycle will be adjusted so the time-averaged TVS energy removal rate equals the background tank heat leak (~20 percent duty cycle). Intermittent operation proportionately lowers the time-averaged TVS flowrate. The time period for each TVS duty cycle will be less than the residence time of fluid in the TVS tube to insure no liquid is vented from the TVS and so the TVS energy removal rate is relatively steady. A steady energy removal rate will insure that most of the heat leak on the tank wall is intercepted and a minimum amount of energy enters the tank fluid.

An internal wall-mounted TVS heat exchanger will be used in Tanks 1 and 2. The TVS heat exchanger on Tank 3 is externally mounted to evaluate any performance degradation which results. Liquid fill levels of 65 and 10 percent will be studied in Tank 1. Liquid fill levels of 75 and 25 percent will be evaluated in Tanks 2 and 3. The effect of three different acceleration levels will be investigated.

To conclusively indicate the performance of the TVS, each test will be long enough so that a significant increase in the tank pressure (34.5 kPa) would occur if the TVS were not operating. A schematic of the expected tank pressure profile is shown in Figure 3-1.

Passive TVS, Thermal Conditioning Tests

Each of these tests will follow a thermal stratification test so the tank fluid will initially be thermally stratified. In Tanks 2 and 3 the TVS will be operated continuously, so the TVS energy removal rate will be greater than the background heat leak into the tank. In Tank 1 the heater power will be set lower than the TVS energy removal rate. The TVS will operate continuously and the mixer will be off. Half-way through the test in Tank 1, the mixer will be turned on briefly to remove any thermal stratification so the second half of the test will begin with the fluid in thermal equilibrium. A schematic of the expected pressure profile in Tank 1 is included in Figure 3-2. The TVS design, liquid fill levels, and acceleration levels are similar to those used during the Passive TVS constant pressure tests described above.

Mixer Destratification Tests

These tests will be performed in Tank 1. The fluid will initially be thermally stratified. The degree of stratification will depend on the heat flux level used in the prior thermal stratification test. Three heat flux levels will be considered. The TVS will not be operating during the mixing tests. The axial-jet mixer will first be operated at the lowest flowrate, where complete mixing is not expected.

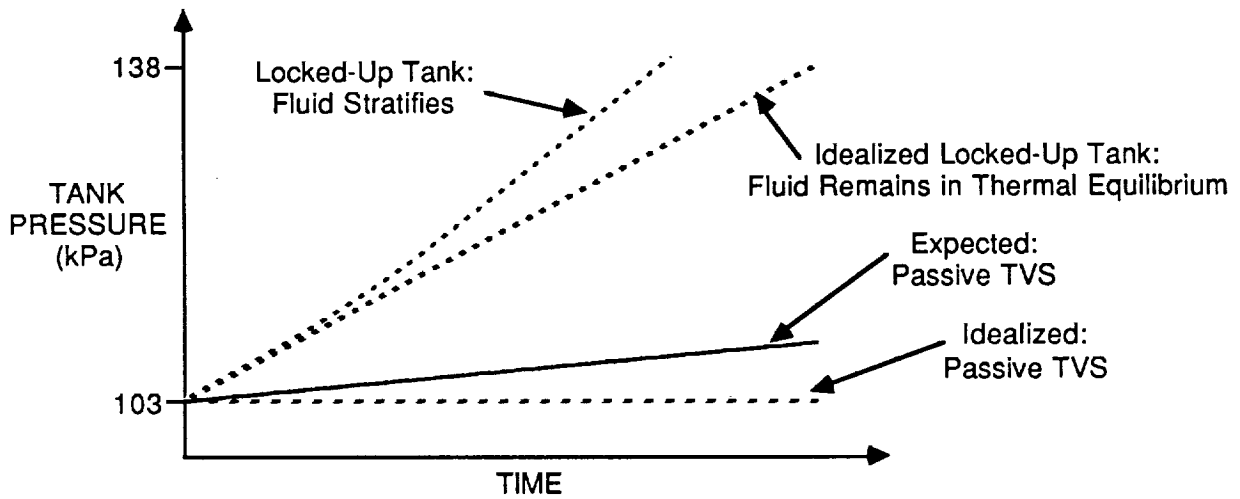


Figure 3-1. Tank Pressure Profile expected during Passive TVS, Constant Pressure Experiments

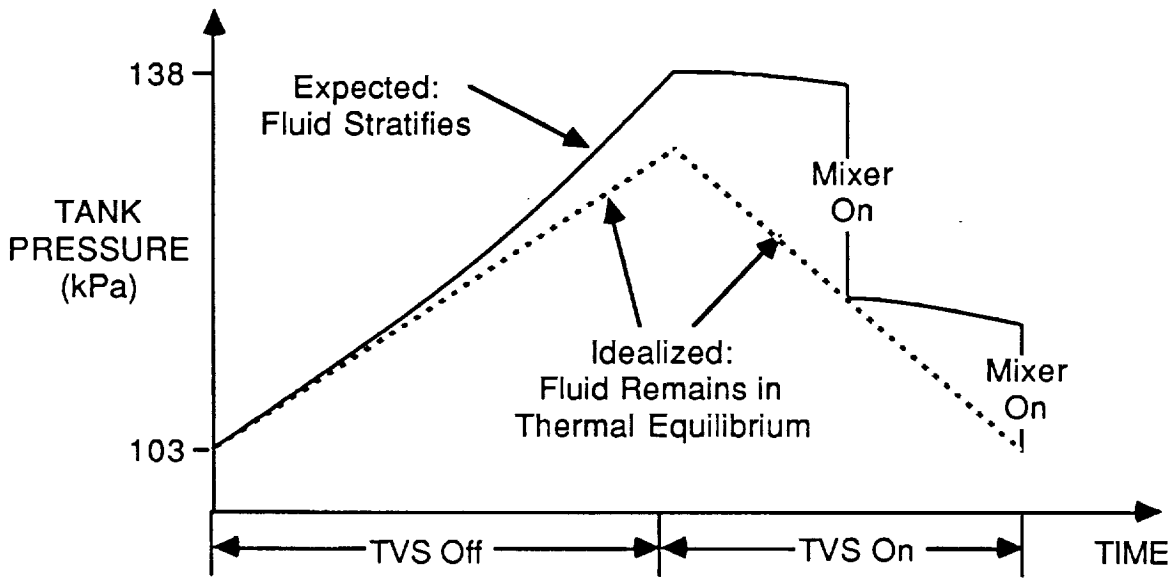


Figure 3-2. Pressure Profile expected in Tank 1 during Thermal Stratification and Passive TVS, Thermal Conditioning Experiments

Once the tank pressure levels out or begins to rise, the jet flowrate will be increased to the medium level, and then to the highest level. Mixing of the bulk liquid only is expected at the lower flowrates. The system will be designed to produce ullage disruption and complete mixing of the tank fluid at the highest flowrate. A schematic of the expected tank pressure profile during the mixing tests is included in Figure 3-3. Mixing tests will be performed at four liquid fill levels and three acceleration levels.

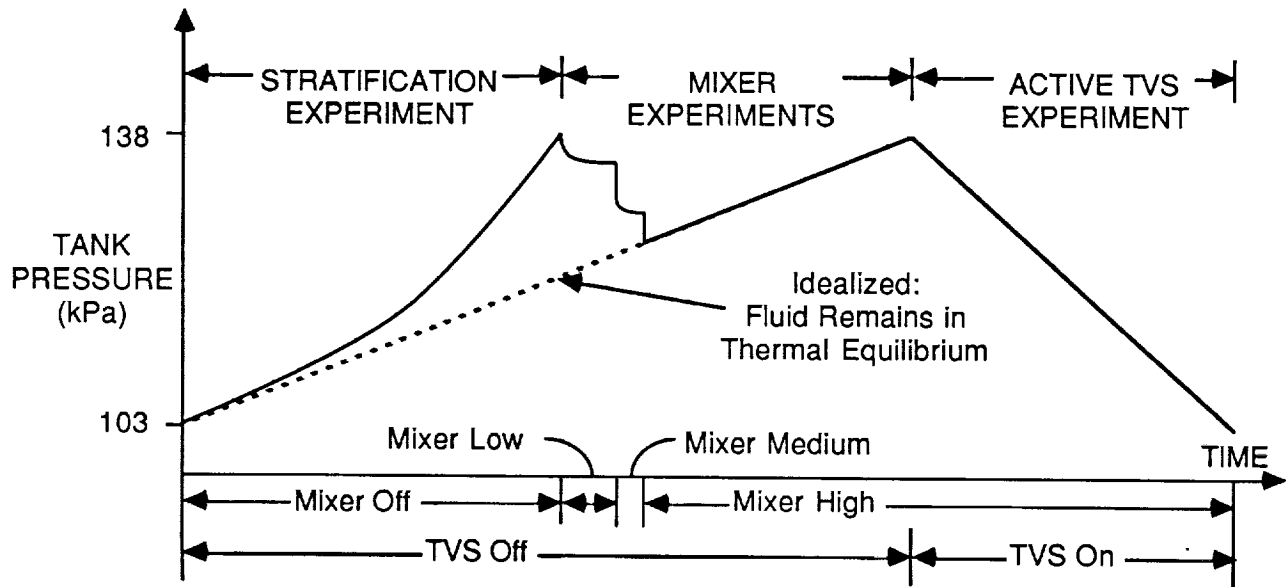


Figure 3-3. Tank Pressure Profile Expected during Thermal Stratification, Mixer, Destratification, and Active TVS Thermal Conditioning Experiments

Active TVS Thermal Conditioning Tests

Following the mixing tests, the TVS heat exchanger will be used in conjunction with the axial-jet mixer to thermally condition the tank pressure by 34.5 kPa. Separate tests will investigate the effectiveness of the compact heat exchanger and the wall-mounted heat exchanger. A schematic of the expected tank pressure profile during these tests is included in Figure 3-3.

3.2.2 Tank Chillydown

3.2.2.1 Discussion of Experiment. The objectives of this experiment are:

(1) To provide a better understanding of tank chillydown in zero g, and to determine techniques which minimize the LH₂ required for this process. This will include determination of the effects of the following:

- Tank thermal mass to volume ratio and shape;
- Nozzle orientation and flowrate;
- Mass injection profile and staged venting;
- G-level.

(2) To provide subscale modeling data of representative tank configurations which can be applied to flight tankage systems.

The key parameters and ultimate experimental data to be evaluated in the Tank Chillover experiment are shown below.

KEY PARAMETERS

1. Tank thermal mass to volume ratio
2. Mass injection profile
3. Nozzle configuration and flowrate
4. Supply liquid temperature and pressure
5. Tank g level
6. Venting procedure including cyclic venting parameters
7. Tank configuration and features

ULTIMATE EXPERIMENTAL DATA

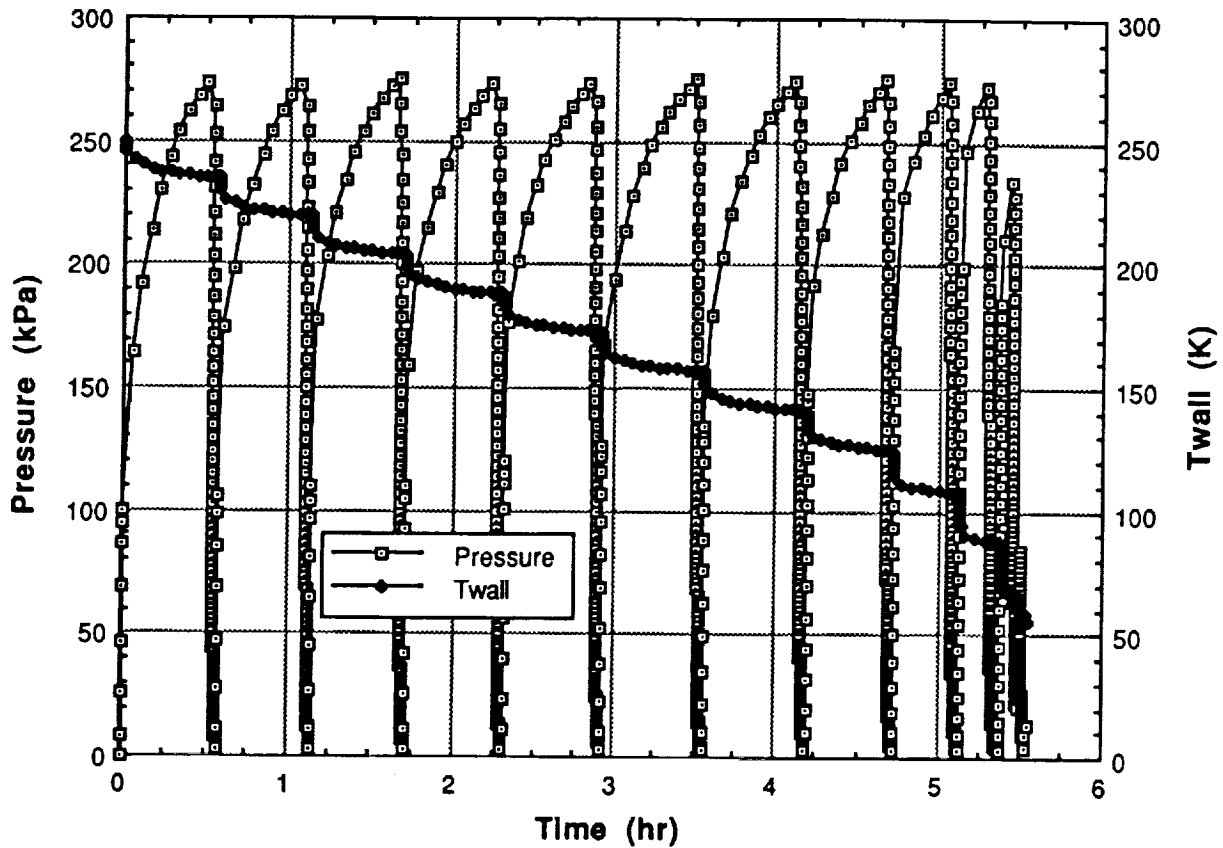
1. Pressure profiles
2. Temperature profiles
3. Total liquid mass used, and time required for chillover
4. Number of charge/hold/vent cycles required
5. Effect of staged venting
6. Effect of mass injection profile
7. Heat transfer coefficients

It is desirable that zero g chillover of cryogenic tankage be performed with the least LH₂. In the absence of settling acceleration, the most promising method for doing this is the "charge/hold/vent" procedure. The warm, evacuated tank is initially charged with a pre-determined quantity of liquid, which vaporizes and cools the tank. If the charge is too large, tank pressure will exceed the maximum allowable and venting will occur before full cooling of the tank wall occurs. If too small, the rate of tank chillover will be reduced and the time to achieve the specified target temperature will be increased. The fluid is held in the tank until it is no longer cooling the tank, or the tank pressure rises to a specified level. At this point the tank is vented to space, either completely or in stages. These steps comprise one cycle, which is repeated until the tank temperature is reduced to a predetermined "target" temperature. This is the initial system temperature required for a subsequent no-vent fill of the tank (Section 3.2.3).

In order to conserve fluid during the process, the heat transfer from the tank to the chillover fluid must be maximized so that the fluid is dumped to space at the highest possible temperature. This process must take into account, not only the heat capacity of the tank, but the rate of heat transfer to the insulation and outer structure of the tank. The heat capacity of the tank relative to the volume of the tank is an important parameter in the process.

In the process of charge/hold/vent chillover, the question to be answered is how the cooling of the tank will be affected by the difference in flow patterns from the nozzles and the zero g effect on the heat transfer and fluid distribution in the tanks. The venting can be accomplished in several steps to extract additional heat from the fluid, and the effect of this "staged venting" will also be investigated.

The results will be correlated with ground tests and codes will be established for the prediction of tank chillover performance. The NASA/LeRC code for modeling chillover is CRYOCHIL and the General Dynamics code is GDNVF. Typical results of the GDNVF program are shown in Figure 3-4. The largest unknowns are the heat transfer rates between the tank fluid and the tank wall during the three phases of a cycle. The hold phase is particularly dependent on the duration of the fluid motion persistence from the charge phase, since any fluid motion will greatly enhance the heat transfer. Experiment data will be correlated with the analytical models.



Curve based on GDNVF results for Test I-3.1, Table 3-3:
 Tank 3, Spherical tank diameter = 1.07m, $M/V = 53 \text{ kg/m}^3$,
 Variable charge mass to achieve a constant tank pressure during each cycle,
 Single vent for each cycle.

Figure 3-4. Typical GDNVF Tank Chilldown Results

3.2.2.2 Summary of Tests. Two tanks will be used in the chilldown experiment. One tank will be the bare spherical Tank 3, which has a full complement of axial, radial and tangential spray nozzles, although the axial nozzles will not be used in these tests. This tank does not have a LAD, but has the lower M/V ratio of the two test tanks being used for this experiment. The M/V is approximately 47 kg/m^3 . For comparison, similar tests will be performed in Tank 2. It is cylindrical in shape, has radial and axial nozzles, a total communication LAD, and a higher M/V ratio of about 54 kg/m^3 .

The tests performed will evaluate the effects of the different spray nozzles operating at different flowrates. The mass of LH_2 injected into the tanks will be varied from cycle to cycle during any one test. The effect of acceleration level on chilldown performance will also be evaluated.

The preliminary test conditions for the chilldown tests are shown in Table 3-3. The charge masses and chilldown times were calculated by the GDNVF code for Tanks 2 and 3. A target temperature of 56 K was assumed. The best heat transfer throughout the cycle will probably result if the initial velocity is maximized. Thus it is expected that the maximum flowrate will give maximum turbulence and momentum for the highest and most prolonged heat transfer between the incoming liquid and the tank wall.

Table 3-3. Tests for the Tank Chilldown Experiment

TEST NO.	NOZZLE SET USED	TOTAL H ₂ MASS INJECTED (KG)	LH ₂ FLOWRATE (KG/S)	NO. OF VENTS PER CYCLE	EST. CHILL-DOWN TIME (HRS)	G LEVEL x10 ⁻⁶	BOND NO.	NOTES
TANK 3: SPHERICAL, DIA=1.07 M, VOL=0.62 M³; WITH AXIAL, RADIAL, AND TANGENTIAL NOZZLES.								
I-3.1	RADIAL	4.0	0.0227	1	5.5	~0.3 (NOTE 2)	~0.03	RADIAL NOZZLE USING MAXIMUM FLOW RATE
I-3.2	RADIAL	3.6	0.0227	2	7.7	~0.3	~0.03	MAXIMUM FLOW RATE WITH STAGED VENTING
I-3.3	RADIAL	4.0	0.0136	1	6	~0.3	~0.03	MODERATE FLOW RATE
I-3.4	RADIAL	4.0	0.0068	1	6.2	~0.3	~0.03	LOW FLOW RATE
I-3.5	TANGNTL	4.0	0.0136	1	6	~0.3	~0.03	MODERATE FLOW RATE
I-3.6	TANGNTL	4.0	0.0068	1	6.2	~0.3	~0.03	LOW FLOW RATE
I-3.7	RADIAL	3.5	0.0136	1	2.0	100 (NOTE 1)	10	ARTIFICIAL G IMPOSED ALONG SPACECRAFT AXIS, HIGH G LEVEL, MODERATE FLOW RATE
I-3.8	RADIAL	3.6	0.0136	1	2.3	50 (NOTE 1)	5	ARTIFICIAL G IMPOSED ALONG SPACECRAFT AXIS, INTERMEDIATE G LEVEL, MODERATE FLOW RATE
I-3.9	TVS	4.0	TBD	N/A	TBD	~0.3	~0.03	TEST OF TANK CHILLDOWN BY LIQUID FLOW THRU THE TVS. 4.0 KG MASS IS A GUESS AND IS TBD
TANK 2: CYLINDRICAL, DIA=1.02 M, LEN.=1.83 M, VOL.=1.27 M³, WITH AXIAL AND RADIAL NOZZLES.								
I-3.10	RADIAL	12.9	0.0227	1	17.9	~0.1 (NOTE 2)	~0.01	RADIAL NOZZLE USING MAXIMUM FLOWRATE
I-3.11	RADIAL	12.9	0.0136	1	18.9	~0.1	~0.01	MODERATE FLOW RATE
I-3.12	AXIAL	12.9	0.0227	1	17.9	~0.1	~0.01	AXIAL NOZZLE MAXIMUM FLOWRATE
I-3.13	AXIAL	12.9	0.0136	1	18.9	~0.1	~0.01	MODERATE FLOW RATE
TOTAL		86.3		TOTAL	115.5			

NOTES:

1. ACCELERATION VECTOR IS ALIGNED WITH SPACECRAFT AXIS AND DIRECTED AFT.
2. APPROXIMATE BACKGROUND ACCELERATION RESULTING PRIMARILY FROM ORBITAL PITCH RATE.
3. ESTIMATED TEST TIMES WERE BASED ON EARLIER ANALYSIS USING TANK MASS/VOLUME RATIOS OF 85 AND 53 KG/M³ FOR TANKS 2 AND 3, RESPECTIVELY

The general procedure for these experiments is as follows. At the beginning of each test, the tank will be at ambient temperature and evacuated. The transfer line will be chilled and the appropriate valves will be opened to allow the desired flow to enter through the selected nozzle system. The total quantity of fluid injected will be monitored and controlled by the flowmeters in the transfer lines. Following the injection of the mass for each cycle of the process, the temperatures and pressures will be monitored during the hold period as the tank wall cools and the vapor temperature rises. At a predetermined pressure level or tank wall cooling rate (as measured by temperature differentials), the tank will be vented. Following tank chilldown, other tests will usually be run, such as no-vent fill or vented fill.

Prior to each of the tank chilldown tests, the tanks will be allowed to warm up to space equilibrium temperature (~250 K). The tank heaters will be used in the warming of the tanks to reduce the time required. However, the tanks will be allowed to reach equilibrium temperature prior to the tests with the heaters turned off.

The instrumentation for these tests includes: MLI and penetration temperatures; tank wall and internal temperatures; tank pressure; inflowing liquid temperature, pressure and flowrate; vented vapor temperature, pressure and flowrate; acceleration level; and internal fluid velocity (if a suitable sensor is available).

3.2.3 No-Vent Fill

3.2.3.1 Discussion of Experiment. The objectives of this experiment are:

- (1) To determine the effects of nozzle orientation, nozzle flowrates, g level, and tank fill level on the no-vent fill process,
- (2) To obtain the data needed to determine the correct algorithms and input variables for use in the analytical models of the process.

The key parameters and ultimate experimental data to be evaluated in the No-Vent Fill experiment are shown below.

KEY PARAMETERS

1. Nozzle configuration and flowrate
2. Tank g level, Bond Number, and orientation of the fluid in the tank
3. Initial tank temperature (target temperature of the chilldown process)
4. Tank configuration
5. Tank fill level

ULTIMATE EXPERIMENTAL DATA

1. Maximum fill level achievable
2. Pressure as a function of time
3. Final tank temperature
4. Time required for the fill

Conventional tank filling techniques cannot be applied to a tank located in a low gravity environment because liquid will migrate to the vent system and be carried out of the tank. This experiment will investigate a no-vent fill process in which the tank is pre-chilled to a specified target temperature, and then locked up and filled without venting. This process depends on the target temperature, the mass-to-volume ratio of the tank, the inflow rate, the inflow configuration, the g level, and the orientation of the injection nozzle relative to the acceleration vector. The interrelationships and optimum values of these parameters have not been established.

The efficiency of the process depends on good mixing between the incoming liquid and the tank contents, and heat transfer between the liquid, vapor and tank walls. Initially the incoming liquid will flash as it strikes and chills the relatively warm tank wall and internal hardware. Tank pressure will rise rapidly until the tank is chilled to near liquid temperature. As liquid begins to accumulate it will absorb heat from the vapor causing some of the vapor to condense. The no-vent fill procedure will result in a final saturation condition of the fluid in the receiver tank which is higher than that of the fluid transferred from the supply tank. One goal of this experiment is to minimize the resulting increase in saturation temperature of the transferred liquid.

An analytical prediction of the pressure rise in Tank 3, by the General Dynamics program GDNVF, is shown in Figure 3-5. Analyses indicate that it should be possible to fill the tank to at least the ninety-five percent level without exceeding the tank pressure limit if sufficient mixing of the liquid and vapor can be achieved. This is related to the incoming liquid flowrate and flow configuration, the heat transfer between the incoming liquid and the fluid in the tank, and the tank configuration. The efficiency of the process also depends on the thermodynamic condition of the incoming liquid, but the effect of this variable should be analytically predictable.

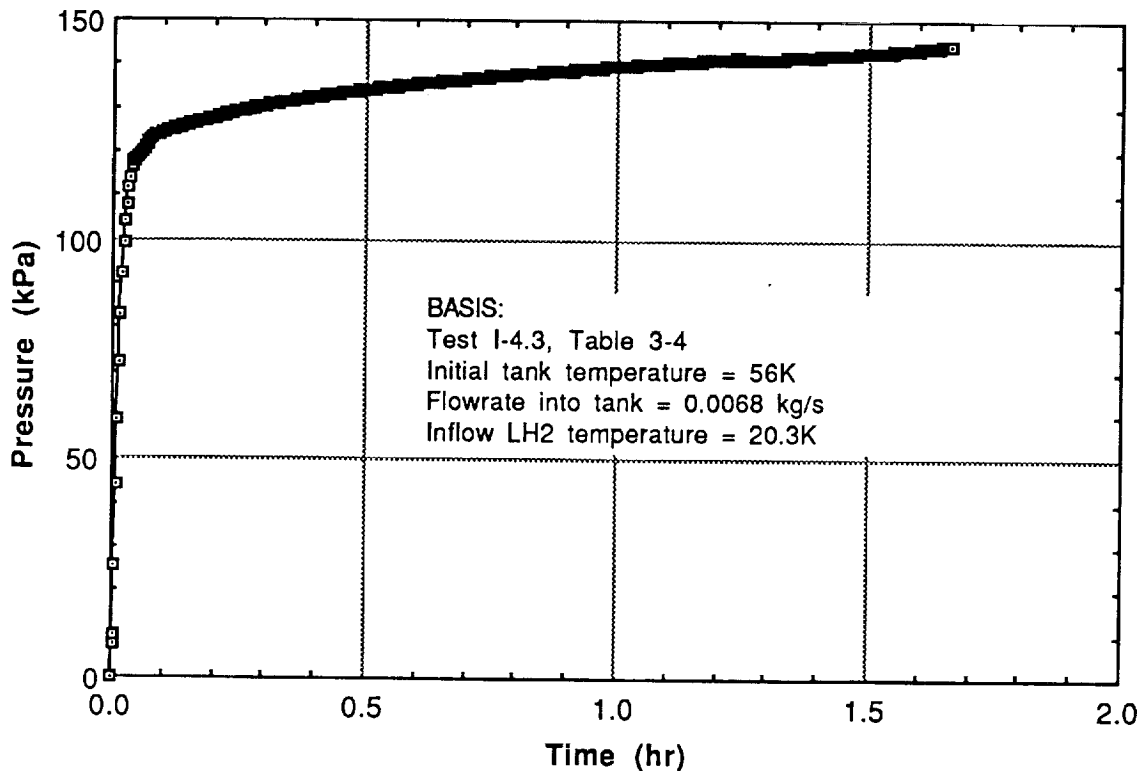


Figure 3-5. Typical GDNVF Pressure Rise Results for No-Vent Fill Process

Determining the dominant mechanisms in the no-vent fill process will help improve the models of this process and increase confidence in predictions for the effects of tank size and other design features on performance. Another currently available model for this process is NVFILL. However, this program uses a limited number of fluid nodes and incorporates a number of assumptions, such as the interface area for mass transfer between the vapor and liquid in the tank is spherical. This is undoubtedly conservative since one objective in the design of the no-vent fill nozzles is to fragment the ullage as much as possible to promote good heat and mass transfer. The experiment will provide data on the actual interface area and the overall heat transfer coefficient. The temperature distribution measurements during the zero-g tests will allow any stratification to be determined and these effects can then be incorporated into the models.

3.2.3.2 Summary of Tests. This experiment will investigate optimum values for the velocity and spray configuration of the incoming liquid. These are emphasized in the tests, which are listed in Table 3-4. Also, the effects of tank size and shape will be investigated through the use of two tanks of different volume and geometry. This experiment uses both the receiver Tanks 2 and 3, with the latter being used for the majority of the tests.

Tests I-4.1 to I-4.3 with Tank 3 are to investigate the effects of the axial nozzle flowrate and determine a best value for use in subsequent tests. These tests are conducted with a thrust applied to settle the fluid away from the nozzle. This will simulate a radial spray configuration in a larger tank with the liquid accumulating on the tank walls.

The best flowrate will be tested again with no settling and with settling over the nozzle (Tests I-4.4 & I-4.5). These tests will determine the effects of the fluid orientation on the filling process and establish data for comparison with the partially filled tank test, which will be done with the liquid settled over the nozzle (Test I-4.7). In partially full tanks, the orientation of the initial liquid in the tank can have an impact on the effectiveness of the nozzles. Liquid settled over the nozzles is expected to produce the greatest negative effect. Test I-4.6 is to determine the effect of a higher target temperature on the process.

Tests I-4.8 to I-4.10 will compare the effectiveness of combined radial and tangential nozzle injection with that of the axial nozzle. The total flow through the radial and tangential nozzles will be equal to the best flow found for the axial nozzle. Fifty percent and 200 percent of this value will also be used.

The tests conducted in the cylindrical tank will emphasize the use of the axial nozzle. The nozzle used will be typical of a radial spray nozzle on a full scale space transfer vehicle or propellant depot. Its flowrate will be scaled based on the flowrates found in the tests on Tank 3. Ground tests during the experimental nozzle design effort may provide information to assist in scaling the flowrate. Other axial nozzle flowrates to be tested will include 50 percent and 200 percent of the scaled value. One test will be conducted with the tank 70 percent full and the liquid settled over the nozzle.

Test I-4.14 will utilize the set of radial nozzles in Tank 2, and the last experiment will utilize the LAD in the no-vent fill process, with the liquid unsettled. The LAD no-vent fill is being performed to determine if this process could be accomplished without the use of nozzles.

Most of the no-vent fill tests will be conducted in sequence with the tank chilldown tests of Section 3.2.2. Prior to each of the no-vent fill tests, the receiver tank will be initially pre-chilled to a specified target temperature and then completely evacuated. The transfer line will be pre-chilled to assure the presence of liquid with the proper temperature and pressure at the inlet to the receiver tank main and nozzle flow control valves. The appropriate inlet valves will be opened to provide the desired flow to the nozzles or LAD.

During the filling process, the internal tank and fluid temperatures and tank pressure will be monitored. Approximate liquid orientation will be determined by the liquid vapor detectors. Liquid flow will be terminated when the tank reaches a specified fill level as determined by the flow meters, or the tank pressure rises to the upper limit.

The instrumentation for these tests includes: MLI and penetration temperatures; tank wall and internal temperatures; tank pressure; inflowing liquid temperature, pressure and flowrate; and acceleration level.

Table 3-4. Tests for the No-vent Fill Experiment

TEST NO.	INITIAL FILL LEVEL %	FLUID ORIENT.	INITIAL TANK TEMP (K)	INFLOW LH2 TEMP (K)	NOZZLE SET USED	# OF NOZ. ZLES	TOTAL* INFLOW RATE (KG/S)	MAX TANK PRESS (KPA)	EST. TEST TIME (MIN)	G LEVEL x10 ⁻⁶	BOND NUMBER	NOTES
TANK #3: SPHERICAL, DIA=1.07 M, VOL=0.62 M3 ; WITH AXIAL, RADIAL, AND TANGENTIAL NOZZLES.												
I-4.1	0	SETTLED AWAY FROM NOZZLE	55.56	20.3	AXIAL	1	0.0227	145	30	100	10	SETTLED AWAY FROM AXIAL NOZZLE TO SIMULATE RADIAL SPRAY INTO A LARGER TANK @ 0-G WITH LIQUID ON THE WALL
I-4.2	0	SETTLED AWAY FROM NOZZLE	55.56	17.8	AXIAL	1	0.0136	145	50	100	10	TEST I-4.1 WITH MODERATE NOZZLE FLOW RATE AND MORE SUBCOOLING
I-4.3	0	SETTLED AWAY FROM NOZZLE	55.56	20.3	AXIAL	1	0.0068	145	100	100	10	TEST I-4.1 WITH LOW NOZZLE FLOW RATE
I-4.4	0	UNSETTLED	55.56	20.3	AXIAL	1	BEST	145	100	-0.3**	-0.03	BEST OF THE ABOVE FLOW RATES BUT WITH THE LIQUID UNSETTLED
I-4.5	0	SETTLED OVER NOZZLE	55.56	20.3	AXIAL	1	BEST	241	100	100	10	BEST FLOW DETERMINED ABOVE BUT WITH THE LIQUID SETTLED OVER THE NOZZLE (WORST CASE)
I-4.6	0	UNSETTLED	-67	-20	AXIAL	1	TBD	-	-	-	-	STUDY THE EFFECT OF A HIGHER TARGET TEMP ON THE FILL PROCESS (ONLY PERFORM IF P _{MAX} < TBD ON ABOVE TESTS)
I-4.7	50	SETTLED OVER NOZZLE	-20	-20	AXIAL	1	BEST	241	80	100	10	BEST FLOW RATE WITH THE TANK INITIALLY 50% FULL AND THE LIQUID SETTLED OVER THE NOZZLE.
I-4.8†	0	UNSETTLED	55.56	20.3	RADIAL & TANGENTIAL	3 & 2	0.0136	241	50	-0.3**	-0.03	RADIAL AND TANG NOZZLES, MODERATE FLOW
I-4.9	0	UNSETTLED	55.56	20.3	RADIAL & TANGENTIAL	3 & 2	0.0068	241	100	-0.3**	-0.03	RADIAL AND TANG NOZZLES, LOW FLOW
I-4.10	0	UNSETTLED	55.56	20.3	RADIAL & TANGENTIAL	3 & 2	0.0227	241	30	-0.3**	-0.03	RADIAL AND TANG NOZZLES, HIGH FLOW
TANK #2: CYLINDRICAL, DIA=1.02 M, LEN=1.83 M, VOL=1.27 M3, WITH AXIAL AND RADIAL NOZZLES.												
I-4.11	0	SETTLED AWAY FROM NOZZLE	55.56	-20	AXIAL	1	-SCD/2	193	205	100	9	ABOVE BUT WITH 50% OF SCALED FLOW (NOTE 4)
I-4.12	0	SETTLED AWAY FROM NOZZLE	55.56	-20	AXIAL	1	-SCD*2	186	65	100	9	ABOVE BUT WITH 200% OF SCALED FLOW (NOTE 4)
I-4.13†	70	SETTLED OVER NOZZLE	-20	-20	AXIAL	1	-SCD*2	241	50	100	9	ABOVE BUT WITH TANK PARTIALLY FULL AND LIQUID SETTLED OVER NOZZLE (WORST CASE) (NOTE 4)
I-4.14	0	UNSETTLED	55.56	-20	RADIAL	9	TBD	241	205	-0.1**	-0.01	TEST OF THE RADIAL NOZZLES FOR FILLING TANK #2.
I-4.15	0	UNSETTLED	55.56	-20	LAD	-	TBD	241	205	-0.1**	-0.01	THIS IS A NO-VENT FILL TEST WITH THE LAD.
										TOTAL TIME 1370 680 AT 1E-4 G		

* TOTAL INFLOW RATE OF ALL THE NOZZLES AND INCLUDING THE LAD IN TANK #2 WHERE APPLICABLE

** APPROXIMATE BACKGROUND ACCELERATION RESULTING PRIMARILY FROM ORBITAL PITCH RATE

† CAN ONLY BE DONE WITH 24 HOUR OPERATIONS

- 1 FOR ALL TESTS WITH INITIAL LIQUID IN THE TANKS, 30 MINUTES OF SETTLING HAS BEEN INCLUDED IN THE ESTIMATED TEST TIMES
- 2 FLUID LOSSES AFTER EACH NO-VENT FILL TEST ARE ESTIMATED AT: 8%, OR -7 LBS FOR TANK #3 AND 3%, OR -6 LBS FOR TANK #2
- 3 THE ESTIMATED TEST TIMES AND MAXIMUM TANK PRESSURES WERE OBTAINED FROM THE GDNVF PROGRAM BASED ON A TANK 2 MV OF 86 KG/M3, AND A TANK 3 MV OF 53 KG/M3.
- 4 TIMES FOR THESE TESTS ASSUMED FLOW RATES OF 0.0068 KG/S FOR THE HALF SCALE TEST, AND 0.0227 KG/S FOR THE TWICE SCALE TESTS

3.2.4 LAD Fill/Refill Experiment

3.2.4.1 Discussion of Experiment. The objective of this experiment is to determine whether a total communication liquid acquisition device (LAD) can be filled in low-g, and what the governing parameters are that affect the filling process.

The key parameters and ultimate experimental data to be evaluated in the LAD fill and refill experiment are shown below.

KEY PARAMETERS

1. Inflow rate.
2. LAD configuration and features.
3. Tank fill level.
4. Initial tank/LAD temperature.
5. Pressurant species.

ULTIMATE EXPERIMENTAL DATA

1. Tank pressure effects on the collapse of the vapor in the LAD.
2. Mass flow effects on LAD filling success.
3. Tank fill level effects on LAD filling.
4. TVS venting effectiveness on LAD filling.

The filling of the LAD may ultimately depend on the collapse of trapped vapor bubbles in the LAD. The rate of bubble collapse has been studied by several investigators (References 3-1 to 3-4), and is based on calculating the rate at which the latent heat of condensation is conducted from the bubble surface to the liquid. The time to collapse bubbles has been analyzed and typical results are shown in Figure 3-6. These results were determined from the GDSS computer program CONDENS. Hydrogen bubble collapse times are shown as a function of initial bubble radius for 35-207 kPa of liquid subcooling and an initial tank pressure of 138 kPa. The figure shows that for 69 kPa of subcooling above an initial tank pressure of 138 kPa, it would take approximately 32 seconds to completely collapse the largest spherical bubble that could exist in a LAD channel with a depth of 2.54 cm.

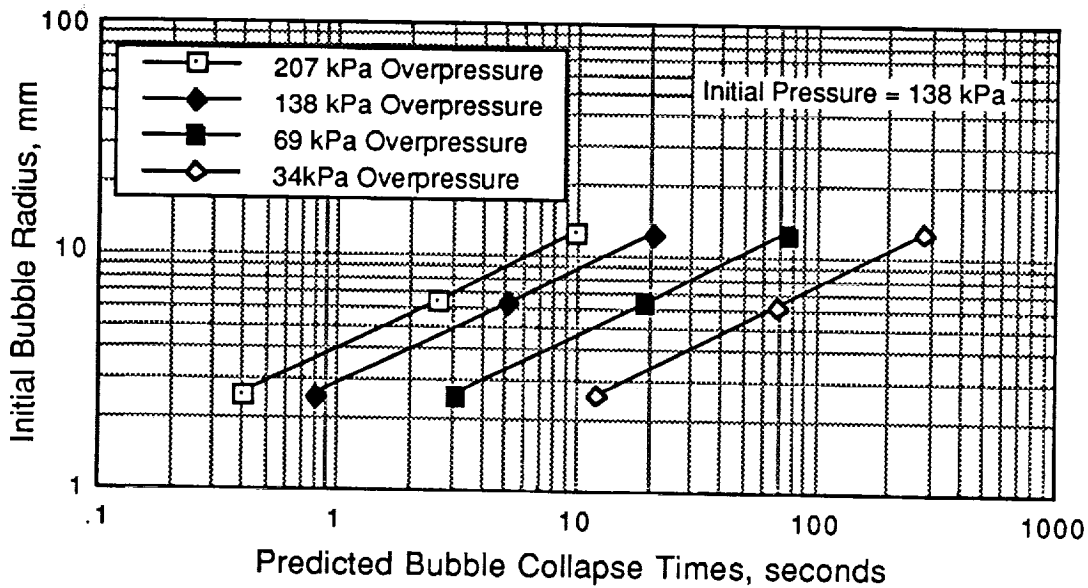


Figure 3-6. The Effect of Subcooling and Initial Bubble Radius on Bubble Collapse Time for Liquid Hydrogen in a Low-G Environment

3.2.4.2 Summary of Tests. Tests will be conducted primarily on the LAD in Tank 2. This tank will have a total communication LAD which is scaled, and characteristic of a depot tank. However, near the end of all COLD-SAT testing, one test will be conducted in Tank 1 which contains a different LAD design. The tests planned for LAD filling are shown in Table 3-5. Tests will be conducted on

Table 3-5. Tests for the LAD Fill and Refill Experiment

(SOME OF THESE TESTS MAY BE PERFORMED DURING TANK CHILLDOWN AND NO-VENT FILL TESTS)

TEST NO.	INITIAL TANK LAD T PRESS. (K)	APPROX. TANK PRESS. (kPa)	INITIAL TANK FILL (%)	INFLOW LIQUID TEMP (K)	FLOW RATE	TANK PRESS-URANT	GLEVEL x10 ^{^6}	BOND NO	NOTES

TANK #2: CYLINDRICAL, DIAMETER=1.02 m, LENGTH=1.83 m, VOL=1.27 m³, TOTAL COMM. LAD									
I-5.1	~20	TBD	0%	~37	TBD (HI)	H2	~0.1	~0.001	LAD FILL OF EMPTY TANK USING HIGH FLOW RATE
I-5.2	~20	TBD	0%	~20	TBD (LO)	H2	~0.1	~0.001	LAD FILL OF EMPTY TANK USING LOW FLOW RATE
I-5.3	~20	TBD	0%	~20	TBD (HI)	H2	~0.1	~0.001	LAD FILL WITH TVS VENT, HIGH LAD INFLOW RATE
I-5.4	~20	TBD	0%	~20	TBD (LO)	H2	~0.1	~0.001	LAD FILL WITH TVS VENT, LOW LAD INFLOW RATE
I-5.5	~20	103	10%	~20	TBD	H2/He	~0.1	~0.001	LAD FILL WITH A NON-EMPTY TANK AND WITH TVS VENT AND He TO COLLAPSE VAPOR
I-5.6	56	TBD	0%	~20	TBD (HI)	H2	~0.1	~0.001	WARM LAD FILL FROM TARGET TEMPERATURE, HIGH INFLOW RATE
I-5.7	56	TBD	0%	~20	TBD (LO)	H2	~0.1	~0.001	WARM LAD FILL FROM TARGET TEMPERATURE, HIGH INFLOW RATE

TANK #1: ELLIPSE OF REVOLUTION, DIA=2.42m, LENGTH=1.73m, VOL=5.38m³, TVS AND TOTAL COMMUNICATION LAD									
NOTE: TANK #1 LAD FILL TESTS WILL ONLY BE DONE AFTER ALL OTHER TESTS ARE COMPLETED.									
I-5.8	~20	TBD	TBD (LOW)	~20	TBD (HI)	H2	~0.1	~0.005	REFILL TEST OF THE LARGER SCALE LAD IN THE SUPPLY TANK UNDER ZERO-G CONDITIONS; HIGH FLOW
I-5.9	~20	TBD	TBD (LOW)	~20	TBD (LO)	H2	~0.1	~0.005	REFILL TEST OF THE LARGER SCALE LAD IN THE SUPPLY TANK UNDER ZERO-G CONDITIONS; LOW FLOW

NOTES:

- 1 APPROXIMATE BACKGROUND ACCELERATION RESULTING PRIMARILY FROM ORBITAL PITCH RATE.
- 2 OUTFLOW TESTS FOLLOWING LAD FILL WILL BE PERFORMED AT MAXIMUM LIQUID DESIGN FLOW OUT OF THE TANK
- 3 A LAD TEST IS ALSO INCLUDED IN THE NO-VENT FILL TESTS

the effects of the filling flowrate, TVS venting, a partially full tank, and an initially warm LAD. The notes on the table indicate the parameters which are being varied in each test listed.

The general procedure during the LAD fill tests will be to; 1) introduce a metered quantity of subcooled liquid into the LAD; 2) initiate outflow from the tank to determine whether vapor is detected; 3) if vapor is detected pressurize the tank and attempt to collapse the bubbles in the LAD; 4) try another outflow sequence; and 5) finally use settled outflow to remove the liquid if LAD filling hasn't succeeded. If the LAD was successfully filled, at the conclusion of LAD outflow the TVS will be operated to determine the amount of liquid left in the tank. The tank heaters will be operated and the tank fluid will be vented through the TVS until the tank pressure and temperature indicate that only vapor remains.

LAD fill and refill tests will be done in conjunction with the tank chilldown and no-vent fill tests. Consequently, this experiment will be integrated with those described in Sections 3.2.2 and 3.2.3. All of the tests will be conducted with background acceleration.

The instrumentation required for these tests will include tank and fluid temperatures, pressures, flowrates, pressurant conditions, LAD temperatures and liquid/vapor detection, and tank outlet liquid/vapor detection.

3.3 CLASS II EXPERIMENTS

3.3.1 Tanker Thermal Performance

3.3.1.1 Discussion of Experiment. The objective of this experiment is to determine the performance of a thermal protection system typical of an Earth-to-orbit cryogenic propellant resupply tanker. This includes demonstrating the ascent venting characteristics of a thick multilayer insulation system design, determining the time required to achieve space thermal equilibrium conditions, and measuring the thermal performance of a combined resupply tanker/orbital propellant depot cryogenic insulation system. This experiment will investigate the heat transfer characteristics of a representative tanker thermal control system using helium-purged multilayer insulation confined in a purge enclosure. This will include evaluation of the performance of the fluid, structural, and electrical penetrations as well as the insulation system. Measurements of pressures, temperatures, and mass flowrates will be made for comparison with analytical predictions.

3.3.1.2 Summary of Tests. This test will be performed using the COLD-SAT experiment supply tank, Tank 1. Tanker tank thermal performance will be determined on the ground, during ascent, and in the space environment. Following insertion of the spacecraft into orbit, data will continue to be taken on the temperatures of the MLI, tank pressure, and the tank boiloff until the temperatures within the MLI stabilize. From these data, the transient performance of the MLI will be determined. Preselected, key system temperatures will be recorded and plotted, then compared to analytical model predictions to indirectly determine heat flow. System thermal performance will be inferred from measured liquid boiloff rates. Following initiation of the COLD-SAT experiments, most of the MLI performance data will be taken during the Class I pressure control experiments, and possibly several of the other experiments to cover a range of fill levels. Temperatures of the support structure will be taken to evaluate the heat leaks through penetrations. After most of the Class I experiments are completed, and at several discrete time intervals over the life of the spacecraft, additional data will be taken to determine whether any changes have occurred in the tank thermal protection system.

The instrumentation required for this experiment is listed in the Experiment Requirements Document, Reference 3-5. A flight-worthy ionization gage could possibly be made to measure the change in pressure in the rarified gas regime (10^{-2} to 10^{-8} torr). It would be difficult to measure the interstitial pressure in the multilayer insulation by this method, however it could measure the pressure under the

MLI blanket (between the tank and MLI blanket). From this measurement an estimate of the interstitial pressure in the MLI could be made to evaluate system performance.

3.3.2 Tank Pressurization

3.3.2.1 Discussion of Experiment. The objective of this experiment is to determine the amount of pressurants required for LH₂ transfer processes in low-g, under varying conditions of flow, g-level, fill-level, and tank pressure.

Important parameters in low-gravity tank pressurization include, 1) g-level, 2) pressurant inlet temperature, 3) pressurant injection technique, 4) ortho/para hydrogen composition, 5) pressurant type (i.e., He or GH₂), 6) liquid fill level, 7) transfer pressure, 8) ramp time, and 9) outflow rate. The ultimate experimental data is the pressurant mass required for ramping and outflow as a function of these parameters. Both ortho and para hydrogen pressurization tests will be conducted by using the stored high pressure hydrogen and the autogenous hydrogen as the pressurant. The relatively warm high pressure gaseous hydrogen will contain a high percentage of ortho hydrogen, whereas the autogenous hydrogen, will be nearly all para hydrogen. Pressurant mass requirements for each of these two forms will be compared. A total of 11 tests have been designed to examine the parameters listed above and these are given in Table 3-6.

3.3.2.2 Summary of Tests. Tests II-4.1 through II-4.4 use cold para-hydrogen from the autogenous pressurization system. Tank 2 is pressurized using evaporated liquid from the supply tank. Power limitations on the evaporator (approximately 300 W) determine the minimum ramp times which can be used in the tests. During Test II-4.1, the pressure will be ramped from 103 kPa to 137 kPa. Estimates of the average pressurant flowrates required during ramping are provided in Table 3-6. The inlet temperature of the pressurant gas is not controllable, and will require detailed thermal analysis before it can be predicted. However, for purposes of preliminary design and analysis a constant value of 29K has been used. Test II-4.1 is performed using a maximum tank pressure of 137 kPa and a liquid outflow rate of 0.009 kg/s. The test will take approximately 39 minutes and will be conducted under a background g-level of approximately 1×10^{-7} . Tests II-4.2 through II-4.4 will provide data on pressurant collapse under other conditions of ramp time, maximum tank pressure, outflow rate, and initial ullage volume.

Pressurization for tests II-4.5 through II-4.9 will be accomplished using gaseous normal hydrogen (75% ortho and 25% para), from high pressure bottles. As in the case of the autogenous pressurization, the inlet temperature of the pressurant is not precisely known, and an assumed value of 208K was used in the determination of flowrates. Due to the higher flow capacity of high pressure bottles, faster ramp times are used.

The majority of the tests are performed at a background g-level of approximately 1×10^{-7} , which is due primarily to the orbital pitch rate of the satellite. However, Tests II-4.8 and II-4.9 are performed with an imposed acceleration of $50 \times 10^{-6}g$, and are done with the warmer pressurant which is expected to undergo greater collapse than the cold vapor pressurant.

Pressurization Tests II-4.10 and II-4.11 use high pressure stored Helium. The tank is ramped to a pressure consistent with a pressurized transfer, and different initial ullage volumes are used in each of the two tests.

The pressurant requirements for Tests II-4.1 through II-4.9 can be calculated using several different approaches. Discussion and results of these calculations are given in Section 6.4.

Table 3-6. Tests for the Pressurization of Cryogenic Tankage in Low G Experiment

(SOME OF THESE TESTS MAY BE PERFORMED IN CONJUNCTION WITH FLUID TRANSFERS BETWEEN OTHER EXPERIMENTS)

TEST NO.	PRESSURANT (NOTE 1)	APPROX PRSNT TEMP. (K)	INITIAL FILL (%)	FINAL FILL (%)	INITIAL TANK PRESS (kPa)	TANK XFER PRESS (kPa)	RAMP TIME	AVE. RAMP PRESENT FLOW (kg/hr)	OUTFLOW RATE OF LH2 (NOTE 4) (kg/sec)	EST. TEST TIME (MIN)	G LEVEL BOND NUMBER x10 ⁻⁶	NOTES	
II-4.1	H2 (PARA)	29	80%	60%	103	138	LONG (NOTE 3)	0.4	0.0091	39	~0.1 (NOTE 2)	COLD GH2 PRESSURIZATION TO LOW PRESSURE, HIGH FILL LEVEL, SLOW RAMP (TBD), & BCKGND G	
II-4.2	H2 (PARA)	29	80%	60%	103	138	SHORT	1.6	0.0227	15	~0.1	SAME AS II-4.1 BUT FAST RAMP (TBD) AND HIGHER OUTFLOW RATE	
II-4.3	H2 (PARA)	29	80%	60%	103	241	LONG	0.5	0.0091	53	~0.1	SAME AS II-4.1 BUT PRESSURIZATION TO HI PRESS	
II-4.4	H2 (PARA)	29	30%	10%	103	138	LONG	1.47	0.0091	39	~0.1	SAME AS II-4.1 BUT LOW FILL LEVEL	
II-4.5	H2 (ORTHO)	208	80%	60%	103	241	LONG	0.2	0.0091	39	~0.1	STORED, HI TEMP GAS FOR PRESSURIZATION TO HI PRESS, HI FILL LEVEL, SLOW RAMP (TBD), BCKGND G	
II-4.6	H2 (ORTHO)	208	80%	60%	103	241	SHORT	3.2	0.0227	15	~0.1	SAME AS II-4.5 BUT FAST RAMP (TBD) AND HIGHER OUTFLOW RATE	
II-4.7	H2 (ORTHO)	208	30%	10%	103	241	LONG	0.6	0.0091	43	~0.1	SAME AS II-4.5 BUT LOW FILL LEVEL	
II-4.8	H2 (ORTHO)	208	80%	60%	103	241	LONG	0.2	0.0091	43	50	4.7	SAME AS II-4.5 BUT 50 MICRO-G IMPOSED
II-4.9	H2 (ORTHO)	208	30%	10%	103	241	LONG	0.8	0.0091	TBD	50	4.7	SAME AS II-4.8 BUT LOW FILL LEVEL
II-4.10	He	208	80%	60%	103	241	DESIGN	TBD	0.0091	TBD	~0.1	~0.1	STORED He FOR PRESSURIZATION TO HI HIGH PRESS, HI FILL LEVEL, DESIGN RAMP TIME, BCKGND G
II-4.11	He	208	30%	10%	103	241	DESIGN	TBD	0.0091	TBD	~0.1	~0.1	SAME AS II-4.10 BUT LOW FILL LEVEL

* TANK #2: CYLINDRICAL, DIA=1.02 m, LEN=1.83 m, VOL=1.27 m³, NO MIXER, TVS WITH WALL MOUNTED HX, & ONE VCS.

* TANK #2 IS THE PRIMARY TANK FOR THE PRESSURIZATION TESTS. HOWEVER, PRESSURIZATION DATA WILL BE TAKEN DURING ALL TRANSFERS BETWEEN TANKS. THIS, DATA WILL BE TAKEN ON TANKS #1, #2, AND #3.

- NOTES:
- 1 ORTHO REFERS TO EQUILIBRIUM PARA/ORTHO COMPOSITION OF THE BOTTLED GAS.
 - 2 APPROXIMATE BACKGROUND ACCELERATION RESULTING PRIMARILY FROM ORBITAL PITCH RATE.
 - 3 RAMP TIMES LISTED AS "LONG" AND "SHORT" ARE NOT NECESSARILY THE SAME FOR PARA H2, ORTHO H2 AND HE
 - 4 ALL LIQUID TRANSFERS ARE PLANNED TO BE PUMP ASSISTED.

3.3.3 Low-G Settling and Outflow

3.3.3.1 Discussion of Experiment. The objective of this experiment is to investigate low-g liquid settling accelerations and times, and the quantity of liquid remaining in a tank following outflow under these conditions. The latter involves the phenomenon of "pull through" which is the appearance of vapor at the outlet due to vortex formation and/or curvature of the liquid/vapor interface above the outlet. The key parameters and ultimate experimental data to be evaluated in this experiment are shown below.

KEY PARAMETERS

1. G level and time (including the effects of pulsed acceleration)
2. Outflow rate
3. Tank configuration and baffling
4. Tank fill level

ULTIMATE EXPERIMENTAL DATA

1. Settling times and g levels
2. Tank residuals after outflow
3. Mass flow and tank level effects on residuals

The settling of the liquid over a tank outlet is discussed in References. 3-6 to 3-10. A GDSS computer program called PROPSET, which is based on empirical equations presented by Sumner and Bowman, was used to evaluate settling times for COLD-SAT. The program computes the time required to "flood-the-drain" and "clear-the-vent" for Bond Numbers from 2 to 15. The time to "flood-the-drain" is that required for the liquid to flow to the bottom of tank and for the geysers to disappear. The time to "clear-the-vent" is the sum of, the time for the ullage bubble to reach the top of the tank, and for the liquid film in this area to disperse. For the low g-levels considered for this experiment, a Bond number of 5 gives the fastest settling and the time for settling to occur in Tank 3 is approximately 30 minutes.

After settling and the initiation of outflow, vapor "pull-through" can necessitate the premature termination of flow, resulting in higher tank residuals and resulting liquid loss. Short term low-g testing and immiscible liquid testing have been performed to investigate these effects (References 3-11 to 3-14). A computer program named PULL is available at GDSS based on the procedure suggested by Stark, and uses a critical height (the depth of liquid over the drain at the time of "pull-through") based on empirical equations of Bereyni. The program is for an unbaffled outlet, and is therefore not strictly applicable to the outlet configuration of Tank 3. However, the program was used to estimate conservative residuals and the effects of flowrate and g-level on these residuals. Typical results are shown in Figure 3-7.

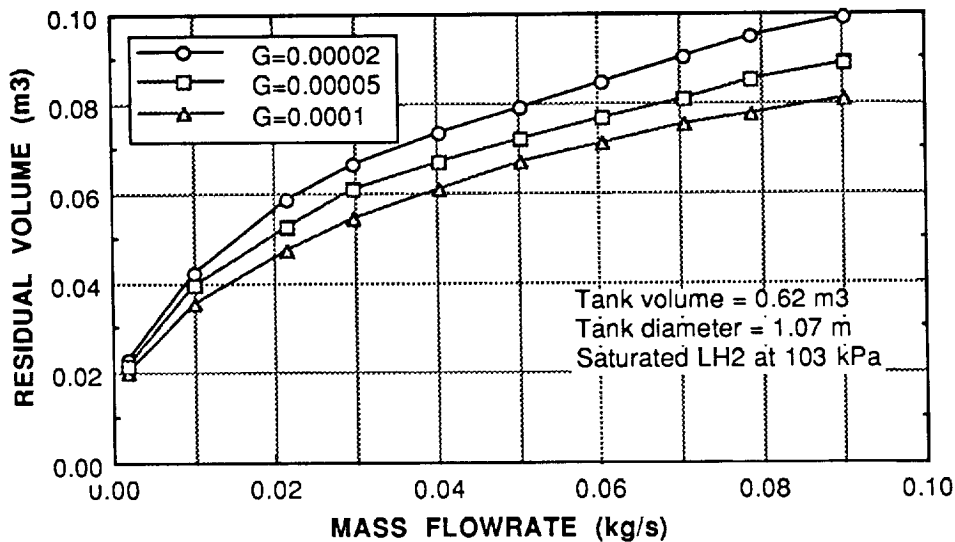


Figure 3-7. Effect of Mass Outflow Rate on the Residual Volume in Low-G

3.3.3.2 Summary of Tests. A list of eight tests for the settled outflow experiment is shown in Table 3-7. All tests will be performed in Tank 3, the only tank without a LAD. Pressurization will be accomplished by cold hydrogen vapor. Thrusting will be required during the tests to settle the liquid. Tank fill levels at 30 and 70% have been selected to provide information on the effects of the fill level on "pull through". The effect of pulsed acceleration will be determined and compared with data obtained under conditions of constant acceleration. Two liquid outflow rates will be tested.

Prior to each test, the test tank will be filled to the initial fill level and allowed to come to thermal equilibrium in a background g-level environment. When equilibrium is achieved, axial thrust will be applied to settle the liquid over the outlet end of the tank. The gas/liquid configuration during settling will be monitored by vapor/liquid detectors positioned within the tank.

The liquid will be transferred from the receiver tank back into the supply tank. The flow will continue until vapor is detected in the outlet of the tank. At this time, outflow will be terminated and the amount of liquid remaining in the tank will be determined. This can be done for large residuals by the liquid level sensors in the tank, and for low residuals by use of the TVS and flow meter.

Instrumentation for this experiment will include, 1) tank pressure, temperatures and vapor/liquid detectors, 2) pressurant temperature, pressure and flowrate, 3) liquid outflow rate and quality, and 4) spacecraft acceleration.

3.3.4 LAD Performance

3.3.4.1 Discussion of Experiment. The objective of this experiment is to determine the effect of heat input to the LAD, g-level and flowrate on the quantity of vapor-free LH₂ that can be removed from a cryogenic storage tank using a total communication LAD.

Parameters which affect the performance of a total communication LAD include, 1) the fluid properties, 2) liquid orientation inside the tank, 3) acceleration level, 4) heat input to the LAD, 5) liquid fill level, 6) channel cross-sectional area, 7) screen mesh size, and 8) liquid outflow rate. Parameters other than those mentioned will not be tested due to limitations of equipment and resources. The ultimate experimental data is the expulsion efficiency of the LAD as a function of these parameters.

3.3.4.2 Summary of Tests. The LAD performance tests are shown in Table 3-8. Tests are included for two different flowrates, two different g-levels, and two different heating rates. Low initial fill levels are specified to minimize potential fluid losses. Tank pressure is H₂ at 103 kPa. Breakdown of the LAD will be determined by the appearance of vapor in the outlet line from the tank.

In Test II-6.1 and II-6.2 outflows of approximately 0.023 kg/s and 0.009 kg/s are used at background g-levels and no heat is applied to the LAD. Tests II-6.3 and II-6.4 will be conducted with imposed acceleration levels of 100×10^{-6} g and 20×10^{-6} g, respectively. The direction of the imposed acceleration will be such that the liquid in the tank settles away from the tank outlet, representing a worst condition for the LAD.

In Tests II-6.5 and II-6.6, heat will be applied to the LADs near the tank outlet during outflow. These tests will attempt to determine what heat levels result in vapor formation in the outlet. Future analyses will be required to determine the appropriate heat flux levels and outflow rates for these tests.

Table 3-7. Tests for the Low Gravity Settling and Outflow Experiment

(SOME OF THESE TESTS WILL BE PERFORMED DURING FLUID TRANSFERS BETWEEN TANKS FOR OTHER EXPERIMENTS)

TEST NO.	PRESS-URANT	INITIAL FILL (%)	ULLAGE PRESS (kPa)	WT FLOW RATE (kg/s)	EST. SETTLING TIME (MIN)	EST. XSFER TIME (MIN)	EST. TOTAL TIME (MIN)	GLEVEL x10 ⁶	BOND NUMBER	NOTES	
II-5.1	H2	70%	103	0.01	30	53	83	100	10	CONTINUOUS G, LOW FLOW, MAX BOND NO.	
II-5.2	H2	70%	103	0.01	30	53	83	20	2	CONTINUOUS G, LOW FLOW, LOWER BOND NO.	
II-5.3	H2	70%	103	0.023	30	21	51	100	10	CONTINUOUS G, HIGH FLOW, MAX BOND NO.	
II-5.4	H2	70%	103	0.023	30	21	51	20	2	CONTINUOUS G, HIGH FLOW, LOWER BOND NO.	
II-5.5	H2	70%	103	0.023	30	21	51	20	2	PULSED ACCELERATION FOR COMPARISON WITH TEST II-5.4. (FREQ AND LEVEL OF THRUST TBD)	
II-5.6	H2	30%	103	0.023	30	22	52	20	2	CONTINUOUS ACCELERATION, LOWER FILL LEVEL LOWER BOND NUMBER AND HIGH FLOW	

TOTALS FOR TANK #3									180	191	371

Table 3-8. Tests for the LAD Performance Experiment

TEST NO.	INITIAL FILL %	TANK ULLAGE PRESS (kPa)	TANK PRESS URANT	WEIGHT FLOW, SAT LH2 (kg/sec)	EST. TRANSFER TIME (min)	EST. SETTLING TIME (min)	HEAT INPUT	G LEVEL x10 ⁴	BOND NUMBER	NOTES

TANK #2: CYLINDRICAL, DIAMETER=1.02 m, LENGTH=1.83 m., VOL=1.27 m3, TOTAL COMMUNICATION LAD.										
II-6.1	20%	103	H2	0.0227	12	-	ND	~0.1 (NOTE 1)	~0.01	HIGH FLOW, BACKGROUND G LEVEL (WILL BE DONE DURING OTHER OPS) AS ABOVE BUT LOWER FLOW RATE
II-6.2	20%	103	H2	0.0091	30	-	ND	~0.1	~0.01	
II-6.3	20%	103	H2	TBD	TBD	30	ND	100	9	LIQUID SETTLED OPPOSITE TO OUTLET OF LAD, HI G LEVEL
II-6.4	20%	103	H2	TBD	TBD	30	ND	20	2	SAME AS II-6.3 BUT LOWER G LEVEL
II-6.5	20%	103	H2	TBD	TBD	-	MCD	~0.1	~0.01	HEAT INPUT, BACKGROUND G LEVEL
II-6.6	20%	103	H2	TBD	TBD	-	MAX	~0.1	~0.01	SAME AS II-6.5 BUT MAXIMUM HEAT INPUT

NOTES:

- 1 APPROXIMATE BACKGROUND ACCELERATION RESULTING PRIMARILY FROM ORBITAL PITCH RATE.
- 2 LAD PERFORMANCE DATA WILL BE OBTAINED ON THE LAD IN TANK #1 DURING MANY OPERATIONAL TRANSFERS.

3.3.5 Line Chillover

3.3.5.1 Discussion of Experiment. The objective of this experiment is to investigate the chillover of cryogenic fluid transfer lines in the space environment.

In the past, special designs have been proposed to enhance the chillover of cryogenic fluid transfer lines, and also to keep the lines chilled. At this time, this experiment does not address such special designs, but does address the issue of the performance of line chillover. Since the process of line chillover involves forced convection, it is important that the low-gravity tests be well coordinated with those performed on the ground.

The main issue related to line chillover is the proper venting of superheated vapor, rather than liquid, so that the amount of liquid hydrogen used in the process can be minimized. Also, the line must be chilled and then filled with zero quality fluid before a transfer process can proceed. This will require consideration of the source tank fluid condition and of the final condition of the transfer line. For our tests, the chillover temperature will correspond to the temperature of the fluid to be introduced into the line, and the fluid will be subcooled enough to compensate for the parasitic heat leak into the transfer lines.

Another issue is the potential use of the boiloff from line chillover for tank chillover. In most operational scenarios line chillover will be performed in conjunction with the chillover of a tank. However, in some cases the receiver tank will already be chilled or partially full, and the venting of the fluid through a tank will not be applicable. Therefore, line chillover with and without venting through a tank will be investigated. Other alternatives are to vent the fluid through a tank TVS or VCS.

The liquid inflow rate must be compatible with the chillover heat transfer rate to avoid venting liquid at the downstream end. In general, very low flowrates will be used. The effectiveness of intermittent inflow will be evaluated.

The initial temperature of the line can have an effect on the approach used for chillover and may affect the flowrate and the amount of fluid required for the process. A second consideration with a line previously used and containing liquid is what to do with the liquid. It is assumed that if residual fluid is left in a transfer line, it will be vented and the line refilled before any transfer process requiring 100% liquid is performed. However, the venting of the line can be done in a manner to take advantage of the cooling capability of the fluid and possibly make use of the vented fluid.

3.3.5.2 Summary of Tests. This experiment will be performed in the fluid transfer systems between Tank 1 and each of the two smaller receiver tanks. A listing of the tests is shown in Table 3-9. Two different flowrates and initial line temperatures will be tested. For one of the tests, the line will be vented through Tank 2 so that a combined line and receiver tank chillover will be performed. The test of the line at about 170 K will be performed after a transfer and when the line has reached the required temperature. The chillover history of the line at the lower initial temperature will be compared with that at the higher temperature.

The line chillover experiment will be performed in conjunction with the Class I experiments since chillover of the fluid transfer system will be required for these experiments. The list shown in Table 3-9 is considered to be the minimum number of tests that will be performed. The final list of tests may expand to fit the chillovers which are required in the Class I experiments, but will depend on the overall sequencing of experiments and tests. One of the parameters affecting chillover time and liquid consumed is the size of the line being chilled. To evaluate this aspect of the process, the lines between Tanks 1 and 2 and between Tanks 1 and 3 will be tested.

Table 3-9. Tests for the Transfer Line Chilldown Experiment

(THESE TESTS WILL BE PERFORMED DURING FLUID TRANSFERS ON THE OTHER EXPERIMENTS)

TEST NO.	LINE INITIAL TEMP (K)	TANK #1 PRESS (KPA)	FLOW RATE (KG/S)	TEST TIME (MIN)	G LEVEL	NOTES

LINE CHILLDOWN TESTS WHICH WILL BE CONDUCTED ON THE 1.91 cm DIAMETER LINE BETWEEN TANKS #1 AND #2.						
II-7.1	~250*	138	HIGH**	TBD	BKGRND	CONTINUOUS HIGH FLOW, DIRECT VENT
II-7.2	~250	138	LOW	TBD	BKGRND	CONTINUOUS LOW FLOW, DIRECT VENT
II-7.3	~170	138	LOW	TBD	BKGRND	CONT LOW FLOW, DIRECT VENT, LINE @ LOWER UNIFORM TEMP
II-7.4	~250	138	LOW	TBD	BKGRND	VENT THROUGH TANK #2, CONTINUOUS FLOW
II-7.5	~250	138	HIGH	TBD	BKGRND	INTERMITTANT FLOW, VENT THROUGH TANK #2

LINE CHILLDOWN TESTS WHICH WILL BE CONDUCTED ON THE 1.91 cm DIAMETER LINE AND THE 1.27 cm DIAMETER LINE BETWEEN TANKS #1 AND #3.						
II-7.6	~250*	138	HIGH**	TBD	BKGRND	CONTINUOUS HIGH FLOW, DIRECT VENT
II-7.7	~250	138	LOW	TBD	BKGRND	CONTINUOUS LOW FLOW, DIRECT VENT
II-7.8	~170	138	LOW	TBD	BKGRND	CONT LOW FLOW, DIRECT VENT, LINE @ LOWER UNIFORM TEMP
II-7.9	~250	138	LOW	TBD	BKGRND	VENT THROUGH TANK #3, CONTINUOUS FLOW
II-7.10	~250	138	HIGH	TBD	BKGRND	INTERMITTANT FLOW, VENT THROUGH TANK #3

* LINES WILL BE ALLOWED TO WARM UP TO APPROX. THIS TEMPERATURE PRIOR TO EACH ~250K TEST. (HEATERS MAY BE REQUIRED)

** RELATIVE TO THE LOW LINE CHILL DOWN FLOWRATES AND TBD

*** THE BACKGROUND ACCELERATION IS ON THE ORDER OF 1.E-7 G

For the tests at the space equilibrium temperature, the line will be allowed to warm and stabilize. Flow will be introduced into the transfer line by pressurizing Tank 1. The flowrate will be set by the main Tank 1 orificed valves and monitored by the tank flowmeter. For Tests II-7.1 and II-7.2, the line initial temperature will be approximately 250 K. Test II-7.3 will be conducted following Test II-7.2 when the line has recovered to an average temperature of approximately 170 K. The first three tests will be conducted by venting fluid from the transfer line into the vent manifold. Tests II-7.4 and II-7.5 will vent the fluid through Tank 2 to accomplish chilldown of this tank. The last of these tests will use intermittent flow and venting. During all of the tests the flowrate and quality of the fluid flowing into the transfer line will be monitored, and during the tests including tank chilldown, flow into the tank and tank temperature and pressure will be monitored. Line chilldown tests will terminate when the line has reached the temperature of the chilldown fluid.

The instrumentation for these tests includes: inlet liquid temperature, pressure, flowrate and quality; transfer system temperatures and pressures; acceleration level; tank temperature and flowrate; and vent flowrate.

3.3.6 Outflow Subcooling

3.3.6.1 Discussion of Experiment. The objective of this experiment is to evaluate the effectiveness of a compact heat-exchanger in subcooling tank outflow. Tank fluid is throttled to a lower pressure and temperature prior to entering the cold-side of the heat-exchanger. All the liquid flowing through the cold-side is vaporized prior to the exit.

The dominant heat transfer mechanisms in the compact heat-exchanger are single-phase forced convection on the hot-side, and two-phase forced convective boiling on the cold-side. Both of these phenomena are dominated by viscous and inertial forces. The micro-g space environment is expected to have little effect on the compact heat-exchanger effectiveness. Both continuous and intermittent flow on the cold-side of the heat-exchanger will be evaluated.

KEY PARAMETERS

1. Hot-side flowrate
2. Cold-side flowrate and duty-cycle
3. Heat exchanger design
4. Acceleration level

ULTIMATE EXPERIMENTAL DATA

1. Temperature drop of the liquid flowing through the hot-side
2. Temperature and quality of the fluid entering and exiting the cold-side
3. Location of the "dry-out" point on the cold-side
4. Heat exchanger effectiveness

3.3.6.2 Summary of Tests. A summary of the minimum experiment requirements for the outflow subcooling tests is shown in Table 3-10. Outflow subcooling tests can be conducted in conjunction with liquid transfers required for other tests, such as tank chilldown and no-vent fill. Many more outflow subcooling tests with much longer test times can be accommodated if tests are run concurrently with other experiments. All tests will be performed under the background acceleration level. Fluid to the compact heat exchanger will be supplied by the LAD in Tank 1. The hot-side flowrate will be controlled by a pump. Three different liquid flowrates will be investigated. The cold-side flowrate will be intermittent and controlled by a valve. The duty cycle will decrease as the hot-side flowrate decreases to maintain the same level of subcooling. The time period for each duty cycle will be less than the residence time of the cold-side fluid in the heat exchanger to insure no liquid is vented. The duration of each experiment needs to be long enough to insure "steady-state"

Table 3-10. Tests for the Class II Outflow Subcooling Experiment

(THESE TESTS WILL BE CONDUCTED DURING FLUID TRANSFERS REQUIRED FOR OTHER EXPERIMENTS. THE TEST CONDITIONS SHOWN REPRESENT THE MINIMUM TEST REQUIREMENTS.)

TEST NO.	TANK SAT PRESS (kPa)	HOT-SIDE FLOW RATE (KG/SEC)	COLD-SIDE DUTY CYCLE (%)	MINIMUM TEST TIME (MIN)	G LEVEL x10 ⁶	NOTES
II-8.1	103	0.0227	100	5	~0.1	HIGH FLOW RATE.
II-8.2	103	0.0136	60	10	~0.1	MEDIUM FLOW RATE.
II-8.3	103	0.0068	30	10	~0.1	LOW FLOW RATE.

TANK 1: SHORT CYLINDER, DIA.=2.41 M, LEN.=1.73 M, VOL.=5.38 M³, THERMAL CONTROL SYSTEM, MIXER, VCS, COMPACT TVS HX, AND INTERNAL WALL MOUNTED HX

NOTES:

- 1 APPROXIMATE BACKGROUND ACCELERATION RESULTING FROM ORBITAL PITCH RATE.
- 2 ALL TESTS WILL BE PERFORMED WITH H₂ AS THE PRESSURANT.
- 3 ALL TEST PERFORMED IN AN EXTERNAL, ANNULAR COILED, COMPACT HEAT EXCHANGER.
- 4 COLD-SIDE FLOW IS THROUGH THE INNER TUBE. HOT-SIDE FLOW IS THROUGH ANNULAR RING BETWEEN TUBES.
- 5 COLD-SIDE FLOW IS INTERMITTENT AND CONTROLLED BY A VALVE.
- 6 THE DUTY CYCLE PERIOD WILL BE LESS THAN THE RESIDENCE TIME OF THE FLUID IN THE HEAT EXCHANGER.
- 7 COLD-SIDE FLOW RATE IS 0.00121 KG/SEC WHEN THE VALVE IS OPEN.

conditions have been reached. Intermittent flow tests will be run longer to insure the flow and thermal variations are periodic.

Fluid temperatures will be measured at the inlet and exit of each side of the heat exchanger. Temperature sensors will be required at regular intervals along the cold-side to determine the location of the "dry-out" point. For intermittent flow tests, data sampling rates will be greater than the duty cycle frequency.

3.3.7 Low-Gravity Vented Fill

3.3.7.1 Discussion of Experiment. The objective of this experiment is to determine the operational parameters under which a low-gravity filling operation can be performed, and the resulting fill level that can be achieved prior to the appearance of liquid in the vent.

The ultimate parameter to be evaluated in this experiment is the final fill level of the tank. This will depend on the conditions of the inflowing liquid, the initial temperature of the receiver, the g level, and the configuration of the inlet and outlet hardware in the tank (baffles, vent inlet design, etc.). For a low-gravity vented fill, the initial temperature of the receiver could be near space equilibrium requiring a tank chilldown prior to tank fill. The process to be studied in this experiment is the fill, but to achieve the low initial tank temperature a chilldown must also be performed. This chilldown could be performed by either a vented low-g process or a zero-g "charge/hold/vent" process. The determination of which process will be used will be the subject of further analysis and study. In the event that a low-g vented chilldown is used, this experiment will be inherently included in the tests. For these fills, the initial temperature of the tank will be near the fluid saturation temperature at the tank pressure. The higher initial tank temperature is included in the tests to evaluate the case where the "charge/hold/vent" process is terminated at a higher target temperature.

During the tests, tank pressure will be maintained relatively constant by the vent line valves. The tank pressure will be kept at the same value for all of the tests. The optimum gravity level is the lowest that results in complete tank filling without liquid venting. Tests will be conducted at g levels of 1×10^{-4} , which is the maximum COLD-SAT acceleration level, and at 5×10^{-5} for comparison.

The type of flow for maximum filling is one dimensional, with liquid entering the "bottom" of the tank at minimum velocity and vapor venting from the opposite end. The flow into Tank 3 will be introduced through a baffled inlet to diffuse the inflow energy. The baffle configuration will be the subject of further analysis and design.

3.3.7.2 Summary of Tests. This experiment will be performed using Tanks 2 and 3 as the receivers and Tank 1 as the supply. A listing of the tests to be performed is shown in Table 3-11. The cold vent gas from the tank will be vented overboard through the vent valve and liquid/vapor detectors which will be used to detect the presence of liquid in the vent.

Tank 3 will be chilled to the required initial temperature. The specified acceleration level will be applied to the spacecraft, and the filling of the tank will be initiated. A tapered inlet section or a "coolie hat" fitting will be used on the vent line to discourage the entrainment of liquid, and the vent rate will be controlled to maintain the desired tank pressure. Venting will be terminated when liquid is detected in the vent line. At this point, low-gravity filling will be terminated and the quantity of liquid in the tank determined. The flow meter measurements, as well as the liquid/vapor detector readings in the tank (after the liquid is allowed to settle), will be used to determine the mass of the fluid in the tank. If the tank is found to be less than 95 percent full of liquid, the tank will be locked up and the spray nozzle system will be activated to complete tank filling. Once again the liquid level and the final fluid conditions in the tank will be determined. Two acceleration levels and two initial tank temperatures will be tested as shown in Table 3-11.

Table 3-11. Tests for the Low-G Vented Fill Experiment

TEST NO.	INITIAL TANK (K)	PRESSURANT (K)	URGENT (KPA)	ULLAGE PRESS. (KPA)	FLOW RATE (KG/S)	EST. TIME (MIN)	G LEVEL x10 ⁶	BOND NUMBER	NOTES
TANK #3: SPHERICAL, DIA=1.07 M, VOL=0.62 M3; WITH BAFFLED INLET									
II-9.1	21	H2	104	104	0.0227	30	50	5	MOD G, INITIAL TEMPERATURE CORRESPONDING TO FINAL SATURATION TEMP. HIGH FLOW RATE
II-9.2	21	H2	104	104	0.0068	100	50	5	MOD G, INITIAL TEMPERATURE CORRESPONDING TO FINAL SATURATION TEMP. LOW FLOW RATE
II-9.3	21	H2	104	104	0.0227	30	100	10	HIGHER G, INITIAL TEMPERATURE CORRESPONDING TO FINAL SATURATION TEMP. HIGH FLOW RATE
II-9.4	56	H2	104	104	0.0227	30	100	10	HIGHER G, HIGH TANK INITIAL TEMPERATURE, HIGH FLOW RATE
II-9.5	56	H2	104	104	0.0136	50	100	10	HIGHER G, HIGH TANK INITIAL TEMPERATURE, MODERATE FLOW RATE
II-9.6†	56	H2	104	104	0.0068	100	100	10	HIGHER G, HIGH TANK INITIAL TEMPERATURE, LOW FLOW RATE
TANK #2: CYLINDRICAL, DIA=1.02 M, LEN=1.83 M, VOL=1.27 M3; WITH FULL COMMUNICATION LAD									
II-9.7	21	H2	104	104	0.0227	63	50	5	FILL THROUGH THE LAD, MODERATE G AND HIGH FLOW RATE
II-9.8	21	H2	104	104	0.0068	210	50	5	FILL THROUGH THE LAD, MODERATE G AND LOW FLOW RATE
II-9.9	21	H2	104	104	0.0227	63	100	10	FILL THROUGH THE LAD, HIGHER G AND HIGH FLOW RATE
II-9.10†	21	H2	104	104	0.0068	210	100	10	FILL THROUGH THE LAD, HIGHER G AND LOW FLOW RATE

TOTAL TIME 886

† CAN ONLY BE COMPLETED WITH 24 HOUR OPERATIONS

If the tests performed in Tank 3 are deemed successful, Tank 2 will be used to evaluate vented fill through the liquid acquisition device. The effects of both low and high imposed g levels will be investigated.

The instrumentation for these tests includes: liquid temperature, pressure, and flowrate; tank pressure, temperature, and liquid level; pressurant temperature, pressure, and flowrate; transfer line temperature; acceleration level; and vent line flowrate, quality, pressure, and temperature.

3.3.8 Fluid Dumping

3.3.8.1 Discussion of Experiment. The objective of this experiment is to evaluate the effectiveness of dumping fluid from a tank in a micro-g, space environment. These tests will focus on procedures applicable to unsettled tanks containing no special equipment for dumping.

The tank can be emptied in the shortest time when liquid is dumped. The dump rate decreases when vapor is ingested into the outflow line, which becomes more likely for high outflow rates and as the liquid fill level decreases during the dump. Besides vapor ingestion, hydrogen freezing in the tank and/or outflow line will also decrease the dump rate. The effectiveness of heaters for minimizing hydrogen freezing during the dump will be investigated. The distribution of liquid in the tank and LAD will be much different in the micro-g space environment as compared to 1-g earth environment. Consequently, hydrogen freezing in these locations cannot be adequately tested on the ground. Conditions under which the vent line freezes are not expected to be strongly dependent on the acceleration level.

KEY PARAMETERS

1. Tank outlet geometry (baffle or LAD)
2. Tank heater power level
3. Outflow line heater power level
4. Tank pressurization

ULTIMATE EXPERIMENTAL DATA

The time history of the following quantities will be monitored during each test

1. Outflow mass flowrate
2. Temperature and quality of outflow
3. Tank and outflow line pressure
4. Liquid fill level
5. Acceleration level

3.3.8.2 Summary of Tests. Hydrogen used during a fluid dump cannot be recovered. To conserve hydrogen, fluid dumping tests will only be performed when an operational dump is required or as part of a liquid transfer. A summary of the fluid dumping tests is shown in Table 3-12. All fluid dumping tests will be performed under background acceleration. Dumping will be initiated by opening the vent valve.

Hydrogen freezing in the LAD and/or tank will be investigated in both receiver tanks. During the dump, hydrogen freezing in the LAD and/or tank is expected to decrease the rate of outflow. When the rate of outflow stabilizes or stops, the tank heater will be turned on to melt the solid hydrogen and provide tank pressurization. The outflow line heater power will be on during these tests to prevent hydrogen freezing in the outflow line.

Hydrogen freezing in the outflow line is not expected to be strongly dependent on the acceleration level and could be adequately tested on the ground. However this test can be performed in space with no penalty as part of an operational dump. The procedure for this experiment will be the same

Table 3-12. Tests for the Fluid Dumping Experiment

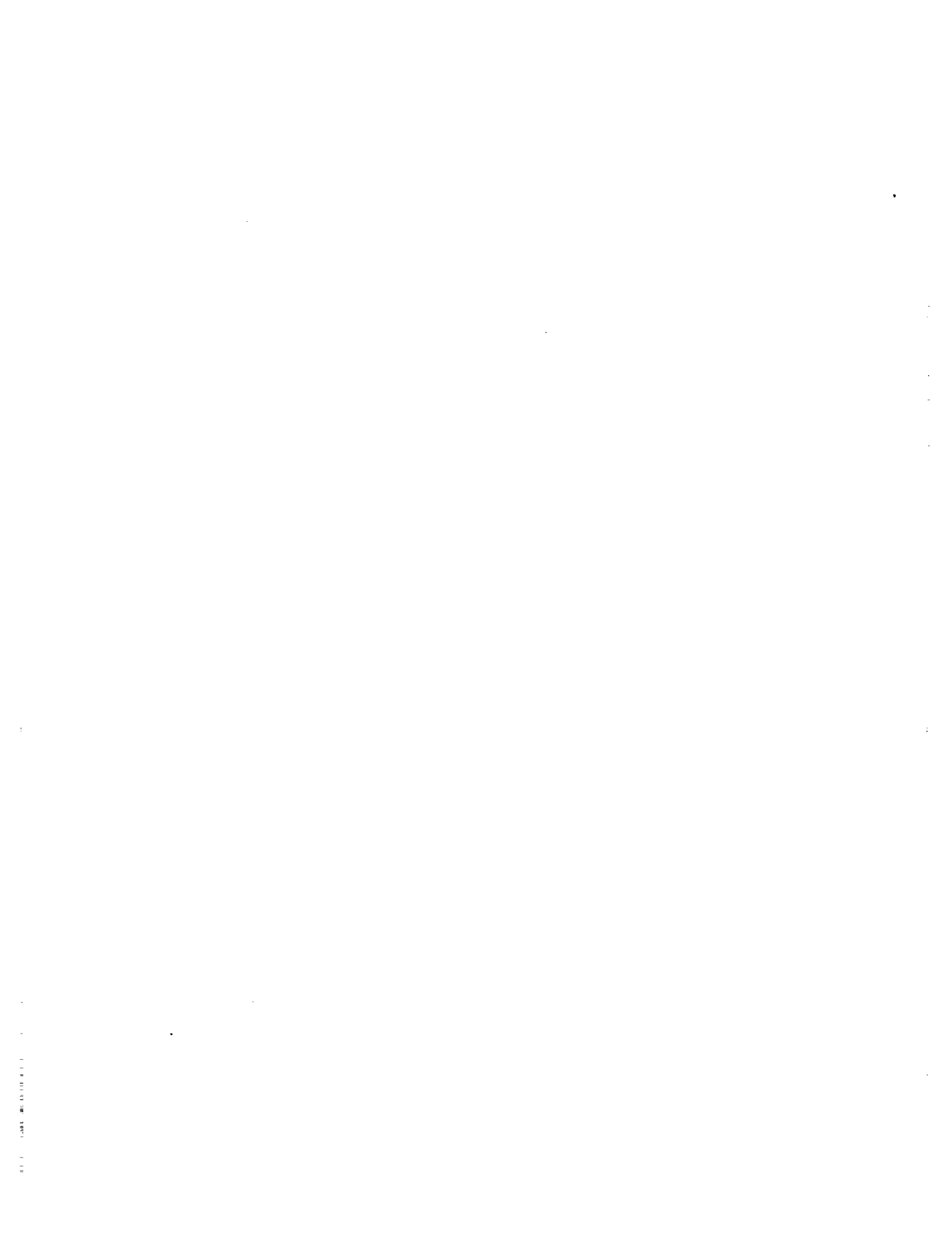
TEST NO.	INITIAL FILL (%)	ACC. LEVEL (Gx10 ⁻⁶)	ULLAGE PRESSURIZATION	ULLAGE PRESS. (KPA)	OUTLET LINE USED	OUTFLOW LINE HEATER	EST. TIME	NOTES
TANK 2: CYLINDRICAL, DIA.=1.02 M, LEN.=1.83 M, VOL.=1.27 M3.								
II-10.1	5%	~0.1	NO	120 (INITIAL)	LAD	ON	TBD	HYDROGEN FREEZING IN TANK AND LAD.
TANK 3: SPHERICAL, DIA=1.07 M, VOL=0.62 M3.								
II-10.2	10%	~0.1	NO	120 (INITIAL)	BAFFLED	ON	TBD	HYDROGEN FREEZING IN TANK.
II-10.3	10%	~0.1	YES	35.0	BAFFLED	OFF/ON	TBD	HYDROGEN FREEZING IN OUTFLOW LINE.
II-10.4	>20%	~0.1	YES	120.0	BAFFLED	OFF	TBD	VAPOR INGESTION TEST, LOW FLOW RATE. (PUMP-ASSISTED TRANSFER)
II-10.5	>20%	~0.1	YES	120.0	BAFFLED	OFF	TBD	VAPOR INGESTION TEST, HIGH FLOW RATE. (PUMP-ASSISTED TRANSFER)

NOTES:

- 1 APPROXIMATE BACKGROUND ACCELERATION RESULTING PRIMARILY FROM ORBITAL PITCH RATE.
- 2 OUTFLOW RATE, PORT GEOMETRY, AND ACCELERATION LEVEL WILL AFFECT THE FILL LEVEL WHICH CAN BE ACHIEVED BEFORE VAPOR PULLS-THROUGH THE OUTLET.
- 3 BACK PRESSURE AND LINE HEATER OPERATION WILL AFFECT WHEN THE VENT FREEZES-UP WITH SOLID HYDROGEN.
- 4 ULLAGE PRESSURIZATION AND TANK WALL HEATER OPERATION WILL AFFECT WHEN SOLID HYDROGEN FORMS IN THE TANK.
- 5 LAD PERFORMANCE IS EXTENSIVELY TESTED AS PART OF OTHER EXPERIMENTS.
- 6 CONDITIONS UNDER WHICH THE VENT LINE FREEZES-UP ARE NOT EXPECTED TO BE STRONGLY DEPENDENT ON THE ACCELERATION LEVEL AND COULD BE ADEQUATELY TESTED ON THE GROUND.
- 7 CONDITIONS UNDER WHICH VAPOR PULLS-THROUGH THE VENT ARE DEPENDENT ON THE ACCELERATION LEVEL AND WILL BE DIFFICULT TO TEST ON THE GROUND.
- 8 THE AMOUNT OF HYDROGEN THAT FREEZES IN THE TANK IS DEPENDENT ON THE ACCELERATION LEVEL AND WILL BE DIFFICULT TO TEST ON THE GROUND.
- 9 TANK WALL HEATER USED ONLY IF NECESSARY TO THAW TANK.

as for the tank freezing experiment described in the previous paragraph, except the line heater power will be varied. The tank will be pressurized during this test to prevent freezing in the tank.

The liquid fill level when vapor is ingested into the outflow line cannot be determined during a dump without losing "usable" hydrogen. To conserve hydrogen, these tests will be performed during an operational transfer of liquid between tanks. The tanks will be pressurized and unsettled during these tests. Tests to determine the liquid fill level when vapor is ingested into a simple baffled outlet will be conducted in Tank 3. Two different outflow rates will be investigated. The outflow rate will be controlled by the transfer pump. Once vapor is ingested into the outlet, the remainder of the transfer can be completed under settled conditions to increase the amount of liquid transferred.



4
MISSION DESCRIPTION

4.1 MISSION REQUIREMENTS

The mission of the COLD-SAT spacecraft is to carry out liquid hydrogen experiments under low-g conditions. The spacecraft bus must provide a stable orbital platform in low-Earth orbit for the cryogenic experiments and provide the necessary support services for the experiment operation. These services include data acquisition, telemetry, operation and control, electrical power, attitude control, accelerations at specified levels, thermal control of experiment electronics, and radiation protection for the electronics. Micrometeoroid and debris protection, although not an explicit NASA requirement, should be provided if necessary to meet system reliability goals. The operational mission lifetime is one year and the ground storage life is also one year. The overall mission reliability for accomplishing the Class I experiments must be 0.92 or better.

The orbit and the operation of the spacecraft provide a very quiet, low-g working background for the experiment with an acceleration of 5×10^{-7} g or less. Launch will be with an expendable launch vehicle from Kennedy Space Center in 1997. At the end of the mission the spacecraft must either have an orbital lifetime of 500 years or it must be disposed of safely. This disposal could be either retrieval by the STS or a re-entry which would not endanger populated areas. Unless COLD-SAT is to be retrieved as the means of disposal, it is not to be designed for reuse, recovery or repair.

The primary communication link is through the TDRSS Multiple Access Service, and the STDN network is used for launch operations and for backup ground command. Normal communications through the TDRS system is limited to ten minutes per orbit to avoid potential TDRS scheduling problems. Data storage for the experiment telemetry must be provided for periods when the TDRS system is not available.

The attitude control system will maintain an attitude pointing accuracy of 5 deg. or better in each axis. In addition to the low background acceleration, acceleration levels between 10^{-5} and 10^{-4} g will be provided by thrusters for periods of up to 45 hours.

4.2 LAUNCH VEHICLE PERFORMANCE

The Atlas I expendable launch vehicle will be used to place COLD-SAT into a 28.5 deg. inclination circular orbit at an altitude of 1300 km. Two Centaur upper stage burns will be used to provide the lift capability shown in Figure 4-1. The Atlas I lift capability provides greater than a 34 percent margin in lift capability for the mission.

4.3 PAYLOAD FAIRING

Figure 4-2 shows the COLD-SAT spacecraft packaged within the 4.2 m diameter, 64.4 m^3 Atlas I payload fairing. The cylindrical section of the payload fairing provides 4.2 m of length. The cylindrical section is topped by a 14.5 degree conical nose cone which provides generous envelope for the spacecraft.

4.4 PAYLOAD MASS AND CENTER OF GRAVITY ENVELOPE

Figure 4-3 shows the Atlas I launch vehicle payload center of gravity location limit as a function of payload mass. The critical structural limit is set by the Centaur stage equipment module to which the payload adapter is attached. The payload mass thus includes the payload adapter and separation

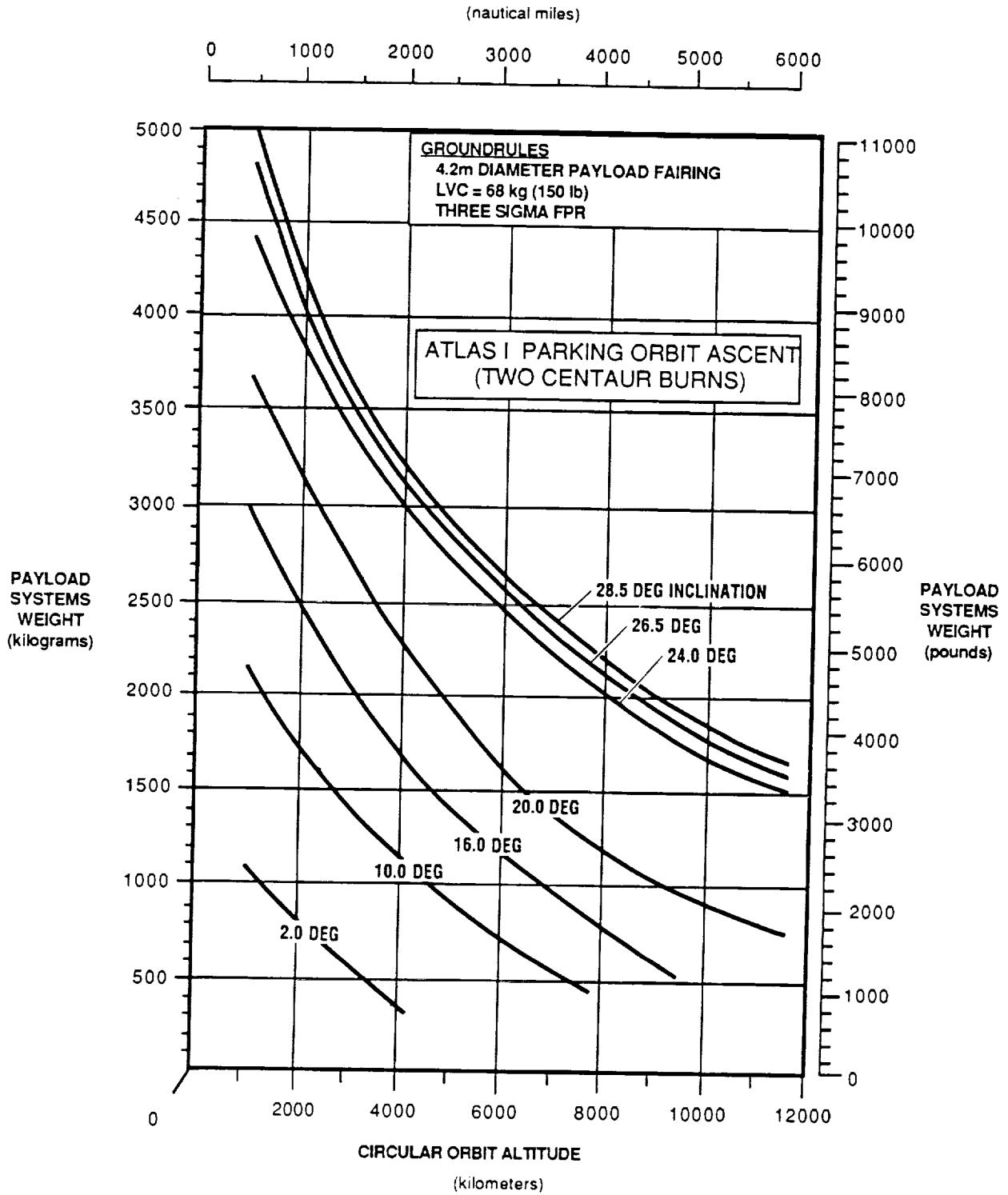


Figure 4-1. Atlas I Parking Orbit Ascent Payload Capability to Circular Orbit

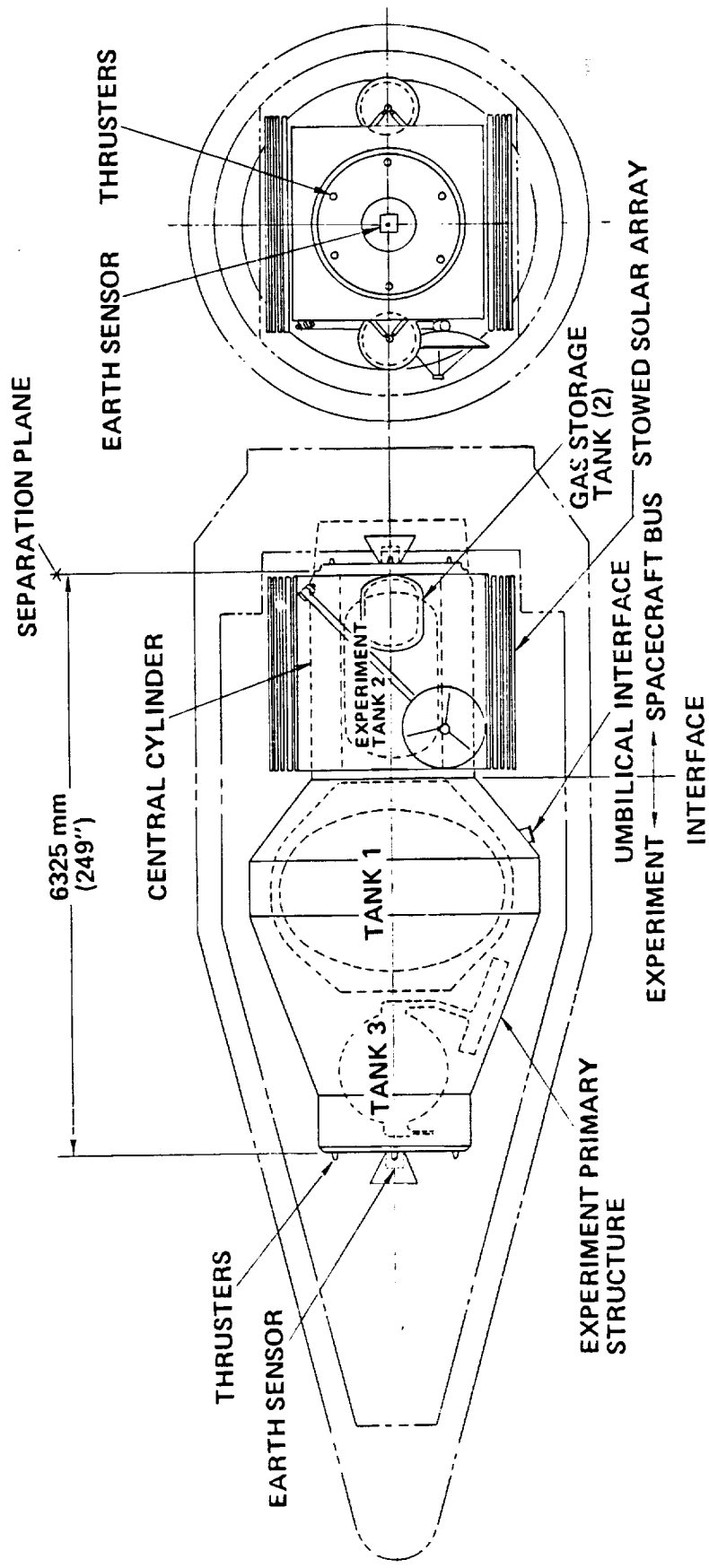


Figure 4-2. COLD-SAT Configuration within the Atlas I Payload Fairing

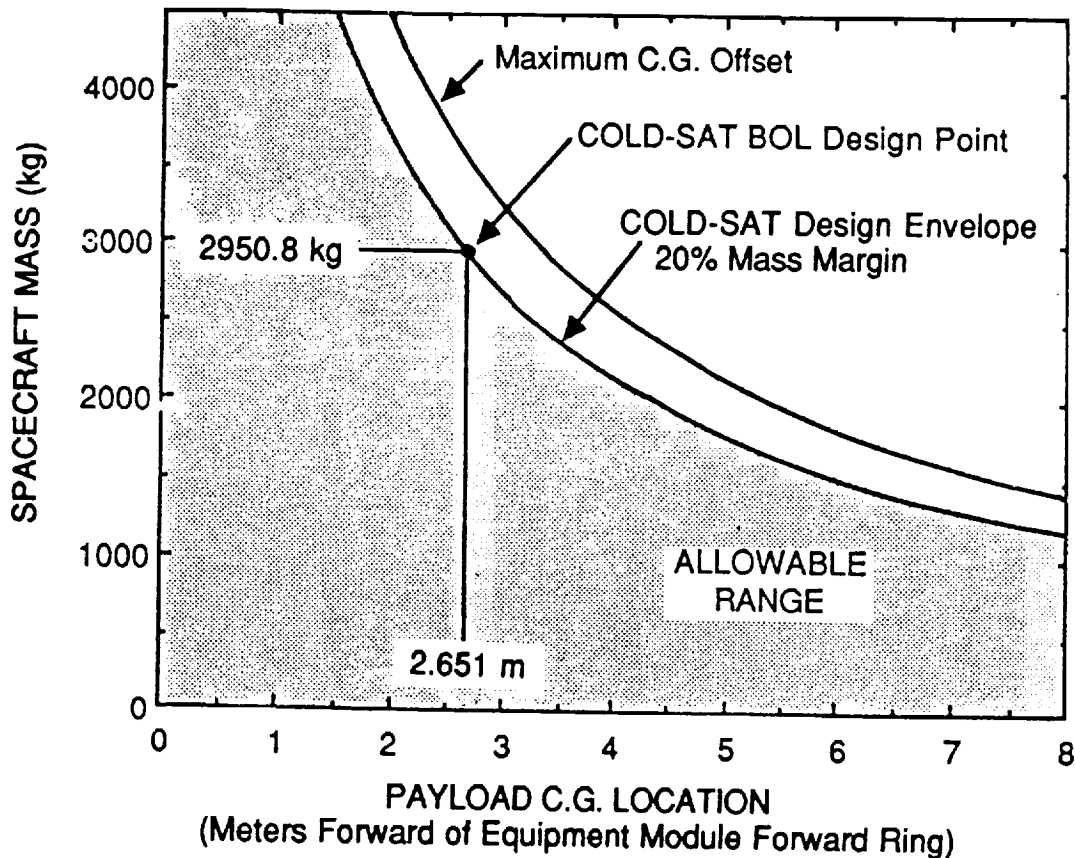


Figure 4-3. Atlas I Payload Mass/Center of Gravity Envelope

system as well as the COLD-SAT spacecraft. The COLD-SAT mass properties satisfy the launch vehicle constraint with the required 20 percent margin.

4.5 ORBIT ANALYSIS

4.5.1 Baseline Orbit

The 1300 km altitude selection is the result of a trade study to minimize atmospheric disturbances, and satisfy lifetime and launch vehicle constraints. Since the COLD-SAT mission requirements are not significantly influenced by orbit inclination, the standard due-east launch (28.5 deg. inclination) from the Eastern Test Range has been selected. At altitudes lower than 350 km the atmospheric drag would induce unacceptable background accelerations, and at altitudes above 1800 km, the charged particle radiation environment becomes excessive. Within this range of altitudes, the Atlas I lift capability does not impose any constraints. The concentration of man-made orbital debris varies with altitude. Therefore, the selected altitude was chosen to satisfy the 500 year orbital lifetime, and achieve a relatively low concentration of orbital debris.

A list of the orbital characteristics are given in Table 4-1. The maximum eclipse duration is 35.2 minutes but varies cyclicly due to the nodal regression rate as shown in Figure 4-4. The solar angle variation over the same twelve month period is shown in Figure 4-5. The long period cyclic motion is caused by the solar declination variation, and the short period variation is a result of the orbit plane regression.

The 1300 km altitude is above the TDRSS zone of exclusion (ie. where the Earth occults the COLD-SAT/TDRS line-of-sight. This higher altitude also increases the contact time with a STDN ground station if contingency communications were required. Figure 4-6 shows when TDRSS and each of the STDN and Deep Space Network ground stations will be visible to COLD-SAT in a typical 24 hour period. Three satellites in the TDRS system are expected to be available in 1997; the operational satellites TDRS-East and TDRS-West, and a spare. There will be three STDN ground stations for launch and backup communications located at Wallops Island, Virginia; Merritt Island, Florida; and Bermuda. The three DSN stations, although they are not planned to be used, could be used for backup command transmissions. Figure 4-7 indicates how many ground stations will be within COLD-SAT's field-of-view on a typical day. The worst case scenario results in no ground station contacts for as many as 3 orbits per day utilizing both the DSN and STDN networks, and up to 6 orbits per day utilizing just the STDN network. This raises serious satellite control implications if for any reason the TDRS system is not available. However, the COLD-SAT bus has the capability to operate autonomously with SCE firmware and stored commands for up to 28 days.

4.5.2 Orbit Perturbations

The perturbations affecting the COLD-SAT orbit are external environmental disturbances (atmospheric drag, solar radiation pressure, triaxiality), and internal disturbances due to experiment thrusting requirements. At 1300 km altitude, the external disturbances are negligible. The largest of these perturbations is the atmospheric drag which imparts a disturbance acceleration of 2×10^{-9} g during the operational phase of the mission. Figures 4-8 and 4-9 show the disturbance accelerations and orbital lifetime as a function of altitude for a range of COLD-SAT ballistic coefficients. The experiment thrusting, on the other hand, will generate large in-plane accelerations for extended periods of time. The net effect of these thrusting maneuvers will be to either increase or decrease the circular orbit altitude depending on the specified direction of the required acceleration (ie., a thrust vector in the +X direction increases the altitude, and a thrust vector in the -X direction decreases the altitude). Figure 4-10 shows the increase in altitude as a function of the net change in velocity due to experiment thrusting. Currently it is expected that there will be a net propellant consumption in the +X direction of 337 kg which would increase the altitude by 610 km. Since this large an increase is unacceptable, the spacecraft will occasionally rotate to fly in the -X direction for some of the firings. The orbital lifetime of the vehicle based on a 1300 km orbit is 684 years.

4.5.3 Orbital Environment

There are three potential environmental hazards that the spacecraft design must consider for low Earth orbits: atomic oxygen corrosion, micrometeoroid and debris impacts, and charged particle damage. Atomic oxygen impinging on the spacecraft at orbital velocities is extremely reactive or erosive to some materials such as Kapton, graphite epoxy and silver. The atomic oxygen environment (Figure 4-11) is sufficiently low at the proposed altitude that most likely no specific protection will be required.

The micrometeoroid and debris environment is described in Reference 4-1. The debris flux profile in terms of both particle density and particle size as a function of orbital altitude is a function of time with significant changes occurring within a time span of one or two years. The debris density profile for particles (Figure 4-12) greater than 100 mm in diameter shows a minima in the measured debris flux in the vicinity of 1300 km. The flux of small particles is generally assumed to follow a similar

Table 4-1. Orbit Parameters and Characteristics

INITIAL ALTITUDE (KM)		1300
INCLINATION (DEGREES)		28.5
ECCENTRICITY		0
PERIOD (MINUTES)		111.5
NODAL REGRESSION RATE (DEGREES/DAY)		4.58
MAXIMUM ECLIPSE DURATION (MINUTES)		35.2
MINIMUM ECLIPSE DURATION (MINUTES)		16
ORBITAL LIFETIME (YEARS)		684
TYPICAL DRAG ACCELERATION (G)		3.5×10^{-9}
AVERAGE GROUND STATION CONTACT DURATION (MINUTES)		15.8
PERCENTAGE OF ORBITS HAVING GROUND STATION CONTACT		
AVAILABLE (PERCENT)	STDN PLUS DSN	77
	STDN ONLY	54
TYPICAL BETA = ZERO DEG. CROSSINGS PER YEAR		11

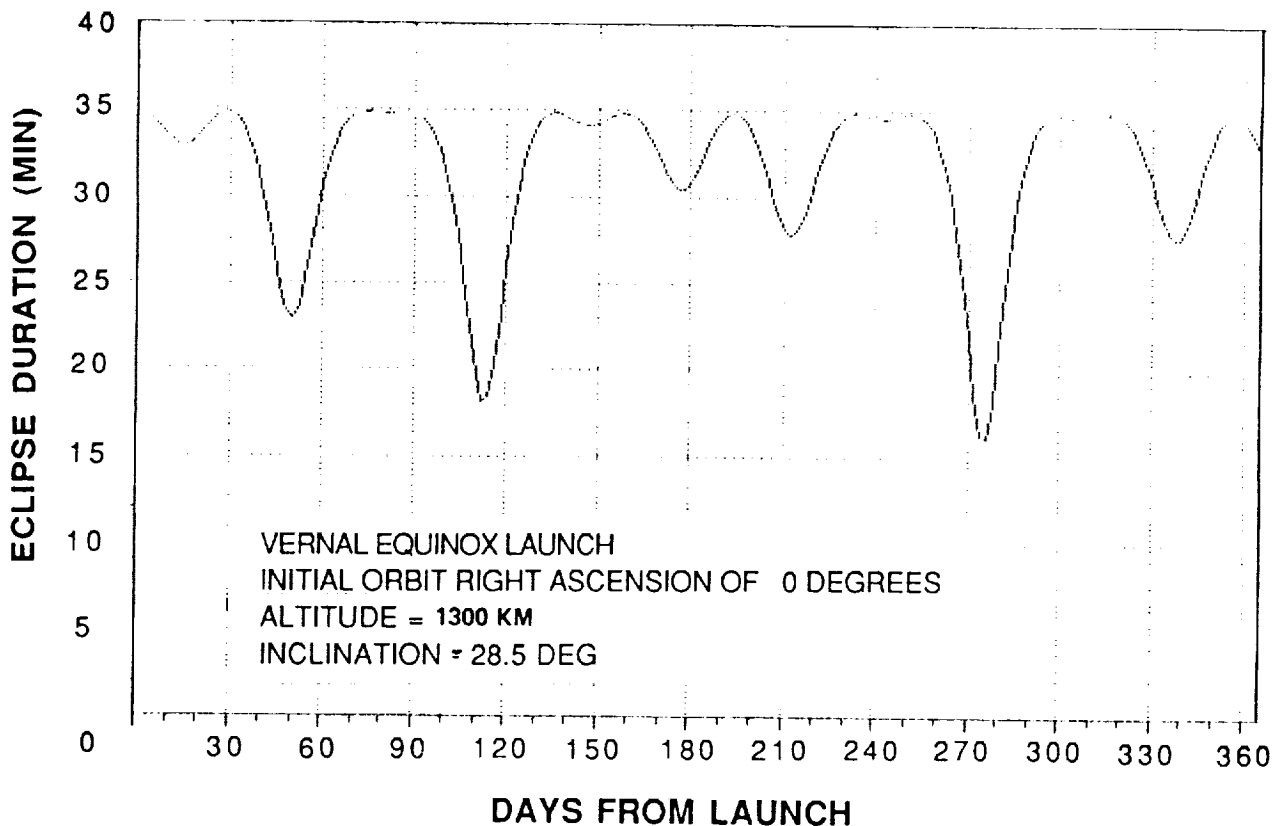


Figure 4-4. Eclipse Durations for an Initial Orbit Right Ascension of Zero Degrees

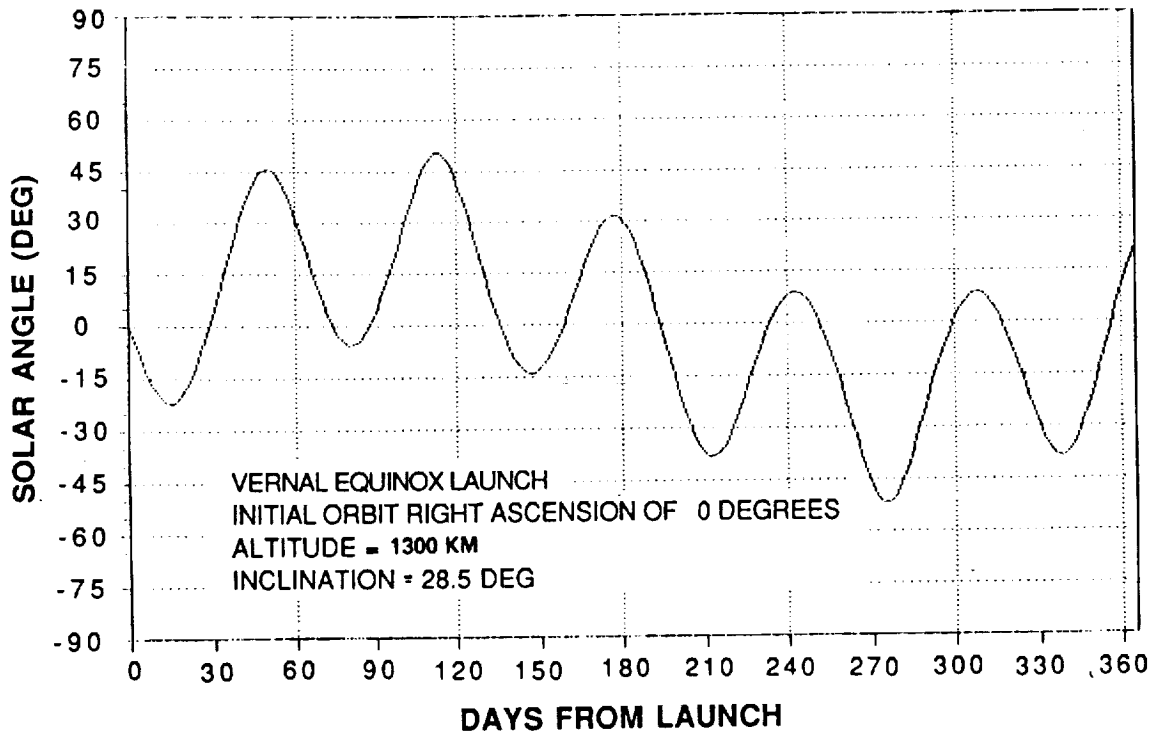


Figure 4-5. Beta Angle for an Initial Orbit Right Ascension of Zero Degrees

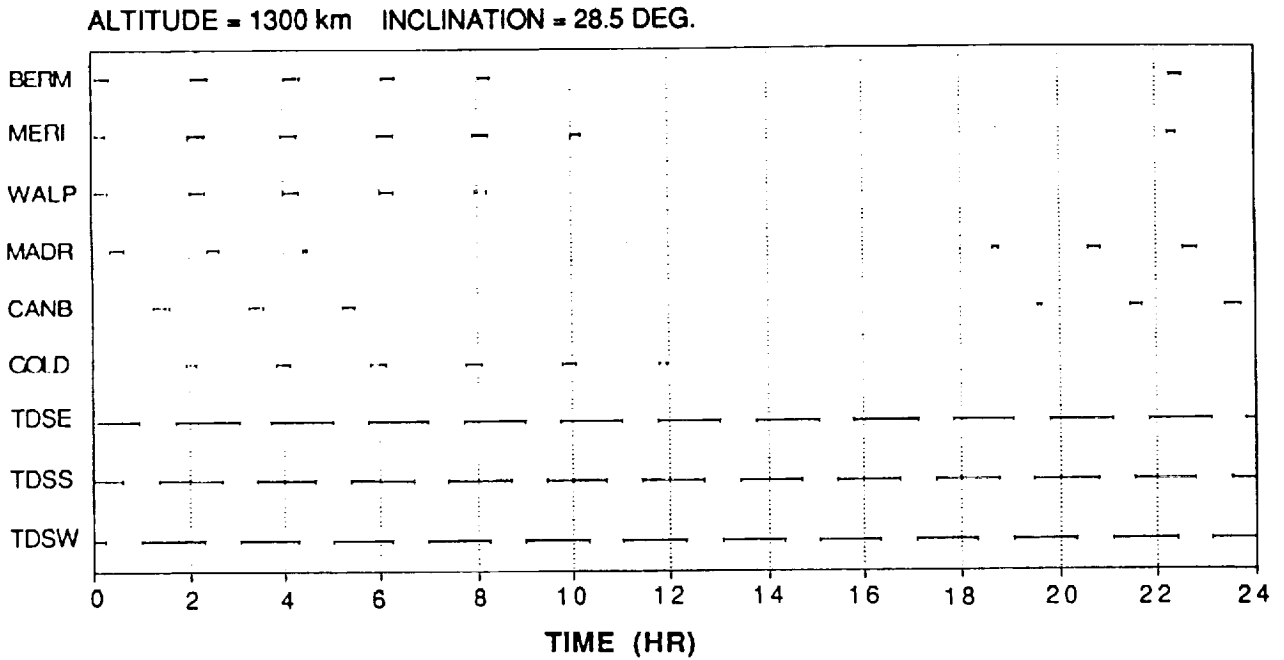


Figure 4-6. Tracking Station and TDRS Visibility

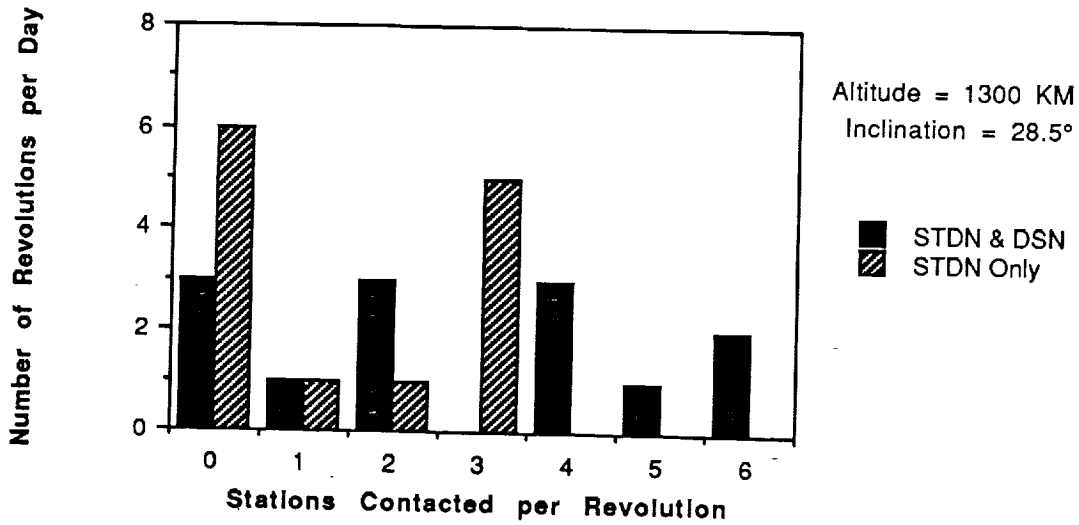


Figure 4-7. Typical Daily Tracking Station Contacts

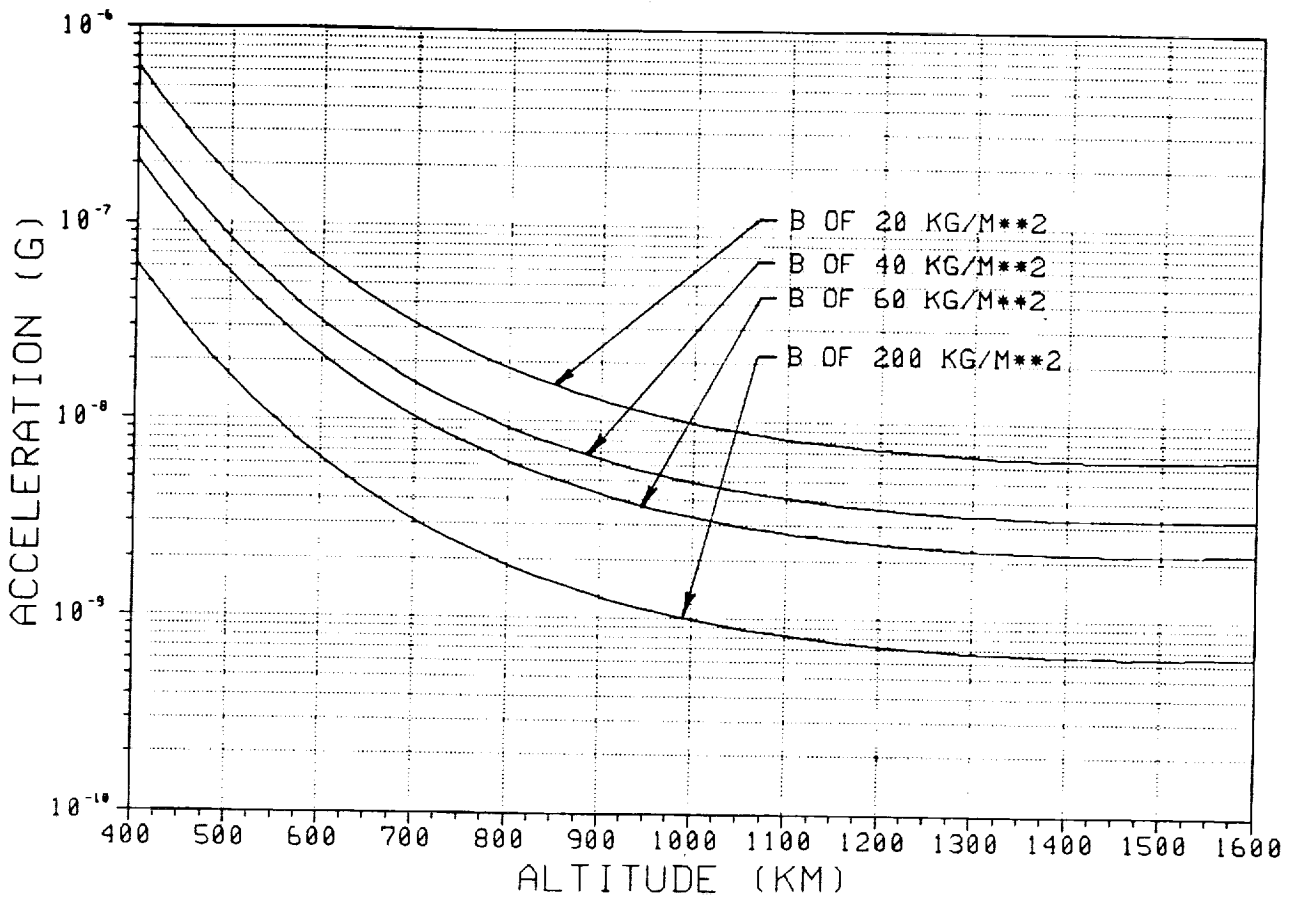


Figure 4-8. Accelerations Induced by Atmospheric Drag

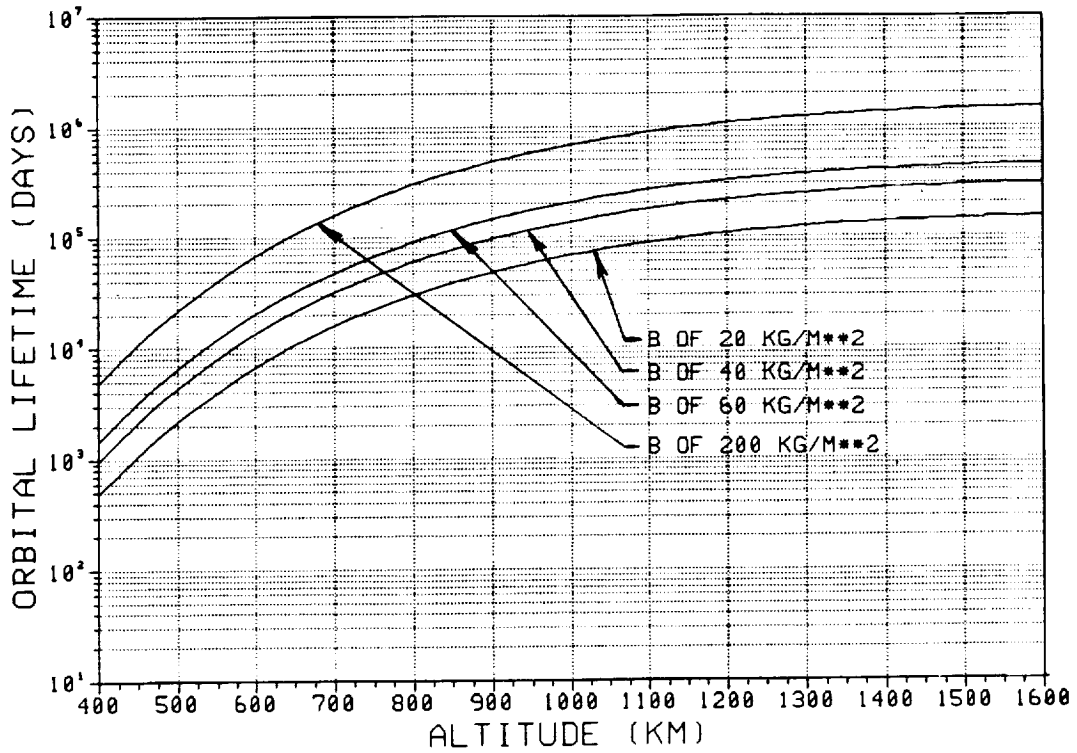


Figure 4-9. COLD-SAT Orbital Lifetime from an Initial Circular Orbit

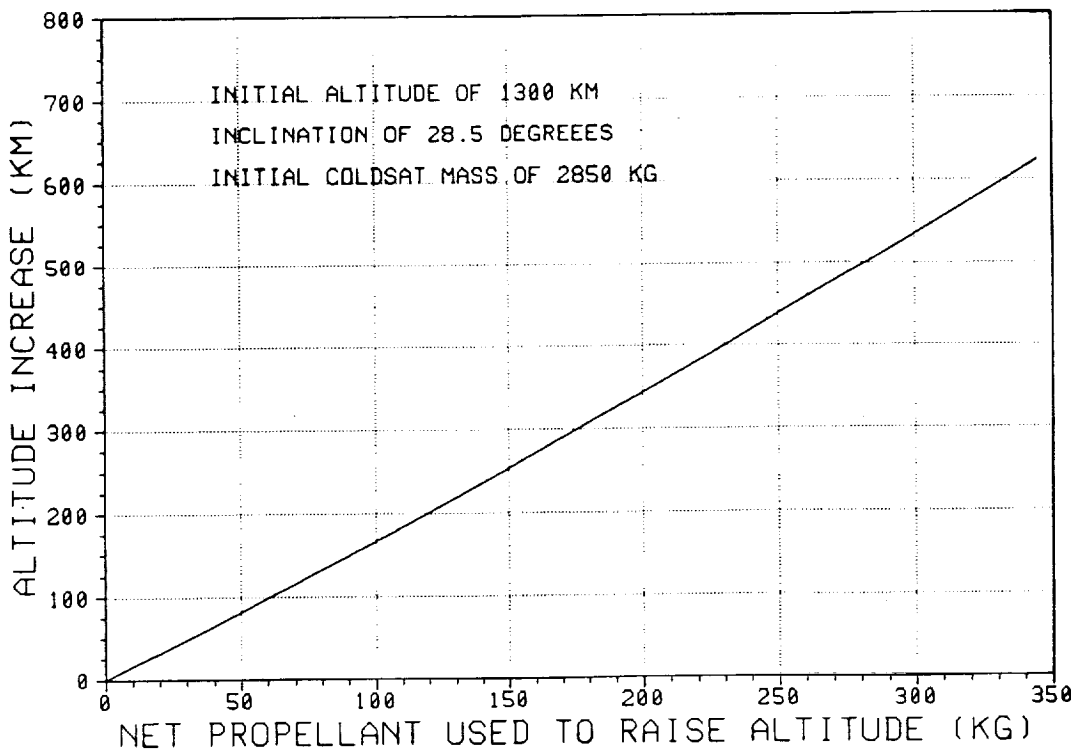


Figure 4-10. COLD-SAT Altitude Increase due to Experiment Thrusting

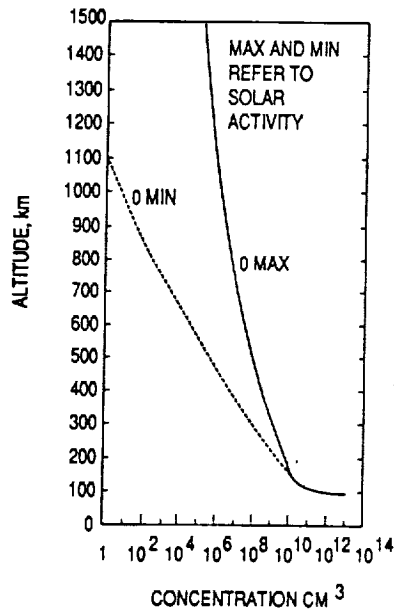


Figure 4-11. Distribution of Atomic Oxygen

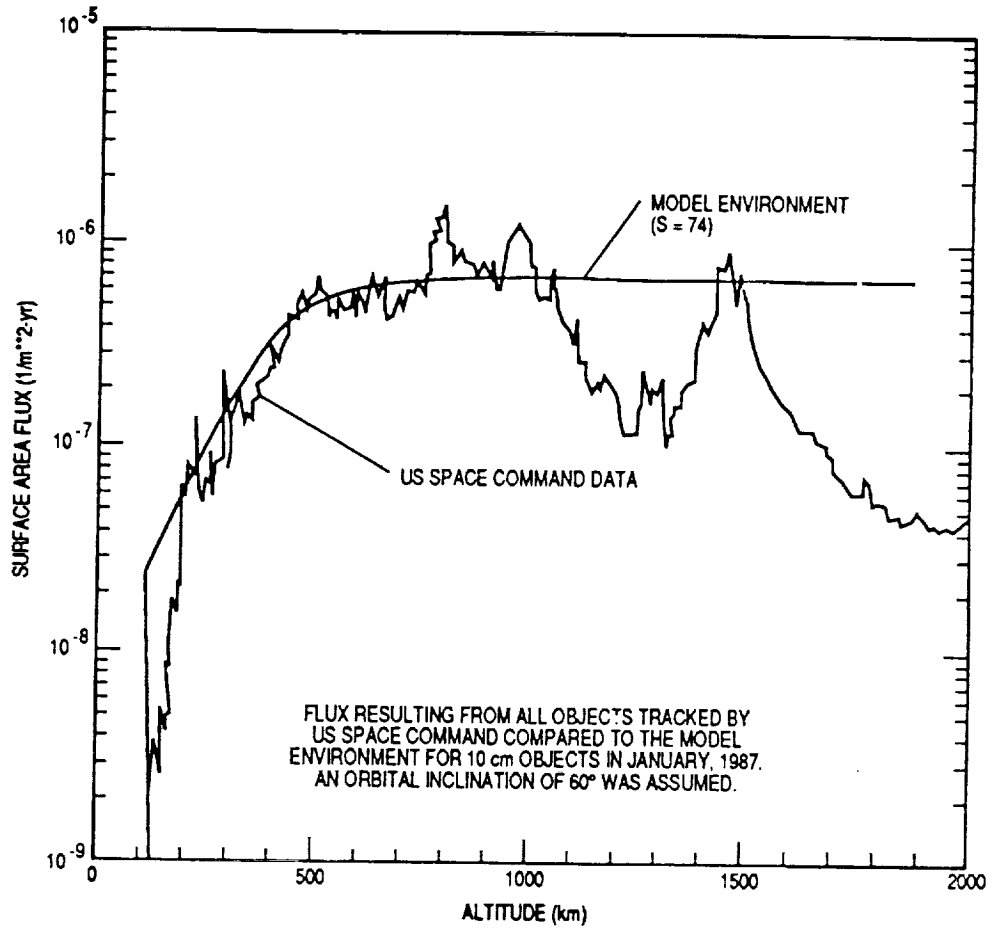


Figure 4-12. Distribution of Orbital Debris

profile due to a lack of measured data. The experiment module and the partially exposed gaseous hydrogen pressurization tanks will require micrometeoroid and debris shielding to meet mission reliability requirements. The spacecraft bus honeycomb panels will provide sufficient protection for components mounted within the bus.

The charged particle environment poses two types of threats to the spacecraft. First, the electron plasma at the orbital altitude can cause low voltage differential charging of the spacecraft, potentially leading to discharges which could damage hardware or cause spurious electrical signals. Ford Aerospace geosynchronous spacecraft have protection designed for the high differential voltages which can be generated by the energetic electrons found at that altitude. Grounding, electrical shielding, and materials selection methods used for protecting these vehicles apply to the COLD-SAT environment. The other threat from charged particles is radiation damage to the electronics. The total radiation dose as a function of the thickness of the aluminum shielding is shown in Figure 4-13. This curve represents an idealized spherical shielding geometry which yields a higher dosage rate than is achieved by the actual hardware. The effective shielding within the bus is equivalent to 2.5 mm of aluminum, providing a maximum one year dose rate of 12 krad - Silicon at the 1300 km altitude. The dose rate is within the usual capabilities that the bus electronics hardware will withstand.

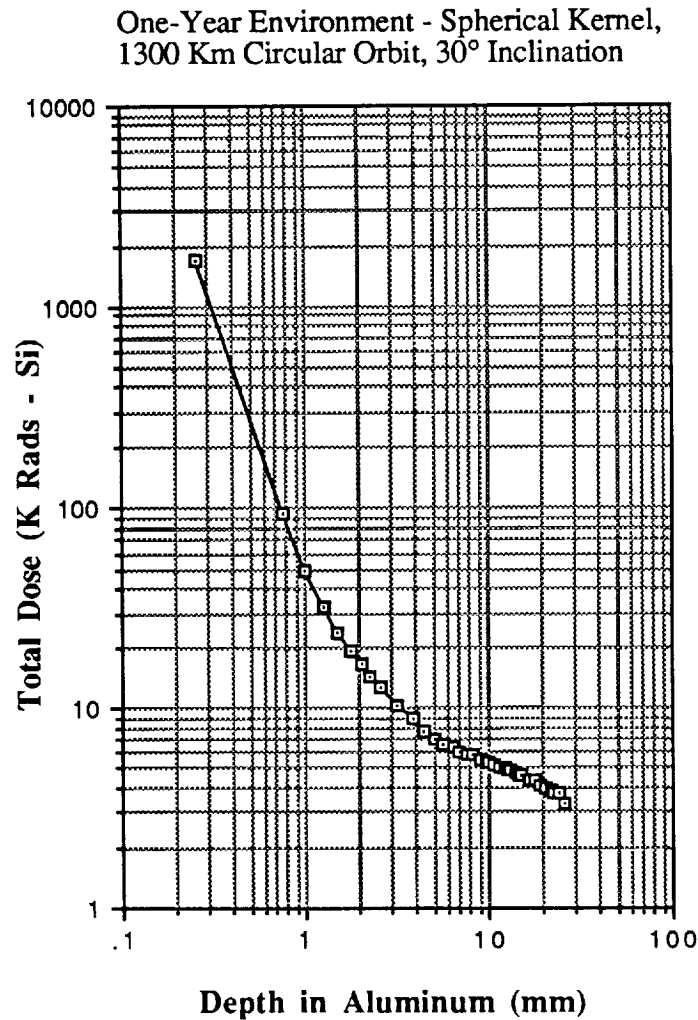
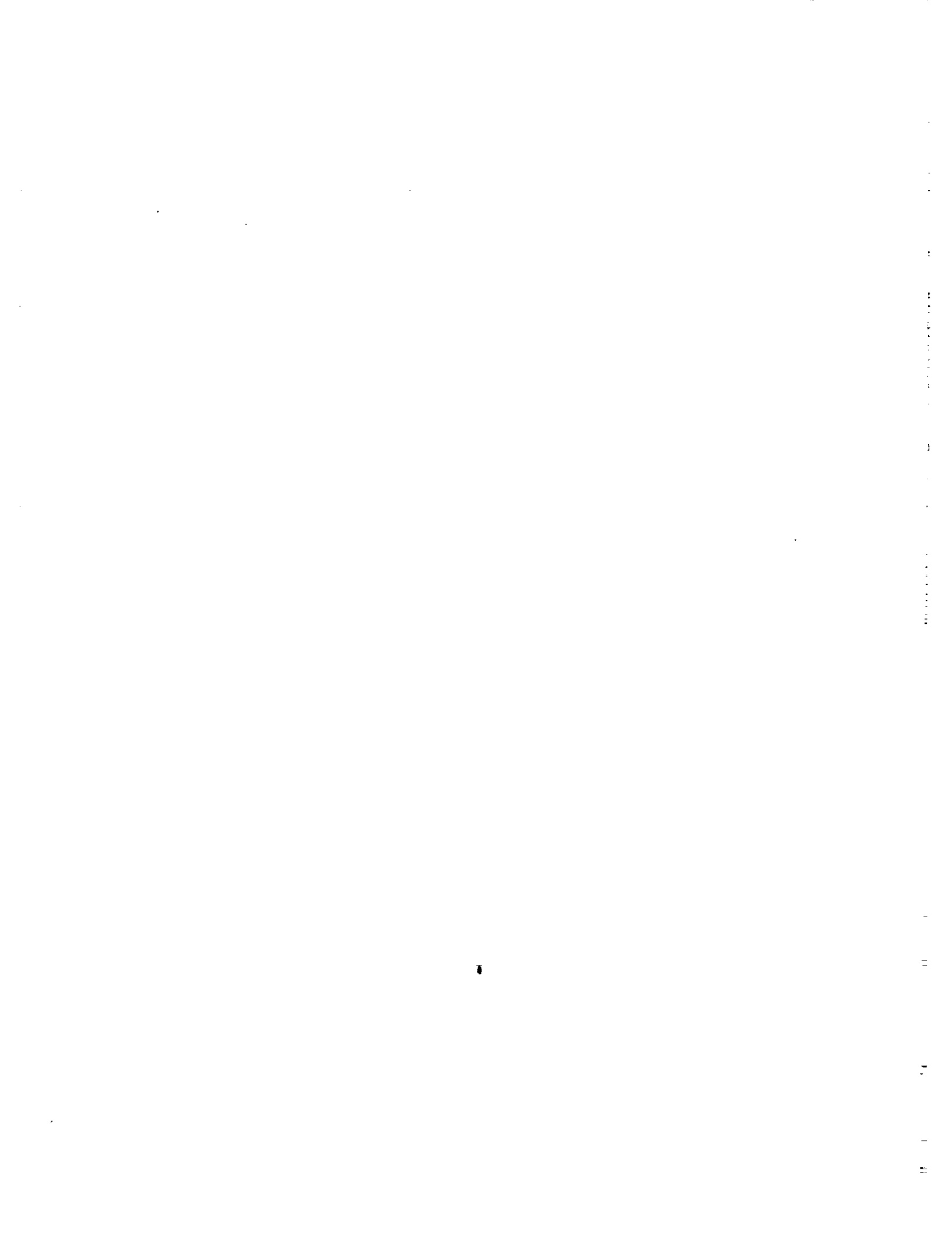


Figure 4-13. Annual Radiation Dose



5
EXPERIMENT MODULE DESIGN

This section presents the experiment subsystem design, fabrication, operation, tank details, fluid components, and hardware development status. The electrical power system, instrumentation, and control systems are also discussed.

5.1 EXPERIMENT SUBSYSTEM OVERVIEW

The experiment requirements developed during the program, which are discussed in Section 3.0, were used to determine the basic design of the experiment subsystem. In addition to the requirements which were derived from the experiment definition and design analysis activities, other guidelines were mutually agreed upon or stipulated by NASA during the course of the study. The more pertinent NASA guidelines which had effects on the design of the experiment subsystem are listed below.

- Limited the number of experiment tanks to three.
- Limited the maximum size of the tanks to:

Supply Tank 1	5.38 m ³ (190 ft ³)
Receiver Tank 2	1.27 m ³ (45 ft ³)
Receiver Tank 3	0.708 m ³ (25 ft ³)
- Allowed the use of He-purged multilayer insulation (MLI) for the supply tank in place of a vacuum-jacketed tank.
- Eliminated the use of tangential spray nozzles, vapor-cooled shield (VCS), mixer, and para-to-ortho converter with Tank 2.
- Required the inclusion of sufficient stored high pressure hydrogen gas to provide for at least 25 percent of the experiment pressurization requirements.
- Stipulated the inclusion of tests of an outflow subcooling heat exchanger.
- Stipulated a nominal heat leak for the receiver tanks of 1.58 watt/m² (0.5Btu/hr-ft²).
- Recommended that cryo-formed stainless steel not be used for high pressure gaseous hydrogen storage because of hydrogen embrittlement potential.

The experiment fluid system consists of three experiment tanks, including the supply tank which is launched wet, and two receiver tanks which are launched dry. The schematic of the fluid system is presented in Section 5.2. Transfer between the tanks is accomplished by supply tank pressurization with the assistance of a transfer pump which is capable of pumping fluid between any of the tanks in either direction. Pump-assisted flow is controlled by pump speed. As an alternative, purely pressurized transfer can be used, with the flowrate controlled by tank pressure and sets of orificed valves in the tank transfer lines.

The experiment tanks are normally pressurized by an autogenous cold vapor generation system which takes fluid from the supply tank, pumps it to higher pressure and vaporizes it in an electrically-heated helical evaporator. The autogenous pressurant is supplied at approximately 345 kPa to all of the tanks. High pressure gas, stored at 27.6 MPa, is provided as a back-up to the autogenous system and will provide enough pressurant to conduct 25 percent of the experiments using solely pressurized fluid transfers. This capability, in addition to the redundancy in the pump configuration, gives the system dual failure tolerance in its ability to transfer fluids between tanks. High pressure helium is also stored for use in several of the experiments. The high pressure H₂ bottles are made with an aluminum liner over-wrapped with graphite epoxy for stiffness and strength. A glass cloth scrim is used between the graphite/epoxy and the aluminum to prevent corrosion. These bottles are commercially available. For the helium high pressure bottle, a CRES liner is acceptable since hydrogen embrittlement is not a potential problem.

A summary of the design features of the experiment tanks is given in Table 5-1. Also shown are the experiments supported by each of the tanks. The supply tank is 1.73 m long and 2.42 m in diameter, and is an oblate spheroid. It is insulated with 76 mm of MLI which is purged with helium on the ground to prevent cryopumping. This approach is cheaper than a vacuum jacket, and is made possible by the hydrogen tanking and venting provisions of the Atlas I launch vehicle Centaur upper stage. The tank also has a vapor-cooled shield (VCS), a total communication liquid acquisition device (LAD), an internally-mounted wall thermodynamic vent system (TVS) heat exchanger, a compact TVS heat exchanger, and a mixer. The exterior of the tank is covered with flexible strip heater elements to provide uniform heating for the pressure control experiments. The tank is fabricated from 2219 aluminum alloy. The access openings for this tank and the two receiver tanks are welded in place around two upstanding rings at the perimeter of each opening. These openings can be removed by grinding off the weld and can be replaced by re-welding. The tank contains forward and aft fairings to support the MLI outside the envelope of the tank wall, in order to enclose the fluid components within the MLI. All external fluid lines are CRES and the transitions to the tank wall bulkhead fittings are made by diffusion-bonded blocks of aluminum-to-CRES material. This same all-welded approach is used for all the tanks and plumbing with the exception of some of the vent lines.

Tank 2 is cylindrical with a length of 1.8 m and a diameter of 1.02 m. The length facilitates testing of an axial spray nozzle which would simulate a radial nozzle in a larger tank fitted with radial spray nozzles. The tank is insulated with 38 mm of MLI. The tank contains a total communication LAD, an internally wall-mounted TVS heat exchanger, axial and radial spray nozzles, a LAD heater, and instrumentation. A heater is also provided on the exterior of the tank for evacuating and warming the tank. The tank contains plumbing which allows the TVS to vent the LAD for use during LAD filling tests. Like Tank 1, fairings are used to extend the insulated volume at both ends of the tank for housing valves, flowmeters, lines, and electrical equipment. The fairings on Tanks 1 and 2 make it easier and less costly to install the MLI, while reducing the amount of individual insulation which must be applied to fluid components.

Tank 3 is the smallest tank, and is a 1.07 m diameter sphere. It is relatively bare on the inside since it doesn't contain a LAD, and the TVS heat exchanger tubes are on the outside of the tank. It contains sets of axial, radial, and tangential spray nozzles for chilldown and no-vent filling. Unlike Tanks 1 and 2 this tank does not have a fairing. The MLI is mounted to the tank walls around the periphery of the tank, and the valves are housed in a separately-insulated module off to the side of the tank. This MLI installation will provide a comparison to that of Tanks 1 and 2, and also decreases the effective length of the tank, providing for its installation farther aft in the spacecraft.

A number of insulated valve modules are used in the fluid system and located within the experiment enclosure. Most of the valve functions in the system are satisfied by common latching solenoid valves, thus minimizing the number of valve types and eliminating the need for complex regulators and control valves.

The experiment tanks, plumbing, and electrical equipment are housed in an outer structure which also serves as a micrometeoroid and debris shield. It is a ring-stiffened, semi-monocoque, aluminum honeycomb structure with inner and outer aluminum skins, the inner being the thicker load-carrying skin. The experiment structure contains access openings, a removable forward cap, umbilical connectors, and a special baffled opening for the venting of the MLI and the interior of the enclosure during ascent. The configuration of this structure, its interfaces with the spacecraft and the experiment equipment, and the details of its construction are given in Section 5.8.

The experiment system instrumentation includes platinum resistance temperature sensors, strain gage-type pressure transducers, electrostatic micro-g accelerometers, and carbon resistor liquid/vapor detectors for the tanks. The major measurement problems include gauging the amount of fluid mass in the tanks and measuring hydrogen two-phase flowrate. Direct gauging of tank fluid mass will

Table 5-1. COLD-SAT Experiment Tank Configurations and Experiments Supported

TANK NO.	DESIGNATION	SIZE	LH2 CAPACITY	SHAPE	INSULATION & SHIELDS	MIXER	LAD	TVS	SPRAY NOZZLES	OTHER EQUIPMENT	TESTS SUPPORTED	
											CLASS I	CLASS II
1	"Supply"	D=2.42m L=1.73m V=5.38m ³ A= 15.1m ² Vol ratio=1.0	372 kg LH2 (365 kg @ 98% full)	Elliptical heads Tank L/D=0.71 Head a/b=1.38	MLI (76mm) VCS (one) Purge System Fairings	Turbine axial pump	4 rectang. screend channels	Internal wall mounted HX Compact HX (internal)	None	Outflow sub-cooling heat exchanger Wall mounted heaters	I-1 Pass Press Control I-2 Active Press Control I-4 No-Vent fill I-5 LAD Fill	II-1 Tanker Thermal Perf. II-4 Pressurization II-6 LAD Performance II-7 Line Chillover II-8 Outflow Subcooling II-11 Adv Instrument
2	"Depot" (Receiver)	D=1.02m L=1.83m Lcyl=1.09m V=1.27m ³ A=6.15m ² Vol ratio=.24 M/V=54kg/m ³	88 kg LH2 (84 kg @ 95%)	Cylindrical Tank L/D=1.8 Elliptical heads a/b=1.38	MLI (38mm) Fairings	None	4 rectang. screend channels	Internal wall mounted HX	Axial & Radial	Wall mounted heater	I-1 Pass Press Control I-3 Tank Chillover I-4 No-Vent Fill I-5 LAD Fill	II-4 Pressurization II-6 LAD Performance II-7 Line Chillover II-9 Vented Fill II-10 Fluid Dumping II-11 Adv Instrumentation
3	"Bare" (Receiver)	D=1.07m L=1.07m V=0.62m ³ A=3.58m ² Vol ratio=.12 M/V=47kg/m ³	43 kg LH2 (41 kg @ 95%)	Spherical	MLI (25mm) No fairings	None	None	External wall mounted HX	Axial, Radial, & Tangential	Wall mounted heaters Heaters on outflow lines for fluid dumping	I-1 Pass Press Control I-3 Tank Chillover I-4 No-Vent Fill	II-4 Pressurization II-5 Settled Outflow II-7 Line Chillover II-9 Vented Fill II-10 Liquid Dump II-11 Adv. Instrument.

NOTES: 1. All LH2 capacities are based on saturated liquid at 138 kPa with a density of 69.5 kg/m³.
 2. Tank 1 LH2 capacity is based on a free internal tank volume of 5.35 m³ (0.03 m³ internal equipment volume). Both 100% and 98% fill levels are given. The effective density including the effect of the bubbles on the launch pad (99.6% of saturated) has not been accounted for in the table and will cause a slight rise in the liquid level.

require settling and tank liquid/vapor detectors unless a zero-g mass gauge becomes available. A two-phase flowmeter is under development and was assumed to be available for use. However, the fluid system can be configured to use single-phase liquid and vapor flowmeters, along with detectors for sensing liquid in vapor flow and vapor in liquid flow.

Data acquisition and experiment control is performed by the spacecraft control electronics (SCE) that are part of the spacecraft bus, along with some additional signal conditioning, voltage regulation, and data concentrator units (DCUs). These electronics are derived from the Ford Aerospace Intelsat VII SCE with voltage regulation provided by existing, developed components. The experiment electronics have been placed within the spacecraft bus in order to take advantage of its stable thermal environment.

5.2 FLUID SYSTEM SCHEMATIC AND OPERATION

The baseline fluid system schematic (see Appendix B for component definitions) for COLD-SAT is shown in Figure 5-1. This system consists of three tanks with interconnecting plumbing designed for flexibility and reliability in conducting the COLD-SAT experiments at a reasonable cost. In general, the plumbing shown in the lower half of the schematic is used for fluid transfer between tanks and the plumbing in the top half is for tank pressure control. The tanks and plumbing are designed to a maximum operating pressure of 350 kPa with the exception of the autogenous pressurization system plumbing which is designed for 500 kPa and the pressurization gas supplies which operate up to 27.5 MPa.

5.2.1 Thermal Control

Each tank is surrounded by multi-layer insulation (MLI) to reduce heating in orbit. A vapor-cooled shield is included in the insulation for Tank 1 which routes hydrogen from the tank to intercept heat within the insulation and vent the warmer gas overboard. Most of the valving for Tanks 1 and 2 are located beneath their MLI enclosures while the components and transfer lines for Tank 3 are packaged in independent modules with their own MLI.

Electric resistance heaters are attached to each tank wall to augment tank evacuation and wall conditioning between tests. The heaters for Tank 1 are distributed over most of the tank surface and specially designed to produce uniform heating at several different flux levels for the pressure control experiment.

5.2.2 Tank Pressure Control

Tank pressure reduction (energy removal) is primarily achieved using a thermodynamic vent system (TVS) for each tank. Each tank has tubing attached to its wall which is used as a heat exchanger for passive TVS operation. This tubing is attached to the inner surface of Tanks 1 and 2 and to the exterior of Tank 3. Tank 1 also has a compact TVS system using a mixer to augment contact with a small heat exchanger. Each TVS is supplied through a Joule-Thomson orifice to expand and cool the flow. The TVS supplies for Tank 1 are redundant to enhance their reliability since conditioning of the fluid in this tank is central to the COLD-SAT experiments.

Each tank also has a direct vent system. Tank 1 uses this direct system to vent gas during tanking and ascent. The direct vent systems of Tanks 2 and 3 are used for tank evacuation experiments and, when the liquid has been settled can also be used for gas venting.

Redundant valves in these vent systems enhance their reliability. Typically, three shutoff valves are arranged such that a backup valve can be used for control if the primary valve fails in any

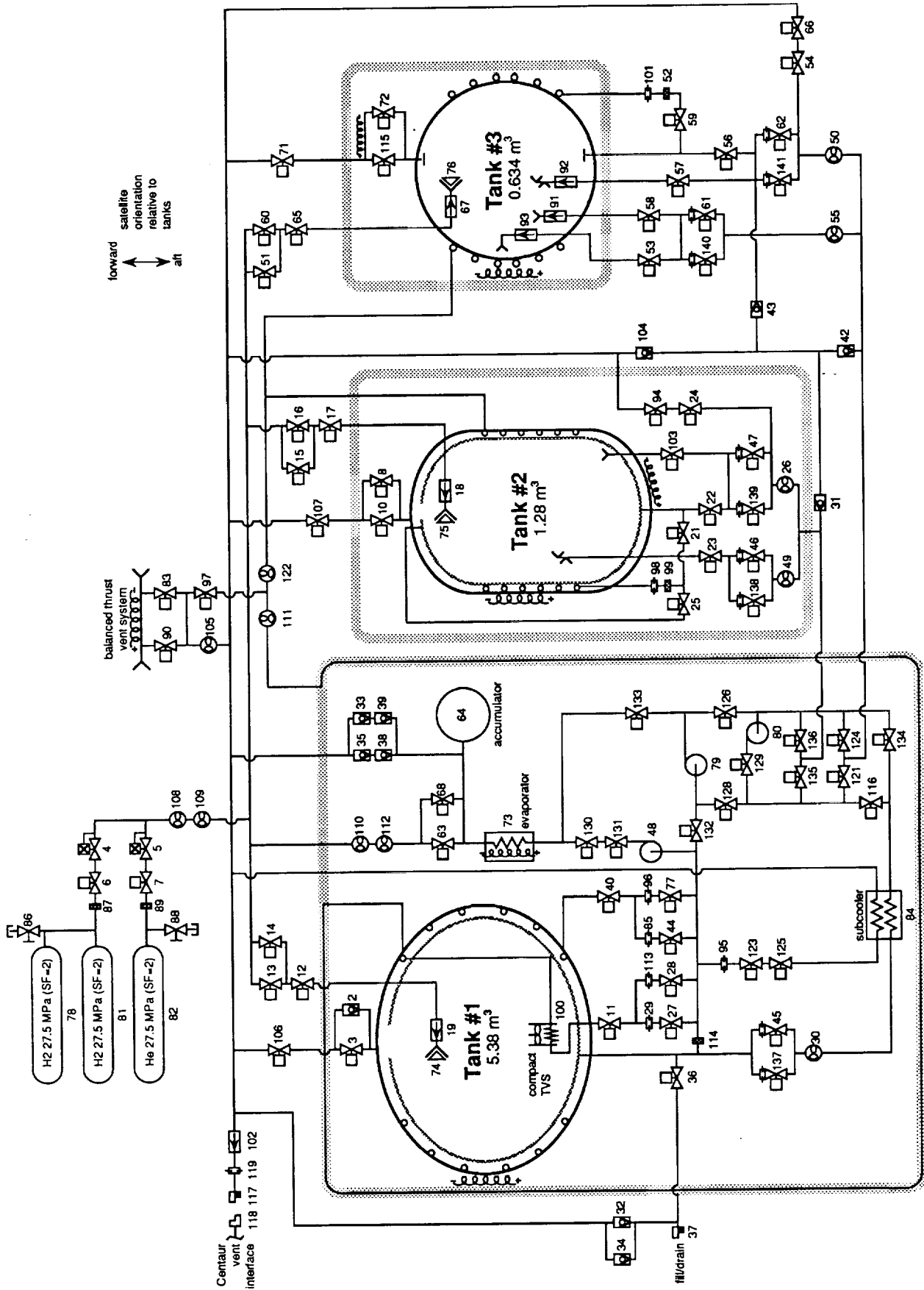


Figure 5-1. COLD-SAT Fluid System Schematic

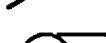
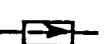
LEGEND	
	disconnect half
	self-sealing disconnect half
	filter
	flowmeter
	nozzle
	orifice
	diffuser
	pump
	baffle
	pressure regulator
	check valve
	relief valve
	shutoff valve
	shutoff valve with orifice
	manual valve
	multi-layer insulation
	vapor-cooled shield
	heater

Figure 5-1 (cont.). COLD-SAT Fluid System Schematic Legend

configuration (open, closed or partway). Since the backup valves are dormant (not actuated) unless the primary valve has failed, they are much less likely to fail in another position during normal operation. (e.g. Valve 107 in the direct vent system of Tank 2 can't realistically stick in the closed position since it is never closed during normal operations.)

In orbit, vent flow exits the system through a balanced-thrust vent system which directs equal amounts of flow in opposing directions to minimize its impact on attitude control for COLD-SAT. Shutoff valves near the exit control the vent line pressure to be 15-20 kPa to preclude freezing of hydrogen in the lines. An electric heater prevents freezing downstream of these valves. A heater is also provided on the Tank 3 direct vent valve module to prevent freezing during the tank dump experiment.

Tank pressurization is provided through a diffuser in each tank with flow controlled by redundant shutoff valves. The diffuser is located in the central region of each tank and will be designed to minimize heat and mass transfer between the ullage and liquid in the tank as pressurant is introduced. Check valves are located just upstream of each diffuser to avoid the heat leak which could otherwise develop through percolation of fluid in the line.

Most pressurization gas is supplied by an autogenous system which vaporizes liquid pumped from Tank 1. The evaporator uses electrical resistance heating controlled to a constant outlet temperature. Pump 48 nominally supplies the flow with Pump 79 providing backup capability. The generated hydrogen vapor flows through an accumulator which provides a relatively constant pressure to the pressurization valves. Redundant relief valves protect the system from overpressure.

Closer control of the pump and evaporator and/or a larger accumulator volume could eliminate the requirement for pressure regulators. Further evaluation of this trade is recommended.

An independent supply of gaseous hydrogen and helium is also available to pressurize the experiment tanks. This supply satisfies requirements for certain experiments and also acts as a backup to the autogenous system.

Flowmeters are included in the pressurization and vent lines to satisfy experiment requirements. Pressurization and TVS vent flowmeters are designed to measure gas flow while flowmeters for the direct tank vent should be able to measure two-phase flow.

5.2.3 Fluid Transfer

A centrifugal pump is normally used to transfer fluid between the tanks. Transfer lines from each tank are connected to the pump module which can, through valving, provide pumping between any two tanks in either direction. Pump 80 is normally used with Pump 79 providing backup capability for this operation. Transfer flowrate is controlled by varying pump speed. Alternately, fluid transfer can be accomplished by tank pressure control using the orificed shutoff valves in the transfer lines to provide incremental flow control. Flowmeters in the transfer lines are designed to measure two-phase flow to provide experiment data.

Tanks 1 and 2 each contain a liquid acquisition device (LAD) for low-g liquid acquisition. An electric resistance heater is attached to Tank 2 in the vicinity of the LAD outlet to satisfy the LAD performance experiment. Tank 3 has a baffled outlet to promote the acquisition of liquid during settled outflow.

All transfer flow in and out of Tank 1 is through its LAD with forced convection within the tank being provided by the mixer of the compact TVS. Tanks 2 and 3 have various nozzles which are used to inject flow into these tanks at different locations and orientations. Each set of nozzles is controlled independently by orificed shutoff valves. Both tanks have nozzles which are oriented

axially and radially; Tank 3 also has a set which spray tangential to the tank wall. Check valves are used on the nozzle supplies to Tank 3 to reduce heat leak (similar to the pressurization system).

The transfer lines are connected to the vent system through redundant shutoff valves (24, 94, 54 and 66) near Tanks 2 and 3. This allows the transfer lines to be chilled without chilling the intended receiver tank by flowing directly to the vent.

A subcooler is located in the transfer line from Tank 1. When desired, outflow cooling is provided by flowing some hydrogen through Joule-Thomson Orifice 95. This flow is vented overboard after absorbing heat from the flow being transferred between tanks.

Between fluid transfer operations, the liquid in the transfer lines is vented through the line chilldown vent (e.g. Valves 24 and 94) only as required to relieve excess pressure. Relief valves provide backup protection from overpressure of these transfer lines. The transfer line for Tank 1 is within the vapor-cooled shield and will remain open to the tank when not in use.

5.2.4 Tanking

The gaseous hydrogen and helium supply bottles will be charged through the manual shutoff valves prior to closeout of the surrounding payload fairing. These valves are then closed and the connections capped to provide redundant sealing.

Prior to launch, Tank 1 is loaded with liquid hydrogen through the Fill/Drain Disconnect (37). The tanking flow from the ground supply is controlled by ground system valves based on the pressure and liquid level in Tank 1. Hydrogen vapor generated during chilldown and tanking will be vented through the Vent Disconnect (117) which interfaces with the Centaur vent line to share the ground and ascent vent provisions of the Centaur hydrogen tank.

These interfaces and tanking operations are described more fully in Sections 8 and 9, respectively.

5.3 OVERALL MODULE ARRANGEMENT AND MASS PROPERTIES

Prior to determining the final configuration for our experiment system and tanks, nine alternative arrangements were studied. These arrangements were compared for their overall mass, c.g., volume utilization, and high pressure gas bottle location desirability. The layouts and discussion of these alternatives is presented in Appendix A.

The inboard profile view of the COLD-SAT baseline experiment configuration attached to the spacecraft bus and located within the Atlas I payload fairing is shown in Figure 5-2. The major components are one large LH₂ supply tank; two smaller LH₂ receiver tanks, two hydrogen gas storage bottles, one helium gas storage bottle, three valve modules, electronic packages, and an outer support structure equipped with micrometeoroid/debris shielding. The three LH₂ experiment tanks are equipped with multilayer insulation (MLI) and the LH₂ supply tank has an MLI purge enclosure. Other components include accelerometers, a pump control package, a destruct unit, and plumbing.

The spacecraft bus consists of a central cylinder which carries the thrust load, and rectangular panels surrounding this cylinder which provide a volume to house other bus components. The bus is described in detail in Section 7. Tank 2 of the experiment module is located inside the bus central cylinder and the three gas storage bottles and a pressure control module are attached to the outside of the central cylinder. Electronic packages for the experiment are located on the inboard side of the bus anti-Earth panel (-Z). The supply tank (Tank 1) and a second receiver tank (Tank 3) are located forward of the bus and are supported from an outer structure which attaches to the bus central cylinder. This outer structure has a parting line at the base of the forward conical section which

allows installation of Tank 1 and permits a separate buildup of the forward section during assembly. A valve module for Tank 3 and a fluid line junction module are located between Tanks 1 and 3 and are also attached to the outer structure. Tanks 1, 2 and 3 are supported with adjustable low conductive struts equipped with spherical bearing end fittings. The center lines of these struts are directed tangentially to the tank walls.

The bus central cylinder attaches to the Atlas I equipment module forward ring with an adapter equipped with a "V" band release system, tank springs, an electrical disconnect, and a hydrogen vent disconnect.

Figure 5-2 summarizes the mass and c.g. locations of each component including the bus and the propellants. Also included are the c.g. location and mass for the total spacecraft loaded with consumables. This is shown on a plot which also includes the Centaur equipment module-limited mass and c.g. curve, as well as a lower curve which provides a 20 percent mass margin compared to the maximum load-carrying capability. For a more precise curve and discussion of the values on this plot, see Section 4.4. The 20 percent margin was used as the design point for COLD-SAT at the direction of NASA.

A mass summary and c.g. location of each component for the experiment only is presented in Table 5-2. The 45.4 kg mass for electrical harnessing is for external runs between the tanks, the modules and the electronic boxes on the anti-Earth panel. Additional allowances for electrical wiring and sensors are included in the masses for the tanks and modules. For example, the four modules attached to the aft bulkhead on Tank 1 each have a wiring allowance plus an additional allowance for interconnecting these four modules. The 313.4 kg mass for Tank 1 also includes mass for instrumentation, wiring, and electrical pass-throughs. Detailed mass breakdowns for the tanks and the outer structure are given in Appendix A.

For our baseline configuration, design details were developed in order to insure that the assumptions which had been made during our trade comparisons were valid and that the more detailed design met the required envelope, mass and c.g. requirements. The overall length of the experiment system is related to how much room is required for the system components located under the MLI on Tanks 1, 2 and 3. Also, the size of the forward section of the support structure is influenced by how much room is required for components located outside of the tanks.

To obtain a realistic set of packaging volumes, detailed hardware type layouts were made for eleven sections of the system as summarized in Figure 5-3. In most cases, these sections were packaged into modules which were supported from the tank bulkheads, the outer structure, and/or from the bus central cylinder. These modules typically contain fluid components such as valves, flowmeters, heat exchangers, pumps and accumulators. These components are usually mounted on a waffle panel with interconnecting plumbing. For Tank 2, the components are bench-mounted to the fairings and the entire assembly slipped onto the tank.

Throughout the fluid system, off-the-shelf, standard fittings designed for orbit arc welding are used for the tubing connections. The material is 304L CRES (corrosion resistant steel) and tube wall gauges are 0.50 mm minimum. The length of the valves from the inlet side to the outlet side are a conservative 100 mm, and clearances between lines and components are such as to permit the use of orbit arc welding heads. The flow meters are located so that flow straightening sections of tubing can be used both upstream and downstream of the meters. The fluid component mounting techniques compensate for tolerances and dimensional changes. Also included with each module is a mass breakdown and a schematic.

Table 5-2. Experiment Module Mass Properties

SUBSYSTEM/ITEM	MASS (KG)	MOMENT ARM (CM) FROM EQUIPMENT MODULE RING	MOMENT (CM-KG)
PAYLOAD:			
OVERBOARD VENT SYSTEM	5.9	698.5	4127.5
TANK 3 VENT VALVES	5.0	668.0	3340.1
TANK 3 ASSEMBLY	36.0	599.4	21578.4
TANK 3 PLUMBING	3.6	533.4	1939.6
TANK 3 VALVE MODULE	38.6	533.4	20608.6
JUNCTION MODULE	29.0	520.7	15100.3
TANK 1 VENT SYSTEM	5.4	492.8	2661.1
OUTER SUPPORT STRUCTURE	284.6	455.4	129606.8
TANK 1 ASSEMBLY	313.4	391.2	122602.1
EXTERNAL PLUMBING	18.1	378.5	6850.9
UMBILICAL +F&D	8.8	345.4	3039.5
OVERALL ELECT HARNESS	45.4	332.7	15104.6
DESTRUCT UNIT	.9	312.4	284.0
TANK1 SYSTEM EQUIPMENT	90.7	312.4	28334.7
TANK 1 PUMP CONTROL UNIT	3.9	271.8	1050.1
TANK 2 VENT SYSTEM	5.4	262.9	1419.7
ACCELEROMETERS	7.5	251.5	1886.0
HELIUM GAS BOTTLE	27.2	226.1	6149.9
ELECTRONICS	33.6	215.9	7262.1
TANK 2 ASSEMBLY	83.5	165.1	13785.9
H2 GAS STORAGE BOTTLES	108.9	116.8	12719.5
PRESSURATION CONTROL MODULE	16.5	109.2	1807.1
TANK 2 SYSTEM EQUIPMENT	27.5	74.9	2064.0
DRY EXPERIMENT MODULE	1199.4	353.7	423364.7
DRY SPACECRAFT	1983.8	285.5	566285.4
LIQUID HYDROGEN	364.5	403.9	147221.6
HYDRAZINE PROPELLANT	530.5	124.5	66020.4
SPACECRAFT BOL	2878.8	270.8	779527.4
20% CONTINGENCY	575.8	270.8	155926.6
PAYLOAD ADAPTER AND CLAMP	72.0	38.1	2743.2
TOTAL PAYLOAD AND CONTINGENCY	3526.6	266.0	938197.2

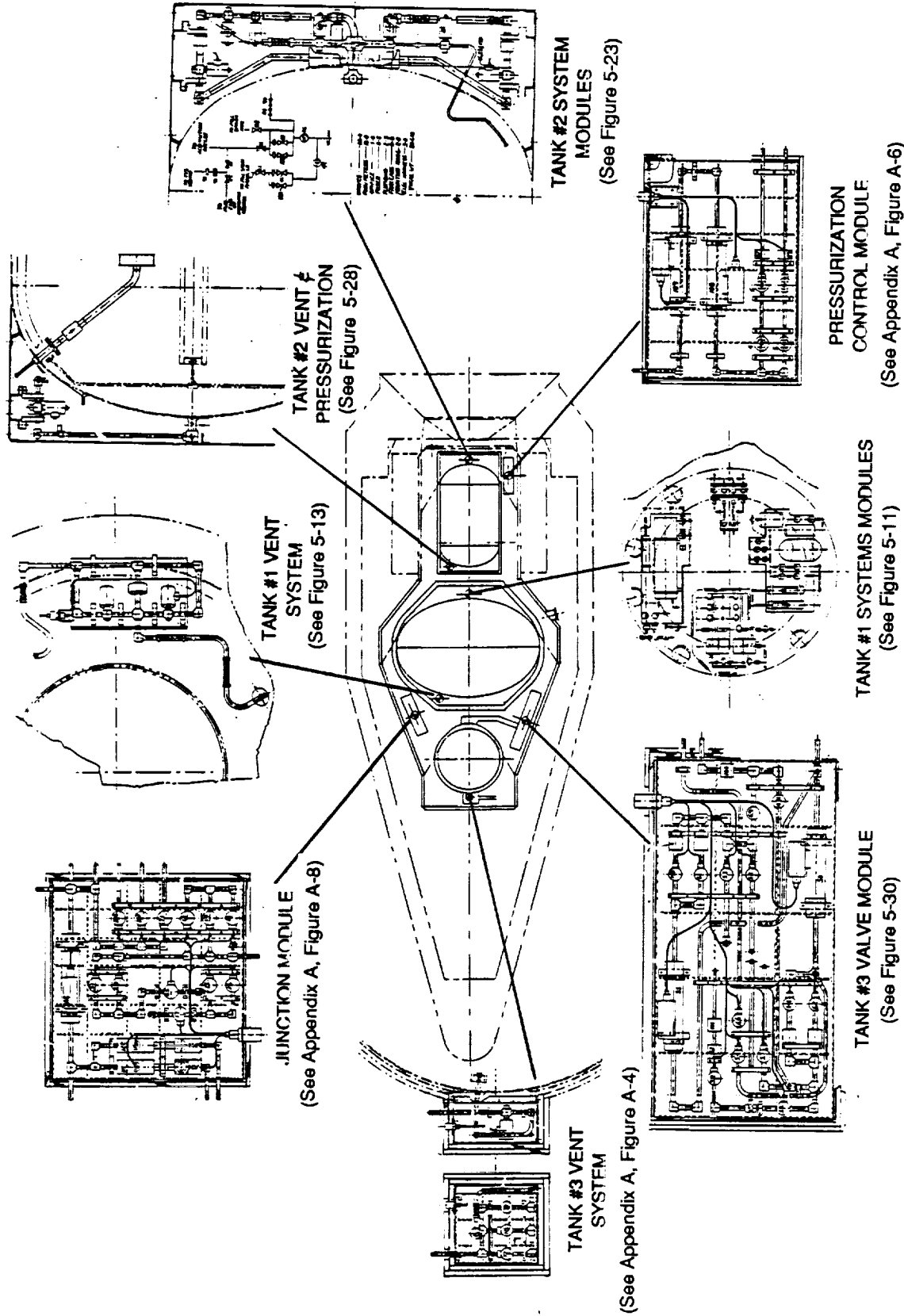


Figure 5-3. Systems Hardware Definitions

5.4 SUPPLY TANK (TANK 1)

5.4.1 Supply Tank General Arrangement and Internal Components

The basic shell for Tank 1 consists of two spun-formed elliptical bulkheads welded at the equator (Figure 5-4). The material is 2219 aluminum alloy. This shell is equipped with internal and external components. Internally, the tank contains wall-mounted TVS tubing, a four-channel liquid acquisition device (LAD), an instrumentation tree, a TVS/mixer assembly and a pressurization diffuser. Details for the TVS tubing and the LAD system are the same as those for Tank 2. The installation configuration for the TVS/mixer assembly is outlined in Figure 5-5, however, the sketch of the device is not to scale. More details on the size and design of the TVS/mixer are contained in Section 5.9.1.

Externally, a fairing is attached to the tank at each end. The profile of these fairings was determined by the system equipment installed on each bulkhead, and the requirement to keep the overall length of the tank as short as possible. Each fairing is equipped with a "T" ring near the base which in turn attaches to a series of fittings welded to the bulkheads. The ends are capped off with stiffened flat panels.

The tank is supported from the aft bulkhead with six fittings which are oriented so that the support strut center lines are directed tangentially to the bulkhead wall. These fittings are equipped with spherical bearings and are welded to the bulkhead just aft of the equator.

The exterior surface of the tank is equipped with heaters which provide a uniform heat flux. These heaters are applied in flat strips bonded to the tank wall and interconnect to form redundant circuits. Both bulkheads have several penetrations required for systems and for access to the tank interior. The primary penetration for the forward bulkhead is the access opening which is configured for welding. Entry is accomplished by cutting the weld off and then rewelding. The penetration for the pressurization diffuser is similar to that described in the pressurization and vent system installation for Tank 2 and is presented in Section 5.5. All external plumbing is corrosion-resistant steel (CRES). Therefore, fittings which penetrate the tank wall are machined from diffusion-bonded blocks of aluminum-to-CRES as outlined for Tank 2.

The primary penetrations through the aft bulkhead are for the electrical and LAD connections. The electrical pass-through fittings are configured for welding (see Tank 2) similar to that for the access opening. The LAD and TVS systems penetrate the tank wall with aluminum to CRES transition fittings.

5.4.2 Tank 1 Insulation Features

5.4.2.1 Tank 1 MLI Design. Referring to Figure 5-6, Tank 1 (including system equipment installed on both bulkheads) is completely enveloped with two blanket layers of MLI. The MLI blankets are applied over the fairings in 45 deg. gore sections running continuously along the side wall and in single flat sections at the ends. Each blanket is a pre-formed, trimmed, assembly incorporating hard points for attachments. A typical blanket construction is described for the MLI system of Tank 2, see Section 5.5.3.

The joints between the gore blankets are butt type and are held together with "velcro" fasteners and tape strips. Mitered joints are used at the end caps with the outboard face sheet of each gore blanket overlapping the outboard face sheet of each cap blanket.

The inboard blankets are attached at the forward and aft ends only to the fairings with epoxy/fiberglass pins. Polyphenylene Oxide (PPO) pins are an alternative with lower thermal

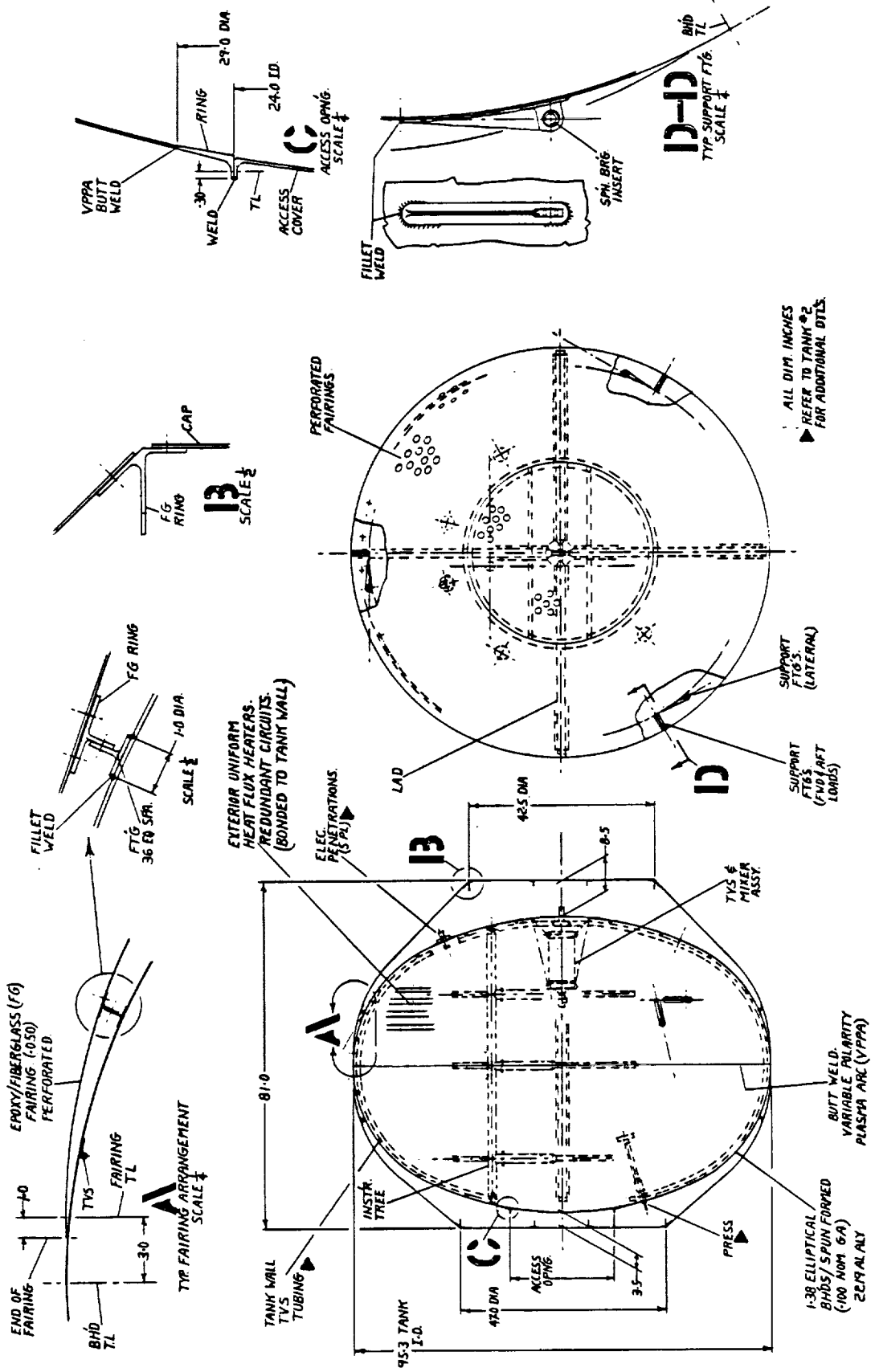


Figure 5-4. Tank 1 General Arrangement

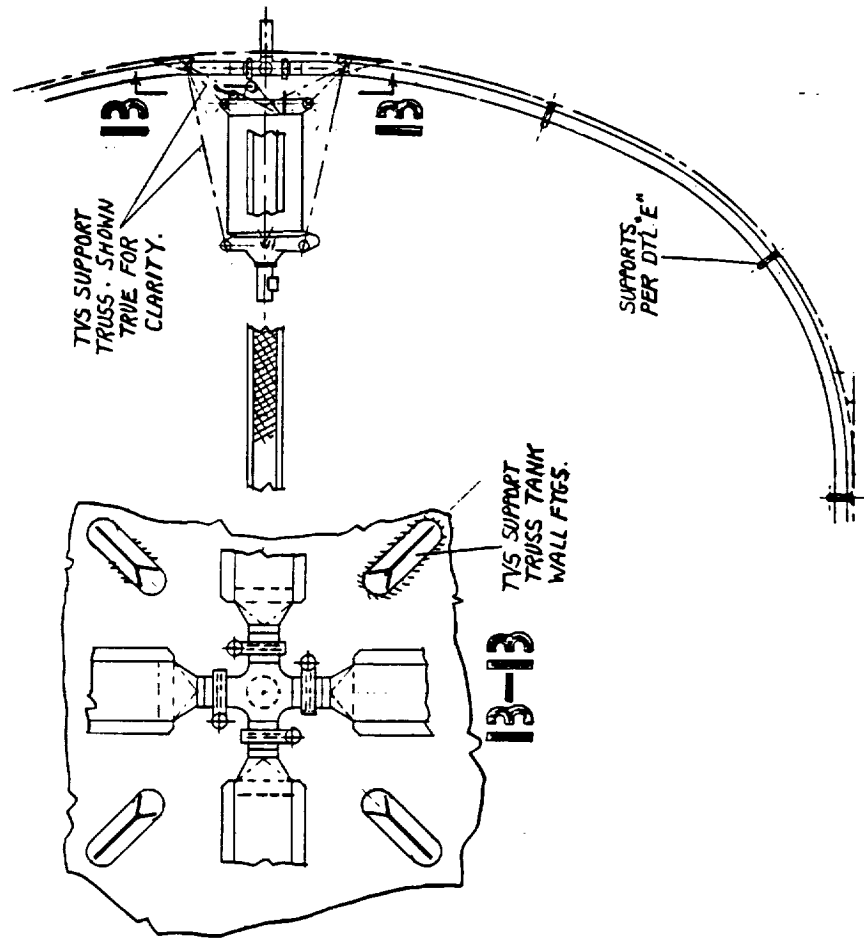


Figure 5-5. Tank 1 TVS/Mixer Assembly Installation

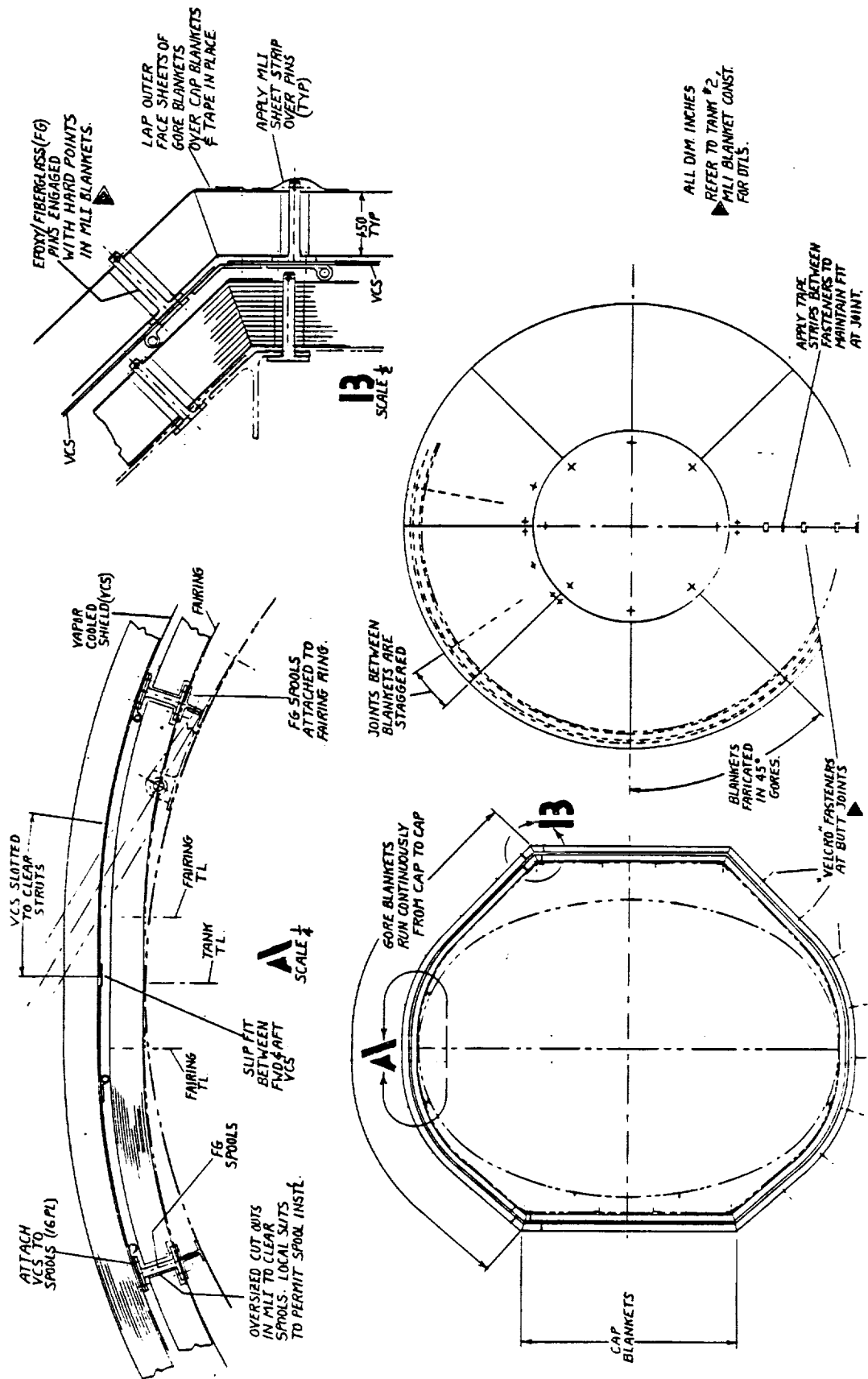


Figure 5-6. Tank 1 Insulation

conductivity. The outboard blankets are attached similarly to the vapor-cooled shield (VCS) which is located between the two blanket layers.

Figure 5-7 outlines some typical MLI penetrations for plumbing and tank support struts. The tank is supported with low-conductive struts which penetrate the MLI blankets. The staggered cutouts in the MLI blankets are located near the blanket edges so that a slit can be made from the cutout to the edge. This permits fitting the blanket to the side wall with the struts in place. After installation, these slits are taped over with Kapton pressure-sensitive tape.

After the first side wall MLI blanket is in place, the strut MLI wrap is installed and the first split close-out boot taped in place. The same procedures are followed for the second blanket layer.

Plumbing penetrations are located near the edge of the MLI blankets so that the blankets can be slit from the cutout to the edge, thus permitting a blanket fit with the tubes in place. The blanket cutouts and the MLI wrap on the tubes are configured for a staggered butt joint.

A typical low conductive strut consists of two CRES spools interconnected with a composite tube. MLI discs are placed inside the tube to intercept tunnel radiation and the end spools are equipped with fittings having left and right hand threads.

5.4.2.2 Tank 1 Vapor-cooled Shield. Tank 1 is completely enveloped with a VCS located between the inboard and the outboard MLI blanket layers (Figure 5-8). This VCS consists of two cap assemblies and two body assemblies. Each body assembly is attached to the fairing "T" rings with fiberglass spool-type fittings shown in the insulation drawing for Tank 1. The inboard surfaces of both caps and the two body sections are equipped with tube extrusions routed as shown in Figure 5-8 and attached by spot or seam welding. These tubes provide additional stiffness to each of the sections.

The aft body section has slot-type cut-outs to permit installation with the tank struts in place. Most of the slots can be covered over after the VCS is installed using thin aluminum sheet patches attached with blind fasteners or bonding.

At installation, a slip fit stove pipe joint exists between the two body sections which compensates for movement and tolerances. The tubing is interconnected between sections by stripping back the flanges at the ends, forming the ends, and welding. Local cut-outs in the VCS and the MLI permit these connections. The formed ends on the tubing are configured for flexibility so that the ends can be easily aligned for welding, and to permit movement between sections with minimum strain.

5.4.2.3 Tank 1 Ground Purge Enclosure. The ground purge for Tank 1 (Figure 5-9) is basically a bag type enclosure equipped with helium and nitrogen supply lines, a pressure relief valve, and two 152 mm diameter vent openings (one on each end). The enclosure is spaced approximately 12.7 mm from the MLI and consists of a rigid forward section and a flexible aft section. Both sections are equipped with rigid flat caps and are supported from the outer structure. This enclosure arrangement permits movement of Tank 1 without compressing the MLI. Purge gas injection and venting is accomplished at both ends of the enclosure.

The purge supply lines start at the umbilical disconnect and run to the forward and aft cap sections. The lines penetrate each cap section at two places, one for inboard injection and one for outboard injection. Referring to View "C-C", the inboard injection introduces conditioning (either nitrogen or helium) gas into the fairing cavity (under the MLI, between the tank and MLI) using a PPO tube which routes under the outboard MLI blanket before penetrating the VCS and the inboard MLI blanket. This arrangement minimizes heat leak and provides flexibility between the tank fairing and the enclosure cap. The MLI and the VCS are locally slotted to clear the tube and an extra-large hole is provided in the enclosure caps to allow for misalignment at assembly. The outboard injection, View "D-D", introduces or exhausts the purge gas through the enclosure cap wall. This outboard

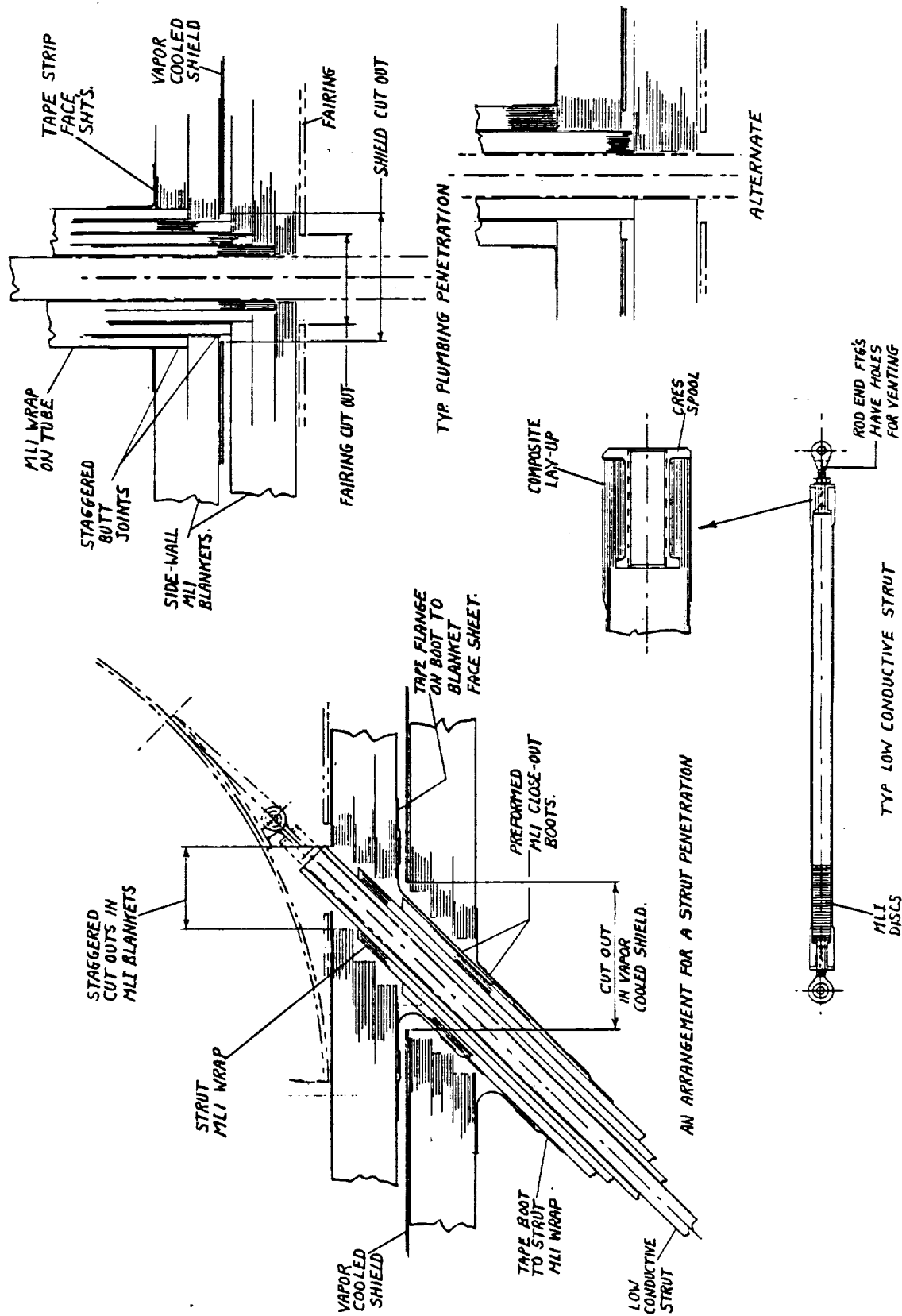


Figure 5-7. Tank 1 Insulation/Typical Penetrations

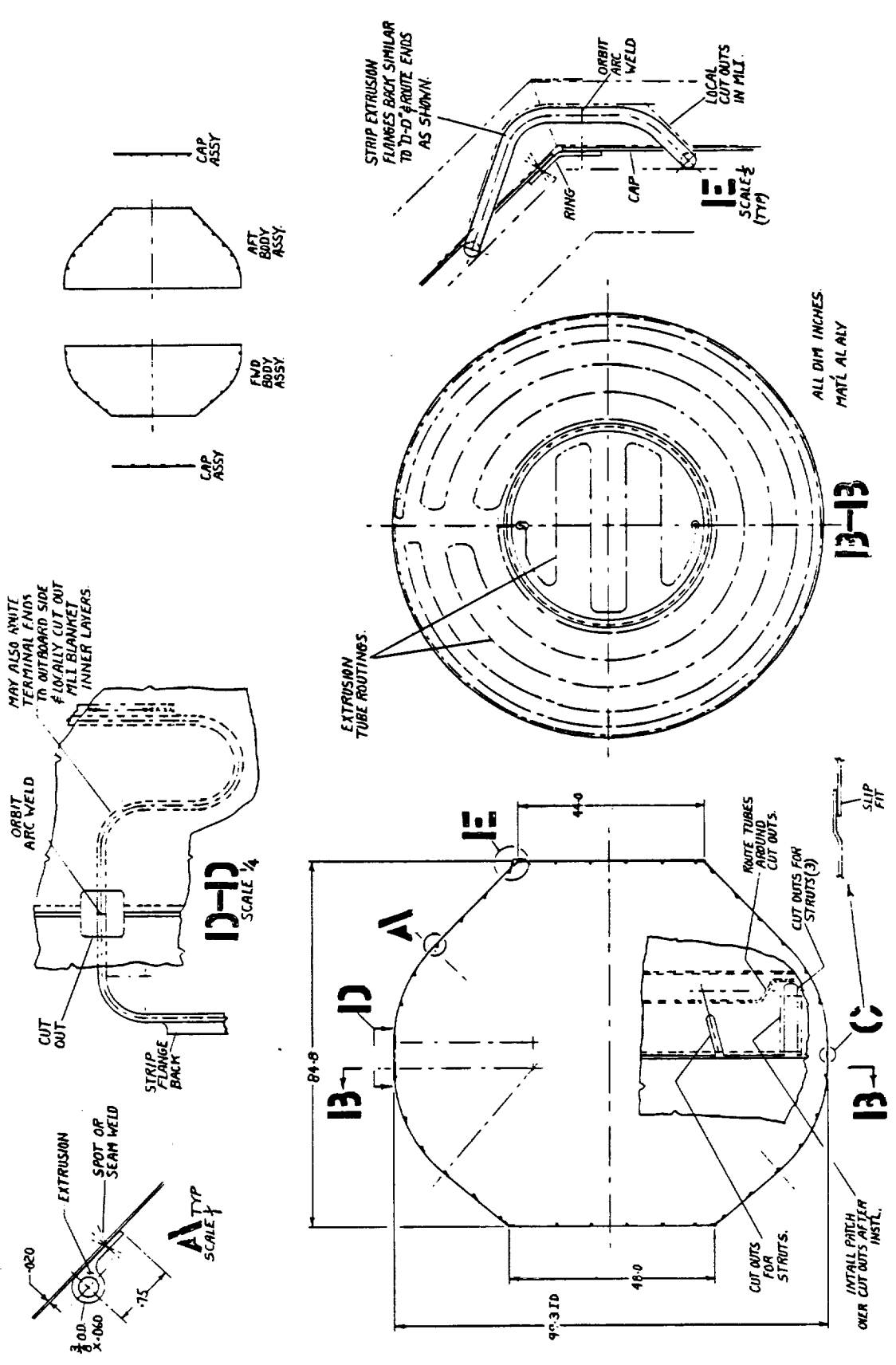


Figure 5-8. Tank 1 Vapor-Cooled Shield

injection is used to provide the helium gas make-up that leaks through the containment enclosure during ground hold and features a deflector plate to prevent local impingement on the MLI.

The purge system is connected to the ground supply/exhaust through an umbilical disconnect and a ground control valve module that regulates flow conditions. The sequence of events for the GN₂ and GHe ground purge conditioning is discussed in Section 9.4.3. During prelaunch conditioning, GN₂ is introduced on the outside of the containment blanket under the micrometeoroid/debris shield as well as through the payload fairing. To prevent cold gas under the shield from entering the spacecraft bus area, which contains temperature-sensitive electronics, a separation containment diaphragm is installed at the forward end of the bus central cylinder.

Each enclosure cap section has a relief valve which can be directly mounted on the cap or on the outer structure with a tube running from the cap to the valve. The latter method may be required if the relief valve envelope is larger than the clearance between Tanks 1 and 2. This relief valve, set at 3.45 kPa differential pressure, prevents over pressurization of the purge bag. Normally the pressure in the purge bag will be held at 2.07 kPa differential.

Referring to Views "A-A" and "E-E" on Figure 5-9, both caps are equipped with a valve which provides a 152 mm diameter opening when in the open position. The valve is a visor type, driven by a torsional spring actuator and released by a pyrotechnic pin puller with dual squibs for redundancy. The fiberglass honeycomb visor is sandwiched between retainer beams attached to the cap stiffeners and the cap wall and is equipped with a soft Teflon or KEL-F seal. All surfaces in contact with the visor and seal are Teflon coated.

The side wall of the forward section is an epoxy/fiberglass lay-up with the forward end bonded to the cap section as shown in Figure 5-9, View "J-J". The aft end is bonded to a continuous ring as indicated in Detail "F". Both the side wall and the cap section are lined with 25.4 mm of MLI. Referring to Figure 5-9, Detail "B", the side wall is stiffened by two "Z" shaped rings bonded to the outboard surface. The total rigid forward assembly is supported from the outer structure with struts having adjustable lengths and ends equipped with spherical bearings.

The aft soft section of the enclosure is a thin 0.051 mm thick scrim-reinforced Kapton wall (double aluminized) with the aft end bonded to the rigid cap section and the forward end bonded to a three piece ring (see Details "F" and View "J-J" on Figure 5-10). The wall has cut-outs and slits to permit installation over the tank struts. A typical strut penetration is shown in View "H-H" and Detail "G". The cap section is supported from the outside structure with adjustable struts and the three piece ring is bolted to the continuous ring on the forward rigid section. Techniques for sealing at the rings and cut-outs are shown in Figure 5-10.

Tank assembly is done in the vertical position by three rods screwed into fittings on the forward bulkhead. The flat MLI blankets on the forward fairing are locally deflected around these rods, therefore three hand holes will be required through the enclosure forward cap to inspect the MLI when the rods are removed. These holes are sealed off with plates after tank assembly installation. During tank assembly, the support rods run through these hand holes and the forward rigid section is held above the tank. After the tank assembly is completed, the rigid section of the enclosure is lowered into position and locked into place on the rods. The aft flexible section is then positioned, bolted to the single piece flange on the forward section and sealed off as shown in Figure 5-10. The entire assembly (tank and purge enclosure) with struts attached is lowered into the structure and attached. Holes in the structure permit access to the strut attachments for the aft purge enclosure cap.

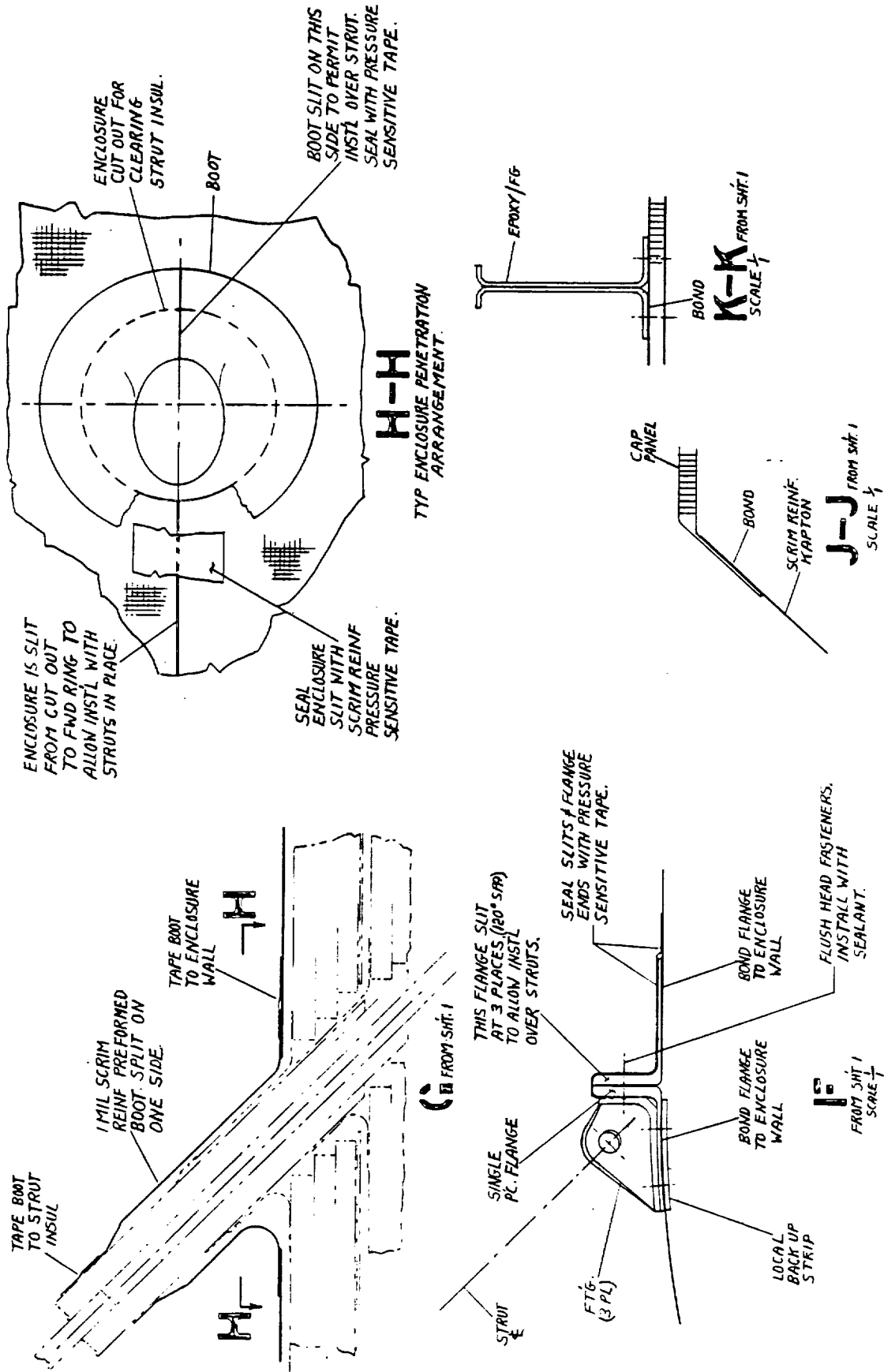


Figure 5-10. Tank 1 Ground Purge Enclosure

ORIGINAL PAGE IS OF POOR QUALITY

5.4.3 Tank 1 Aft Bulkhead Equipment Installation

The corresponding system schematic locates numerous valves, pumps, heat exchanger, evaporator, accumulator and flow meters inside the Tank 1 insulation. To minimize fairing size and the quantity of attachment fittings, the circuitry was divided into four sections and packaged into modules.

The four modules are located on the aft bulkhead of Tank 1 as shown in Figure 5-11, and attached to fittings which are welded to the bulkhead. The center area of the bulkhead is kept as clear as practical because this area will be needed for activities such as plumbing between modules, plumbing to the tank bulkhead penetration fittings, and electrical harnessing. The electrical penetration fittings for the tank instrumentation are located outboard of the modules, which provides a clear circular path for harnessing.

5.4.4 Tank 1 Valve Module on Aft Bulkhead

The system circuitry for Tank 1 has a cluster of valves and orifices which serve the internal TVS/mixer assembly, the tank wall heat exchanger tubing, the pump module, the heat exchanger module, and the evaporator module. These valves and orifices are packaged together as shown in Figure 5-12 and mounted on a waffle panel, which in turn, is supported from the tank bulkhead. Similar to the other modules, the valves and orifices are interplumbed using standard fittings and the orbit arc welding process. Fairleads are used to clamp the welded assembly to the waffle panel.

5.4.5 Tank 1 Vent System on Foreward Bulkhead

The vent system consists of a valve module attached to the tank forward bulkhead and plumbed to a tank wall penetration fitting and to an overboard vent line (Figure 5-13). The valve module which is shown consists of one shut off valve, one rupture disk and a relief valve mounted on a waffle panel (Figure 5-14). A fluid system configuration change was made late in the program which deleted the rupture disk, and this is not reflected in the diagram.

Referring to Figure 5-13, the vent fitting which penetrates the tank wall is machined from a CRES/aluminum diffusion-bonded block. This fitting is located outboard of the tank access opening. The inlet side of the vent module is connected to the tank wall penetration fitting with a 304L CRES line equipped with two short flex hose sections for absorbing tolerances and dimensional changes. The orbit arc-welding process is used for the end connections. The outlet side of the vent module is equipped with a CRES hose which routes to a coupling located on the fairing ring. This coupling transitions from CRES to Teflon through a mechanical connection which is commonly used on commercially-available, high-pressure Teflon flex hoses. The pressure in this vent line will always be well below the design pressure of the Teflon tubing. The Teflon tube section (no braid, to minimize the conduction heat leak) is routed through the MLI and to the overboard vent. The electrical wiring is converted to a ribbon configuration at the one end and penetrates the first MLI blanket. This ribbon is then attached to the VCS and is routed aft where it penetrates the outer MLI blanket at the purge enclosure ring flanges. Figure 5-13 shows that the forward fairing cap can be located 88 mm from the tank bulkhead which allows room for stiffeners on the fairing cap section.

5.4.6 Tank 1 Heat Exchanger Module

The Tank 1 heat exchanger module consists of one subcooler, one flow meter, four valves, one orifice, and one filter mounted on a waffle panel (Figure 5-15). This assembly is mounted off the aft bulkhead of Tank 1 and is located under the MLI. The components are interconnected with 304L

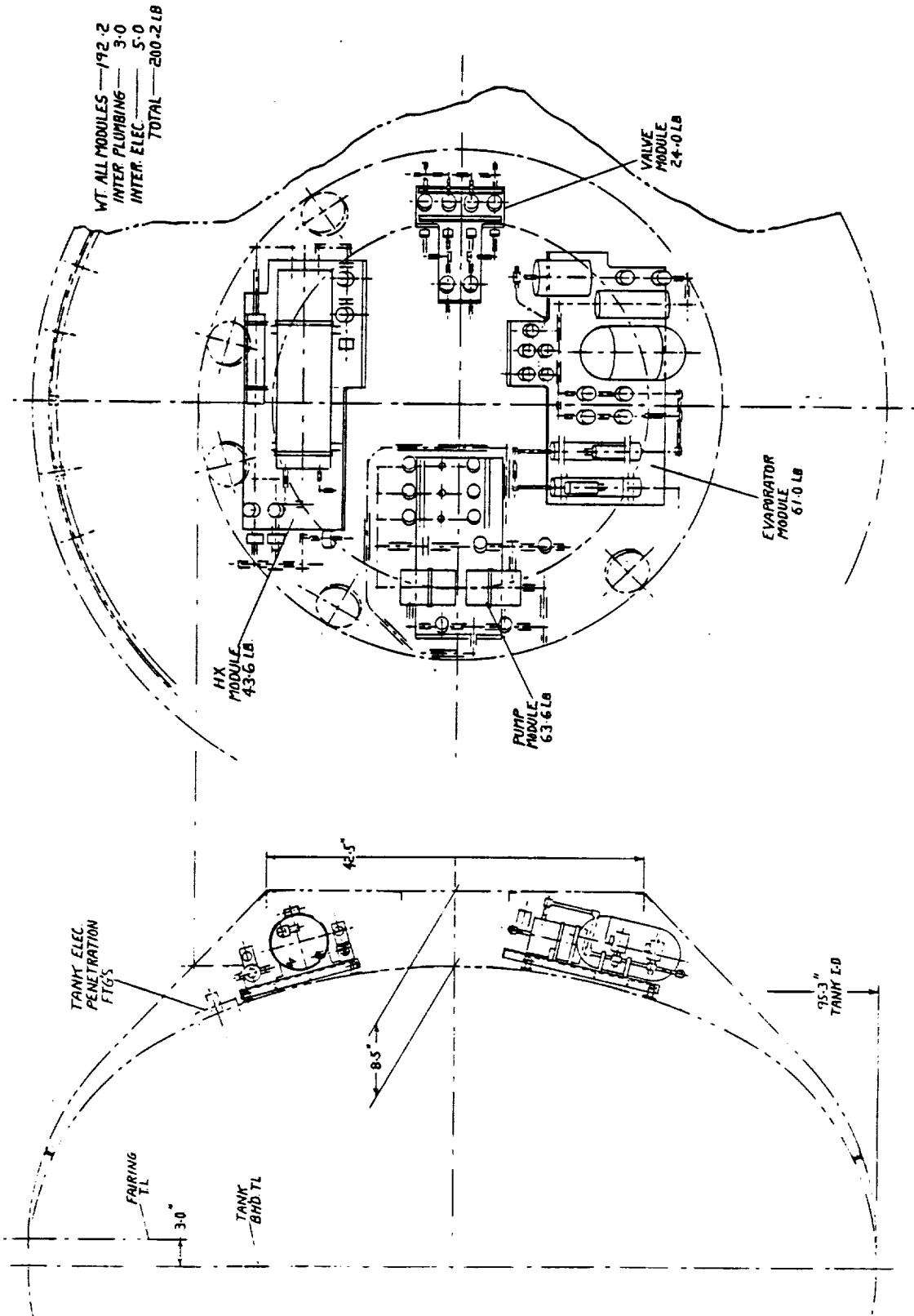
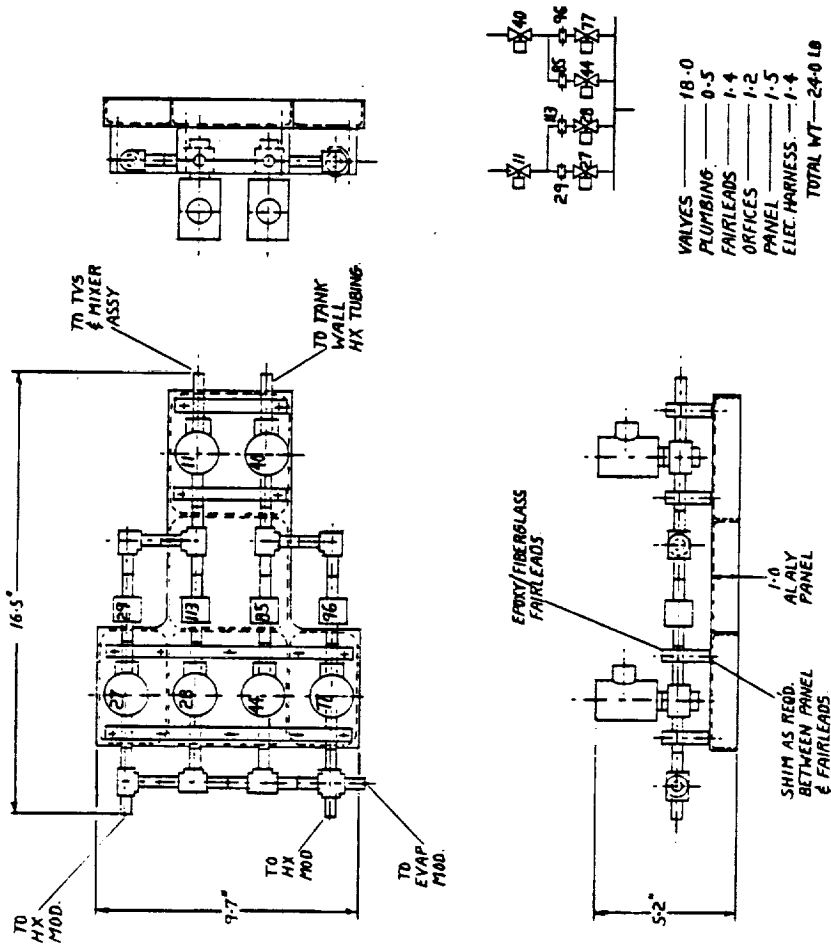


Figure 5-11. Tank 1 Aft Bulkhead Equipment Installation



PLUMBING 304L CRES/STD FTGS.
ALL CONNECTIONS ORBIT ARC WELDED.

Figure 5-12. Tank 1 Valve Module/Aft Bulkhead

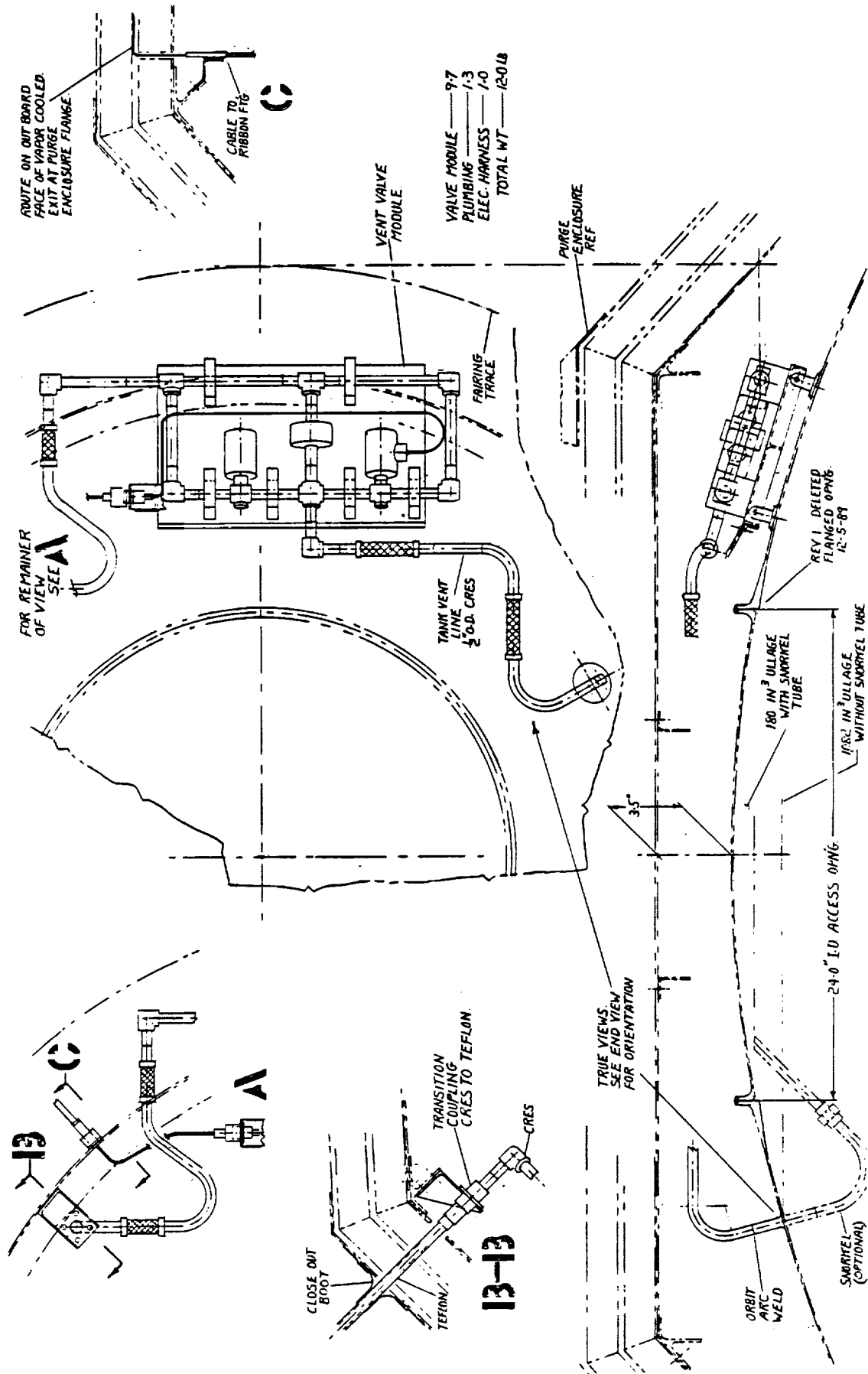
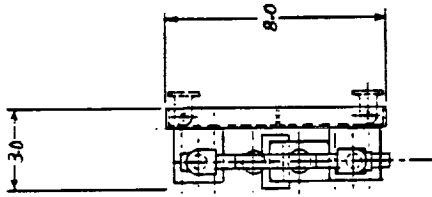
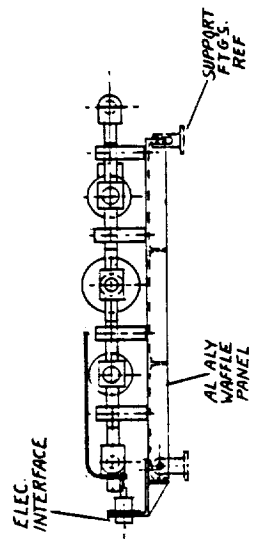
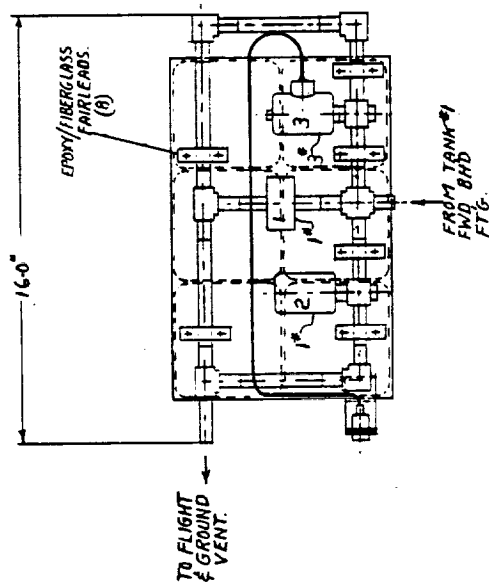


Figure 5-13. Tank 1 Vent System/Forward Bulkhead



NOTE:
ALL JOINTS ORBIT ARC WELDED
USING STD. FTGS.
1/2" LINE SIZE / .020 WALL
304 L CRES



VALVES & RIPTURE DISK	6.0
FRAME	2.0
PLUMBING	5
WIRING	4
MOUNTING HONEY/FAIRLEADS, BUS, ETC.	8
TOTAL	9.7 LB

Figure 5-14. Tank 1 Vent Valve Module

CRES plumbing using standard fittings designed for orbit arc-welding. After the plumbing is completed and checked out, the assembly (plumbing and components) is mounted on a waffle panel using fiberglass fairleads, saddles and CRES bands. Shimming between the fairleads/saddles and the panel is performed when required to compensate for tolerances and to prevent the introduction of preloading when the fairleads and saddles are bolted in place. The end result of this mounting technique is that the components are clamped in place rather than hard-mounted. This clamping allows slippage at the saddles and fairleads during dimensional changes. Figure 5-15 also includes a system schematic and a weight breakdown.

5.5 TANK 2

5.5.1 Tank 2 General Arrangement

The basic shell for Tank 2 is a 1.02 m diameter cylinder (rolled sheet with a single weld) equipped with a single piece, spun-formed elliptical bulkhead at each end (Figure 5-16). The material is 2219 aluminum alloy. This shell is equipped with internal and external accessories and has several penetrations through the walls.

The internal accessories include tank wall heat exchanger tubing, a four channel liquid acquisition device (LAD), a combination fill spray manifold/instrumentation tree, a pressurant inlet diffuser and a single spray nozzle.

The tank external accessories include an insulation fairing at each end, support fittings and tank wall heaters. The length of the fairings were determined by system hardware layouts and the requirement to minimize overall length. Each fairing is equipped with an angle ring which in turn attaches to a series of fittings welded to the bulkhead. The ends are capped off with stiffened flat panels.

The tank is supported with three fittings located on the aft bulkhead and three located at the forward end of the cylindrical section. The fittings are oriented so that the support strut center lines are directed tangentially to the tank walls. The fittings are equipped with spherical bearings and are fillet welded to the walls.

The exterior surface of the tank walls are equipped with heaters for drying and warming the tank. These heaters are applied in flat strips bonded to the tank wall. Both bulkheads have numerous penetrations for systems and access to the tank interior. The primary penetration for the forward bulkhead is the access opening which is welded in place. For removal of the cover from the access opening and re-entry into the tank, the weld is ground off the upstanding legs. Replacement of the cover is accomplished by rewelding the legs. All external plumbing is corrosion-resistant steel (CRES). Therefore, plumbing penetrations through the walls (the pressurization line for example) are made by machining fittings from diffusion-bonded blocks of 2219 alloy and 304L CRES.

5.5.2 Tank 2 Internal Components

5.5.2.1 Tank 2 Spray Fill and Instrumentation Tree. One of the filling and chilldown techniques for Tank 2 is to radially spray LH₂ at three different stations along the length of the tank. To accomplish this, three clusters of three equally spaced spray nozzles (Figure 5-17) are mounted on a feed tube which connects to a penetration fitting through the aft bulkhead. The feed tube is CRES and the diameter is oversized due to vibration considerations. To compensate for dimensional changes while permitting access to the tank, the forward end of the feed tube has a blind fitting which slides into a tank access cover fitting (Detail C). The aft end has a universal type flex joint equipped with a flange for "V" band connection to the tank wall penetration fitting.

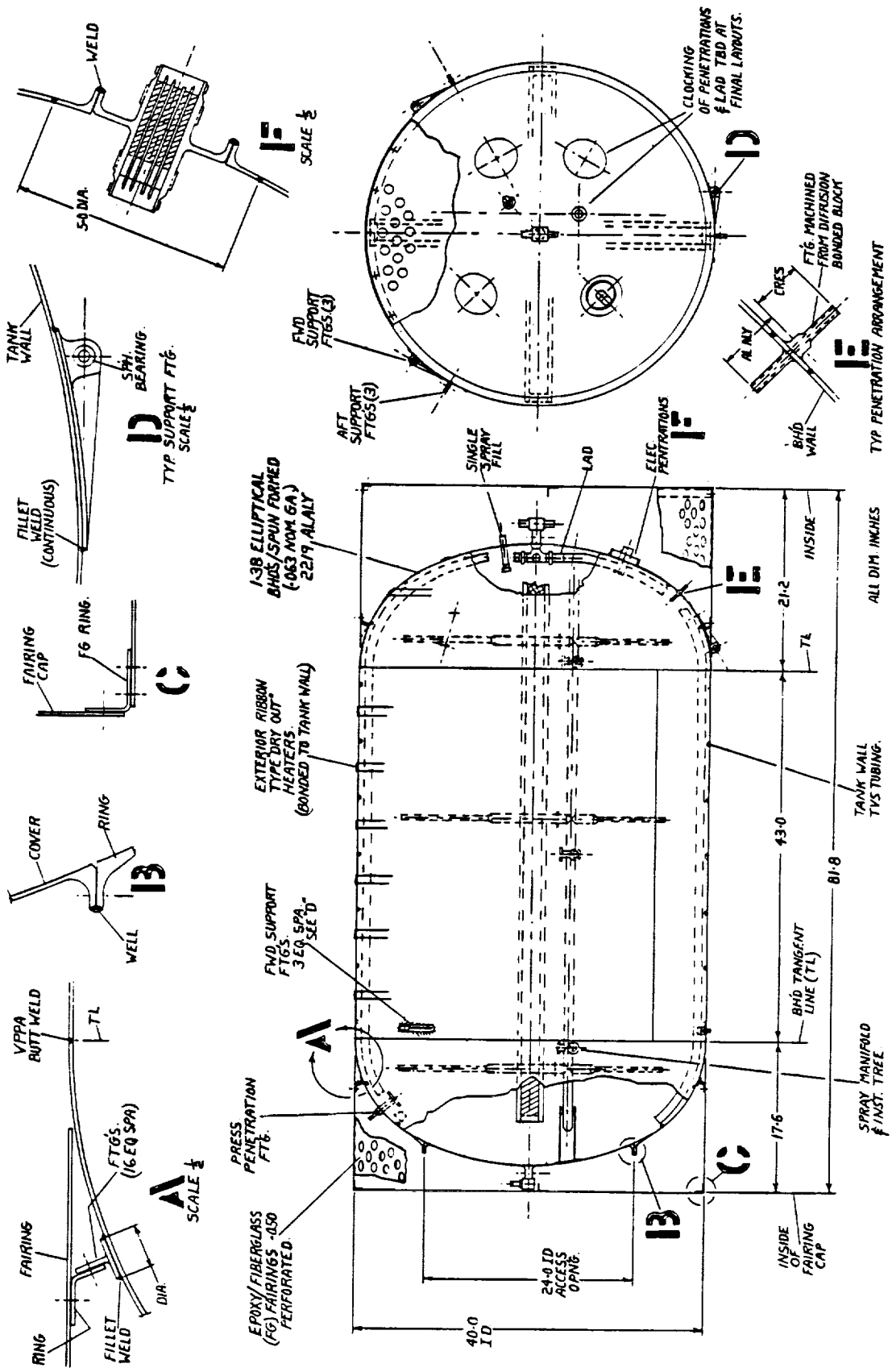


Figure 5-16. Tank 2 General Arrangement

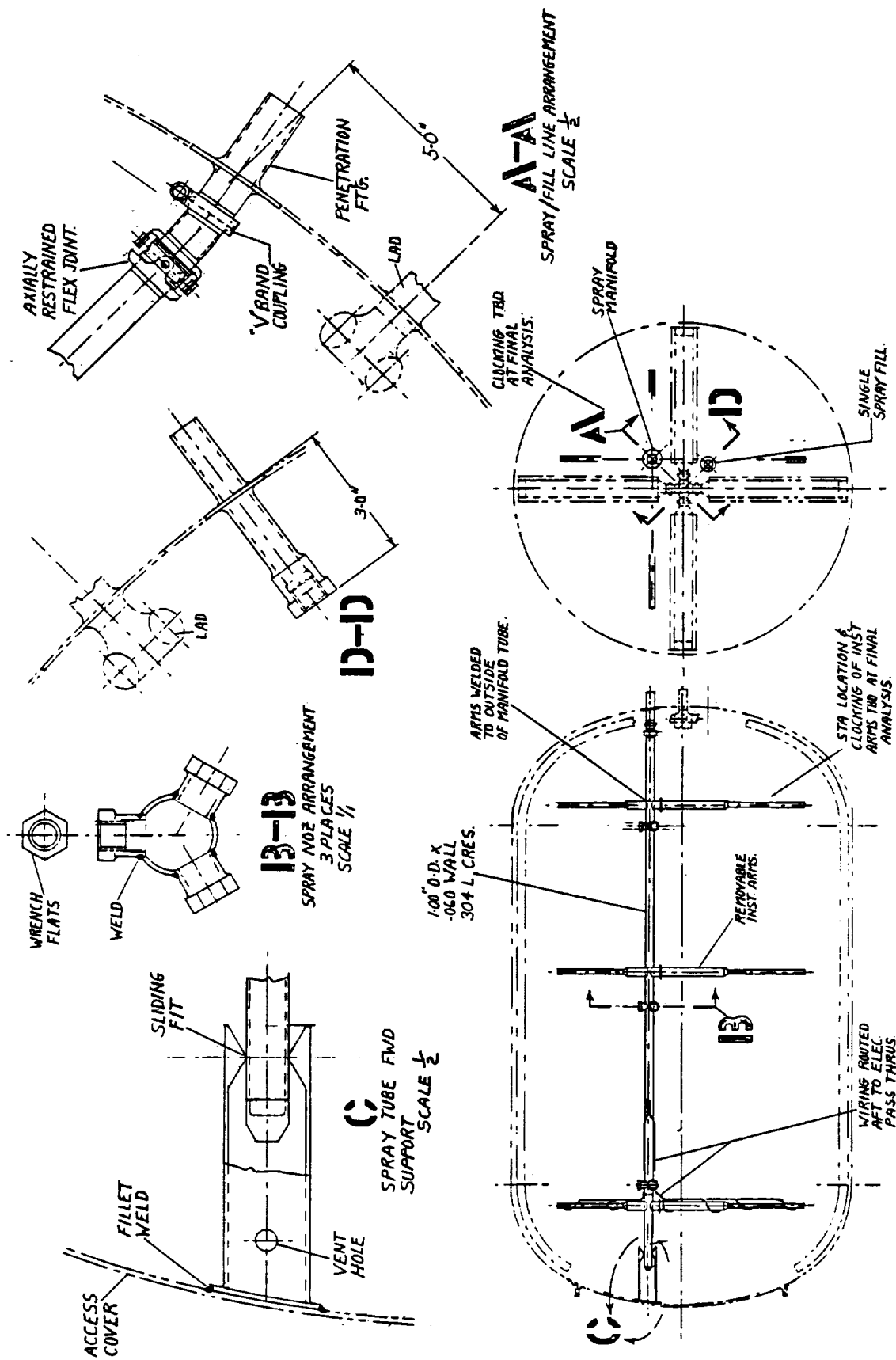


Figure 5-17. Tank 2 Spray Fill and Instrumentation Tree

This feed tube also serves as an instrumentation tree, therefore, radial arms are attached for supporting instrumentation and wiring. Some of these arms are removable to permit installation through the tank access opening. The quantity, length, clocking, and station location of these arms will be determined in the final design phase.

5.5.2.2 Tank 2 TVS Wall Heat Exchanger. TVS tubing is required over the entire tank including the end bulkheads. The tubing is located inside the tank with the ends connected to two tank wall penetration fittings (Figure 5-18).

The TVS tube is an aluminum extrusion having a single flat fin located tangentially on the tube. This tube extrusion is spot welded to the tank wall.

The tube extrusions are welded to each bulkhead and to the cylindrical section prior to tank assembly. The fins are stripped back at the ends and the tube portion formed to mate with the tank wall penetration fittings and with the ends between the cylindrical section and the bulkheads. The orbit arc-welding process is used for joining.

The tube routing shown is not necessarily the final routing since more analysis must be performed on TVS operation and performance. However, the configuration shown is representative and would generally be applicable to other routings such as a double pass arrangement with both penetration fittings in the aft bulkhead.

5.5.2.3 Tank 2 Liquid Acquisition Device. The liquid acquisition device is described in Figures 5-19 and 5-20. This device consists of four channels that follow the tank wall and converge at a penetration fitting through the aft bulkhead. The channels are fabricated from 304L CRES and are supported from the tank wall with low conductive links.

A typical channel cross section is shown in view "C-C." Three walls of the channel are formed from sheet stock with flanges on two legs for attaching the fine mesh screen. The screen is continuously seam welded to the channel flanges using a backup strip. The channels end near the tank access opening and are supported from the tank wall at 16 places (four for each channel). To permit installation, each channel is connected to a cross fitting at the aft bulkhead using "V" bands. The aft end of each channel has an adapter section which transitions from a rectangular to a round cross-section.

The LAD channels are supported from the tank walls by an arrangement shown in Figure 5-20 (view E-E) which uses two radial links and one drag link. Low thermal conductivity between the tank wall and the LAD is accomplished by using fiberglass parts. A fiberglass/epoxy support fitting equipped with self-locking threaded inserts is riveted to the channel walls. This fitting is bolted to two fiberglass links which are attached to aluminum clevis fittings. These clevis fittings are fillet-welded to the tank wall. For lateral support, a drag link is added which connects the channel support fitting to the tank wall fitting. The arrangement shown in view "E-E" is used at three places on each channel and the detail "G" design is used at one place on each channel. Detail "G" is the same as view "E-E" except the drag link is deleted.

A backup strip is used when seam welding the fine mesh screen to the channel flanges. Detail "D" shows the backup strip configuration. The strip is cut from flat sheet stock and features cross ribs and end close outs. This configuration permits continuous seam welding around the ends and along the sides.

5.5.3 Tank 2 Insulation Features

Tank 2 is completely enveloped with a multi-layer insulation (MLI) system which is presented in Figures 5-21 and 5-22. The MLI is applied in prefabricated blanket assemblies which are formed

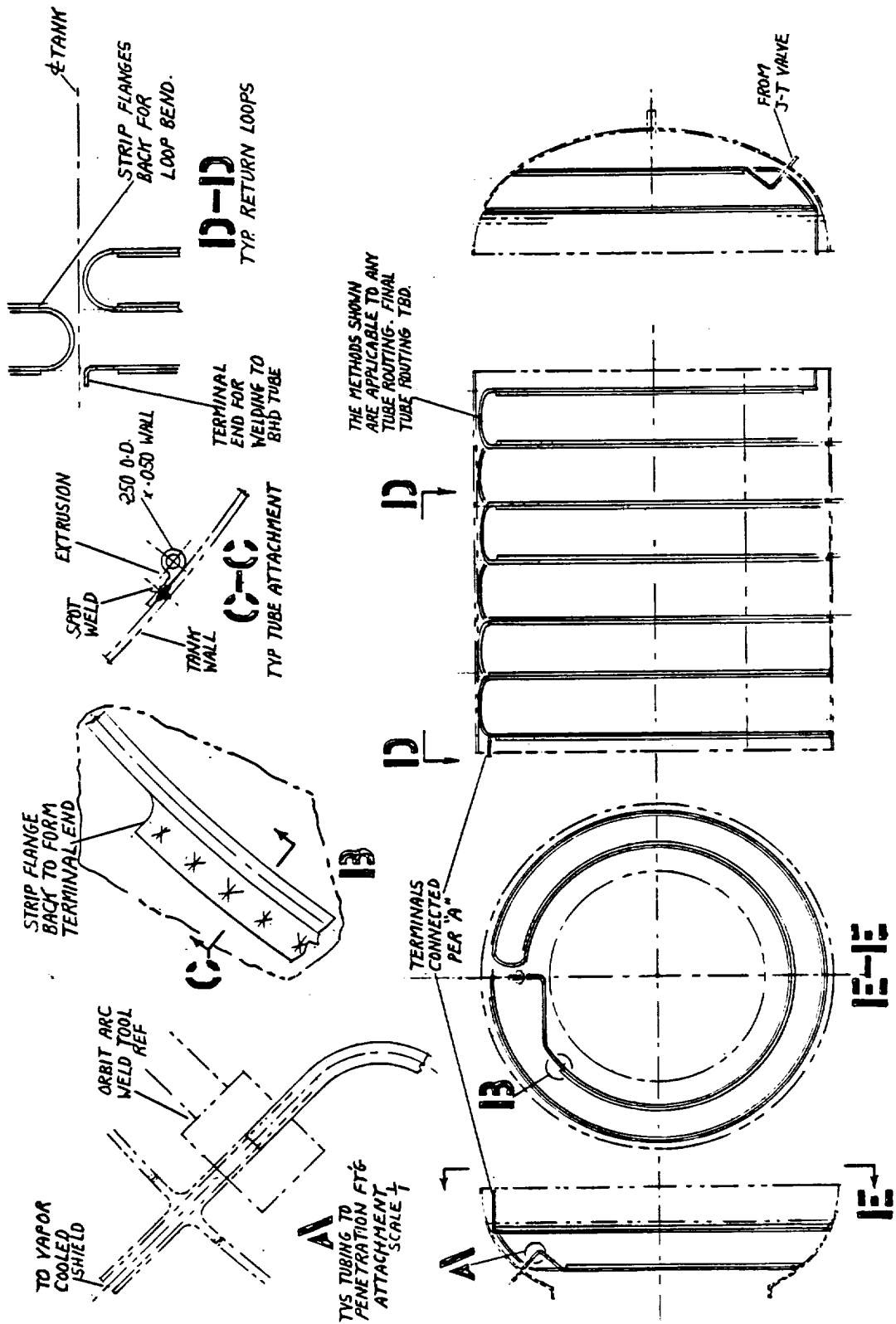


Figure 5-18. Tank 2 Wall Heat Exchanger and TVS

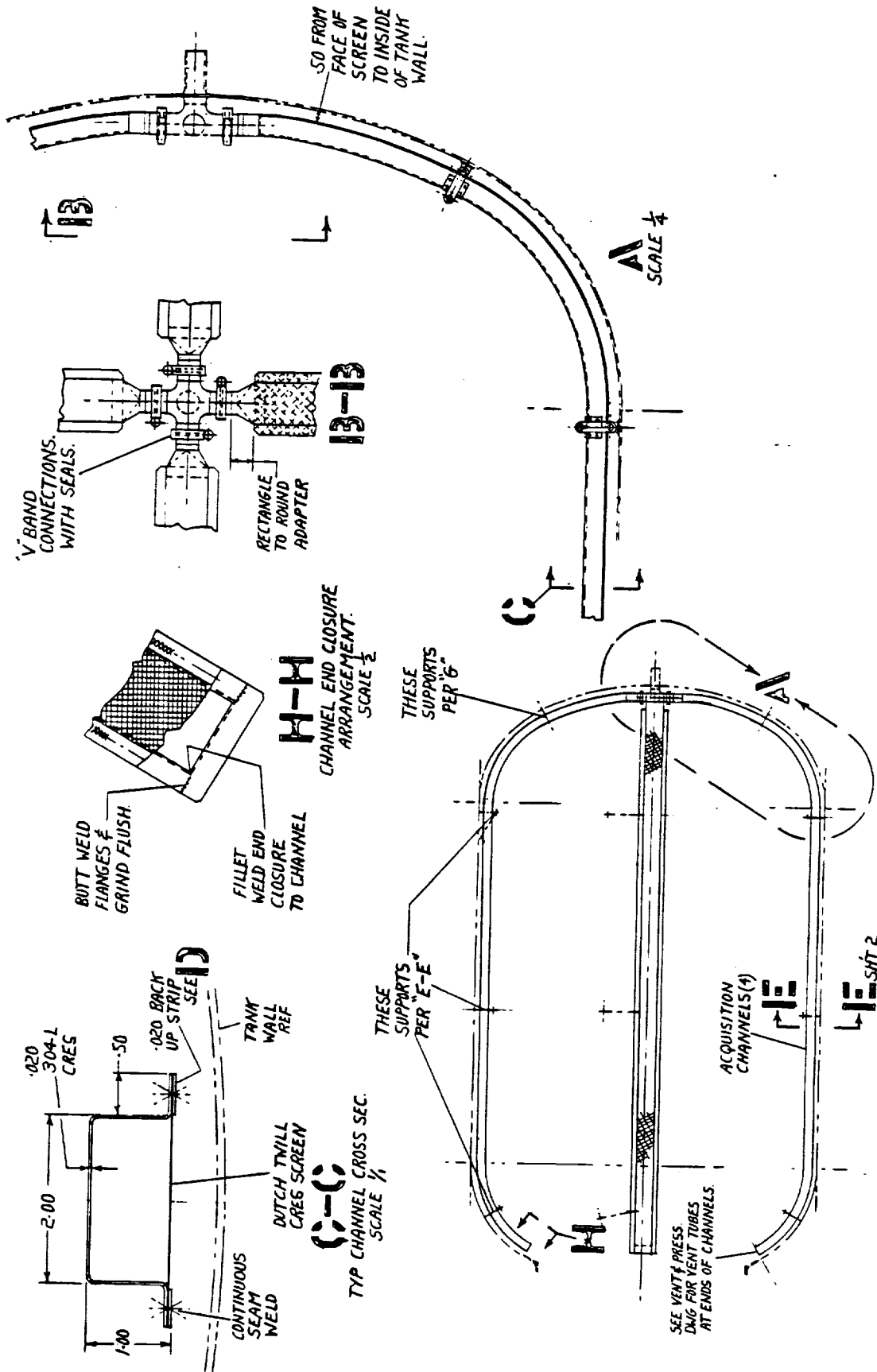
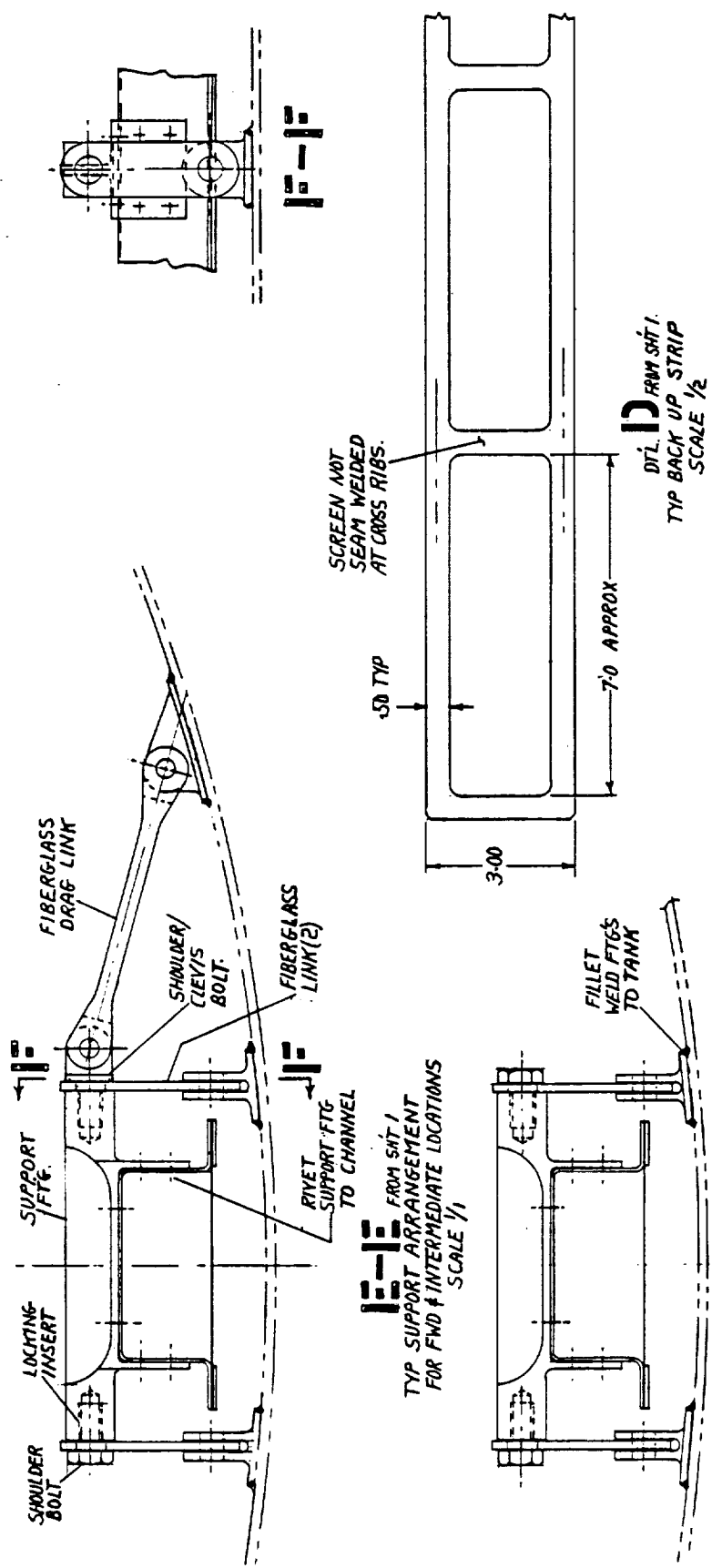


Figure 5-19. Tank 2 Liquid Acquisition Device/LAD



A-A FROM SHIT 1
 TYP SUPPORT ARRANGEMENT
 FOR FWD & INTERMEDIATE LOCATIONS
 SCALE 1/1

B FROM SHIT 1.
 TYP BACK UP STRIP
 SCALE 1/2

C FROM SHIT 1
 SUPPORT FOR AFT LOCATION.
 SAME AS E-E EXCEPT AS
 SHOWN.

Figure 5-20. Tank 2 Liquid Acquisition System Device/Additional Details

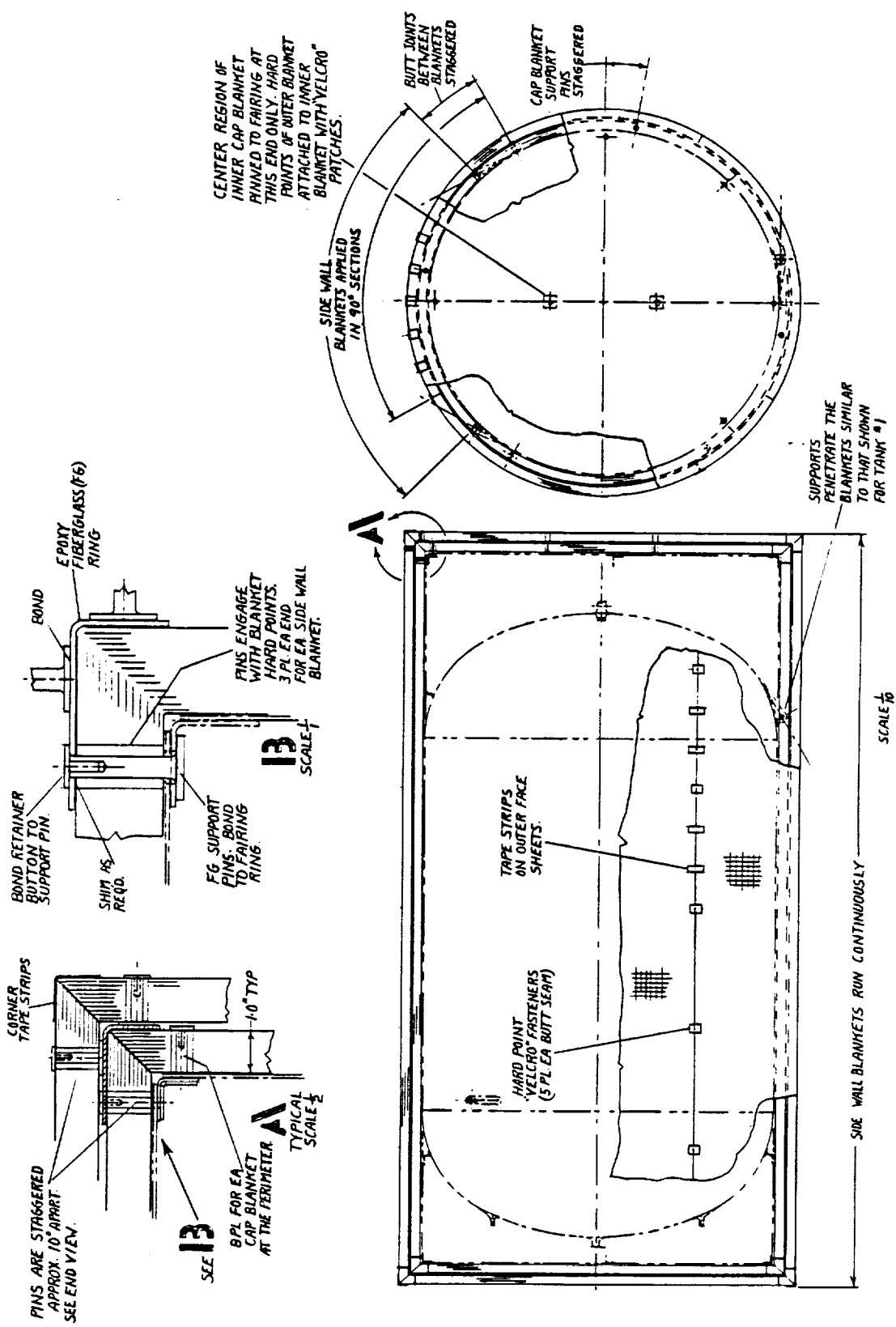


Figure 5-21. Tank 2 Insulation

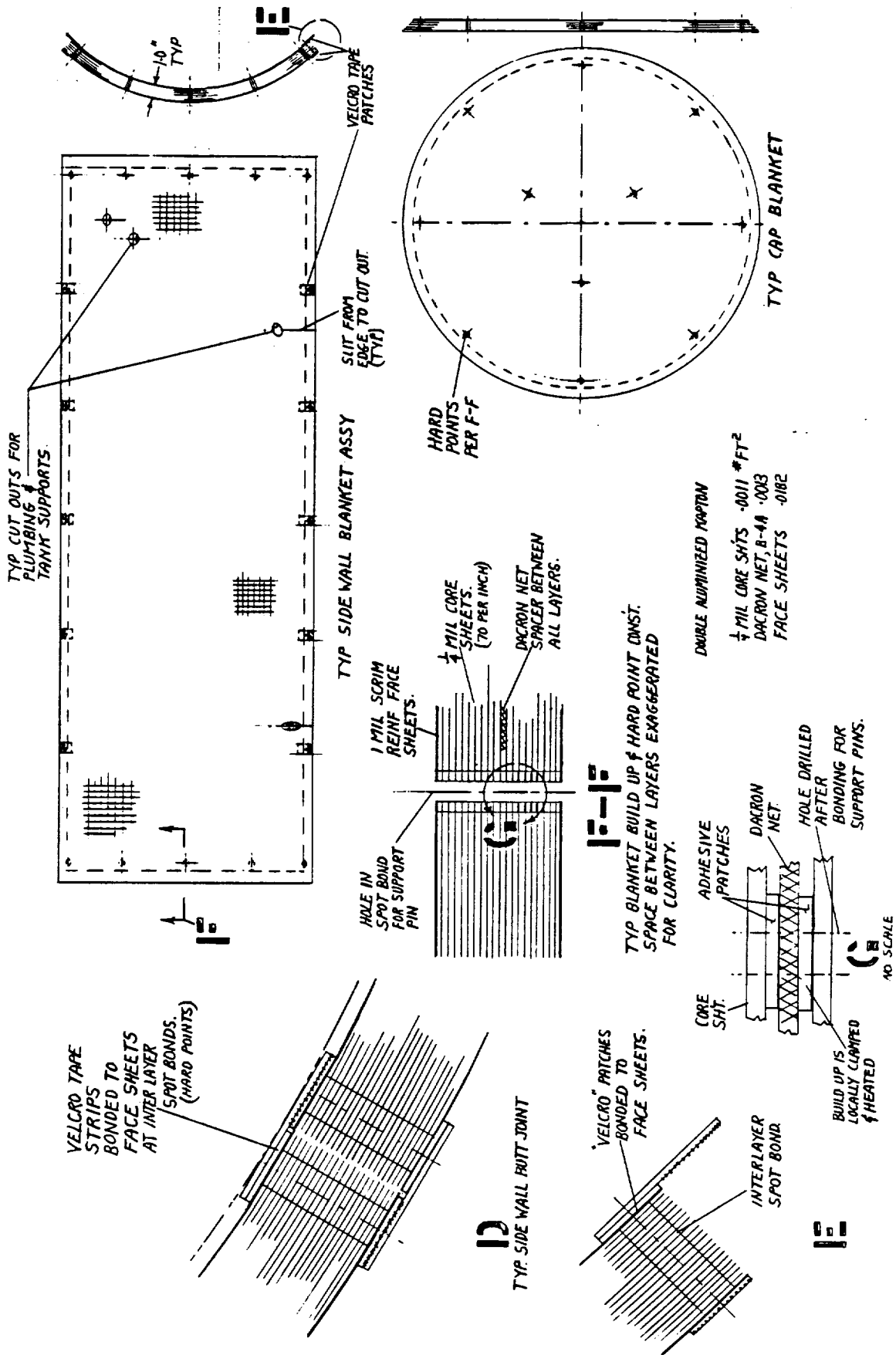


Figure 5-22. Tank 2 Insulation and Typical Blanket Construction

and trimmed to fit the side wall and the flat ends. The MLI is applied in two blanket layers and attached to the tank fairings with fiberglass or PPO pins. The side wall blankets run continuously from cap to cap with the butt joints and support pins staggered between layers. "Velcro" fasteners are used to hold the butt joints together, and tape strips (located on the outboard surfaces) are used between these fasteners to insure a uniform fit. The ends of the side wall blankets fit with the end cap blankets through mitered joints equipped with corner tape strips. On the aft end only, the cap blankets have two additional supports located near the center. The support pins at the perimeter of the cap blankets are staggered between blanket layers.

Figure 5-22 shows a cross section of a typical MLI blanket containing many layers of thin core sheets of double-aluminized Kapton (DAK). The MLI blanket has about 2.76 layers per millimeter. These layers are sandwiched between the outer scrim-reinforced face sheets. The DAK sheets are separated by dacron netting. As shown in View F-F and Detail G, hard points are built into each blanket by local interlayer bonding using adhesive patches inserted between each layer of material. The hard points at the ends are drilled for mating with support pins at installation.

A typical side wall blanket is layed up over a mold to match the contour at installation. The blanket has 16 hard points, cutouts for plumbing and tank supports, trimmed edges, and has Velcro fasteners bonded to the hard points along the sides (Detail E). A typical fastener arrangement at a butt joint is shown in Detail D.

The same fabrication procedures as described above are used for the flat cap blankets.

5.5.4 Bulkhead Equipment and Installation

5.5.4.1 Tank 2 System Equipment Installation on the Aft Bulkhead. The system equipment installation for the aft fairing compartment on Tank 2 is presented in Figure 5-23. The installation establishes the length of the fairing and demonstrates that the volume allocated provides room for making connections to the tank and for flexibility in the plumbing between components.

Most of the components and interconnecting plumbing are mounted on the fairing. The remaining components are supported from the tank penetration fittings and from clips attached to fittings on the tank bulkhead. All plumbing is corrosion resistant steel (CRES) and connections are made with the orbit arc-welding process. Valves and flowmeters are not bolted directly to the structure, but are supported by a clamping action through fiberglass fairleads and saddles. Dimensional changes due to temperature gradients are compensated for by slippage at the saddles and fairleads. Flexibility in the plumbing is provided by short flex hose sections and by the routing configuration.

Two electrical harnesses will be required, one for the tank instrumentation and one for the valves and flowmeters. The tank wall penetration fittings for the instrumentation are located outboard from the tank center so that access will be provided for the final plumbing connections. The clocking position for these instrumentation fittings will be determined at final design.

Valves, flowmeters and fairing are built up into a separate assembly and checked out. After the valves and related parts are installed on the tank bulkhead and checked out, the fairing assembly is slipped into position, attached to the tank and the final welds made. The electrical harnessing is next installed and checked out.

5.5.4.2 Tank 2 Vent and Pressurization Installation on Forward Bulkhead. Two solenoid valves (a late change in the study deleted one of the solenoid valves, which is not reflected in the drawing), and a relief valve are manifolded together and located under the MLI on Tank 2 at the forward bulkhead. The Figure 5-24 layout shows the arrangement along with the tank pressurization assembly and vent lines for the LAD system. The valves and manifold are supported from the tank fairing with two epoxy/fiberglass fairleads and a section of a ring having a channel cross section.

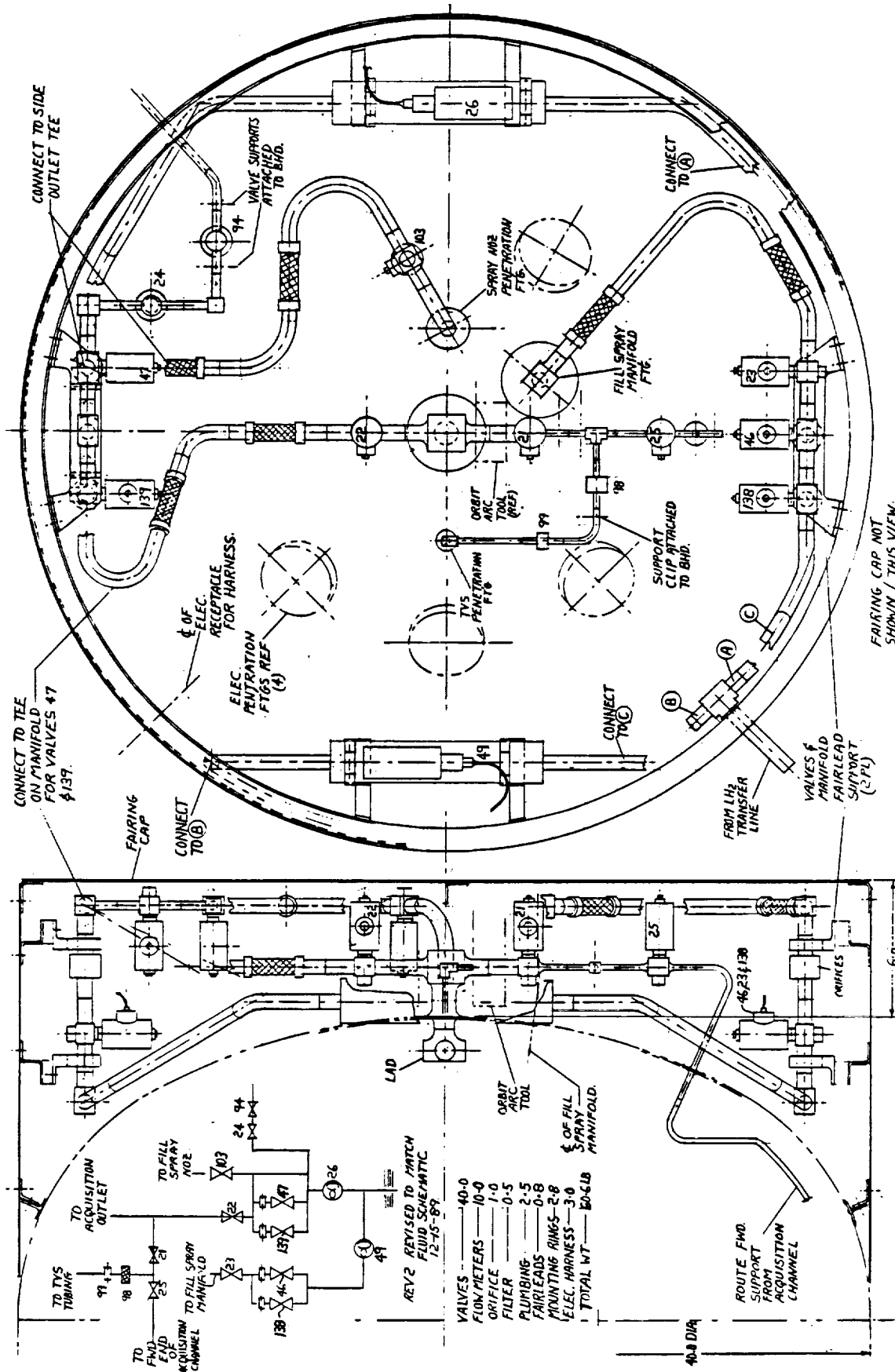


Figure 5-23. Tank 2 System Equipment Installation/Aft Bulkhead

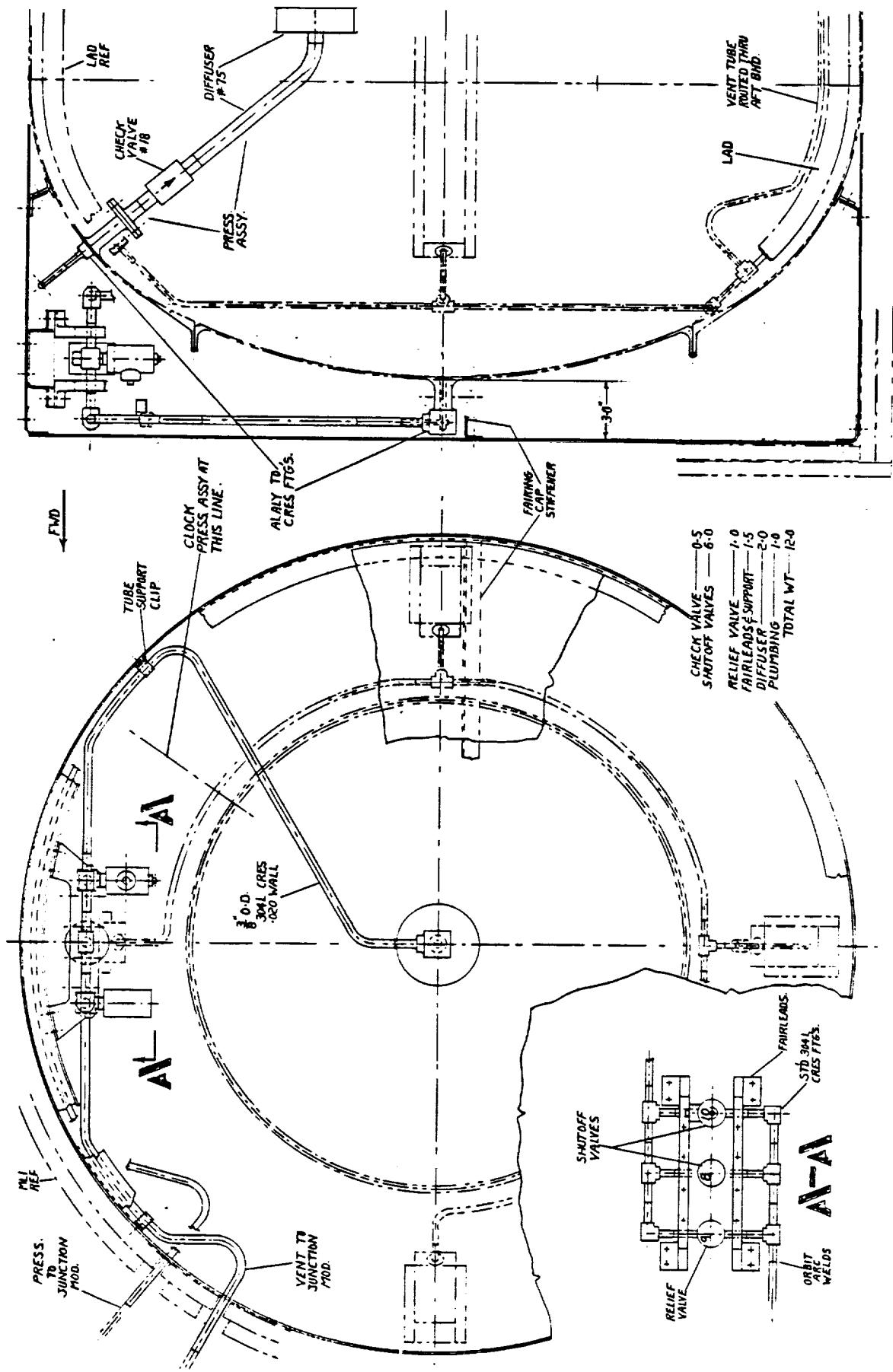


Figure 5-24. Tank 2 Vent and Pressurization Installation

The ring section distributes the loads into the fairing and acts as a spacer for locating the valves slightly inboard for accessibility. One end of the manifold is routed through the fairing and the opposite end is plumbed to a CRES-to-aluminum transition fitting located in the access opening cover. This transition fitting is machined from a diffusion-bonded block and the aluminum portion welded to the cover. Line sizes are small and there is adequate room for the tubing. The tubing has sufficient flexibility without the use of flex hose sections. The material is 304L CRES, and all connections are made with the orbit arc-welding process.

A CRES-to-aluminum transition fitting is also used for the pressurization line. The fitting is located outboard of the access opening and one end is plumbed through the fairing with 6.35 mm diameter tubing. The opposite end is equipped with a flange for attaching a section of the tubing containing a check valve and a diffuser. The tubing for the check valve and diffuser is oversized for structural reasons.

The forward ends of each LAD channel are vented with 6.35 mm diameter tubing manifolded together and routed through the aft bulkhead. One of the tubes at the end of a channel has a tee fitting. The branch end of this tee fitting is connected to a vent tube which is supported from the LAD channel and routed through the aft bulkhead. The vent tube is spaced from the channel wall and is attached with epoxy/fiberglass clips. This line ultimately vents through the tank wall-mounted TVS.

5.6 TANK 3

5.6.1 Tank 3 General Arrangement and Internal Components

Tank 3 is a 1.07 m inside diameter aluminum alloy (2219) sphere fabricated from two single spun hemispheres. The aft end is equipped with an access opening through which most of the electrical lines and tubes pass. One vent line equipped with a baffle penetrates the forward bulkhead. Figure 5-25 is an overall layout of Tank 3, and the various views and details called out on the layout are included in other figures in this section. The assembly of the tank and details on the nozzles and vent arrangements are described in Appendix A.

Equipment attached to the exterior surface includes a heat exchanger, fittings for attaching a small fairing on the aft end, support fittings for attaching six struts, and flat strip heaters bonded to the wall.

The interior is equipped with a tubular cross structure which supports fluid lines, nozzles, a pressurant diffuser, electrical wiring, and instrumentation for conducting a variety of fill, drain, and vent experiments. The cross structure has two flanged connections to permit assembly through the access opening.

Unlike Tanks 1 and 2, there are no system components installed under the MLI on Tank 3. Instead, the system components are packaged into a module and interconnected to the penetrations at the aft end of the tank with several lines, which are collected into a bundle and wrapped with MLI. The location of the valve module relative to Tank 3 was presented earlier in Section 5.3 in the overall experiment general arrangement, Figure 5-2.

5.6.2 Tank 3 Insulation

The MLI is applied in two preformed blanket layers with the seams staggered between layers. The hard points built into the blankets (per that described for Tank 2) are equipped with Velcro fasteners (Figure 5-26).

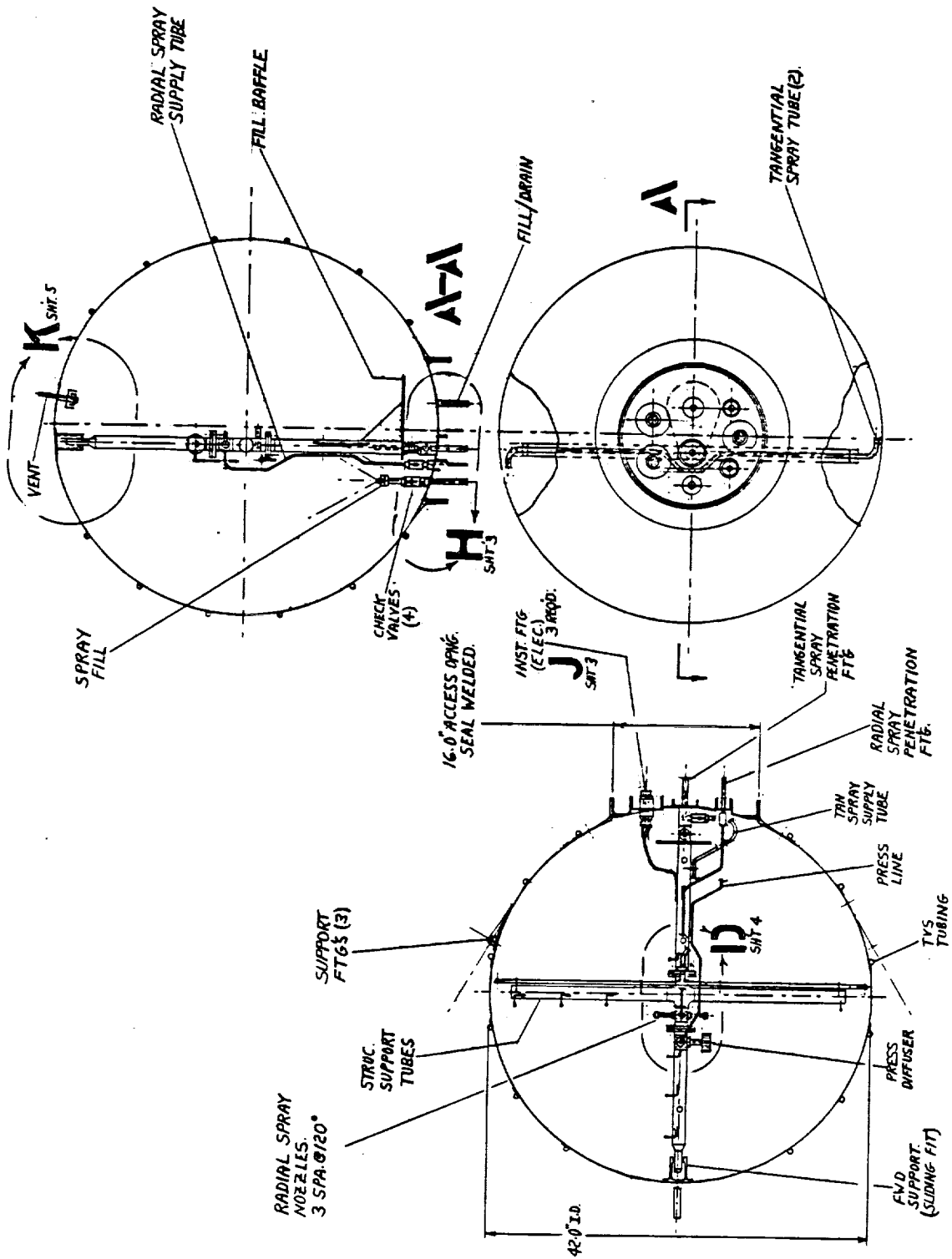


Figure 5-25. Tank 3 General Arrangement

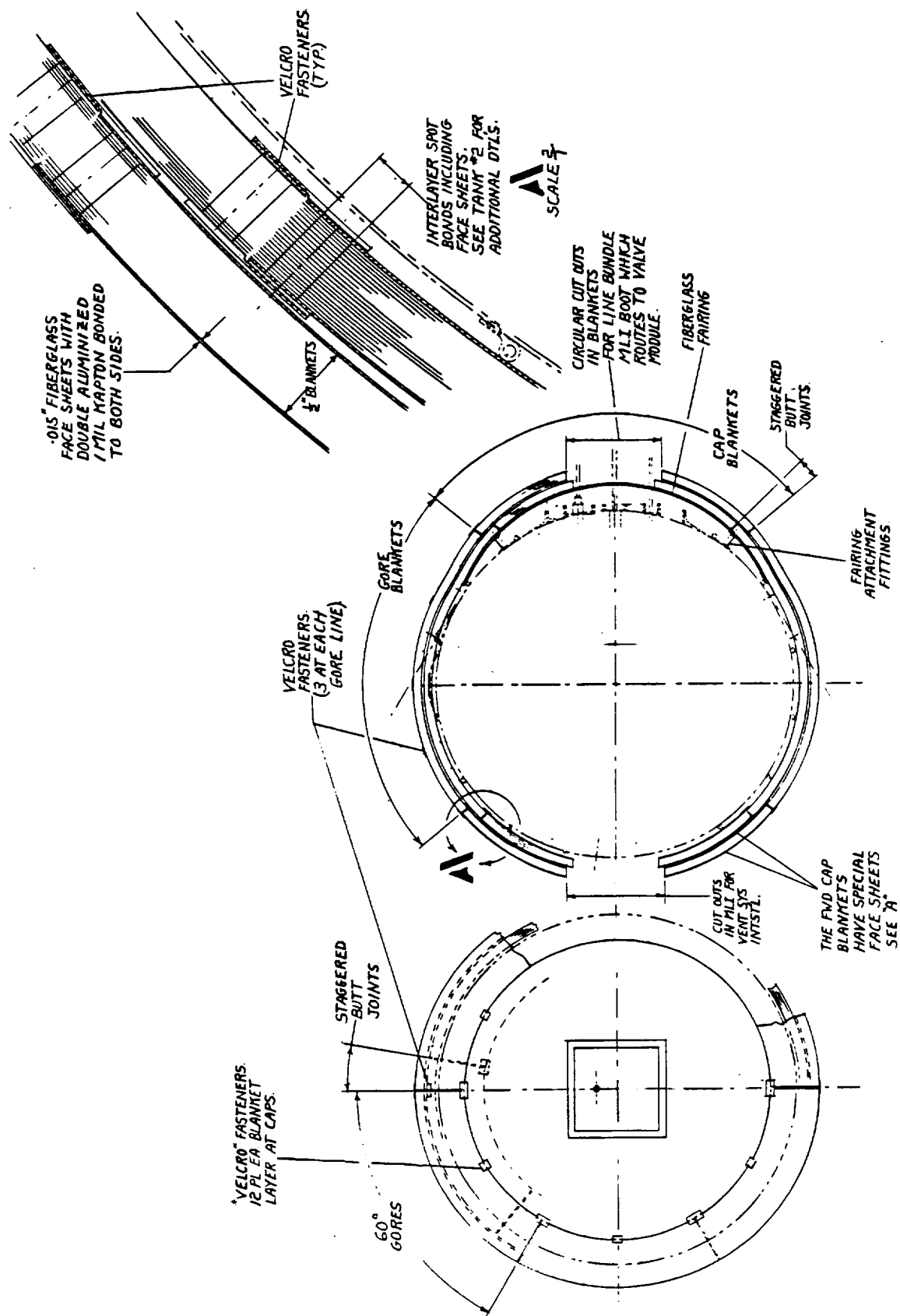


Figure 5-26. Tank 3 Insulation

The small fiberglass fairing at the aft end of the tank provides a uniform surface for mounting the MLI. The fairing is supported from the tank wall with fittings which are welded to the tank. These fittings have floating self-locking nut plates. The external surface of the tank is not uniform due to the TVS tubing, therefore the forward cap blankets have thicker face sheets which permit the MLI to span over the tubes without compressing and/or wrinkling in local areas. A typical blanket layer consists of two cap blankets and six gore blankets interconnected with Velcro fasteners at the hard points. Penetrations at the support struts are similar to that shown for Tank 2.

5.6.3 Tank 3 Bulkhead Fittings and TVS Heat Exchanger

5.6.3.1 Tank 3 Aft Bulkhead Penetrations and Accessories. The aft bulkhead of Tank 3 has an access opening through which pass several penetrations (Figure 5-27, Detail "H"). These penetrations and the access opening cover are sealed by welding the ends of the upstanding flanges machined into each part. For access, the welds are cut off and the upstanding flanges rewelded.

The penetration fitting for the tangential spray manifold also provides support for the internal cross structure by a tongue/clevis connection featuring a spherical bearing insert (views B-B and C-C). This penetration fitting also has an interface for installing the check valve and supply tube. The supply tube has a flex hose section which absorbs dimensional changes and permits easy alignment at assembly. A second penetration fitting for a spray nozzle is shown in Detail "H" which is machined to receive a check valve and a spray fitting.

A minimum of three electrical penetrations (Detail "J") are required. The receptacle features a flange with upstanding legs for welding into the access opening cover. All penetration fittings for tubes are machined from diffusion-bonded aluminum-to-CRES transition blocks so that CRES lines can be welded to the outboard ends.

5.6.3.2 Tank 3 Forward Bulkhead Penetration Fittings. Figure 5-28 is a view at the forward end of the Tank 3 (Detail K), which has one vent penetration and a support fitting for the internal cross structure.

The vent penetration is a fitting machined from a steel-to-aluminum diffusion-bonded block, and is equipped with a baffle assembly on the inboard end. The design of this vent and baffle is preliminary, and will be the subject of further review, based on the specific tests which are required in the experiments.

The end of the cross structure tube is equipped with an end fitting which slip fits with a support which is welded to the tank wall. The assembly is configured to allow angular deflections as well as length changes.

5.6.3.3 Tank 3 External Wall-Mounted Heat Exchanger. The wall-mounted TVS heat exchanger tubing shown in Figure 5-29 is basically the same as that described for Tank 2. However, the tubes are on the outside of the tank wall. Like Tank 2, the tubing is an extrusion which has a fin for spot or seam welding to the tank (Detail "A"). The fins are stripped back at the ends and the tubing formed to interface with the adjacent part. The tubing ends at the tank equator are formed to allow clearance for an orbit arc tool (Detail "C"). The insulation is cut locally for clearance. The exact routing and length of tubing will be determined at final analysis.

5.6.4 Tank 3 Valve Module

The valve module for Tank 3 is shown in Figure 5-30, and follows the same design approach used on other modules. The valves, flowmeters, orifices, etc. are interplumbed with 304L CRES tubing and standard fittings designed for orbit arc-welding. The plumbed assembly is then supported from

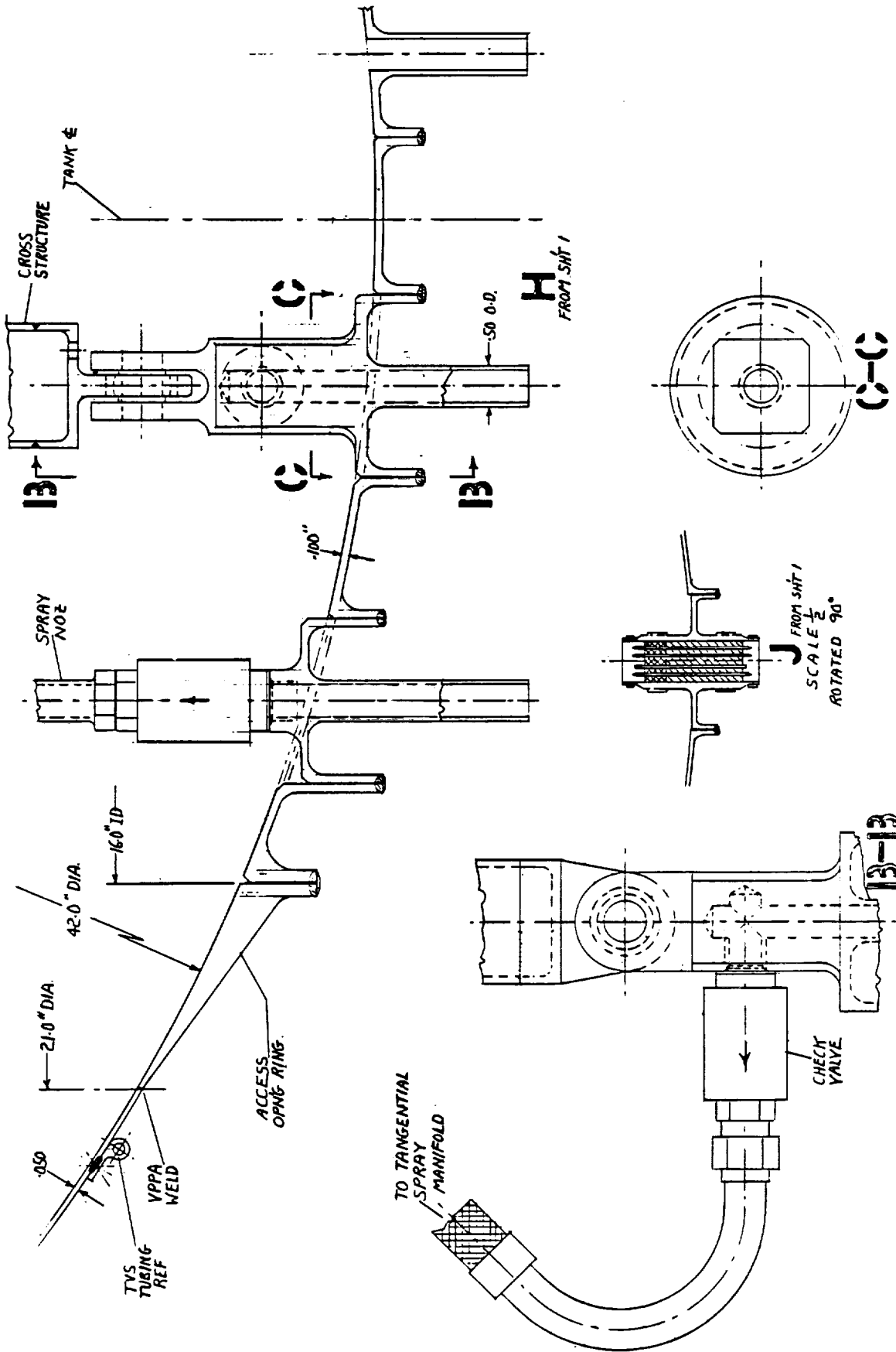


Figure 5-27. Aft Bulkhead Penetrations and Accessories

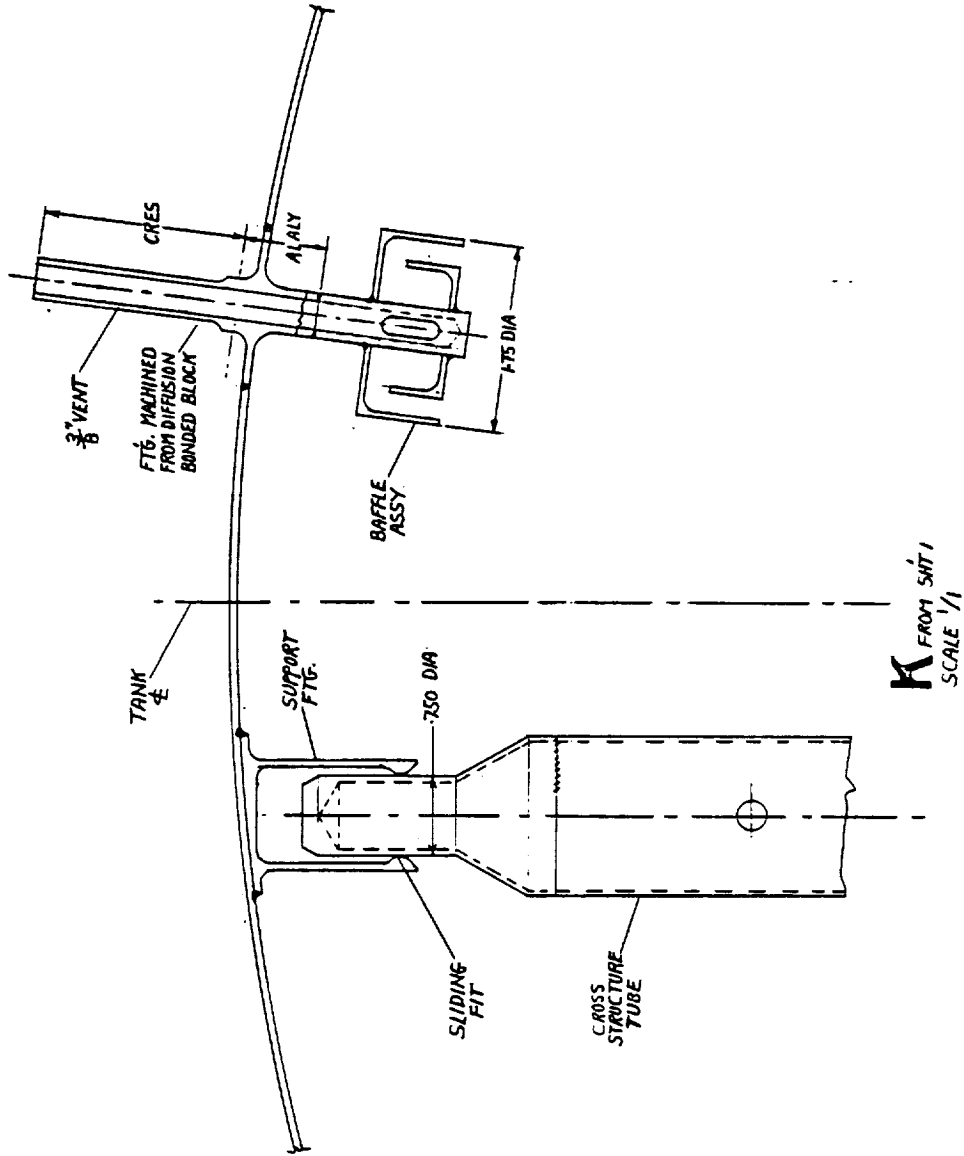


Figure 5-28. Tank 3 Forward Bulkhead Penetration and Accessories

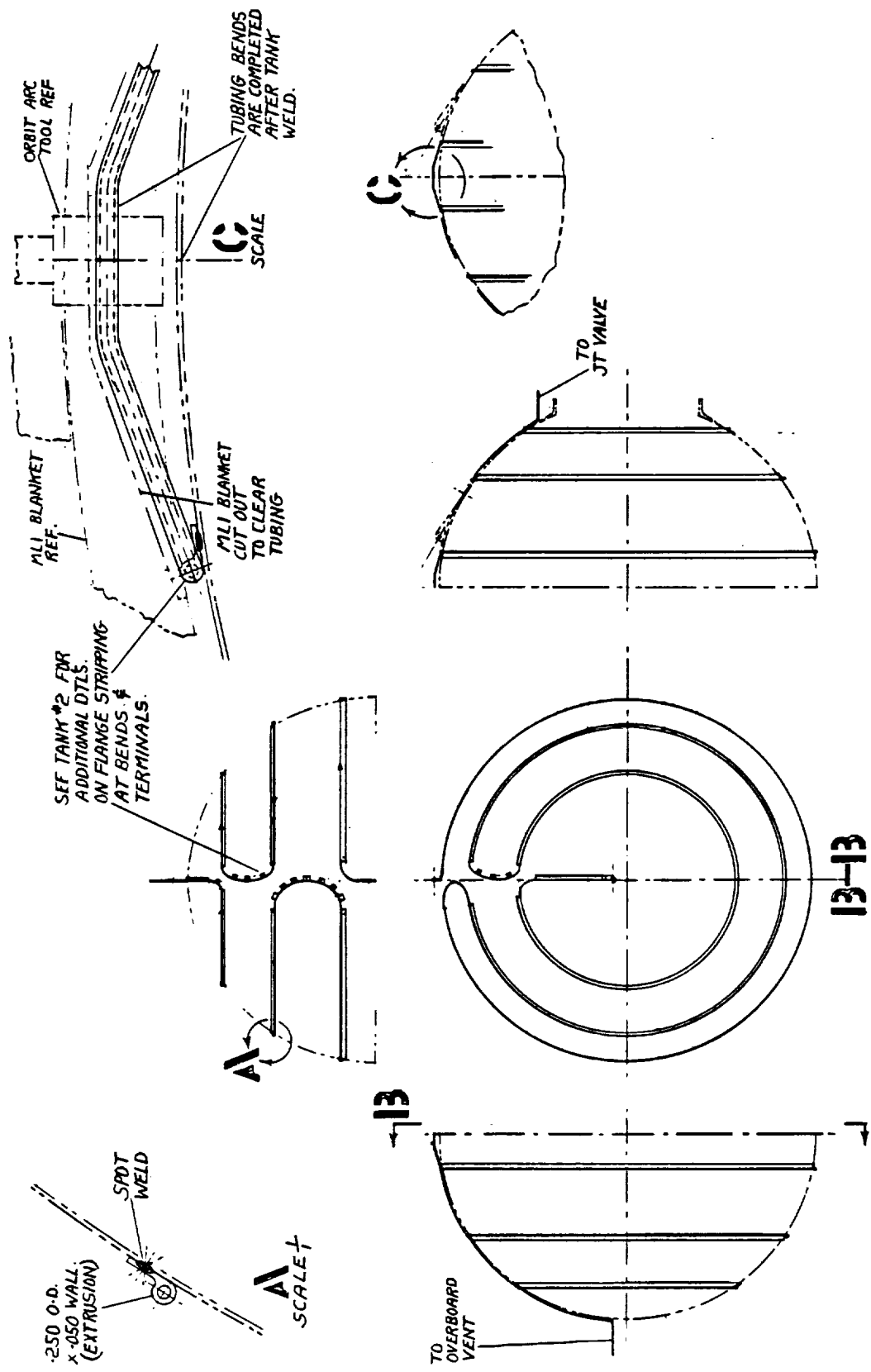


Figure 5-29. Tank 3 Wall Heat Exchanger/TVS

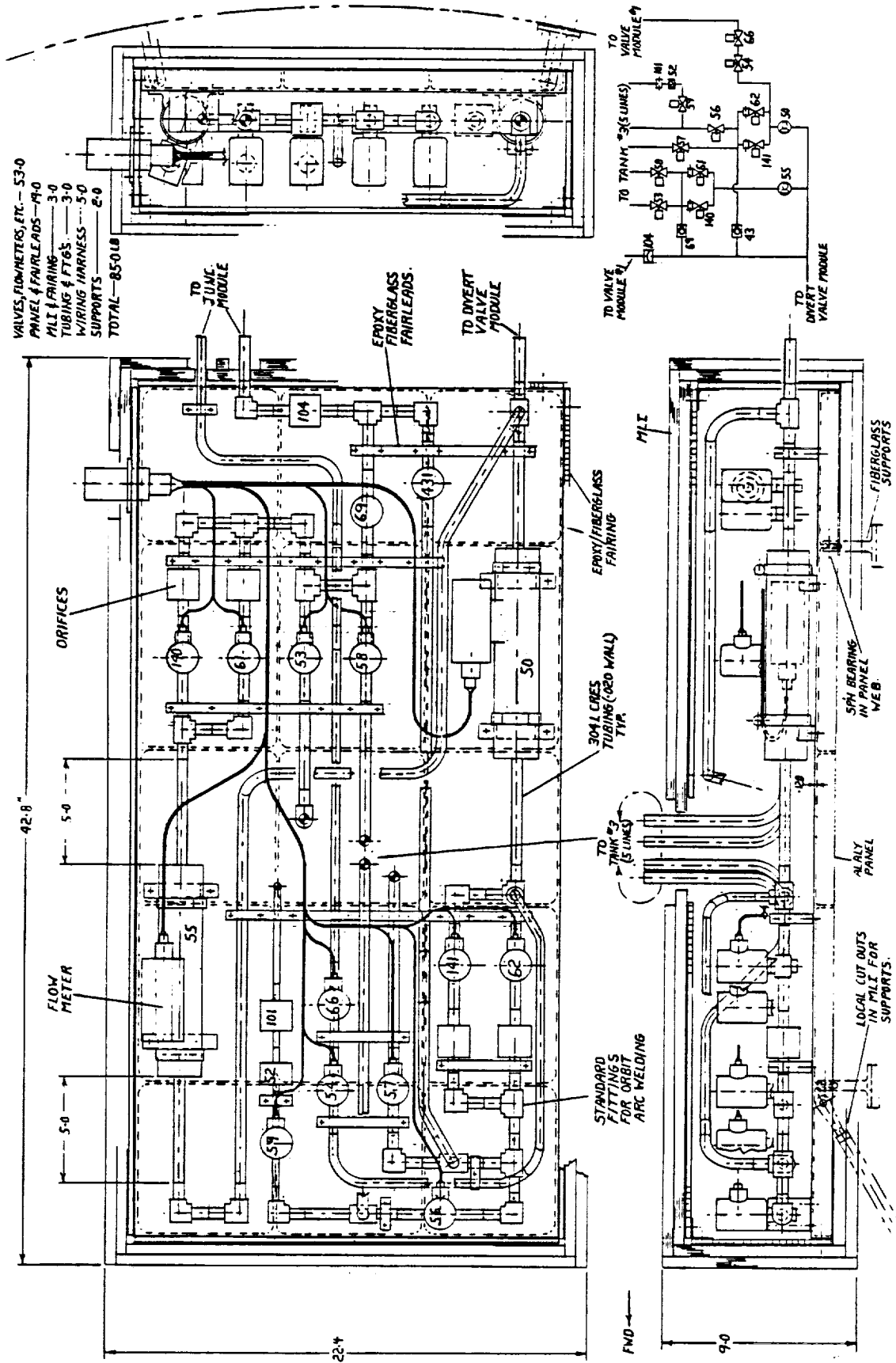


Figure 5-30. Tank 3 Valve Module

a waffle panel using fiberglass/epoxy fairleads and saddles. With this mounting approach, the assembly is basically clamped to the waffle panel rather than hard-mounted. This allows dimensional changes. The five tubing stub-ups located near the center of the assembly are plumbed to Tank 3 using CRES lines equipped with flex hose sections. These lines are approximately 760 mm long and are clamped together with fairleads forming a bundle which is wrapped with MLI. A MLI close out boot is used at each end which interfaces with the insulation on Tank 3 and the valve module. The entire valve module assembly is enveloped with MLI and a vented fiberglass honeycomb fairing which is attached to the waffle panel. The MLI is attached with fiberglass or PPO pins bonded to the fairing and to the waffle panel.

The module is supported from the outer structure with fiberglass fittings and adjustable length struts that attach to the webs of the waffle panel. Spherical bearing inserts are used at the attachment points to allow for angular misalignments. The MLI is cut out locally to clear the supports.

5.7 FLUID LINES AND FLUID COMPONENT MODULES

5.7.1 LH₂ Fill, Drain, and Ground Vent Arrangement

The LH₂ fill and drain line for Tank 1 runs from the umbilical panel disconnect to the shut off valve located near the tank outlet. The arrangement for this system is shown in Figure 5-31. To avoid trapping LH₂ in this fill and drain line, a vent line is used which has one branch running aft to the Centaur ground vent and a second branch running forward to the junction module, which in turn connects to the flight vent. The branch which runs aft is equipped with relief valves (view A-A) and a disconnect which crosses the separation plane. This disconnect is located on the outboard side of the bus central cylinder and is clocked slightly off the "Y" axis. Local micrometeoroid/debris shielding may be required for the relief valve manifold and the aft vent line.

The fill and drain line penetrates the cap section of the Tank 1 purge enclosure and hard mounts to the tank fairing ring as shown in Detail "B." The line is equipped with flex hose sections to account for tolerances in fabrication and dimensional changes. The oversized hole in the purge enclosure cap is sealed off with a preformed boot which attaches to the fill and drain line insulation.

5.7.2 LH₂ Transfer Circuit Plumbing

A plumbing layout for the LH₂ transfer circuit which interconnects Tank 1, Tank 2, and the Tank 3 valve module is presented in Figure 5-32. The central junction for this circuit is at the relief valves, which are equipped with manifolds and packaged into an insulated module. The relief valve module is located in the forward section of the the outer structure so that the plumbing to the Tank 3 valve module and stub-ups for runs to Tanks 1 and 2 can be completed prior to mating the forward section of the structure to the aft section. Also, this location permits tubing runs of approximate equal lengths for fabrication purposes. The exception is the length of the run to Tank 2. Lines extend from the relief valve module to the vent valve module on the forward bulkhead of Tank 1. These lines contain flex sections and are connected on final assembly.

In the aft section, the run from Tank 2 at the aft fairing crosses over to the bus central cylinder through two flex sections and routes forward to the structure access opening where final connections are made. The line is orbit arc-welded to a hard-mounted stub up on the Tank 2 fairing (Detail "G"), and wrapped with MLI which intersects with the Tank 2 insulation through staggered butt joints. The line is supported from the bus central cylinder and the aft structure per Detail "B".

Two lines are routed to the aft end of Tank 1. Referring to Detail "F", the lines are orbit arc-welded to stub ups which are hard mounted to the aft fairing and wrapped with insulation which intersects with the tank MLI through staggered butt joints. An oversized hole in the purge enclosure cap

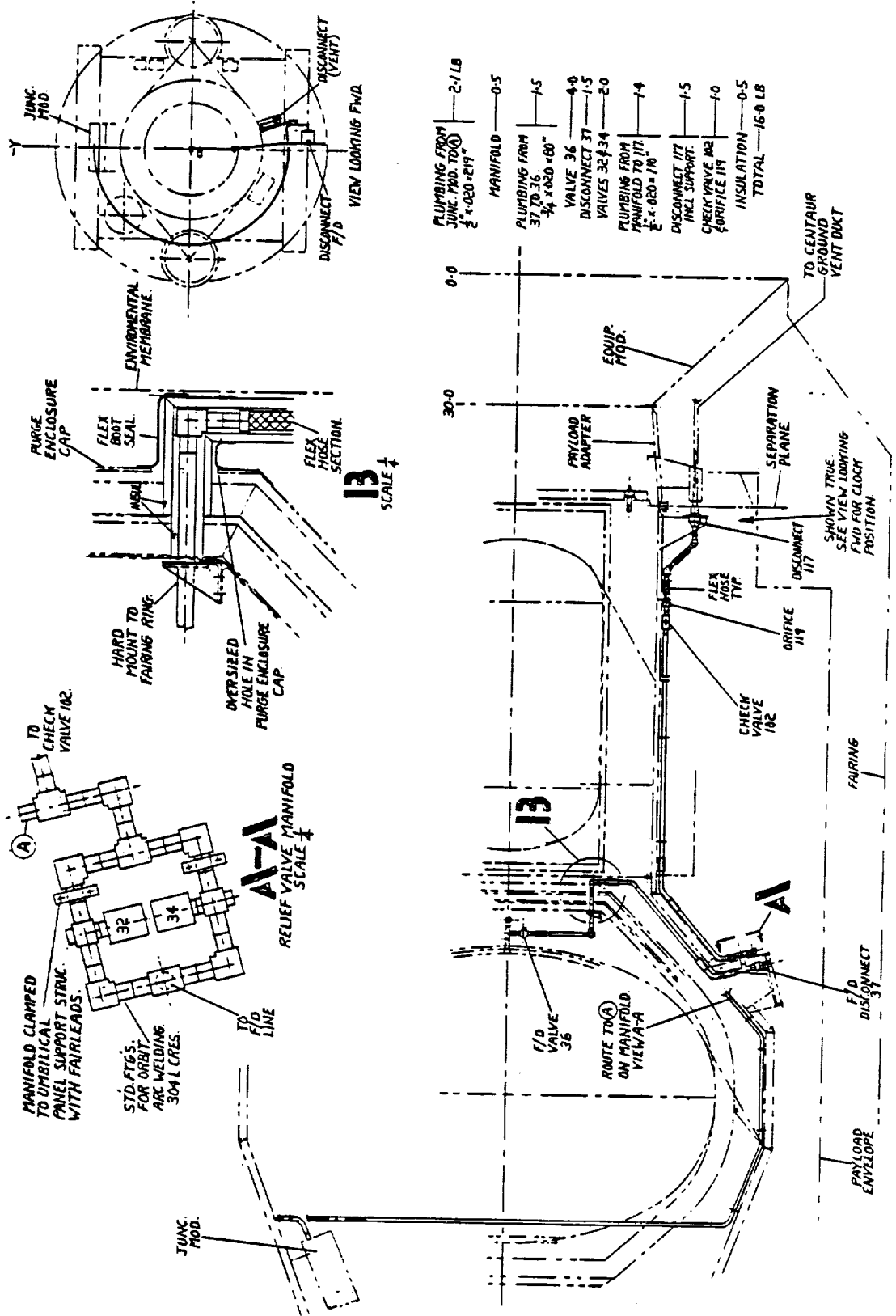


Figure 5-31. LH2 Fill, Drain, and Ground Vent Arrangement

section and an insulation closeout boot permits movement between supports on the structure and the purge enclosure. The work required to achieve the assembly which is shown in Detail "F" must be performed prior to the installation of Tank 1 assembly. Therefore, the two lines are clamped together with a fairlead (view "C-C"), the "Z" clip attached to the fairlead (view "D-D"), and insulation applied before the tank is lowered into the structure. Nut plates on the "Z" clip will permit attachment to the outer structure through small tool access holes with Tank 1 in place.

5.7.3 Vent and Pressurization Plumbing

The junction module is a collection of valves which control venting and pressurization for the three tanks. It also contains flowmeters for monitoring the venting of the Tank 1 VCS; the Tank 2 TVS; and the TVS for Tank 3. The junction module is located between Tanks 1 and 3, and is plumbed to the balanced thrust system at the forward end of the spacecraft and to the pressure control module at the aft end. It is also plumbed to both ends of all three tanks. Figure 5-33 shows the arrangement of this plumbing and includes a weight breakdown.

Except for the vent line on Tank 1 (which is Teflon), all lines are corrosion resistant steel (CRES) using standard fittings designed for orbit arc-welding. To allow for tolerances and movement between the tanks and the outer structure, the lines incorporate flex hose sections. These are generally placed in the tubing where it crosses between the outer structure and a tank. Most of the lines are attached to the outer structure using a combination of clips, brackets and fairleads. The lines are collected together at the aft section of the structure so that final assembly orbit arc-welds can be made through the access opening. All connections to the tanks are orbit arc-welded to stub-ups which are hard-mounted to the tank fairings for reacting loads created by line weights and flexures.

The balanced thrust vent system consists of three valves manifolded together as shown in views "A-A" and "B-B" (Figure 5-33). The valves and manifold are mounted on a waffle panel and the entire package attached to the inboard side of the forward cap on the outer structure. The lines will incorporate heaters to prevent and correct for freeze-up of the H₂.

In the final design, the clock position of the junction module relative to the pressure control module and Tank 3 valve module, can be varied in the pursuit of more favorable line runs. Likewise, the clock position for stub-ups on the tanks can be varied. Openings through the forward section of the outer structure provide access to the valve modules and to tank stub-ups. These openings are located adjacent to the valve modules. Access to the pressure control module at the aft end is provided by removal of the bus body panel or through an access opening in the body panel. Access to the aft stub-ups on Tank 1 and forward stub-ups on Tank 2 is available through hand holes in the outer structure and through hand holes in the bus central cylinder (located between the stringers). Removal of the bus aft closure panel or hand holes through the central cylinder provides access to the aft stub-ups on Tank 2.

Other details of the fluid component modules are contained in Appendix A.

5.8 EXPERIMENT MODULE STRUCTURE GENERAL FEATURES

The baseline concept for the experiment module outer structure is a ring frame-stiffened, semi-monocoque, aluminum honeycomb with inner and outer skins. This structure also provides protection against micrometeoroids and debris. An alternative graphite/epoxy structure design is presented in Appendix A.

Referring to Figure 5-34, a 3.05 m diameter short cylinder coupled with a short cone frustum makes up the aft section of the outer support structure. Similarly, the forward section is a 1.52-m diameter short cylinder equipped with a cap at one end and a long cone frustum at the opposite end. Both

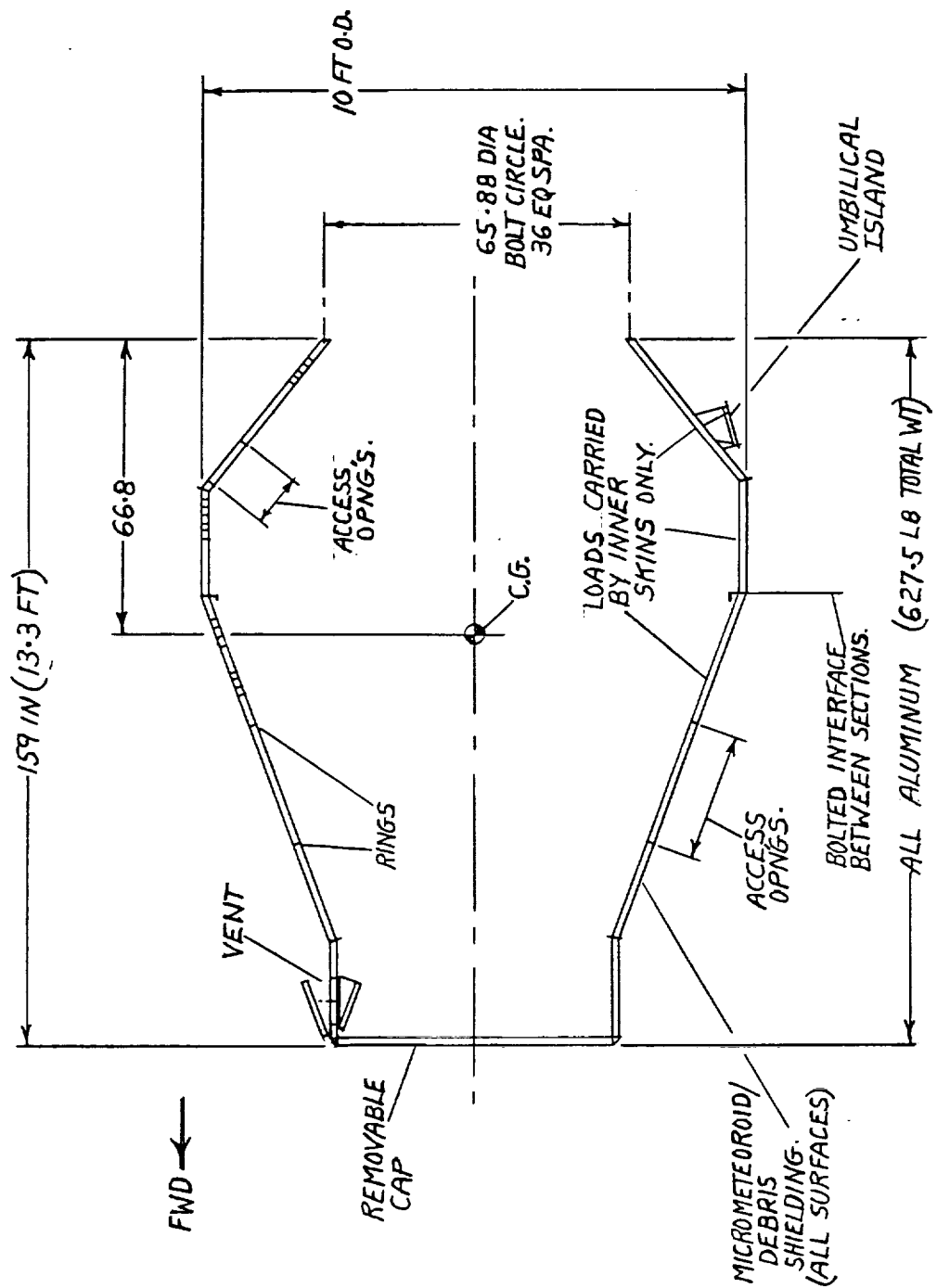


Figure 5-34. Outer Structure/All Aluminum/Baseline/General Features

sections feature micrometeoroid/debris shielding and access openings. The loads in both sections are carried by the frame-stiffened inner skins only with the micrometeoroid shielding added on as an accessory. Aluminum is used for both sections. Other features include an umbilical island, a removable forward cap, a baffled vent opening, a bolted interface between the forward and aft sections, and a 36-point interface at the aft end for attaching to the bus central cylinder.

5.8.1 Experiment Module Outer Structure

Figure 5-35 presents details of the aft interface, which attaches to the bus central cylinder at 36 points. This interface consists of one "Z" ring, and 36 fittings. Each fitting is equipped with a floating type nut plate, and the bolts which engage with these nut plates are loose-fitted to the holes. Shear loads are therefore reacted by a raised, conical-shaped boss on each fitting which engages with a matching recess machined into each of the bus central cylinder longerons. All parts are aluminum alloy.

Referring to Detail "C", the mitered ends of the aft cone and the cylinder are interconnected with a "T" ring and two angle rings. Three tank support fittings equipped with spherical bearings are attached to the "T" ring flanges. In Detail "D", the forward cone is bolted to the cylinder kick ring using floating-type nut plates. Since the inner skin only reacts loads, the outer skin is not connected to the cylinder. Three clevis-type tank support fittings are attached to the cylinder kick ring. Holes through the forward cone outer skin and honeycomb core provide tool access. Local patches are applied over these holes after installation.

Attachments between the forward cone, the forward cylinder, and the end cap are outlined in Figure 5-36. Since the skins and honeycomb core are bonded into sub-assemblies, a two-ring arrangement (Detail "G") is required to permit assembly at the cone/cylinder junction. Tank support fittings are attached to the inboard side of the ring assembly. For the end cap shown in Detail "H", a two-ring arrangement is also required to permit assembly. The end cap is bolted to the channel ring on the cylinder and the corner closed out with a thin skin that can be applied in sections.

5.8.2 Outer Structure Vent Arrangement

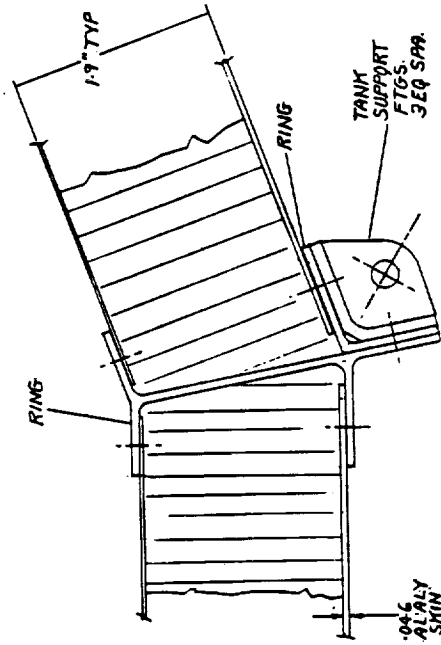
A vent arrangement for the outer structure is shown in Figure 5-37. This design allows venting of the volume inside the structure while providing micrometeoroid/debris shielding. A fitting is installed in the wall of the structure, forming a 254-mm inside diameter opening. Baffles are positioned on both sides of this opening to prevent particles from entering through the hole. The baffles are supported on the forward sides by brackets and near the center by a pair of struts positioned in a "v" arrangement. The inboard baffle is equipped with side baffles to intercept any particles which pass the outboard baffle in a lateral direction.

5.9 FLUID SYSTEM COMPONENTS

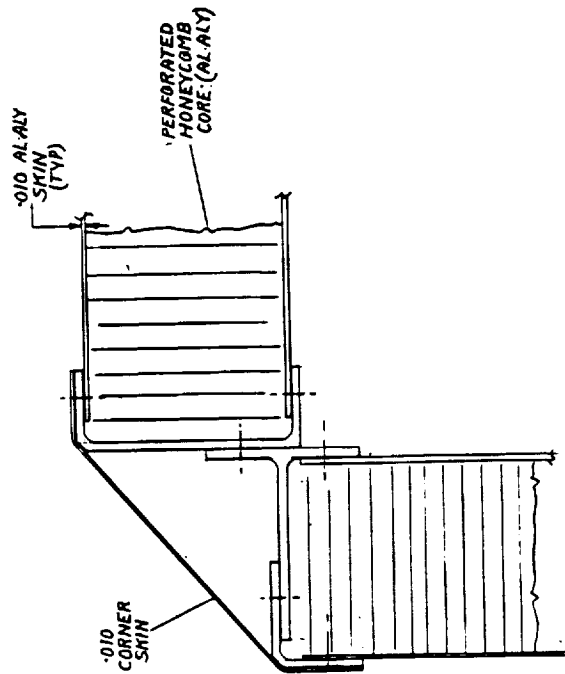
This subsection describes major components of the fluid systems within the experiment module. Addressed are the thermodynamic vent systems, the transfer and pressurization pumps, the autogenous pressurization system, the outflow subcooler, the stored gas pressurization system, and valves and regulators.

5.9.1 Thermodynamic Vent Systems

Each tank is equipped with a passive TVS to control tank pressure. The supply tank also has an active TVS. Fluid from the tank is throttled to a lower pressure and temperature through a J-T valve.



G
SCALE ↑



H
SCALE ↑

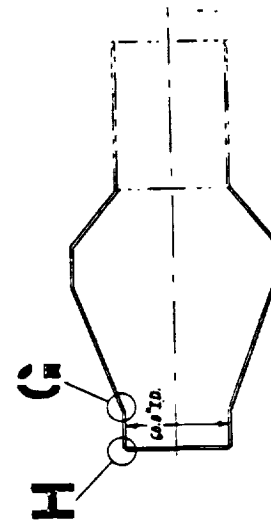


Figure 5-36. Outer Structure/All Aluminum/Baseline

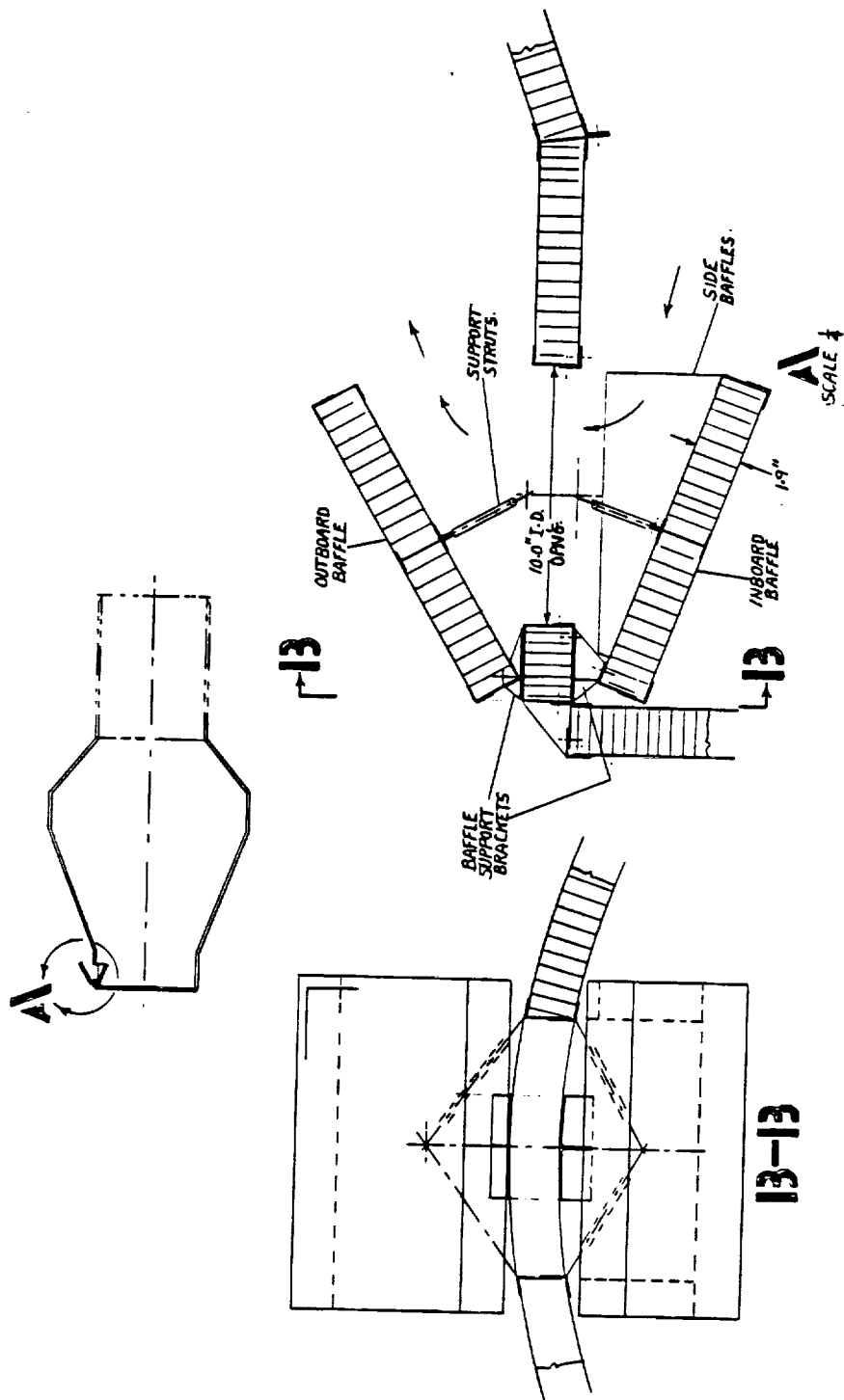


Figure 5-37. Outer Structure Vent Arrangement

The TVS fluid will then be routed through a heat exchanger to intercept or remove heat leak into the tank. The TVS pressure will be maintained at 34.5 kPa. To minimize hardware, each TVS will utilize a single throttling valve (plus redundant valves). Due to the low TVS flowrates, Viscojets are being considered for the throttling devices. As compared to an ordinary orifice with the same amount of flow restriction, Viscojets have much larger passages, which are less susceptible to clogging. Viscojets are manufactured by the Lee company, and have been tested in TVS's with liquid nitrogen at flowrates lower than 1.26×10^{-5} kg/s (Reference 5-1).

The heat exchanger for each passive TVS will consist of a length of tubing mounted to the tank wall. The tubing will be mounted internally on Tanks 1 and 2, and externally on Tank 3. The TVS tube must be long enough to completely vaporize the TVS fluid to insure no liquid is vented. The required tube lengths are 44.2, 66.4, and 43.6 meters for Tanks 1, 2, and 3, respectively. Analyses for the TVS are presented in Section 6.3. The majority of the TVS tubing will be routed perpendicular to the acceleration vector to take advantage of a greater free convective heat transfer coefficient. The TVS tube will have an OD of 9.525 mm and a 1.27 mm wall thickness. The pressure drop through the TVS for Tanks 1, 2, and 3 will be 3.5, 11, and 3.5 kPa, respectively. In order to maintain the TVS exit pressure greater than 13.8 kPa, a pressure drop below 20.7 kPa is considered acceptable.

The passive TVS for the supply tank will operate continuously at a flowrate of 6.63×10^{-5} kg/s. A constant tank pressure will be maintained, provided the tank wall heat flux is set at 1.9 W/m^2 , using the tank wall heaters. When the tank wall heat flux is reduced by a reduction in heater power, the TVS will have the capacity to thermally condition the tank fluid and reduce the pressure. For a tank wall heat flux of 0.32 W/m^2 , the time to condition the tank fluid from 137.9 to 103.4 kPa will vary from 41 hours, for a tank that is initially 95 percent full, to 14 hours for a 10 percent full tank. The amount of hydrogen used to thermally condition the tank by 34.5 kPa varies from 10 kg, for a tank that is initially 95 percent full, to 3 kg for a 10 percent full tank.

The TVS flowrates for Tanks 2 and 3 are 1.12×10^{-4} and 6.51×10^{-5} kg/s, respectively. The heat leak cannot be controlled, but is expected to be no greater than 1.58 W/m^2 . When operated continuously, the TVS in both receiver tanks has the capacity to thermally condition a 95 percent full tank from 137.9 to 103.4 kPa in less than 6 hours. The mass of hydrogen used to condition the tank is 2.5 kg for Tank 2 and 1.2 kg for Tank 3. The conditioning time decreases to less than 2 hours for a 10 percent full tank. Similarly, the mass boiled off decreases to 0.8 kg and 0.4 kg for Tanks 2 and 3, respectively. To intercept the tank heat leak and maintain a constant tank pressure, the TVS in each of the receiver tanks will be operated intermittently, on a 20 percent duty cycle. The duty cycle frequency must be high to achieve nearly "steady" thermal conditions in the tank. A duty cycle period of 150 seconds will be used. The TVS will be "on" for 20 percent of this time, or 30 seconds per cycle. The residence time of the TVS fluid within the TVS tube is about 40 seconds, so it will take about 1.25 cycles for each fluid molecule to pass through the TVS tube. Intermittent TVS operation is discussed in greater in Section 6.3.2.1.

The supply tank also contains an active TVS, which includes an internally-mounted, compact heat exchanger and an axial-jet mixer. Analyses for the active TVS are presented in Section 6.3. A counterflow, helically wound, concentric tube configuration for the compact heat exchanger was considered for sizing purposes. The TVS flowrate will be 1.2×10^{-3} kg/s and will flow within the inner tube of the heat exchanger. Tank fluid, obtained from the LAD, will be circulated through the annular gap between the inner and outer tubes to decrease the temperature by 2.5 K. The subcooled liquid will be discharged through a 25.4 mm diameter jet. The axial jet mixer will be capable of operating at three different flowrates. The highest flowrate will be 0.023 kg/s, which should be sufficient to disrupt the ullage and establish a flow pattern of complete circulation in the tank under the most extreme COLD-SAT conditions. For lower mixer flowrates the TVS will be operated intermittently to insure no liquid is vented overboard. The outside diameters of the inner and outer

tubes will be 25.4 mm and 12.7 mm, respectively. The tube wall thickness is 1.27 mm. Tube lengths of 6.7 meters are required. The concentric tubes will be coiled into a helix, 305 mm in diameter and 175 mm in length. The compact heat exchanger will be mounted internally along the tank axis. A short heat exchanger is desirable to keep the exit of the axial jet submerged. The pressure drop through both sides of the heat exchanger will be less than 3.5 kPa.

At the highest mixer flowrate, the time required to completely mix the tank fluid will vary from 25 minutes for a tank that is 95 percent full, to 3 minutes for a 10 percent full tank. A 95 percent full tank can be thermally conditioned from 137.9 to 103.4 kPa in 2 hours using the active TVS. Less than 9 kg of hydrogen will be boiled off. For a 10 percent full tank, the conditioning time and mass boiled off will decrease to 36 minutes and 2.7 kg, respectively. These results are valid for a tank wall heat flux of 1.9 W/m².

5.9.2 Transfer and Pressurization Pumps

As the names indicate, the transfer pump transfers liquid between the supply and receiver tanks while the pressurization pump provides liquid to the evaporator which produces pressurant. The baseline requirements for these pumps (assuming a saturated or subcooled liquid with a fluid density of 70.48 kg/m³) are given in Table 5-3.

Table 5-3. COLD-SAT Pump Requirements

		Transfer Pump	Pressurization Pump
Volumetric Flow Rate	m ³ /s	3.155x10 ⁻⁴	9.464x10 ⁻⁶
Pressure Rise	Pa	3.447x10 ⁵	2.757x10 ⁵
Mass Flow Rate	kg/s	2.224x10 ⁻²	6.670x10 ⁻⁴
Head Rise	m	498.6	399.0
Ideal Input Power	W	109	2.61
Estimated Input Power	W	260	10

Both of these pumps have relatively low flowrates with high pressure rises which tends to drive the design toward a positive displacement type, especially for the pressurization pump. This can be seen by examining the specific speed, a dimensionless parameter used to compare pumps. It is defined as:

$$n_s = \frac{\omega \sqrt{Q}}{(gH)^{0.75}} \quad (5-1)$$

Figure 5-38 shows the various types of pumps and their best efficiencies as a function of specific speed. The lower specific speed pumps (piston or vane) are classified as positive displacement pumps. In these pumps, the fluid is moved to a higher pressure region by reducing the volume of a chamber which is momentarily sealed off from the lower pressure region. The other pumps are classified as non-positive displacement, in which the static pressure is increased by adding kinetic energy and then diffusing the flow e.g., centrifugal.

Since the flow and head requirements for COLD-SAT have been fixed, only the rotational speed is left as a variable. In order to use a centrifugal pump ($n_s = 0.2-2.0$), the rotational speed must be

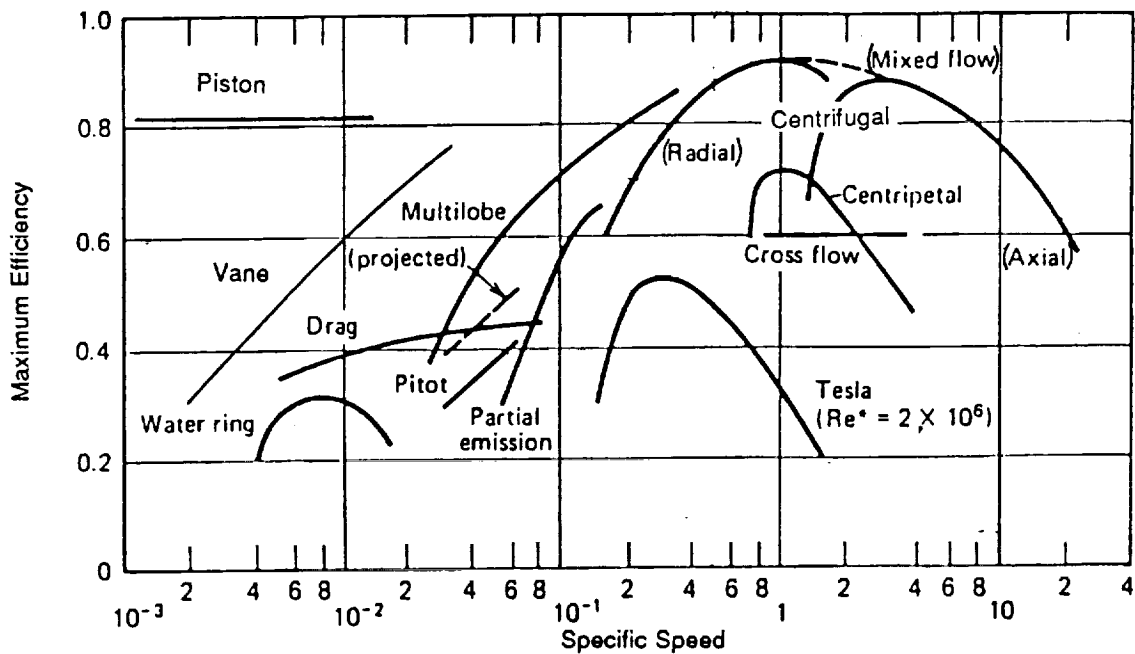


Figure 5-38. Maximum Efficiency versus Specific Speed for Various Pump Types (References 5-2 and 5-3)

Table 5-4. Development Pump Specifications

		Sundstrand: Dual Lobed, Vane with Boost Stage 3 Ø Induction Motor Ball Bearings		AiResearch: Centrifugal Permanent Magnet Motor Foil Bearings	
		Transfer Pump	Pressurization Pump	Transfer Pump	Pressurization Pump
Rotational Speed	Rad/s	795.9	397.9	6283-7330	6283-7330
Specific Speed		0.0242	0.00256	.191-.223	.0392-.0456
Motor Efficiency		0.88	0.8	.90-.95	.90-.95
Vane Stage Efficiency		0.35	0.5	-	-
Centrifugal Stage Eff.		-	-	0.7	0.6
Overall Efficiency		0.25	0.35	0.50-0.60	0.40-0.50
Input Power	W	444	7.5	185-222	5.2-6.5
Weight	kg	2.95	2.22	2.04	2.04
Size Envelope	m	0.109 Dia X .155 Lg	0.109 Dia X .142 Lg	0.0635 Dia X .140 Lg	0.0635 Dia X .140 Lg

high (> 6580 rad/s). High rotational speeds necessitate non-contacting bearings, e.g. magnetic or gas, for high reliability since bearing life is a function of rotational speed. A vane pump ($n_s = 0.002-0.04$) would run at much lower rotational speeds (< 987 rad/s). Thus, a more conventional ball bearing system could be used.

No off-the-shelf pumps exist that can meet the COLD-SAT requirements. Table 5-4 summarizes preliminary size, weight, and power information for development pumps. This information is based on design points of 3.447×10^5 Pa at 2.224×10^{-2} kg/s and 2.757×10^5 Pa at 6.670×10^{-4} kg/s for the transfer and pressurization pumps respectively. Note that the development transfer pump has a higher pressure rise than the current COLD-SAT requirements shown in Table 5-3.

The proposed Sundstrand pumps are based on work which they performed for NASA/LeRC on the LOX/LH₂ Boost/Vane Pump for the Advanced Orbit Transfer Vehicle Auxiliary Propulsion System (Reference 5-4) in 1979. This pump was built (without the boost stage) and tested in LN₂ (Reference 5-5). It apparently operated well but its performance was slightly less than predicted. Predicted overall efficiency for the vane stage of the test pump was about 50 percent while the measured efficiency was only about 40 percent. The three phase induction motors which would drive the Sundstrand pumps are based on the Space Shuttle LH₂ recirculation pump motor. A motor controller/power converter would be needed for each of the drives.

AiResearch proposes a centrifugal design based on their experience with centrifugal compressors/pumps and foil bearings. Higher rotational speeds are necessary for these pumps, hence the requirement for non-contacting bearings. AiResearch proposes to use the same basic pump for both transfer and pressurization applications, substituting a smaller impeller for the pressurization pump. This would result in a specific speed well below that normally found with centrifugal pumps, and could degrade pump efficiency.

Creare, Inc. has developed and tested two LHe pumps (Reference 5-6) for ground applications. These were high speed ($\sim 10,000$ rad/s) centrifugal pumps with gas bearings. Currently they are working on a lower speed (2500 rad/s) LHe pump with ball bearings. Also, they are developing electromagnetic bearings for high speed turbomachinery. These technologies could be applied to the COLD-SAT pumps.

Sundstrand's vane with boost stage design may be better suited for the low flow, high head requirements of COLD-SAT, since its specific speed is low. Also, it is capable of ingesting 10 percent vapor by volume. However, the three phase induction motor would require additional power conditioning equipment.

Based on the above considerations, the present recommendation for the COLD-SAT pumps is to use the Sundstrand pump design with a DC motor drive system. The present fluid subsystem design, as described throughout this report, is based on this approach with separate transfer and pressurization pumps. However, a single pump option was also considered in which one pump would provide both the liquid transfer between tanks and the liquid supply for the evaporator. This pump would be sized to the transfer pump requirements and the small flowrate required by the evaporator would be obtained by tapping into the transfer line downstream of the pump. This option reduces the pump development effort by eliminating one of the pumps. However, the initial pressure ramping of the supply tank would require either stored pressurant or a boot strap start-up to prevent cavitation at the pump inlet. This option should be more thoroughly analyzed in future COLD-SAT studies.

5.9.3 Autogenous Pressurization System

The autogenous pressurization system is used to generate cold hydrogen gas to be used as pressurant during four of the pressurization tests and during liquid transfers. This system consists of a pump,

an evaporator, an accumulator, and some valves as shown in the Fluid System Schematic, Figure 5-1. The pump provides the evaporator with liquid hydrogen which is then vaporized and slightly superheated. The hydrogen gas at about 0.4 MPa then flows either to the accumulator or to the tank being pressurized as required by demand.

5.9.3.1 Pressurization Pump. This pump provides liquid hydrogen at $9.46 \times 10^{-6} \text{ m}^3/\text{s}$ with a 0.276 MPa pressure rise and it is described in further detail in Section 5.9.2.

5.9.3.2 Evaporator. The evaporator shown in Figure 5-39 consists of a 76.2 mm diameter, 203 mm long helical coil with a 6.35 mm square flow channel. An electric heater is attached to the outside of the coil. This heater provides about 300 W which is needed to vaporize and slightly superheat the hydrogen. The approximate calculations used to obtain this preliminary design are described below.

As a conservative estimate of the boiling heat transfer coefficient, the Dittus-Boelter forced convection correlation was used.

$$\text{Nu} = \frac{hd}{k} = 0.023 \text{ Re}^{0.8} \text{ Pr}^{0.4} \quad (5-2)$$

This should be conservative since the heat transfer coefficient for boiling heat transfer changes with the flow regime (Reference 5-7) as shown in Figure 5-40. The heat transfer coefficient peaks in the annular flow regime with the subcooled liquid and superheated vapor heat transfer coefficients being about the same. The Schmidt correlation for helical flow passages (Reference 5-8) was used to adjust h to account for the helix.

$$\frac{h_c}{h} = 1 + 3.6 \left(1 + \frac{d}{D_p}\right) \left(\frac{d}{D_p}\right)^{0.8} \quad 20,000 < \text{Re} < 150,000 \quad (5-3)$$

Using this heat transfer coefficient (h_c) and assuming a ΔT (between the wall and fluid) of about 4 K, gives a heat transfer area requirement of 0.0685 m^2 . This can be accomplished with a 76.2 mm diameter coil which is 203 mm long assuming a fin efficiency of zero on the radial fins.

To insure that the design of the evaporator wouldn't produce film boiling, the minimum ΔT for stable film boiling (or Leidenfrost point) was calculated. This condition is given by Berenson in Reference 5-9 as:

$$\Delta T_{\min} = 0.127 \frac{\rho_v h_{fg}}{k_v} \left[\frac{g(\rho_l - \rho_v)}{(\rho_l + \rho_v)} \right]^{\frac{2}{3}} \left[\frac{g_c \sigma}{g(\rho_l - \rho_v)} \right]^{\frac{1}{2}} \left[\frac{\mu_v}{g(\rho_l - \rho_v)} \right]^{\frac{1}{3}} \quad (5-4)$$

For our case this yields a value of about 92 K, thus there is no danger of film boiling.

As a "rule-of-thumb", the upper bound of the pressure drop can be obtained by assuming pure vapor flow throughout the evaporator and doubling the resulting value. The straight pipe friction factor is modified by the Schmidt correlation for helical passages (Reference 5-8).

$$\frac{f_c}{f} = 1 + 0.0823 \left(1 + \frac{d}{D_p}\right) \left(\frac{d}{D_p}\right)^{0.53} \text{ Re}^{0.25} \quad 22,000 < \text{Re} < 150,000 \quad (5-5)$$

The resulting total pressure drop through the evaporator is less than 11.8 kPa.

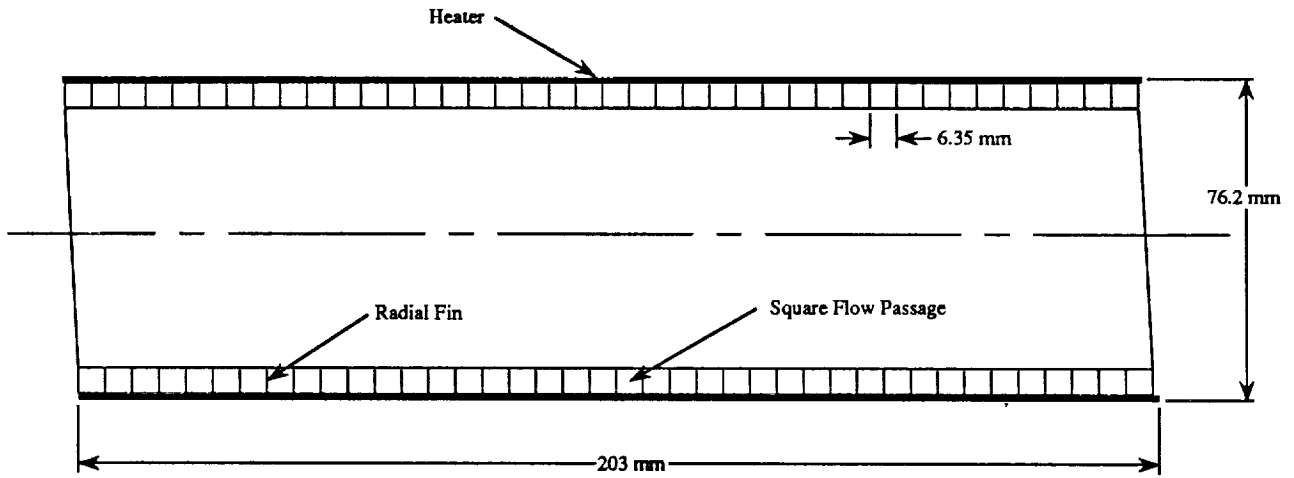
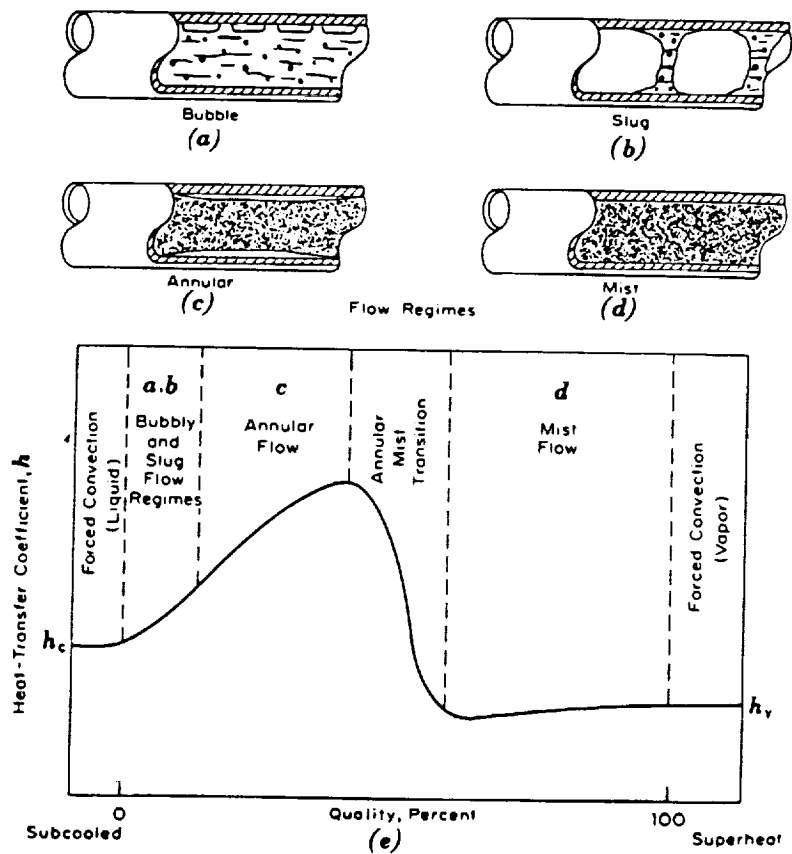


Figure 5-39. Cross Section of Helical Evaporator



(Taken from Reference 5-7)

Figure 5-40. Forced Convection Boiling Heat Transfer Coefficients

5.9.3.3 Accumulator. The cylindrical accumulator has a volume of 0.00439 m³. It provides a capacitance for the system so that pressurant flowrate transients can be accommodated without a serious drop in pressure. A larger accumulator volume may be desirable to reduce the duty cycle of the pressurization pump. This should be the subject of future analysis in conjunction with detailed control system design for the autogenous pressurization system.

5.9.3.4 Control Scheme. The control scheme for the autogenous pressurization system is to turn the pressurization pump on and off depending on the accumulator pressure and to control the evaporator heater with temperature sensors in both the exit flow stream and the evaporator wall. Control logic will turn on the evaporator heater prior to starting the pump if the evaporator temperature is too low. This will prevent heater power from being absorbed by the thermal mass of the evaporator when the pump is on. Thus, liquid will not exit the evaporator due to start-up transients. A detailed control analysis has not been done but this scheme appears feasible.

5.9.4 Outflow Subcooler

The outflow subcooler will be used to subcool liquid for transfers between tanks. It will consist of a throttling valve and a counterflow, concentric tube heat exchanger. Liquid from the supply tank LAD will be subcooled as it flows through the annular gap between the inner and outer tubes. Fluid from the supply tank will be throttled to a lower pressure (~34.5 kPa) and temperature through a J-T valve and routed through the inner tube of the subcooler heat exchanger. The maximum liquid flowrate expected is 0.0227 kg/s. To subcool the liquid by 2.6 K, a TVS flowrate of 0.00122 kg/s is required. Due to this low flowrate, Viscojets are being considered for the throttling device. For lower liquid flowrates, the TVS will be operated intermittently to insure no liquid is vented.

The subcooler heat exchanger is similar in design to the compact heat exchanger used for the active TVS described in Section 6.3. The inner and outer tubes will have 1.27 mm wall thicknesses and outside diameters of 12.7 and 25.4 mm, respectively. The tube length required to completely vaporize the TVS fluid is 9.75 meters. When coiled into a 152.4 mm diameter helix, the overall length of the subcooler heat exchanger will be 520 mm. The pressure drop for the TVS flow through the inner tube will be less than 3.5 kPa. Less than 0.9 kPa of pressure drop was calculated for the liquid flow through the annular gap between the inner and outer tubes.

5.9.5 Stored Gas Pressurization System

5.9.5.1 Hydrogen Gas Storage Bottles. Two high pressure hydrogen gas storage bottles are located aft on the Earth/anti-Earth axis of the spacecraft, and are supported by the spacecraft bus primary load-carrying structure called the central cylinder (Figure 5-41). The bottles are manifolded together and plumbed to a hand-operated loading valve located on the Earth panel and to a pressure control module which is located in the same vicinity. Cut outs in bus body panels permit locating the bottles inboard to minimize the length of the structural supports. Each bottle has a micrometeoroid/debris shield which is attached to the bus body panels after the bottles and plumbing have been installed and checked out.

The bottle design uses a thin aluminum alloy liner in the form of a cylinder with elliptical bulkheads at each end. At the end of one bulkhead is a fitting machined from a diffusion bonded block of aluminum-to-CRES material, which provides a CRES stub-up for attaching plumbing by the orbit arc welding process. The opposite bulkhead is equipped with an aluminum fitting for attaching supports. This fitting is not attached to the bulkhead but is held in place by the outer windings. The aluminum liner and fittings are covered with glass scrim cloth and the entire assembly wound with carbon filaments. The glass scrim is needed for electrolytic corrosion protection between the graphite and the aluminum.

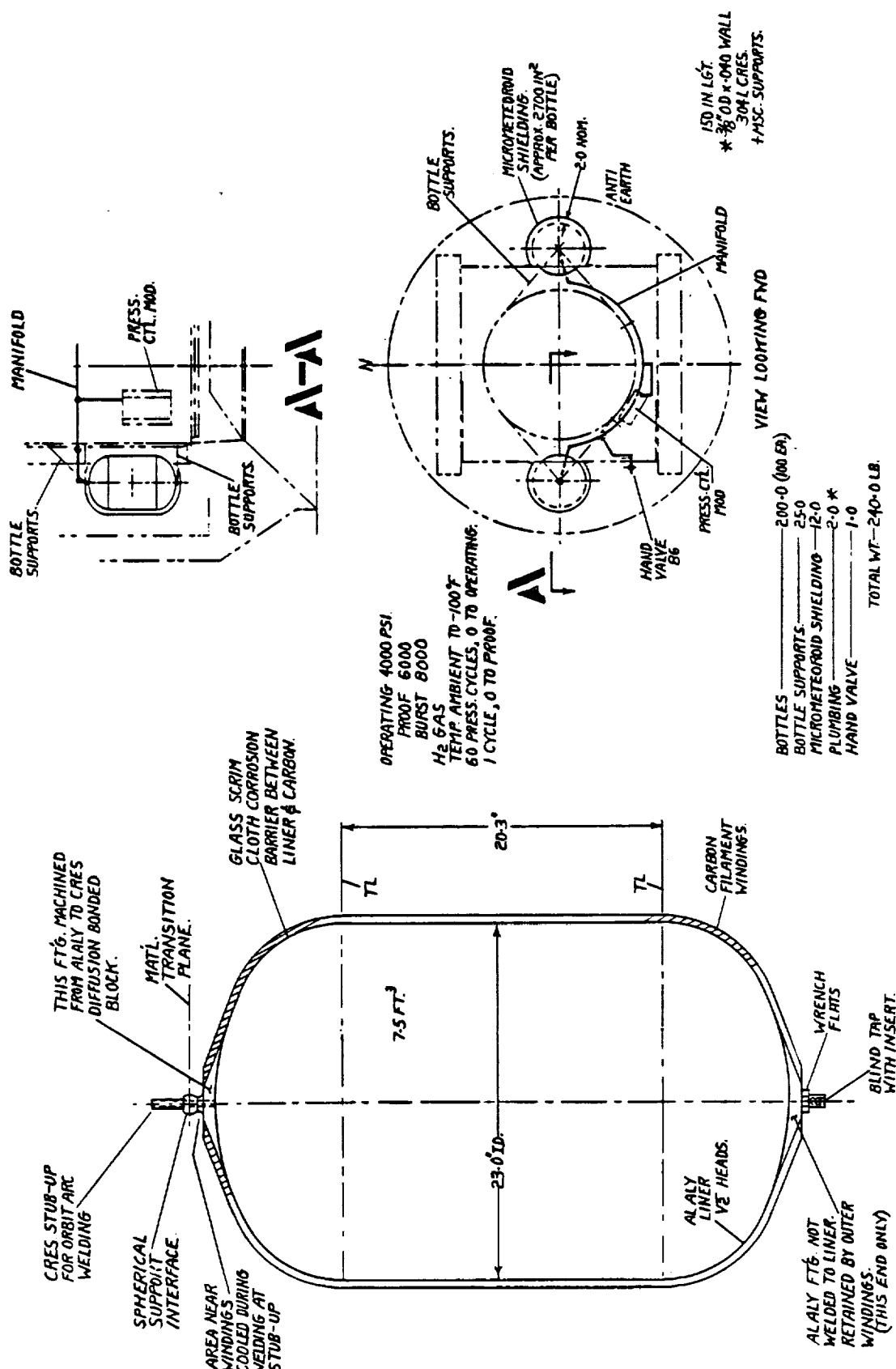


Figure 5-41. Hydrogen Gas Storage Bottles

During the study other high pressure bottle materials were considered, but were found to be unacceptable. Earlier in the program we were considering the use of cryo-formed CRES bottles, but these are susceptible due to potential hydrogen embrittlement. Also, the use of Kevlar was found to be unacceptable with an aluminum liner since the stretch of the Kevlar can cause unacceptable stresses in the liner, leading to failure. Thus, the use of an aluminum liner with a graphite wrap was adopted as the best approach.

5.9.5.2 Helium Gas Storage Bottle. One high pressure helium gas storage bottle is located near the forward end of the bus central cylinder in the corner formed by the Earth panel and north panel (Figure 5-42). The bottle is supported from the central cylinder and is plumbed to a hand-operated loading valve and to the pressure control module.

The bottle design uses a thin corrosion resistant steel (CRES) liner consisting of a short cylinder with an elliptical bulkhead at each end. One bulkhead is attached to a fitting which incorporates a stub-up for orbit arc welding and an interface for supports. The opposite bulkhead is equipped with a fitting for attaching supports only. This fitting is not attached to the liner but is held in place by the outer windings. The CRES liner assembly is wound with carbon filaments.

5.9.6 Valves and Regulators

As evident in the fluid system schematic, Figure 5-1, the COLD-SAT design incorporates many different components. These components are listed by identification number in Appendix B. Table 5-5 summarizes the component types with the quantity required and the mass allocated to each item. This section discusses the requirements for the generic components such as valves and regulators including the current design baseline and alternatives.

5.9.6.1 Cryogenic Valves. These valves are used for control of tank-to-tank transfer and of cold-vapor pressurization flow. To perform these functions, the valves must be qualified for liquid hydrogen (LH₂) service with a maximum operating pressure of 350-500 kPa. External leakage must be very low to avoid hazards associated with hydrogen but some small internal leakage can be tolerated (<20 scc/min).

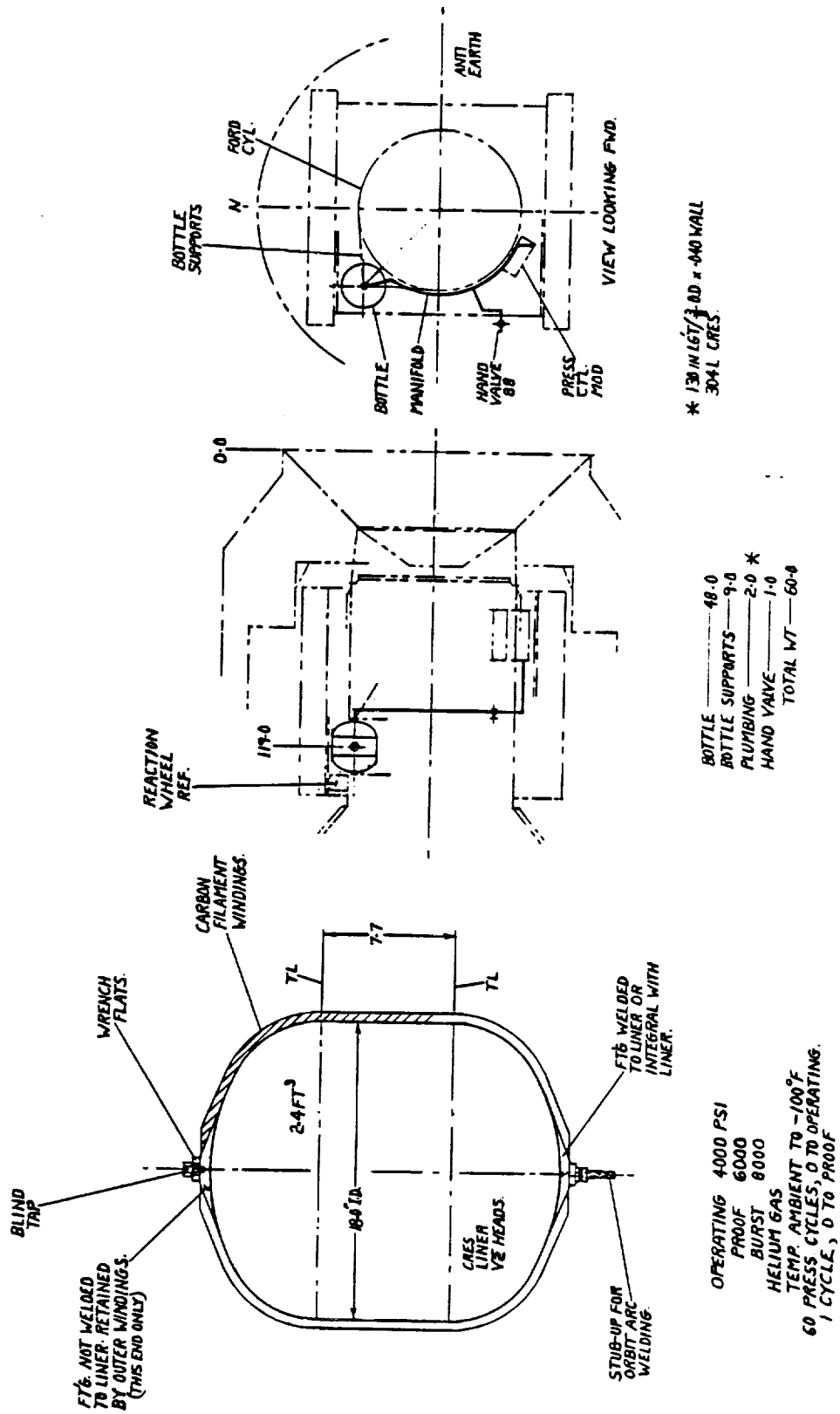
Shutoff valves are used throughout the fluid system to control flow direction, to isolate subsystems and to regulate flowrate. In general, the valves must be capable of flowing and sealing in both directions and must operate fairly quickly (<1 second to change position). Power consumption and heat input to the LH₂ should be minimized in the actuator design.

Flow requirements for the shutoff valve applications vary considerably. A preliminary trade study indicated that a total of two valve sizes would provide the best combination of performance and development cost. For nominal line sizes of 6.4-9.5 mm (0.25-0.38 inches), a valve with an equivalent sharp-edged orifice diameter of 6.1 mm is specified. For line sizes of 12.7-19 mm (0.5-0.75 inches), the specified orifice diameter is 10.4 mm.

The baseline shutoff valve design is a floating-seal gate valve based on a Valcor concept shown in Figure 5-43. The gate valve configuration provides for a relatively light and compact package and, with the floating seal, can provide adequate isolation in both directions when closed.

Poppet valve concepts were also investigated such as the concept provided by Consolidated-Eaton Corp. shown in Figure 5-44. In general, the poppet valves designed to these requirements are more complicated and more expensive than the gate valve.

The selected actuator design uses a latching solenoid as shown in the Valcor drawing (Figure 5-43).



* 1/30 IN LST/3 RD x .040 WALL
304L CRES.

BOTTLE SUPPORTS	48-0
PLUMBING	9-0
HAND VALVE	2-0 *
TOTAL WT	1-0
	60-8

OPERATING 4000 PSI
 PROOF 6000
 BURST 8000
 HELIUM GAS
 TEMP AMBIENT TO -100°F
 60 PRESS CYCLES, 0 TO OPERATING.
 1 CYCLE, 0 TO PROOF.

Figure 5-42. Helium Gas Storage Bottle

Table 5-5. Summary of Fluid Component Types being used on COLD-SAT

TYPE	NOMINAL LINE DIAMETER, mm (inches)	QUANTITY	MASS (kg)	COMMENTS
LH2, 350-500 kPa max				
accumulator	---	1	2	
diffuser	9.5/6.4 (0.38/0.25)	3	1	
disconnect, self-sealing	19/12.7 (0.75/0.5)	2	0.5	
disconnect, non-sealing	12.7 (0.5)	1	0.5	
evaporator	9.5 (0.38)	1	1	
filter, cryogenic	6.4 (0.25)	3	0.5	
flowmeter, 2-phase	19/12.7 (0.75/0.5)	6	3	Bi-directional
flowmeter, gas	9.5/6.4 (0.38/0.25)	6	2	Uni-directional
orifice	12.7 (0.5)	1	0.2	
	9.5 (0.38)	1	0.2	
	6.4 (0.25)	6	0.1	
pump	19 (0.75)	2	3	
	6.4 (0.25)	1	3	
subcooler	---	1	5	
TVS, compact	6.4 (0.25)	1	9	
valve, check	12.7/9.5/6.4 (0.5/0.38/0.25)	7	0.2	
valve, relief	12.7/9.5 (0.5/0.38)	11	1	
valve, shutoff, cryogenic	19/12.7 (0.75/0.5)	31	2	Orifice* = 1.04 cm
	9.5/6.4 (0.38/0.25)	37	1.5	Orifice* = 0.61 cm
GH2/GHe, 27.5 MPa max				
bottle, helium	---	1	27	Incl. shield. & supprt.
bottle, hydrogen	---	2	55	"
filter, high-pressure	9.5 (0.38)	2	0.2	
regulator, high-pressure	9.5 (0.38)	2	3	
valve, manual	9.5 (0.38)	2	0.5	
valve, shutoff, high-pressure	9.5 (0.38)	2	1.5	

* Equivalent Sharp Edged Orifice Size

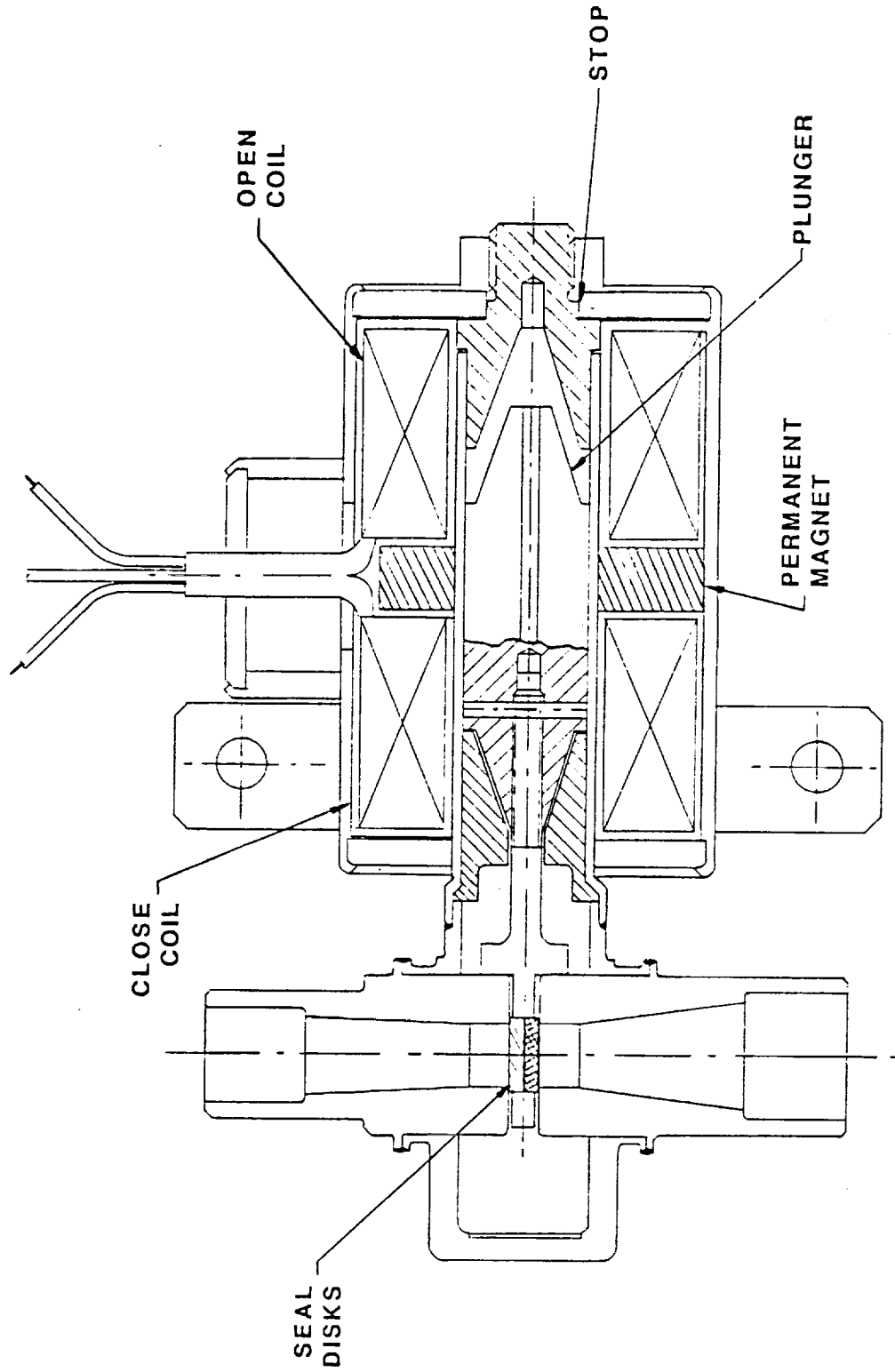


Figure 5-43. Valcor's Floating Seal Gate Valve Concept

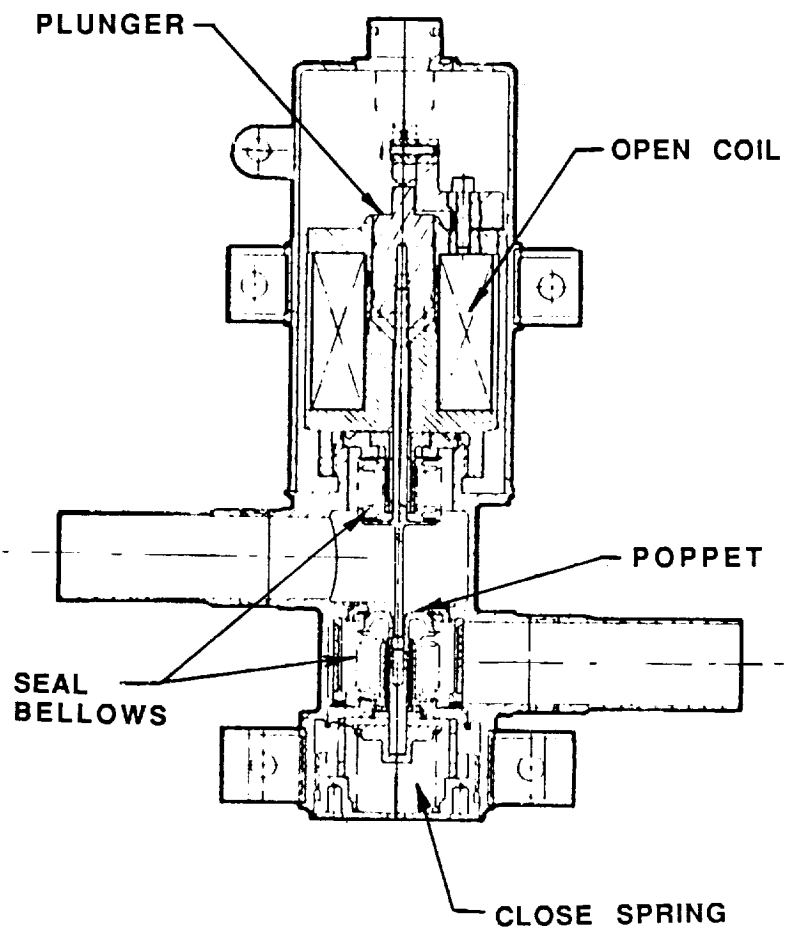


Figure 5-44. Consolidated's Poppet Valve Concept

This approach uses two coils; one to open and one to close. A permanent magnet "latches" the valve to the last commanded position. A single solenoid with an opposing spring is less desirable since it would continuously draw current and add too much heat to the LH2 flow when the valve was actuated. Motor-driven and pneumatic actuation concepts tend to be more complex and not justified for small applications such as this.

Relief valves provide mechanical backup for pressure relief of tanks and lines. This valve must be adjustable to relieve at a pressure in the range of 300-600 kPa within 20 kPa of the set pressure. Flow requirements for these valves have not yet been analyzed but it is expected that a nominal 12.7 mm (0.5 inch) size will be adequate.

Check valves are used primarily to minimize heat leak into the tanks by preventing backflow of the pressurization and nozzle supply lines. To reduce development costs, one check valve will be designed to meet all system requirements. This valve will be for a nominal 12.7 mm (0.5 inch) line diameter.

5.9.6.2 High-Pressure Components. The components for the stored gas pressurization system must be qualified for GH₂ and GHe at temperatures as low as ~160 K. The maximum operating pressure is 27.5 MPa.

The shutoff valves for this system will be used to isolate the high-pressure gas supplies from the pressurization system when it is not being used to provide the pressurant. These valves are required to flow and seal in just one direction but against a high pressure difference (27.5 MPa).

Similar shutoff valves are required to isolate the bottles from their charge port to allow the ground supply to be disconnected and capped after the bottles are filled. Since this is a manual operation, these valves can use manual screw-type stems. These valves must flow in both directions but need only seal in one direction to prevent significant leakage from the bottles.

Many existing valve designs are under consideration for both the remote and manual shutoff application. Poppet valves are preferred to provide low-leakage ability. A latching solenoid actuator design as described for the cryogenic shutoff valves is baselined for the remotely-controlled valves.

The pressure regulator for the stored gas pressurization system has to regulate its downstream pressure to ~400 kPa. The inlet pressure to the regulator can be as high as 27.5 MPa when the bottles are fully charged. To accommodate this large reduction in pressure, a two-stage design which controls to an intermediate pressure within the component may be advantageous. The set point of the regulator must be adjustable with a maximum error of ± 20 kPa.

5.10 INSTRUMENTATION, POWER AND CONTROL

5.10.1 Instrumentation Summary

5.10.1.1 Requirements. The instrumentation measurement requirements, summarized in Table 5-6, consist predominantly of the parameters required to monitor status of the experiments. The list also includes those measurements which monitor the health of the power conversion equipment.

5.10.1.2 Instrumentation System Design. The instrumentation system, illustrated in Figure 5-45, consists of dual redundant DCUs, a signal conditioner, the transducers and the associated wiring. The data concentrator units (DCUs), signal conditioner, accelerometers and flow meter electronics are physically located in the spacecraft bus. The remainder of the transducers are distributed throughout the experiment module. Signal types include low-level analog, high-level analog, bi-level and serial digital. A description of the various circuit configurations is provided in the following paragraphs and a block diagram of each configuration is provided in Appendix C.

Table 5-6. COLD-SAT Measurement Requirements

MEASUREMENT TYPE	TANK 1	TANK 2	TANK 3	OTHER	TOTAL
ACCELERATION				18	18
CURRENT	1	2	2	13	18
FLOW	1	2	2	7	12
LIQUID/VAPOR STATE	33	24	27		84
PRESSURE	8	6	6	11	31
TEMPERATURE	145	79	56	47	327
VALVE STATUS	31	17	17	5	70
VOLTAGE				4	4

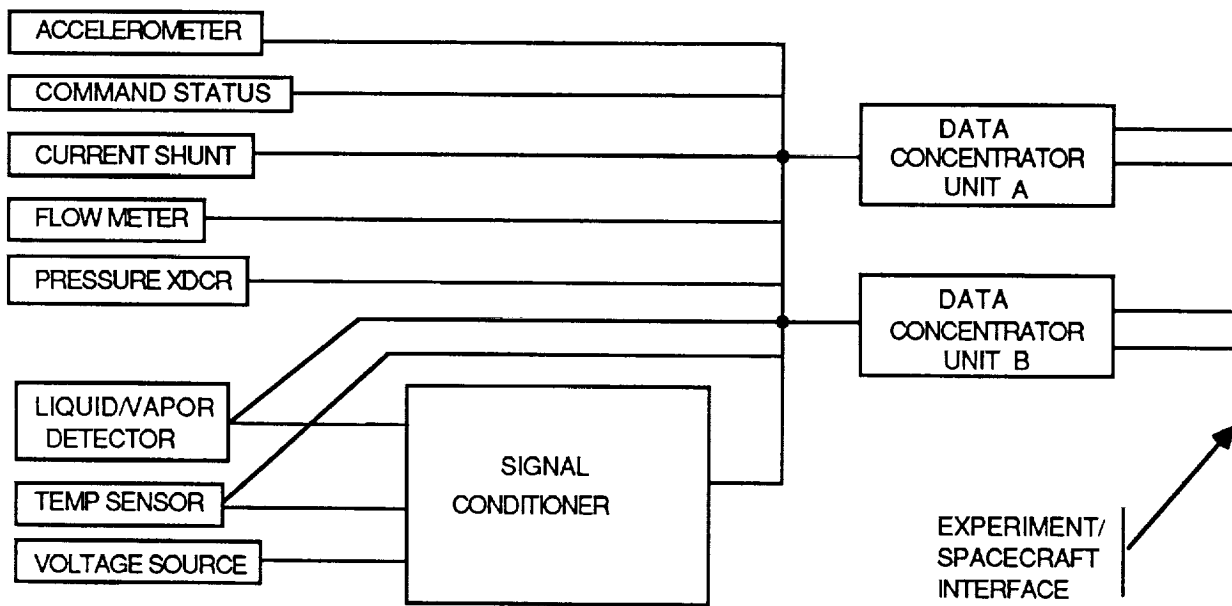


Figure 5-45. Instrumentation Block Diagram

Acceleration

Measurement of micro-G accelerations is required in many of the experiments. The miniature electrostatic accelerometer (MESA), manufactured by Bell Aerospace - Textron was selected for this measurement. The MESA provides three ranges with autoranging. The unit will have ranges of +/- 100, +/- 250 and +/- 500 micro-G. The output voltage will be scaled to provide 0 to 5 V for compatibility with the high-level analog input of the DCU. The axial acceleration will be sampled at 8 samples per second (SPS) and the other axes will be sampled at 4 SPS. Triple redundancy will be utilized to satisfy reliability requirements. The temperature environment will be maintained within the specified 250 K to 344 K operating range of the accelerometer.

Command Status

Command status signals for activities such as valve operation are monitored on bi-level channels of the DCU at a sample rate of 1 SPS.

Current

Current shunts were selected as the transducer for the current measurements primarily for reliability reasons. The shunt output signal is connected to a low-level analog input of the DCU and sampled at 1SPS.

Flowrate

The transducer proposed to measure two-phase fluid flow is being developed by Quantum Dynamics. The output signal is serial digital RS-232, sampled at 2 SPS. The transducer electronics are mounted in the temperature-controlled environment of the spacecraft bus. Other recommended flowmeters for measuring single-phase liquid and vapor flows are described in Section 5.11.

Liquid/Vapor State

The liquid/vapor detector (57-01004) designed for Titan/Centaur is proposed for the COLD-SAT application. The sensor is a deposited carbon resistor that changes resistance when submerged in liquid hydrogen. The sensor forms part of a voltage divider so that when the sensor resistance changes, the voltage to the DCU changes to identify the change in fluid state. The excitation for the circuit is provided from the instrumentation 5 Vdc. The signal output is monitored on a bi-level channel and sampled at 1 SPS.

Pressure

The pressure measurements are made with the Statham model PA8224 cryogenic pressure transducer which utilizes a sputtered thin film strain gage technology. Statham can provide temperature compensation of these units down to 27 K. The unit, excited from the instrumentation 10 Vdc power supply, provides a nominal 30 mV full scale output. The signal output is monitored on a low level analog channel of the DCU. These parameters are also sampled at one second intervals.

Temperature

Most of the experiment parameters are temperatures. Platinum resistance sensors will be used for these measurements. For those parameters that require high precision in the region of liquid hydrogen temperatures, a narrow temperature range will be used together with a large sensor resistance. The temperature multiplexer of the DCU will provide dual, matched, multiplexed, constant current sources for the sensor excitation and amplification of the sensor output. These measurements will be sampled at intervals ranging from 1 to 300 seconds.

Voltage

The various buss voltages will be monitored to determine the status of the experiment power conditioning equipment. Voltage dividers will be used for voltages greater than 5 V. These parameters will be monitored on high-level analog channels and will be sampled at one second intervals.

5.10.2 Experiment Power Requirements

The power requirements of the experiment equipment are summarized in Table 5-7. The table shows the major power consuming components, the voltage required for their operation, and the number of individual units in the system. For each type of component, three sets of power values are indicated. The first is the power consumption of an individual unit when it is on. The second is an estimate of the maximum average power required during an orbital period of approximately 112 minutes. The third is the estimated average power during the entire mission, which lasts approximately 64 days. Both the regulated and unregulated power is indicated, and the efficiency of conversion for all dc-to-dc converters was assumed to be 90%. This is consistent with existing hardware.

The system has three accelerometers, two of which are operational at any one time. The Data Concentrator Units (DCUs) operate on unregulated power and, only one of the two units is normally on. Twelve flowmeters are contained in the system but the equivalent of only three are on continuously. Over selected orbital periods, as many as 7 could be used simultaneously.

The estimates for the average power required for the evaporator heater are based on the calculated pressurant requirements for the mission and for a typical pump-assisted no-vent fill of Tank 2. The resulting values are 100 watts during the orbital period and 13 watts over the mission. Most of the heaters can be operated on unregulated power. However, the Tank 1 heater is provided 28V regulated power because of the accurate control required for the supply tank pressure control experiments. Similar to the evaporator heater, the pressurization pump average power was calculated based on the cold vapor pressurant requirements of the experiments. The transfer pump, together with the transfer pump controller power requirements, are based on the test sequence for our experiments and the predicted transfer times. This pump can be on during about 2/3 of the orbit period, but is only on about 3 percent of the time overall. The liquid/vapor detectors and the pressure transducers require very little power and are assumed to be on continuously. Valves require substantial power during actuation, but very little on average.

Of particular interest is the maximum average power during any one orbit period, for this must not exceed the available 800 watts unregulated power from the spacecraft. Peak loads, somewhat greater than the 800 watts can be accommodated as long as the average is less than the 800 watts. An approximate value for the power required for experiment operations during an orbital period can be obtained by adding up the values in the table with double asterisks on them. This total is 503 watts and is considerably under the 800 watt available average power. However, at particular times during the experiment operations, the power requirements can exceed the 503 watt value. For example, the transfer pump, the pressurization pump, the evaporator heater, and the several other units could be operating simultaneously. This would require approximately 1kw, but this short term power level can be accommodated as long as the orbital average remains under the 800 watts.

Due to the wide voltage range, 30 to 42 V, of the unregulated voltage from the spacecraft, it is necessary to regulate the voltage for most of the experiment power requirements. The experiment power distribution schematic is illustrated in Figure 5-46. Power is supplied to the DCUs and all of the heaters, except the Tank 1 heater, from the unregulated power buss. The DCU is designed to operate from the unregulated power. The 28 V dc/dc converter is primarily required to provide power for the ECU, the accelerometer and the Tank 1 heater. The Tank 1 heater is powered from the regulated 28 V to permit a more accurate record of the input power. Also, the input power to the Tank 1 heater is only about 30 W. However, to derive the other voltages from the unregulated power buss would require substantial design/development costs. So, in an attempt to eliminate these costs, the inverter, the 5 V and 10 V converters are driven by the 28 V converter. This will improve the probability of obtaining off-the-shelf hardware.

Table 5-7. Experiment Equipment Power Requirements

Components	Voltage	Number of Units	Unit Power Required when ON		Estimated Average Power for the Units that are Operating				Notes
			Reg. (watts)	Unreg.* (watts)	Max. During an Orbit		During Mission		
					Reg. (watts)	Unreg.* (watts)	Reg. (watts)	Unreg. (watts)	
Accelerometers	28	3	8	9	16	18**	16	18	2 of 3 operating continuously
Data Concentration Unit (DCU)	30-42	2	-	7.5	-	7.5**	-	7.5	One unit operating
Flowmeters	28	12	10	11	70	78**	30	33	
Heater, Evaporator	30-42	1	-	300	-	100**	-	13	
Heater, LAD, Tank 2	30-42	1	-	100	-	33	-	negl	
Heater, Tank 1	28	1	30	33	30	33	5	6	
Heater, Tank 2	30-42	1	-	200	-	200	-	8	
Heater, Tank 3	30-42	1	-	200	-	200	-	21	
Heater, Vent line	30-42	1	-	200	-	TBD	-	TBD	
Heater, Tank 3 line	30-42	1	-	200	-	TBD	-	TBD	
Liquid/Vapor Detectors	5	84	0.02	0.02	2	2**	2	2	All units on, 20 milliwatts each.
Pressure Transducers	10	31	0.3	0.37	9	11**	9	11	All units on, 286 milliwatts each.
Pump, Pressurization	28	1	10	11	3	3**	<1	<1	
Pump, Transfer	28	1	260	289	173	192**	9	10	
Tank 1 Mixer	28	1	~5	<1	2	<1	<1	<1	
Transfer Pump Controller	28	1	29	32	20	22**	1	1	
Valves	28	70	24	27	2	2**	1	1	3 amp maximum for 0.3 secs during actuation

* All dc/dc converter efficiencies were taken as 90%. Five and ten volt power requires the use of two converters, and therefore results in an 81% efficiency.

** Approximate values of simultaneous power consumers. Their total is 503 watts, compared to 800 watts available from the spacecraft.

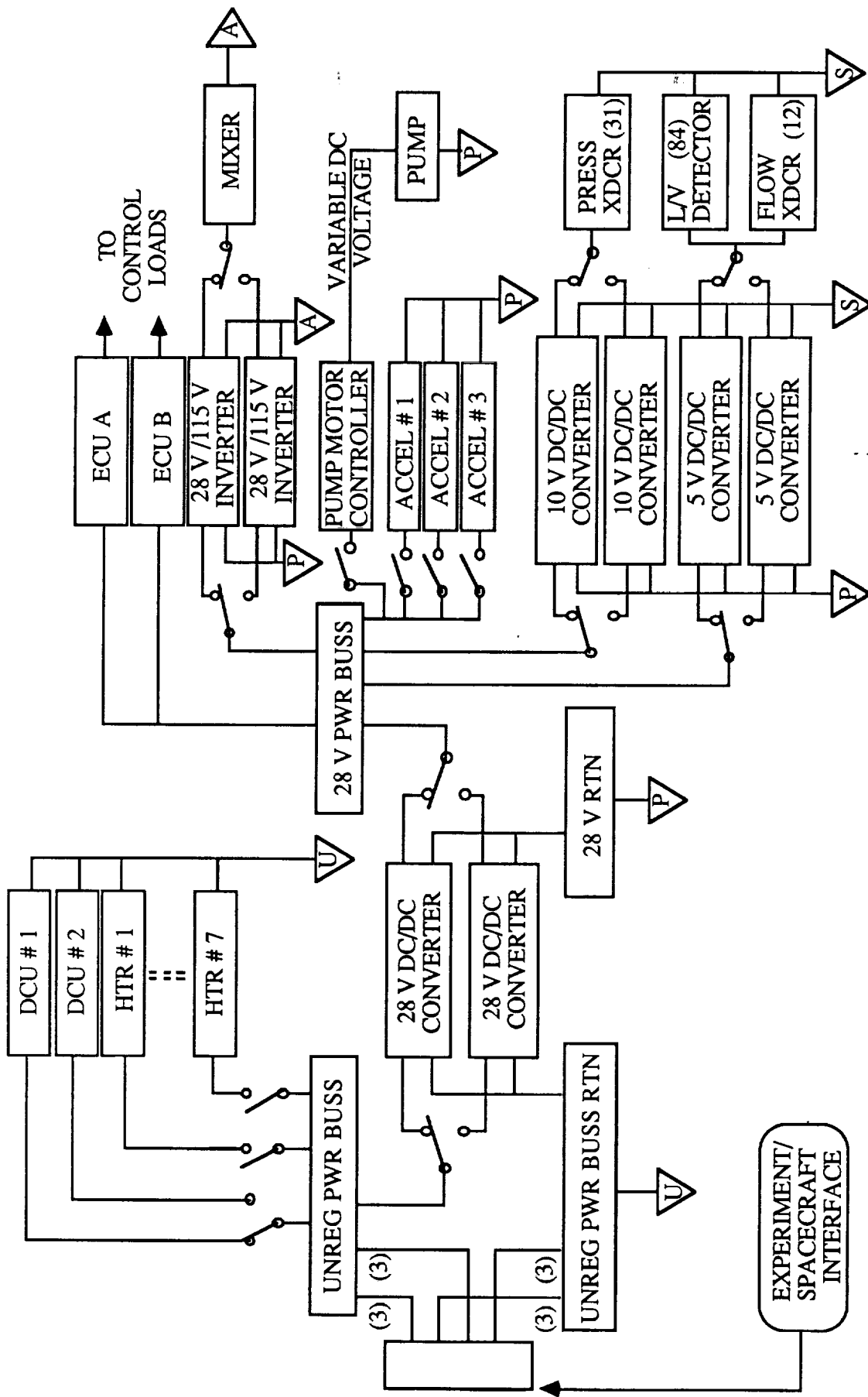


Figure 5-46. Power Distribution Block Diagram

5.10.3 Experiment Control Concept

Figure 5-47 is a block diagram that identifies that portion of the control system for which GDSS is responsible and Table 5-8 provides a summary of the experiment commands. Operations required to perform the experiments are under the control of the experiment software which resides within the control processor of the spacecraft electronics. For example, a command is issued from the control processor, in the sequence programmed in the experiment software, to the DCU. The DCU decodes the command to determine the command type and the destination of the command. The command is then routed to the experiment control unit (ECU) where it operates a power control device to supply the required power to the appropriate component. Latching valves are used to conserve power. Also, valve commands are issued sequentially where ever possible to reduce peak power requirements. Although the experiment functions are primarily performed autonomously, the capability exists to modify the experiment software from the ground via a command uplink.

5.11 EXPERIMENT COMPONENTS AND DEVELOPMENT STATUS

COLD-SAT experiment components are grouped into two categories for the purpose of listing development status. The first category is avionics, and includes instrumentation hardware such as pressure, temperature, and flow measurement transducers, harnesses, and associated signal conditioning equipment and control electronics. The second category is mechanical equipment, and includes hardware such as valves, regulators, tanks, filters, and fluid mixers. Table 5-9 and Table 5-10 list the components in these two categories.

The development status of each component is rated in accordance with the NASA/LeRC statement of work guidelines for categorizing risks. Development status is rated A thru D according to the following definitions: Category A contains those elements for which existing hardware or qualified designs may be used. Category B contains those elements which require new designs but for which existing, proven design techniques are available. Category C contains those elements which require new designs and are at or near the state-of-the-art for the technical discipline involved. Category D contains those elements which require new designs which are beyond the current state-of-the-art.

Sources for the components were selected after an evaluation of many alternatives, and considered reliability requirements and the technical risks. Those items listed as Categories C and D were reviewed for alternative solutions. The Category D mass gage which was under development by Ball Aerospace was eliminated from the experiment. In addition, alternative flowmeters were identified as possible replacements for the Category D flowmeters now in development by Quantum Dynamics.

Most of the selected instrumentation, such as temperature and pressure transducers, was developed to fly on the Atlas family of launch vehicles, or developed under other aerospace programs. Where possible, the development heritage of a particular component is stated.

Accelerometers, dc/dc converters, and low power airborne system inverters are not considered to be high risk items. These items are off-the-shelf, mature, and are not anticipated to require further development. These items are assigned a Category A status.

Liquid/vapor detectors flown on early Titan/Centaur missions were built to a General Dynamics design. A new specification was written for the procurement of liquid/vapor verification instrumentation for the current Titan/Centaur missions, and Tayco Engineering has been selected as a vendor. We intend to use these detectors for COLD-SAT, but the redesign of this component causes it to be rated as Category B.

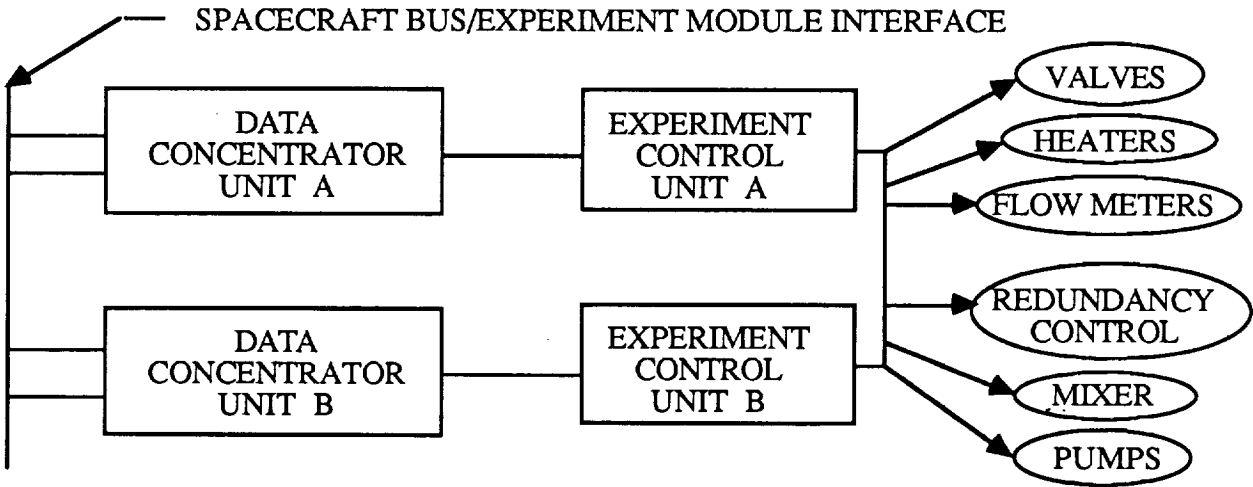


Figure 5-47. Experiment Control Subsystem Block Diagram

Table 5-8. Experiment Commands

COMMAND TYPE	QUANTITY
VALVE CONTROL	140
AVIONICS POWER CONTROL	20
HEATER POWER CONTROL	14
FLOWMETER POWER CONTROL	24
PUMP POWER CONTROL	6
ACCELEROMETER POWER CONTROL	6
TOTAL	210

Table 5-9. Development Status Assessment - Avionics Category

DEVELOPMENT CATEGORY	DESCRIPTION	SOURCE		COMMENTS
		YES	NO	
A	ACCELEROMETER, TRIAX	X		FLOWN ON SHUTTLE; EXPLORER, USAF S73-5, SATURN, ETC.
A	CONVERTER, DC/DC (10V)		X	SOURCE IS TBD-NOT CONSIDERED HIGH RISK
A	CONVERTER, DC/DC (28V)		X	SOURCE IS TBD-NOT CONSIDERED HIGH RISK
A	CURRENT SHUNT		X	OFF THE SHELF HIGH QUALITY RESISTOR
B	EXPERIMENT CONTROL UNIT (ECU)	X		IN-HOUSE DESIGN AND FAB USING QUALIFIED PIECE PARTS
A	INVERTER		X	SOURCE IS TBD
B	LIQUID/VAPOR DETECTOR	X		TAYCO ENGINEERING
D	METER, FLOW		X	CURRENTLY IN TECHNOLOGY VERIFICATION
A	PRESS XDCR (0-30mV)	X		GENERAL DYNAMICS-FLOWN ON CENTAUR
B	DATA CONCENTRATOR UNIT (DCU)	X		FAC DEVELOPED FOR INTELSAT-VII, DELTA QUAL REQD
A	TEMP XDCR, PROBE	X		GENERAL DYNAMICS-FLOWN ON CENTAUR
A	TEMP XDCR, SURFACE	X		GENERAL DYNAMICS-FLOWN ON CENTAUR
A	TEMP XDCR, ZERO-G	X		GENERAL DYNAMICS-FLOWN ON CENTAUR

Table 5-10. Development Status Assessment - Mechanical Category

DEVELOPMENT CATEGORY	DESCRIPTION	SOURCE		COMMENTS
		YES	NO	
B	ACCUMULATOR	X		DESIGNED AND BUILT IN-HOUSE TO MIL-STD-1522A
B	BOTTLE, GASEOUS HELIUM	X		DESIGNED TO MIL-STD-1522A
B	BOTTLE, GASEOUS HYDROGEN	X		DESIGNED TO MIL-STD-1522A
B	DIFFUSER	X		DESIGNED AND FABRICATED IN-HOUSE
B	DISCONNECT, SELF SEALING		X	EATON IS CANDIDATE (ALT. NON SELF SEALING PLUS VALVE)
B	EVAPORATOR	X		IN-HOUSE DESIGN AND FABRICATION
A	FILTER, CRYOGENIC	X		AVAILABLE OFF SHELF FROM MANY VENDORS
A	FILTER, HIGH PRESSURE GAS	X		AVAILABLE OFF SHELF FROM MANY VENDORS
A	HEATER, ACCUMULATOR	X		RAYCHEM, TAYCO ARE SOURCES
A	HEATER, TANK 1	X		RAYCHEM, TAYCO ARE SOURCES
A	HEATER, TANK 2 LAD	X		RAYCHEM, TAYCO ARE SOURCES
A	HEATER, TANK 2 WALL	X		RAYCHEM, TAYCO ARE SOURCES
A	HEATER, TANK 3 VENT	X		RAYCHEM, TAYCO ARE SOURCES
A	HEATER, TANK 3 WALL	X		RAYCHEM, TAYCO ARE SOURCES
A	HEATER, VENT SYSTEM	X		RAYCHEM, TAYCO ARE SOURCES
C	LAD, TANK 1	X		SYSTEM DEVELOPMENT REQUIRED
C	LAD, TANK 2	X		SYSTEM DEVELOPMENT REQUIRED
A	MULTIPLE LAYER INSULATION	X		SHELDahl, NATIONAL METALIZING, APEX MILLS, IN-HOUSE FIT
A	ORIFICE	X		VISOJET
C	PUMP, CRYOGENIC		X	SUNSTRAND & ALLIED SIGNAL ARE CANDIDATES
B	REGULATOR, CRYOGENIC		X	VALCOR, CONSOLIDATED ARE CANDIDATES
B	REGULATOR, HIGH PRESSURE	X		HTL, VALCOR, CONSOLIDATED, PARKER
B	SUBCOOLER	X		IN-HOUSE DESIGN AND FABRICATION REQUIRED
B	TANK 1	X		DESIGNED AND FABRICATED IN-HOUSE TO MIL-STD-1522A
B	TANK 2	X		DESIGNED AND FABRICATED IN-HOUSE TO MIL-STD-1522A
B	TANK 3	X		DESIGNED AND FABRICATED IN-HOUSE TO MIL-STD-1522A
A	TRANSITION JOINT, EXPLOSION WELDED, 2219 TO 304	X		EXPLOSIVE FABRICATORS IS MATURE SOURCE
A	TUBING 1/2" MIL-T-8808A		X	OFF-SHELF SS 304L EXTRUSION TUBING
A	TUBING 1/4" MIL-T-8808A		X	OFF-SHELF SS 304L EXTRUSION TUBING
A	TUBING 3/8" MIL-T-8808A		X	OFF-SHELF SS 304L EXTRUSION TUBING
C	TVS, COMPACT	X		SUNSTRAND IS CANDIDATE
C	TVS, TANK 1	X		IN-HOUSE DEVELOPMENT REQUIRED
C	TVS, TANK 2	X		IN-HOUSE DEVELOPMENT REQUIRED
C	TVS, TANK 3	X		IN-HOUSE DEVELOPMENT REQUIRED
B	VALVE, CHECK, CRYOGENIC	X		CONSOLIDATED CONTROLS, HTL
B	VALVE, SHUTOFF, CRYOGENIC	X		PARKER, VALCOR, CONSOLIDATED CONTROL
B	VALVE, SHUTOFF, HIGH PRESSURE	X		PARKER, VALCOR, CONSOLIDATED CONTROL
A	VALVE, MANUAL	X		PARKER, CONSOLIDATED, VALCOR
B	VALVE, RELIEF		X	VALCOR IS CANDIDATE
C	VAPOR-COOLED SHIELD	X		IN-HOUSE DEVELOPMENT REQUIRED

Flowmeter selection has been given considerable study. Table 5-11 gives the flow condition ranges for the experiment. Some experiments require the ability to measure flowrate in two-phase flow conditions. Fourteen flowmeter vendors with experience in NASA, DOD, commercial airborne vehicle, space vehicle, and ground flow measurement instrumentation were contacted to determine if they had an off-the-shelf capability to support the COLD-SAT flowmeter requirements. Only one vendor, Quantum Dynamics in Woodland Hills, California, indicated the ability to measure two-phase flowrate. Three vendors who have the capabilities to meet preliminary requirements, are Flow Technology Inc. in Phoenix, Arizona, Hoffer Flow Measurement Systems in Port Monmouth, New Jersey, and Thermal Instrument Co. in Trevese, Pennsylvania. Table 5-12 indicates the vendor model number for a particular flowmeter.

The turbine flowmeter was selected as the best alternative for every flowmeter except meters numbered 105 (two-phase), 111 and 122. Flowmeters 111 and 122 measure the amounts of gas passing through the tank TVS vents and are expected to operate at pressures of approximately 20 kPa. Thermal flowmeters are available to satisfy requirements for these two meters.

Quantum Dynamics is developing a dual turbine two-phase flowmeter for NASA, and has indicated that all the COLD-SAT liquid, vapor and two-phase flow conditions could be met with two versions of their meter. Testing of the flowmeter at NASA/JSC has revealed accuracy and calibration problems, and there are doubts about its ability to accommodate flow conditions that range from all-liquid through the full range of two-phase quality to all-vapor. Further development work with these meters is required in the areas of accuracy verification, calibration techniques and qualification for flight. COLD-SAT could benefit if a developed meter becomes available because it includes all the data acquisition and signal processing to produce instantaneous measurement of quality and total flow. We currently are specifying use of this meter for the two-phase flows in the experiment system. For some of these applications, an acceptable replacement might be a conventional liquid flowmeter in conjunction with a vapor detector (such as a capacitance device).

Category A mechanical components are essentially risk-free. These items are either available in components that satisfy COLD-SAT applications, or have a low risk process to convert these items for use on the COLD-SAT spacecraft.

Most of the valves considered are rated within Category B with the exception of the Category C cryogenic regulators and the Category A manual valve. Valve attributes and requirements were studied. Several valve manufacturers were contacted and no valve was found which could be used for COLD-SAT as an off-the-shelf item. Detailed valve results are discussed in Section 5.9.6.

The experiment Tanks 1, 2, 3 and the accumulator are made of aluminum alloy. They will be designed, fabricated, and tested in accordance with the philosophy of MIL-STD-1522 and MIL-STD-1540B. All spacecraft aluminum tanks are considered low risk. The gas storage bottles are also considered low risk and use mature technology. The gas storage bottles are cylindrical with ellipsoidal ends and use carbon-carbon filament wound over a thin metallic liner. Liner material for the high pressure gaseous helium bottle is CRES and the liner material for the high pressure gaseous H₂ bottle is aluminum alloy with a fiberglass corrosion barrier. Similar gas storage bottles are currently used on the Centaur high energy upper stage. The filament wound bottles will be tested and qualified per approved test plans.

The cryogenic pump is rated Category D. The vane pump was considered primarily because of the low flowrates required by the COLD-SAT mission. Sunstrand designed and built a technology development vane pump to conduct ground tests for LH₂ and LOX service. The Sunstrand pump was delivered to NASA/LeRC where it was tested using LH₂ and LN₂ as the test fluids. The test results showed adequate agreement with the performance prediction code developed to model this type of pump. Further development is required to close the gap between the present state of cryogenic pumps and a qualified pump ready for COLD-SAT. Although NASA/LeRC used a

Table 5-11. Preliminary Flowmeter Requirements

METER #	PRESS (KPa)	FLUID	INLET TUBE (MM)	LOW FLOW (Kg/SxE-03)	HIGH FLOW (Kg/SxE-03)	LOW FLOW GAS (M ³ /SxE-03)	HIGH FLOW GAS (M ³ /SxE-03)	LOW FLOW LIQUID (M ³ /SxE-03)	HIGH FLOW LIQUID (M ³ /SxE-03)	TEMP (°K)
26	103.42	LH2	19.1	2.27	45.40	-	-	33.71	674.21	-
30	103.42	LH2	19.1	2.27	45.40	-	-	33.71	674.21	-
49	103.42	LH2	19.1	2.27	45.40	-	-	33.71	674.21	-
50	103.42	LH2	12.7	2.27	22.70	-	-	33.71	337.11	-
55	103.42	LH2	12.7	2.27	22.70	-	-	33.71	337.11	-
105	20.68	H2-2P	12.7	2.27	22.70	-	-	33.71	337.11	-
108	344.73	GH2	9.53	0.10	1.01	0.25	5.04	-	-	208
108	344.73	GHe	9.53	0.19	0.91	0.23	2.28	-	-	208
109	344.73	GH2	9.53	0.10	1.01	0.25	5.04	-	-	208
109	344.73	GHe	9.53	0.19	0.91	0.23	2.28	-	-	208
110	344.73	GH2	9.53	0.06	1.27	0.02	0.03	-	-	111
111	20.68	GH2	9.53	0.05	0.45	3.62	36.18	-	-	222
111	20.68	GH2	9.53	0.05	0.45	1.78	17.79	-	-	111
112	344.73	GH2	9.53	0.06	1.27	0.02	0.03	-	-	111
122	20.68	GH2	9.53	0.03	0.32	2.53	25.33	-	-	222
122	20.68	GH2	9.53	0.03	0.32	1.25	12.45	-	-	111

0.254M X 0.102M DIA + 10 TUBE DIAMETERS @ INLET & OUTLET

28 VDC

TBD

0 TO 5 VDC OR SERIAL DIGITAL WORD

4000 Gs ABOVE 1500 Hz

2.7 Grms

142 dB OASPL

101.3 kPa TO 0 kPa

USE 100dB MICRO V/M FOR INITIAL EMC EVALUATION

NO EXTERNAL LEAKAGE ALLOWED

278 TO 300 °K

22 TO 300 °K

MAX ENVELOPE (L X DIA)

INPUT VOLTAGE

POWER DISSIPATION

SIGNAL INPUT

LAUNCH ENVIRONMENT

SHOCK

VIBRATION

ACOUSTIC

PRESSURE

EMI

OPERATION ENVIRONMENT

FUNCTIONAL

THERMAL VACUUM

THERMAL CYCLING

AVIONICS

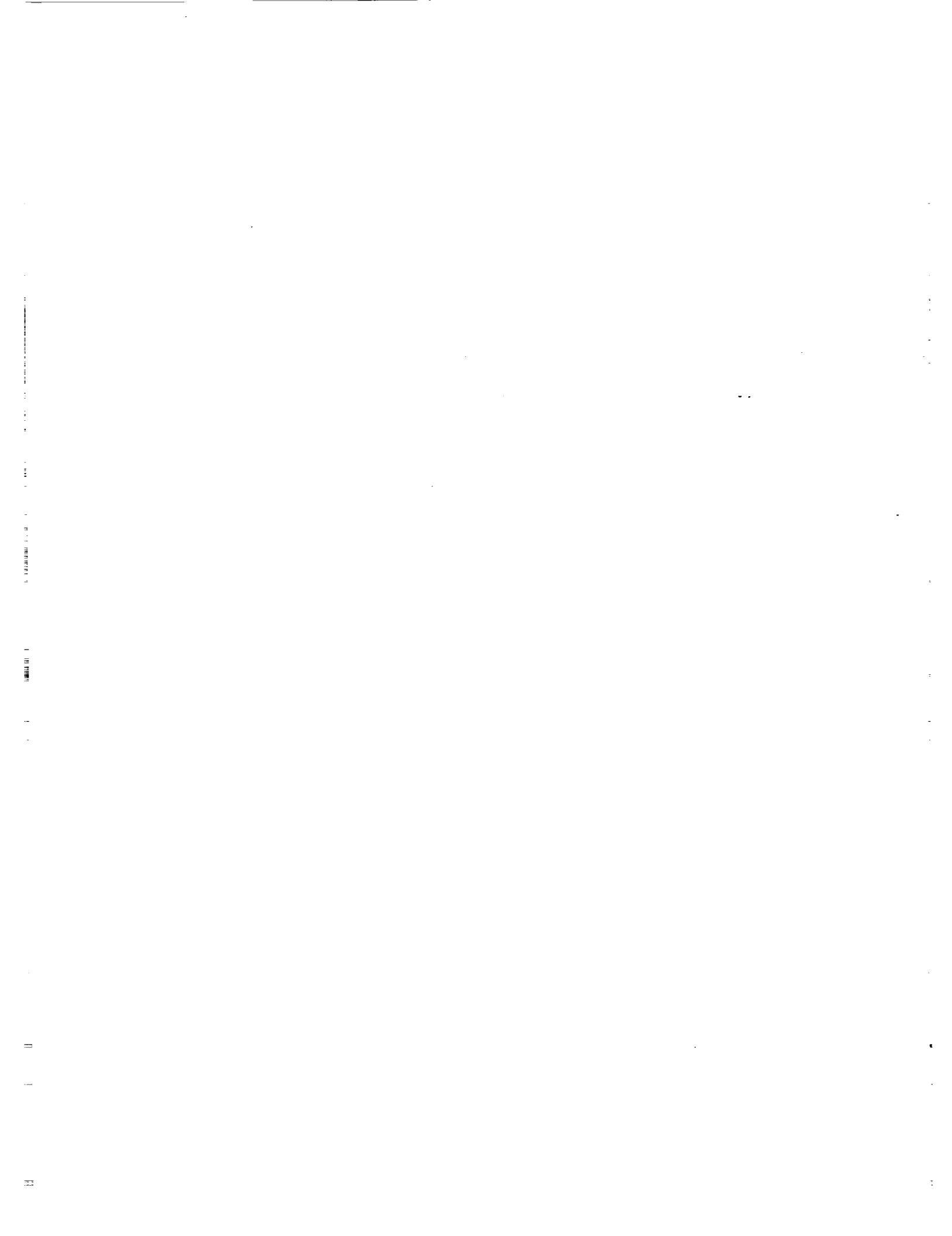
WETTED COMPONENTS

Table 5-12. Recommended Flowmeters

FLOWMETER #	HOFFER FLOWMETER MODEL #	FLOW TECHNOLOGIES FLOWMETER MODEL #	THERMAL INSTRUMENT Co. FLOWMETER MODEL #
26	HO1/2X1/2-.6-10.7-1MXB-B-5	FT-10	-
30	HO1/2X1/2-.6-10.7-1MXB-B-5	FT-10	-
49	HO1/2X1/2-.6-10.7-1MXB-B-5	FT-10	-
50	HO1/2X3/8-.53-5.4-B-1MXB-B-5	FT8-8	-
55	HO1/2X3/8-.53-5.4-B-1MXB-B-5	FT8-8	-
105	-	-	-
108	HO3/4X3/4-20-B-IMC3PXB-B-5	FT-08	-
109	HO3/4X3/4-20-B-IMC3PXB-B-5	FT-08	-
110	HO1/2X3/8-20-B-IMC3PXB-B-5	FTM5GB	-
111	-	FT-20	600
112	HO1/2X3/8-20-B-IMC3PXB-B-5	FTM5GB	-
122	-	FT-20	600

hydraulic drive to power the pump for validation tests, various motor and control schemes are possible. Sunstrand also has the ability to design and integrate a control system with the pump which accepts either digital or analog command and feedback signals. A pump system closed loop stability analysis is also required as part of the development effort.

Liquid acquisition devices (LADs) will require only minimal development before they are suitable for COLD-SAT. The present day liquid acquisition systems are well understood for use with storable propellant systems. However, because of the low surface tension of LH₂, sensitivity to heat conducted through LAD tank wall mounts, and bubble entrapment within the LAD screen mesh, the LAD systems for Tanks 1 and 2 will require some testing using LH₂. The COLD-SAT design utilizes low thermal conduction fiberglass/epoxy links and struts to minimize boiloff from heat conduction into the LAD.



EXPERIMENT MODULE SUPPORTING ANALYSES

This section provides design/sizing and performance analyses for some of the experiment module subsystems and components presented in Section 5. Subjects covered include fluid system pressure drop, measurement requirements and accuracies, thermodynamic vent system sizing and performance, performance of the pressurization and transfer systems, venting of the helium-purged insulation on the LH2 supply tank, overall performance of the experiment module thermal management features, sizing of the micrometeoroid/debris shielding, and analysis of design requirements for the major structural features of the experiment module.

6.1 FLUID SYSTEM PRESSURE DROP

6.1.1 Results and Implications

The pressure drop in the fluid system lines has an important effect on system performance and must be considered when arranging the system components. For example, the pressure drop between the LAD in Tank 1 to the entrance of the transfer pump has an impact on the suction head requirement of that pump.

Initially, the pressure drop in the fluid system lines and components was only approximated for determination of tank pressure, pressurization system requirements and line sizes. Pressure drop characteristics of the nozzles, the flowmeters and some of the valves were unknown.

Later in the program, estimates of these pressure drop characteristics were obtained from vendors and a more detailed analysis of the pressure drop in the liquid transfer lines was performed. System layouts which indicate line lengths, fittings and component placement were used as input to this analysis. The results of this preliminary analysis indicated that the major components (especially the nozzles and flowmeters) were the dominant source of pressure drop and that the selected sizes met flow requirements. Table 6-1 summarizes these results.

Table 6-1. Liquid Transfer Pressure Drop Summary

TRANSFER FLOW PATH	PRESSURE DROP (kPa)*		
	Line	Nozzles	Total
Tank 1 to Tank 2	14	25	39
Tank 1 to Tank 3	29	35	64
Tank 2 to Tank 3	30	35	65

* for maximum liquid hydrogen flowrate = 0.023 kg/s

The fluid system has been updated somewhat since this detailed analysis was performed. Most significantly, shutoff valves were removed from the Tank 1 transfer line and a four-way valve in the pump module was replaced by a shutoff valve network. These changes represent relatively small reductions in the overall system pressure drop. The analysis will be updated to reflect these changes and the rest of the fluid system will be analyzed in similar detail as the system development continues. The results of these analyses will be used to further define the requirements and design of the fluid system, including redundancy determinations, component specifications and selection, and system performance evaluations.

6.1.2 Analysis Technique

To calculate the pressure drop of the main liquid transfer lines, the lines were divided into the major segments between each tank and the pump module. From the layout drawings, the major components, line lengths and fittings for each of these segments were listed.

The valve pressure drop data was obtained from the vendor for valves similar to those being proposed. The Valcor gate valve design discussed in Section 5.9.6.1 was estimated at that time to have a loss coefficient (K) of 0.59. To account for uncertainty in this estimate, a factor of two was applied to the coefficient used in the pressure drop calculations (K=1.18). Current valve requirements (specified in Section 5.9.6.1) reflect a loss coefficient of 0.91 which is greater than originally estimated but well within the allocated tolerance.

Flowmeter pressure drops were estimated based on the Quantum Dynamics development unit described in Section 5.11. This information is preliminary, since the meter was not fully calibrated.

For the nozzles in the tanks, a preliminary assessment was made of their requirements for the experiments and led to the selection of the nozzles shown in Table 6-2. These nozzles were selected from Catalog 50A (1988) of Spraying Systems Co., Wheaton Ill. The pressure drops for the nozzles were based on scaling relations which were presented by the manufacturer. Prior to any detailed design or fabrication, the nozzles would be tested with LH₂ to acquire actual performance data.

Flow resistance of the fittings were determined using standards readily available from handbooks. These were expressed in terms of equivalent pipe diameter lengths (Le). To simplify the pressure drop calculation, the pressure drop for the valves and flowmeters was also converted to equivalent length. The overall pressure drop was then calculated using this equation:

$$\Delta P = f(L/D_{\text{TUBING}} + \sum L_{\text{COMPONENTS}}) \rho v^2 / 2 + \Delta P_{\text{NOZZLE}} \quad (6-1)$$

6.2 MEASUREMENT ACCURACY REQUIREMENTS

6.2.1 Instrument Accuracy

The measurement accuracy for each measurement category is identified in Table 6-3. All errors are specified as a percent of the instrument range. Instrumentation and control lists are presented in Appendix C. The total error has been subdivided into three parts; measurement error, processing error, and quantizing error. Since the processing and quantizing errors remain constant for each case, the measurement error is responsible for the difference in accuracy for each category. For high level analog measurements, the ± 0.5 percent error is due to voltage dividers. If greater precision is required for any measurements in this category it is possible to eliminate this error component through calibration, thereby reducing the total error to ± 0.18 percent. For acceleration measurements, the specified accuracy of the Textron accelerometer is ± 1.0 percent under worst case conditions. For current measurements, the ± 1.0 percent error is the specified shunt tolerance and if desired can also be eliminated through calibration. For the flow measurements, ± 0.2 percent error is the specified accuracy of the Quantum Dynamics flow meter. For the pressure measurements, the major error sources are the transducer, excitation and amplifier. The excitation and amplifier errors can be eliminated by monitoring the excitation voltage through the amplifier. The transducer error consists of a ± 0.5 percent static error and a ± 0.0054 percent per Kelvin temperature coefficient. The transducers are located in three general areas; under the MLI of Tank 1 at 19.4 K to 25.0 K, under the MLI of Tanks 2 and 3 at 13.9 K to 250 K and outside the MLI at 211 K to 222 K. The worst case environment, under the MLI of Tanks 2 and 3 has a temperature variation of ± 116 K. This

Table 6-2. Nozzle Requirements and Characteristics

TANK NO.	REQUIREMENTS					CHARACTERISTICS**				
	TYPE	QUANT	FLOWRATE		TYPE	FLOW 1E-06 m ³ /s	PRESS DROP		NOTES	
			TOTAL kg/s	PER NOZZLE kg/s			WATER kPa	LH2*** kPa		
2	radial	9	0.0227 0.0113	0.0025 0.0013	36 18	WHIRLJET 1/4 SIZE 3	241 62	17.1 4.4	hollow cone standard with ~60° to 70° incl angle	
2	axial	1	0.0227 0.0136	0.0227 0.0136	322 193	FULLJET 3/4 SIZE 3050	352 103	24.9 7.3	full cone narrow with 26° to 30° incl angle	
3	radial	3	0.0227 0.0034	0.0076 0.0011	107 16	WHIRLJET 1/4 SIZE 5	689 21	48.8 1.5	hollow cone wide with ~100° to 126° incl angle	
3	axial	1	0.0227 0.0068	0.0227 0.0068	322 97	WHIRLJET 3/8 SIZE 20	427 41	30.3 2.9	hollow cone standard with ~63° to 73° incl angle	
3	tangential	2	0.0136 0.0034	0.0068 0.0017	97 24	VEEJET 1/4 SIZE 11010	621 40	43.9 2.8	full cone oval with up to 103° incl angle on wide axis	

** Spraying Systems Co. nozzle catalog 50A, 1988

*** Calculated assuming that the pressure drop is proportional to the liquid density.

Table 6-3. Measurement Accuracy Expressed as a Percent of Instrument Range

MEASUREMENT CATEGORY	MEASUREMENT ERROR (%)	PROCESSING ERROR (%)	QUANTIZING ERROR (%)	TOTAL RSS ERROR (%)
ANALOG (HI LEVEL)	±0.5	±0.17	±0.05	±0.53
ACCELERATION	±1	±0.17	±0.05	±1.02
CURRENT	±1	±0.17	±0.05	±1.02
FLOW	±0.1	±0.17	±0.05	±0.2
PRESSURE	±0.8	±0.17	±0.05	±0.82
TEMPERATURE	±0.1	±0.17	±0.05	±0.2

accounts for the worst case error of ± 0.8 percent. For the temperature measurements a similar technique can be used to eliminate the errors due to the constant current sources and amplifier leaving only the transducer error of ± 0.2 percent.

6.2.2 Uncertainty Analysis for Pressure Control Experiments

The quantities directly measured during the pressure control experiments are pressure, temperature, and flow rate. Analyses were performed to quantify how uncertainties in these measured quantities propagate into the uncertainties of calculated quantities, such as the heat transfer coefficient and pressure rise rate. A summary of the results is described below.

For these uncertainty analyses, the following instrument accuracies were assumed: ± 0.7 percent for pressure, ± 0.5 percent for temperature and ± 1 percent for flowrate. These instrument accuracies differ slightly from the updated values quoted in Section 6.2.1 and Table 6-3. The updated values were not available when the following uncertainty analyses were performed. The instrument accuracies are based on the percent of the full-scale range of the instrument. Pressure will be measured with an instrument having a full-scale range of 69 kPa (see Table C-1 in Appendix C). Therefore the absolute accuracy for the pressure measurement is ± 0.5 kPa. The full-scale range of the temperature transducer is 14 K (see Table C-1), so the absolute accuracy for the temperature measurement is ± 0.07 K. Since the range of the measurement must be less than the instrument range, the measurement accuracy, which is based on the percent of the measured value, will be less than the instrument accuracy, which is based on the percent of instrument range. The quality of a measurement is best indicated by the measurement accuracy, based on the percent of the measured value not the instrument accuracy. In the following sections, measurement accuracies are determined and presented.

6.2.2.1 Thermal Stratification Experiments. During the thermal stratification experiments the tank will be locked-up with the heaters on and the TVS off. The tank pressure will be allowed to rise 34.5 kPa, from 103.4 kPa to 137.9 kPa.

Average Pressure Rise Rate

The primary results of this experiment will be the actual pressure rise rate and the equilibrium pressure rise rate:

$$dP/dt \approx (P_2 - P_1) / \Delta t \quad (6-2)$$

$$dP/dt_{\text{equil}} \approx (P_{2,\text{equil}} - P_1) / \Delta t \quad (6-3)$$

The final equilibrium pressure ($P_{2,\text{equil}}$) can be measured after mixing the tank fluid following the stratification experiment. The time necessary for the tank pressure to rise by 34.5 kPa will take hours, consequently the time (Δt) will be known with much greater precision than pressure. As a result, the actual and equilibrium pressure rise rates can be determined with accuracies of ± 2 percent. The fluid mass in the tank must also be measured to correlate the measured pressure rise rates.

Distribution of Energy in the Stratified Fluid

Temperature measurements at numerous locations within the tank will be required to quantify the distribution of energy in the stratified fluid. The maximum possible temperature difference that can exist in the liquid will be 1.02 K, which corresponds to the difference in the saturation temperature at 103.4 kPa and 137.9 kPa. The maximum temperature difference in the vapor may be greater. A

1.02 K temperature difference can be resolved to ± 6.5 percent using temperature sensors with ± 0.07 K accuracy.

Passive Heat Transfer Coefficient

The passive heat transfer coefficient on the heated tank wall will require measurements of the tank wall temperature, "bulk" fluid temperature, and the local wall heat flux:

$$h = Q'' / (T_{\text{wall}} - T_{\infty}) \quad (6-4)$$

The heat rate into the tank will be inferred from the electrical power dissipated in the heaters attached to the outer surface of the tank wall. The heater heat rate can be determined with an accuracy of ± 1.4 percent from measurements of voltage and current. An analysis of the tank wall, presented in Section 6.3.1.1, indicates that the heat flux distribution on the tank wall inner surface will be uniform, within ± 10 percent.

The heat transfer coefficient uncertainty decreases as the wall-to-bulk fluid temperature difference increases. Assuming free convection is the dominant heat transfer mechanism, this temperature difference will depend on the acceleration level, free convective length scale, and phase of the fluid adjacent to the wall. The precise magnitude of the convective length scale (L) is difficult to determine, but is limited by the size of the tank. The wall-to-bulk fluid temperature differences were estimated using an empirical correlation for laminar free convection on a heated vertical plate and are listed in Table 6-4. The corresponding free convection coefficient uncertainties were determined from an error analysis of Equation 6-4 and are also listed in the table.

Table 6-4. Free Convection Coefficient Uncertainties

		L = 2.4 meters		L = 0.076 meters	
		ΔT	h uncertainty	ΔT	h uncertainty
Liquid	$g/g_0 = 10^{-7}$	1.4 K	$\pm 12\%$	0.72 K	$\pm 17\%$
	$g/g_0 = 10^{-4}$	0.35 K	$\pm 29\%$	0.18 K	$\pm 55\%$
Vapor	$g/g_0 = 10^{-7}$	7.8 K	$\pm 10\%$	3.9 K	$\pm 10\%$
	$g/g_0 = 10^{-4}$	2.0 K	$\pm 11\%$	1.0 K	$\pm 14\%$

The results presented in Table 6-4 indicate that the free convection coefficient on the heated tank wall can be determined accurately (less than ± 20 percent uncertainty), except for the high acceleration liquid case. These results are valid for a tank wall heat flux of 1.9 W/m^2 . For lower heat flux levels the temperature differences will be lower, causing greater uncertainty in the convection coefficients. The wall-to-bulk fluid temperature difference will also be lower if other convective mechanisms are significant, i.e., fluid motion due to spacecraft disturbances, fluid motion persistence, and surface tension effects.

6.2.2.2 Mixing Destratification. Following the thermal stratification experiments, the axial jet mixer will be operated with the TVS off. Mixing will reduce thermal stratification causing a decrease in the tank pressure. The primary result of this experiment will be the time variation of the tank pressure. The accuracy of the pressure measurement is ± 0.5 kPa, which corresponds to ± 1.4 percent of the 34.5 kPa range from 137.9 kPa to 103.4 kPa. Time can be measured with negligible error.

Temperature measurements will be required to quantify the changing distribution of energy in the tank fluid while the mixer is operating. Temperature distribution measurement in the tank fluid was discussed in Section 6.2.2.1. The maximum possible temperature difference in the liquid was found

to be 1.02 K, which can be resolved to ± 6.5 percent. However, while the mixer is in operation temperature gradients in the tank fluid will be reduced to nearly zero.

The heat transfer coefficient on the heated tank wall while the mixer is operating cannot be accurately determined. With the mixer on, the convection on the tank wall will be enhanced, decreasing the wall-to-bulk fluid temperature difference relative to those given in Table 6-4 for the case of pure free convection. The magnitude of the convective velocity on the tank wall will depend on the mixing pattern established in the tank by the axial jet mixer, but is expected to be on the order of the jet velocity (0.03 – 0.3 m/sec). The analysis presented in Section 6.3.1.3 indicates these velocities are more than 70 times greater than the maximum velocity expected in a buoyancy driven flow field near a heated tank wall. An empirical correlation for laminar forced convection indicates that the maximum wall-to-bulk fluid temperature difference will be 0.10 K while the mixer is operating. This temperature difference cannot be adequately resolved using temperature sensors with ± 0.07 K accuracy.

6.2.2.3 Wall-Mounted TVS Performance. The heat transfer rate to the TVS fluid can be determined from the TVS flow rate and the enthalpy change between the inlet and outlet:

$$Q_{\text{TVS}} = m_{\text{TVS}} (h_{\text{exit}} - h_{\text{inlet}}) \quad (6-5)$$

Temperature measurements are required to determine the inlet and outlet enthalpies. At the inlet, subcooled or saturated liquid from an LAD will be ingested. The TVS tube length will be sized to insure the exiting TVS fluid is saturated or superheated vapor. Taking into account uncertainties in temperature, flow rate, and fluid properties, the heat transfer rate can be determined with an uncertainty of ± 1.8 percent.

The overall heat transfer coefficient between the TVS fluid and the tank fluid is defined below:

$$U_i = \frac{Q_{\text{TVS}}}{A_i \Delta T} = \frac{Q_{\text{TVS}}}{\pi D_i L_{\text{TVS}} (T_{\text{TVS}} - T_{\text{tank}})} \quad (6-6)$$

The heat transfer coefficient is based on the tube inner surface area, A_i . For a 103.4 kPa tank pressure and a 34.5 kPa TVS pressure, the temperature difference between the TVS fluid and tank fluid will be 3.2 K. An error analysis, which takes into account the uncertainties of all these quantities, indicates that the heat transfer coefficient can be determined with an accuracy of ± 4 percent. The heat transfer coefficient will be relatively constant in the region upstream of the "dry-out" point in the TVS tube, where the temperature difference ($T_{\text{TVS}} - T_{\text{tank}}$) is constant.

6.2.2.4 Compact Heat Exchanger Performance. The compact heat exchanger has TVS fluid on the "cold-side", and flow to the mixer on the "hot-side". The mixer flow is obtained from a LAD, and is saturated liquid. The heat transfer rate to the TVS fluid can be determined in the same manner and with the same accuracy (± 1.8 percent) as for the wall-mounted heat exchanger.

The overall heat transfer coefficient between the TVS fluid and the mixer fluid is dependent on the heat transfer rate, heat transfer area, and the log-mean temperature difference, similar to the definition given in Equation 6-6. An error analysis indicates the log-mean temperature difference can be measured with an accuracy better than ± 9 percent using temperature sensors with ± 0.07 K accuracy. The total uncertainty for the overall heat transfer coefficient associated with the compact heat exchanger was found to be ± 10 percent.

6.2.3 Tank Chill and No-Vent Fill Uncertainty Analysis

The GDNVF code was run with different liquid injection temperatures in order to determine the influence of uncertainty in the liquid temperature measurements. Table 6-5 shows the impact of a 0.055 K and a 0.278 K increase in the injected liquid temperature on both the chilldown and no-vent fill processes in Tank 3.

Table 6-5. Liquid Transfer Sensitivity to Temperature Uncertainty

Temperature (K)	CHILLDOWN		FILL	
	Time (sec)	Mass of Liquid (kg)	Time (sec)	Max. Pressure (kPa)
20.338	35680	4.227	1800	141.6
20.393	35703	4.225	1799	143.7
20.616	35861	4.227	1792	152.2

The results indicate that the chilldown process is relatively insensitive to the temperature uncertainty in that even a 0.278 K uncertainty in the liquid injection temperature only causes a 0.5 percent difference in the chilldown time and essentially no difference in the amount of liquid required to chill the tank. The fill process is more sensitive, but the 7.5 percent difference in the maximum tank pressure with a temperature uncertainty of 0.278 K is acceptable. Thus the ± 0.07 K uncertainty in the liquid temperature measurements appears to be adequate for the tank chills and no-vent fills.

6.3 PRESSURE CONTROL

6.3.1 Thermal Stratification

6.3.1.1 Supply Tank Heaters. Heaters will be necessary on the LH₂ supply tank to provide a controlled uniform heat flux. These heaters are expected to be similar to the thin, flexible, "ribbon" type heaters manufactured by TAYCO. The vendor has indicated that heaters of this type have been used in the past for similar low temperature applications. The effects of heater width and spacing on the heat flux uniformity have been investigated, along with the transient response of these heaters. A summary of the results is presented here.

A two-dimensional, finite difference, transient conduction code, developed under GDSS IRAD, was used to analyze this problem. The heater configuration shown in Figure 6-1 was analyzed first. Heaters are attached directly to the tank wall outer surface. The tank wall is thin (~2.54 mm) relative to the tank diameter (~2.4 m) so a rectangular coordinate system was used. The computational domain was reduced by assuming symmetry exists through the center of the heaters and through the tank wall between adjacent heaters. The heat flux across the width of the heater is assumed to be constant and uniform. The tank wall outer surface not covered by the heater and the symmetry lines are treated as adiabatic surfaces. A uniform convective condition was assumed to exist over the entire tank wall inner surface.

This investigation is ultimately concerned with the maximum heat flux variation across the tank wall inner surface. The magnitude of this variation is indicated by the range in the heat flux, non-dimensionalized by the average heat flux through the tank wall, as indicated by Equation 6-3. q''_{\max} and q''_{\min} are the highest and lowest values of the heat flux on the tank wall inner surface, q''_H is the

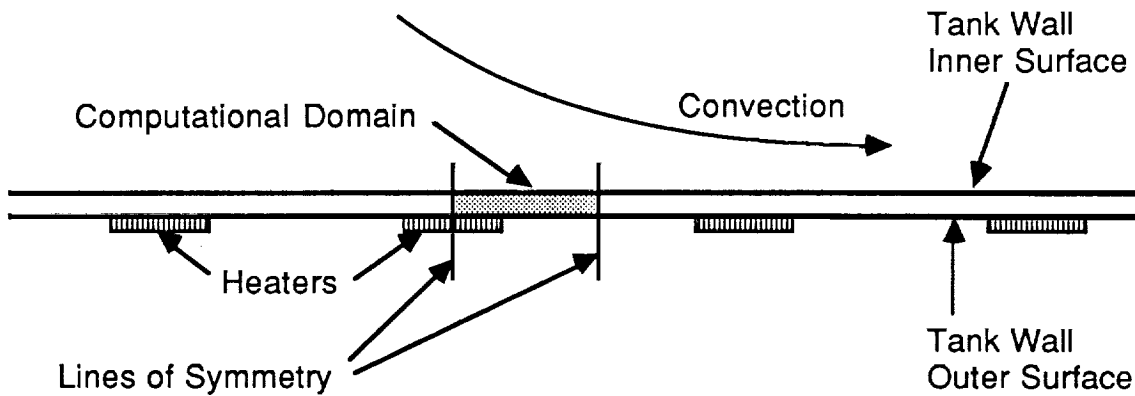


Figure 6-1. Configuration of Tank with Heaters

heater heat flux, W is the heater width, and L is the centerline-to-centerline spacing between adjacent heaters.

$$\frac{q''(\text{range})}{q''(\text{avg})} = \frac{q''_{\max} - q''_{\min}}{q''_H (W/L)} \quad (6-7)$$

A dimensional analysis of the steady-state, two-dimensional, heat conduction equation and boundary conditions indicates that the normalized heat flux variation across the tank wall inner surface is dependent on only three dimensionless groups: W/L , B/L , and hL/k , where B is the tank wall thickness, h is the convection coefficient on the tank wall inner surface, and k is the thermal conductivity of the tank wall. A parametric study was carried out for a wide range of conditions: $W/L = 0.1$ to 1 , $B/L = 0.05$ to 0.5 , and $hL/k = 0.02$ to $20,000$. The following general trends were apparent from the results:

1. The heat flux variation decreases as the convective resistance becomes large relative to the conductive resistance, i.e., $hL/k \rightarrow 0$.
2. The heat flux variation decreases as the fraction of the outer tank surface covered by the heaters increases, i.e., $W/L \rightarrow 1$.
3. The heat flux variation decreases as the heater spacing becomes small relative to the tank wall thickness, i.e., $L/B \rightarrow 0$.

For low values of hL/k , i.e., $hL/k < 0.2$, the heat flux variation was found to primarily dependent on only two dimensionless groups: hL/k and $(L-W)/B$. This observation is apparent from Figure 6-2. The COLD-SAT supply tank is made of aluminum, which has a thermal conductivity of 17.3 W/m-K at 22.2 K . The heater spacing is expected to be less than 305 mm . The largest convection coefficient expected on the tank wall inner surface during thermal stratification experiments was estimated to be $\sim 11.35 \text{ W/m}^2\text{-K}$. This value of h was estimated using a laminar free convection correlation, and the following conditions: saturated liquid hydrogen at 137.9 kPa , $g/g_0 = 10^{-4}$, and an average tank wall heat flux of $q''(\text{avg}) = 1.9 \text{ W/m}^2$. The free convection coefficient will be smaller for lower acceleration levels and lower heat flux levels. For the COLD-SAT supply tank, the parameter hL/k will be less than 0.2 , consequently the heat flux distribution will primarily depend on only two parameters as shown in Figure 6-2.

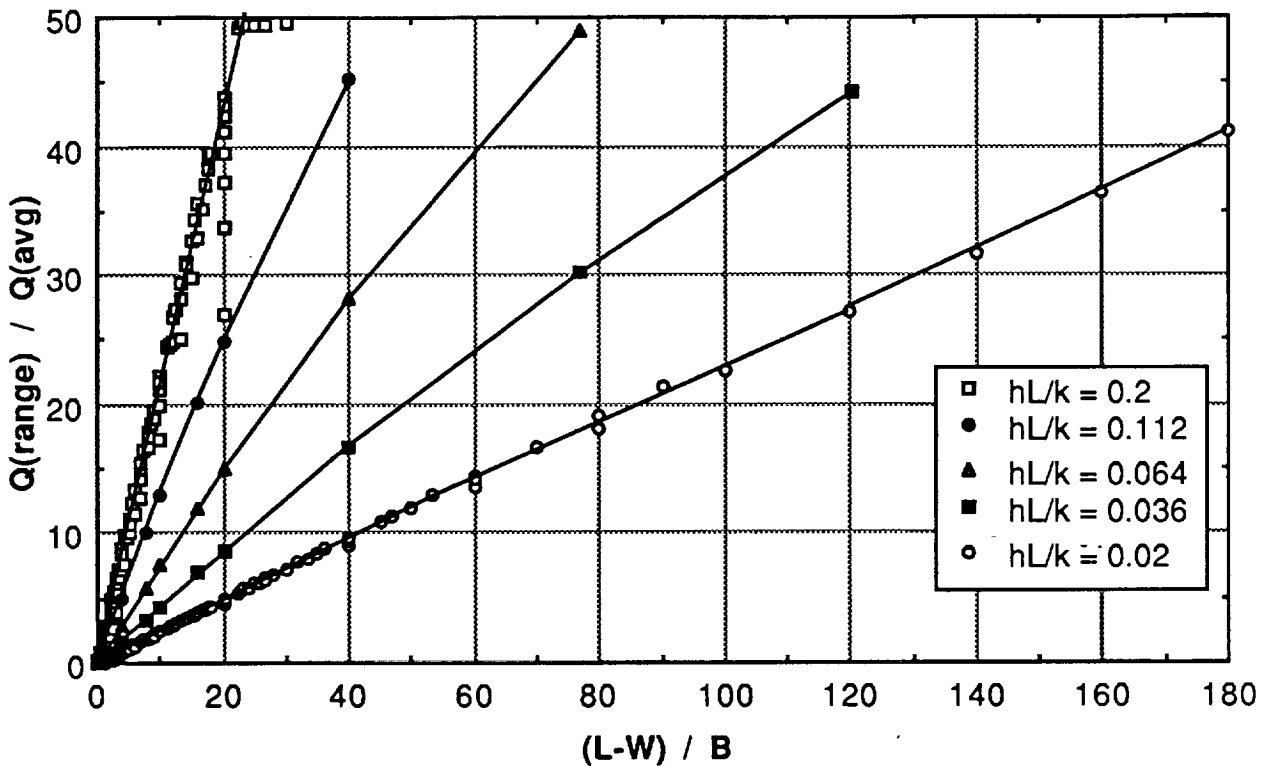


Figure 6-2. Heat Flux Variation for Low Values of the Parameter hL/k

The tolerable limit for the heat flux variation on the tank wall inner surface is expected to be about ± 10 percent, which roughly corresponds to a heat flux range of 20 percent. Figure 6-3 indicates that the percentage of the tank wall outer surface which must be covered by heaters to achieve a 20 percent heat flux variation on the tank wall inner surface decreases as the heater spacing decreases. The heater width is equal to the product of the heater spacing and the fraction of the tank wall covered by heaters. Results for two convective conditions on the tank wall inner surface are shown. The high convection coefficient, $h = 11.3 \text{ W/m}^2\text{-K}$, represents the maximum expected value, while $h = 2.3 \text{ W/m}^2\text{-K}$ represents a lower limit expected if vapor contacts the tank wall. As indicated in Figure 6-3, when the convective coefficient is high the heaters must cover a greater percentage of the tank wall outer surface to insure a "uniform" heat flux distribution on the tank wall inner surface.

For large heater spacing, i.e., $\sim 300 \text{ mm}$, the heat flux uniformity on the tank wall inner surface can be made acceptable without high heater coverage by sandwiching a layer of thermally-conducting material and a layer of thermally-insulating material between the heaters and the tank wall outer surface. These heater configurations have also been investigated, but are not recommended because of the additional weight and complexity.

Figure 6-3 indicates that the heat flux variation on the tank wall inner surface will be less than 20 percent if the heater spacing is 76.2 mm or less, regardless of the width of the heater, i.e., the heater can be made infinitesimally narrow. This result is valid for the maximum convection condition expected during the thermal stratification experiments, therefore the heat flux variation will be less than 20 percent for lower convective coefficients. For a given average heat flux level through the tank wall, the "heater" heat flux increases as the width of the heater decreases. The heat flux distribution on the tank wall inner surface will vary less than 15 percent for 12.7 mm wide heaters

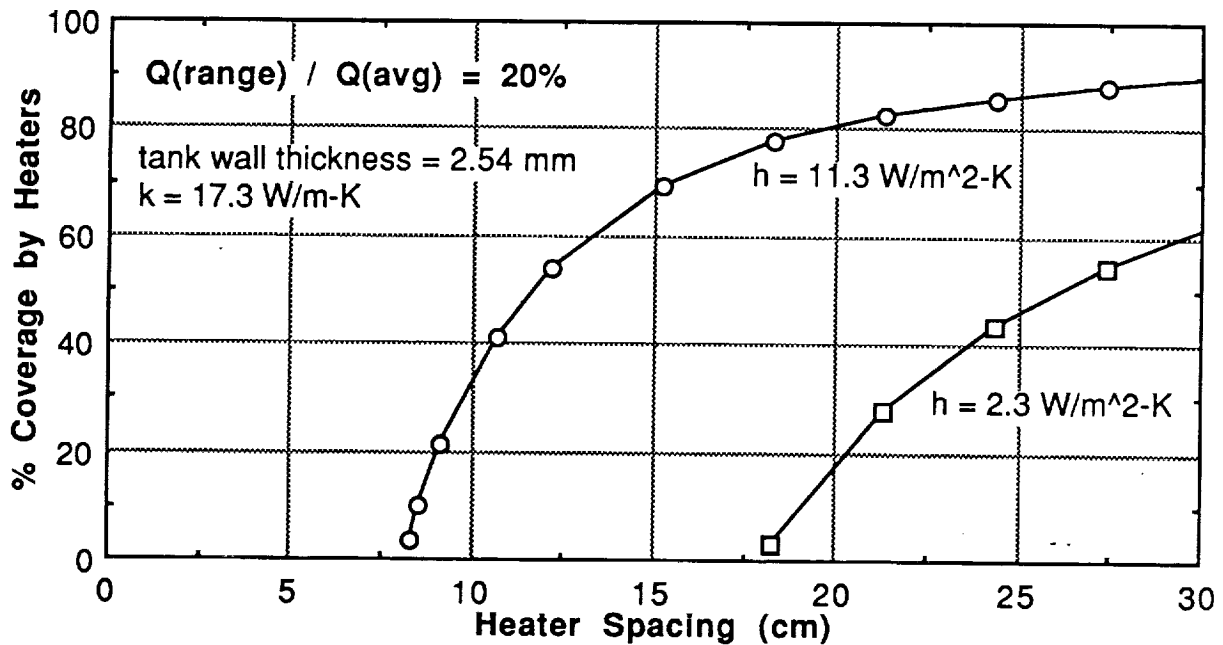


Figure 6-3. Heater Coverage Required on the Tank Wall Outer Surface to obtain 20 percent Heat Flux Variation on the Inner Surface

spaced 76.2 mm apart on the tank wall outer surface. This is the recommended design for the supply tank heaters. The heater heat flux will have to be 11.35 W/m^2 to obtain a 1.9 W/m^2 average heat flux through the tank wall for this configuration.

The heat flux distributions on the tank wall inner surface for two example heater configurations, both having a 20 percent heat flux variation, are shown in Figure 6-4. Examples of low and high heater coverage are shown. The local heat flux is normalized by the average heat flux, and the x-coordinate is measured from the center of a heater. The heat flux distribution on the tank wall inner surface varies in a periodic manner. Although the average heat flux and the heat flux variation are the same for these two cases, the spatial frequency of the heat flux distribution is greater for smaller heater spacing. The spatial frequency is an additional parameter which describes the "heat flux uniformity".

For small heater spacing, and therefore low heater coverage, the heater heat flux is much higher than the average heat flux through the tank wall. Consequently, the heat flux distribution in the small region beneath the heaters rises to a steep peak and varies gradually over the large region between adjacent heaters. For large heater spacing, and therefore high heater coverage, the heater heat flux is only slightly higher than the average heat flux. The heat flux distribution in the large region beneath the heaters varies gradually and drops to a relatively sharp minimum in the short region between adjacent heaters.

Figure 6-5 shows isotherms in a tank wall having the recommended heater configuration; 12.7 mm wide heaters, spaced 76.2 mm apart on the tank wall outer surface. The coordinate system is compressed in the x-direction and has the origin on the tank wall outer surface at the center of the heater. The temperature distribution in the tank wall is nearly one-dimensional, i.e., the temperature variation through the thickness of the tank wall is insignificant relative to the temperature variation in the x-direction. The maximum temperature difference in the tank wall is 0.028 K.

The transient behavior of the heat flux immediately after the heaters are turned on is shown in Figure 6-6, for two convective conditions. The initial tank wall temperature was assumed to be

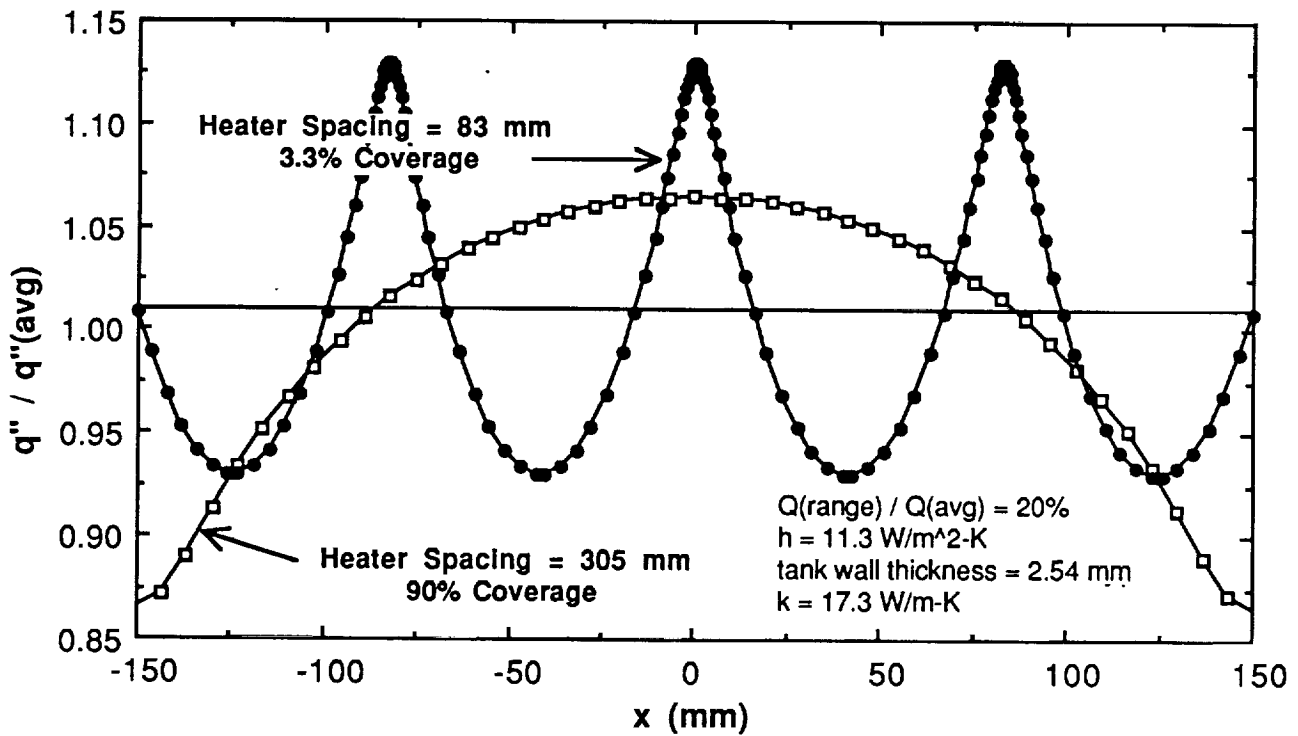


Figure 6-4. Heat Flux Distributions on the Tank Wall Inner Surface

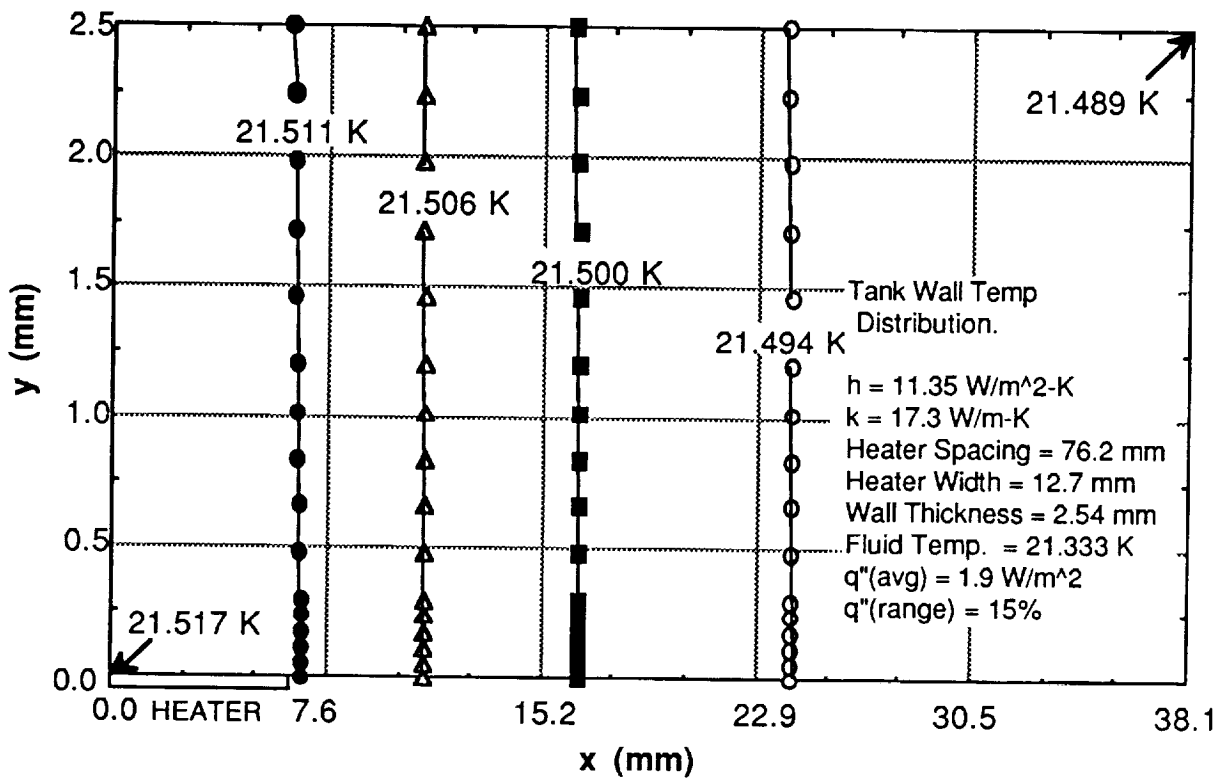


Figure 6-5. Isotherms in the Tank Wall

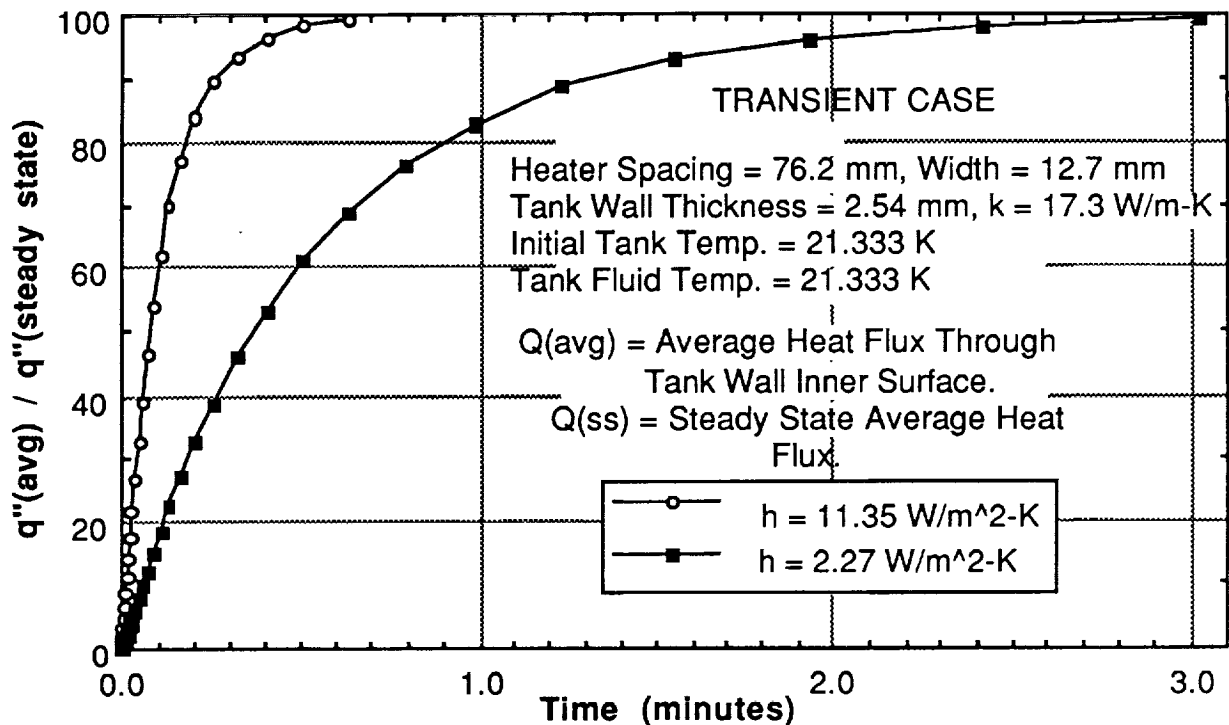


Figure 6-6. Transient Behavior of the Heat Flux Through Tank Wall

uniform and equal to the tank fluid temperature. Once the heaters are turned on, the average heat flux through the tank wall inner surface monotonically increases from zero to the steady-state value. Three minutes after the heaters are turned on, the average heat flux through the tank wall inner surface is 99 percent of the steady-state value for the lowest expected convection condition, $h = 2.27 \text{ W/m}^2\text{-K}$. The time required for the heaters and tank wall to reach steady state decreases as the convective coefficient increases, because the steady-state tank wall temperatures are lower. The transition time is less than 40 seconds for the maximum expected heat transfer coefficient, $h = 11.35 \text{ W/m}^2\text{-K}$.

6.3.1.2 Heat Flux to Initiate Nucleate Boiling. The heat flux level on well-insulated cryogen storage tanks in the micro-g space environment is expected to be less than 0.3 W/m^2 . Nucleate boiling is not expected to be significant at these low heat flux levels. The dominant heat transfer mechanism is expected to be convection. Even during "quiescent" periods, when the tank mixer is not operating, convective fluid motion will exist in the tank as a result of buoyancy forces, spacecraft disturbances, persistence from earlier mixer operation, and possible variations in surface tension.

In order to reduce the duration of thermal stratification experiments performed on COLD-SAT, the tank wall heat flux level for many experiments will be set higher than 0.3 W/m^2 . However, the heat flux level must not be increased beyond the point where nucleate boiling becomes significant, otherwise the results of the experiments will not be directly applicable to cryogen storage depots, where conduction and convection are expected to be the dominant heat transfer mechanisms.

The approximate heat flux level that initiates significant nucleate boiling was estimated by matching the free convective coefficient with the heat transfer coefficient for nucleate boiling, as shown schematically in Figure 6-7. The onset of nucleate boiling (ONB) occurs when the heat flux

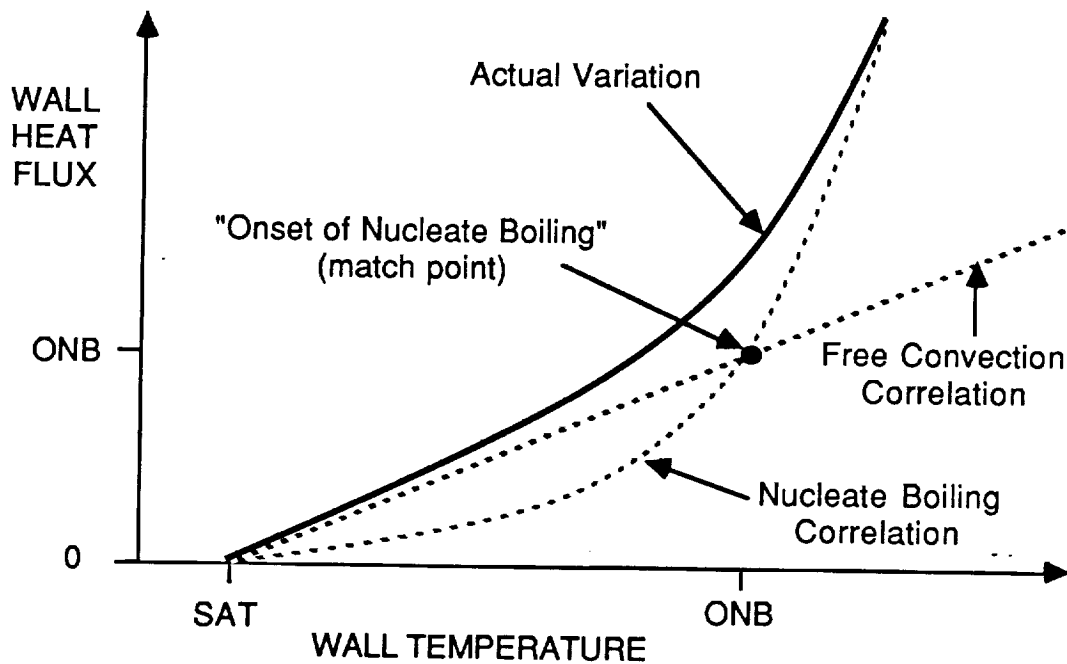


Figure 6-7. Relationship between Wall Heat Flux and Wall Temperature

increases to the point where vapor bubbles form and detach from the wall, enhancing the convection and causing a decrease in the wall temperature. The heat flux level when nucleate boiling is initiated is estimated as the heat flux where the convective capacity due to free convection is equal to that of nucleate boiling.

The Rohsenow correlation (Reference 6-1) was used to indicate the relationship between the wall temperature (T_w) and the tank wall heat flux (q'') for nucleate boiling heat transfer. T_{sat} is the saturation temperature corresponding to the tank pressure, C_{sf} is an empirical constant that depends on the nucleation properties of the liquid-surface combination (typically $C_{sf} = 0.013$), g is the acceleration level, and c_{pf} , h_{fg} , μ_f , k_f , ρ_f , Pr_f , ρ_g , σ are fluid properties. The exponents k and m recommended by Rohsenow are 0.33 and 0.7, respectively.

$$\frac{c_{pf}(T_w - T_{sat})}{h_{fg}} = C_{sf} \left[\frac{q''}{\mu_f h_{fg}} \left(\frac{\sigma g_c}{g(\rho_f - \rho_g)} \right)^{0.5} \right]^k Pr_f^{(1+m)} \quad (6-8)$$

The relationship between the wall temperature and the tank wall heat flux for laminar free convection is shown in Equation 6-9 (Reference 6-2). L is the free convective length scale, C and n are empirical constants that have values of 0.6 and 0.25, respectively. The "bulk" liquid temperature is assumed to be at the saturation temperature corresponding to the tank pressure.

$$\frac{q'' L}{(T_w - T_{sat}) k_f} = C \left[\frac{g \beta_f \rho_f^2 (T_w - T_{sat}) L^3 Pr_f}{\mu_f^2} \right]^n \quad (6-9)$$

Solving Equation 6-8 for T_w in terms of q'' and substituting into Equation 6-9 results in an equation for the heat flux when nucleate boiling is initiated (q''_{ONB}). This equation is dependent only on fluid properties, free convective length scale, and gravity level.

$$q''_{\text{ONB}}^{(1-kn-k)} = \quad (6-10)$$

$$C C_{\text{sf}}^{(n+1)} g^{(n-kn/2-k/2)} L^{(3n-1)} Pr_f^{(n+mn+m)} \mu_f^{(1-k-nk-n)} k_f^{-n} (\beta_f \rho_f^2)^n \left[h_{fg}^{(1-k)} \left(\frac{\sigma g_c}{\rho_f - \rho_g} \right)^{k/2} \right]^{(n+1)}$$

As shown in Figure 6-8, the heat flux which initiates nucleate boiling increases as the acceleration level increases and as the free convective length scale decreases. Properties of saturated hydrogen at 103.4 kPa were used for this figure. The free convective length scale is difficult to determine for this complex geometry, however, it must be smaller than the tank, i.e., 2.4 m. Figure 6-8 indicates that significant nucleate boiling is not expected for heat flux levels less than 1 W/m² when the acceleration level is greater than $g/g_0 = 10^{-9}$. However, nucleate boiling may occur at the highest heat flux level used during the COLD-SAT thermal stratification experiments, i.e., $q'' = 1.9 \text{ W/m}^2$, particularly at low acceleration levels. This analysis has considered only buoyancy-driven convection. If other sources of convective fluid motion are significant, e.g., spacecraft disturbances, the onset of nucleate boiling will occur at higher heat flux levels.

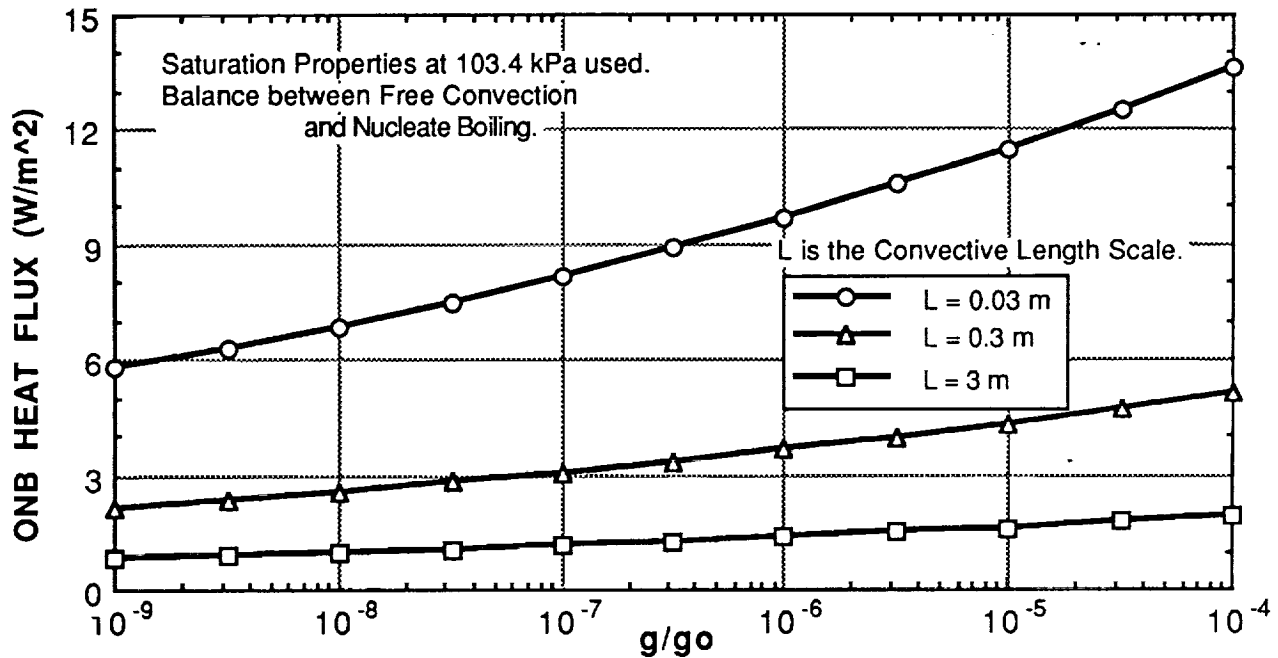


Figure 6-8. Heat Flux to Initiate Nucleate Boiling on a Heated Wall

6.3.1.3 Buoyancy-Driven Fluid Velocity. Two different analyses have been performed to indicate the magnitude of the buoyancy-driven fluid velocity near a heated wall. The free-convection correlation given in Equation 6-11 (Reference 6-2) indicates the relationship between the convection coefficient and the tank wall heat flux in a laminar, buoyancy-driven flow. L_B is the free convection length scale.

$$\frac{h L_B}{k} = 0.6 \left[\frac{g \beta \rho^2 q'' L_B^4 Pr}{k \mu^2} \right]^{0.2} \quad (6-11)$$

In general, the convection coefficient is a fluid mechanic quantity that depends primarily on the flow field near the wall and the fluid properties. The fluid velocity is the dominant characteristic of a flow field. The laminar forced-convection correlation given in Equation 6-12 (Reference 6-2) indicates the

relationship between the convection coefficient and the fluid velocity. L_P is the convective length scale of the flow.

$$\frac{h L_P}{k} = 0.664 \left(\frac{U \rho L_P}{\mu} \right)^{1/2} Pr^{1/3} \quad (6-12)$$

Equations 6-11 and 6-12 can be combined to eliminate h . The result is an expression for the buoyancy-driven fluid velocity magnitude in terms of the acceleration level, wall heat flux level, fluid properties, and convective length scales. This expression is shown in Equation 6-13, where the convective length scales have been assumed to be equal, i.e., $L_B = L_P = L$.

$$U = 0.82 \left(\beta^2 \mu / k^2 \rho \right)^{0.2} Pr^{-0.27} (q'' g)^{0.4} L^{0.6} \quad (6-13)$$

The expression given in Equation 6-13 is based on empirical correlations for free and forced convection. A theoretical analysis of the boundary layer on a heated tank wall was performed to provide a second estimate of the velocity magnitude expected when buoyancy forces drive the flow. This analysis is not dependent on an empirical correlation for forced convection. Listed below is the differential form of the momentum equation applicable to a two-dimensional laminar boundary layer flow (Reference 6-3):

$$\rho U \frac{\partial U}{\partial x} + \rho V \frac{\partial U}{\partial y} = -\frac{dP}{dx} + \frac{\partial}{\partial y} \left(\mu \frac{\partial U}{\partial y} \right) - \rho g \quad (6-14)$$

where x is the coordinate measured in the flow direction, y is measured perpendicular to the wall, P is the static pressure, and U and V are the fluid velocities in the x and y directions, respectively. For a buoyancy-driven flow, the pressure gradient in the boundary layer equals the hydrostatic pressure gradient outside the boundary layer:

$$\frac{dP}{dx} = -\rho_\infty g \quad (6-15)$$

where ρ_∞ is the bulk fluid density outside the free convection boundary layer. The velocity is zero at the wall and in the "freestream". The peak velocity occurs at some location near the heated wall where the velocity gradient is zero:

$$\frac{\partial U}{\partial y} = 0 \quad (\text{at the peak velocity point in boundary layer}) \quad (6-16)$$

For free convection flows the following simplified equation of state is applicable:

$$\rho_\infty - \rho = \rho \beta (T - T_\infty) \quad (6-17)$$

Substituting Equations 6-15 through 6-17 into Equation 6-14 results in a differential relationship between the peak velocity (U_{peak}) and the flow coordinate (x):

$$U_{\text{peak}} \frac{\partial U_{\text{peak}}}{\partial x} = g \beta (T - T_\infty) \quad (6-18)$$

The viscosity term in Equation 6-14 has been neglected, consequently Equation 6-18 represents an overestimate of the peak velocity. Equation 6-18 can be integrated from the origin of the free convection boundary layer ($x = 0$), where $U_{\text{peak}} \approx 0$, to $x = L$ where the peak velocity is U_{peak} :

$$U_{\text{peak}} \approx \sqrt{2 g \beta (T_{\text{wall}} - T_{\infty}) L} \quad (6-19)$$

The variation in the x-direction of the fluid temperature at the maximum velocity point has been neglected and assumed equal to the wall temperature (T_{wall}). This approximation will result in high estimates of the peak velocity in the boundary layer near the heated tank wall. The free convection correlation given in Equation 6-11 indicates the relationship between the wall-to-bulk fluid temperature difference and the wall heat flux for a buoyancy-driven flow. Substituting this correlation into Equation 6-19 results in the following expression:

$$U = 1.83 \left(\beta^2 \mu / k^2 \rho \right)^{0.2} \text{Pr}^{-0.1} (q'' g)^{0.4} L^{0.6} \quad (6-20)$$

Equations 6-13 and 6-20 are rough order-of-magnitude estimates of the fluid velocity in a buoyancy-driven flow near a heated wall in terms of the fluid properties, wall heat flux, acceleration level, and convective length scale. The precise size of the convective length scale is difficult to predict, but is limited by the size of the tank (2.4 m). The predicted velocity will be less for smaller length scales.

Fluid velocities in a buoyancy-driven flow near a heated wall for a range of acceleration levels are shown in Figure 6-9. The velocity estimates based on the theoretical analysis of the buoyancy-driven boundary layer are higher, but the same order-of-magnitude as the estimates based on the empirical correlations. Fluid velocities in vapor are higher than in liquid. The highest tank wall heat flux expected on the COLD-SAT supply tank was used for these calculations, $q'' = 1.9 \text{ W/m}^2$. The velocities will be lower for smaller heat flux levels. The highest velocity expected in the liquid for a background acceleration level of $g/g_0 = 10^{-7}$ is less than 0.4 mm/s.

These small velocities indicate that buoyancy forces will cause negligible circulation within the tank liquid. Fluid motion persistence from earlier mixer operation and/or small spacecraft disturbances could cause fluid velocities of this magnitude or greater, enhancing the heat transfer coefficient. Consequently, free convection may not be the dominant heat transfer mechanism during the thermal stratification experiments.

6.3.1.4 Maximum Thermal Stratification Times. Thermal stratification tests will be performed in a heated, locked-up tank. The tests will begin with the tank fluid in thermal equilibrium at 103.4 kPa, and end when the tank pressure has risen to 137.9 kPa. The pressure rise time is proportional to the mass in the tank and inversely proportional to the heat leak into the tank. The lowest pressure rise rate, and therefore the maximum pressure rise time, will occur if the tank fluid remains in thermal equilibrium. For this idealized case, pressure rise times were calculated using the conservation of energy equation. The fluid mass in the tank and the tank volume remain constant during these tests. Figure 6-10 shows the maximum time for the tank pressure to rise 34.5 kPa for a range of initial liquid fill levels in each of the three COLD-SAT tanks. Results are shown for the three heat flux levels to be imposed on the supply tank, and the single background heat flux level on the receiver tanks. The pressure rise times for the receiver tanks are less than the supply tank due to the smaller amount of fluid mass contained in the receiver tanks. These results were used to estimate the maximum time required to perform the thermal stratification tests shown in Table 6-6. The actual test times are expected to be shorter since the fluid is not expected to remain in thermal equilibrium.

6.3.2 Passive TVS

6.3.2.1 Flow Rate and Duty Cycle. The TVS flow rate required to maintain a constant tank pressure is dependent on the heat leak rate into the tank and the thermodynamic states of the tank fluid and exiting TVS fluid. Assuming the tank fluid remains in thermal equilibrium, the

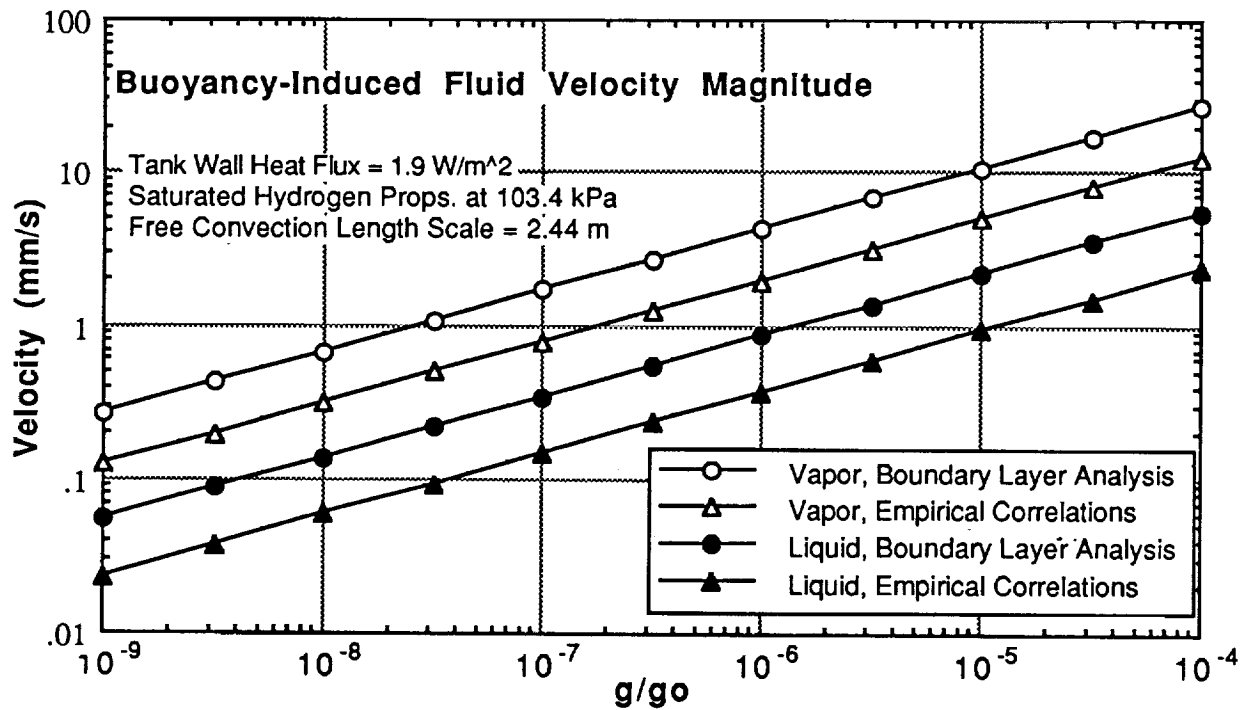


Figure 6-9. Magnitude of the Fluid Velocity in a Buoyancy-Driven Flow Near the Heated Wall

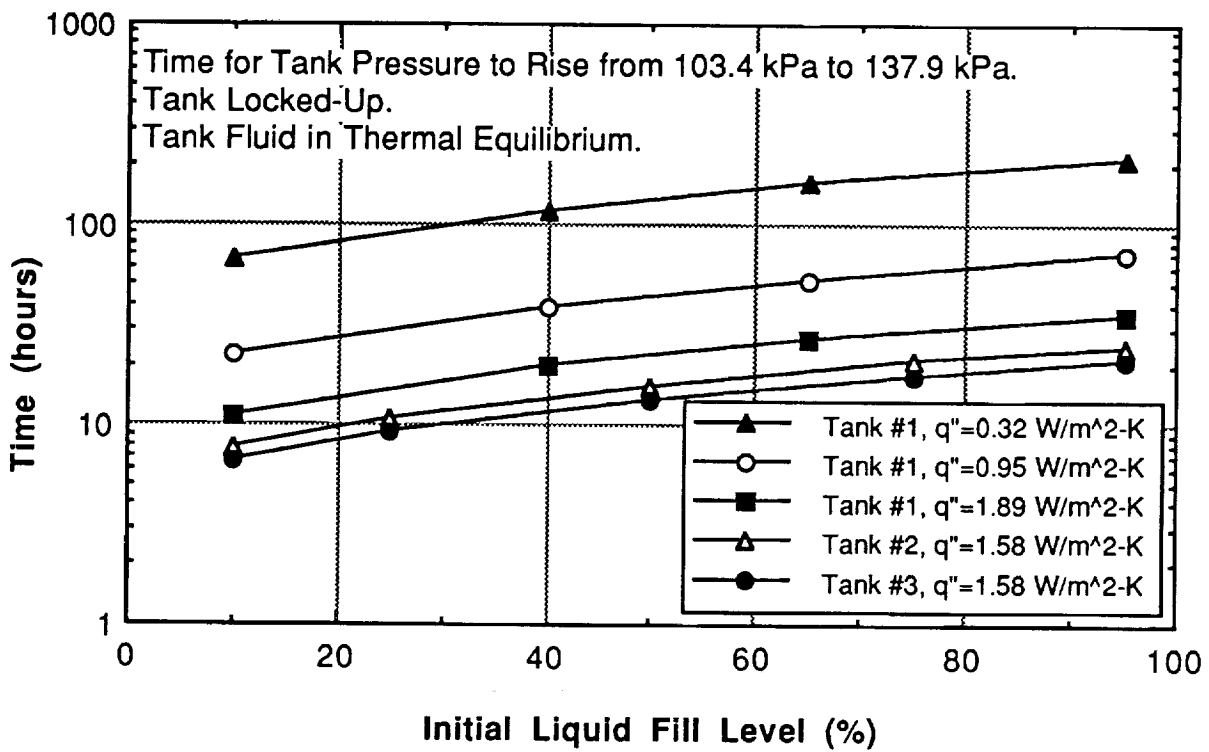


Figure 6-10. Maximum Pressure Rise Times

conservation laws for mass, energy, and tank volume can be combined to calculate the steady-state boiloff rate (m_{TVS}). The steady state boiloff rate is not dependent on the liquid fill level.

$$m_{TVS} = \frac{q'' A}{h_{exit} - \frac{u_g}{1 - v_g/v_f} - \frac{u_f}{1 - v_f/v_g}} \quad (6-21)$$

The heat leak into the tank is equal to the product of the heat flux, q'' , and the area it acts on, A . The fluid properties, u_g , u_f , v_g , and v_f are evaluated at the tank pressure. The enthalpy of the exiting TVS fluid is denoted h_{exit} . The steady state boiloff rates for the three COLD-SAT tanks over a range of heat flux levels are shown in Figure 6-11. The tank pressure is 103.4 kPa and the exiting TVS fluid is assumed to be saturated vapor at 34.5 kPa.

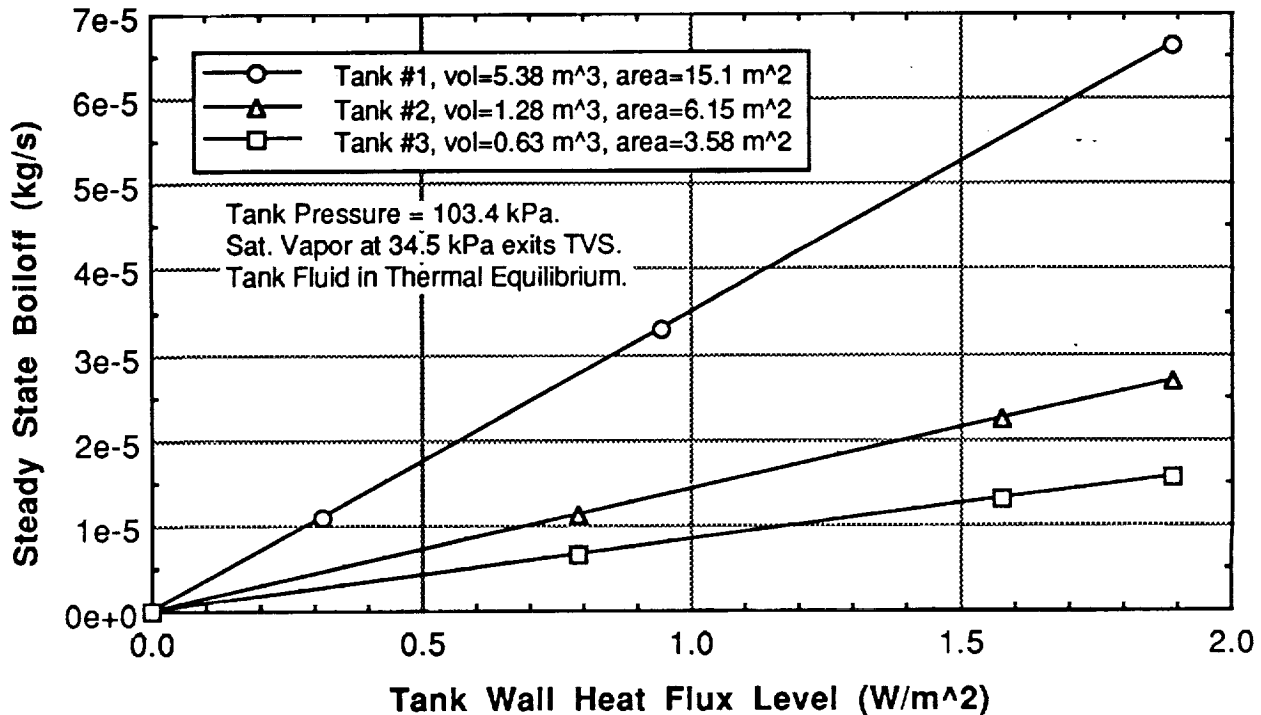


Figure 6-11. Steady State Boiloff

Each tank is equipped with a wall-mounted TVS heat exchanger to control tank pressure. To minimize hardware, each heat exchanger will have a single throttling valve (plus redundancy valves), consequently only a single flow rate for each wall-mounted heat exchanger can be used for a given set of tank and TVS pressures. The TVS flow rate will vary slightly as the tank pressure varies. Varying the TVS back pressure was considered as a means to vary the TVS flow rate, but this procedure is not feasible for the planned tests.

For constant tank pressure tests, the TVS energy removal rate must equal the tank heat leak rate, while for pressure reduction tests, the TVS energy removal rate must be greater than the tank heat leak rate. In the supply tank, heaters will be used to vary the tank heat leak rate relative to the TVS energy removal rate. For constant tank pressure tests, the wall-mounted TVS will operate continuously at a flow rate of 6.63×10^{-5} kg/s, corresponding to a heat flux level of 1.9 W/m^2 (see Figure 6-12). For pressure reduction tests, the heat flux level will be decreased to 0.315 W/m^2 , so the TVS energy removal rate will be greater than tank heat leak rate.

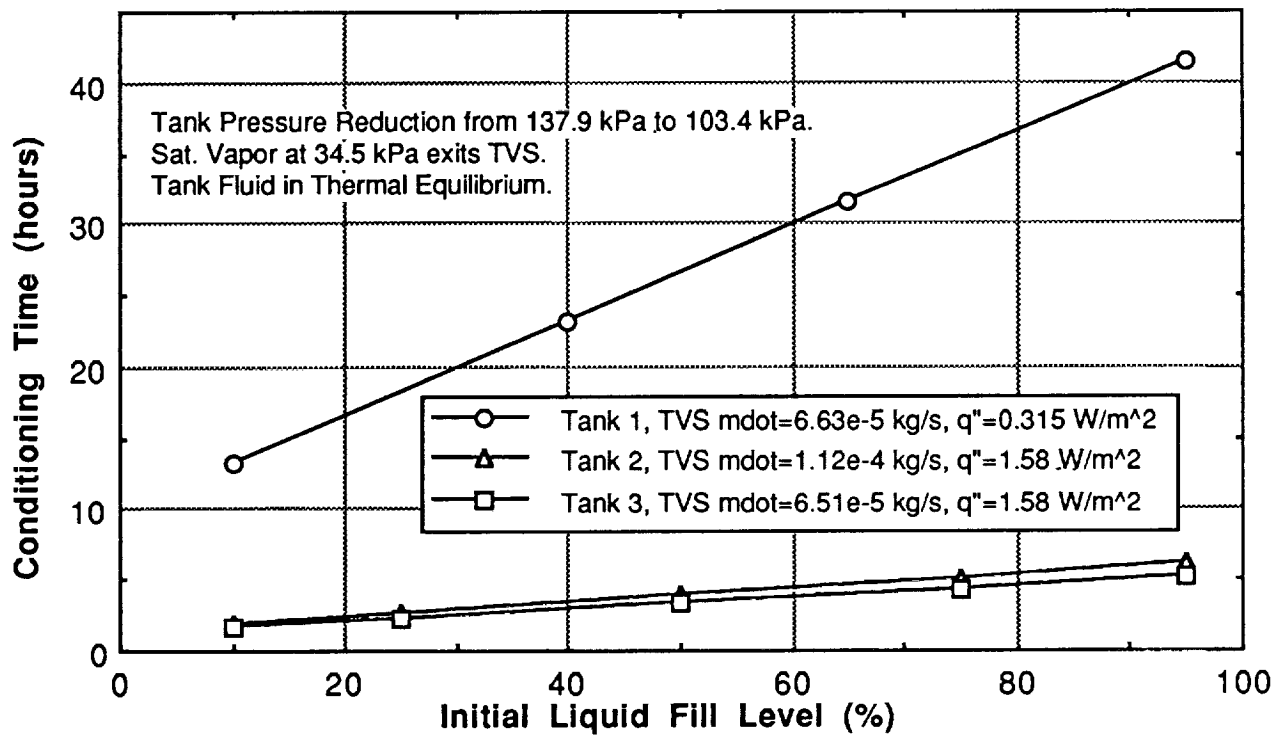


Figure 6-12. Time for Each Pressure Reduction Test

For the two receiver tanks, heaters cannot be used to vary the tank heat leak rate relative to the TVS energy removal rate. Instead, the TVS will operate intermittently for the constant tank pressure tests and continuously for the pressure reduction tests. The TVS flow rate, when operating, will be set at five times the steady-state flowrate corresponding to the background heat flux level of 1.58 W/m^2 , i.e., $11.2 \times 10^{-5} \text{ kg/s}$ for Tank 2 and $6.51 \times 10^{-5} \text{ kg/s}$ for Tank 3 (see Figure 6-11). During the constant tank pressure tests, the TVS will be operated on a 20 percent duty cycle, so the time-averaged TVS flow rates will be $2.24 \times 10^{-5} \text{ kg/s}$ for Tank 2 and $1.30 \times 10^{-5} \text{ kg/s}$ for Tank 3. As a result, the time-averaged TVS energy removal rates will equal the tank heat leak rates.

The duty cycle frequency will be high so that the TVS energy removal rate will be nearly constant with time and to insure that no liquid will be vented from the TVS heat exchanger. A high frequency corresponds to a duty cycle time period that is short relative to the residence time of fluid in the heat exchanger. This residence time is dependent on the mass flowrate, quality distribution along the TVS tube, and the TVS tube length. Table 6-6 indicates the actual residence time for the fluid in the TVS tube is about 40 seconds, as predicted by the FLUIDTVS program. This program and the TVS tube length calculations will be discussed later in this section. Table 6-6 also shows the lower and upper limit for the residence time. The lower limit is about 10 seconds and was calculated by assuming the TVS fluid is superheated vapor at the tank temperature through the entire tube. The upper limit is around 30 minutes and was calculated by assuming the TVS fluid remains as saturated liquid at the TVS saturation temperature through the entire tube. To be conservative, the duty cycle time period will be set at 150 seconds. The TVS will be "on" for 20 percent of this time every cycle, i.e., 30 seconds per cycle. Each fluid molecule is expected to take over 1.25 cycles to pass through the TVS tube. The periodic behavior of the intermittent TVS operation will be monitored with measurements of pressure, temperature, and flowrate taken at one second intervals.

Table 6-6. Residence Time of Fluid in Wall-Mounted TVS Heat-Exchanger

	TVS Flow Rate (kg/sec)	TVS Tube Length (m)	Residence Time Lower Limit. Vapor 34.5 kPa, 21.4 K	Actual Residence Time	Residence Time Upper Limit. Sat. Liquid 34.5 kPa
Tank 2	1.12×10^{-4}	66.4	9.1 sec	37.3 sec	28 min
Tank 3	6.51×10^{-5}	43.6	10.3 sec	43.8 sec	32 min

Energy is required to open and close the solenoid valves that will be used to control the TVS. These valves "latch" in the open and closed position, so no energy is required except to change position. The current design calls for a valve that energizes for 0.3 seconds to change position, and uses 2.5 amps at 28 volts. For the constant tank pressure tests, the valve will be energized twice every duty cycle, i.e., every 150 seconds. The time-averaged energy dissipation rate is 0.28 Watts. Most of this energy is expected to be absorbed by the TVS fluid. For Tank 2, this amounts to less than 3 percent of the time-averaged TVS energy removal rate during constant pressure tests. For Tank 3, the power to switch the valves is less than 5 percent of the TVS energy removal rate. These valves are the same as other valves required on COLD-SAT. They were selected to reduce the number of different kinds of valves required. Valves which require only 0.02 seconds to change position are available. The time-averaged power required to switch these faster-latching valves would be less than 0.4 percent of the time-averaged TVS energy removal rate during constant tank pressure tests. The final valve selection will be delayed until the impact of the power dissipated by valves and other parasitic heat leaks into the tanks have been evaluated in greater detail.

During the constant tank pressure tests in Tanks 2 and 3, the TVS control valve will be cycled on and off every 150 seconds. To perform all of the constant tank pressure tests currently planned (see Table 3-2), the valve controlling the Tank 2 TVS will be energized less than 3100 times. Similarly,

the Tank 3 TVS valve will be energized less than 2600 cycles. From the standpoint of reliability, the intermittent operation of the TVS should present little problem.

During the passive TVS pressure reduction tests the wall-mounted TVS will be run continuously in an attempt to reduce the tank pressure from 137.9 to 103.4 kPa. During these tests, the tank wall heat flux will be reduced to 0.315 W/m^2 on the supply tank. Only the background heat flux, $q'' = 1.58 \text{ W/m}^2$, will be applied to the receiver tanks. Conditioning times were estimated using the conservation equations for energy, mass and tank volume. The tank fluid was assumed to be in thermal equilibrium for these calculations. Predicted conditioning times and the total boiloff mass are shown in Figures 6-12 and 6-13 for a range of initial liquid fill levels. The conditioning time and boiloff is much higher in the supply tank as compared to the receiver tanks due to the greater mass of fluid. The TVS flow rates were assumed constant for these calculations. In reality, the TVS flowrate will decrease by about 18 percent as the tank pressure decreases from 137.9 to 103.4 kPa. The TVS pressure was assumed constant at 34.5 kPa. As discussed in Section 3.2.1, if free convection is the dominant heat transfer mechanism in the micro-g space environment, the tank fluid will probably not remain in thermal equilibrium as assumed here. Operating the TVS with an energy removal rate greater than the tank heat leak will likely subcool the surrounding liquid and cause no immediate decrease in the tank pressure. However, if other convective mechanisms are significant, the passive TVS may be successful in reducing the tank pressure. The times and boiloff amounts shown in these figures were used to estimate the duration and amount of hydrogen used during the passive TVS pressure reduction tests shown in Table 3-2. The actual time and boiloff required to reduce the tank pressure by 34.5 kPa using the passive TVS could be much greater than these estimates. Consequently, the tests will be terminated after the times shown in Figure 6-12, unless a significant reduction in the tank pressure has occurred.

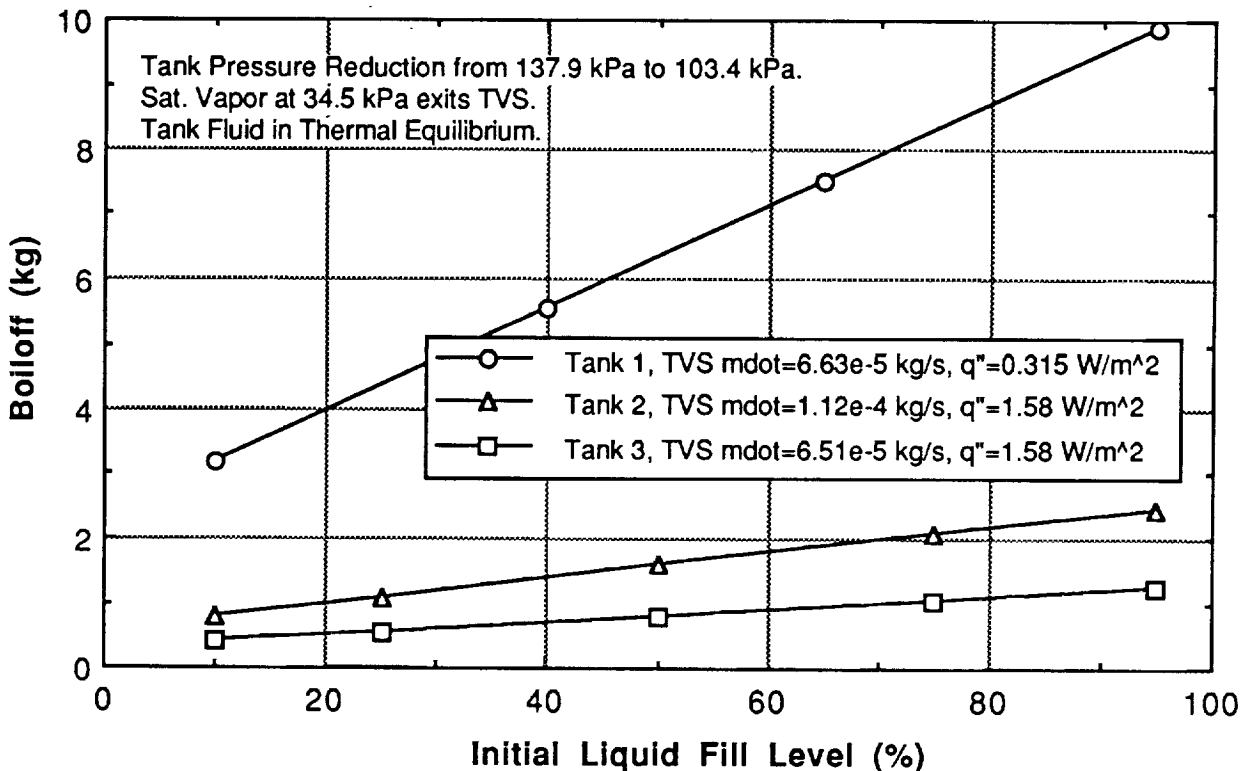


Figure 6-13. Boiloff Amount for Each Pressure Reduction Test

6.3.2.2 Wall-Mounted TVS Tube Length. The TVS tube must be sufficiently long to remove enough energy from the tank fluid to completely vaporize the TVS fluid. The computer program FLUIDTVS, developed under GDSS IRAD (Reference 6-4), was used to analyze the heat transfer between the tank fluid and the TVS fluid and determine the tube length necessary to completely vaporize the TVS fluid, i.e., saturated vapor is assumed to exit the TVS. This program takes into account the axial variation in conditions along the tube. Heat is transferred from the tank fluid to the TVS tube by free convection, and from the TVS tube to the TVS fluid by two-phase forced convection. The conductive resistance through the tube wall is over 100 times smaller than the convective resistances on the inner and outer surfaces of the tube. As a result, the thickness of the tube wall does not significantly influence the heat transfer. A tube wall thickness of 1.27 mm was assumed, and is typical based on fabrication considerations. The thermal resistance on the tube inner surface, due to two-phase forced convection, is as much as 10 times less than the outer surface thermal resistance due to free convection.

Figure 6-14 indicates the effect of a wide range of acceleration levels on the tube length required to vaporize a given TVS flowrate. The minimum acceleration level expected during the COLD-SAT experiments is $g/g_0=10^{-7}$. The required TVS tube length for the supply tank is 44.2 meters. Table 6-6 showed the tube lengths required for Tanks 2 and 3. The required tube length decreases by about 25 percent for an order of magnitude increase in the acceleration level. These results are valid for free convection from a horizontal tube submerged in liquid. The majority of the TVS tube will be mounted perpendicular to the acceleration vector, i.e., horizontal, to take advantage of the greater convective coefficient, as compared to a vertically-mounted tube. The TVS tube will actually be mounted to the tank to take advantage of the wall as an extended heat transfer area. An approximate analysis of a wall-mounted TVS tube has indicated that the results shown in Figure 6-14 represent worse case values for the actual TVS configuration. If fluid motion from sources other than buoyancy forces are significant, shorter tube lengths would be sufficient.

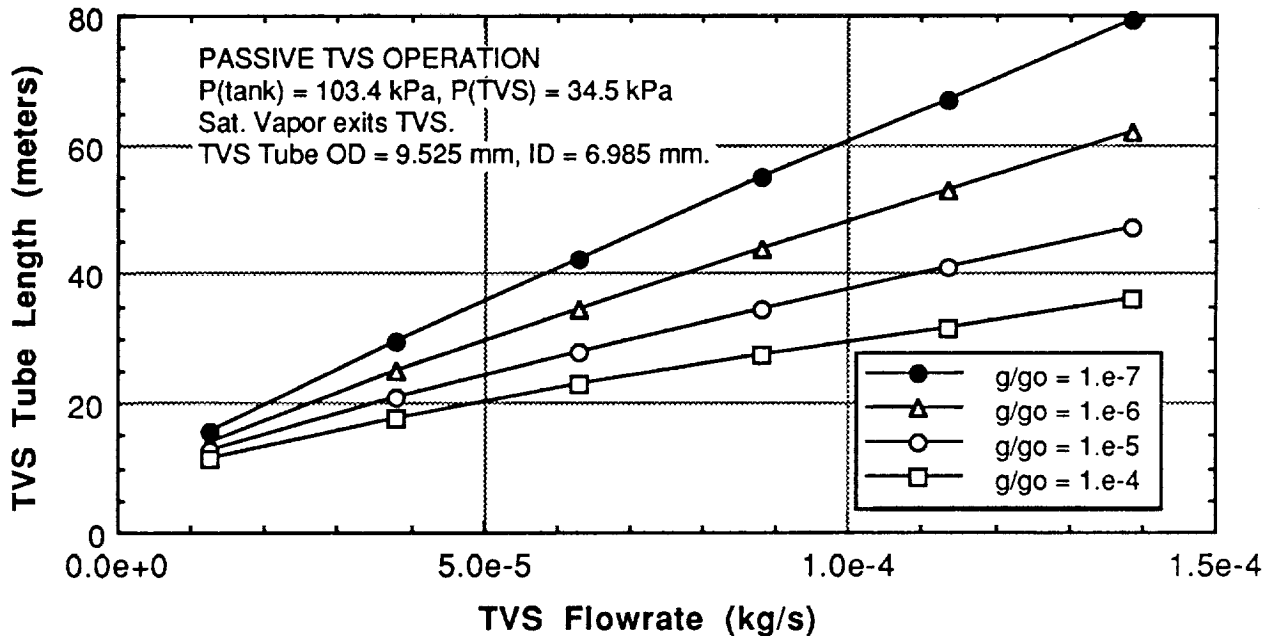


Figure 6-14. TVS Tube Lengths

The tube diameter has little effect on tube length required to vaporize a given TVS flowrate. However, the pressure drop through the tube is a strong function of the tube diameter. The frictional pressure drop through the tube can be expressed in terms of the mass flowrate (m):

$$\Delta P = f \left(\frac{L}{D} \right) \frac{\rho V^2}{2} = \frac{8}{\pi^2} \frac{f L m^2}{D^5 \rho} \quad (6-22)$$

where f is the friction factor, V is the fluid velocity, and ρ is the fluid density. The pressure drop is inversely proportional to the tube diameter raised to the fifth power, neglecting the variation of the friction factor. Estimated pressure drops through the TVS tube are shown in Table 6-7. The Lockhart-Martinelli correlation (Reference 6-1) has been used to estimate the pressure drop for the two-phase flow. To prevent freezing, the back-pressure in the vent will be maintained above 13.8 kPa. To allow a TVS pressure of 34.5 kPa or less, the total pressure drop through the tube must be less than 20.7 kPa. A 6.35 mm OD tube (3.81 mm ID) is too small for Tank 2, and will likely be too small for the supply tank due to the length of VCS tubing which follows the TVS. To have a consistent tube size, 9.53 mm OD (6.99 mm ID) tubing will be used for the wall-mounted TVS on all three tanks.

The minimum tube length necessary to vaporize the TVS flow is also dependent on the phase and temperature of the surrounding fluid. Due to the low acceleration level and the wettability of hydrogen, the majority of the wall-mounted TVS tube is expected to be in contact with liquid, even at low liquid fill levels. Regions of the TVS tube that are in contact with vapor will have elevated heat transfer coefficients due to condensation, consequently TVS tube lengths shorter than those shown in Figure 6-14 would probably be adequate. For the results shown in the figure, the temperature of the liquid surrounding the TVS tube was assumed to be 20.3 K, i.e., the saturation temperature corresponding to 103.4 kPa. At higher liquid temperatures, the heat transfer rate between the tank fluid and TVS fluid will increase. Predictions using the program FLUIDTVS indicate that the required TVS tube length decreases by 30 percent compared to those shown in Figure 6-14 when the liquid temperature is 21.4 K, which corresponds to a saturation pressure of 137.9 kPa.

6.3.3 Supply Tank Mixing

Correlations developed by Aydelott from low-g experiments in a drop tower (Reference 6-5) were used to size the axial jet mixer in the supply tank. The relationships between the mixer flowrate, liquid fill level, and jet diameter are shown in Figure 6-15. The flowrate shown is the minimum flowrate required to disrupt the ullage and establish a flow pattern of complete circulation in the tank. The required flowrate decreases as the liquid fill level decreases. For jet diameters greater than 25.4 mm, the flowrate becomes greater than the flow rates used during liquid transfers between tanks, and are considered too high. For low acceleration levels, $g/g_0 < 10^{-5}$, the acceleration level has little effect on the flowrate required to establish a flow pattern of complete circulation in the tank. As shown in Figure 6-16 the required flowrate increases as the acceleration level increases above $g/g_0 = 10^{-5}$. A 25.4 mm diameter axial jet mixer will be used on the COLD-SAT supply tank. The highest flowrate will be 0.0227 kg/s, which is adequate to handle the most extreme COLD-SAT conditions, i.e., $g/g_0 = 10^{-4}$ and 95 percent liquid fill level. The times required to completely mix all the fluid in the supply tank are shown in Figure 6-17, as a function of liquid fill level. The mixing time decreases as the fill level decreases. Mixing times are short relative to the thermal stratification times, previously shown in Figure 6-10. These results are valid for the highest mixer flowrate, 0.0227 kg/s. Tests will also be performed at two lower flow rates to bracket the optimum mixer power required to thermally destratify the tank fluid. The lowest mixer flowrate will be selected to cause no ullage disruption and mix only the bulk liquid.

Table 6-7. Pressure Drop Through Wall-Mounted TVS Tube

TVS Tube ID 6.985 mm	TVS Flow Rate (kg/s)	TVS Tube Length (meters)	ΔP (kPa) Liquid Flow	ΔP (kPa) Two-Phase Flow	ΔP (kPa) Vapor Flow
Tank 1	6.63×10^{-5}	44.2	0.0117	0.502	0.541
Tank 2	1.12×10^{-4}	66.4	0.0298	1.72	2.06
Tank 3	6.51×10^{-5}	43.6	0.0113	0.482	0.518

TVS Tube ID 3.810 mm	TVS Flow Rate (kg/s)	TVS Tube Length (meters)	ΔP (kPa) Liquid Flow	ΔP (kPa) Two-Phase Flow	ΔP (kPa) Vapor Flow
Tank 1	6.63×10^{-5}	44.2	0.132	8.08	9.87
Tank 2	1.12×10^{-4}	66.4	0.347	28.0	38.2
Tank 3	6.51×10^{-5}	43.6	0.128	7.76	9.44

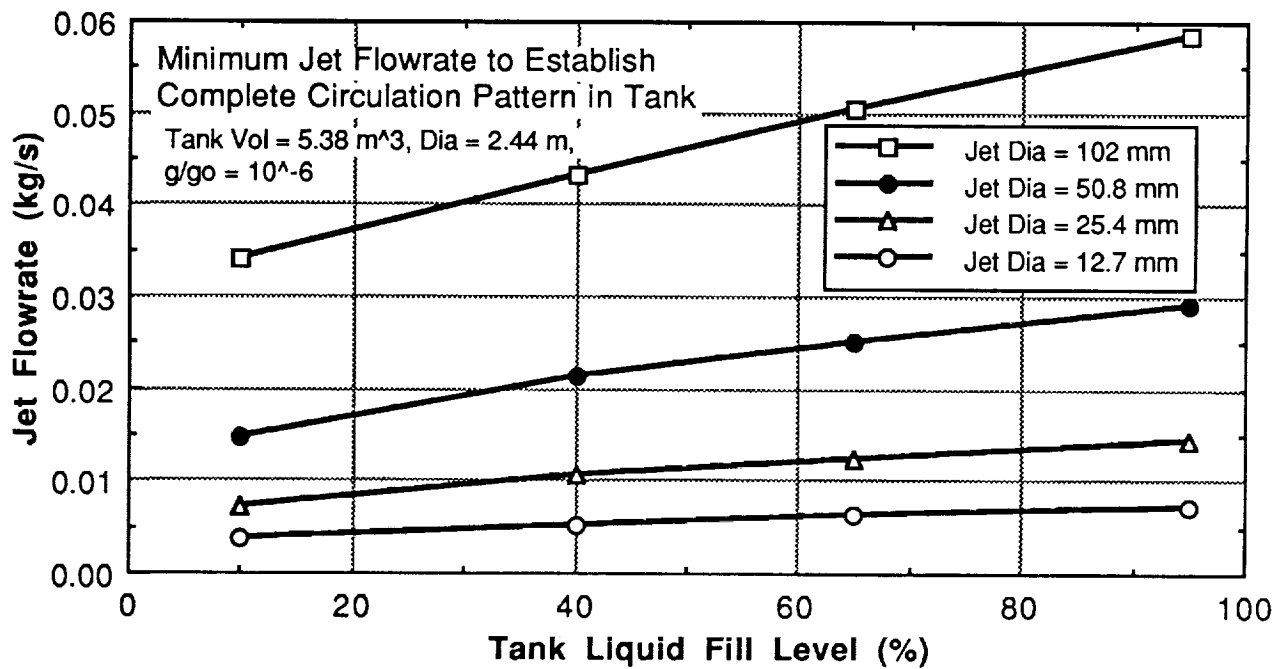


Figure 6-15. Jet Diameter Effects on Axial Jet Mixer

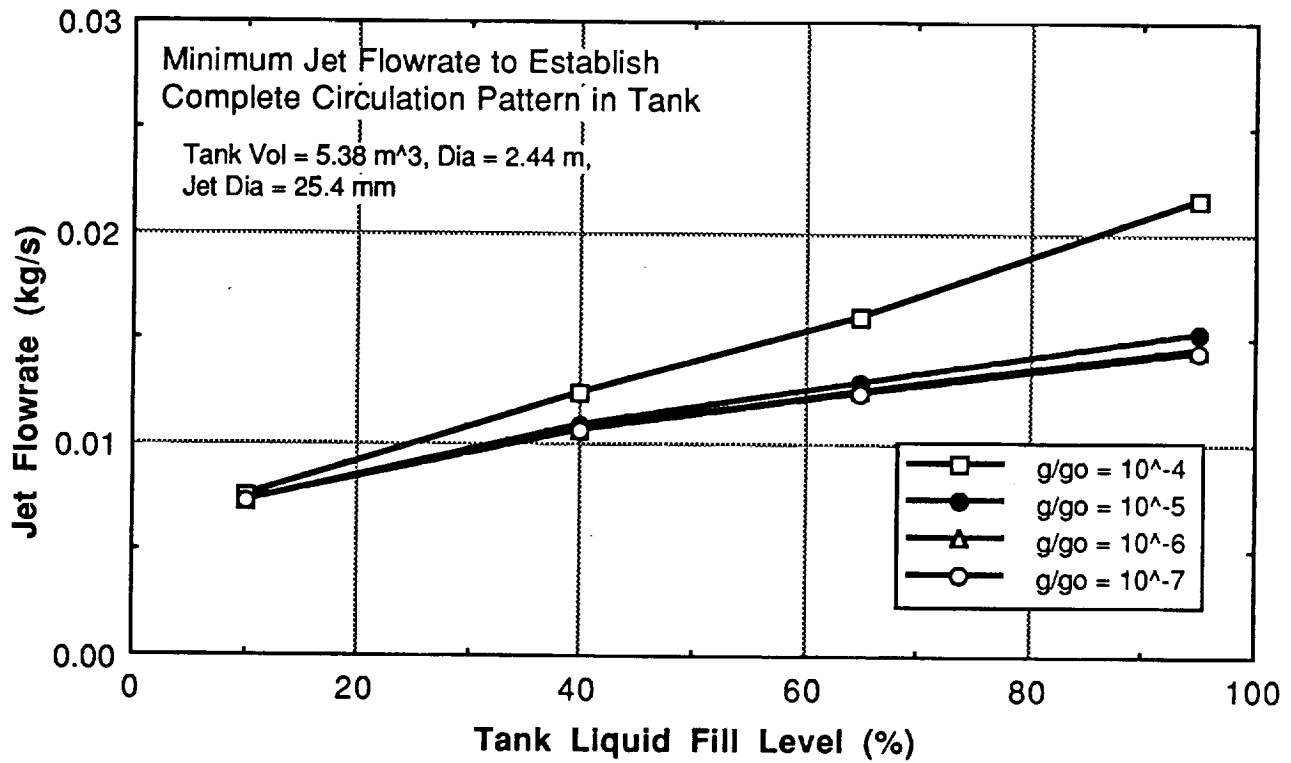


Figure 6-16. Acceleration Level Effect on Axial Jet Mixer

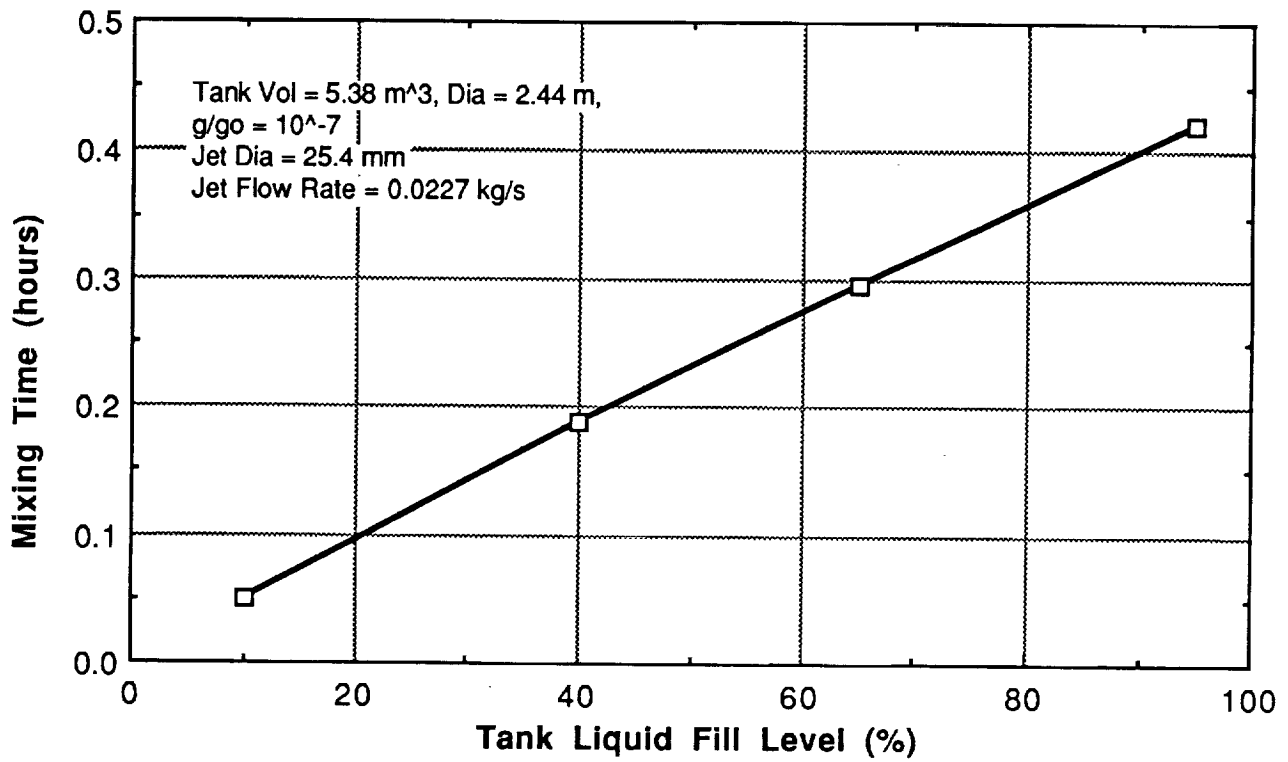


Figure 6-17. Mixing Time Using Axial Jet Mixer

6.3.4 Active TVS

The main uncertainty associated with the active TVS thermal performance is associated with mixing the tank fluid to remove any thermal stratification. The mixing process was discussed above. The sizing of the compact heat exchanger will be discussed here. The heat exchanger will be sized to subcool the liquid flowing to the mixer, and to completely vaporize the TVS flow. For sizing purposes, a counterflow, concentric tube heat exchanger will be considered. The TVS flow will be inside the inner tube and the mixer flow will be in the annular gap between the inner and outer tubes. The entire concentric tube assembly will be coiled into a helix to force any liquid in the TVS fluid to the wall and improve heat transfer on both sides of the heat exchanger. The maximum mixer flowrate will be 0.0227 kg/s. An energy balance indicates that the TVS flowrate must be 1.20×10^{-3} kg/s to subcool the mixer flow by 2.5 K. The heat transfer rate between the mixer fluid and the TVS fluid is $q = 510$ W. The length of concentric tube (L_{tube}) required to transfer this amount of energy will be determined from the heat transfer rate equation:

$$q = U A \Delta T_{\text{lm}} = \left(\frac{\pi D_i L_{\text{tube}}}{1/h_i + 1/h_o} \right) \Delta T_{\text{lm}} \quad (6-23)$$

where U is the overall heat transfer coefficient based on the inner tube diameter, D_i . The conduction resistance through the inner tube wall is small relative to the convective resistances and has been neglected. The two-phase TVS flow remains at 17.11 K, the saturation temperature corresponding to 34.5 kPa. The mixer fluid enters at 20.34 K, the saturation temperature corresponding to the tank pressure (103.4 kPa), and exits at 17.84 K. For these conditions the log-mean temperature difference (ΔT_{lm}) equals 1.67 K. The forced convection coefficient on the outside surface of the inner tube is calculated using a correlation for turbulent flow in concentric annuli (Reference 6-6):

$$h_o = 0.023 \left[0.87 \left(\frac{D_o}{D_i} \right)^{0.53} \right] \frac{k}{D_h} \left(\frac{\rho V D_h}{\mu} \right)^{0.8} \text{Pr}^{1/3} F_S \quad (6-24)$$

where D_h is the hydraulic diameter, and D_o and D_i are the outer and inner tube diameters of the annulus. The quantities ρ , μ , Pr and k are subcooled liquid properties and V is the mean velocity in the annular gap. To this equation the correction factor of Schmidt (Reference 6-7) has been applied to account for the improved heat transfer due to turbulent flow in a helical coil:

$$F_S = 1 + 3.6 \left[1 + \left(\frac{D_h}{D_p} \right) \left(\frac{D_h}{D_p} \right)^{0.8} \right] \quad (6-25)$$

where D_p is the helix pitch diameter. The heat transfer coefficient on the inner surface of the inner tube is calculated using the two-phase convection correlation of Chen (Reference 6-1):

$$h_i = 0.023 \frac{k_f}{D_i} \left[\frac{G (1-x) D_i}{\mu_f} \right]^{0.8} \text{Pr}_f^{1/3} \left[2.35 \left(\frac{1}{X_{\text{tt}}} + 0.213 \right)^{0.736} \right] \quad (6-26)$$

where G is the quotient of the mass flowrate and the cross-sectional area of the tube, X_{tt} is the Lockhart-Martinelli correlation factor, and x is the quality of the flow. The quantities k_f , Pr_f , and μ_f are properties of the saturated liquid.

A 25.4 mm OD outer tube and a 12.7 mm OD inner tube were chosen to keep the pressure drop through the heat exchanger low (discussed in the next paragraph). Both tubes have a wall thickness of 1.27 mm. A tube length of less than 6.7 meters is adequate to insure no liquid is vented from the

TVS side of the heat exchanger. When the concentric tubes are coiled into a 304.8 mm diameter helix, the length of the heat exchanger package becomes less than 174.7 mm. The heat exchanger will be internally mounted along the tank axis. A short heat exchanger is desirable to keep the exit of the axial jet submerged.

The pressure drop through the mixer-flow side of the heat exchanger was calculated using the following turbulent flow correlation:

$$\Delta P = f \left(\frac{L}{D_h} \right) \frac{\rho V^2}{2} C_s \quad \text{where } f = 0.184 \left(\frac{\rho V D_h}{\mu} \right)^{-0.2} \quad (6-27)$$

The Schmidt helical flow pressure drop correction (Reference 6-7) has been applied to this correlation to account for the greater pressure drop associated with a helical flow:

$$C_s = 1 + 0.0823 \left(1 + \frac{D_h}{D_p} \right) \left(\frac{D_h}{D_p} \right)^{0.53} \left(\frac{\rho V D_h}{\mu} \right)^{0.25} \quad (6-28)$$

The Lockhart-Martinelli correlation (Reference 6-1) was used to estimate the pressure drop for the two-phase TVS flow through the inner tube. The pressure drop through both sides of the heat exchanger is less than 34.5 kPa.

The conservation equations for energy, mass, and tank volume were used to calculate the time and boiloff required for the active TVS to condition the supply tank fluid and lower the tank pressure from 137.9 to 103.4 kPa. During active TVS tests the mixer will be on so the tank fluid will be in thermal equilibrium. Figures 6-18 and 6-19 indicate that the conditioning time and boiloff decrease as the fill level decreases. Results for three heat flux levels on the tank wall are shown. The heat flux level has little effect on the conditioning times and boiloff because the TVS energy removal rate is much greater than the heat leak rate into the tank. These results were used to estimate the duration and amount of hydrogen used during the active TVS tests shown in Table 3-2.

6.4 PRESSURIZATION AND TRANSFER

The analysis presented in this section is for the low-g pressurization of a tank containing subcritical cryogenic fluid, for the purpose of expelling liquid from the tank. The amount of pressurant needed for the process can be divided into, 1) that needed to increase the pressure of the tank to that desired for the expulsion process (referred to as the ramp pressurant requirement), and 2) the pressurant needed to maintain the tank pressure during the outflow of liquid.

During tank pressurization, heat and mass transfer from the pressurant to the tank and liquid can result in a significant reduction in the pressurant temperature. This effect is referred to as "pressurant collapse". The extent of the pressurant collapse is often expressed in terms of a "collapse factor". For this study the collapse factor is defined as the ratio of the actual pressurant mass required to the pressurant mass required under zero heat and mass transfer conditions. The minimum value of the collapse factor is 1.0 and the maximum value is reached when the temperature of the pressurant drops to the saturation temperature of the liquid at the transfer pressure.

The analytical and experimental results from Moore (Reference 6-8) represent a simplified solution to the problem of determining pressurant requirements. Moore conducted a total of 8 experiments in which GH₂ was used as a pressurant to expel LH₂ at transfer pressures ranging from 189.6 kPa to 792.9 kPa. Outflow rates were high; ranging from 0.139 kg/s to 2.52 kg/s. All of the tests were conducted with an initially full tank (i.e., no initial ullage) and no variations were made in the pressurant inlet temperature. Because of these conditions, the Moore data has limited application to

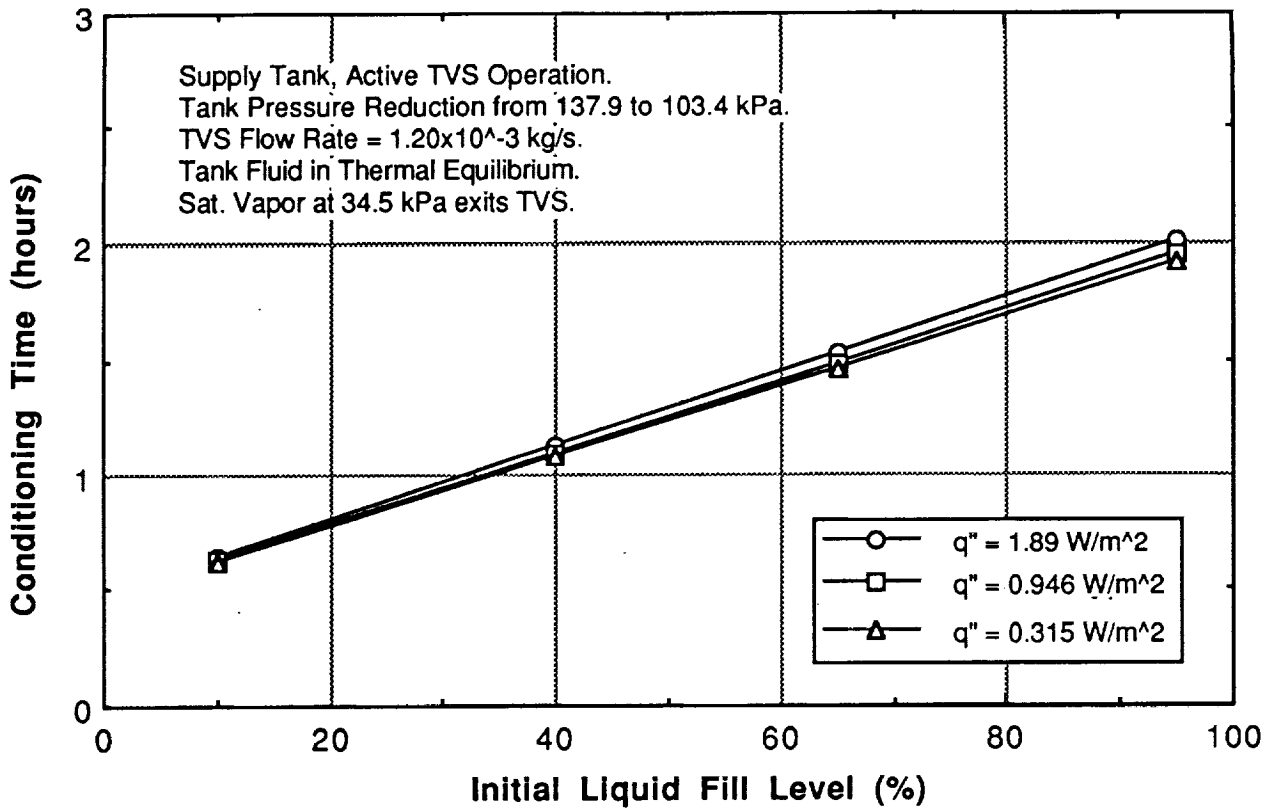


Figure 6-18. Active TVS Test Duration

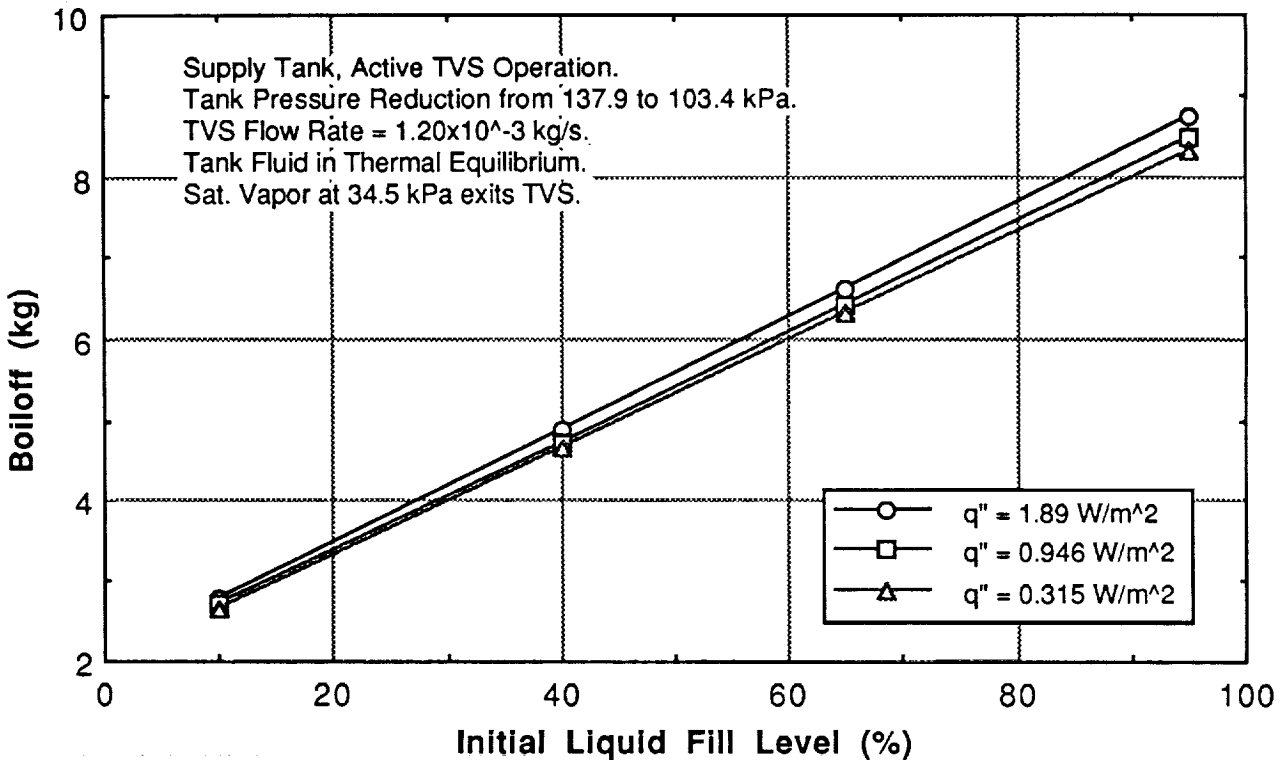


Figure 6-19. Mass Boiloff to Perform Active TVS Tests

the COLD-SAT pressurization analyses. However, it was used as a comparison to other approaches.

Epstein, et al. (Reference 6-9) developed an excellent mathematical model of tank pressurization that included many of the physical processes left out in previous studies. The computer program TNKTHRM, which GDSS is using in-house, is based on this mathematical model. One of the basic shortcomings of the model has been its dependence on indeterminate physical parameters and constants. During the development of the Saturn launch vehicle Nein and Thompson (Reference 6-10) obtained experimental data at the Marshall Space Flight Center which allowed the determination of these previously unknown quantities.

Following the work of Nein and Thompson, Epstein (Reference 6-11), presented a single analytic equation for the collapse factor, based on computations from the above mentioned program, which allowed for the prediction of total pressurant requirements in any liquid hydrogen or oxygen cylindrical propellant tank system pressurized autogenously or with helium vapor.

6.4.1 Analytical Methods

Pressurant requirements for COLD-SAT were estimated using 1) an approximation based on experimental data presented by Moore, 2) the Epstein correlation, and 3) the TNKTHRM computer model.

6.4.1.1 Approximation Based on Moore's Data. Based on the experimental data of Moore, pressurant requirements are estimated to be 1.75 times the ideal pressurant requirement. The ideal ramp pressurant requirement is calculated as:

$$m_{\text{ramp}} = \frac{P_1 V_{v1}}{ZRT_i} \left[\left(\frac{P_2}{P_1} \right)^{\frac{1}{\gamma}} - 1 \right] \quad (6-29)$$

and the ideal outflow pressurant mass requirement as:

$$m_{\text{outflow}} = \rho_i (V_{v2} - V_{v1}) \quad (6-30)$$

with, P = pressure, Pa
 V = volume, m³
 T = temperature, K
 Z = compressibility factor, -
 m = mass, kg
 R = gas constant, J/kg K
 h = specific enthalpy, J/kg
 u = specific internal energy, J/kg
 ρ = density, kg/m³
 γ = ratio of specific heats, -

with subscripts: 1-prior to pressurization, 2- after pressurization, v-vapor, and i-inlet condition.

6.4.1.2 Epstein Correlation. The Epstein correlation is an analytical expression which allows the determination of a collapse factor, CF. Pressurant mass is calculated directly from this collapse factor using the definition of the ideal pressurant mass requirement.

$$CF = \frac{m_{\text{actual}}}{m_{\text{ideal}}} \quad (6-31)$$

It is important to remember that the Epstein correlation is only valid for a limited range of operating conditions and is not intended for ramp pressurant calculations. For these reasons, the generalized computer program TNKTHRM, from which the Epstein correlation was derived, was used to further evaluate pressurant requirements.

6.4.1.3 TNKTHRM Computer Model. The TNKTHRM program was used extensively for analyses of the COLD-SAT pressurization system. Figure 6-20 illustrates the autogenous and stored gas pressurization systems that may be analyzed using TNKTHRM. For the autogenous system the pressurant is stored as a liquid and evaporated in a heat exchanger. The pressurant gas can be identical to or different from the liquid in the tanks being pressurized.

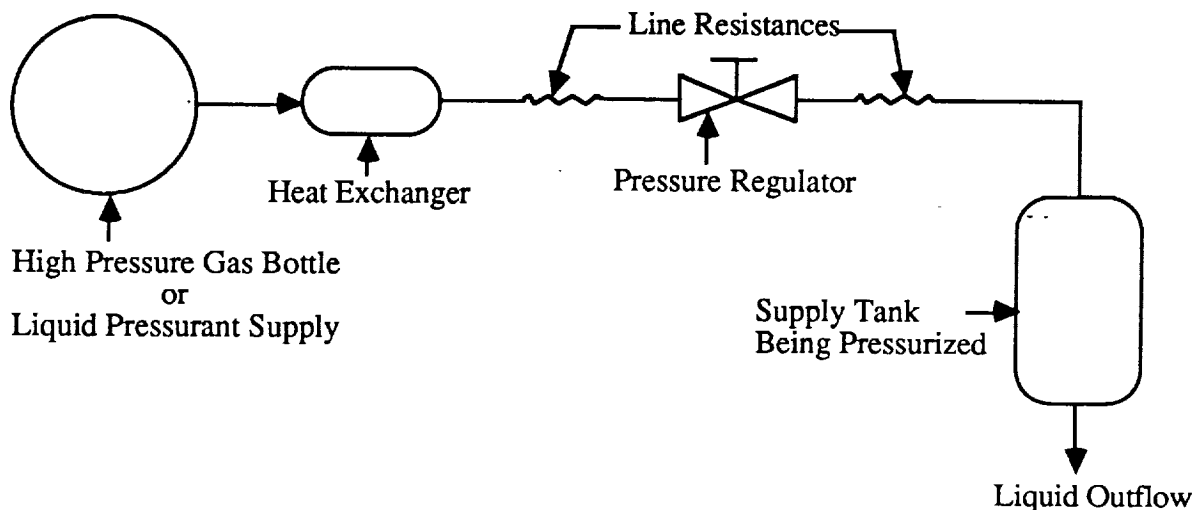


Figure 6-20. TNKTHRM Model of Pressurization Using Stored Gas or Liquid Supply

The assumptions made in the TNKTHRM computer model are summarized below.

1. The liquid is a pure substance.
2. The gas may be a mixture of He and H₂ vapor.
3. The liquid is settled over the drain regardless of the g-level.
4. Condensation and evaporation occur only at the gas-liquid interface.
5. No bulk boiling of the liquid can occur.
6. Gas total pressure throughout the tank is uniform.
7. Gas, liquid, and wall temperatures are a function of time and axial distance, but not radial or circumferential locations.
8. Insulation temperature is a function of time and axial and radial distance, but not circumferential location.
9. Axial heat transfer in the wall and insulation is neglected.
10. Heat transfer modes:

Conduction: between gas nodes, between liquid nodes, through wall and insulation

Convection: gas-to-liquid, liquid-to-wall, gas-to-wall, and wall or insulation-to-ambient

Radiation: wall or insulation-to-ambient

11. Vapor and liquid are in thermodynamic equilibrium at the interfaces.
12. The effective thermal conductivity, mass diffusivity, and heat transfer coefficients vary exponentially with distance from top of tank.
13. Liquid density is independent of temperature and pressure.
14. Momentum and kinetic energies of the flows are ignored.

15. Thermal properties of the liquid, wall, and insulation are functions of temperature.
16. The coordinate system is stationary with respect to the tank.

Assumption 3 implies there is a flat liquid/vapor interface regardless of the g-level, and is perhaps the most limiting assumption in TNKTHRM. In a low-gravity environment the surface area of liquid exposed to the pressurant gas would be increased and would therefore affect the heat and mass transfer processes. No modifications have been made to TNKTHRM to account for this phenomena. However, there are several modifications being considered which would better simulate the conditions expected in low-g.

6.4.2 Effect of System Parameters on Pressurant Requirements

6.4.2.1 Pressurant Temperature. Of all the parameters investigated, the pressurant inlet temperature had the strongest influence on pressurant mass requirements. Increases in pressurant inlet temperature always result in lower pressurant mass requirements.

Figure 6-21 shows an estimate of the total mass of hydrogen pressurant needed on COLD-SAT for a range of pressurant inlet temperatures. The maximum pressurant requirement is also shown for comparative purposes.

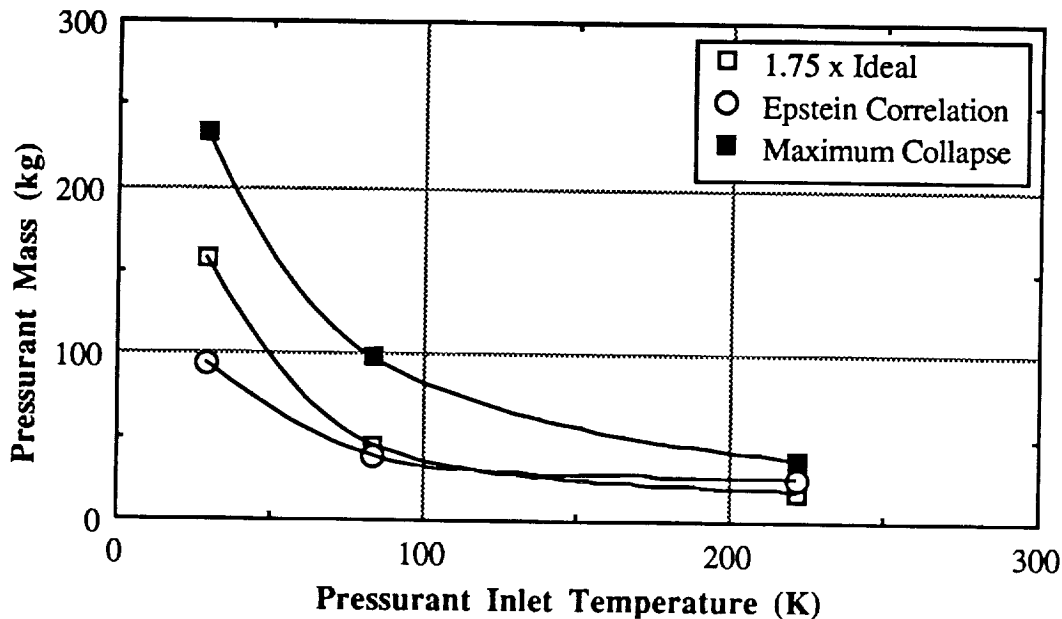


Figure 6-21. Effect of Pressurant Temperature on Pressurant Requirements

The maximum pressurant requirement results when the temperature of the injected pressurant drops to the saturation temperature of the liquid at the transfer pressure. Equations have been derived in Reference 6-12 for the calculation of this quantity and are stated as

$$m_{\max} = \rho_{L2} V_T - \left(\frac{A_3 - A_2}{A_1} \right) \left[\frac{\rho_{L2}}{\rho_{V2}} - 1 \right] - m_{L1} - m_{V1} + m_e \quad (6-32)$$

where,

$$A_1 = uv_2 - h_i + \frac{\rho_{L2}}{\rho_{V2}} (h_i - u_{L2}) \quad (6-33)$$

$$A_2 = m_e h_{L2} + \rho_{L2} u_{L2} V_T - m_{v1} u_{v1} - m_{L1} u_{L1} \quad (6-34)$$

$$A_3 = h_i (\rho_{L2} V_T - m_{L1} - m_{v1} + m_e) \quad (6-35)$$

with,

m = mass, kg

h = specific enthalpy, J/kg

u = specific internal energy, J/kg

ρ = density, kg/m³

V = volume, m³

with subscripts: e - exit condition, i - inlet condition, 1 - before ramp, 2 - after the expulsion, L = liquid, V = vapor, and T = tank.

The maximum ramp pressurant requirement is found by setting m_e to zero in Equations 6-32, 6-34, and 6-35.

Total pressurant mass requirements have not been estimated using TNKTHRM, however, preliminary studies indicate that the Epstein correlation and TNKTHRM computer model are in close agreement for pressurant inlet temperatures ranging from 30 K to 220 K.

6.4.2.2 G-Level. Pressurant requirements are dependent on heat transfer from the ullage to the tank walls and liquid as well as mass transfer from the ullage to the liquid. These heat and mass transfer processes are affected by the g-level and the liquid-vapor interface shape.

Below are the heat and mass transfer equations used in the TNKTHRM computer program. The basic forms of the equations are derived from a theoretical 1-g analysis. The constants were determined empirically from experimental pressurization tests conducted at the Marshall Space Flight Center (Reference 6-10).

The ullage gas-to-wall heat transfer coefficient is expressed as a sum of the free and forced convection coefficients.

$$h_{gw} = h_c + h_{co} e^{-\beta_w Z} \quad (6-36)$$

where,

$$h_c = .13 k_g \left[\frac{g c_{p_g} \rho_g^2 (|T_g - T_w|)}{T_g \mu_g k_g} \right]^{.333} \quad (6-37)$$

$$\frac{h_{co} r}{k_g} = .06 \left(\frac{r \dot{M}}{A_D \mu_g} \right)^{.8} \left(\frac{\mu_g c_{p_g}}{k_g} \right)^{.333} \quad (6-38)$$

The ullage gas-to-liquid heat transfer coefficient is expressed as a sum of the free and forced convection coefficients.

$$h_s = h_{sc} + h_{so} e^{-\beta_s Z_i} \quad (6-39)$$

where

$$h_{sc} = .13 k_g \left[\frac{g c_{p_g} \rho_g^2 (|T_g - T_L|)}{T_g \mu_g k_g} \right]^{.333} \quad (6-40)$$

$$\frac{h_{so} r}{k_g} = .06 \left(\frac{r \dot{M}}{A_D \mu_g} \right)^.8 \left(\frac{\mu_g c_{p_g}}{k_g} \right)^.333 \quad (6-41)$$

$$h_c = .13 k_L \left[\frac{g c_{pL} \beta_L \rho_L^2 (|T_L - T_w|)}{\mu_L k_L} \right]^ .333 \quad (6-42)$$

with, h_c = gas-to-wall free convection heat transfer coefficient, W/m²·K
 h_o = gas-to-wall forced convection heat transfer coefficient, W/m²·K
 h_{sc} = gas-to-liquid free convection heat transfer coefficient, W/m²·K
 h_{so} = gas-to-liquid forced convection heat transfer coefficient, W/m²·K
 $\beta_w = 3.313 \times 10^{-5} r^{-2}$, m⁻¹
 r = tank radius, m
 z = axial distance from the tank top, m
 k = thermal conductivity, W/m·K
 g = effective gravity, m/s²
 c_p = specific heat, J/kg·K
 ρ = density, kg/m³
 T = temperature, K
 μ = viscosity, Pa·s
 \dot{M} = pressurant mass flowrate, kg/s
 A_D = pressurant diffuser area, m²
 β_L = liquid thermal expansion coefficient, K⁻¹

The mass transfer at the gas-to-liquid interface is calculated as

$$Y_s = Y_{sc} + Y_{so} e^{-\beta_s Z_i} \quad (6-43)$$

where,

$$Y_{sc} = .13 \bar{D} \left[\frac{g k_g \rho_g (|\Phi_g - \Phi_i|)}{\mu_g^2 c_{p_g} \bar{D}} Pr \right]^ .333 \quad (6-44)$$

$$\frac{Y_{so} r}{\bar{D}} = .06 \left(\frac{r \dot{M}}{A_D \mu_g} \right)^.8 \left(\frac{\mu_g}{\rho_g \bar{D}} \right)^.333 \quad (6-45)$$

with, Y_{sc} = gas-to-liquid free mass transfer coefficient, m/hr
 Y_{so} = gas-to-liquid forced mass transfer coefficient, m/hr
 Φ = mole fraction, -
 \bar{D} = diffusion coefficient, m²/hr

with subscripts: g-gas, l-liquid, i-gas-to-liquid interface, and w-wall.

The effect of the g-level on GH₂ ramp pressurant requirements is shown in Figure 6-22 for a range of pressurant inlet temperatures. Cold vapor GH₂ pressurant requirements are not strongly affected.

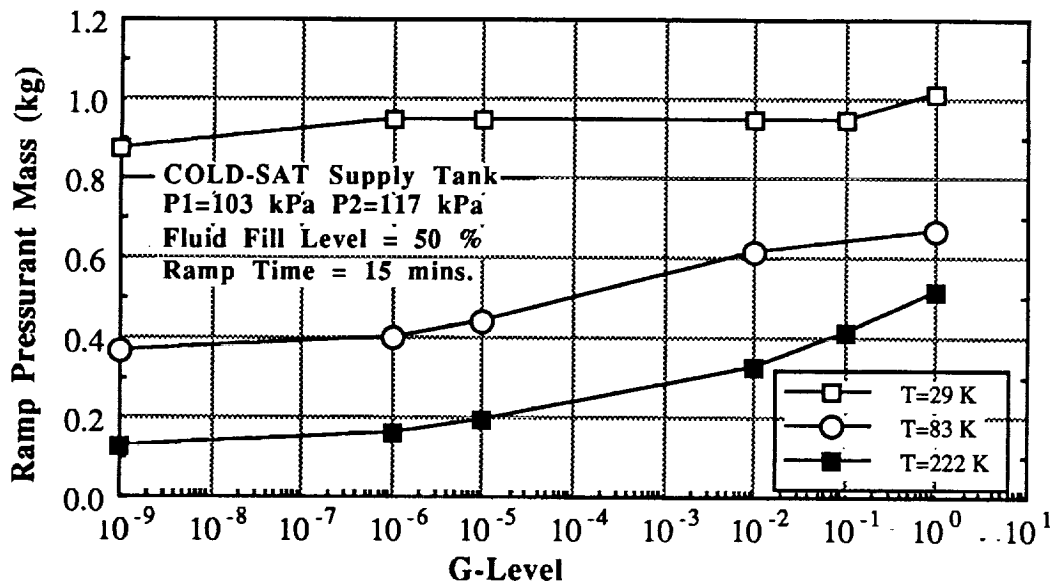


Figure 6-22. Effect of G-level on Ramp Pressurant Requirements

This is due to the relatively small temperature differential between the ullage and the surrounding tank walls and liquid. Conversely, warm GH₂ ramp pressurant requirements show a strong dependence on the g-level.

6.4.2.3 Pressurant Inlet Velocities. The pressurant inlet velocities are dependent on the mass flowrate of pressurant and the pressurant diffuser area. The total area of the diffusers used in the supply tank pressurization system was modeled in TNKTHRM as $A_D = .0734 \text{ m}^2$. For pump-assisted and pressurized transfers the resulting pressurant inlet velocities ranged from 0.15 m/s to 1.52 m/s, respectively.

Pressurant inlet velocities influence the magnitude of the forced convection coefficients. With TNKTHRM these coefficients decrease exponentially from the top of the tank. This type of spatial variation would be expected if the pressurant diffuser was located at the top of the tank and the liquid settled over the drain. However, this is not the case with the COLD-SAT pressurization system. Further analyses and modifications to TNKTHRM will be required to account for the effect of pressurant diffuser orientation on the pressurant gas velocity distributions.

The gas-to-wall forced convection heat transfer coefficient is largely controlled by the diffuser area. For a given pressurant temperature and ramp time, reducing the diffuser area results in increased pressurant inlet velocities and lower mean ullage temperatures. Increasing the diffuser area has the opposite effect. There does exist, however, a point beyond which further increases in the diffuser area will not result in significantly higher mean ullage temperatures.

6.4.2.4 Fill Level and Ramp Time. The initial liquid fill level and the duration of the ramp time significantly affect pressurant mass requirements. Figures 6-23 and 6-24 show cold GH₂ pressurant requirements for pump-assisted and pressurized transfers, respectively, over a range of liquid fill levels. For pump-assisted transfers the supply tank is pressurized from 103 kPa to 117 kPa, while for pressurized transfers the tank is pressurized from 103 kPa to 241 kPa. The results were generated using TNKTHRM.

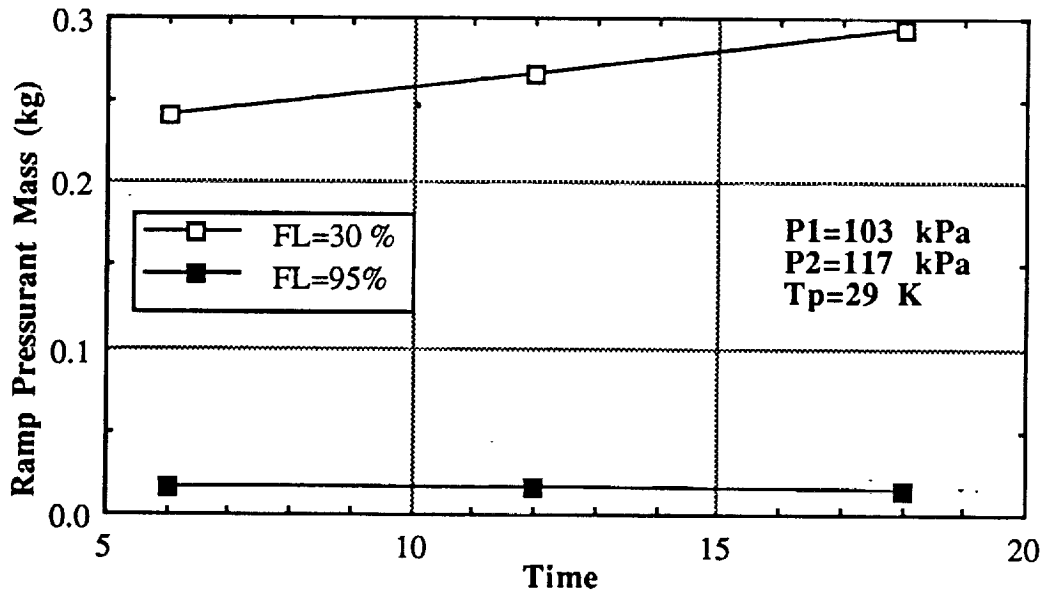


Figure 6-23. Effect of Ramp Time and Fill Level on Cold Gaseous Hydrogen Ramp and Pressurant Mass Requirements (Pump-assisted Transfer)

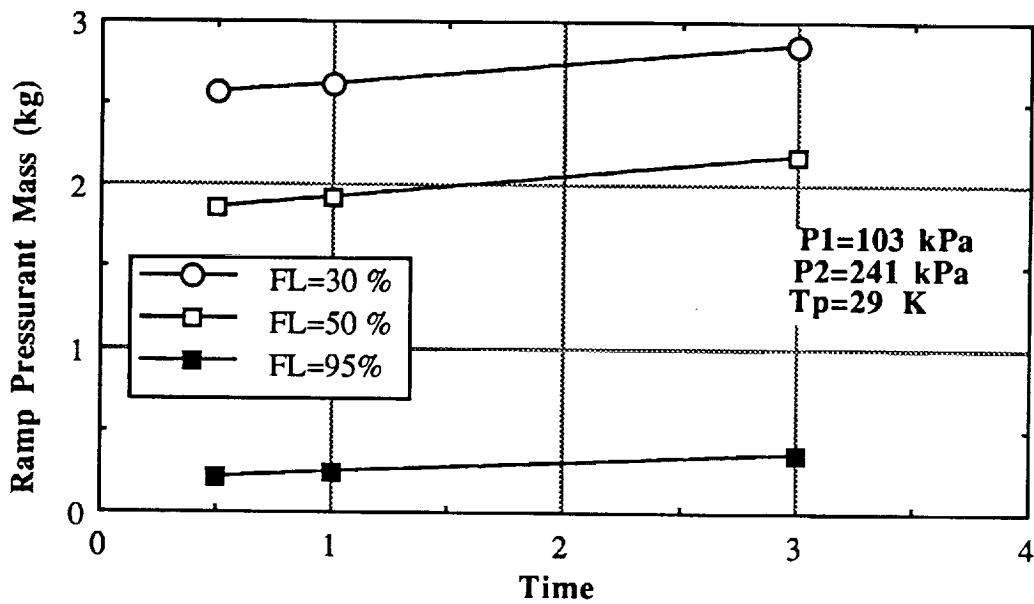


Figure 6-24. Effect of Ramp Time and Fill Level on Cold Gaseous Hydrogen Ramp and Pressurant Mass Requirements (Pressurized Transfer)

For a given ramp time TNKTHRM predicts that pressurant collapse is greater at low liquid fill levels. Large ullage volumes allow for more gas-to-wall heat transfer due to the increased tank wall area exposed to gas. In addition, pressurant gas inlet velocities are higher since larger mass flow rates are needed for ramping. This results in higher gas-to-wall and gas-to-liquid forced convection heat transfer coefficients. Much less pressurant collapse occurs at high liquid fill levels. In a low-g environment these trends are not necessarily the same. Modifications to TNKTHRM will be required to determine the effect of the ullage volume on pressurant collapse in low-g.

6.4.2.5 Ambient Heat Flux. Parametric studies with TNKTHRM have shown that an ambient heat flux of 0.3 W/m^2 uniformly distributed to the supply tank does not appreciably change pressurant mass requirements. This was observed for both pump-assisted and pressurized transfers at pressurant inlet temperatures ranging from 29 K to 208 K and g-levels ranging from 1.0 to 10^{-9} . Ramp times varied from 6 to 18 minutes for pump-assisted transfers and from 30 to 180 minutes for pressurized transfers. Outflow times ranged up to 60 minutes.

6.4.3 Boiloff Requirements for Thermal Conditioning

After pressurization and transfer, the TVS will be used to thermally condition the tank fluid. The mass required to condition the tank for a range of pressurant inlet temperatures is shown in Figure 6-25. Results for pressurant that enters as para-hydrogen, ortho-hydrogen, and an equilibrium mixture of ortho and para-hydrogen at the inlet temperature are shown. The pressurant mass is also shown for comparison with the conditioning mass. The pressurant mass is not expected to be highly dependent on the para-ortho composition of the hydrogen since the conversion time is much longer than the pressurization time. For these calculations, the supply tank was assumed to be 50 percent full, with the fluid initially in thermal equilibrium at 103.4 kPa. A pump-assisted transfer at 117.2 kPa of 81.6 kg of liquid at 20.3 K is performed. Following the transfer, the TVS is used to condition the tank fluid back to thermal equilibrium at 103.4 kPa. The vapor vented from the TVS is assumed to be saturated at 34.5 kPa.

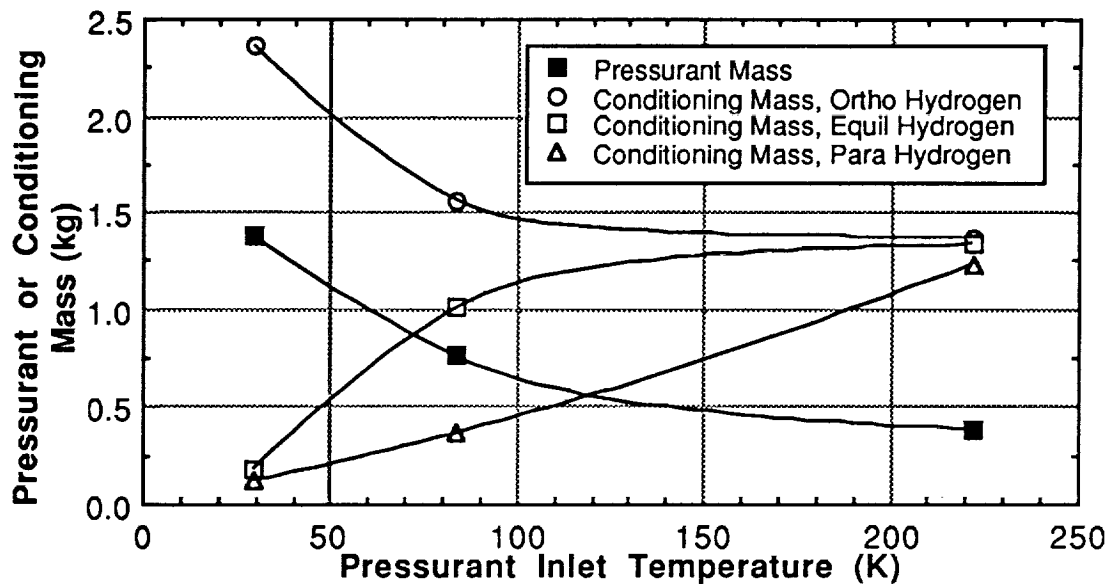


Figure 6-25. Conditioning Mass Requirements

The results for para-hydrogen, shown in Figure 6-25, are applicable to autogenous pressurization. Liquid from the tank is evaporated and used for pressurant. The conversion from para to ortho is slow, so the pressurant gas will be mostly para-hydrogen. The mass required for pressurization decreases as the injectant temperature increases, however, the conditioning mass increases, as shown in Figure 6-25.

The equilibrium hydrogen results shown in Figure 6-25 are more applicable to pressurization using stored high pressure GH₂. Over an extended period of time, the warm GH₂ stored in high pressure bottles will convert from para to an equilibrium mixture of para and ortho hydrogen at the storage temperature. After pressurization, the pressurant gas will reconvert to the para form. The energy released must be removed by the TVS, which results in greater conditioning mass requirements, as compared to pressurant that enters as pure para-hydrogen. The high-pressure GH₂ bottles used on COLD-SAT will be stored at about 250 K. The initial bottle pressure will be around 25 MPa. For these conditions, the Joule-Thomson coefficient is small and negative, i.e., the temperature of the gas will increase slightly as it flows through the throttling device. The bottle pressure will decrease below 700 kPa during use. As a result, the temperature of the bottled gas will also decrease as it undergoes a nearly isentropic expansion; however, this will be offset by heat transfer to the bottle, which will reheat the contents in the interim period between tank pressurizations.

Figure 6-25 also shows the conditioning mass required if the pressurant entered as pure ortho-hydrogen. These results represent an idealized upper limit. For temperatures less than 30 K, the enthalpy difference between ortho and para hydrogen is greatest, so the conditioning mass required for ortho pressurant is much greater than for para pressurant. At these low temperatures, the equilibrium composition is mostly para, so the conditioning mass requirements for equilibrium-hydrogen are only slightly more than the para-hydrogen case. For temperatures greater than 230 K, the difference between the enthalpy of para and ortho hydrogen is relatively small, so the conditioning mass required is nearly the same for all three cases. At these high temperatures, the equilibrium composition is about 75 percent ortho.

6.4.4 Energy Requirements for Pumped and Pressurized Transfers

The total energy required to transfer 81.6 kg of LH₂ from the supply tank using pressurant at 29 K is shown in Table 6-8 for a range of initial liquid fill levels. Included is a breakdown of the energy required by each pump and the evaporator. For this analysis the total energy is defined as the sum of the energy required to operate the evaporator, pressurant pump and transfer pump.

Table 6-8. Energy Requirements for Pumped and Pressurized Transfers

		Pumped Transfer Energy (W-hr)				Pressurized Transfer Energy (W-hr)			
		Time (min)	Fill Level (%)			Time (min)	Fill Level (%)		
			30	50	95		30	50	95
Pressurization Pump ($\Delta P=276$ kPa, eff=.25)	Ramp	12	1.16	0.71	0.073	60	11.3	8.38	1.06
	Outflow	60	5.15	5.15	5.15	60	11.3	11.3	11.3
Transfer Pump ($\Delta P=159$ kPa, eff=.25)	Outflow	60	204	204	204	60	-	-	-
Evaporator Heater	Ramp	12	40.4	24.6	2.60	60	305	226	29.0
	Outflow	60	179	179	179	60	305	305	305
Total		72	430	413	391	120	633	551	346

Average evaporator power requirements as a function of fill level and ramp time are shown for pump-assisted and pressurized transfers in Figures 6-26 and 6-27, respectively.

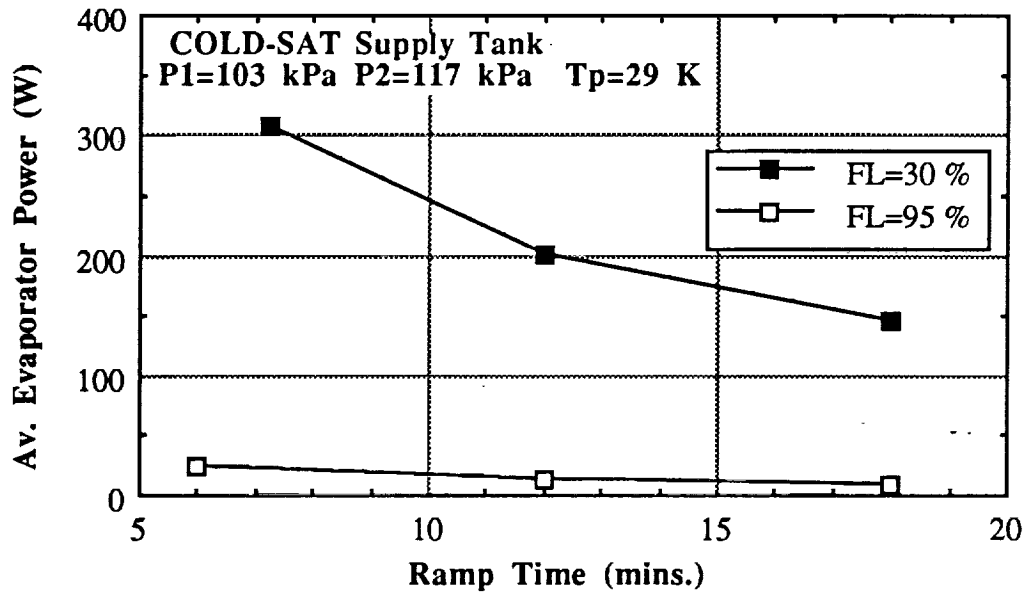


Figure 6-26. Effect of Ramp Time and Fill Level on Average Evaporator Power (Pump-assisted transfer)

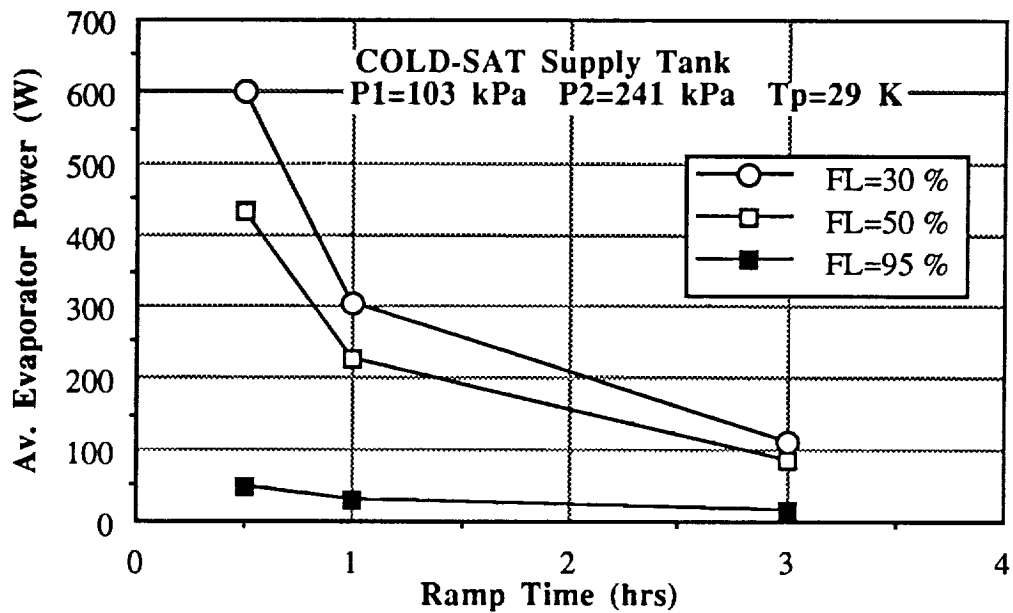


Figure 6-27. Effect of Ramp Time and Fill Level on Average Evaporator Power (Pressurized transfer)

The analyses confirm that except for very high fill levels (≥ 95 percent), considerable energy savings can be realized using pumps. Several other observations were made and are summarized below.

1. For pressurized transfers the power requirement of the evaporator constitutes the majority of the total power requirements, while for pump-assisted transfers the transfer pump power requirement constitutes the majority of the total power requirements.
2. Ramp pressurant mass requirements for pressurized transfers are much greater than those needed for pumped-assisted transfers due to the longer ramp times and higher transfer pressures. Because of this, total power requirements are also higher for pressurized transfers.
3. The lower power requirements for pump-assisted transfers permit shorter ramp times.
4. Power requirements for pumped-assisted transfers are relatively insensitive to the liquid fill level as shown in Figure 6-28. The opposite is true for pressurized transfers.
5. For both types of transfers the power required by the pressurization pump is negligible compared to the power required by the transfer pump and evaporator.

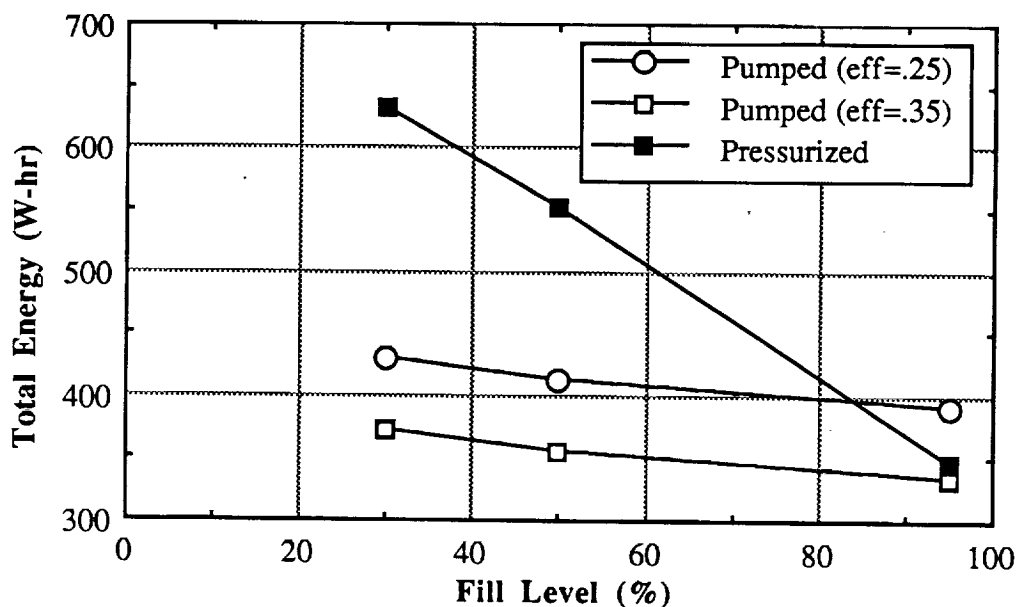


Figure 6-28. Effect of Fill Level on Total Energy Requirements for Pump-assisted and Pressurized Transfers

6.4.5 Summary of GH₂ Pressurant Requirements for the Class II Pressurization Experiment

Ramp and outflow pressurant mass requirements were calculated for all the pressurization tests (see Section 3.2.2.2) using the three methods of analysis previously mentioned. The results of these computations are summarized in Table 6-9. The low-g computations made with TNKTHRM involved changing an input g-level appearing in the free convection heat and mass transfer equations (see Equations 6-37, 6-40, 6-42 and 6-44 in Section 6.4.2.2). No attempt was made to model the effects of a low g-level on fluid orientation.

Table 6-9. Summary of the Pressurant Mass Requirements

Exp. No.	Pressurant Mass Requirements (kg)						
	1.75 x Ideal (Moore)		Epstein Corr.	TNKTHRM (low-g)		TNKTHRM (1-g)	
	Ramp	Outflow	Total	Ramp	Outflow	Ramp	Outflow
II-4.1	0.09	0.55	0.39	0.04	0.31	0.05	0.35
II-4.2	0.09	0.55	0.39	0.04	0.30	0.04	0.30
II-4.3	0.35	1.03	0.85	0.17	0.56	0.19	0.55
II-4.4	0.32	0.55	0.54	0.15	0.30	0.16	0.30
II-4.5	0.05	0.13	0.24	0.02	0.08	0.06	0.17
II-4.6	0.05	0.13	0.24	0.03	0.08	0.03	0.19
II-4.7	0.16	0.13	0.40	0.09	0.09	0.20	0.54
II-4.8	0.05	0.13	0.18	0.04	0.13	0.06	0.54
II-4.9	0.16	0.13	0.29	0.13	0.16	0.20	0.54
Subtotal	1.30	3.31	3.53	0.71	2.03	0.99	2.36
Total		4.61	3.53		2.74		3.35

As mentioned earlier, the Epstein correlation was derived entirely from computations made with TNKTHRM, and therefore is only valid over a limited range of conditions; outflow times of 200 - 500 secs., pressurant inlet temperatures of 55 K - 667 K, and tank pressures of 207 kPa - 690 kPa. In addition, the Epstein correlation is not intended for calculation of ramp pressurant requirements. Our studies show, however, that the Epstein correlation is useful for estimating pressurant collapse factors in cases which involve operating conditions outside the ranges mentioned above.

In comparison to the average collapse factor of 1.75 used in the approximation of the Moore experimental data, average collapse factors of 1.34, 1.04, and 1.27 may be calculated for the Epstein correlation, TNKTHRM (low-g), and TNKTHRM (1-g) methods of analysis (based on results presented in Table 6-9). A collapse factor of 1.75 was used to size the high pressure GH₂ bottles based on direction from NASA. All studies done thus far indicate this is a conservative estimate and should therefore provide an adequate supply of pressurant for the scheduled tests and transfers.

Future analyses of COLD-SAT pressurization requirements will center on modifying TNKTHRM to account for the increased liquid surface area exposed to pressurant gas in low-g as well as the effect of low-g on free convection heat and mass transfer.

6.5 TANK MLI VENTING

Prior to filling the LH₂ tank, the thick MLI surrounding the supply tank is purged with dry nitrogen to drive out excess moisture. Then helium is pumped under the MLI to drive the nitrogen out from between the layers of MLI to prevent nitrogen freezing and cryopumping. Hence, during the prelaunch phase of the mission, the free volume within the supply tank MLI system is completely filled with helium. Upon ascent, the helium gas is allowed to evacuate through blanket seams and perforations within the shields. The rate of helium evacuation significantly impacts the heat flow through the MLI, since gas conduction effects remain dominant until pressure has dropped below 0.0133 Pa.

The evacuation of the nitrogen purge gas within the micrometeoroid/debris shield (MMS) was assumed to follow the Atlas payload fairing evacuation profile down to approximately 1330 Pa, after which an isentropic evacuation was assumed. The ensuing evacuation rate reduced pressure an order of magnitude every 4 seconds, with the nitrogen pressure reaching a negligible level 140 seconds after launch. The helium pressure within the MLI was assumed to match the nitrogen pressure profile until it reached a rarified state at about 1.33 Pa, after which it decayed slowly to 0.0013 Pa 600 seconds after launch. At this point, helium gas conduction ceases to make a significant contribution to overall heat flow through the MLI system.

The MLI interlayer evacuation time of 10 minutes was an estimate loosely based upon past data from Titan/Centaur and Shuttle/Centaur insulation vacuum chamber tests. (References 6-13 and 6-14) However, the real helium evacuation rate will depend upon numerous factors, such as MLI layer density and seam length, and should be modeled for the specific COLD-SAT geometry during the next phase of analysis. A plot of the pressure profiles assumed for this analysis is given in Figure 6-29.

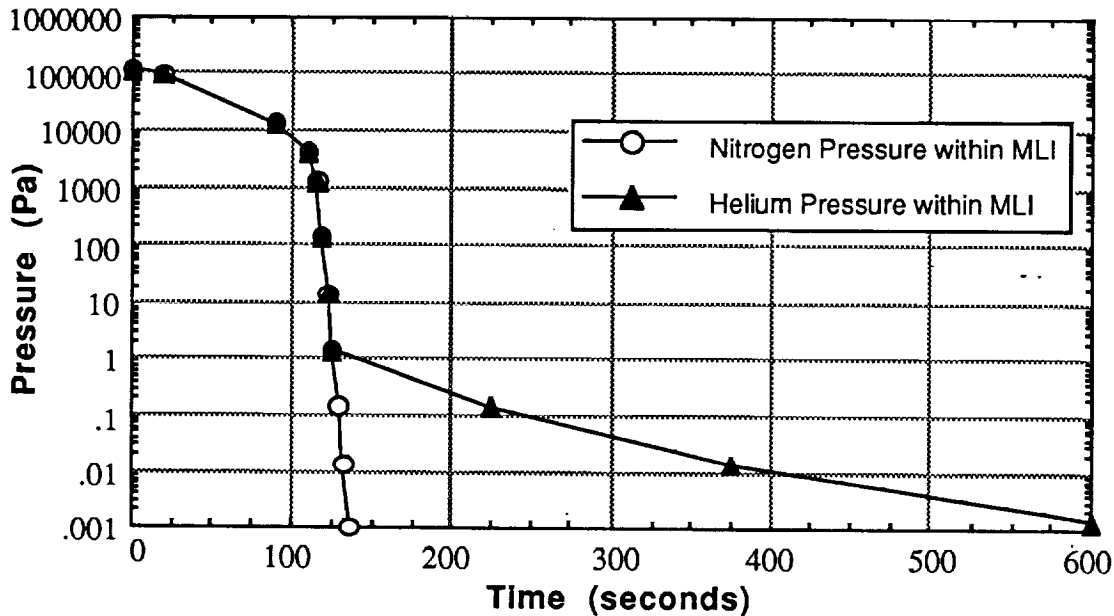


Figure 6-29. Pressure Profiles for Nitrogen under Micrometeoroid Shield and Helium within MLI

6.6 THERMAL PERFORMANCE

The three tanks comprising the COLD-SAT experiment tank set will be subjected to parasitic heating due to incident solar radiant energy and internal heat generation. Since all parasitic heat loads result in LH₂ boiloff, which reduces the useable LH₂ inventory, the prelaunch, ascent, and on-orbit heat leaks to the experiment tanks must be kept within acceptable limits. Various thermal modeling techniques were used to calculate space heating loads and tank heating levels throughout the COLD-SAT mission.

6.6.1 Space Heating and External Temperatures.

Space heating is the combination of direct solar, albedo, and Earth thermal radiation, and varies with orbital altitude and inclination, length of mission, and geometry and attitude of the spacecraft. COLD-SAT will fly in a 1300 km circular orbit at an inclination of 28.5 degrees. The solar angle, beta, varies between 0 degrees, taken as the minimum heating orbit, and 52 degrees, the maximum heating orbit. A surface model of the COLD-SAT configuration was generated to determine surface temperature profiles for the experiment module, which can be described as a forward cone, a middle cylinder, and a rear cone. The space heating program Vector Sweep (Reference 6-15) was used to calculate incident fluxes at 10 minute intervals throughout the orbit.

A grey body analysis accounting for incident flux and the surface-to-surface heat exchange yielded absorbed flux profiles for each section of the experiment module. Solar absorptance and emittance values of 0.44 and 0.88, respectively, were assumed based upon NASA test data for white paint (Reference 6-16). The absorbed surface fluxes were converted to radiative equilibrium temperatures by the formula:

$$q_{\text{abs}} = \epsilon \sigma T^4 \quad (6-46)$$

where q_{abs} is the absorbed heat flux in Watts per square meter, ϵ is the surface emissivity, σ is the Stefan Boltzmann constant with units of Watts per square meter per degree Kelvin to the fourth power, and T is the temperature in degrees Kelvin. Quadrant temperatures were obtained for each section and averaged to provide section temperatures as a function of time. Temperature histories are given in Figures 6-30 and 6-31 for the maximum and minimum heating orbits respectively; orbital average section temperatures and overall average temperature for the MMS are listed in Table 6-10.

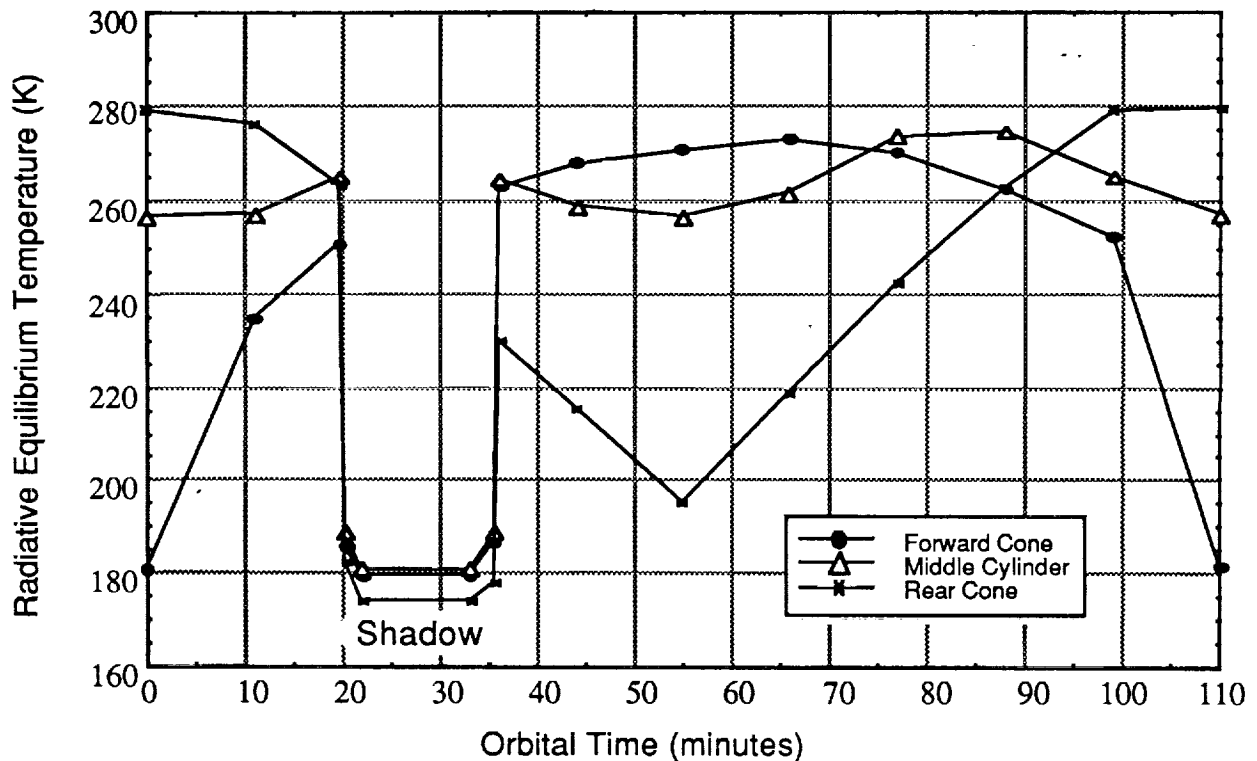


Figure 6-30. Average Surface Temperature Profile for Maximum Heating Orbit (Beta=52)

The values of radiative equilibrium temperature are dependent on the levels of incident flux, and abrupt changes in flux due to spacecraft shadowing or Earth eclipse cause abrupt changes in surface temperature. These temperatures represent extreme ranges of surface temperature; the actual magnitude and variation of the surface temperature will be damped by the thermal capacitance of the MMS.

6.6.2 Earth -To-Orbit Performance

The supply tank undergoes a wide range of parasitic heating levels during the transition from the prelaunch to the ascent to the on-orbit phases of the mission. During the ground-hold, heat is

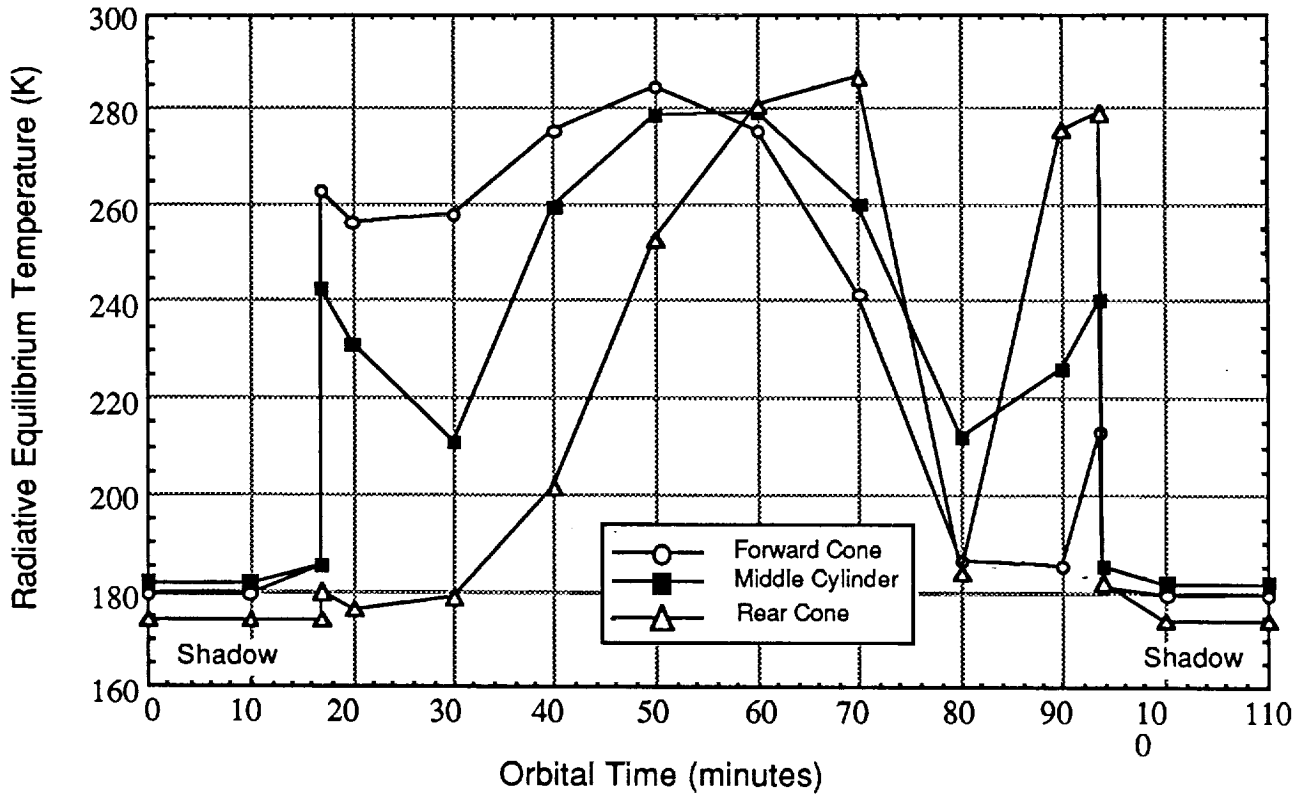


Figure 6-31. Average Surface Temperature Profile for Minimum Heating Orbit (Beta=0)

Table 6-10. Orbital Average Temperature Summary

SECTION	TEMPERATURE (K)	
	$\beta = 52$ deg.	$\beta = 0$ deg.
Forward Cone	241	227
Middle Cylinder	251	226
Rear Cone	236	214
Spacecraft	243	223

transferred to the supply tank by a warm, dry gaseous nitrogen purge flowing along the inside of the payload fairing. Gaseous helium is supplied to the MLI to prevent nitrogen from condensing and cryopumping into the insulation system. The ground-hold heating rate determines both the LH₂ resupply flowrate needed prior to supply tank lockup, and the post-lockup LH₂ boiloff before launch. During ascent, the purge gases within the MMS and insulation evacuate to space; the resulting heat flow across the MLI drops significantly as the main heat transfer mode changes from helium gas conduction to radiation across low-emittance shields.

A transient one-dimensional thermal model of the COLD-SAT/Atlas I payload fairing cross section was developed, simulating the point of highest purge gas flow velocity and maximum prelaunch heat transfer to the supply tank. A schematic of the model is shown in Figure 6-32. Atlas payload fairing temperatures from Reference 6-17 were used for radiative and convective boundary conditions for heat exchange with the MMS during prelaunch and ascent. After payload fairing jettison 225 seconds after launch, the surface flux profile calculated by the space heating analysis was assumed through two orbits for a total simulation time of 14,200 seconds. The heat flow predicted by this model was conservatively taken as the flux to the supply tank through the ground-to-orbit phase of the mission. As shown in Figure 6-33, the supply tank heat rate drops rapidly from a prelaunch level of 350 W/m² to an average on-orbit heating rate of 0.10 W/m². Analysis was conducted assuming both maximum and minimum heating orbit flux profiles, but the heat leak to the supply tank remained essentially constant, attesting to the effectiveness of the thick insulation.

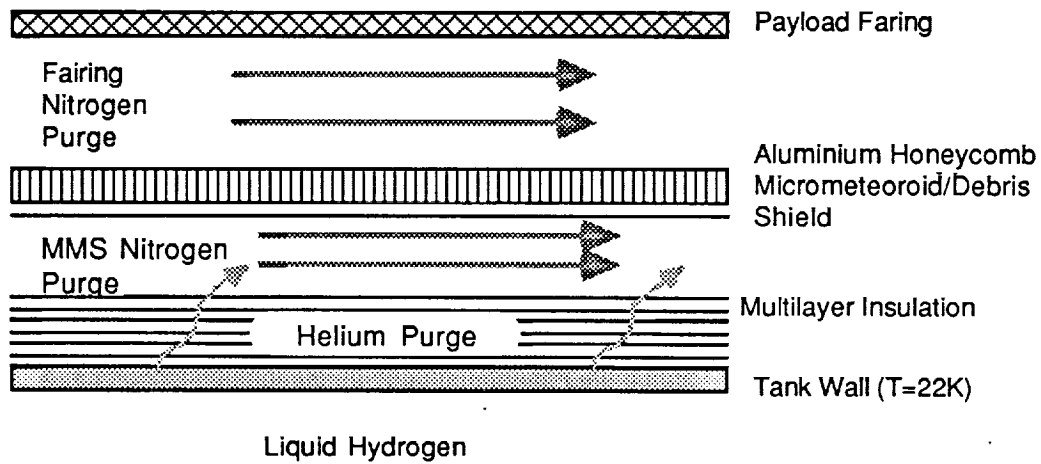


Figure 6-32. Schematic of Prelaunch-To-Orbit Thermal Model

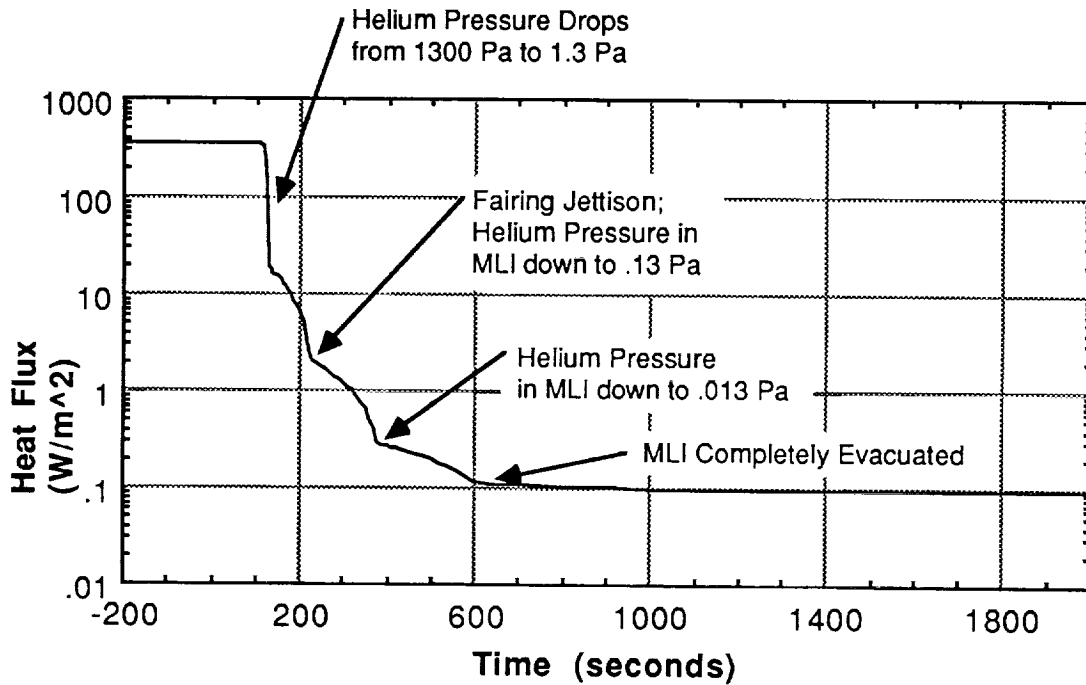


Figure 6-33. Supply Heating Profile from Prelaunch through Ascent

6.6.3 On-Orbit Tank Heating

The on-orbit thermal performance of the insulation system was analyzed to determine average heat loads for the three experiment tanks. The analysis examined both heat flow through the MLI and heat leaks through structural, electrical, and fluid penetrations.

6.6.3.1 MLI Performance Analysis. A steady-state, one-dimensional model of each insulation system was developed using the finite difference code MLISYS (Reference 6-18) which calculates shield radiation, pin conduction, spacer conduction, gas conduction and seam radiation through an MLI system, given a cold boundary temperature and either a warm boundary temperature or an incident heat flux. For this analysis, the MLI outer surface temperature was conservatively assumed to be slightly less than the average MMS temperature calculated from the space heating analysis. For Tanks 1 and 3, the warm boundary temperatures used were 240 K and 217 K, representing maximum and minimum orbital heating conditions, respectively. The warm boundary temperature for Tank 2 was between 240 K and 300 K due to its placement in the thermally-controlled environment of the spacecraft bus.

A parametric analysis was performed for the supply tank insulation system, consisting of 76 mm of double aluminized Kapton (DAK) with a layer density of 2.80 layers/mm. The study examined the impact of interstitial gas pressure, pin material, and shield perforations on MLI performance. It was found that the helium gas pressure within the MLI must drop below 0.0133 Pa before the gas conductivity can be neglected, which is supported in technical literature (Reference 6-19). Support pin conduction was found to contribute significantly to overall heat flow and low conductance polyphenylene oxide (PPO) pins are recommended over fiberglass pins. Perforations placed in the MLI shields allow for broadside evacuation of purge gases during ascent, but degrade radiative resistance by increasing the effective emittance of the shields. From Reference 6-19, the following equation was used to account for the increased emittance:

$$\epsilon_{\text{eff}} = \epsilon(1-\tau) + 2\tau \quad (6-47)$$

where ϵ_{eff} is the effective shield emittance, ϵ is the un-perforated shield emittance, and τ is the perforation grade, which is a ratio of shield open area over total area. In order to minimize radiative performance degradation, the shields were assumed to be slit rather than perforated with holes. The perforation grade assumed for the slits was $t = 0.01$, resulting in a performance degradation of only 10 percent.

Although the parametric analysis of MLI design options was conducted on the supply tank insulation system only, the results can be directly applied to the receiver tank insulation systems as well. Therefore, all three tanks will use PPO pins and be slit to facilitate broadside pumping. The insulation thickness for the receiver tanks was sized based upon orbital heating loads, since they are both dry until the spacecraft has reached orbit. The effects of MLI thickness on heat flux through the MLI is shown in Figure 6-34. The baseline insulation thicknesses for Tank 2 and Tank 3 have been tentatively set at 38.1 mm and 25.4 mm, respectively.

6.6.3.2 Penetration Heat Flow Through MLI. Heat leak through MLI penetrations can be a significant portion of the overall heat load on the experiment tanks. Heat conducts directly from the outer spacecraft environment to the tank through structural supports, through fluid lines, and along electrical wiring. Emphasis was placed on using passive techniques to minimize penetration heat leaks, such as through the use of low-conductance materials and selective routing of the penetrations to increase the heat path length. The constraints on these techniques include excessive weight, electrical wire resistance requirements, and ease of insulation system assembly. Active cooling of penetrations using boiloff vapor was not considered a viable option due to the intermittent venting cycle planned for the experiment tanks.

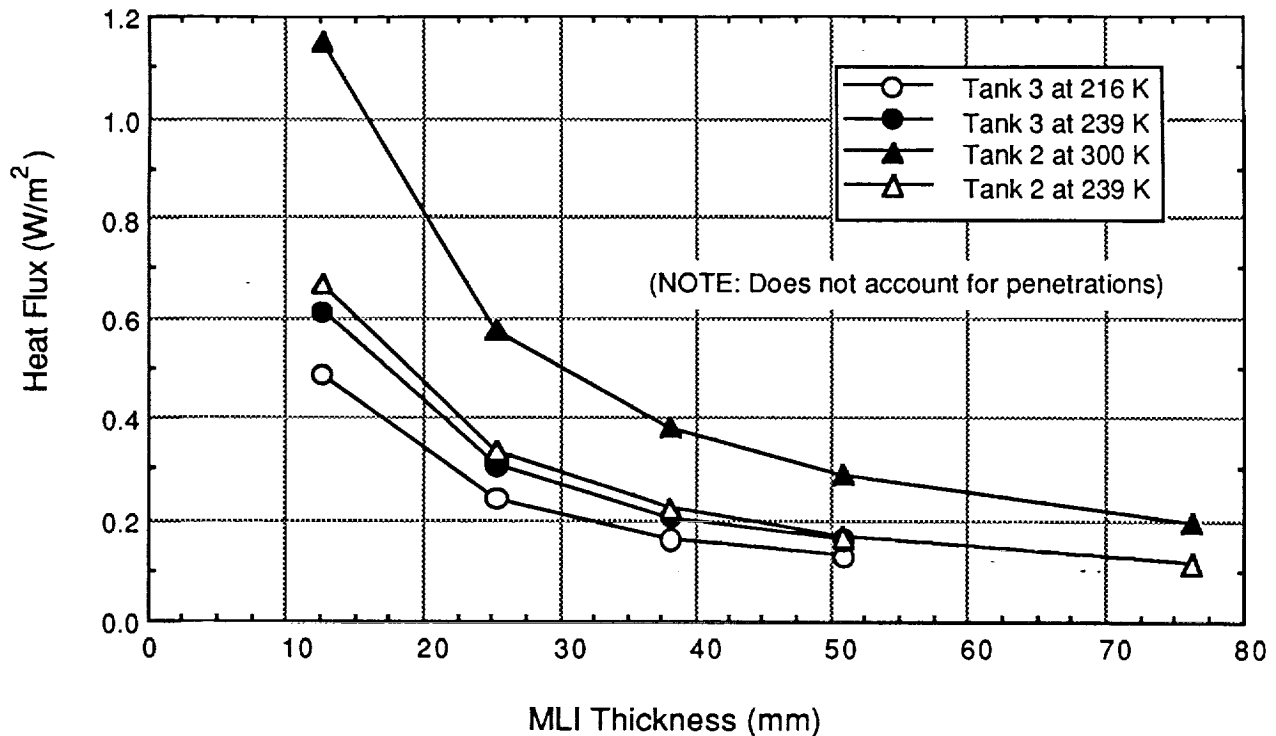


Figure 6-34. Receiver Tank Insulation Performance Summary

Tank support struts have been designed to have a high thermal resistance; they are wound using S2/E788 glass/epoxy and have MLI spacers within the strut to prevent radiation tunneling. The struts were sized to handle launch loads on the experiment tanks. A one-dimensional conduction analysis was performed on a typical strut, assuming known end temperatures. Because of the large temperature gradient between tube end points, thermal conductivity integrals from Reference 6-20 were used to calculate heat flow according to the following equation:

$$Q = \pi/4 (d_o^2 - d_i^2)/L_t \int k(T) dT \quad (6-48)$$

where the heat flow Q is in Watts, d_o and d_i are the strut outer and inner diameter in meters, L_t is the tube length in meters, and $\int k(T) dT$ is in Watts per meter. Tabulated values for $\int k(T) dT$ were multiplied by the ratio of strut cross-sectional area over length to find heat flow through the strut. A summary of strut geometry and heat flow is shown in Table 6-11.

There are three types of wire used for the experiment tank control and data measurement. Low current instrumentation and valve position indicator leads will use 0.64 mm diameter manganin wire; valve coil leads will also be 0.64 mm in diameter, with the first 380 mm running from the valve through the MLI being manganin and copper comprising the remaining length. High current leads, required for pumps and receiver tank heaters use 1.0 mm diameter pure copper wire. All wires were assumed to run from the tanks to the Data Concentrator Unit (DCU), which is housed in the spacecraft bus. For this reason, the warm end temperature of all the wires was assumed to be 300 K. Table 6-12 lists the length and number of wires used for the analysis of each tank. Heat flow through individual wires was calculated using the same procedure as for the support struts, then multiplied by the number of wires. This yielded a conservative summary of the electrical heat leak for each tank, which is summarized in Table 6-13.

Table 6-11. Structural Penetration Heat Flow Summary

	TANK 1	TANK 2	TANK 3
No. of Struts	6	6	6
Outer Diameter (mm)	50.8	25.4	25.4
Wall Thickness (mm)	0.89	0.45	0.45
Length (mm)	460	300	660
Heat Flow per Strut (W)	0.029-0.037	0.017	0.005-0.006
TOTAL Heat Flow (W)	0.172-0.222	0.104	0.028-0.039

Table 6-12. Electrical Lead Thermal Analysis Parameters

NUMBER OF WIRES

	Wire Length (mm)	Valve Leads		Instrument Leads	High Current Leads
		Coil Leads	Position Indicators		
TANK 1	3660	68	64	214	16
TANK 2	1220	44	44	150	4
TANK 3	4980	38	38	96	4

Table 6-13. Electrical Penetration Heat Flow Summary

HEAT FLOW (W)

TANK	Valve Leads	Instrument Leads	High Current Leads	TOTAL Heat Flow
1	0.185	0.082	0.533	0.800
2	0.193	0.170	0.393	0.756
3	0.097	0.041	0.100	0.238

The fluid lines that connect the experiment tanks create a thermal path between tanks and from the tanks to the spacecraft fairing. Heat is conducted between tanks when one or both of the receiver tanks are empty. In addition, both radiative and conductive thermal exchange occurs continuously between the tanks and the spacecraft MMS. The fluid penetration heat flow, therefore, could not be analyzed with the same analytical technique as used for previous analyses. Instead, a two-dimensional steady-state thermal model was developed using Thermal Analyzer (Reference 6-21). A schematic of the model is shown in Figure 6-35. It should be noted that this analysis was performed based upon an early configuration that places the spherical receiver Tank 3 in the spacecraft bus and the cylindrical receiver Tank 2 in the forward end of the experiment module. The overall heating of Tank 1 will be representative of that for the current configuration, however. The receiver tanks were assumed to be either filled, at a constant 22.2 K, or empty and acting as fins. A summary of the heat flows calculated with this model is shown in Table 6-14.

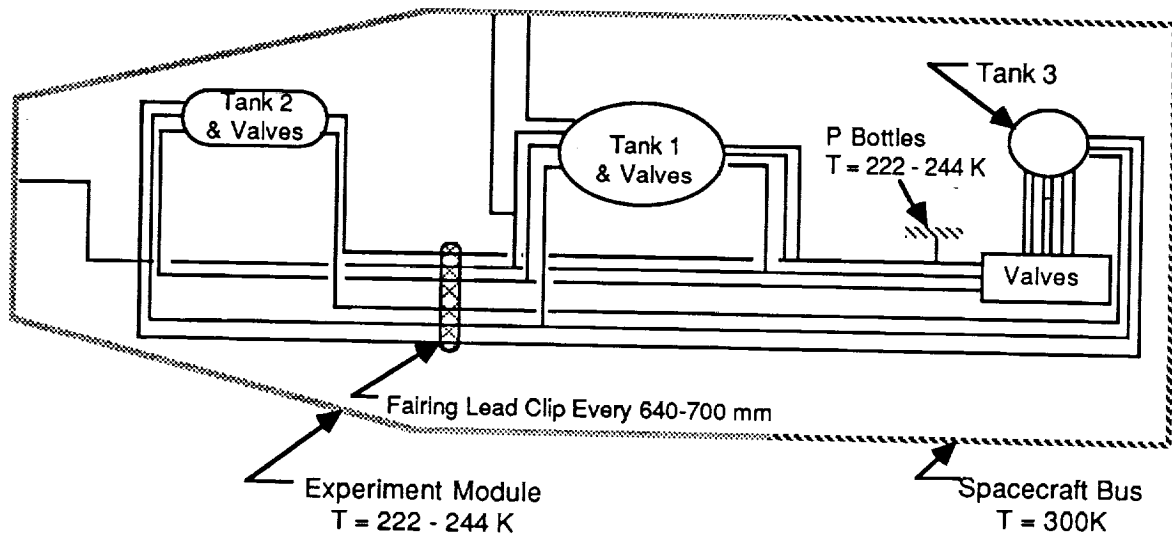


Figure 6-35. Schematic of Fluid Penetration Thermal Model

Table 6-14. Summary of Heat Flow into Filled Tanks through Fluid Penetrations

RECEIVER TANK FLUID OPTIONS	HEAT FLOW (W)		
	TANK 1	TANK 2	TANK 3
<u>T = 222 K*</u> Both Tanks Full	0.064	0.040	0.169
Tank 2 Empty, Tank 3 Full	0.070	N/A	0.170
Tank 3 Empty, Tank 2 Full	0.082	0.040	N/A
Both Tanks Empty	0.088	N/A	N/A
<u>T = 244 K*</u> Both Tanks Full	0.081	0.051	0.175
Tank 2 Empty, Tank 3 Full	0.088	N/A	0.176
Tank 3 Empty, Tank 2 Full	0.100	0.052	N/A
Both Tanks Empty	0.107	N/A	N/A

* Temperature of the inner surface of the micrometeoroid shield.

N/A = Not Applicable

The total on-orbit heat flow is summarized in Table 6-15. The relatively large amount of instrumentation on the tanks is reflected by the significant percentage of overall heat flow to the tanks attributed to penetrations.

Table 6-15. Total On-Orbit Heat Flow to Experiment Tanks

Penetration Type	HEAT FLOW (W)		
	TANK 1 (Surface Area = 18m ²)	TANK 2 (Surface Area = 8.3 m ²)	TANK 3 (Surface Area = 3.6 m ²)
Fluid	0.064 - 0.107	0.040 - 0.052	0.169 - 0.176
Electrical	0.800	0.756	0.238
Structural	0.172 - 0.222	0.104	0.028 - 0.039
Overall Penetration	1.04 - 1.13	0.90 - 0.91	0.44 - 0.45
Equivalent Flux (W/m ²)	0.058-0.063	0.108-0.109	0.122-0.125
MLI with VCS* w/o VCS*	2.05 - 2.54	1.83 - 3.17	0.88 - 1.11
	3.80 - 5.06		
TOTAL with VCS* w/o VCS*	3.09 - 3.67	2.73 - 4.08	1.32 - 1.56
	4.84 - 6.18		
Equivalent Flux (W/m ²)	0.172 - 0.204 0.269 - 0.343	0.329 - 0.492	0.367 - 0.433
Percent Total Due to Penetrations	31 - 33 18 - 22	22 - 33	29 - 33

* Based on MLI Thickness of 76 mm for Tank 1, 38 mm for Tank 2, 25 mm for Tank 3

6.6.4 Spacecraft Bus / Experiment Module Thermal Exchange

In order to protect electrical components from exposure to cryogenic temperatures, they will be placed in the more benign environment of the spacecraft bus. The supply tank and receiver Tank 3 will be housed in the experiment module, where the thermal environment will be driven mainly by the incident space heating level. Since the experiment module will tend to be much colder than the spacecraft bus, heat will flow across the interface, directly impacting the heating requirements of the spacecraft bus.

A steady-state two-dimensional model of the interface area was developed to simulate heat flow from the spacecraft bus connecting ring through an interface structure and into the rear cone. A schematic of the interface heating model is shown in Figure 6-36. The rear cone structure, part of the MMS, consists of a 76.2 mm thick 2219 aluminium honeycomb core with 9.53 mm hexagonal cells sandwiched by inner and outer faceplates of 2219 aluminium with thicknesses of 2.03 and 0.25 mm, respectively. Solar heating of the rear cone, corresponding to the minimum heating orbit, was assumed, since this yields the most conservative heat flow estimate. The inside surface and the forward end of the rear cone were treated as adiabatic, while the spacecraft bus was simply modeled as a 289 K constant temperature heat source. At the interface point, there are 36 contact points around a 1680 mm bolt circle. Heat flows via conduction through the bolt and into a nut plate, then is distributed around the circumference of the rear cone along continuous reinforcement bands. Symmetry allowed the model to consider only a 5 degree arc of the bolt circle.

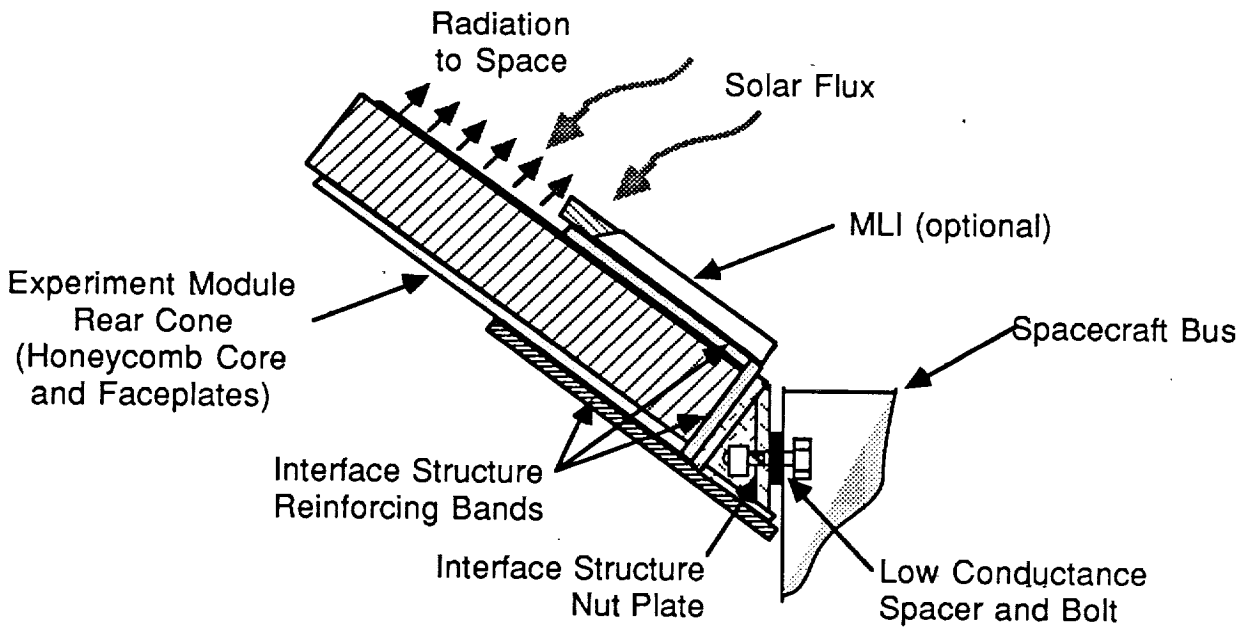


Figure 6-36. Schematic of Interface Heating Model

A parametric analysis was conducted using the interface model to assess the impact of using various materials, specifically titanium, aluminum and T300 graphite epoxy, for components of the interface structure. The effect of partial enclosure of the rear cone with MLI was also examined. The resulting heat leaks from each case examined are given in Figure 6-37. Although significant reductions in thermal exchange were realized by using graphite/epoxy, cost and ease of manufacturing considerations favored the aluminium structure with MLI extending forward 510 mm from the interface point.

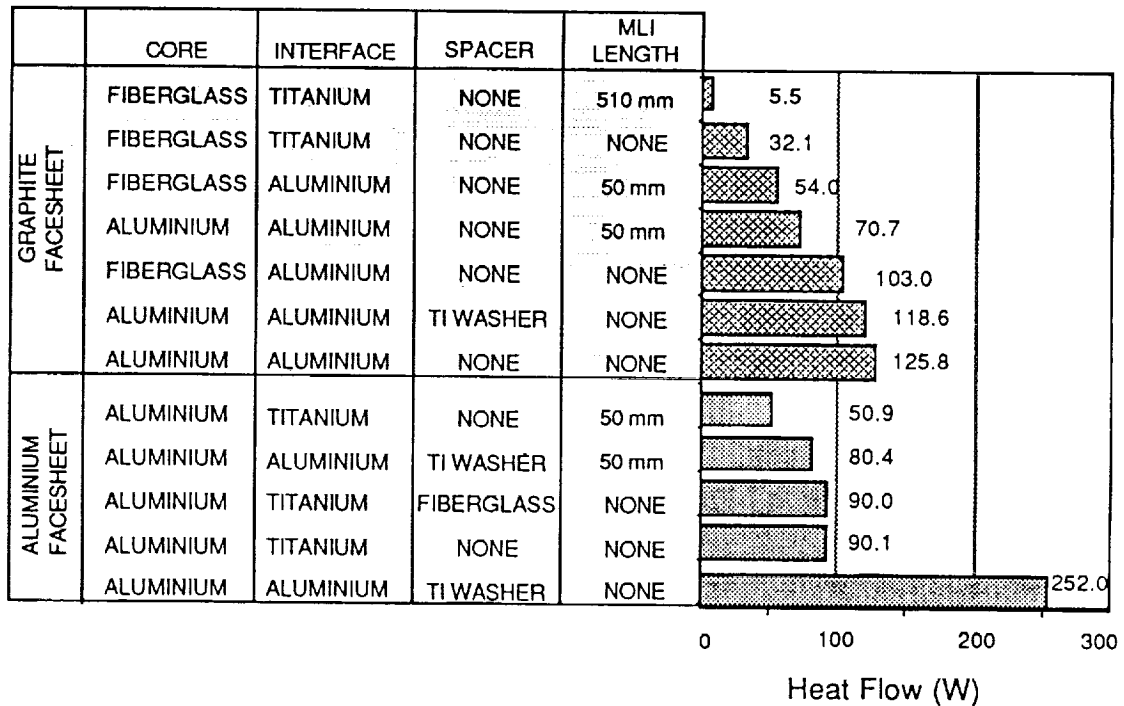


Figure 6-37. Summary of Interface Heat Flow Parametric Analysis

6.7 MICROMETEOROID/DEBRIS SHIELDING

The low-Earth-orbit environment includes hazards caused by micrometeoroids and man-made debris. In order to meet the reliability goal of 0.92 for Class I experiments, analysis indicates the need for shielding around the experiment to prevent penetration of the tanks and fluid lines and/or damage to the insulation. The analysis is based on environmental parameters taken from Space Station design criteria documents, and uses particle penetration models published by NASA/JSC.

Reference 6-22 defines the anticipated mid 1990s debris environment for the Space Station Freedom at altitudes of 400 km and 500 km. Interpolation of this information to an altitude of 463 km (250 NM) gives the following equation for debris particle flux

$$\log_{10} N_{463} = 2.48 \log_{10} D - 8.13 \quad (6-49)$$

where D is the particle diameter in meters and N is the flux of particles of diameter D or greater per square meter per second.

Reference 6-23 provides updated data on debris flux distribution, indicating that the flux at our 1297 km (700 NM) reference altitude is reduced to about 38 percent of the flux at 463 km. Assuming the normalized distribution of particle size to be the same for the two altitudes, the debris flux equation for 1297 km becomes

$$\log_{10} N_{1297} = 2.48 \log_{10} D - 8.56 \quad (6-50)$$

Reference 6-22 indicates an average velocity of 9 km/s for debris and a density of 2800 kg/m³. The debris hazard is strongly anisotropic, with debris only incident from the ram direction and from within the orbital plane.

The sporadic meteoroid environment used is defined in Reference 6-24 as

$$\log_{10} N = -1.22 \log_{10} m - 18.07 \quad (6-51)$$

where m is the particle mass in kilograms. The reference indicates meteoroids can be assumed spherical, with an average density of 500 kg/m³ and an average velocity of 20 km/s. No anisotropy of the meteoroid hazard is considered except for Earth shadowing. Shadowing and a reduction of gravitational focusing with altitude combine to decrease the flux by about 35 percent.

The COLD-SAT experiment module has a dual-wall external aluminum structure, representing a simple yet state-of-the-art impact protection system. It is approximately 25 percent as heavy as a single-wall system. Particles are vaporized or fragmented by the outer wall, and the gap between the walls allows the material to disperse, defocusing the impact energy on the inner wall. The equations for aluminum dual-wall shield thickness requirements are taken from Reference 6-25. The thickness of the inner wall is

$$S = 5.5 \times 10^{-7} (\rho_p \rho_s)^{0.167} m^{0.333} V \quad (6-52)$$

where S is in meters and ρ_p and ρ_s are the density of the particle and wall, respectively in kilograms per cubic meter, and V is the particle velocity in meters per second. The optimal outer wall thickness is about 20 percent the particle diameter for velocities characteristic of orbital debris (9 km/s) and about 5 percent the diameter for velocities characteristic of meteoroids (20 km/s). The inter-wall gap should be at least thirty times the particle diameter.

From Reference 6-26 the probability of not receiving an impact at a given particle flux level is

$$P_o = e^{-NA t} \quad (6-53)$$

where A is the exposed area in square meters and t is the exposure duration in seconds. The analytical approach taken is to determine the shield parameters that yield the desired probability of not being penetrated by the combined micrometeoroid and debris environment. Since these two hazards are unrelated, the penetration probability must be optimally partitioned between them to find the minimum weight shield. Thus Equation (6-53) is used to determine particle flux, Equations (6-50) and (6-51) are used to determine particle diameter, and Equation (6-52) and particle diameter are used to determine the inner and outer wall thicknesses, respectively, and the inter-wall gap.

Figure 6-38 illustrates the resulting relationship between wall mass and probability of not penetrating the shield over the half year reference mission. Based on these results a survival probability of 99 percent was selected. Figure 6-39 gives the relationships between mission duration and shield wall mass and inter-wall gap. Doubling the mission duration to one year will increase the required wall mass by about 27 percent. Figure 6-40 gives the relationships between mission duration and shield wall thicknesses. For a half year mission the inner and outer walls are 1.17 mm and 0.25 mm thick, respectively.

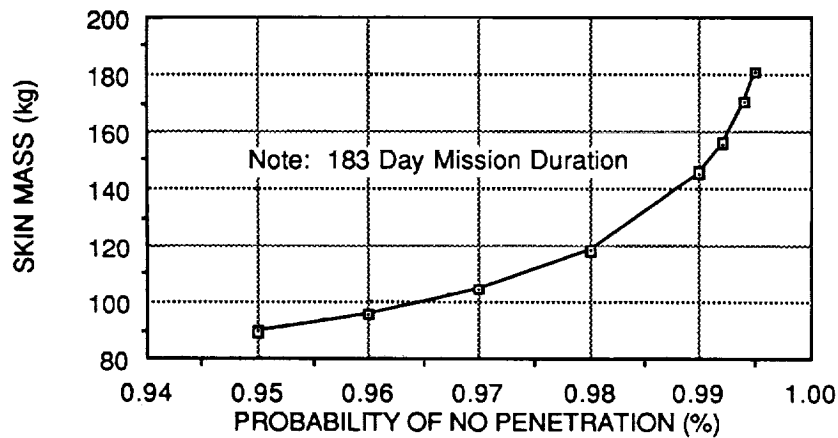


Figure 6-38. Effect of Penetration Resistance on Shield Mass

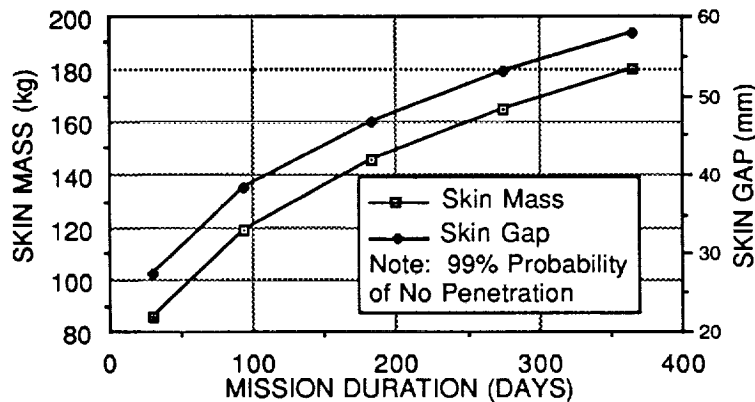


Figure 6-39. Effect of Mission Duration on Shield Mass and Thickness

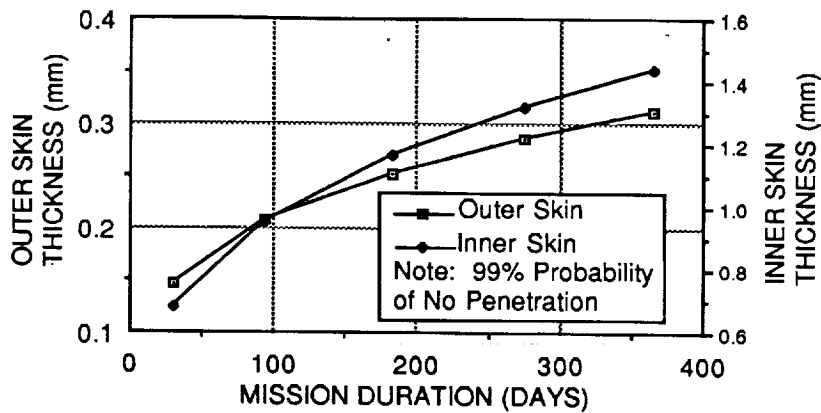


Figure 6-40. Effect of Mission Duration on Shield Skin Thicknesses

6.8 STRUCTURAL REQUIREMENTS

A structural analysis was performed to verify the design of the major COLD-SAT components. The major components analyzed included the micrometeoroid/debris shield, experiment tanks, tank supports, and experiment module separation system. All major structural components of the COLD-SAT system met the design performance requirements.

The structural analysis of the COLD-SAT system was based on the following assumptions: the principle structural material is 2219 aluminum alloy; a 20 percent load knock-up factor was used to account for system weight uncertainties; and, factors of safety were 1.0 yield, 1.25 ultimate for structure, and 1.50 ultimate for pressure vessel structure. Stability analysis was performed per NASA SP-8007, Buckling of Thin Walled Circular Cylinders, Reference 6-27, and NASA SP-8019, Buckling of Thin Walled Truncated Cones, Reference 6-28. The launch vehicle accelerations used for design were taken from the Atlas Mission Planner's Guide Revision 1 March 1989, Reference 6-29. These conditions are listed in Table 6-16.

Table 6-16. Atlas Launch Vehicle Payload Acceleration Factors

LOAD CONDITION	DIRECTION	STEADY-STATE ACCELERATION	DYNAMIC
Launch	Axial	1.2	±1.5
	Lateral	-	±1.0
Flight Winds	Axial	2.2	±0.3
	Lateral	0.4	±1.2
BECO (max axial)	Axial	5.5	±0.5
	Lateral	-	±0.5
BECO/BPJ (max lateral)	Axial	2.5-1.0	±1.0
	Lateral	-	±2.0
MECO	Axial	4.0-0.0	±0.5
	Axial	0.0	±2.0
	Lateral	-	±0.5

6.8.1 Analysis of External Structure

A preliminary analysis was performed to verify the adequacy of the experiment module external structure. This structure carries launch loads, and also provides protection against micrometeoroids and debris. It is a semi-monocoque sandwich structure composed of a thin aluminum outer skin, a low density aluminum honeycomb core, and a structural aluminum inner skin; the sub-component regions are reinforced at the major and minor joint/hard-point regions with aluminum frame extrusions.

The two primary regions of structural concern are diagrammed in Figure 6-41. The upper portions of the sandwich structure were sized for the micrometeoroid/debris shielding requirements. The lower cone and mid-cylinder regions were also analyzed for stability failure considering specific weight contributions of each of the major components of the module to the axial, bending and shear loading distributions within the structural shield during worst-case launch vehicle accelerations.

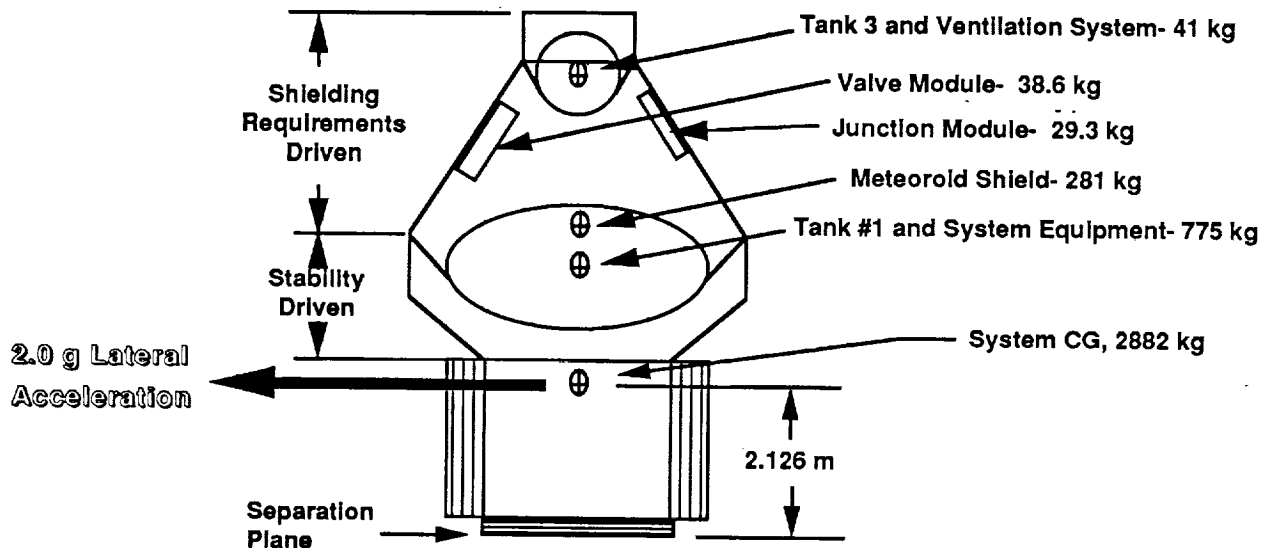


Figure 6-41. Experiment Module External Structure Design Drivers and V-Band Clamp Loads

The stability analysis assumed the inner skin of both the lower cone and cylinder were monocoque structures. This assumption is conservative considering it is a sandwich structure and that rings distribute the component load introductions into the shield i.e. the localized point and kick loads due to Tank 1 strut attachment at the mid-cylinder shield inner skin. The baseline sandwich cross-sectional configurations for each region are diagrammed in Figure 6-42.

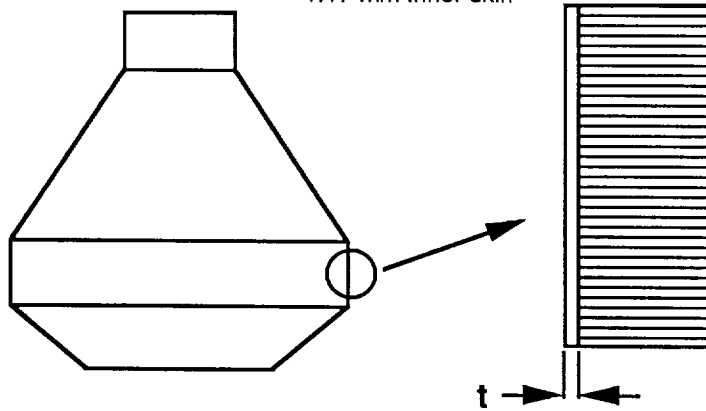
6.8.2 Experiment Module Pressure Vessel Design

The experiment module pressure vessels are made from 2219-T62 aluminum alloy sheet. Due to the welded fabrication with no post-weld heat treatment the skin thickness requirements for the tanks were based upon material properties for the 2219-0 condition. Tensile yield and ultimate strengths for the 2219-0 condition were taken from Battelle's Aerospace Structural Metals Handbook, Reference 6-30, (110 MPa yield strength; 207 MPa ultimate strength).

The tanks skins are yield-critical due to the assumed 1.0 yield factor of safety, and the imposed 1.5 ultimate factor of safety. Tank membrane thicknesses were established using classical stress relations for thin-walled pressure vessel (elliptical) dome, and cylinder regions (GDSS Structures Analysis Manual, Reference, 6-31). Actual tank thicknesses were increased to account for

Debris Shielding Requirement

0.254 mm Outer skin
 48.3 mm, 16 kg/m³ Al core
 1.17 mm Inner skin



Sub-component	t, mm
Cap	1.17
Upper Cylinder	1.17
Upper Cone	1.17
Mid-Cylinder	1.52
Lower Cone	2.16

Structural Inner Skin Requirement

Figure 6-42. External Structure Cross-Section Geometry

discontinuity effects at the dome/cylinder intersections, strut support hard-points, heat-exchanger attach points, and weld land build-up regions.

For ground conditions, the tank differential pressures are expected to be significantly lower than the maximum operating pressure of 345 kPa. The effective burst factor of safety for ground conditions will be 2.00 minimum. Figure 6-43 diagrams the tank configurations and baseline thicknesses.

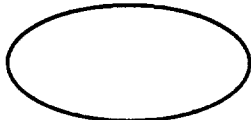
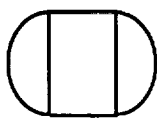
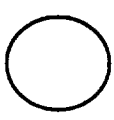
			
	Tank 1	Tank 2	Tank 3
Max. Operating Pressure (kPa)	345	345	345
Dome Thickness (mm)			
Required	1.91	1.14	0.89
Actual	2.54	1.65	1.27
Cylinder Thickness (mm)			
Required	N/A	1.65	N/A
Actual	N/A	1.65	N/A

Figure 6-43. Experiment Tank Wall Thicknesses

6.8.3 Experiment Module Tank Support Struts

Tank support struts were designed considering the axial tensile and compressive loads developed during the launch and flight accelerations. The strut tube diameters were held within limits defined from thermal analysis of the tank heat loads; strut tube thicknesses were developed from the system structural requirements.

The baseline strut is a filament wound glass/epoxy (S2/E788) tube with metal end closures. The laminate consists of 3 deg. and 30 deg. helicals for primary axial stiffness, and secondary torsional rigidity. The glass/epoxy material system has a nominal ply thickness of 0.112 mm, therefore to obtain the preferred ply orientations (± 3 deg./ ± 30 deg.) requires minimum tube thickness increments of 0.457 mm. The strut cross-sections were analyzed for the primary design failure modes of compression shell and Euler buckling. Figure 6-44 outlines the support strut configurational requirements for each experiment tank.

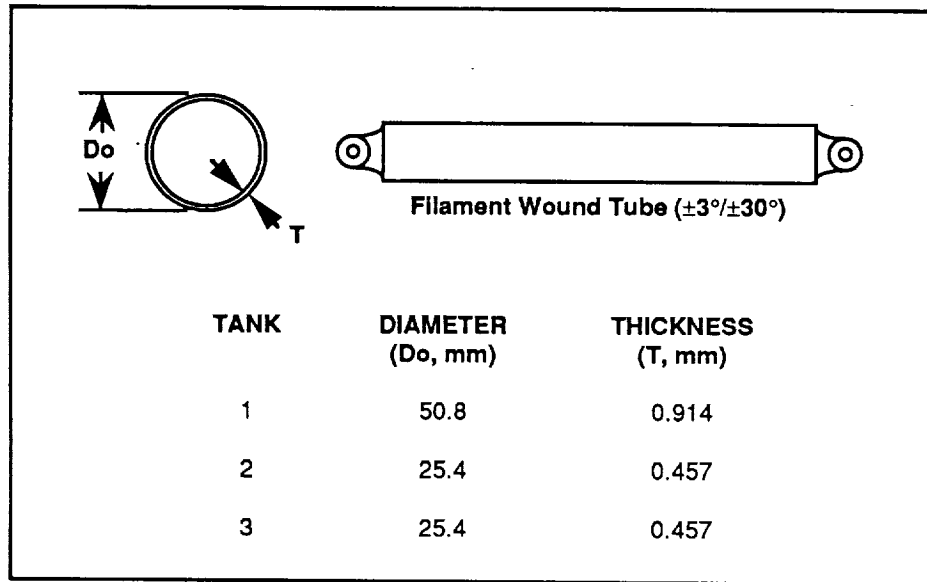


Figure 6-44. Experiment Tank Support Strut Dimensions

6.8.4 Experiment Module Separation System

The V-band clamp load requirements were developed from the worst-case bending loads during the launch vehicle BECO/BPJ (Booster Engine Cut-off/Booster Pod Jettison) events; this worst-case is a 2.0 g lateral acceleration on the experiment module. Figure 6-41 diagrams the condition. The peak tensile axial lineload developed at the clamp region from the lateral acceleration is 80500 N/m ultimate; the transverse shear load developed is 84800 N ultimate. The analysis assumed the weight uncertainty and a 1.25 factor of safety.

There are two (off-the-shelf) V-Band separation systems currently available for the COLD-SAT dimensional restrictions. The systems are produced by Hughes and Saab. The Saab system has been tested to a maximum tensile lineload of 1.39×10^5 N/m (a system proportional limit at test was 87600 N/m). The maximum shear load for the system has not been systematically characterized by Saab. Currently, plans have been established for a GDSS qual test for the Saab clamp (Atlas/Centaur). The test transverse shear load application will be a 67800 N limit condition (85600 N ultimate). The testing will be completed in September of 1991. The tested tensile lineload capacity of the Saab clamp, as well as the GDSS proposed transverse shear test loading bounds the conditions for the baseline COLD-SAT configuration.

7.0 SPACECRAFT BUS DESIGN

The spacecraft bus design is based on the structural arrangement used by Ford Aerospace for most of their recent communications satellites. Most of the subsystems and components specified for the COLD-SAT spacecraft bus have also been employed on previous satellites or will have been used on a satellite several years before COLD-SAT launch. This approach limits risk and development cost.

7.1 DESIGN FEATURES AND HERITAGE

7.1.1 Overall Arrangement

The on-orbit spacecraft configuration is shown in Figure 7-1. The spacecraft is composed of two major modules: the experiment module, and the bus module. The experiment module is a conical and cylindrical structure which contains the major portion of the experiment, and the bus module is a rectangular box structure that houses the major support subsystems for satellite operations. Two of the three experiment tanks are mounted in the forward experiment module, while the third tank is mounted inside the bus central cylinder.

Figure 4-2 shows the spacecraft in profile view within the Atlas I 4.2 m diameter fairing. A standard Atlas 1666 mm diameter V-band separation system, supplied by Saab, joins the spacecraft to the Atlas launch vehicle. During the launch phase, the flat panel solar arrays which are attached to the Solar Array Drive Assemblies (SADA) are stowed on the + Y and - Y panels, while the S-band omni directional antenna and the S-band high gain antenna are mounted on booms and stowed on the + X and - X axis panels of the bus module. These appendages are deployed after spacecraft separation by pyrotechnic devices.

The spacecraft bus module is shown in Figure 7-2. The bus module structure consists of a central cylinder assembly surrounded by a rectangular box. The spacecraft bus equipment is mounted on the internal surfaces of the box while experiment hydrogen and helium pressurant tanks and spacecraft propellant tanks are mounted to the central cylinder. The modular panel type configuration is typical of Ford Aerospace's 3-axis stabilized spacecraft, and allows parallel fabrication, assembly and test of spacecraft subsystems, and provides for straight forward integration of the final system.

The central cylinder is the primary load-carrying structure of the spacecraft bus module and it carries the experiment module loads to the launch vehicle interface. The rolled aluminum sheet central cylinder with stringer and ring construction provide a strong and simple construction at minimum cost. The experiment module is attached to the bus module central cylinder by (24) 0.375 diameter bolts and 12 shear pins, and the pressurant tanks and propellant tanks are fastened to the cylinder by means of fiberglass struts. The rectangular box panels are aluminum honeycomb core/aluminum skin construction. The $\pm Z$ panels and $\pm Y$ panels are joined at their edges by aluminum longerons to form the box. The structural attachment to the central cylinder is through four shear webs in the center of each panel. The $\pm X$ panels complete the box and are also attached to the central cylinder by means of a bolted interface to aluminum rings integral to the cylinder.

7.1.2 Equipment Layout

Figure 7-3 shows the experiment electronics and bus equipment mounted on the six aluminum/honeycomb panels of the spacecraft bus. For optimum thermal performance, the majority of the equipment is mounted on the + Z and - Z panels of the spacecraft body. These panels experience lower average solar incidence and provide the most benign thermal environment. The thermal control system utilizes multi-layer insulation and optical solar reflectors (OSRs) on the

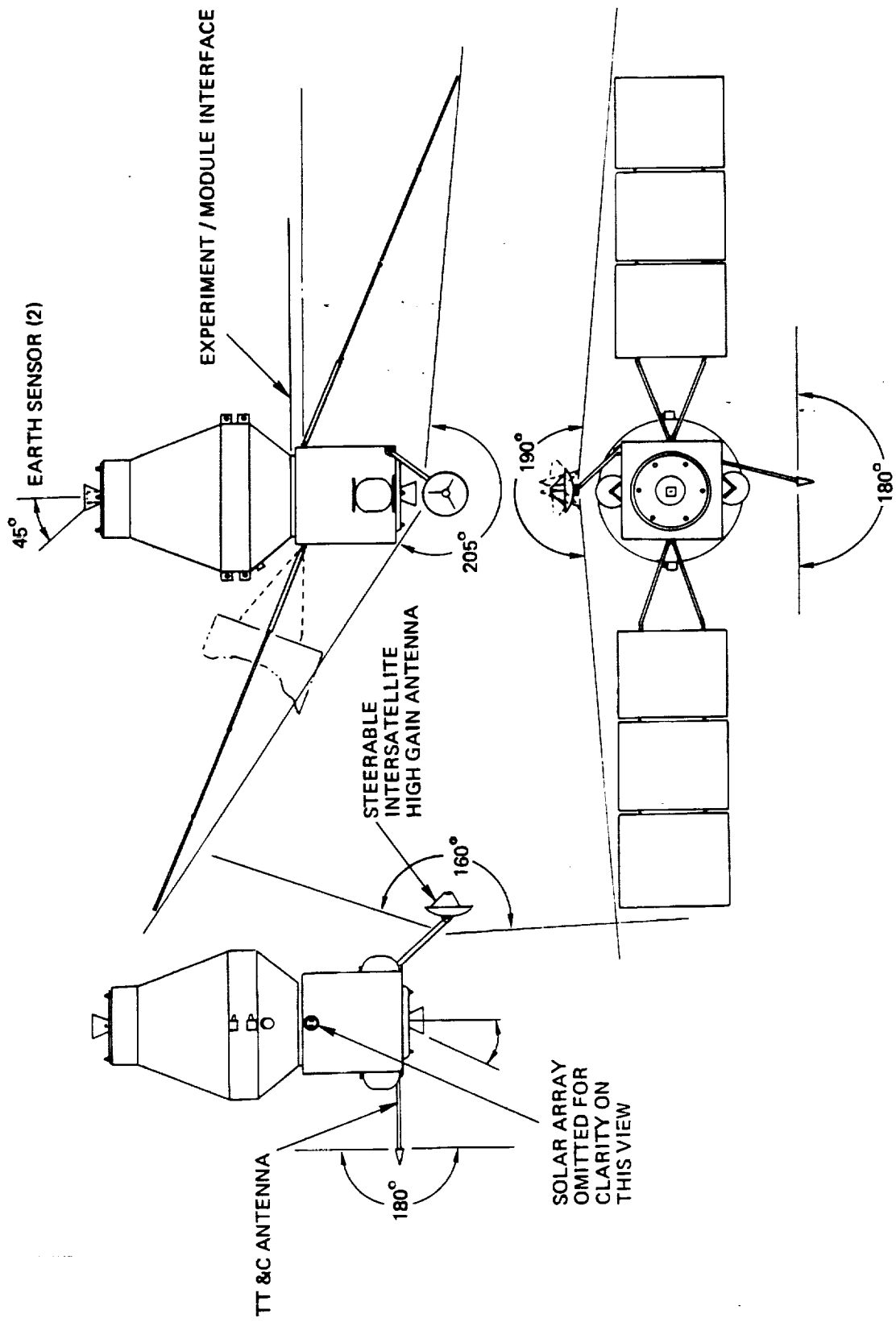


Figure 7-1. COLD-SAT Deployed Configuration Showing Antennae Field-of-View

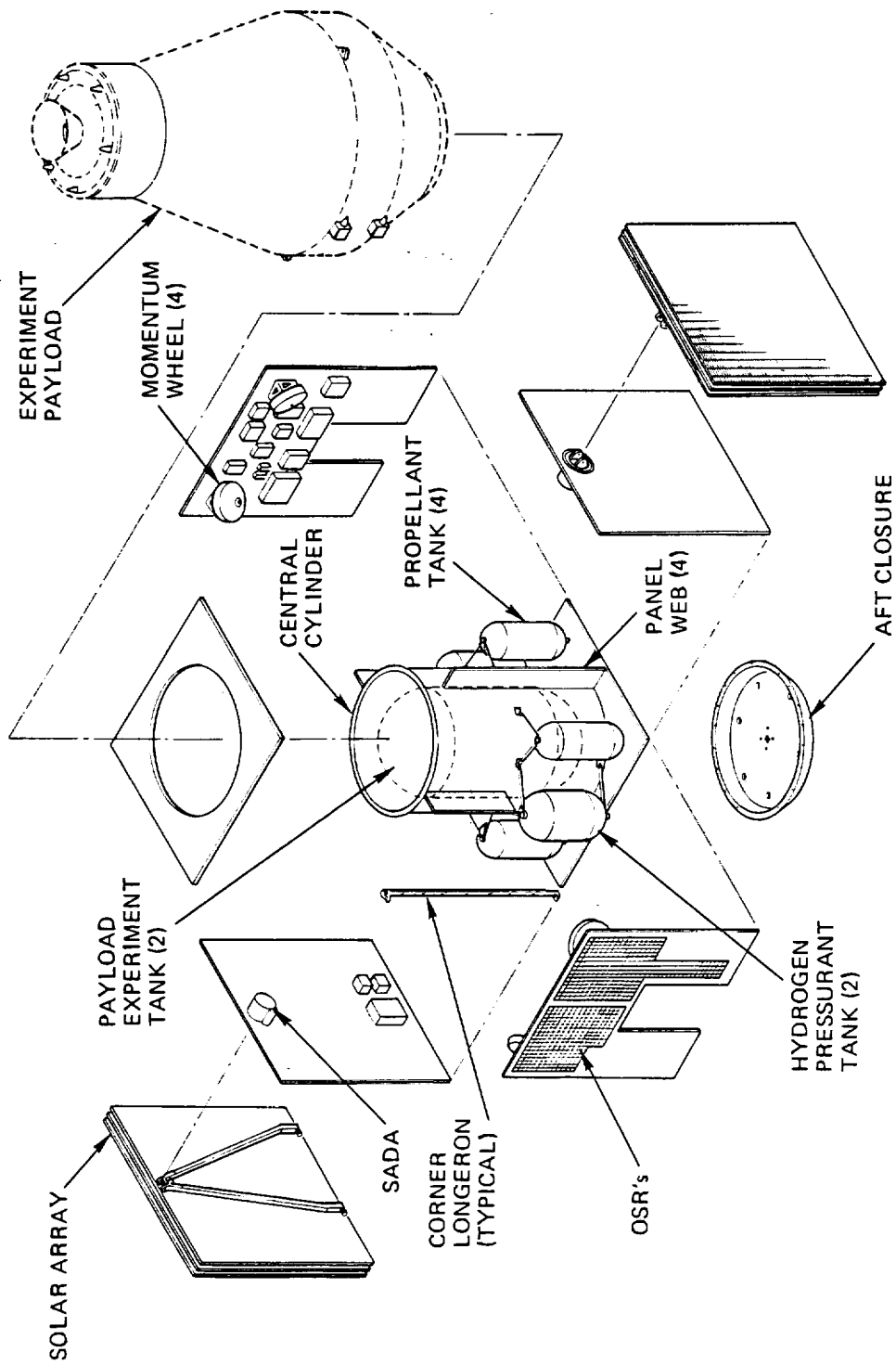
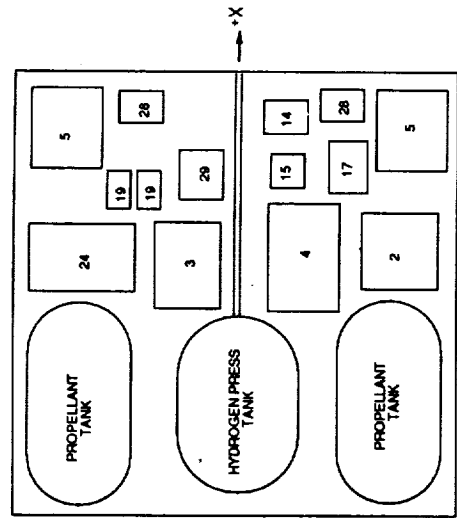
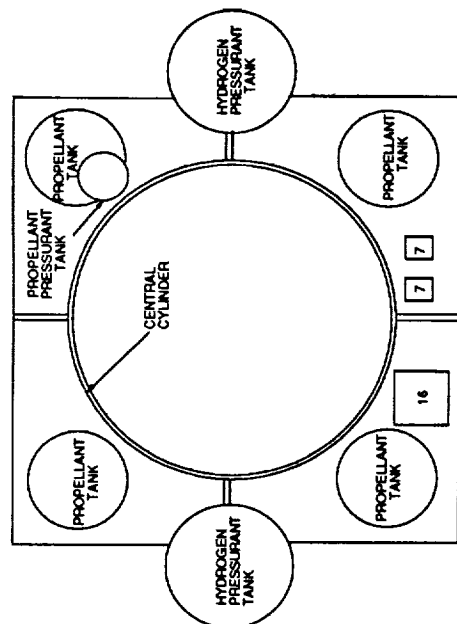


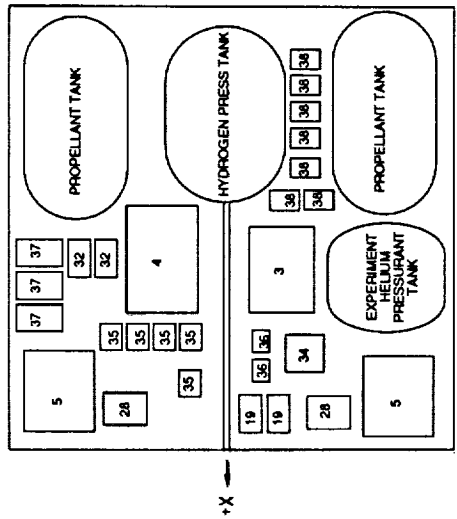
Figure 7-2. COLD-SAT Spacecraft Bus Exploded View



- X PANEL



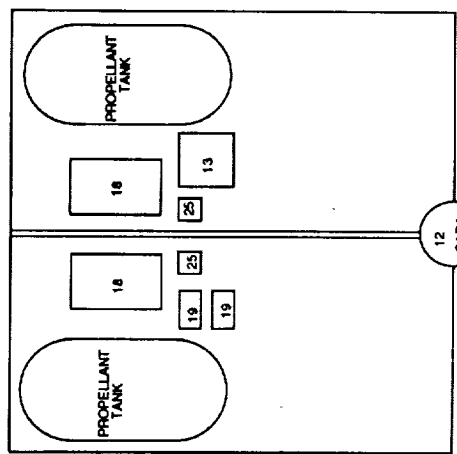
- Y PANEL



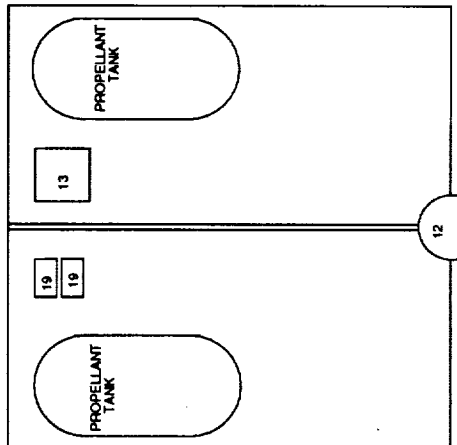
- Z PANEL

- Z PANEL
- 3 BATTERY CHARGE CONTROL
- 4 BATTERY
- 5 REACTION WHEELS (2)
- 19 DATA CONCENTRATOR UNIT (2)
- 28 R W ELECTRONICS (2)
- 32 EXPERIMENT CONTROL UNIT (2)
- 34 SIGNAL CONDITIONER
- 35 CONVERTER (5)
- 36 INVERTER (2)
- 37 TRI-AXIAL ACCELEROMETER (3)
- 38 FLOW METER ELECTRONICS (7)

- X PANEL
 - 7 EARTH SENSOR ELECTRONICS
 - 16 VALVE DRIVER ELECTRONICS
- Y PANEL
 - 12 SADA
 - 13 SADA ELECTRONICS
 - 19 DATA CONCENTRATOR UNIT (2)
- + Y PANEL
 - 12 SADA
 - 13 SADA ELECTRONICS
 - 16 TRANSFORMER (2)
 - 19 DATA CONCENTRATOR UNIT (2)
 - 25 DIPLEXER (2)



+ Z PANEL



+ X PANEL

Figure 7-3. COLD-SAT Equipment Layout

exterior panels of the main body. Some of the equipment is mounted on the + Y and - Y panels, however, the higher power dissipating equipment is mounted on the Z axis panels. The Data Concentrator Units (DCUs) of the SCE are distributed on the four main equipment panels to service COLD-SAT data acquisition, command, and control functions. This distributed architecture facilitates both integration and test, and optimizes weight and reliability by placing the needed processing functions adjacent to the hardware they are servicing. The thrusters and supporting propulsion system components are mounted on the - X panel to produce the required thrust vector for experiment accelerations. The + X panel is used to mount one of the magnetic torquer coils and the bus/experiment interface connectors.

7.1.3 Mass Properties

A spacecraft mass summary that gives mass and center-of-mass position of the spacecraft bus components is presented in Table 7-1. To insure the lowest spacecraft center-of-mass, the heavier equipment is positioned as far aft as possible (in the - X direction). The dry spacecraft bus has a mass of 784.4 kg, and is launched with 530.5 kg of hydrazine propellant, for a bus BOL mass of 1314.9 kg. Added to the experiment module and hydrogen masses, the resulting BOL mass of the entire spacecraft is 2878.8 kg.

7.1.4 System Heritage

The COLD-SAT bus design uses existing flight-proven hardware wherever possible. Although no new technologies are used, it is necessary to modify selected components to provide the capabilities specific to the COLD-SAT mission. These component modifications arise primarily due to the COLD-SAT orbit and eclipse periods; power, processing and stabilization requirements; and launch vehicle constraints. The following is a list of component modifications adapted from existing hardware, or new hardware designs based on developed technology to meet COLD-SAT's performance requirements:

- A new structure is designed using existing technology similar to other Ford Aerospace spacecraft;
- A new hydrazine propellant tank and propellant management device will be designed based on existing technology;
- The propulsion system pressure regulator set point will be adjusted to match the pressure requirements of the COLD-SAT design;
- Intelsat VII data concentrator units are modified to meet the specific data processing and control functions of the experiment module equipment;
- A high gain TDRS tracking antenna system including a dish antenna, gimbals, and pointing control electronics is a new design using existing technology;
- The momentum wheel lubrication system and wheel control electronics are modified to operate the momentum wheel in a reaction wheel mode;
- The magnetic torquers are re-sized (wire size and number of turns) based on the magnetic field strength of the COLD-SAT orbit, and the internal coil area matched to the new structure to provide the required control authority;
- The solar arrays utilize the SCS basic design but changes are made in cell layout and cell interconnect design;

Table 7-1. Spacecraft Bus Mass Properties

SUBSYSTEM/ITEM	MASS (KG)	MOMENT ARM (CM) FROM EQUIPMENT MODULE RING	MOMENT (CM-KG)
EQUIPMENT PANELS	86.5	180.3	15591.2
CYLINDER	54.5	180.3	9836.7
FORWARD CLOSURE	14.4	751.8	10799.2
AFT CLOSURE	20.0	43.2	863.6
MISC	42.8	180.3	7721.8
<i>STRUCTURE TOTAL</i>	<i>218.2</i>		
<i>MECHANICAL INTEGRATION</i>	<i>22.7</i>	<i>180.3</i>	<i>4098.6</i>
<i>ELECTRICAL INTEGRATION</i>	<i>31.8</i>	<i>203.2</i>	<i>6465.5</i>
PRESSURANT TANK	7.9	223.5	1767.8
PROPELLANT TANKS	42.5	124.5	5295.2
FORWARD THRUSTERS	2.6	746.8	1968.7
ROLL THRUSTERS	2.6	447.0	1178.6
AFT THRUSTERS	2.6	40.6	107.1
PLUMBING, VALVES	10.1	83.8	849.6
<i>PROPULSION TOTAL</i>	<i>68.5</i>		
T&C ELECTRONICS	65.2		
OMNI ANTENNA	2.5	152.4	381.0
DIRECT ANTENNA	18.2	172.7	3148.2
<i>T&C TOTAL</i>	<i>86.0</i>		
WHEELS	30.9	251.5	7772.4
SENSORS & ELECTRONICS	39.2	279.4	10947.4
EAST TORQUER COIL	1.4	279.4	381.0
NORTH TORQUER COIL	1.4	172.7	235.5
EARTH TORQUER COIL	1.4	172.7	235.5
FORWARD EARTH SENSOR	1.9	741.7	1415.9
<i>ADCS TOTAL</i>	<i>76.1</i>		
SEQUENTIAL SHUNT UNITS	11.0	210.8	2319.0
BATTERY CHARGE CONTROLLER	22.7	188.0	4271.8
POWER CONTROL UNIT	9.1	185.4	1685.6
BATTERIES	99.1	185.4	18373.4
<i>ELECTRIC POWER TOTAL</i>	<i>141.9</i>		
SOLAR ARRAYS	96.8	170.2	16476.5
YOKES & HOLD DOWN	22.0	170.2	3751.7
<i>SOLAR ARRAY TOTAL</i>	<i>118.9</i>		
FORWARD CLOSURE	2.6	911.9	2404.0
AFT CLOSURE	3.5	40.6	144.1
MAIN BODY THERMAL CONTROL	14.1	172.7	2433.8
<i>THERMAL CONTROL TOTAL</i>	<i>20.3</i>		
DRY SPACECRAFT BUS	784.4	182.2	142920.7
DRY EXPERIMENT MODULE	1199.4	353.7	566285.4
LIQUID HYDROGEN	364.5	403.9	147221.6
HYDRAZINE PROPELLANT	530.5	124.5	66020.4
SPACECRAFT BOL	2878.8	270.8	779579.0
20% CONTINGENCY	575.8	270.8	155926.6
PAYLOAD ADAPTER AND CLAMP	72.0	38.1	2743.2
TOTAL PAYLOAD AND CONTINGENCY	3526.6	266.0	938075.6

- The Ni-Cd batteries are based on the 35 Amp-Hr INTELSAT V design but will be considerably larger.
- The battery charge controller is based on Space Station Freedom technology (developed at Ford Aerospace), but modified for specific COLD-SAT power system specifications;
- Minor modifications to the Intelsat V power control unit are made to remove obsolete functions such as the heater electronics and battery charge sequencer, now performed by the Spacecraft Control Electronics.

A quantitative assessment of the risk associated with each subsystem component, and a component heritage summary is provided in the Section 12.

7.2 TELEMETRY, COMMAND AND DATA HANDLING

The elements comprising the Telemetry, Command and Data Handling (TC&DH) system are shown in Figure 7-4. These elements support three spacecraft functions: spacecraft commands, spacecraft telemetry and ranging, and experiment data handling.

7.2.1 Telemetry, Command and Data Handling Requirements

The Command subsystem must provide the capability for reliable and continuous satellite control during all mission phases, and for recovery operations in response to conditions of attitude instability. The Telemetry and Data Handling subsystem shall collect, process, format, store, and transmit all spacecraft and payload data. Table 7-2 lists the telemetry and command word requirements. The communications link shall be designed for the TDRSS S-Band Multiple Access service with a time constraint of 10 minutes per orbit. Therefore, COLD-SAT must be capable of autonomous operation and onboard data storage.

Table 7-2. TC&DH Telemetry and Command Word Requirement

	TELEMETRY				COMMAND		
	DIGITAL BI-LEVELS (BITS)	SERIAL DIGITAL WORDS	ANALOG	THERMISTOR	DISCRETE PULSE	DISCRETE RELAY	PROPORTIONAL
ACS	229	11	12	0	42	10	15
EPS	12	0	20	2	52	0	0
EXP	152	6	78	327	0	212	0
PROP	4	0	3	0	8	0	0
TCS	0	0	0	62	28	29	0
TT&C	28	0	10	0	18	5	2
TOTAL	431	17	132	391	148	264	17

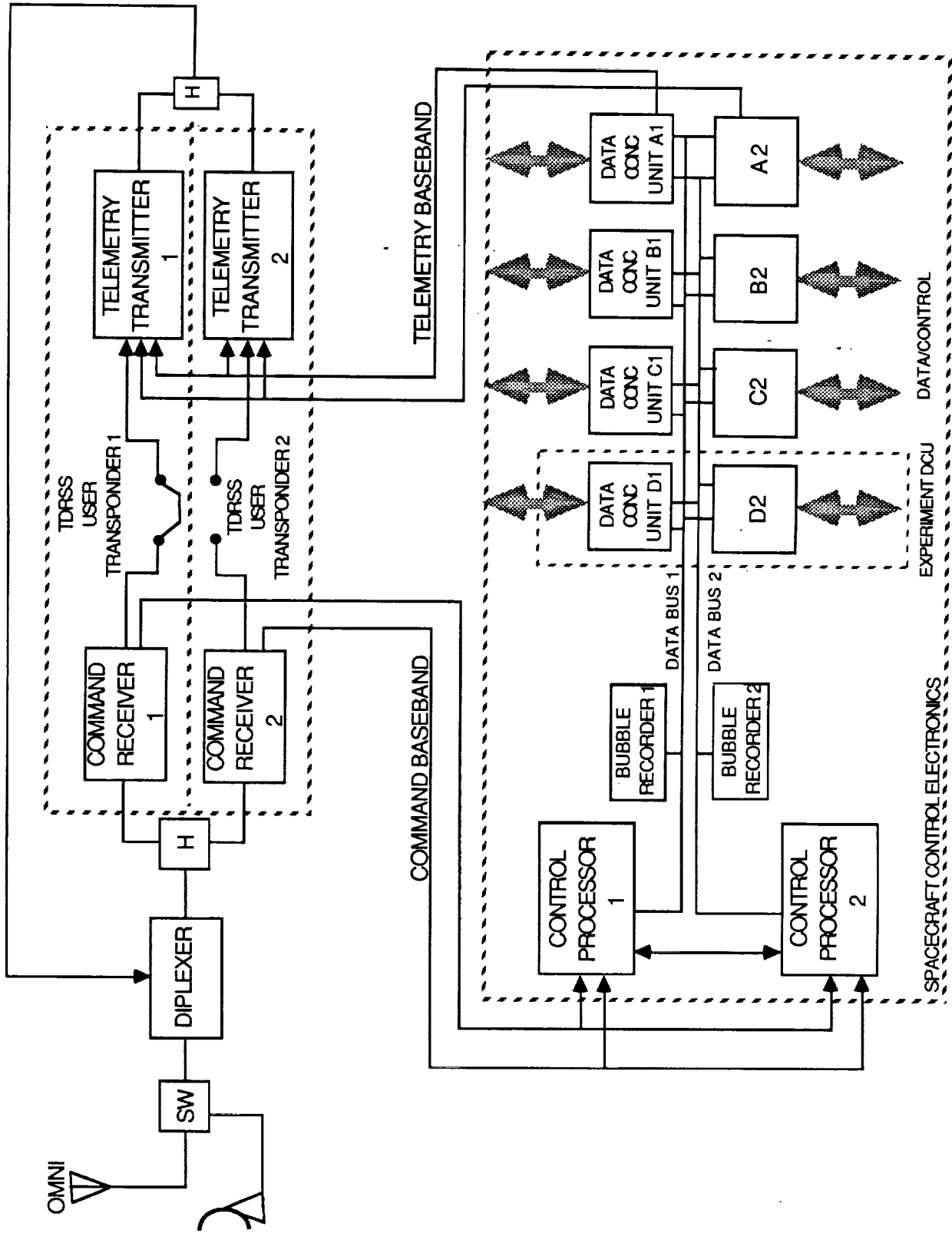


Figure 7-4. Telemetry Command and Data Handling Configuration

7.2.2 Telemetry, Command and Data Handling Description

7.2.2.1 Spacecraft Control Electronics. The Spacecraft Control Electronics (SCE) is an integrated, distributed set of electronics implementing control, command and telemetry functions on the COLD-SAT spacecraft. The SCE consists of four redundant DCUs (Data Concentrator Units) and redundant Central Processor Units (CPUs). The CPU is based on an advanced radiation-hardened CMOS-SOS microprocessor that implements the MIL-STD-1750A instruction set. Each processor has a two wire Mil-STD-1553B data bus to communicate with all eight DCUs. Processor 1 uses data bus 1, and processor 2 uses data bus 2. The normal operating configuration has one CPU and one of each pair of DCUs selected for telemetry and control functions, and is referred to as the "active" mode. The other processor and DCUs are in the "standby" mode. The SCE configuration is selected by ground command.

The CPU controls the system by executing firmware programs contained in its memory. The firmware consists of the operating system and applications programs. All of the modules in both categories are resident in the SCE ROM. The application programs implement the SCE functions such as attitude determination and control, experiment control and execution, telemetry acquisition and formatting, command decoding, verification, distribution and execution, battery management, etc. Since there are many application programs, and they each require execution at different rates, the operating system implements a task scheduler that selects the application programs to be performed in each 62.5 ms basic processing cycle.

The DCUs perform the interfacing function between the processor and the spacecraft equipment to implement the telemetry and command functions required in their local area. Figure 7-5 shows a block diagram of a typical DCU. The smart controller is built around the TI SBR 9000 microprocessor and communicates with the CPU via the Mil-STD-1553B data bus, and with the electronic modules of the DCU via the intra module control bus (IMCB). Each of the electronic modules is tailored to perform a dedicated I/O function, as required to efficiently service the spacecraft and subsystems.

7.2.2.2 Command Subsystem. The command subsystem provides for the reception, decoding, and distribution of spacecraft commands. The RF functions are performed by the redundant command receivers and antennas, and the baseband functions are performed by the redundant elements of the spacecraft controller. The command subsystem consists of two separate command data channels, individually accessible via unique command addresses. Either baseband section can decode, distribute and execute a command. The command receiver is sequentially sampled by the bit detector located in the TDRS User Transponder which is automatically configured to accept S-Band signals from TDRS or from STDN. Detection of a TDRS PN code or a STDN 16 kHz subcarrier signal results in a lockup and subsequent detection of the command message. The transponder outputs to the processor a command bit stream, a clock timing signal, and an "in-lock" signal for address verification and decoding of the command data. User address information is used to distribute the command data to the specific DCU which services the intended user.

Command RF Section

The command RF section receives ground commands on either the high gain directional antenna or the omni antenna and routes them to the receivers within the redundant TDRS User Transponders. During normal operations, the directional antenna receives commands from the TDRS S-Band Multiple Access service. The Omni Antenna is used by the STDN network during launch operations, and is available for on-orbit contingencies as a low rate TDRSS or STDN communications link. In the event of a loss of Earth-lock condition, the SCE will configure COLD-SAT into a safe-mode which includes selecting the omni antenna, and the command receiver will simultaneously attempt to acquire S-Band signals from both the TDRSS and STDN communication networks.

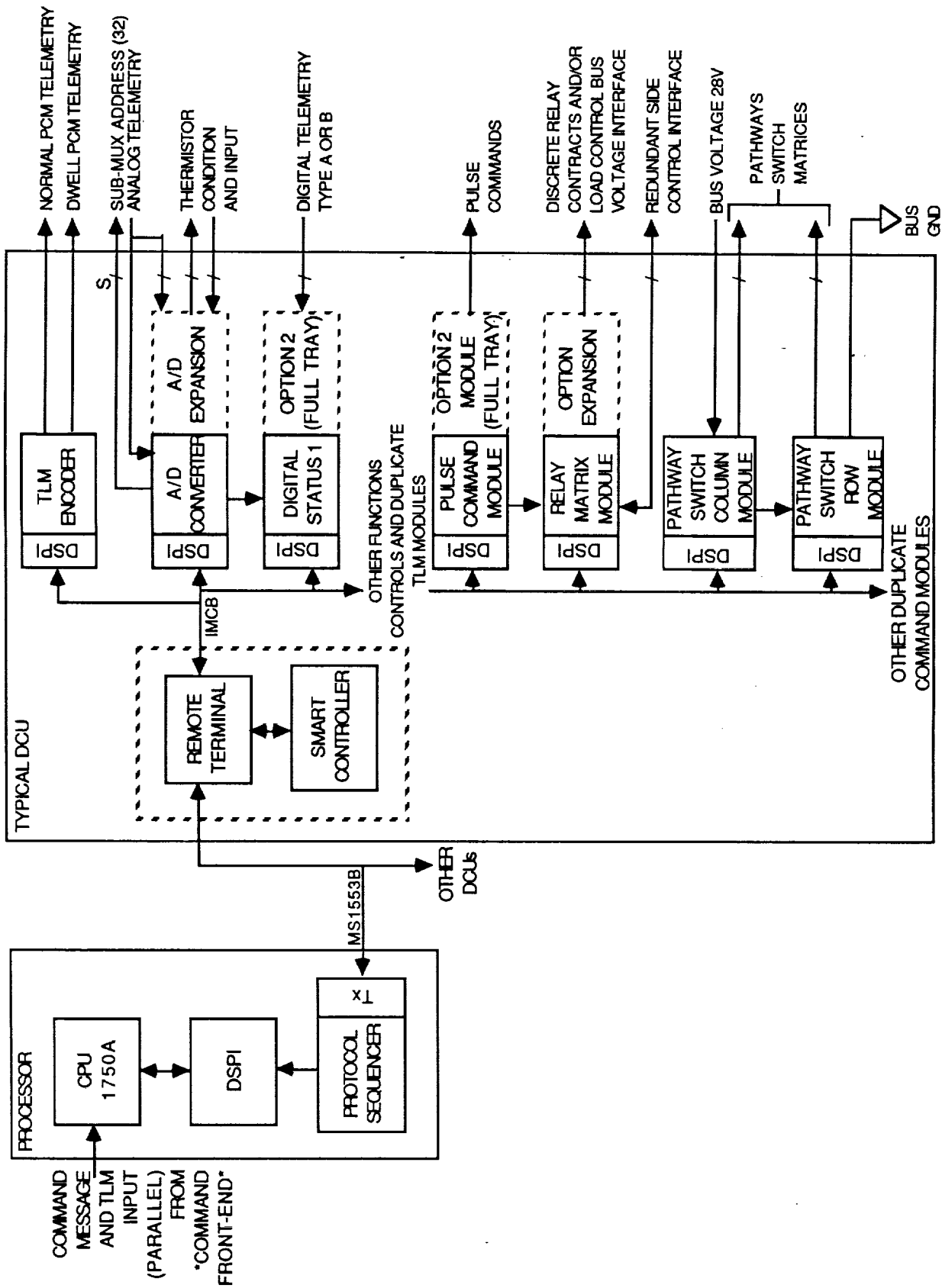


Figure 7-5. DCU Functional Architecture

Command Baseband Section

The command message format is shown in Figure 7-6. A 128 bit preamble of alternating ones and zeros precede the command message to enable acquisition and synchronization of the bit detector clock. Between messages in a multiple command sequence, an idle bit pattern is provided by the command baseband to maintain bit synchronization between intermessage periods. The command data block includes the execute mode, execute parameters, command data, and command vector. Table 7-3 lists the types of execute modes available. The command data is encoded in a 16 bit command data word, and a 6 bit command vector controls its use.

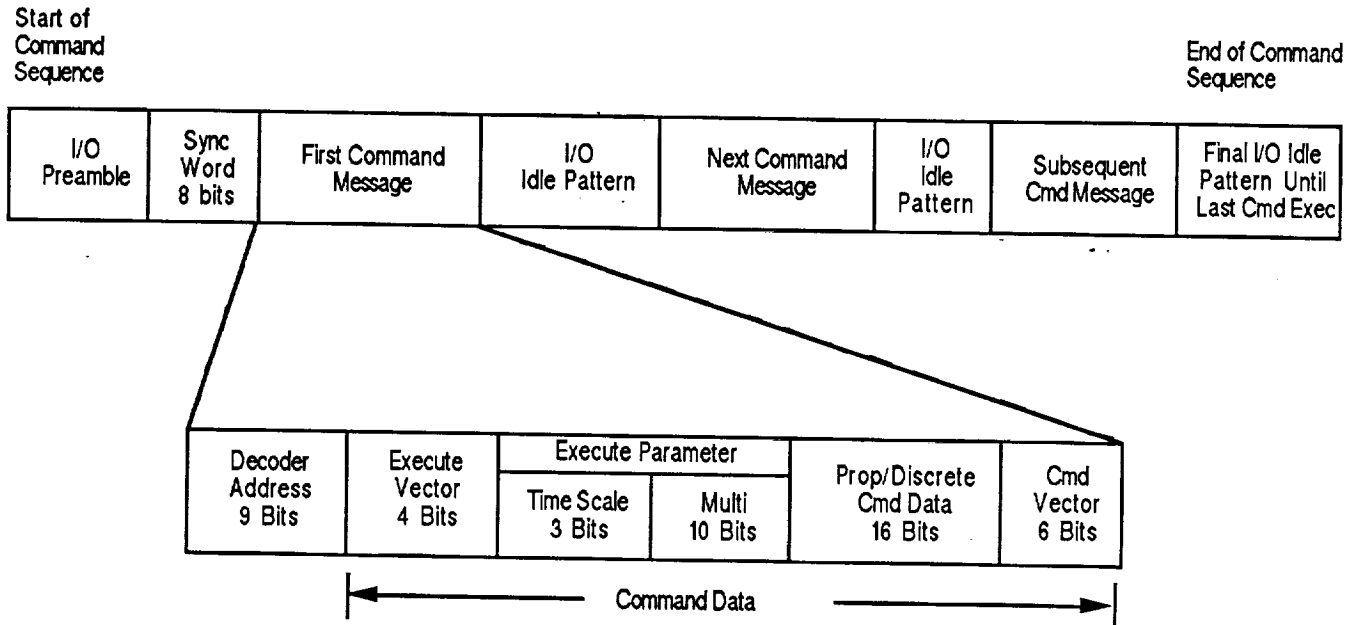


Figure 7-6. Command Message Format

Table 7-3. Command Message Modes

Title	Function
Store	Store current command
Execute & Store	Execute previously stored command; store current command
Multi-function execute 1	Simultaneous execution of multiple functions (eg., experiment switching)
Multi-function execute 2	Sequential execution of stored commands with a single execute (eg., experiment control)
Time tag execute	Auto-execution of stored commands at designated time
Variable length execute	Execute current command with selected pulse length
Multiple execute	Execute current command with selected number, frequency and length of execute pulses
Memory data load execute	Enables routing of continuous 1024 bit data block to designated memory location

The command data words define either a discrete pulse, discrete relay or a 16 bit proportional command. The discrete type commands are used for low power relay and load control. Each pulse command has a nominal 26 V, 300 msec, 90 mA output for low power switching. These commands are obtained by decoding a 10 bit command message at the DCU. The proportional commands have a nominal 26 V, 300 msec, 1 A output, and are obtained by directing a 16 bit command word to the user equipment for processing, without decoding.

Control of the experiment functions is performed by the resident application software of the SCE. The processor issues a discrete relay command to the applicable DCU which in turn decodes it and transmits a 26 V pulse to the appropriate relay circuit in the Experiment Control Unit (ECU). The switching circuits in the ECU apply power to the appropriate flow meters, heaters, valves, and mixers in the experiment module. The baseband design also provides for the upload of memory data by bypassing the normal decode and check process for the selected number of bits, and routes the upload data to processor memory. This feature provides for loading of fixed data blocks into RAM so that new code for experiment sequences can be replaced and executed in place of the resident function.

7.2.2.3 Telemetry and Data Handling Subsystem. The telemetry subsystem consists of the baseband section which performs the collection, processing, storing, formatting, and PCM encoding of spacecraft bus and experiment data, and the RF section to transmit the data to Earth for support of spacecraft operations.

Telemetry Baseband

Spacecraft health, status, performance, and experiment data are collected at the DCU terminals where signal conditioning, A/D encoding, and subcommutation are performed. The processor, a shared resource which services all spacecraft control needs, coordinates the sequential collection of data from the DCUs at the required rates via the data bus, and formats the data into major and minor telemetry frames. The telemetry operation of the SCE is synchronized by the CPU by sending out a broadcast message to all DCUs operating off its data bus at 62.5 ms intervals. The DCUs are able to synchronize their internal 1.667 ms clock to the time synchronization for telemetry data sampling. There are two methods for data collection and processing: normal mode and dwell mode telemetry.

Normal Mode Telemetry. In the normal mode of operation, the DCUs contain all the necessary information needed to sample the required measurements at the correct word intervals (1.666 ms) in order to correlate with designated frame locations. The sampled data is temporarily stored in the microprocessor-controlled RAM of the DCUs to form data blocks, which are transferred to the CPU upon request. The CPU gathers data blocks from the DCUs in a preset sequence at exact intervals, formats it, and stores it for later transmission. During a typical TDRS contact, the formatted data is routed to DCU-A which performs the PCM/BPSK (binary phase-shift keying) encoding and generation of baseband signal for downlink.

Dwell Mode Telemetry. The dwell mode of operation provides a flexible data format to enable additional data monitoring to supplement normal data and for troubleshooting system anomalies. Up to eight main-frame words can be selected for dwell, by command. The remaining operations are the same as for the normal mode. The CPU will access each DCU for its required data words, and then will reformat and store the data in a data block. The block is then sequenced to DCU A where it is encoded and sent to the transmitter.

Telemetry RF Section

The RF section consists of redundant TDRS User Transponders which operate via the high gain directional antenna or the low gain omni antenna. Redundancy is maintained throughout, and the telemetry inputs are cross-strapped with the redundant telemetry encoders, as shown in Figure 7-4. The transponder provides two TDRS telemetry data inputs, one each for the I and Q channels, and a single STDN telemetry modulation input. The two separate TDRSS data input channels are multiplexed to form an QPSK (quaternary phase-shift keying) signal for transmission. The Q channel carries the high data link corresponding to the stored data, and I channel carries either real-time data or dwell data. If dwell data is selected, then the real-time data collection is stored in the redundant Bubble Data Recorder in exactly the same manner as the regular stored data. For contingency purposes, the capability exists to transmit real-time or dwell data via the omni antenna at a reduced capacity.

7.2.2.4 Ranging. The turn-around ranging function is selected by commanding a select switch in the transponder, and is available only when the receiver is locked to a forward link signal. In the TDRSS mode, ranging is obtained by synchronizing the "all 1's" state in the locally generated return link PN code with the "all 1's" state in the received forward link PN code. A coherent turn-around mode provides ground Doppler range rate tracking by a precise 240/221 ratio of the forward link carrier to return link carrier frequency. Ranging capability is not provided in the STDN mode.

7.2.3 Telemetry, Command and Data Handling Performance

Table 7-4 lists the performance parameters for the TC&DH system. During normal operating conditions, the TDRS/high gain directional antenna link is used to receive and transmit telemetry and command data. The TDRS/omni link and STDN/omni link are available for contingency purposes to assure a continuous COLD-SAT command and control capability. In the event of a communications anomaly, the data storage capacity is sufficient to store up to 5 orbits of normal mode telemetry, after which, the spacecraft safe mode is initiated. The SCE has the capability to maintain autonomous spacecraft control for a period of 28 days through a 28 day internal clock, time-tagged commands, and a task scheduler and application programs, all resident in ROM.

7.2.3.1 Command. The primary COLD-SAT command link via TDRSS features a two bit rate capability of 250 and 1000 bps. Robust link margins exist to support these data rates, as shown in Table 7-5. For contingency purposes, command links can be established over the omni antenna through either the TDRS or STDN communications networks.

7.2.3.2 Telemetry and Data Handling. Normal mode telemetry samples all experiment and spacecraft telemetry data within a major telemetry frame. Each major frame contains 64 minor frames for sub-multiplexing of relatively slow time-variant data. The minor frame rate of 0.8532 seconds translates into a real-time data rate of 2.4 kbps. The telemetry format specifications and main frame word allocations are listed in Table 7-6. The analog experiment data is quantized with a 10-bit A/D converter and formatted into the 8-bit word frame by using an overlapping word format approach. This is accomplished by grouping four 10-bit measurements into every five contiguous 8-bit words.

A 2.4 kbps real-time data collection rate input into the Bubble Data Recorder will result in a 16.1 Mega-bit data storage requirement per orbit. Assuming that 7 minutes out of the 10 minute TDRSS contact time is available for the transmission of stored data, the playback rate will be 38 kbps over the I channel TDRSS link. The real-time data or dwell data is transmitted over the Q channel at 2.4 kbps. The sum of these two data channels is well within the 50 kbps capacity of the TDRSS Multiple Access service. The 5 W power amplifier option of the TDRSS User Transponder, and a 0.8 m diameter antenna were selected to achieve acceptable RF link margins, as shown in Table 7-7.

Table 7-4. TC&DH Subsystem Performance

COMMAND		TDRS LINK	STDN LINK
UPLINK FREQUENCY		2106.4 MHz	2026-2120 MHz
PCM FORMAT		NRZ - L	Bi ϕ - L
DATA RATE		1000 bps High 250 bps Low	2000 bps
COMMAND TYPES		Discrete Pulse Discrete Relay Proportional (Multiple-Bit) Block (1024 Bits)	
TELEMETRY			
DOWNLINK FREQUENCY		2287.5 MHz	2200 - 2300 MHz
PCM FORMAT		NRZ - L	Bi ϕ - L
DATA RATES		38 Kbps High 2.4 Kbps Low	280 bps
DOWNLINK RF POWER		5 W	5W
RANGING		PN Code Epoch Sync	None
TELEMETRY TYPES		Analog (A/D Converter Prior to Transmission) Discrete Digital Bus Serial Digital Bus	
TRANSMISSION MODES		Clear (No Encryption)	
DATA STORAGE		2 Bubble Data Recorders 40 MBits per unit	

Table 7-5. Forward Command Link Performance

LINK	ANT. SIZE	ANT. GAIN, dBi	FREQ. GHz	EIRP dBW	NET PATH LOSSES dB	COLDSAT SYSTEM NOISE TEMP. K	COLDSAT G/T dB/K	MODEM LOSSES dB	DATA RATE BPS	AVIL Eb/No dB	FOVD Eb/No DB	LINK MARGIN dB
TDRSS TO HIGH GAIN	0.8 m	22.5	2.1	34.0*	195.8	339	-5.7	2.0	250	37.1	9.9	25.2
TDRSS TO HIGH GAIN	0.8 m	22.5	2.1	34.0*	195.8	339	-5.7	2.0	1000	31.1	9.9	19.2
TDRSS TO OMNI	OMNI	0.0	2.1	34.0*	195.8	339	-27.5	2.0	250	15.3	9.9	3.4
GSTDN TO OMNI	OMNI	0.0	2.1	71.2**	156.3	339	-27.5	2.0	2000	72.4	9.9	60.5

* TDRS EIRP
** GSTDN EIRP

NOTE: THERE IS A 10.4 dB MODULATION LOSS FOR A MOD. INDEX OF 0.5 RAD. ON THE GSTDN COMMAND LINK

Table 7-6. Normal Mode Telemetry Format

	FRAME FORMAT	256	WORDS
	MINOR FRAME RATE	0.8532	SEC
	MAJOR FRAME	64	MINOR FRAMES
	REAL-TIME DATA COLLECTION RATE	2400	BPS
	WORD LENGTH	8	BITS
	DATA QUANTIZATION		
	EXPERIMENT DATA	10	BITS
	BUS DATA	8	BITS
MAJOR FRAME WORD ALLOCATION			
TELEMETRY DATA	MEASUREMENTS		8 BIT WORDS
OVERHEAD			
FRAME SYNC			3
ERROR CODE			2
SUBFRAME ID			2
CMD EXECUTE VERIF			4
EXPERIMENT			
SAMPLE RATE (SEC)		10 BIT WORDS	
0.125	3 ANALOG	21	
0.5	13 ANALOG	26	
0.5	6 SERIAL/DIGITAL	12	
1	92 ANALOG	92	
1	152 DIGITAL	16	
10	140 ANALOG 16 CHANNEL SUBMUX	18	
60	121 ANALOG 64 CHANNEL SUBMUX	2	
300	36 ANALOG 64 CHANNEL SUBMUX	1	
	EXPERIMENT WORD REQUIREMENT	188	235
SPACECRAFT BUS			
	11 SERIAL/DIGITAL 16 CHANNEL SUBMUX		1
	118 ANALOG 16 CHANNEL SUBMUX		7
	273 DIGITAL 16 CHANNEL SUBMUX		2
TOTAL FRAME WORDS			256

Table 7-7. Return Telemetry Link Performance

ANTENNA SIZE	ANTENNA GAIN dBi	FREQ. GHz	DATA RATE	RF POWER WATT	COLDSAT EIRP dBW	NET PATH LOSSES dB	MOD. LOSS dB	MARGIN dB
0.8 m	23.3	2.3	2.4 Kbps	1.0	21.3	194.3	7 *	3.0
0.8 m	23.3	2.3	38 Kbps	4.0	27.3	194.3	1 *	3.0
OMNI	0	2.3	280 Bps	5.0	5.0	194.3	DNA	3.0

DNA - Does not apply

Note: Line loss between COLD-SAT transmitter and antenna is assumed to be 2 dB.

* Due to 4:1 power imbalance.

7.3 ATTITUDE DETERMINATION AND CONTROL

7.3.1 Requirements

The Attitude Determination and Control System (ADCS) is the collection of sensors, actuators, and on-board electronics that provides an attitude reference during all phases of the mission, and provides control of pointing and articulation of all components of the spacecraft.

The ADCS for COLD-SAT has to provide two dynamic environments for the experiment: A very low acceleration field ($<5 \times 10^{-7}g$) meaning that both angular rate accelerations and linear accelerations must be kept small; and thruster-controlled acceleration levels along the +X and -X axes (along the velocity vector) for periods of up to several hours. The high spacecraft reliability required (probability of success > 0.92) dictates a dual-redundant design for critical components, and multiple backup and recovery modes.

Many requirements are imposed by the other subsystems. Thermal control prefers pointing of various surfaces (radiators) toward deep space. The solar arrays require pointing toward the Sun, and periodically, large angle maneuvers (180 deg. roll maneuvers) are required to improve solar array cosine-loss efficiency. The narrow beam antenna must be pointed toward a TDRSS Satellite. All of these requirements are met with a relatively large ± 3 deg. pointing deadband, which allows lower position-loop feedback gains and thus lowers acceleration disturbances to the experiment to within acceptable levels.

7.3.2 Description

Figure 7-7 shows the ADCS design configuration. There are four types of actuators included in the ACS design: Primary attitude control is provided by a set of four reaction wheels arranged in a four-for-three redundant configuration; orbit corrections and low-acceleration longitudinal thrusting for experiments is provided by a dual-redundant monopropellant hydrazine reaction control system; two solar array drive assemblies (SADAs) are needed to slew the solar arrays to track the Sun; and magnetic torquers are used for momentum dumping. Limited backup attitude control is possible using the RCS and the magnetic torquers. There are four types of attitude sensors included in the ADCS design: conical Earth sensors provide roll and pitch attitude data; digital sun sensors mounted on the solar array yokes provide information to an estimator for yaw determination during quiescent on-orbit operations and SADA sun tracking; Dual-redundant three-axis digital integrating rate assemblies (DIRAs or gyros) propagate complete attitude information between attitude sensor updates, and they are especially useful during orbit correction maneuvers, long duration low-acceleration experiment thrusting, and for tumbling spacecraft recovery; and coarse analog sun sensors are used for initial attitude acquisition and during tumbling spacecraft recovery.

The solar arrays have been canted off the SADA drive axis by 26 deg. so that the arrays can track the sun without the need for continuous spacecraft roll maneuvers. However, the spacecraft must be rolled 180 degs. eleven times per year to keep the correct side of the arrays pointed toward the sun. Consequently the Earth-face (+Z) and the anti-Earth face (-Z) switch positions.

7.3.2.1 Subsystem Schematic. A detailed ADCS schematic showing the redundant hardware and data paths is shown in Figure 7-8.

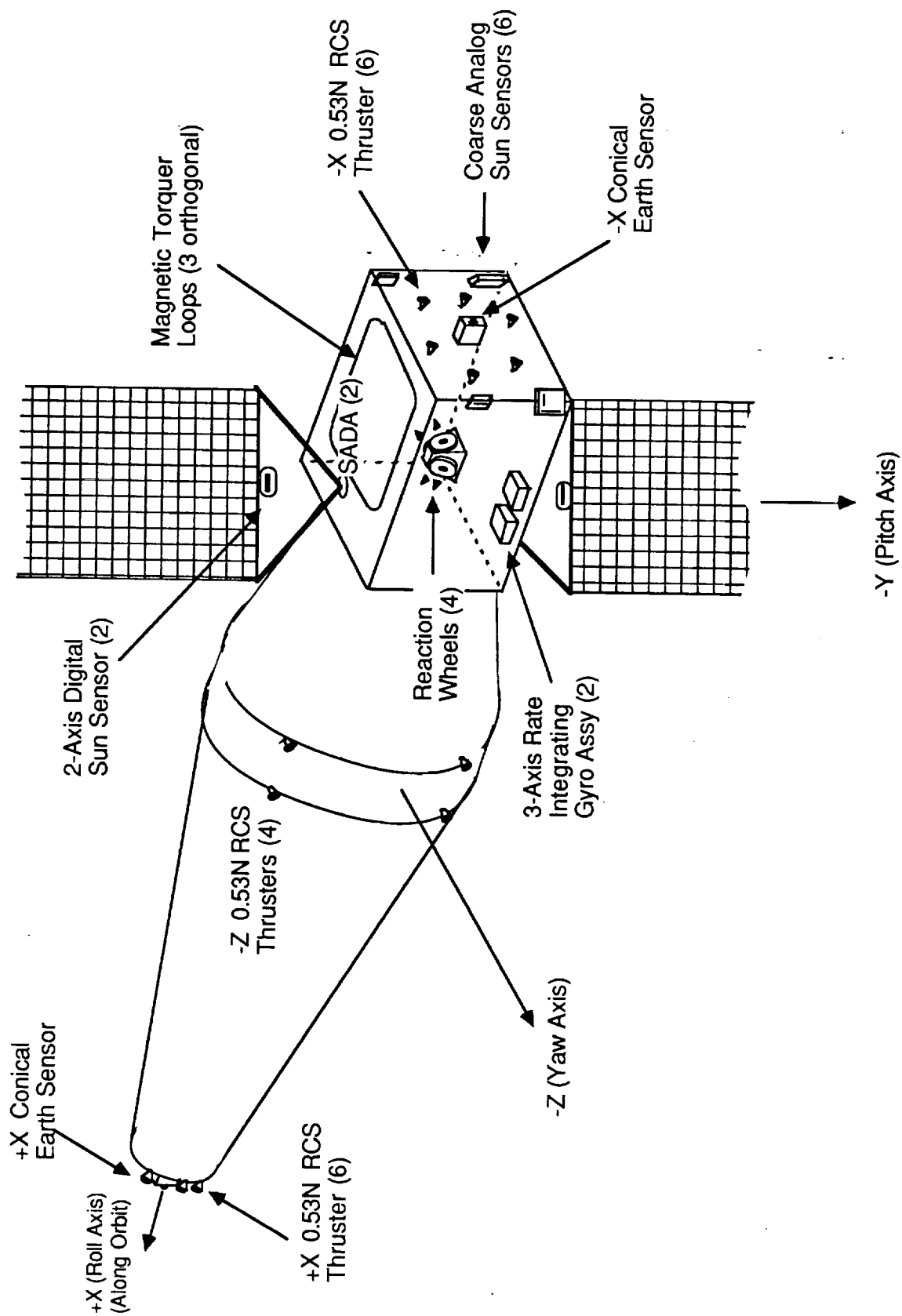


Figure 7-7. Attitude Determination and Control System Equipment Layout

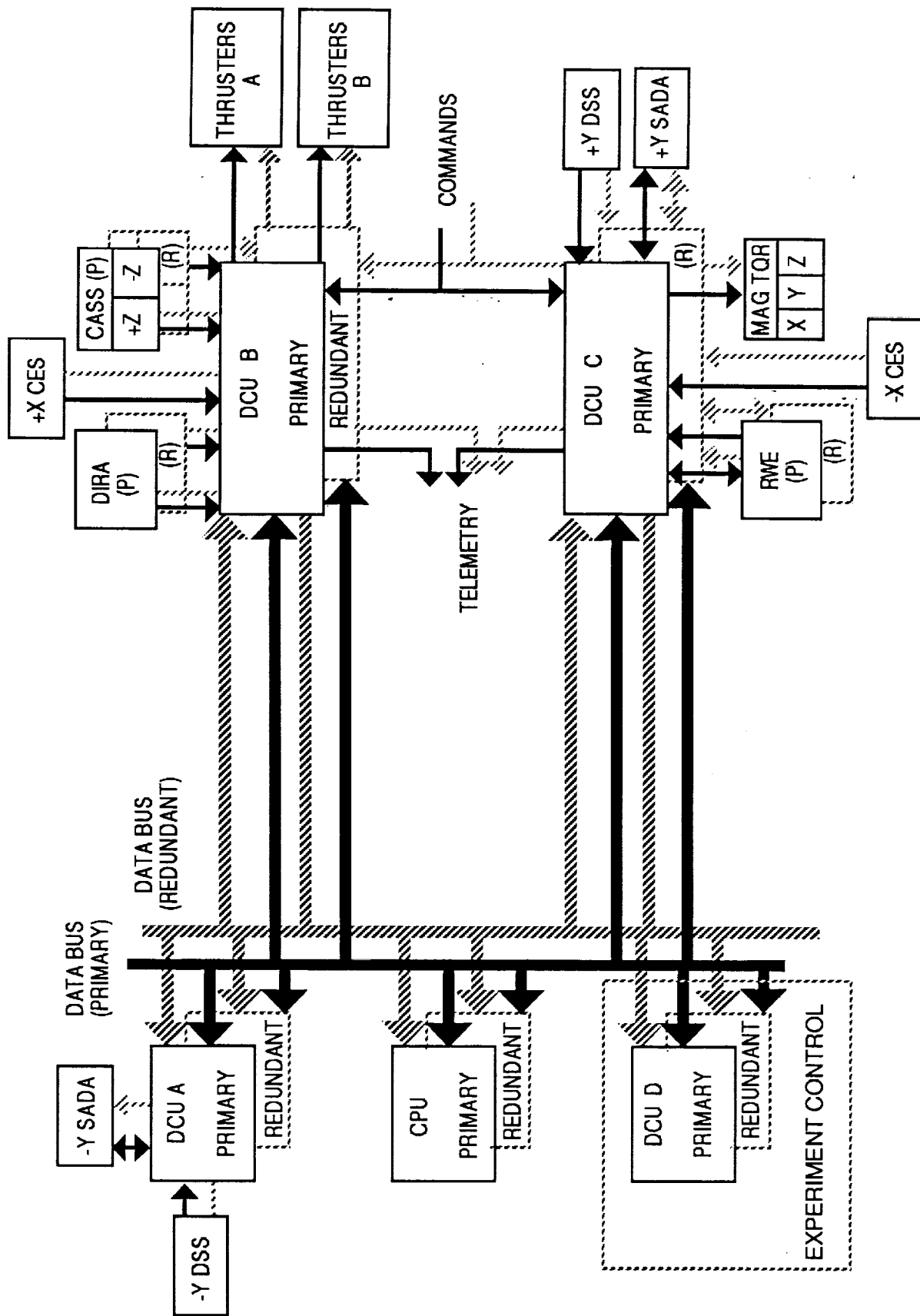


Figure 7-8. Attitude Determination and Control System Schematic

7.3.2.2 Control Concepts. Four operational modes were considered in this design:

(1) The initial attitude acquisition and tumbling spacecraft recovery mode are started by nulling the rates in all three axes of the DIRA using the reaction wheels (and RCS if momentum dumping is necessary). Then search slews are commanded until the sun sensors and then the Earth sensors have acquired their targets.

(2) The quiescent on-orbit storage mode consists of keeping the +X axis aligned with the orbit velocity vector, and tracking the Sun in one axis using the solar array drive assemblies. The primary attitude sensors are the Earth sensors for pitch and roll, digital sun sensors for yaw, and the DIRAs to provide attitude data between sensor updates. The reaction wheels are used to counter cyclic disturbance torques and the magnetic torquers are used to dump secular momentum buildup.

(3) In any situation requiring thrusting (experiments, stationkeeping, etc.), the DIRAs provide complete attitude reference during the burns (calibrated gyro drift 3 degrees in 30 hours). The wide range of desired acceleration levels for the long-duration thrusting maneuvers requires a cluster of multiple small thrusters mounted on the -X and +X faces of the spacecraft bus. The thrusters fire in a round-robin fashion to minimize off-axis disturbance torques such that reaction wheels never saturate. Figure 7-9 demonstrates this methodology using four thrusters for controlling pitch and yaw momentum while maintaining a constant acceleration. Note that no direct feedback from accelerometers is currently planned. However, accelerometer data from the experiments could be used, thus closing the acceleration feedback loop.

(4) The fourth mode is a simple attitude hold using the DIRAs and the reaction wheels during deployment of solar arrays and antennas.

In addition to the dual-redundancy on the critical attitude control system components, many backup control modes are possible using other combinations of sensors and actuators. For example, a complete reaction wheel assembly failure could be replaced by appropriate usage of the magnetic torquers and RCS system. Detailed consideration of backup modes was not pursued during the study.

7.3.3 Performance Analysis

7.3.3.1 Tradeoffs Against Alternate Concepts. The use of thrusters for attitude control was considered briefly but would degrade the experimental results by adding impulsive disturbance torques to the system. For experiments performed in the micro-g range, each thruster pulse will provide an impulse 22 to 110 times the desired background acceleration level (for a short 8 msec time period). (Angular accel = Torque / Inertia = $0.45 \text{ N} * 3 \text{ m} / 12,000 \text{ kg-m}^2 = 0.00011 \text{ rad/s}^2$. Linear accel = ang. accel x moment arm = $0.00011 \times (1 - 5 \text{ m}) = 110 \text{ to } 550 \times 10^{-6} \text{ m/s}^2 = 11 \text{ to } 55 \text{ micro-g}$).

Spinning the spacecraft about the pitch or yaw axis to provide a long-duration acceleration field was briefly considered but was eliminated primarily because of the non-uniform acceleration field produced, and the difficulties in designing a spacecraft that easily handled the nonspinning and spinning experiments. Once it became clear that adequate fuel was available for all the experiments requiring thrusting, the spin option was dropped. Bias-momentum designs are the standard for Ford Aerospace geosynchronous satellites and generate acceleration fields from the nutational dynamics of the rapidly-spinning momentum wheel. Thus this scheme was dropped in favor of the zero-bias momentum design.

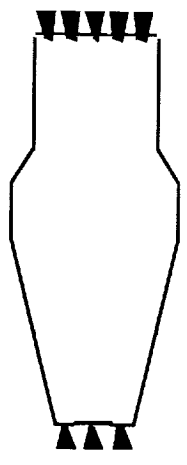
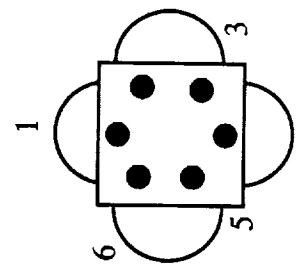
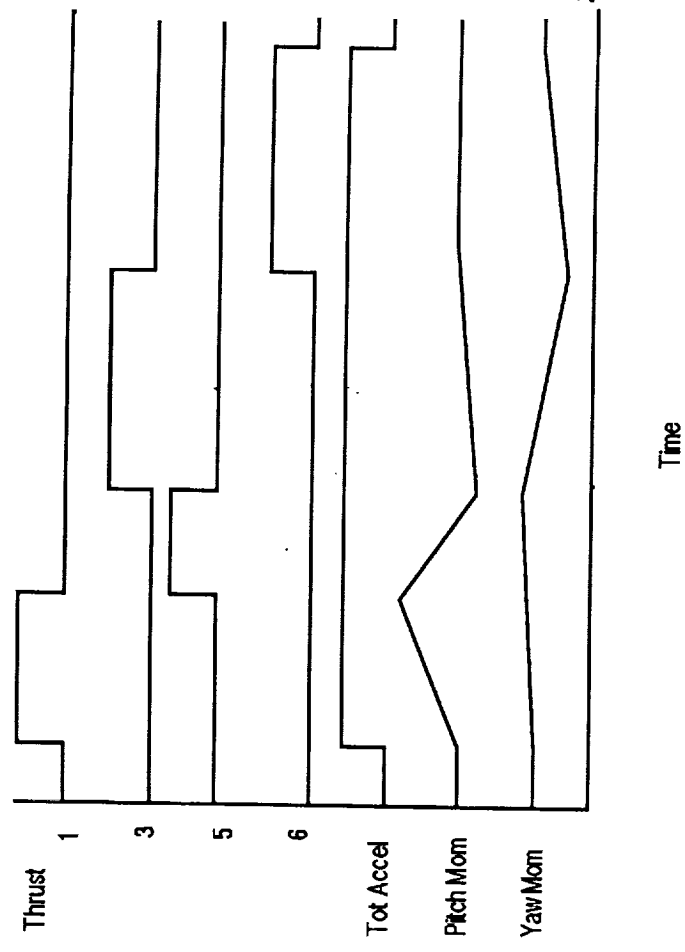


Figure 7-9. Round Robin Thrust Scheme

7.3.3.2 Benefits of Current Concept. The zero-bias momentum reaction wheel design provides the lowest background acceleration disturbances of any design considered. It also uses standard Ford Aerospace ADCS designs and equipment with long heritages. The dual-redundant designs provide for a high probability of success. The round-robin use of the thrusters provides a wide variety of background accelerations for the experiment.

7.3.3.3 Performance Analysis Results. Representative background accelerations have been computed for the 1300 km orbit and are shown in Table 7-8. Accelerations vary around the spacecraft, and detailed development of experiment accelerations is given in the appendix. The accelerations due to aerodynamic forces are negligible compared to the dominant accelerations due to orbit pitch rate and gravity gradient. Note that drag and orbit pitch rate generate accelerations along the $\pm X$ axis and thus are additive in worst case; and gravity gradient and attitude and orbit control activity generate accelerations along the $\pm Z$ axis and thus are additive in the worst case. These two added values are root-summed-squared to give the worst case vector magnitude for each experiment tank. The results are comfortably below the 5×10^{-7} g requirement. The analysis for the disturbance torques on the spacecraft and the resultant reaction wheel sizing is summarized in Table 7-9. The solar torque disturbance was increased 30 percent over sun-alone analyses to cover worst case Earth albedo effects. The aerodynamic torques are negligible at 1300 km. The gravity gradient torque and magnetic dipole torques are the dominant environmentally-caused disturbance. Secular build-up of angular momentum due to gravity gradient was added to account for a possible 6 deg. maximum offset of a principal axes from the local-vertical/local-horizontal reference frame. Off-axis thrusting and internal disturbance torques due to swirling liquid hydrogen during the no-vent fill experiment dominates all disturbance torque sources.

The largest change in angular momentum is in roll, and is due to an internal disturbance from the no-vent fill experiment which sprays two tangential jets of liquid hydrogen on the sides of the receiver tank to pre-cool it. A long experiment can generate an angular momentum disturbance of up to 130 N-m-s, assuming no friction loss during initial fill. Further analysis may allow a 25 percent reduction in the angular momentum, but the full amount is compensated in the current design. The large angular momentum buildup in roll can be absorbed by selecting the size of each of the four reaction wheels to be 50 N-m-s, and choosing cant angles so that most of the momentum capacity is along roll. Note, that internal dissipative forces will eventually reduce the reaction wheel angular momentum buildup back to zero, i.e., no secular angular momentum is imparted (no external forces).

A residual magnetic moment of 30 A-m² (typical value for Superbird-class spacecraft which includes current loops and ferrous materials) causes the torque, angular momentum peaks and angular momentum buildup shown in Table 7-9. Note that it is roughly 4 times larger than solar torque and is the dominant external disturbance torque. The 400 A-m² magnetic coils chosen can easily handle these torques as well as dump secular momentum buildup from other external sources.

7.4 PROPULSION

7.4.1 Requirements

The propulsion system is required to perform two main functions, experiment acceleration and attitude control. Thrusting in support of experiments requires acceleration levels of 20, 50, and 100 micro-g's assuming a nominal BOL on-orbit vehicle mass of 2878.8 kg with a potential maximum of 3454.6 kg. The projected thrust duration at each of the acceleration levels is 67.6, 9.4, and 63.5 hours, respectively, with individual thrusters firing continuously for as long as 46.5 hours. Thruster operation is required for both the steady state and on/off modes. In addition, redundancy is necessary to assure that all thrust levels can be achieved in the event of an individual thruster failure.

Table 7-8. Representative Background Accelerations

<u>LOCATION</u> <u>SOURCE</u>	<u>TANK #1</u> <u>SUPPLY</u> Micro Gs	<u>TANK #2</u> <u>RECEIVER</u> Micro Gs	<u>TANK #3</u> <u>RECEIVER</u> Micro Gs
(1) DRAG (BC=50, 1300 km)	0.002	0.002	0.002
(2) ORBIT PITCH RATE (111.5 MIN ORBIT)	0.13	0.07	0.32
(3) ACS ACTIVITY (EST.) (1.0 DEG DB, MAX DIST.)	0.06	0.03	0.14
(4) GRAVITY GRADIENT	0.22	0.09	0.10
TOTAL (RSS(1+2; 3+4))	0.31	0.14	0.40

Table 7-9. COLD-SAT Environmental Disturbance Torques

	Pitch (Y-Axis)			Roll (X-Axis)			Yaw (Z-Axis)		
	T _{max}	H _{max}	H _{sec}	T _{max}	H _{max}	H _{sec}	T _{max}	H _{max}	H _{sec}
	(N-m)	(N-m-s)	(N-m-s)	(N-m)	(N-m-s)	(N-m-s)	(N-m)	(N-m-s)	(N-m-s)
Solar Torque	1.33x10 ⁻³	2.0	2.0	0	0	0	1.9x10 ⁻³	3.3	3.3
Aerodynamic	6.6x10 ⁻⁶	1.1	1.1	0	0	0	6.6x10 ⁻⁶	1.1	1.1
Grav. Grad.	6.8x10 ⁻⁴	1.17	0.08	5.48x10 ⁻⁵	0.095	0.006	4.43x10 ⁻⁵	0.075	0.005
Off-Axis Thrust	0.41	2.0	0	0.24	1.2	0	0.41	2.0	0
Internal Torq.	3.6x10 ⁻³	13	0	0.036	130	0	3.6x10 ⁻³	13	0
Mag. Dipole	6.4x10 ⁻³	4.3	4.3	6.4x10 ⁻³	4.3	4.3	6.4x10 ⁻³	4.3	4.3
TOTAL	0.422	23.6	7.48	0.283	135.6	4.3	0.422	23.8	8.71

The thrusters can also be used in support of the attitude control system, primarily as a backup for reaction wheel momentum dumping when the magnetic torquers are insufficient.

Another function of the propulsion system is to help maintain a stable spacecraft center of gravity location. Since the hydrazine tanks represent a significant portion of the vehicle's mass, their number, operation, and location affect C.G. perturbations and offsets significantly. This requires that the valve arrangement allow for propellant to be drawn from any tank as necessary to maintain C.G. location.

Other features of the propulsion system required for a successful integration to the spacecraft are shielding of the thrusters to prevent plume interference with the spacecraft's sensitive surfaces (such as the Earth sensors) and proper interfacing with the SCE for control of the pressurization system, propulsion system heaters, thrust level, and firing coordination during attitude control.

7.4.2 Description

The propulsion system is a monopropellant hydrazine system composed of sixteen 0.534 N catalytic thrusters, located on COLD-SAT as shown in Figure 7-7. Twelve of the thrusters are oriented parallel to the X-axis and are located in two thruster groups, one at each end (forward and aft ends) of the spacecraft. Each group is comprised of six equally spaced thrusters configured in a circular pattern to support experiment acceleration requirements.

Roll control of the spacecraft is satisfied by four roll thrusters; two thruster pairs located 180 deg. apart and positioned on the cylindrical section of the spacecraft's experiment module. The thrusters in each pair have an identical orientation with respect to the spacecraft to ensure thruster redundancy in the event of a malfunction. The roll thrusters in each pair are separated from each other by about one meter so that the spacecraft center of mass will always fall between them throughout the mission.

Other propulsion system hardware, shown in the propulsion system schematic (Figure 7-10), include a helium pressurant tank pressurized to 25.511 MPa and four identical hydrazine propellant tanks, each containing a surface tension-type propellant management device. The hydrazine tanks have an operating pressure of 1.378 MPa which gives a nominal thrust value of 0.534 N for each of the catalytic thrusters. Isolation of the propellant tanks is provided by dual coil latching valves at both the pressure inlet and propellant outlet. The latch valves prevent direct propellant migration among the four tanks during launch and zero-g. In addition, the transfer of propellant through cryopumping is prevented by the latching valves at the pressure inlet. Cryopumping results from a temperature difference among the tanks. Propellant vapor generated in warm tanks will migrate and condense in the coldest tank.

The latch valves allow the adjustment of any pressure differentials between tanks due to diurnal temperature excursions. Additionally, the ability to isolate the propellant tanks allow each thruster on the spacecraft to feed from any of the four hydrazine tanks through proper manipulation of the latch valves. Thus propellant usage is optimized and C.G. shift can be controlled.

Helium is metered to the hydrazine tanks via a pressure regulator. As a backup in the event of a regulator failure, a high pressure solenoid valve is routed in parallel to the regulator and is actuated by the Spacecraft Control Electronics (SCE). The bang-bang repressurization features of the solenoid valve combines reliability, simplicity, and cost advantages as opposed to using a second pressure regulator in the system. It also allows thrust tailoring by adjusting the pressure of individual tanks beyond the range made possible by the regulator. The concept was originally incorporated into Ford Aerospace's Intelsat VII program. Analyses conducted so far indicate that pressure regulation to within 1 percent is possible using the solenoid valve, with accuracy increasing as the propellant empties. The solenoid valve is commanded open or closed depending on feedback transmitted to the SCE from the low pressure transducers located just upstream of the hydrazine

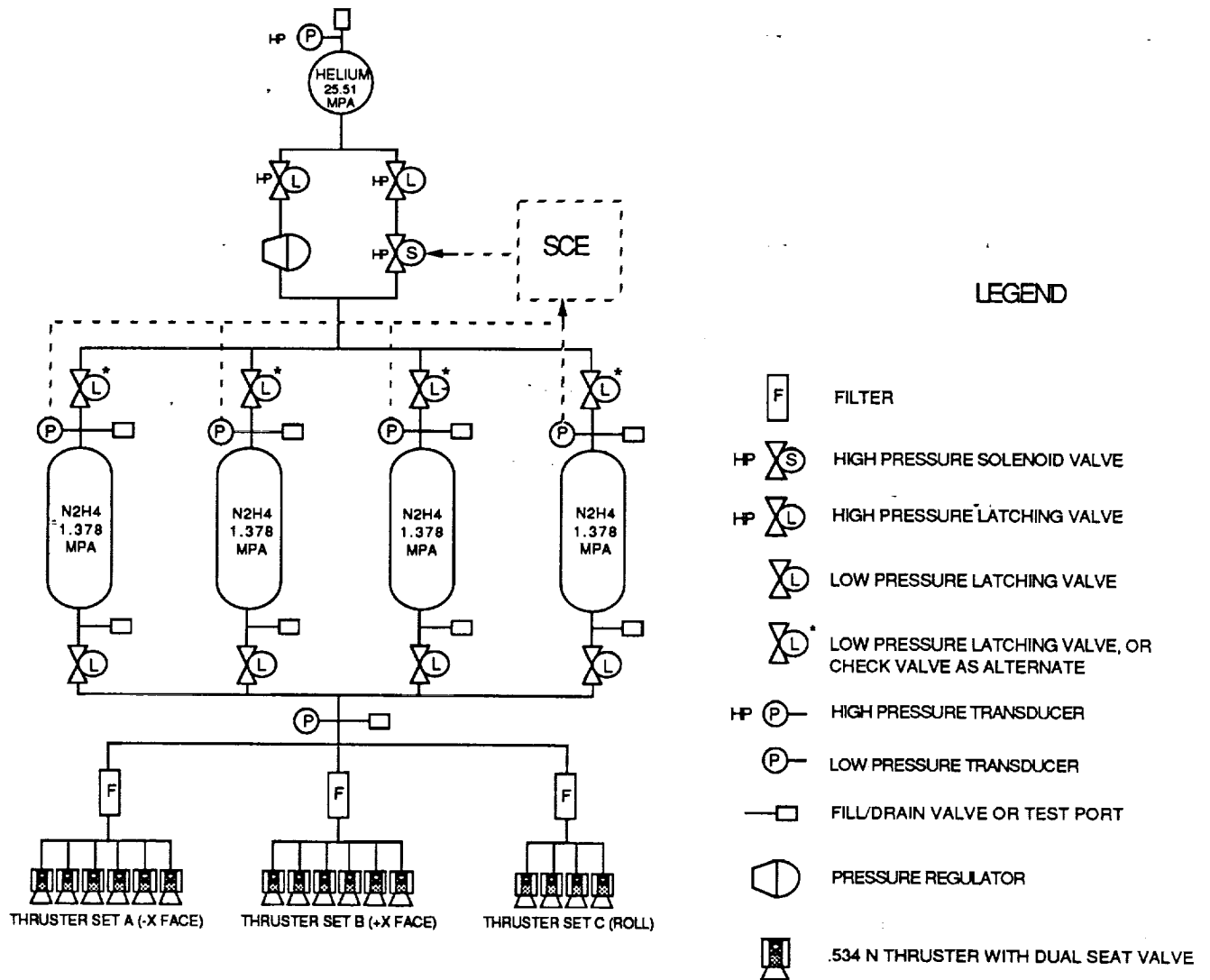


Figure 7-10. Propulsion System Schematic

tanks. For increased reliability, the pressure regulator and the high pressure solenoid valve are isolated from the helium storage tank with high pressure latching valves.

The hydrazine thrusters are of a catalytic variety using dual seat valves for greater reliability and redundancy. Steady state and pulse mode operation is feasible although steady state is preferred due to the greater severity of the thermal and cycling environment of pulsing operation. As mentioned in the previous section, the nominal thrust value of the thrusters is 0.534 N, but the precise thrust level can be varied from about 0.178 N to 0.889 N by adjustments in tank pressure. The tank pressures corresponding to these two thrust levels are 0.4137 and 2.309 MPa, respectively. Thrust level tolerances of ± 5 percent from unit-to-unit are typical.

The maximum anticipated firing duration, being 46.5 hours, is not expected to be a problem. Previous history indicates that a 0.445 N thruster has been fired continuously for 20 hours by Rocket Research, and a 2.224 N thruster of this type was fired in space for 16 hours without incident on the Earth Radiation Budget satellite.

Alternative hardware schemes worthy of further investigation include replacing the propellant tank pressure inlet latch valves with check valves, and using mechanically linked bipropellant valves instead of monopropellant valves. This would reduce the number of valve drivers from 8 to 4.

7.4.3 Performance Analysis

7.4.3.1 System Trades. Four concepts were reviewed for the COLD-SAT propulsion system. The candidate systems were the cold gas, heated gas, bipropellant, and monopropellant systems. With sustained low thrust as the primary requirement, cold gas systems were eliminated because they are excessively heavy and have low performance levels. Some improvement is realized by using electric power to heat the gas, thereby improving specific impulse. However, this requires electric power for extended periods and cannot be accommodated within the COLD-SAT power subsystem design and mission profiles.

A bipropellant system introduces added complexity to the propulsion system, and there are no presently available, space qualified, low level (approx. 0.445 N) thrusters on the market. They also exhibit limited flexibility for maintaining a steady spacecraft center of mass through creative propellant usage among the four tanks.

A catalytic hydrazine thruster system was found to meet all experiment and attitude control requirements. The hydrazine monopropellant system was selected for COLD-SAT because it results in maximum reliability when compared to bipropellants or electrically ignited monopropellants, and much better performance when compared to cold-gas systems.

To meet the steady-state acceleration requirements discussed in Section 7.4.1, a study was undertaken to determine what thruster configuration could meet the requirements for a nominal spacecraft mass of 2878.8 kg, with future growth to a possible 3454.6 kg. A quick survey indicated that the thrust level needed of each individual thruster would be between 0.445 N and 0.578 N with 0.534 N being selected for this study. As can be seen in Figure 7-11, the acceleration requirements of 20, 50, and 100 micro-g's can be met by a cluster of 4, 5, or 6 thrusters. The total thrust values required to meet the three accelerations for an 3454.6 kg spacecraft are 0.678, 1.694, and 3.389 N.

The four-thruster group was dropped because it allows for no redundancy in the event of an individual thruster failure. A comparison between the five and six-thruster configurations shows that the symmetry of the six-thruster configuration about the C.G. appears to provide a more stable acceleration to the spacecraft. Both combinations will require a round-robin operation of the thrusters to prevent momentum wheel saturation, however, the six-thruster configuration will require less switching between thrusters. Therefore, due to its advantages in symmetry and redundancy the six-thruster configuration has been selected. Figure 7-12 shows the firing sequence necessary to achieve the various thrust levels for the six-thruster layout. The thrust levels of 0.534 and 2.669 N require round-robin operation (thrusters denoted by a bar denote round robin operation while the completely darkened thrusters will operate continuously or nearly continuously).

7.4.3.2 Benefits of the Current System. The propulsion system's ability to be flexible in the event of a change in the experiments or a hardware malfunction is an important part of the system design. For instance, the ability to achieve higher or lower thrust levels is provided by adjustments in tank pressure or by pulsing, or round-robin thruster operation.

In the event of a hardware malfunction, redundancy is provided by: a redundant digitally controlled pressurization system provided by the high pressure solenoid valve circuit; a six-thruster group at each end of the spacecraft which provides "engine-out" capability; the thruster valve design incorporates dual series seats to provide a positive seal against leakage; torque-motor latch valve design with two coils, one for opening and one for closing, act as redundant coils when commanded

0.534 N Thruster Acceleration Data

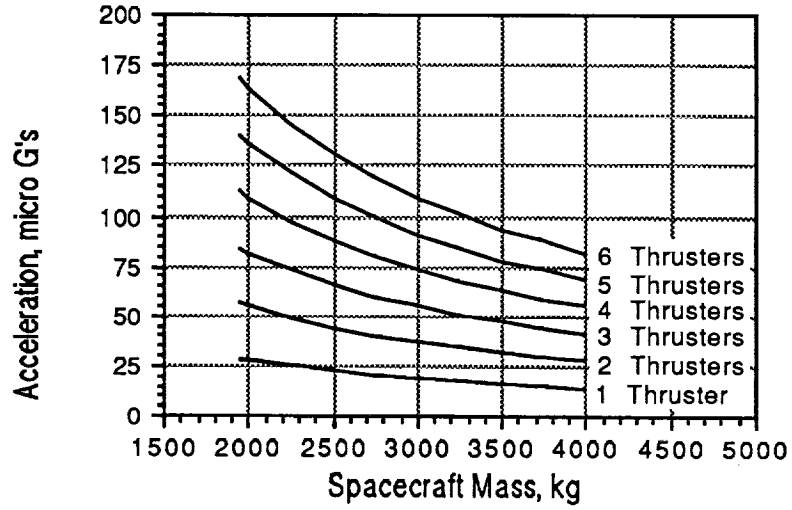


Figure 7-11. Thruster Study to Produce the Required Experiment Accelerations

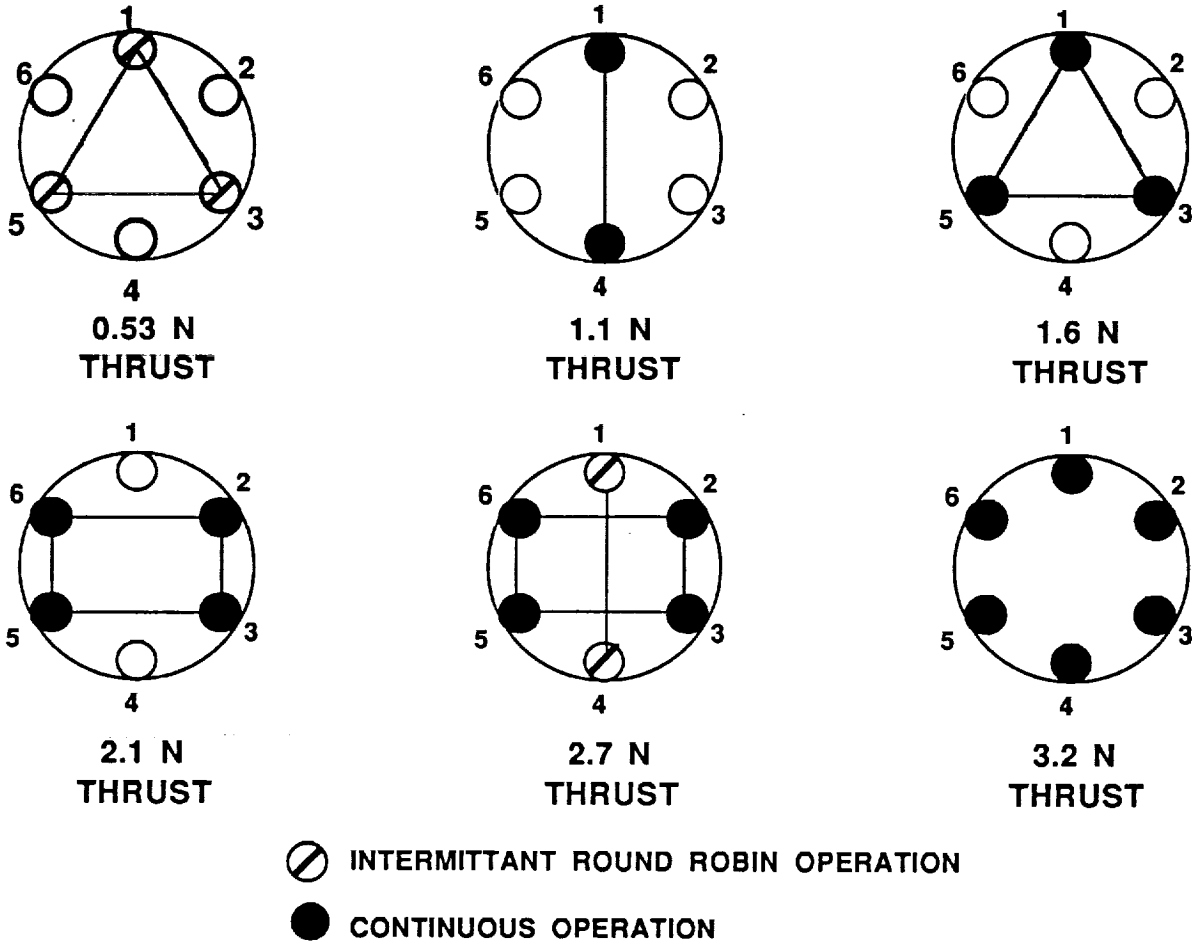


Figure 7-12. Six Thruster Configuration Firing Sequences

with reverse polarity; and a redundant pressure transducer centrally placed at the outlet of the four hydrazine tanks.

Another potential failure which must be accounted for is if the latching isolation valves on both or either end of one of the propellant tanks fails to open. In such an occurrence most, if not all, of the mission requirements can be accomplished by the fact that a monopropellant system is being used with four propellant tanks. If one tank is not operational the tanks immediately adjacent to it are used for thruster operation until depleted. The tank opposite to the crippled tank is then used. Previous calculations show that a maximum vehicle C.G. offset of 80 mm is expected when one hydrazine tank remains full of propellant while the other three are empty. This is well within the design capability of the attitude control system.

7.4.3.3 Propellant Budget. The propellant budget is shown in Table 7-10. The total launch capacity of all four propellant tanks when 90 percent full is 530.5 kg of hydrazine. No additional propellant is necessary for drag makeup. The Class I and Class II experiments require 292 and 67 kg of propellant respectively (Tables 7-11 and 7-12) assuming a specific impulse of 2157.7 N-s/kg. The total amount of propellant required for bus and experiment operations is 416 kg. The initial four tank design has 106 kg excess propellant capacity which may be used to repeat or-add additional experiments. Approximately 1.81 kg of helium gas is required as pressurant.

Table 7-10. Propellant Budget

EVENT	PROPELLANT (kg) ISP = 2157.7 $\frac{\text{N-sec}}{\text{Kg}}$
Initial Attitude Acquisition	6.80
Drag Makeup	NONE*
Reaction-Wheel Unloading	27.22
Experimental Maneuvers	
- Class I	292.35
- Class II	66.89
Unallocated Contingency	22.68
Subtotal	415.94
Residual/Holdup	6.80
Total Propellant (Hydrazine)	422.74
Pressurant (Helium)	1.81
Launch Tankage Capacity (90%) (4 hydrazine propellant tanks)	530.5
Excess Capacity Available	105.95

* Thrusting for experiments totally negates need for drag makeup

Table 7-11. Class I Experiment Propulsive Requirements

EXP. NO	EXPERIMENT TITLE	G-LEVEL (x 10E-6)	TIME @ G-LEVEL HRS	THRUST NEWTONS	IMPULSE NEWTON-SEC	PROPELLANT WT. KG, ISP=2157.7
1-1/1-2	PRESS CONTROL	100	39.8	2.67	382557.60	177.30
		20	46.5	0.53	88722.00	41.12
I-3	CHILLDOWN	100	2	2.67	19224.00	8.91
		50	2.3	1.06	8776.80	4.07
I-4	NO-VENT FILL	100	11.3	2.67	108615.60	50.34
I-5	LAD FILL	NO PROPULSIVE REQUIREMENTS				
I-6	MASS GAGING	DELETED EXPERIMENT				
I-7	SLOSH DYN/CNTL	DELETED EXPERIMENT				
	FLUID RETURN	20	12	0.53	22896.00	10.61
Class I Total					630792.00	292.35

Table 7-12. Class II Experiment Propulsive Requirements

EXP. NO	EXPERIMENT TITLE	G-LEVEL (x 10E-6)	TIME @ G-LEVEL HRS	THRUST NEWTONS	IMPULSE NEWTON-SEC	PROPELLANT WT. KG, ISP=2157.7
II-1	"TANKER" T. P.	No Propulsive Requirements				
II-4	PRESSURIZATION	50	1.4	1.06	5342.40	2.48
II-5	SETTLE/OUTFLO	100	2.2	2.67	21146.40	9.80
		20	4	0.53	7675.20	3.56
II-6	LAD PERFORM	100	1	2.67	9612.00	4.45
		20	1	0.53	1908.00	0.88
II-7	LINE CHILLDOWN	No Propulsive Requirements				
II-8	OUTFLW THERM COND	No Propulsive Requirements				
II-9	VENTED FILL	100	7.2	2.67	69206.40	32.07
		50	5.7	1.06	21751.20	10.08
II-10	FLUID DUMP	No Propulsive Requirements				
II-11	ADV INSTRUMENT	20	2	0.53	3844.80	1.78
	FLUID RETURN	20	2.1	0.53	4037.04	1.87
Class II Total					144523.04	66.89

7.5 THERMAL CONTROL

7.5.1 Thermal Control Requirements

The thermal control system is required to efficiently maintain all of the spacecraft bus components within their design temperature limits during prelaunch, launch, initial attitude acquisition and checkout, and throughout the orbital mission. The thermal design requirements depend on: the planned mission phases, component qualification temperature limits, required thermal design margins, component and subsystem heat loads and duty cycles, reliability considerations, and the integration of the spacecraft. For COLD-SAT the temperature limit margins shown in Figure 7-13 have been adopted. Components with special requirements such as batteries may have modified margins.

7.5.2 Thermal Control System Description

A passive thermal control system will satisfy the COLD-SAT thermal requirements using insulation, surface coatings, and electrical heaters. No louvers, heat pipes, or other active elements will be used. The +Z and -Z panels are the primary radiator elements of the bus because they have the most stable external flux environment throughout the mission. These panels will be covered with a combination of optical solar reflectors (OSRs) and multi-layer insulation (MLI). The +X and -X panels will be covered with MLI and not be used as radiators. The +Y and -Y panels will have some low power equipment mounted on them but will be covered with MLI. The Y panels can not readily be used as radiators because they have long periods where either they will have incident solar flux or where they are completely shadowed. This would require an excessive amount of heater power if they were used as radiators. The backs of the solar array panels have high emittance to limit solar cell temperatures.

The equipment layout within the bus module is strongly influenced by thermal design requirements. The interior of the bus will be painted black to maximize the heat distribution within the bus. The central cylinder will be covered with MLI since it is conductively coupled to the experiment module. The forward portion of the experiment module, containing Tanks 1 and 3, is kept colder than the bus to minimize environmental heat leaks into the hydrogen tanks. Therefore, a significant heat leak from the bus results at the bolted interface between the two modules. The current design to moderate this heat leak uses titanium washers as separators in the interface and MLI on the exterior of the aft portion of the experiment module. Other possibilities for reducing the heat leak were investigated but were considered more costly to implement.

Heaters will be used within the bus to balance out the effects of periodic variations in the external heat fluxes and equipment usage to maintain the components within their operating temperature limits. The hydrazine system must be kept above the freezing point of hydrazine, so propellant tank, propellant line, and thruster valve heaters are used. In addition, the thrusters and propellant lines will be insulated radiatively and conductively from the environment.

7.5.3 Thermal Analysis Results

The technical effort on the COLD-SAT study was halted before a thermal analysis of the present design could be done. However, a thermal analysis was made of the Task III design which is very similar to the present design, so the results of that analysis will be presented here. The main thermal differences in the Task IV design include: the hydrogen pressurant tanks eliminate some potential radiator area on the +Z and -Z panels and significantly reduce the internal radiation within the bus module; the power dissipation within the bus has risen by about 120 watts; and the orbital altitude has been raised to 1300 km from 463 km.

FOR COLD-SAT THE FOLLOWING MARGINS ON TEMPERATURE LIMITS ARE ADOPTED

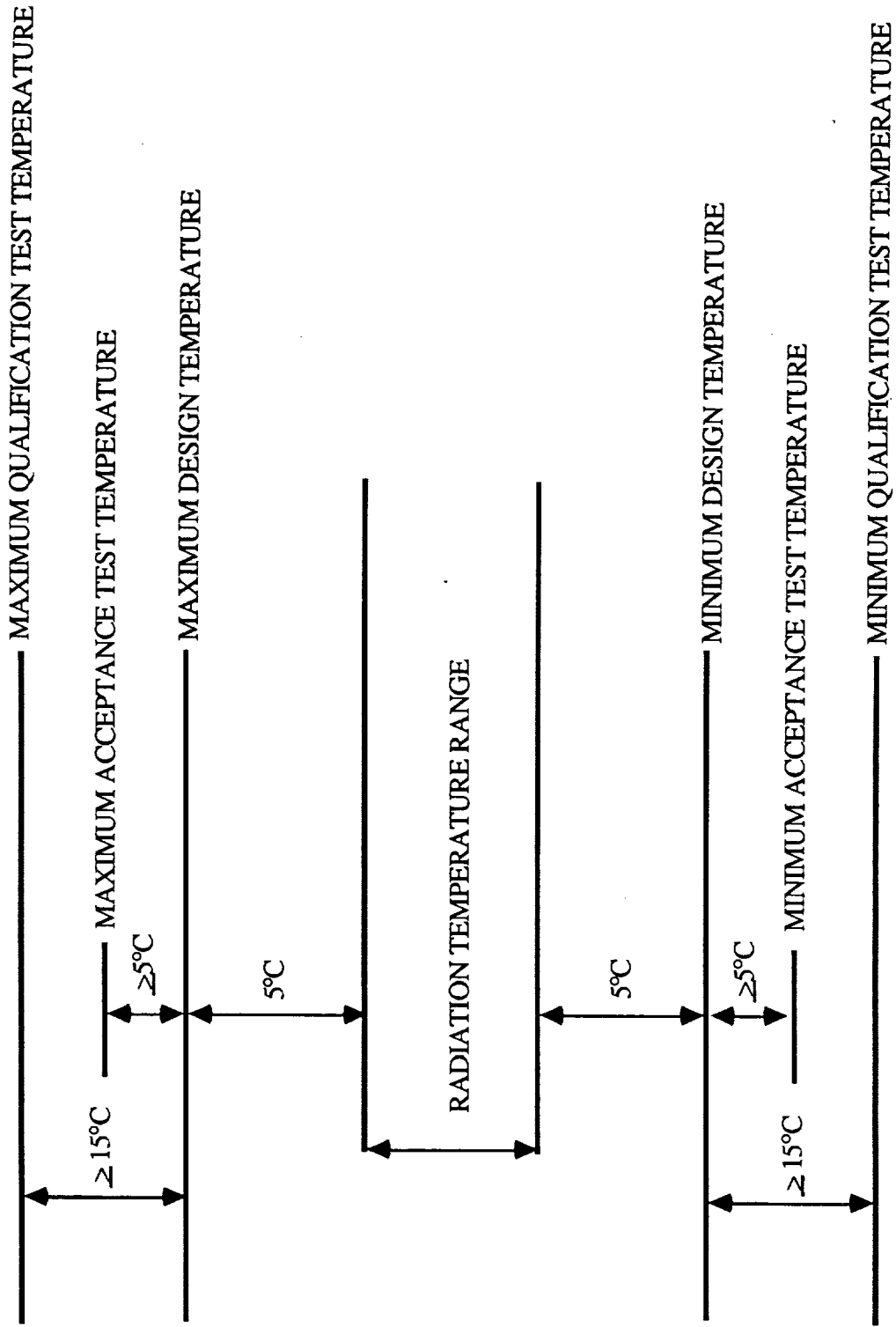


Figure 7-13. Thermal Control Requirements

A 60 node transient thermal model of the bus was constructed. The analysis includes: solar, Earth albedo and Earth infrared external heat rates, and the heat leak between the experiment module and the bus. The Task III bus configuration is similar to the present design except that there were no hydrogen pressurant tanks within the bus. The panel power dissipations are given in Table 7-13. The spacecraft worse hot case occurs while the experiment is being run with thrusters on, and at a 0 deg. Beta angle (angle between the solar vector and the normal to the orbital plane). The worst cold case occurs at a Beta angle of 52 deg. while the experiment is inactive. Twenty-five watts of power from the experiment DC-DC converter was assumed to be the only experiment power dissipated within the bus. Only 42 percent of the available radiator area was required, the remainder was covered with MLI. In the cold case, 50 watts of heater power was required to maintain the panel temperatures within acceptable limits. The results of the analysis are presented in Table 7-14. The orbital temperature variation was small, and the equipment temperatures remained within acceptable limits for both the hot and cold cases.

Table 7-13. Bus Subsystem/Element Heat Loads for the Task III Design

SUBSYSTEM	HOT CASE	COLD CASE
	MAX. HEAT LOAD (EXPERIMENT ON)	MIN. HEAT LOAD (EXPERIMENT OFF)
	W	W
TT&C	182	130
AOCS	169	78
POWER (AVERAGE) ⁽¹⁾	215	215
PROPULSION ⁽²⁾	7	7
PAYLOAD ELECTRONICS ⁽³⁾	25	0
THERMAL CONTROL	0	50
TOTAL	598 W	480 W

- (1) SSU EXTERNAL TO SPACECRAFT. HEAT LOAD NOT INCLUDED.
- (2) THRUSTER EXTERNAL TO SPACECRAFT. HEAT LOAD NOT INCLUDED.
- (3) 32 W THRUSTER VALVE HEATERS AND PROPELLANT LINE HEATERS EXTERNAL TO SPACECRAFT BUS NOT INCLUDED.

Table 7-14. Bus Temperature Predictions for the Task III Design

PANEL	HOT CASE TEMPERATURE, K (0° BETA ANGLE WITH EXPERIMENT ON)		COLD CASE* TEMPERATURE, K (52° BETA ANGLE WITH EXPERIMENT OFF)	
	ORBITAL AVERAGE	ORBITAL MIN./MAX.	ORBITAL AVERAGE	ORBITAL MIN./MAX.
ANTI-EARTH PANEL	300	295/305	278	276/280
EARTH PANEL	299	295/304	286	285/287
NORTH PANEL	298	297/299	283	282/284
SOUTH PANEL	301	300/303	281	280/282

* 50 W COMPENSATION HEATER IS USED TO MAINTAIN THE PANEL TEMPERATURE.

7.6 ELECTRIC POWER

7.6.1 System Requirements

The electrical power system is to continuously provide 1200 watts of DC power to the spacecraft during both the sunlight and eclipse portions of the orbit throughout the one year mission lifetime. The power requirements are defined at the output of the power control unit (PCU) for the worst case orbital situation. This worst case scenario reflects EOL degradation of the solar arrays, Summer Soltice, the 35.2 minute maximum eclipse duration, and the maximum solar incidence angle on the solar array of 26 deg.. The design must accommodate the range of orbital altitudes that the spacecraft will encounter during the mission. Due to the critical nature of the power system, single point failure modes must be minimized to the greatest extent possible. The solar arrays must withstand the effects of the orbital environment (micrometeoroid and debris, charged particle, ultraviolet, and atomic oxygen damage) throughout the operational lifetime. Any maneuvers required for solar array tracking must be compatible with the 5×10^{-7} g background acceleration limit.

7.6.2 System Description

The electrical power system (Figure 7-14) is comprised of two solar array wings, four sequential shunt units (SSUs), one PCU, 2 battery charge converters (BCCs), and 2 NiCd battery assemblies. These units are arranged into two independent primary power buses that may be connected together by command through a high power relay.

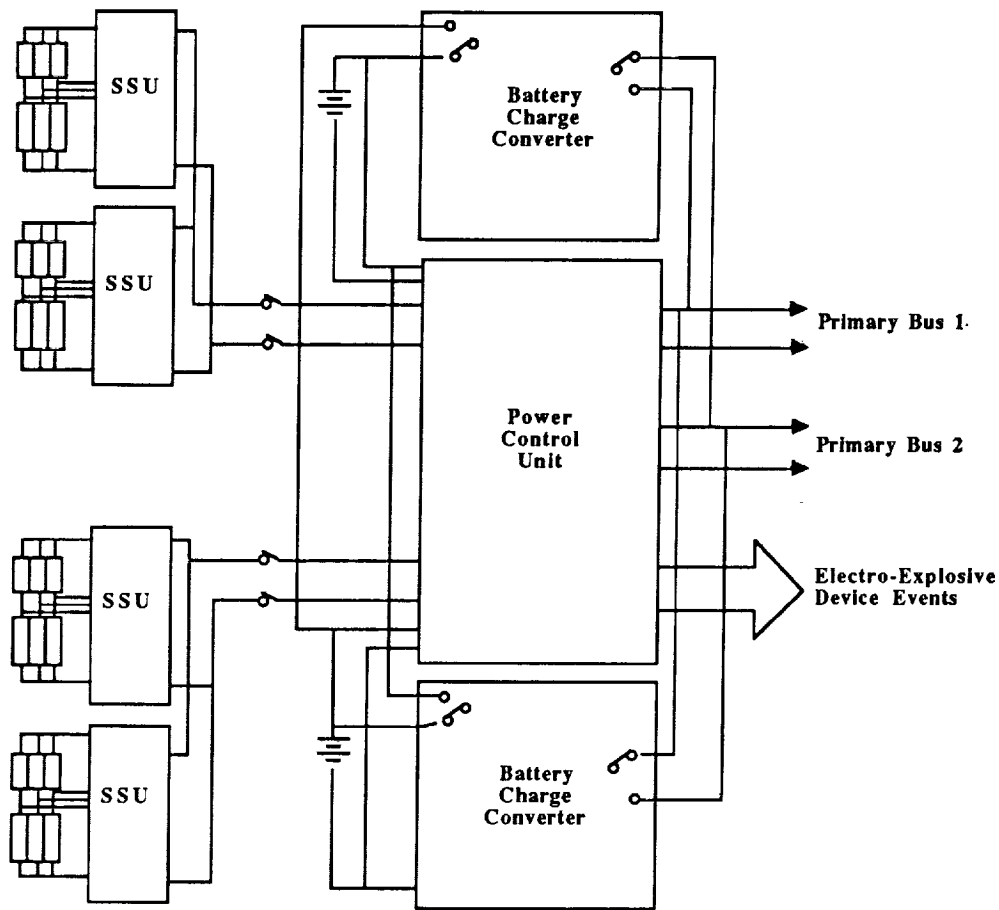


Figure 7-14. Electrical Power System Block Diagram

7.6.2.1 Normal Mode System Operation. Each solar array wing consists of 32 array strings, tapped at the 2/3 voltage point to provide SSU control lines. Two SSU's are provided per wing with each controlling 16 of the 32 array strings. The two SSUs are controlled from a common error bus provided by an error amplifier located in the PCU. The error amplifier senses the bus voltage on each bus, and generates an error signal as a function of the voltage. The error signal is fed across the solar array slipring interface to drive the respective SSUs. Power from each solar cell string is then either directed to return through the shunt element, or directed onto the main bus through a summing diode. The outputs of the two SSUs are connected together to produce a single solar array wing output bus. This bus is routed down the yoke of the array, through the solar array drive assembly (SADA) sliprings, and into the PCU for monitoring, conditioning, and distribution to the loads. Primary bus regulation is performed by the switching of shunt elements on or off in response to load variations. By switching these shunt elements, the solar array wing output current can be adjusted to produce 42.0 ± 0.5 volts across the load impedance. Bus voltage ripple produced as a result of this switching power is reduced to 50 mV by means of a large capacitor bank located in the PCU.

The PCU composes two independent buses, with each bus deriving power from one solar array wing and one battery. Each bus includes an error amplifier, capacitor bank, battery disconnect relay, battery discharge diode, and telemetry required to properly monitor the current and voltage functions of each bus. The two buses may be connected together through cross-strap relays forming a single bus without detrimental effects to the system. The PCU also contains provisions for control of electro explosive discharge (EED) event actuation. This control is provided by redundant actuation relays configured such that EED actuation power may be derived from either bus to insure EED firing. Two "enable" levels are also provided to guard against premature EED event actuation.

Two 26 cell, 53 amp-Hour NiCd batteries are used to provide 1200 watts to the spacecraft during eclipse operation. The batteries are connected onto the bus through isolation diodes, and may be disconnected from the bus by command using series disconnect relays. This configuration allows automatic support of the main bus by the battery during eclipse or during peak loads in the event that load current exceeds solar array output current. In either case, if the main bus voltage falls, forward biasing of the isolation diodes allows the battery to support the load. These diodes also block current from flowing in the reverse direction directly from the main bus to the batteries. Such current flow would be detrimental to the charge control system.

Batteries are charged through the use of the BCC. The BCC is placed like a load on the output of the power system. In this configuration, the primary converter runs off of the regulated bus voltage in sunlight, and automatically shuts off when the bus voltage falls below the regulation range. The output of the converter is hard wired across the terminals of the battery, clamping the converter output to the battery voltage at all times. The converter is essentially a constant power device that converts power from the primary at main bus voltage, to an equivalent power (minus a small conversion loss of 6-8 percent) at the lower battery voltage. Since the output voltage is lower, but the power is the same, converter output current can increase above the input current to allow more charge current to be available at low battery voltages, for a given solar array area. This charge current is controlled by the SCE which monitors discharge current telemetry and sends commands to the BCC to produce an appropriate charge profile.

7.6.2.2 Electro-Explosive Device Controls. Safe and reliable operation of all spacecraft electro-explosive device (EED) actuation functions is ensured by independent and redundant electrical controls. These controls consist of the following: two-level EED enable/inhibit provisions; a minimum of two independent EEDs per EED function; and separate EED power buses and actuation controls for functionally redundant EEDs

The separate EED power buses for EED actuation are provided directly by the two spacecraft batteries. These buses are each connected via independent two-level enable/inhibit functions to the

activation relay circuits for each redundant EED. Pre-separation EED enable/inhibit control is provided by command controlled enabling for each EED bus (level one) and command enabling (level two). Post separation EED enable/inhibit control is provided by enabling relays in series with each EED bus in the PCU that close upon spacecraft separation (level one) and by command enabling (level two). Each EED containing a single bridgewire is controlled by an independent actuation relay which is driven by cross-strapped, dual command inputs. These actuation relays apply a current of 4.5 to 10 amperes from the assigned EED bus upon receipt of a command input. Redundant EEDs for each EED function are divided equally between the two EED buses and are activated by individual relays.

7.6.3 Electric Power System Analysis Results

The electrical power system is designed to provide 1200 W continuously at the output terminals of the PCU to the bus and experiment subsystems. This power is allocated as 400 W for the bus subsystems and 800 W to the experiment at all times except during tests requiring thrusting. During thrusting, 550 W is allocated to the bus and 650 W to the experiment. The overall vehicle power budget is shown in Table 7-15 for experiment thrusting and non-thrusting modes of operation. The bus module component power requirements are shown in Table 7-16.

Two silicon solar cell types (back surface reflector (BSR) and back surface field/reflector (BSFR)) were considered and BSFR solar cells were chosen because they will provide more EOL power. The solar arrays require 32 square meters of area to provide the 1200 W, assuming an 86 percent packing factor and a one year life. The EOL power for worst case conditions including 26 degree solar incidence angle and summer solstice is 2540 W. This results in an EOL solar array power margin of 109 W.

To maximize the efficiency of the solar arrays, they must be kept perpendicular to the incident solar radiation. For the selected orbit and spacecraft orientation, this would require two types of motion: rotation of the solar arrays about their axis using the SADA and in some cases a roll of the entire spacecraft during the orbit. Solar array and spacecraft pointing scenarios have been examined with the objective of keeping the maneuver accelerations on the payload below 5×10^{-7} g. A design using canted solar arrays was chosen to minimize the impact of solar array tracking on the experiment. This design accepts a 10 percent power loss, but does not require 2-axes solar array tracking. However, to keep the solar incidence angle within 26 deg., a 180 deg. spacecraft roll maneuver must be performed eleven times a year (ie., every time the Beta angle passes through zero as shown in Figure 4-4). The timing of this maneuver is not critical, so it can readily be incorporated into the test schedule.

NiCd batteries were chosen since they have been shown to have sufficient lifetime to withstand the large number of charge/discharge cycles that are required in low-Earth orbit due to the frequent eclipses. The two 53 amp-hour batteries will have a maximum depth of discharge of 18 percent in the worst case 35.2 minute eclipse.

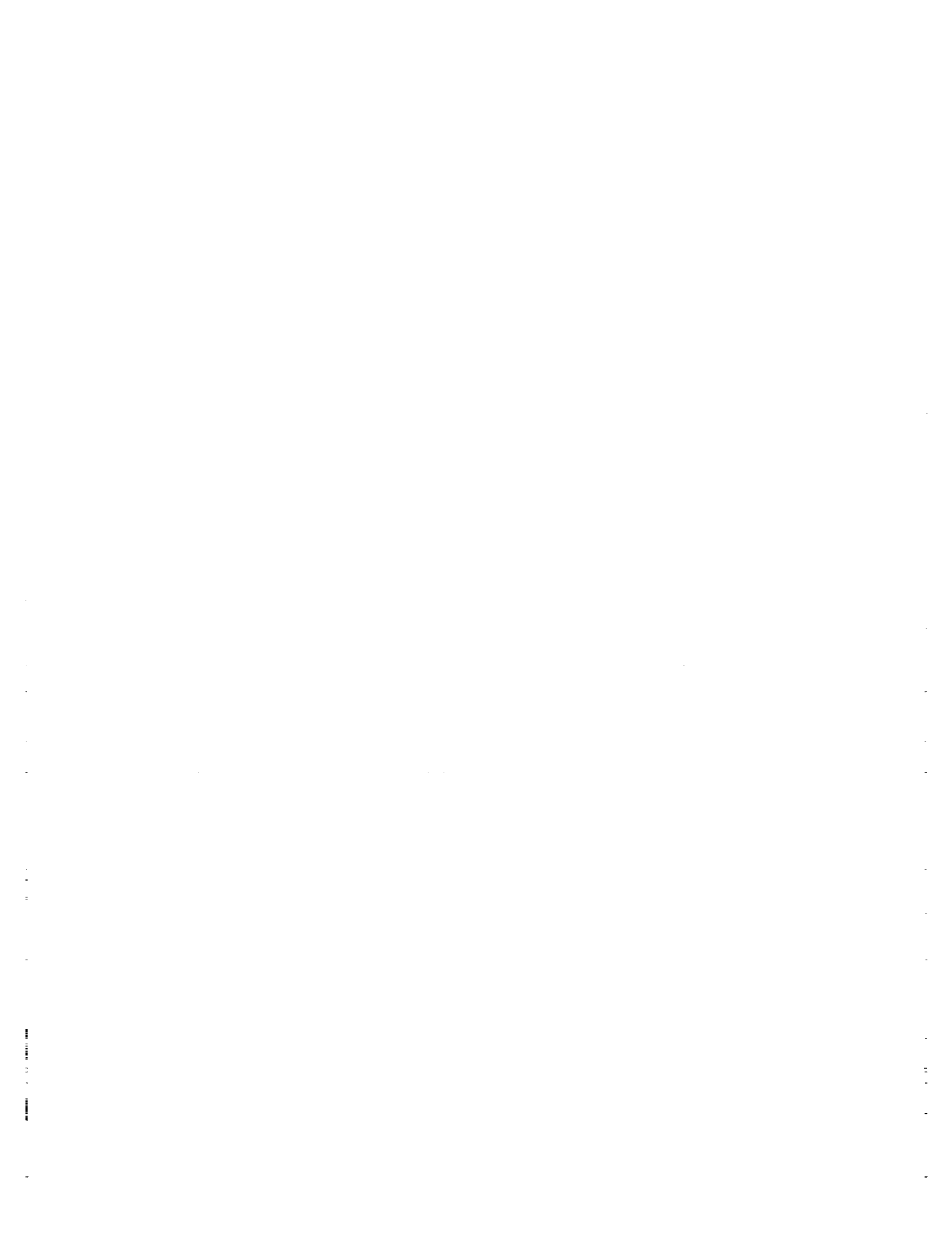
The total bus voltage range is specified to be 26.5 to 42.5 volts. The basis of this range is that the minimum battery voltage at the end of discharge is 30 volts. The minimum bus voltage of 28.9 volts allows for battery interconnect, battery harness, battery diode and current monitor voltage drops. In the unlikely event that a battery cell fails shorted, the minimum battery voltage would be reduced by 1.5 volts due to the lost cell. Under worst case conditions, this allows a 0.9 volt margin between the minimum bus voltage and the minimum specified equipment range.

Table 7-15. Spacecraft Overall Power Budget

	EXPERIMENT THRUSTERS ON (WATTS)		EXPERIMENT THRUSTERS OFF (WATTS)	
	SUNLIGHT	ECLIPSE	SUNLIGHT	ECLIPSE
SOLAR ARRAY OUTPUT POWER	2540	-	2540	
BATTERY OUTPUT POWER	-	1232		1232
POWER SYSTEM LOSSES				
SSU	94	-	94	
BATTERY CHARGE CONVERTER	46	-	46	
BATTERY CHARGING	1080	-	1080	
PCU	11	11	11	11
BATTERY DIODE LOSSES	-	32	-	32
BUS SUBSYSTEMS	490	490	356	356
EXPERIMENT	650	650	800	800
VEHICLE EQUIPMENT MARGIN	60	60	44	44
SOLAR ARRAY MARGIN	109	-	109	-

Table 7-16. Spacecraft Bus Component Power Budget

COMPONENT	EXPERIMENT MODE		COMPONENT	EXPERIMENT MODE	
	THRUST ON	THRUST OFF		THRUST ON	THRUST OFF
TT&C SUBSYSTEM			AOC SUBSYSTEM		
PROCESSOR 1	33.3 W	33.3 W	REACTION WHEELS	100 W	20 W
PROCESSOR 2	20	20	WHEEL ELECTRONICS	20	7
DCU A1	13	13	CONICAL EARTH SENSOR	8	8
DCU A2	0	0	CES ELECTRONICS	4	4
DCU B1	16	16	CASS	0	0
DCU B2	0	0	CASS ELECTRONICS	1	1
DCU C1	16	16	DSS	0	0
DCU C2	0	0	DSS ELECTRONICS	2	2
DCU D1	27	27	SADA/ELECTRONICS	13	13
DCU D2	0	0	DIRA	50	50
TRANSPONDER 1	20	20	DIRA INTERFACE UNIT	1.4	1.4
TRANSPONDER 2	0	0	VALVE DRIVER	0	0
DATA STORAGE UNIT 1	9	9	MAGNETIC TORQUER	10	1
DATA STORAGE UNIT 2	0	0	SUBTOTAL	209.4 W	107.4 W
DIPLEXER	0	0			
OMNI ANTENNA	0	0	PROPULSION		
DIRECTIONAL ANTENNA	0	0	THRUSTERS	88	32
ANTENNA CONTROL ELECT 1	32	32	PRESS TRANSDUCERS	6.6	6.6
ANTENNA CONTROL ELECT 2	0	0	SUBTOTAL	94.6 W	38.6 W
SUBTOTAL	186.3 W	186.3 W	THERMAL CONTROL		
			HEATERS	39	100
			TOTAL BUS POWER	529.3 W	432.3 W



8 INTERFACES

This section addresses the design aspects of COLD-SAT system interfaces, including bus-to-experiment module, spacecraft-to-Atlas launch vehicle, and interfaces with the launch complex.

8.1 BUS-TO-EXPERIMENT MODULE

8.1.1 Fluid and Mechanical Interfaces

The forward body of the experiment module contains two valve modules, Tank 1, and Tank 3. The remaining components, such as Tank 2, the gas storage bottles, and the electronics are distributed throughout the spacecraft bus. Likewise, some of the bus systems, such as thrusters, Earth sensor, propellant lines and electrical lines are located on the forward body section of the experiment module. The purpose for the layout shown in Figure 8-1 is to identify and summarize the interfaces between the bus and the experiment. There are over sixty interfaces, plus numerous small brackets, clips, holes, etc. for plumbing and electrical lines.

One of the primary interfaces is shown in "G". It is the forward body section mated with the bus through 36 attachment points. Also in the area are electrical and plumbing interfaces and provisions for attaching a scrim-reinforced Kapton environmental shield. An interface panel for electrical connectors is also shown.

The installation of Tank 2 inside the bus central cylinder requires six support fittings attached to the cylinder. Also on the inside of the cylinder are mounting interfaces for three accelerometers and one pump controller unit. On the outside of the central cylinder, fifteen attachment fittings and three brackets are required for supporting the gas storage bottles, the pressure control module, and the H₂ ground vent disconnect. Several support clips are also used for attaching gas manifolds, the vent line, and electrical harnessing. Holes through the central cylinder (equipped with grommets) are also required for routing plumbing and electrical lines.

The spacecraft thrusters, along with propellant and electrical lines, are installed on the experiment outer structure. An Earth sensor is also located on the forward cap (view "E-E"). An opening (with a cover) through the forward cap provides additional access for making final connections and inspections. A typical roll thruster arrangement is shown in view "F". Electrical services for the bus are provided by a disconnect located in the umbilical panel which is supported from the experiment outer structure.

8.1.2 Instrumentation, Power and Control

The physical instrumentation interface between the spacecraft bus and the experiment module, shown in Figure 8-2, consists of the two wire, MIL-STD-1553B data buss connecting the control processor in the bus to the DCU in the experiment module. A separate connector is provided for this interface. Another aspect of the interface is the data format. The data format, as shown in Table 7-6, consists of both the bus and experiment module data requirements and resides in the software of the bus electronics. However, the data format interface consists of only the experiment module data requirements. These requirements are presented in Appendix C.

The power interface between the spacecraft bus and the experiment module is illustrated in Figure 8-3. The solar array and batteries in the spacecraft bus supply power for both the bus and the experiment module. This power, supplied to the interface through a separate connector, ranges from 30 to 42 volts. Eight hundred watts of power are allocated to the experiment module.

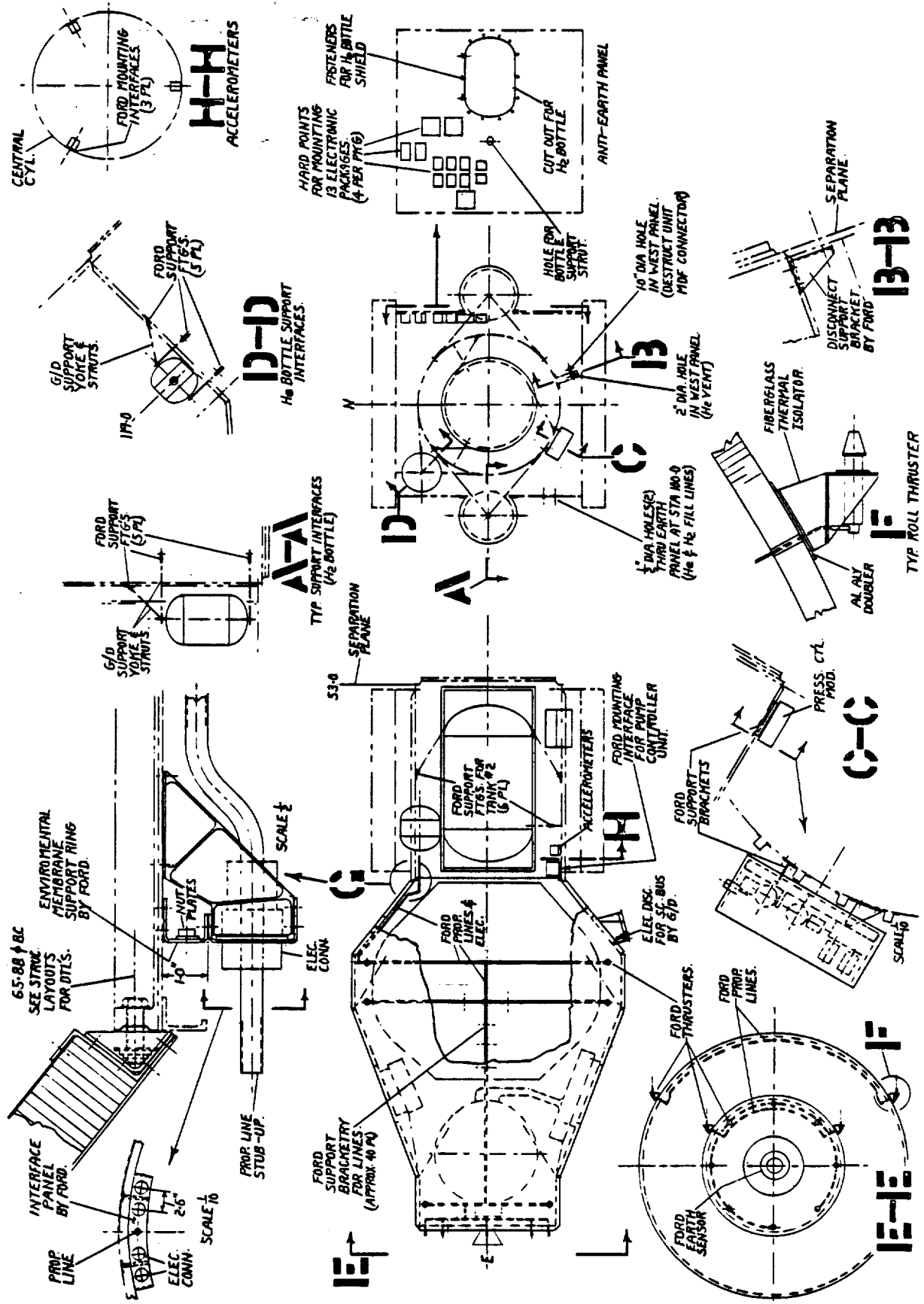


Figure 8-1. Summary of Interfaces Between the Spacecraft Bus and the Experiment

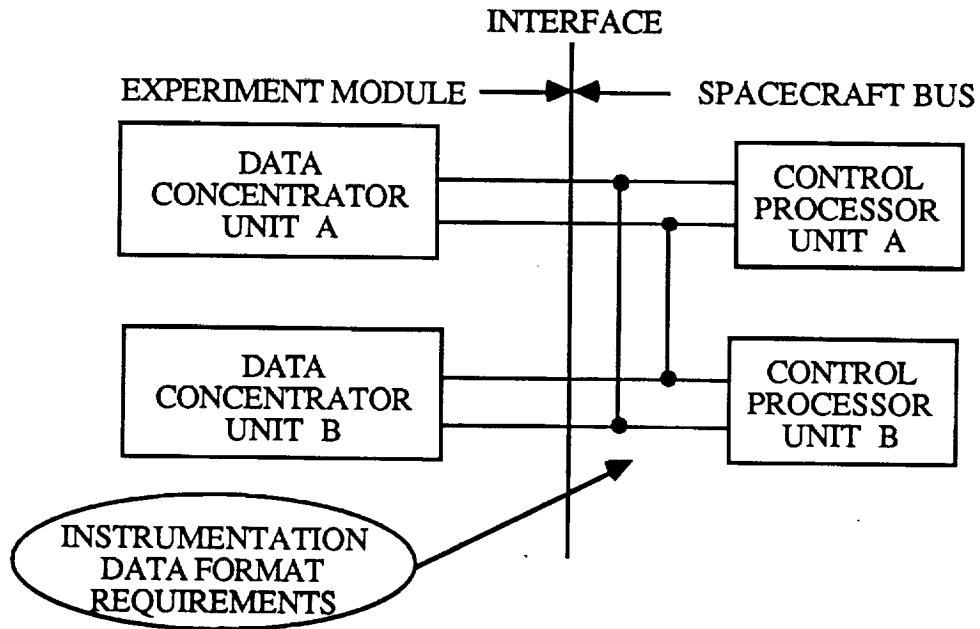


Figure 8-2. Experiment Module / Spacecraft Bus Instrumentation Interface

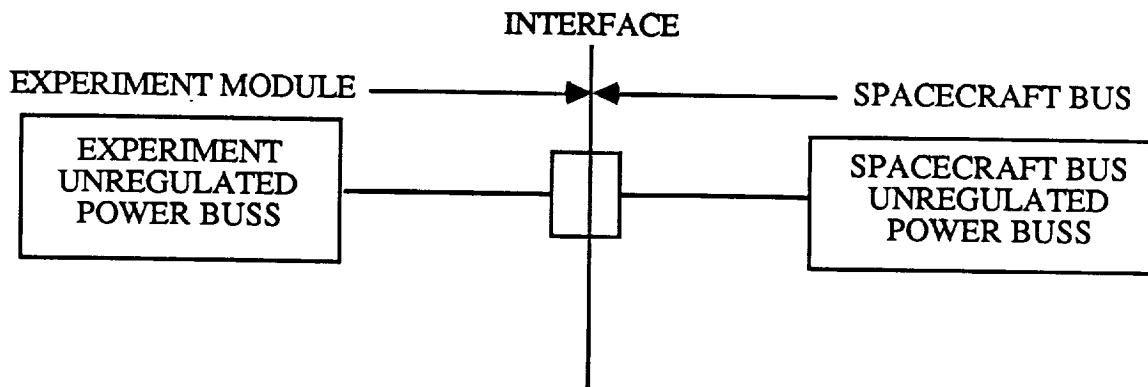


Figure 8-3. Experiment Module / Spacecraft Bus Power Interface

The control interface consists of a physical interface and a software interface as shown in Figure 8-4. The physical interface for the control system, like that of instrumentation, is the MIL-STD-1553B data buss between the control processor in the bus and the DCU in the experiment module. The software interface is made up of the experiment sequences and the experiment timelines which are included in Appendix D.

8.2 SPACECRAFT-TO-ATLAS LAUNCH VEHICLE

8.2.1 Fluid and Mechanical Interfaces

The spacecraft adapter is an aluminum alloy skin-stringer structure, equipped with a ring at the forward end which interfaces with the bus central cylinder. A ring at the aft end interfaces with the

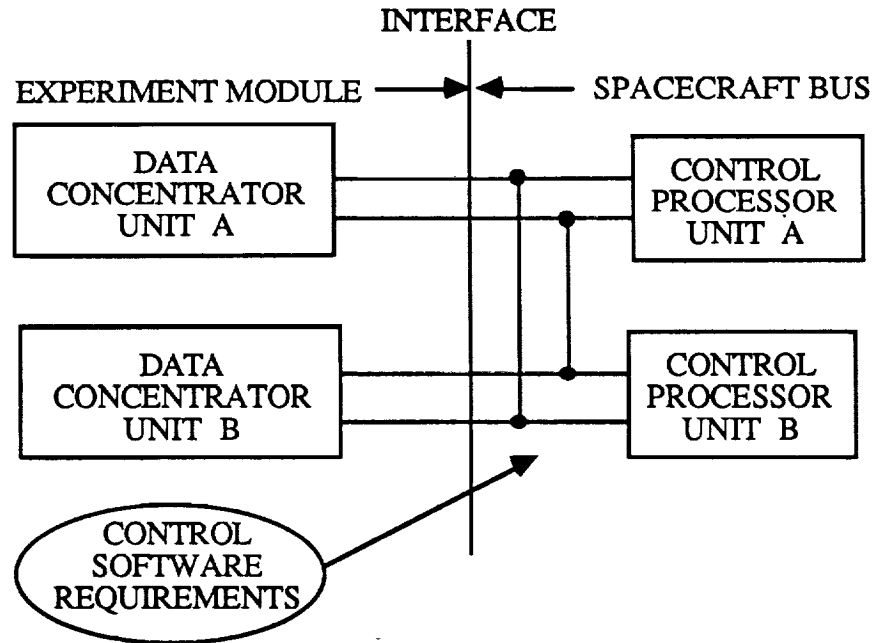


Figure 8-4. Experiment Module / Spacecraft Bus Control Interface

Centaur equipment module (Figure 8-5). The adapter is equipped with a "V" band clamp separation system, four separation springs, and an island structure for the hydrogen gas vent disconnect and a Mild Detonating Fuse (MDF) slip connector.

The "V" band clamp separation system, shown in Figure 8-6, is procured from Saab, and consists of a clamp band set, a matched set of separation spring assemblies, and pyrotechnic bolt cutters. Shear pins are also included which enhance its shear load-carrying capabilities.

The clamp band set joins the spacecraft to the adapter during preflight and flight mission phases until the time of separation of the spacecraft. The connecting bolts are preloaded to provide sufficient tension in the straps to prevent any displacement between the two frames during these phases of operation.

At separation, the two connecting bolts are each cut by a pyrotechnic cutter. The two bands, elongated by the preload, contract and the pressure on the frames is released. The force on the clamps from the frames push the clamps radially outward allowing the frames to separate. The ends of the clamp bands are trapped in the catchers at separation. After separation the clamp band is retained by the catchers and extractors, which are securely fastened to the adapter structure.

The spring assemblies consist of a spring with spring guide and ejector pin in a housing attached to the adapter. These springs bear on the bus aft closure frame and are sized to provide the necessary energy to separate the spacecraft from the adapter. The separation spring assemblies are mounted inside the adapter, are integral with the adapter, and bear on the bus aft closure frame.

Electrical disconnects crossing the separation plane are not required since these functions are furnished at the umbilical panel which attaches to the experiment outer structure. However, a hydrogen gas vent disconnect and three connectors for the destruct unit MDF are required. The three-connector arrangement is part of an Inadvertant Separation Destruct System (ISDS) currently in development for the Atlas I and Atlas II launch vehicles. The adapter is equipped with an island structure on the outboard side which supports these disconnects. The COLD-SAT hydrogen vent line downstream of the disconnect is plumbed to the "Steer Horn" duct assembly of the Centaur

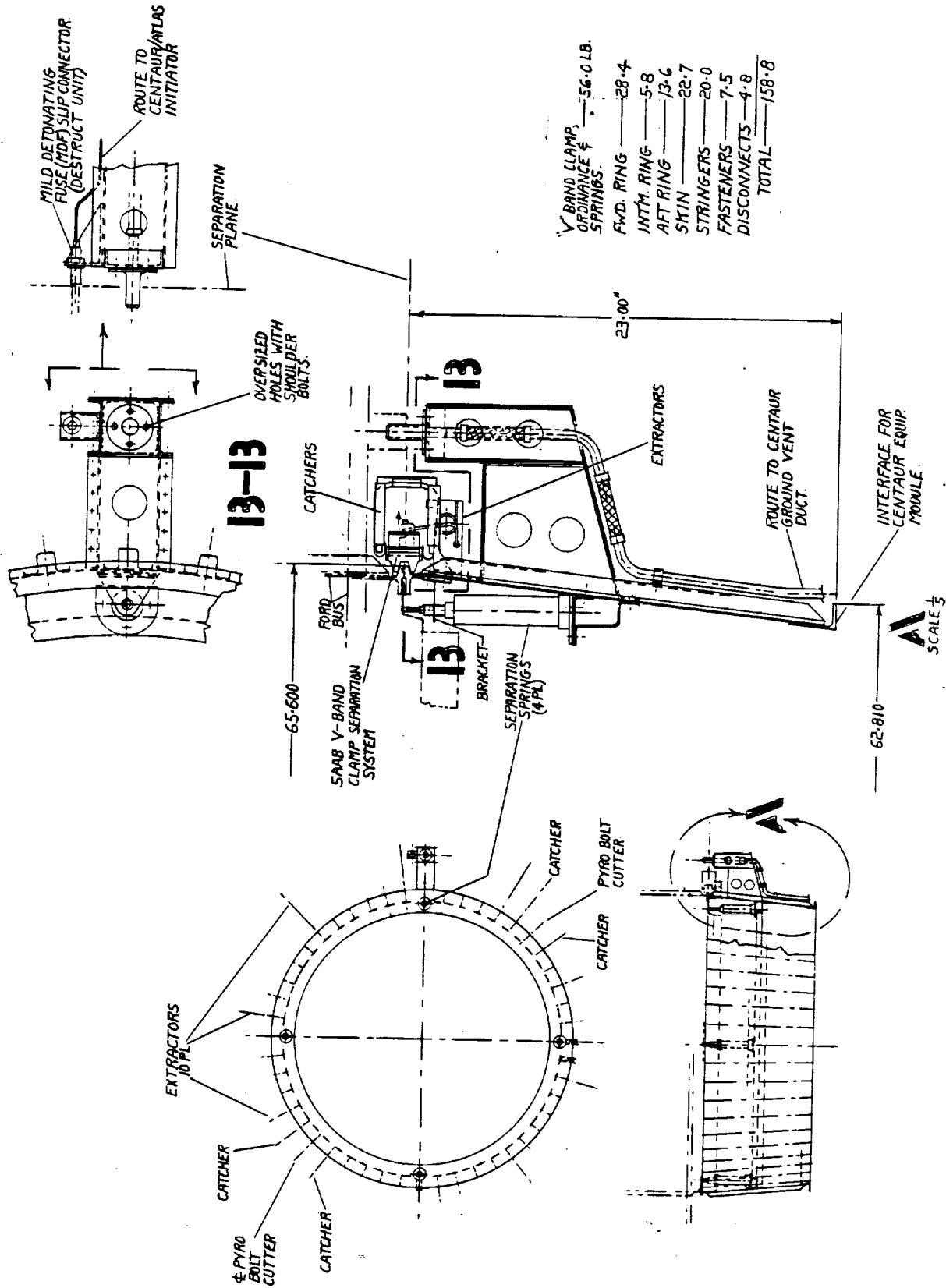


Figure 8-5. Interfaces Between the Spacecraft and the Atlas I Launch Vehicle

ORIGINAL PAGE IS OF POOR QUALITY

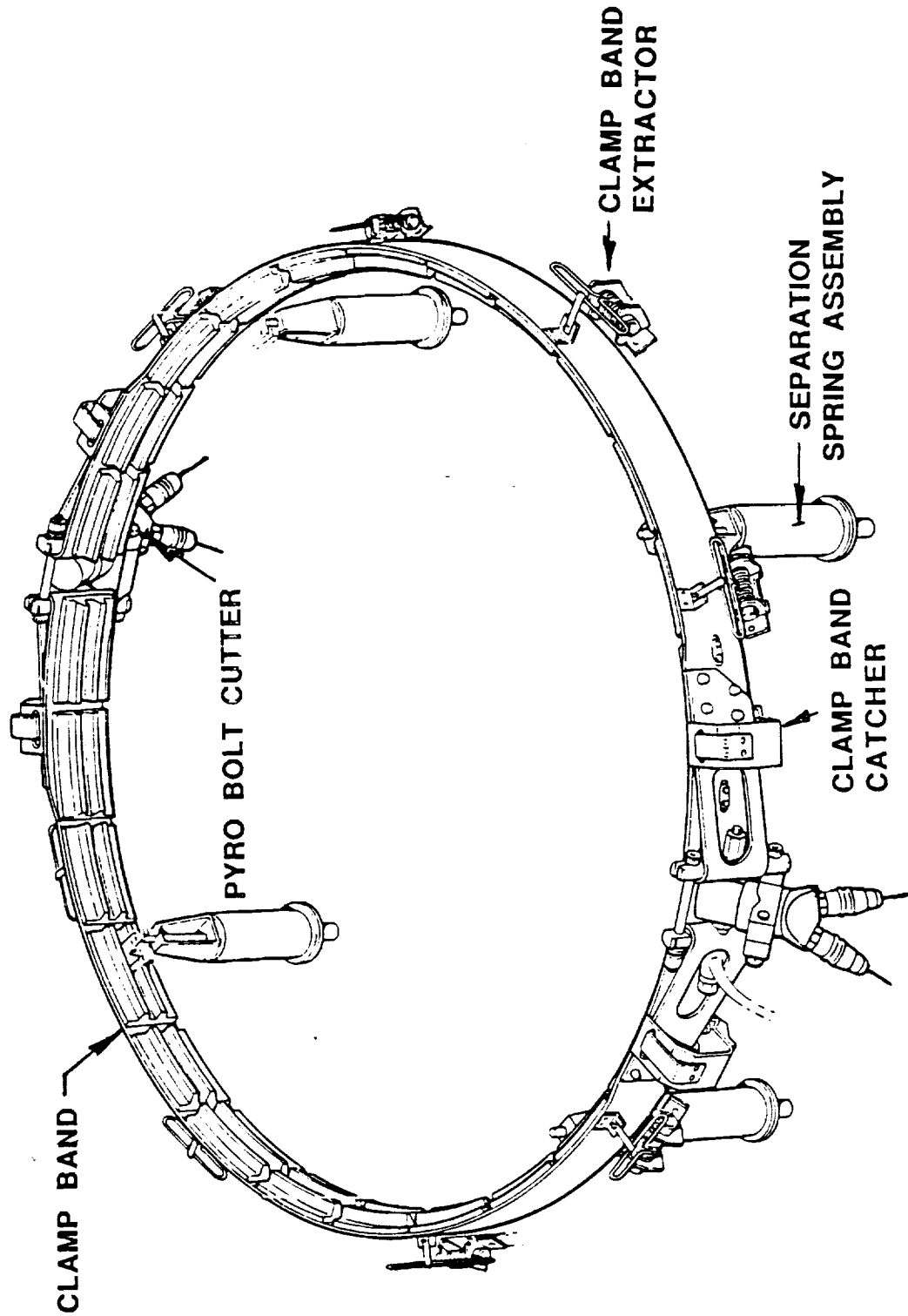


Figure 8-6. Spacecraft "V" Band Clamp Separation System

forward bulkhead. An arrangement for this is presented in Figure 8-7. Referring to view B-B, the COLD-SAT vent tube is routed through the Centaur equipment module to avoid penetration of the Centaur environmental bulkhead. This vent tube connects to the "Steer Horn" duct by adding a boss which is located near the center (View "D") and is supported from the duct and equipment module. Referring to view C-C, the COLD-SAT disconnect is clocked 45 degrees to allow clearances with adjacent components on the spacecraft bus. Further detailed studies may allow an increase of this angle, which would shorten the vent tube. A plan view of the vehicle at launch complex 36-B is included in Figure 8-7. This view shows the clock position of the Centaur vent fin, the Centaur axis, and the relative position of the COLD-SAT spacecraft (view A-A). Further information on the hydrogen gas vent interface with the Centaur upper stage can be found in Section 9.4.2.

8.2.2 Flight Termination System.

In the event that it becomes necessary to terminate the flight, the objective, regarding COLD-SAT, is to open the experiment supply tank to drain the stored hydrogen. To accomplish this, an explosive charge will be installed adjacent to the supply tank. The charge will be detonated by a mild detonating fuse (MDF) from the flight termination system on the launch vehicle. A separable connector on the MDF is installed at the interface to facilitate payload separation.

8.3 LAUNCH COMPLEX INTERFACES

8.3.1 Fluid Interfaces

Preliminary assessment of fluid interfaces required for COLD-SAT launch processing has been summarized in Table 8-1. This summary includes line sizes, flowrates, and preliminary estimates of total usage required for launch. For the LH₂ fill/drain interface, two flowrates are shown because the system will operate at two pressure levels during COLD-SAT operations, as a result of Centaur tanking functions occurring simultaneously. For each fluid required, existing sources located at SLC-36B will be adequate for COLD-SAT supply without impacting Atlas I fluid requirements. Each source will, however, require new flow control and supply piping to service the spacecraft.

Table 8-1. COLD-SAT Launch Facility Fluid Interface Summary

INTERFACE	NOMINAL SIZE (mm)	FLOWRATE (kg/s)	USAGE (kg)	SOURCE
LH ₂ Fill/Drain	19	0.37/0.15	550	• Existing LH ₂ Supply; New Flow control Req'd.
GH ₂ Tank Vent	12	~0.023	-	• Centaur Interface
GN ₂ Insul. Purge	6	~0.0017	[1]	• Existing 5.5 MPa Source; New Flow Control Req'd.
GHe Insul. Purge	6	[2]	45	• Existing 5.5 MPa Source; New Flow Control Req'd.
GHe Fill Line Purge	6	0.0083	-	• Existing 5.5 MPa Source; New Flow Control Req'd.

[1] 0.00125 kg/s Until Switch to GHe purge @ ~ 2 Hours Prior To Launch

[2] 0.0083 kg/s maximum, steady state flow ~ 0.00083 kg/s

A schematic illustration of the fluid interfaces with Centaur and the ground facility is shown in Figure 8-8. Flow to COLD-SAT will be controlled manually by independent modulating valves from a dedicated control console located in the SLC-36 Blockhouse. To control tank and insulation purge flow, a purge control module located on the payload service umbilical will also be required.

Fluid service connections to COLD-SAT will be made through a modified version of the current Centaur T-4 aft umbilical panel, illustrated in Figure 8-9. This panel will carry the ground half disconnects for LH₂, GN₂ and GHe purge supply and exhaust, and an additional electrical interface for COLD-SAT ground power and control to augment the Centaur/COLD-SAT interface at the Centaur forward umbilical panel (see Section 8.3.2). The panel will be attached to the experiment module outer structure using four support legs that are riveted at one end to the panel and attached at the other end to the experiment structure with clips and bolts. Modifications will primarily involve connector downsizing to reflect the smaller COLD-SAT lines, and the substitution of the LH₂ fill/drain line and insulation in place of the current LHe service line and vacuum jacket. The panel contains a few spare disconnect provisions that will be blocked off for COLD-SAT.

Referring to Figure 8-10, the arrangement on the ground side of the panel is basically the same as that for the Titan/Centaur. This ground panel is held to its airborne counterpart by means of a collet/pin assembly. Pulling the pin releases the panel. The pin is connected to a lanyard which, in turn, is attached to a cylinder-operated actuator mounted on the umbilical tower. Upon activation, the cylinder pulls the lanyard at a controlled rate with sufficient stroke to pull the panel clear of the vehicle. A restraint lanyard attached to the umbilical tower helps guide the panel clear of the vehicle while the panel housing acts as a bumper should the assembly strike the mast or the umbilical tower. The panel housing also prevents the ground panel from hanging up in the chute, maintains the door in an open position prior to launch, and provides uniform sliding surfaces for the door and chute during disconnect. Since the umbilical panel is inboard from the payload fairing wall, an opening is required through the fairing cylindrical section, and is equipped with a chute that runs from the opening to the airborne panel. This chute acts as a guide for the ground umbilical and provides a seal for the purge inside the fairing. The chute consists of two sections. The short secondary section attaches to the airborne panel and the longer primary section attaches to the fairing. The two sections interface with a seal. The primary section of the chute is reconfigured from that used for Titan/Centaur in order to meet the geometry arrangement for COLD-SAT. The primary section of the chute also has a door which will require some geometry changes since the present design interfaces with a cone rather than a cylinder.

8.3.2 Telemetry, Power, and Control

During tanking of the COLDSAT supply tank with hydrogen prior to launch it will be necessary to provide ground power to the payload in order to operate fluid control components and monitor the loading procedure on telemetry. Ground power is supplied to the payload via the payload umbilical. The umbilical will be capable of providing up to 1200 watts of power to the payload with a voltage between 30 and 42 Vdc. Activation of the fluid control components during the hydrogen loading procedure will be initiated at the payload control console in the blockhouse and transmitted via landlines and the payload umbilical cable to the test interface on the control processor. The status of the hydrogen loading procedure will be monitored on telemetry. The telemetry signal is transmitted from the test interface of the spacecraft control processor, through the umbilical cable and landlines to the telemetry ground station where it will be decommutated and the parameters of interest will be monitored in real time.

For telemetry retrieval from COLD-SAT on the launch pad, Centaur will interleave the spacecraft PCM and analog data with its master data unit (MDU). The MDU incorporates software programmable, integrated signal conditioning and multiplexing, and multiple-bit rates and PCM formats. Up to 1 KBPS of COLD-SAT data will be interleaved with the launch vehicle data and

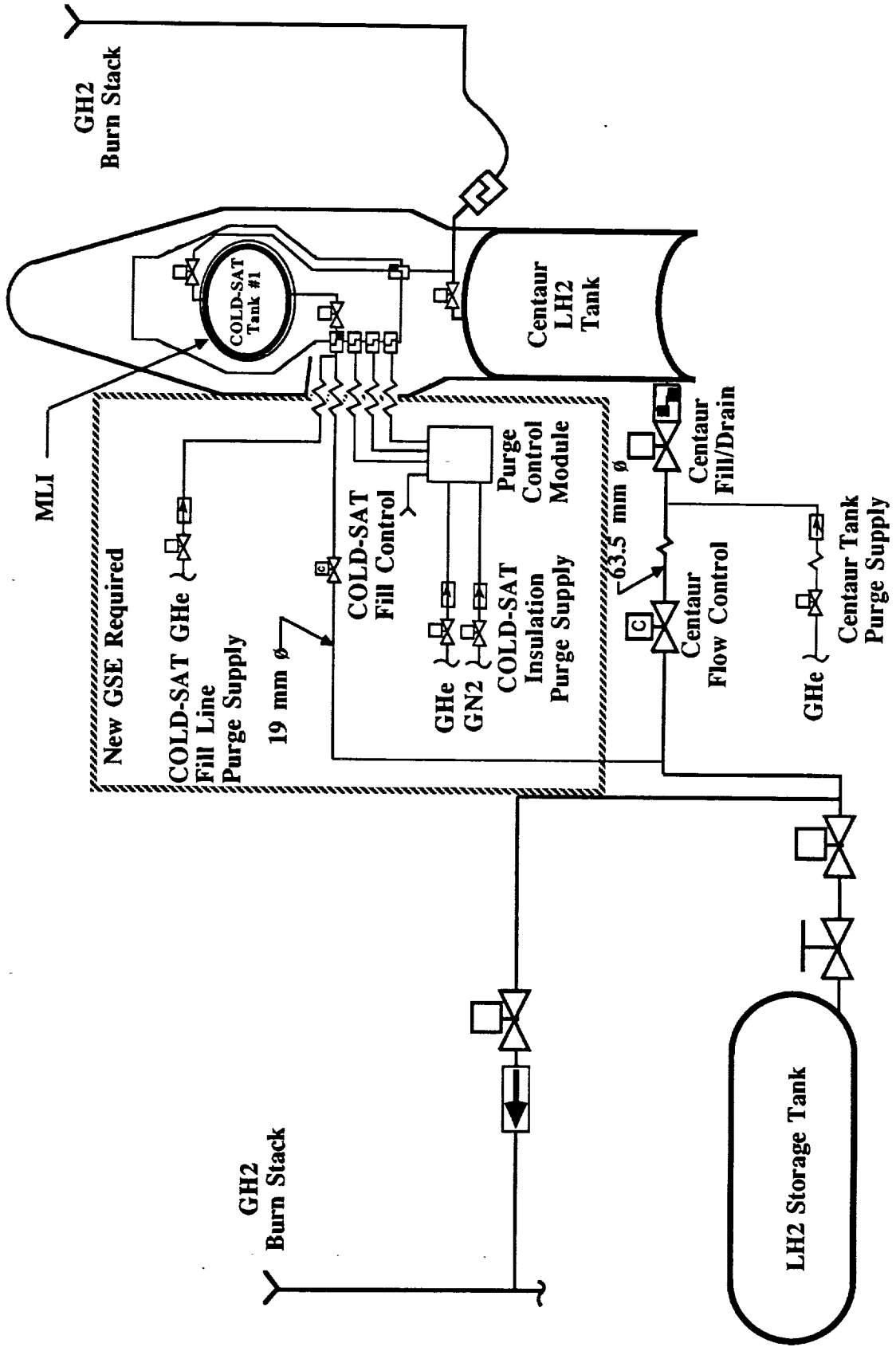


Figure 8-8. Launch Facility Fluid Interfaces

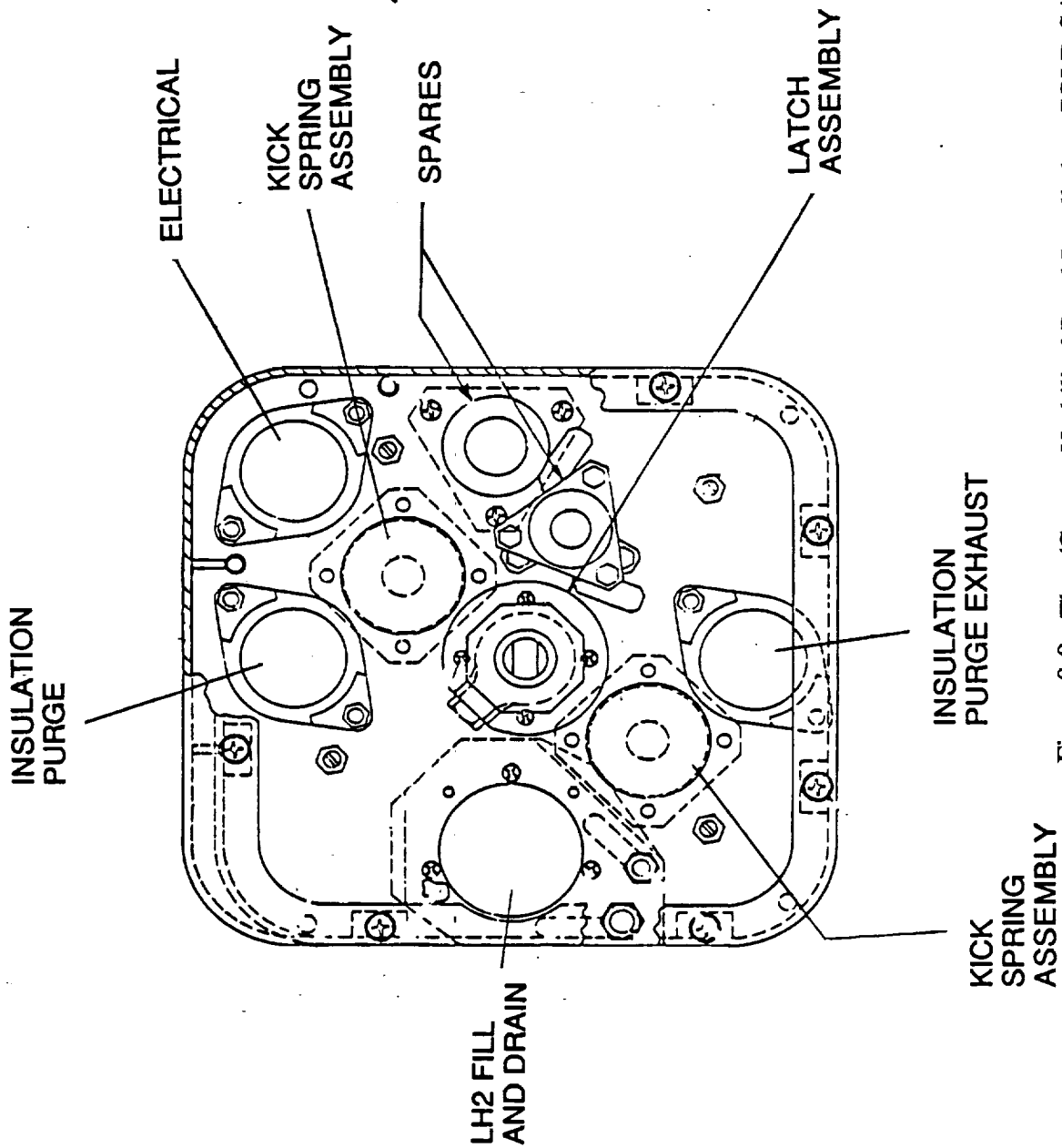
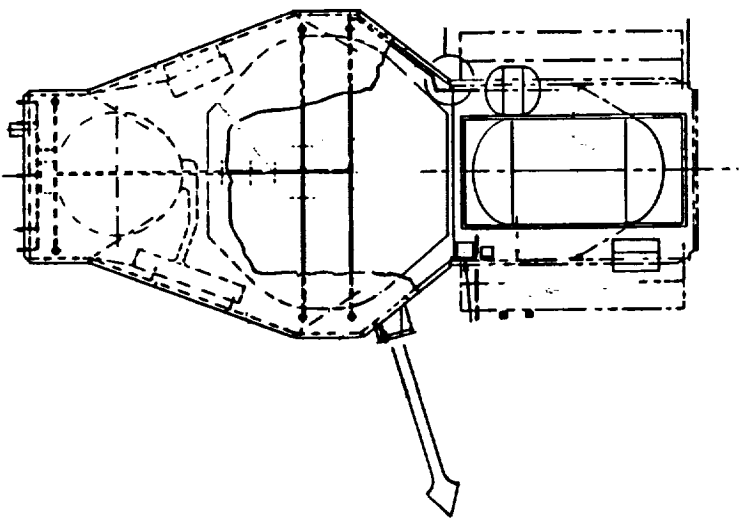


Figure 8-9. Titan/Centaur Umbilical Panel Installed on COLD-SAT Outer Structure

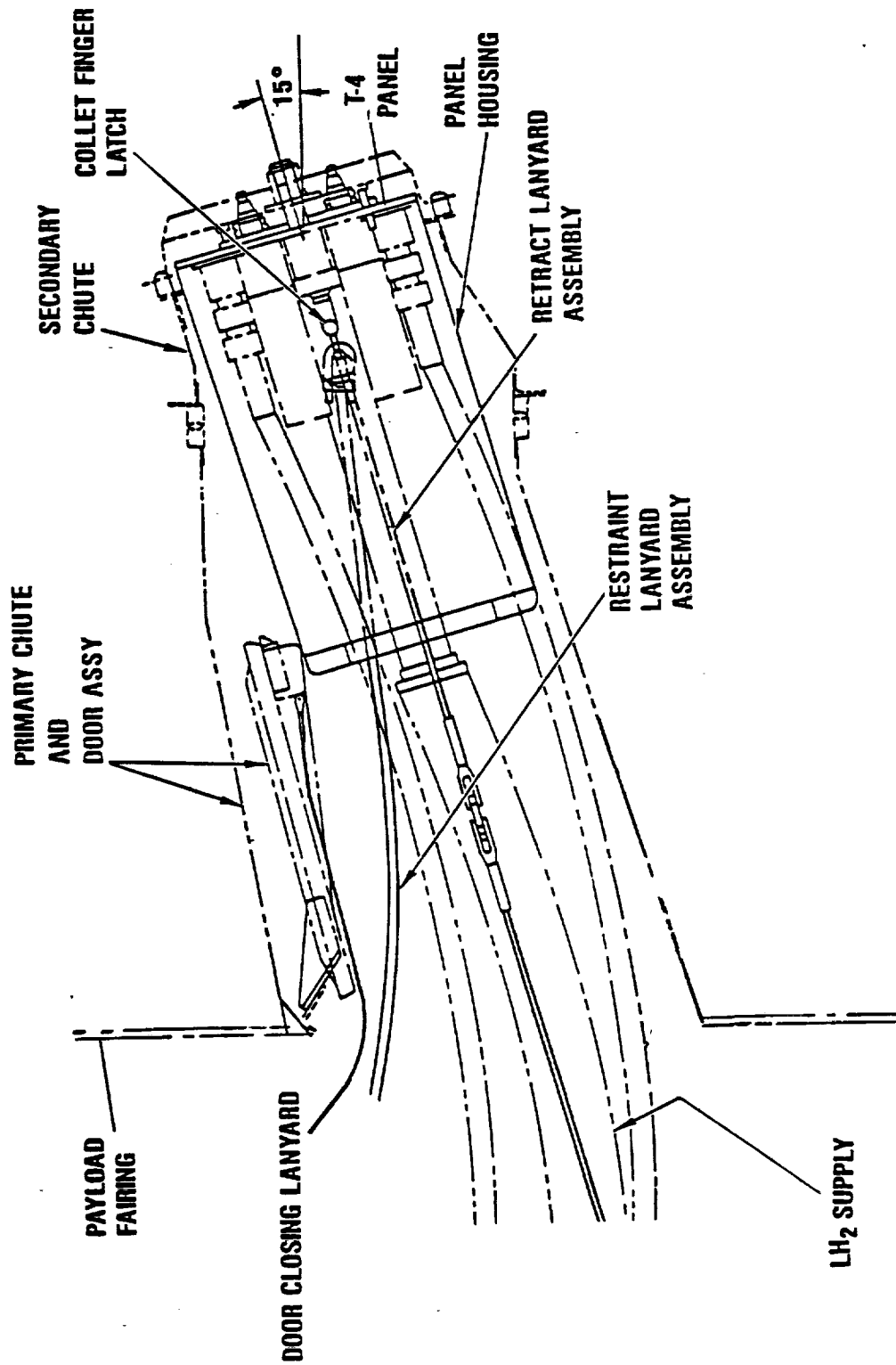


Figure 8-10. COLD-SAT Ground Umbilical Arrangement Using Existing Titan/Centaur Panel

serially transmitted in a PCM bit stream. The PCM link for COLD-SAT GSE exists via hardware to the SLC-36 Blockhouse.

If future analyses determine the need for an RF link, a telemetry re-radiation system can be implemented on the service tower, which will provide direct RF communication between the encapsulated spacecraft and ground stations. This re-radiation capability is provided via the payload fairing-mounted repeater antenna to antenna hat coupling/landline cabling, or through the umbilical tower boom repeater system.

Power and control to COLD-SAT after T-4 umbilical disconnect just prior to launch are provided by a dedicated umbilical disconnect located on the Centaur forward umbilical panel. This umbilical interfaces with two spacecraft dedicated rise-off disconnects located on the spacecraft. This interface provides signal paths between the COLD-SAT and ground support equipment, and also between COLD-SAT and the Centaur for power supply, monitor, and control during pre-launch and launch countdown. The umbilical disconnect separates at liftoff. The two rise-off disconnects separate at COLD-SAT/Centaur separation.

This dedicated umbilical contains the following standard compliment of wires from the umbilical to the launch disconnect:

1. 41 twisted shielded wire pairs-20 AWG
2. 6 twisted shielded wire triplets-20 AWG
3. 4 twisted shielded controlled impedance wire pairs- $75\Omega \pm 10\%$

8.3.3 Ground Support Equipment Interfaces

Floor space is allocated on the operations level of the SLC-36 Blockhouse for installation of a COLD-SAT dedicated ground control console. This console will interface with General Dynamics-provided control circuits through the Centaur umbilical panel to the spacecraft. Control circuits provided for COLD-SAT use will be isolated physically and electrically from those of the Atlas I to minimize EMI effects. COLD-SAT tanking control, telemetry monitoring, and spacecraft control will be performed from this dedicated console during pre-launch and launch operations.

Several types of electrical power are available at SLC-36 for COLD-SAT use. Commercial power is used for basic facility functions with critical supplies connected to an uninterruptable power system (UPS). The dual UPS consists of battery chargers, batteries, and a static inverter. The battery chargers are normally operated from the commercial system, but one may be operated on diesel power during critical testing and operations if required. 28 Vdc UPS power is also available for COLD-SAT use in the blockhouse, launch service building, and umbilical tower.

9.1 MANUFACTURE

Fabrication, buildup and integration of the experiment module and spacecraft bus will require careful planning, scheduling and attention to design. At this early stage of concept development, details cannot be provided, but a general assembly sequence can be described to illustrate the practicality of the structural concepts, layout of the major components, and experiment module-to-bus integration.

9.1.1 Buildup and Integration

Buildup and integration of the COLD-SAT experiment module and the spacecraft bus will be performed at both Ford Aerospace Corporation (FAC) in Palo Alto, California, and General Dynamics Space Systems (GDSS) in San Diego, California. The fabrication process is illustrated in Figure 9-1. Fabrication of the bus cylinder, panels, and solar arrays will be done at Ford while fabrication of the experiment tanks, insulation, fluid components and micrometeoroid shield will be done at General Dynamics. Following their fabrication at Ford, one of the bus panels and the central cylinder will be sent to General Dynamics. The other bus panels and equipment will remain at Ford for later integration into the spacecraft. General Dynamics will install experiment module avionics and wire harnessing on the panel sent from Ford, and will integrate the tanks and the micrometeoroid shield with the central cylinder. Buildup of the central cylinder will include the installation of the following equipment.

1. Experiment Tank 2
2. GH₂ and GHe pressurant bottles and plumbing
3. Pressure control module
4. Pump control module
5. Accelerometer packages (3)
6. Plumbing and harnessing

After this equipment has been installed into the central cylinder, the experiment module will then be assembled and integrated with the central cylinder subassembly in a five-step sequence as illustrated in Figure 9-2. In step 1, the aft section of the outer structure is bolted to the spacecraft bus central cylinder. In step 2, the ends of the tubes at the forward end of the spacecraft central cylinder are extended to the access holes in the outer structure by adding sections. Propulsion lines to the forward thrusters and the harness for the forward Earth sensor are also installed. The Tank 1 assembly (with external lines insulated) is installed next in step 3. In step 4, the forward assembly containing Tank 3 is mated with the aft structural section and the final plumbing connections made through the access openings.

At this point, the experiment module/central cylinder assembly and the separate bus panel containing experiment avionics are transported back to Ford Aerospace for final assembly. The sub assemblies and components installed at this time include:

1. Propulsion system components and plumbing
2. Attitude Control components
3. Avionics panels and interconnecting harnesses
4. Experiment panel and interconnecting harnesses
5. Solar array drives and panel assemblies
6. TT&C antennae
7. Aft closure panel, Earth sensor, and shield
8. Forward Earth sensor and shield

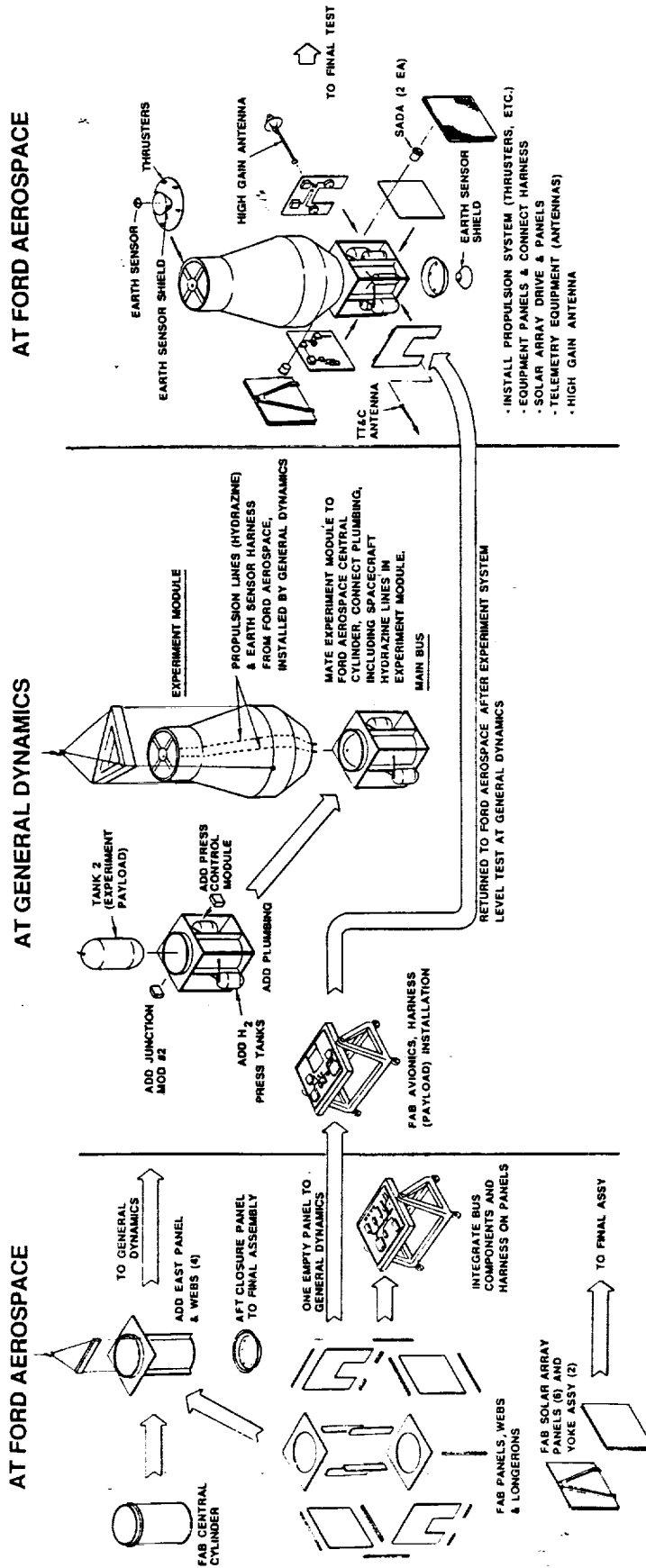


Figure 9-1. Spacecraft Assembly Process

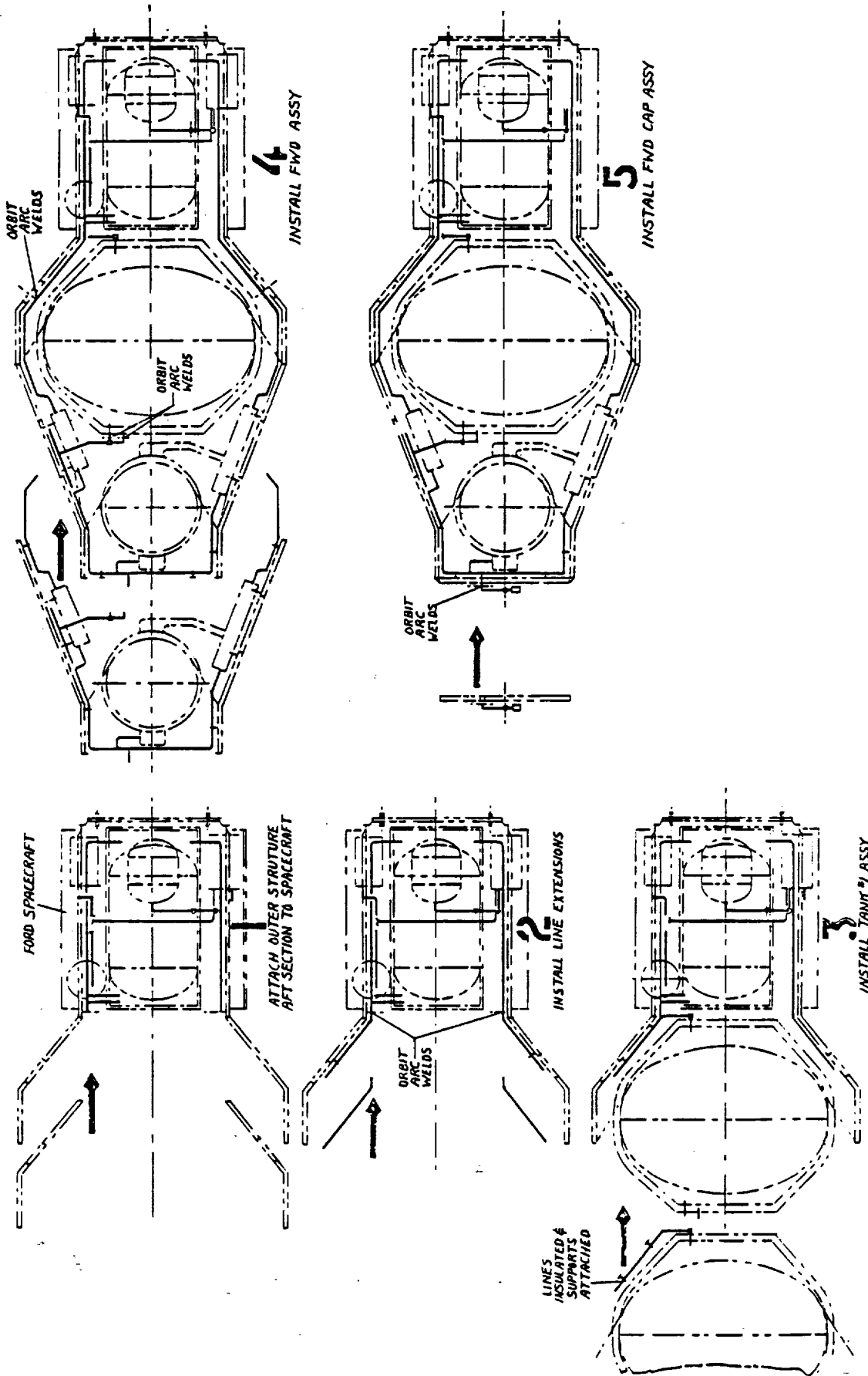


Figure 9-2. Experiment Module-to-Bus Attachment Sequence

After these components are installed, the spacecraft is essentially complete. It is removed from the assembly dolly and is mated to the pressurized vertical/horizontal transporter for movement to final test facilities.

9.1.2 Transport

The integrated spacecraft will be transported on a dedicated vertical/horizontal transport trailer, illustrated in Figure 9-3. This self-contained transporter carries a GN₂ purge supply and control system for spacecraft mechanisms and bearing purges, and a powered tilt mechanism that rotates the spacecraft to a horizontal position for transport and a vertical position for work or removal/installation of the spacecraft on the transporter. During transport operations the transporter cover is installed to provide a sealed enclosure for the spacecraft. Dessicants are placed inside the enclosure which is subsequently pressurized to approximately 13.8 kPa above atmospheric pressure to avoid contamination. The GN₂ purge is used only when the pressurized cover is removed from the transporter.

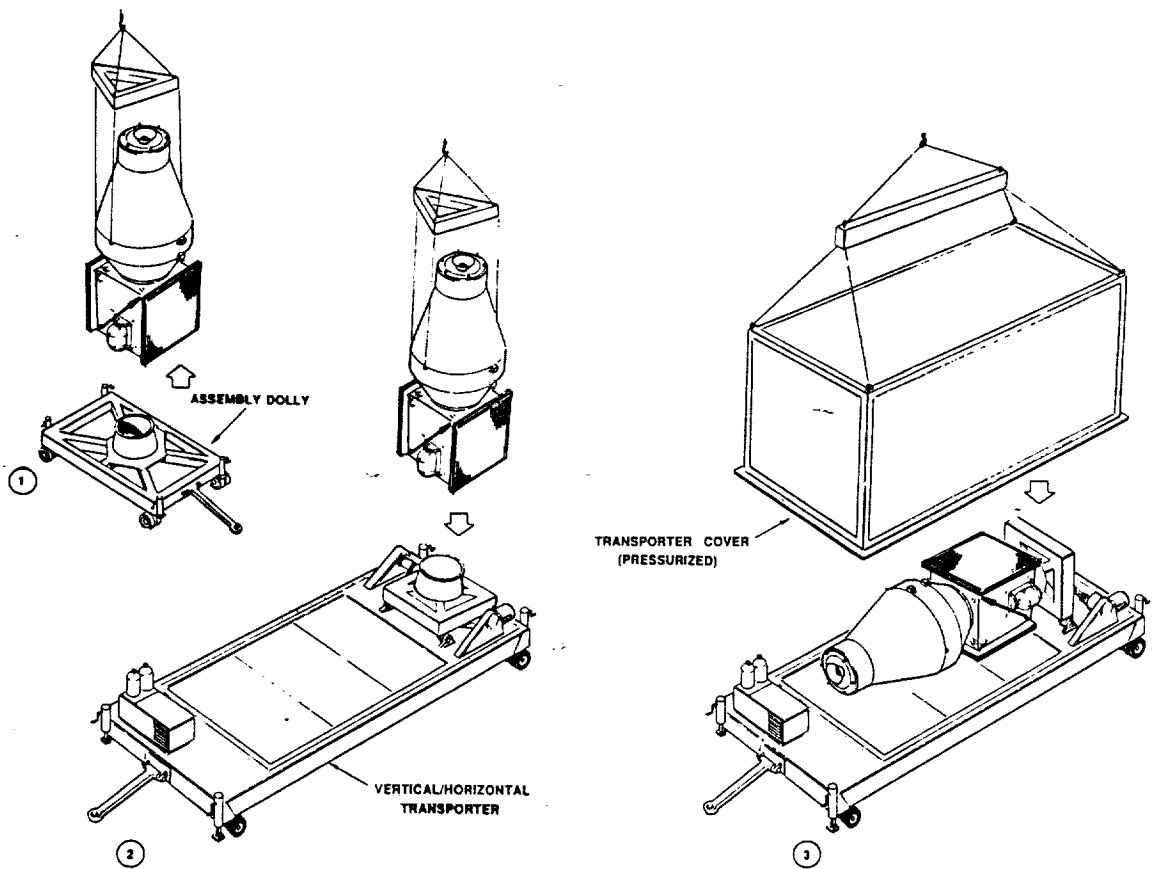


Figure 9-3. Preparation of Spacecraft for Transport

The sealed transporter is small enough to allow transport of the spacecraft by either overland truck or by air. While C-130 and larger aircraft have been used to transport vehicles of similar size, FAC has used overland truck transport for the majority of their spacecraft shipped to KSC. Since there are no identified requirements that would dictate air transport, cost and schedule are perceived as the main drivers for determination of transportation mode to be used.

9.2 LAUNCH PAD MODIFICATIONS

Since the Atlas family of vehicles employs cryogenic propellants, minimal pad modifications will be required to meet COLD-SAT fluid supply and delivery requirements. For fluid supply, current storage capacity for LH₂, GHe, and GN₂ is adequate to meet COLD-SAT requirements.

High pressure GN₂ is supplied to SLC-36B from a constant source pipeline such that COLD-SAT requirements can be met for either Atlas I or II configurations. For GHe, storage capacity for Atlas I allows marginal adequacy for COLD-SAT because of GHe purge requirements for Centaur insulation panels. With Atlas II this purge is no longer required, and scheduled increases in GHe storage capacity will easily satisfy COLD-SAT requirements. LH₂ storage capacity and requirements for Atlas configurations and COLD-SAT are summarized in Table 9-1. Note that all vehicle/spacecraft requirements include LH₂ reserves for a two hour contingency countdown hold. While all LH₂ requirements can be readily met for Atlas I, for Atlas II LH₂ capacity appears marginal. This could be improved by reducing storage facility boiloff losses through modified tanking procedures and schedules. By tanking far enough in advance to allow saturation, and then topping off the facility two to four days prior to launch, boiloff could be compensated, allowing ample LH₂ margin for COLD-SAT tanking.

Table 9-1. SLC-36B LH₂ Capacity and Requirements Summary

LAUNCH VEHICLE	LH ₂ STORAGE CAPACITY (m ³)	LH ₂ REQUIRED (m ³)*	FACILITY BOILOFF (m ³)**	LH ₂ AVAILABLE (m ³)	COLD-SAT LH ₂ REQ'D (m ³)
ATLAS I	106	83	3	20	7.5
ATLAS II	106	91	3	12	7.5

* Includes reserve for two hour contingency countdown hold

** Storage facility boiloff is about 5.7 m³/week

Hardware modifications at SLC-36B required to deliver fluids to COLD-SAT are also minimal. High pressure GN₂ is available on the umbilical tower at the payload service swing boom elevation, and high pressure GHe and LH₂ sources are located at the Centaur service swing boom located below the payload service boom. From these locations, new supply lines would be connected and routed to COLD-SAT along with electrical cables. To accomplish this, a reworked Titan/Centaur (Centaur T4) disconnect panel is attached to the experiment outer structure and mated with a retractable ground panel (see Section 8.3.1 for details). An arrangement for the umbilical lines running between the panel and the launch complex umbilical tower is shown in Figure 9-4. This arrangement uses a retractable boom, higher on the tower than the payload service boom, that is similar to that used for Titan/Centaur. It extends to a position for minimizing the draped line lengths and loads on the experiment disconnect panel while allowing adequate flexibility for movements between the Atlas and the tower. In the final analysis, the station location and clock position of the retractable boom, the drape line lengths, the angular sweep of the payload service swing boom, and the location of the payload fairing air conditioning GSE umbilical would be considered to assure clearances. Lanyard tethers can also be employed to limit the motion of the drape lines after disconnection. Since the drape line sizes are small, additional studies would include an alternate approach which replaces the retractable boom with umbilical drape lines running directly from the tower. In this case, the motion of the drape lines after disconnecting would be limited with tethers.

There is an allowable range for the clock position of the panel on the experiment, thus a position can be chosen which ensures adequate clearance between the swing boom and the drape lines. Some typical Atlas II vehicle umbilical interface locations are summarized in Figure 9-5. Atlas I locations

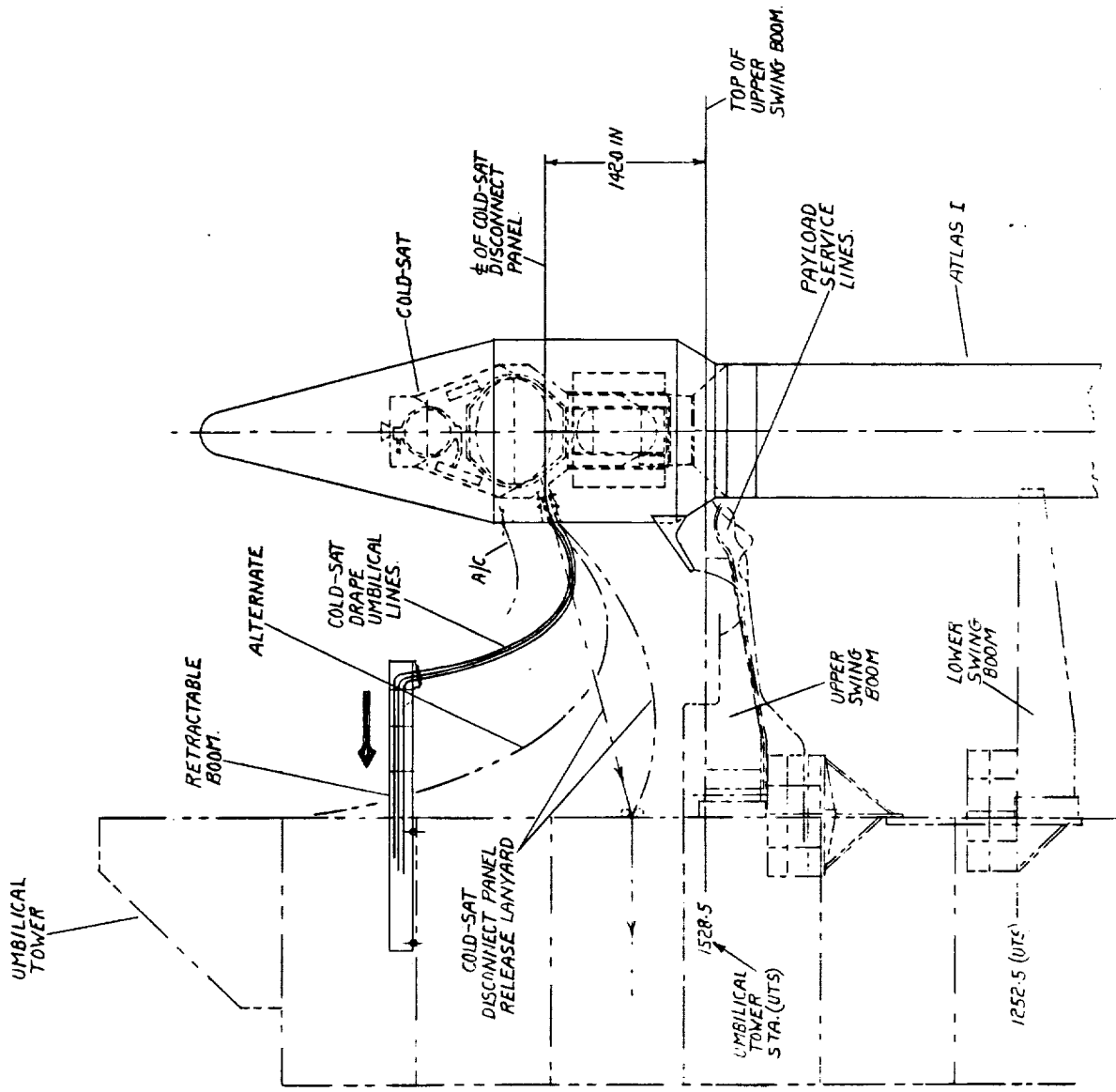


Figure 9-4. Launch Complex COLD-SAT Umbilical Arrangement

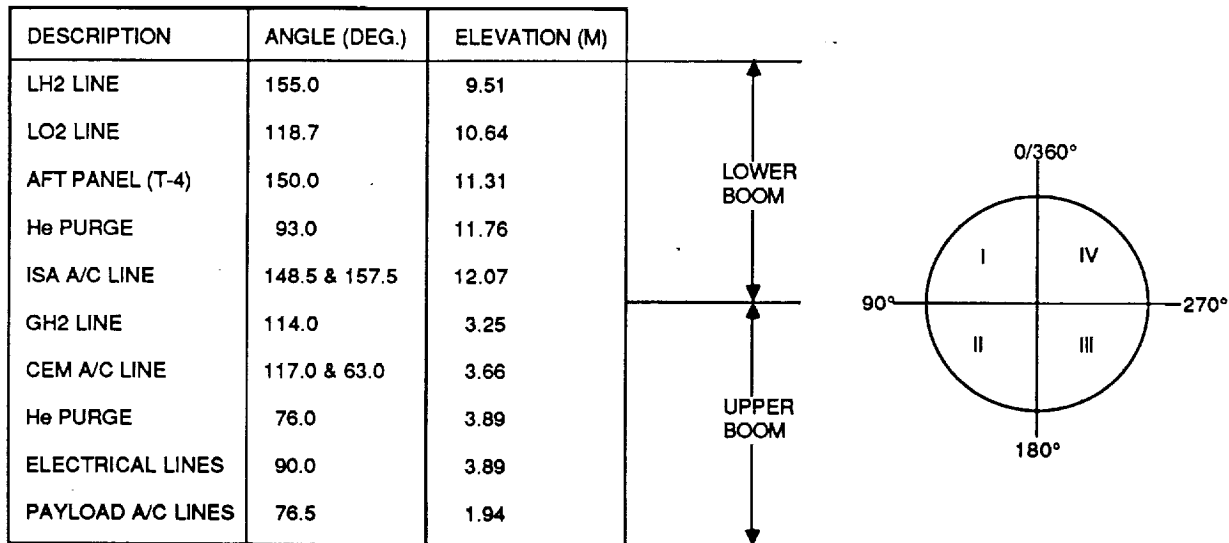


Figure 9-5. Typical Umbilical Interface Locations for Atlas II

would be similar, and these locations for COLD-SAT will need to be determined in future studies. Hydrogen is vented from COLD-SAT through a connection to the Centaur vent line. In addition to the fluid and electrical service lines, the following equipment would also be installed on the boom:

1. Modified Centaur T-4 aft umbilical panel
2. Panel disconnect/retract mechanism
3. COLD-SAT purge control module
4. Purge control module instrumentation and control cables

9.3 GROUND OPERATIONS AND LAUNCH PREPARATION

Launch preparations for COLD-SAT begin with advance team arrival at the launch site approximately 53 days prior to launch. The first eleven days of preparation address test equipment unloading, set up, and calibration prior to arrival of the spacecraft. Spacecraft arrival is scheduled 42 days prior to launch. Battery function tests, RF calibration and Attitude Control System (ACS) checks are made at this time.

Following initial checks and calibration, the spacecraft will be moved into its test stand and prepared for functional and performance testing. ACS performance, solar array, telemetry, tracking, and control (TT&C), electrical power system (EPS), and momentum wheel/Earth sensor systems will be tested at this time. During this testing period, ordinance and electro-explosive device harnessing will also be installed and tested.

Next, the spacecraft will be transported to the Hazardous Processing Facility (HPF), and the Blockhouse Test Set (BTS) will be moved to the blockhouse for continuity and isolation checks. In the HPF, the spacecraft will be prepared for propellant and propellant pressurant loading, and the RF link to the payload processing facility will be established and checked. Following hydrazine testing, loading, and leak checks, the H₂ and He experiment pressurant bottles will be pressurized to flight levels and the spacecraft closeout performed. Next the spacecraft will be mated to the Centaur adaptor and continuity checks will be performed. At this point, the assembly will be transported to SLC-36 for mating to the launch vehicle.

After mating the spacecraft and adaptor to the launch vehicle, functional interface checks will be made on fluid, electrical, and power systems interfaces and spacecraft thermal closeout performed. Spacecraft batteries will be charged and set on a trickle charge and watch schedule, the payload fairing will be installed and launch rehearsals including tanking tests will be conducted. Launch preparation activities come to an end at this point, and the Launch countdown formally begins two days prior to launch.

9.4 LAUNCH COUNTDOWN

Launch countdown operations for COLD-SAT begin approximately 48 hours prior to the scheduled launch time, with initiation of the GN₂ purge for the experiment module, spacecraft bus, solar array drive assemblies (SADA), and the high gain antenna gimbal. The purge process will switch to GHe at approximately one hour prior to tanking operations for COLD-SAT Tank 1.

Twenty-four hours prior to launch, data link configuration, software initialization, and ground control interface checks will be performed. During this period, COLD-SAT telemetry will be available for health checks and real-time monitoring during the launch countdown. At approximately ten minutes prior to launch, the spacecraft will be placed on internal power for final determination of launch status. A chronological summary of countdown events expressed in Launch "minus" time is shown in Figure 9-6. Details of the COLD-SAT tanking, vent, and thermal control purge procedures and timelines are discussed and illustrated in the following sections.

9.4.1 Tanking

COLD-SAT tanking operations will require approximately 65 minutes to complete. This includes a ten minute chill, fast fill to approximately 96 percent of tank volume, followed by topping to 98 percent of tank volume at approximately 0.038 kg/s total flow to compensate for the 0.017 kg/s boiloff rate, and provide sufficient net topping capability to be time efficient. The tanking timeline is shown in Figure 9-7, and compares the nominal Atlas I (Centaur) timeline to the revised requirements necessary for COLD-SAT tanking operations. COLD-SAT chilldown and subsequent tanking have been timed to occur after the completion of Centaur LH₂ chill. This is necessary to avoid impacting the flowrate-critical Centaur chill operation. The result is a ten minute extension of the planned ten minute hold that occurs nominally at the L-15 minute mark in the countdown. The resulting extension does not impact Atlas I operations, and can be accommodated without significant changes in nominal launch operations, or existing SLC-36 resources.

9.4.2 Venting

Analysis of the ground-to-orbit heat flux indicates that approximately 347 W/m² will be input to COLD-SAT Tank 1. Using this as a basis for pressure rise determination, venting of Tank 1 during the ascent portion of the flight will be required until the payload fairing is jettisoned resulting in a significant drop in the heat flux rate.

Two basic options exist for venting Tank 1: (1) using an independent vent fin, and (2) interfacing with the Centaur vent line between the existing vent fin and the Centaur vent valves. The independent vent configuration is considered to be prohibitively expensive in hardware design, and development costs associated with the modification of the payload fairing. While some additional costs will be required for analysis of the Centaur interface configuration to ensure compatibility, it is concluded that this method will be much lower in overall cost to the program.

Examination of the interface vent configuration indicates that the vent pressures for Tank 1 may be driven by Centaur, due to Centaur vent pressures, the desire to keep COLD-SAT tank pressures as

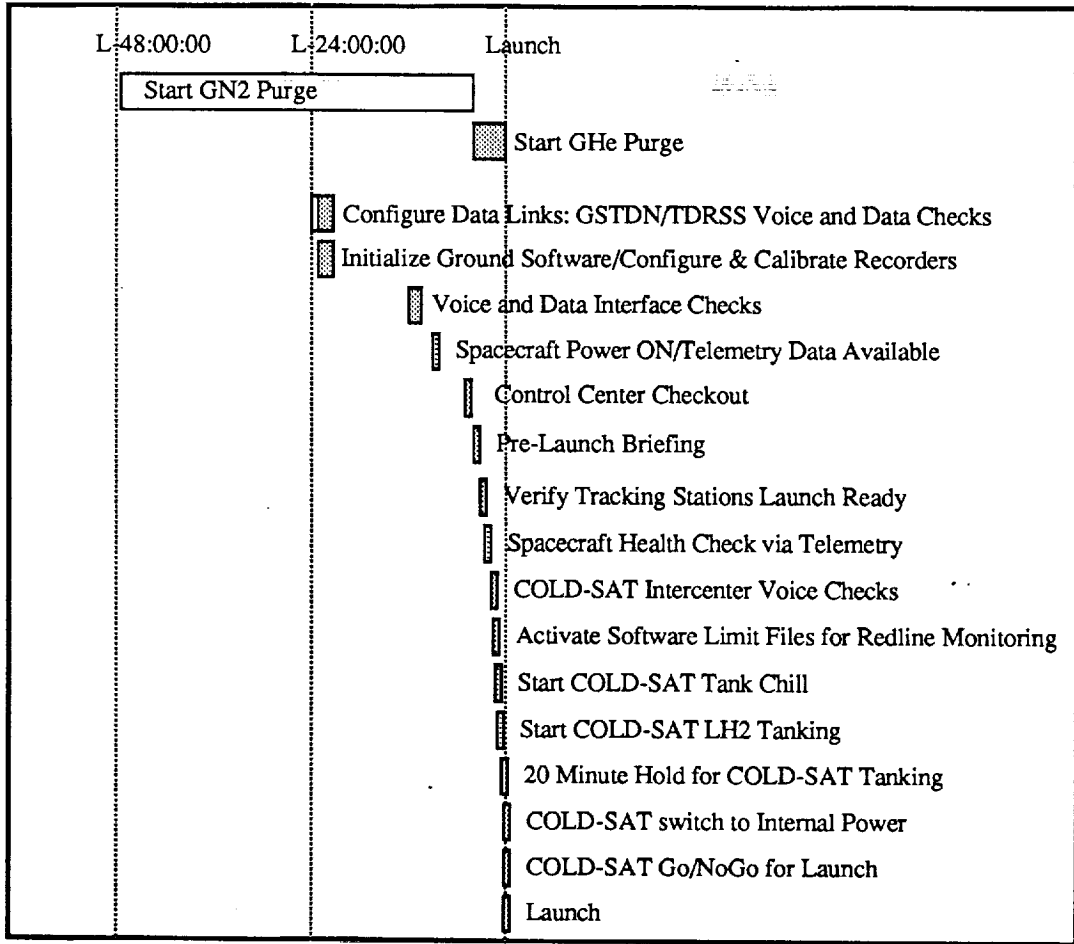


Figure 9-6. Summary Launch Countdown Timeline

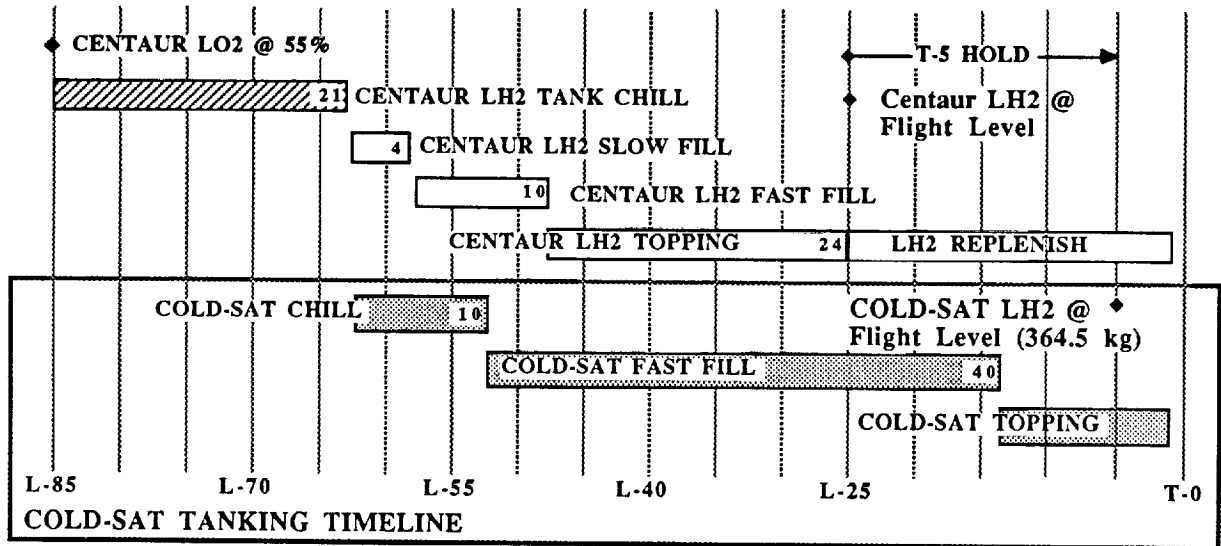


Figure 9-7. COLD-SAT Tanking Timeline

low as possible, and the need to avoid vent backflow between Centaur and COLD-SAT. Potential backflow into the COLD-SAT Tank 1 will be prevented by the check valve installed in the vent line upstream of the connection to the Centaur vent as shown in Figure 9-8. The Centaur H₂ vent function is performed by a self-regulating vent valve that operates between 131 and 145 kPa. This valve has backflow prevention that will prevent the ingestion of vent gas from the vent line. This configuration eliminates the need for active control of the COLD-SAT vent on the launch pad, and allows the Tank 1 vent valve to be held open during tanking, thus keeping Tank 1 pressure as low as possible prior to launch.

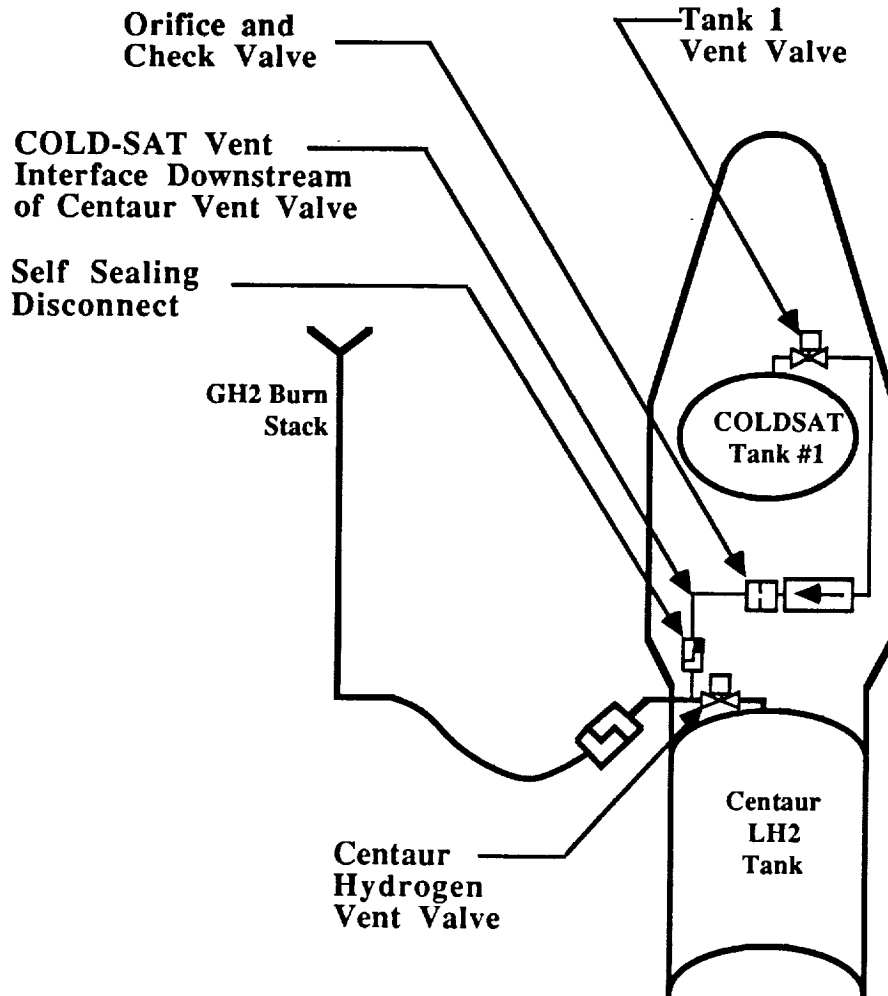


Figure 9-8. COLD-SAT/Centaur Vent Interface Schematic

Just prior to launch, the Centaur vent function switches to a DCU-controlled solenoid valve for flight, and the pressure band shifts upward on a varying flight profile that tops at 200 to 214 kPa. The COLD-SAT Tank 1 vent valve will be activated at this time and the pressure control band will be set to a range of 262 to 276 kPa. To avoid backflow of COLD-SAT vent gas into the Centaur, the orifice in the Tank 1 vent line is used to provide a significant pressure drop in the vent line upstream of the Centaur interface. This venting arrangement will be maintained during the boost phase. At separation from Centaur, the vent path through the Centaur vent fin is closed by the self-sealing

disconnect at the interface. Following this, the COLD-SAT tanks are vented through the COLD-SAT balanced-thrust vent system.

9.4.3 Thermal Control/Purge

The multi-layer tank insulation purge system configuration is described in detail in Section 5.4.2. Key operational features of the airborne purge system include:

1. Inboard purge line to supply conditioning gas
2. Outboard purge line to supply or exhaust conditioning gas
3. Micrometeoroid/debris shield (MMS) purge line
4. Purge containment vent door

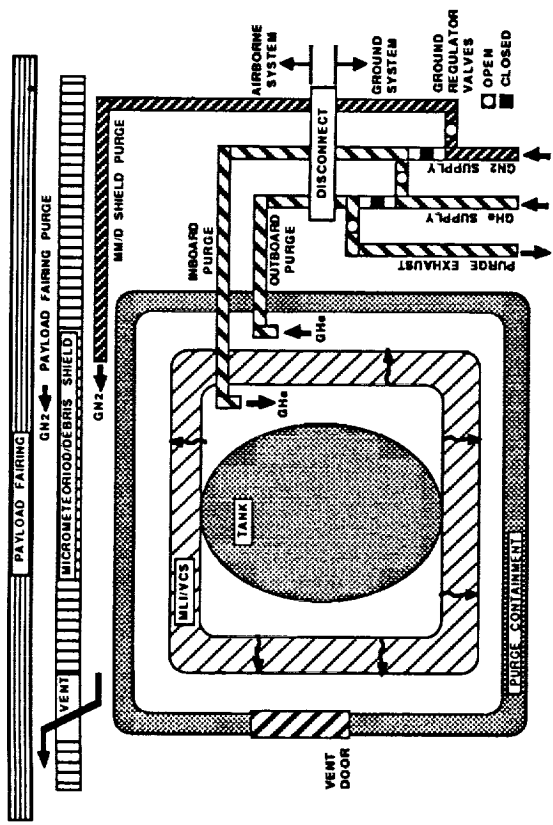
The inboard purge line supplies conditioning gas (GN₂ or GHe) under the multilayer insulation (MLI) and between Tank 1 and the MLI. The MLI is perforated to allow permeation of conditioning gas. The outboard purge line supplies or exhausts conditioning gas between the MLI and purge containment. The purge containment shroud is sealed to minimize leakage of conditioning gas. The MMS purge line supplies GN₂ between the purge containment and MMS. The MMS has an open vent to allow exhaust of GN₂ to the payload fairing. The purge containment vent door allows evacuation of GHe from the MLI during ascent. The vent door remains closed until launch.

The purge system is connected to the ground supply/exhaust through an umbilical disconnect and a purge control module containing five valves. The purge control module regulates the GN₂ and GHe supply flowrates, and interconnects the supply and exhaust lines to provide the required purge sequence. The nominal inlet temperature is approximately 297 K for both the GN₂ and GHe conditioning gas. The sequence of events for the ground purge conditioning is given in Table 9-2 and a schematic representation of the sequence is given in Figure 9-9.

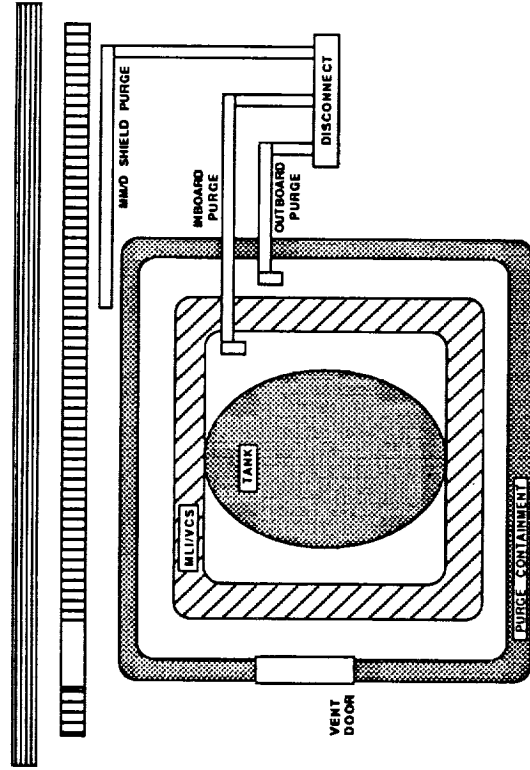
Table 9-2. Sequence of Events for the Ground Purge Conditioning

EVENT SEQUENCE	NOMINAL TIMELINE	NOMINAL* FLOWRATE	DESCRIPTION OF SEQUENCE
A. INITIAL GN ₂ CONDITIONING	Within Two Days Prior to Tanking	Inboard Line GN ₂ at 5 kg/hr	GN ₂ is introduced through the inboard purge line to drive out any water vapor, and is exhausted through the outboard purge line.
B. INITIAL GHe CONDITIONING	One Hour Prior to Tanking	Inboard Line GHe at 27 kg/hr	Conditioning is then switched to GHe to displace the nitrogen in the containment cavity and MLI.
C. MAINTAINANCE GHe CONDITIONING	After Tanking	Outboard Line GHe at 2.3 kg/hr	Inboard purge is discontinued and the outboard purge line supplies GHe to the outside of the MLI to make-up for leakage.
D. ASCENT EVACUATION	At Liftoff	Conditioning Flow Off	At launch all purge conditioning stops and the vent doors on the purge containment shroud are opened to allow helium to flow out from the purge cavity and MLI.

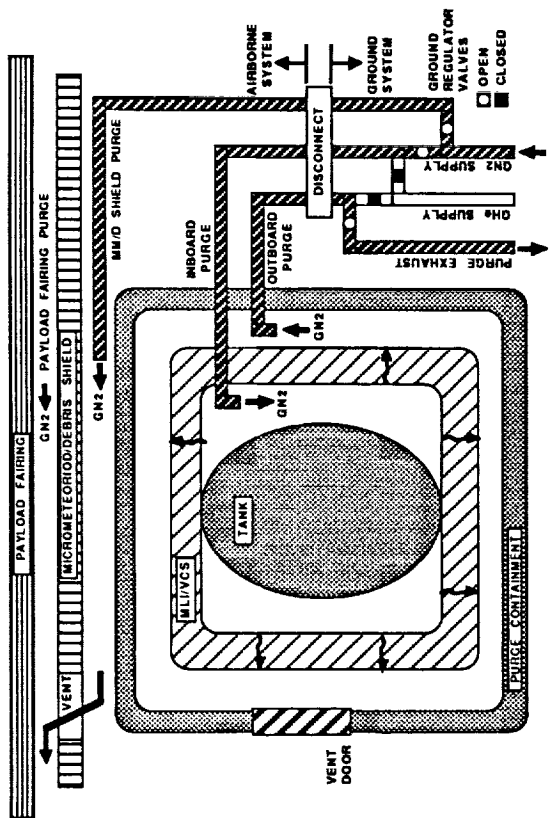
* Nominal flowrate for inboard or outboard purge line only.
 Nominal flowrate for GN₂ micrometeoroid/debris shield purge line is 4.5 kg/min.
 Nominal flowrate for GN₂ payload fairing purge line is 68 kg/min.



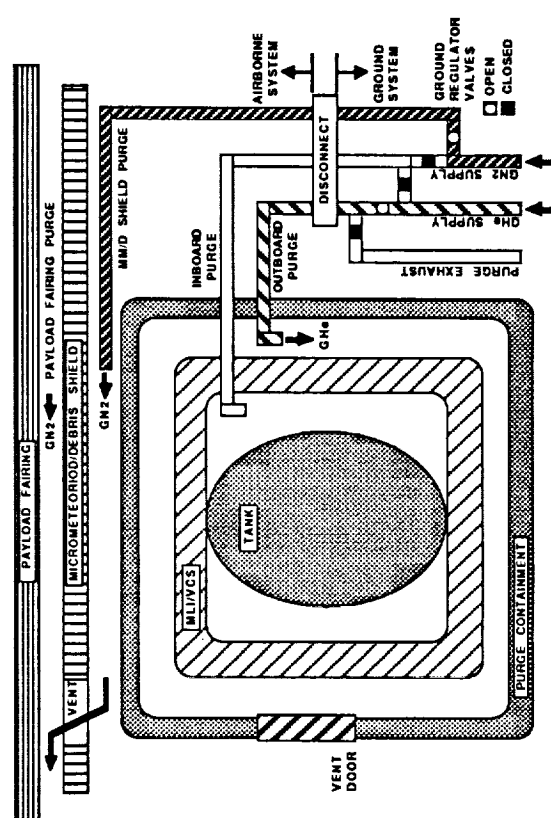
B. Initial GHe Conditioning



D. Ascent Evacuation



A. Initial GN2 Conditioning



C. Maintenance GHe Conditioning

Figure 9-9. Schematic Representation of Insulation Purge Sequence

9.5 ASCENT/TRANSFER ORBIT

During the ascent and transfer orbit flight, COLD-SAT is relatively inactive at standby power levels with limited telemetry of approximately 1 KBPS available through the Centaur interface. Spacecraft guidance, health monitoring, and Tank 1 pressure control are the primary functions performed during this phase of the mission.

Atlas I liftoff officially begins at 51 mm motion (Atlas I 51 mm off the launch pad.). All Atlas engines are operating at liftoff. At two seconds after liftoff, Atlas starts a preprogrammed roll program which continues for thirteen seconds. The Atlas pitch and yaw programs are initiated at fourteen seconds after liftoff and continue until Atlas booster engine cutoff (BECO). Booster engines perform these pitch and yaw maneuvers as the sustainer engine is locked to null. The specific pitch and yaw programs flown are selected on launch day to minimize wind-induced loading on the vehicle. BECO occurs at an accelerometer reading of 5.5 g. The booster package is jettisoned 3.1 seconds after BECO.

The flight control system holds a constant vehicle attitude through payload fairing jettison, which occurs 44 seconds after insulation panel jettison. Sustainer engine cutoff (SECO) occurs when propellant depletion is sensed by either an LO₂ pressure switch or a sensor in the fuel tank. Two seconds after SECO, the pyrotechnic system releases the Centaur from the interstage adaptor.

The Centaur control system begins 3.5 seconds after SECO. At this time, Centaur engine prestart valves are opened, providing control capability and initiating the propulsion system chilldown. The first Centaur main engine start (MES 1) occurs about twelve seconds after SECO. Closed loop guidance starts at twenty seconds after MES 1 and continues until Centaur main engine cutoff (MECO). MECO 1 is directed by guidance when the proper orbit is achieved.

During Centaur coast phase, vehicle attitude and propellant retention is controlled by the smaller reaction control motors. Shortly before MES 2, the reaction motor system orients the vehicle to the proper attitude for ignition. The reaction motors then fire to settle the propellants, and a second chilldown occurs for seventeen seconds before MES 2. MES 2 is initiated by guidance and continues until guidance calculates that the vehicle is properly on the mission orbit.

After separation, Centaur is turned away from the spacecraft. The reaction motors fire for 45 seconds to move Centaur away from the spacecraft. Another motor burn is initiated for 76 seconds until propellant blowdown begins. Blowdown may require several minutes to accomplish, during which time the Centaur is on an orbit considerably different from the COLD-SAT.

9.6 ON-ORBIT OPERATIONS

At separation from the Centaur, COLD-SAT will have an initial roll rate of 2 rpm. Pitch and yaw will be minimal unless tip off rates are encountered. The TC & R antenna and high gain antenna will be pyrotechnically released. The high gain antenna gimbal mechanism will be enabled, allowing the antenna to track TDRS. Commanding from ground stations may then commence, and by either stored or ground initiated command mode, COLD-SAT will be commanded to a stable control mode in preparation for solar array deployment.

9.6.1 Deployment and Checkout

Once the antennae and arrays are deployed, Earth acquisition mode will be commanded. The solar arrays will be slewed to sun normal, and then commanded to run mode. Attitude acquisition events are detailed in Table 9-3 with event times based on local spacecraft time. It is assumed that, (1) eclipses are 35 minutes long, and (2) TDRSS or GSTDN are available for command relay for the

acquisition sequence. If this is not the case, the reconfiguration to on-orbit mode will require more time.

Table 9-3. Attitude Acquisition/Deployment Timeline

Orbit	Time from Eclipse (min)	Event Description
1	0	Turn on AOCS
	10	Checkout DIRAs
	15	Vent Propulsion
	30	Thruster Verification
	45	Initiate Spin-down
	50	Sun Acquisition
2	0	Roll Earth Acquisition
	10	DIRA Attitude Reference Mode
	20	Warm-up North Wing Prior to Deployment
	30	Solar Array North Wing Deployment
	40	North Solar Array Deployment
	50	Warm-up South Wing Prior to Deployment
	60	Solar Array South Wing Deployment
	70	South Solar Array Deployment
3	0	Roll Earth Acquisition
	10	Pitch Earth Acquisition
	20	Slew North Solar Array to Sun
	35	Slew South Solar Array to Sun
	50	Configure Heaters
	60	Transition to On-Orbit Mode
4		On-Orbit Checkout

9.6.2 Spacecraft Bus Operations

Once in on-orbit mode, the spacecraft will require minimum commanding. Under control of the SCE, the spacecraft can function autonomously for up to 28 days. The processor generates necessary signals to maintain attitude for all mission phases, including pointing the spacecraft +X/-X axis along the velocity vector for the experiments, pointing the solar arrays and communication antennae, and maintaining attitude during thrusting maneuvers.

On-orbit operations consist of monitoring spacecraft telemetry data for health and safety, collecting experiment data via the seven minute long data dump each orbit, and uplinking commands to the spacecraft as needed to accomplish:

1. Experiment preparation and operations;
2. Spacecraft housekeeping and experiment support operations;
3. A monthly (approximately) 180 deg. roll maneuver.

Real-time telemetry will be monitored for approximately ten minutes per orbit, simultaneously with the recorder dump. The stored data dump will occur on the TDRS S-band multi-access (SMA) "I" Channel at 38 KBPS, while the real-time data will be carried on the SMA "Q" channel at 2.4 KBPS.

Eleven times per year a 180 deg. roll maneuver (or a 180 deg. pitch maneuver if it is necessary to limit orbit altitude increase caused by thrusting to provide experiment accelerations) is required to keep the solar array near normal to the sun. This maneuver should be performed at or near 6:00 am/pm local spacecraft time to minimize the solar array slew angle. Analyses that must be performed in near real-time prior to the maneuver include:

1. Verification of center of mass offset determined by the SCE;
2. Verification of thermal parameters within limits;
3. Verification of sufficient battery charge to support the maneuver;
4. Verification of thruster performance.

Maneuver timing is determined by power constraints and will require near real-time analysis. The sequence of events is detailed in Table 9-4. Before initiating an experiment, the control system will be reconfigured in one of two ways. First, for no-thrust experiments, which require very low acceleration fields, the spacecraft will be configured to minimize all torque effects. This is accomplished by decreasing control loop gains, and enabling magnetic torquers to provide wheel unloading. Second, for experiments requiring high thrust, the DIRAs will be calibrated and selected for control, thrusters will be enabled such that when activated, continual wheel unloading by off modulation of selected thruster firings is performed to prevent wheel saturation.

Table 9-4. Roll Maneuver Timeline

Step Duration (min)	Event Description
5	Enable Thrusters
20	DIRA Calibration
10	DIRA Attitude Reference Mode
5	Disable SADA
25	180° Roll Bias
1	Verify Attitude
10	Roll Earth Acquisition
10	Pitch Earth Acquisition
15	Slew North Solar Array to Sun
15	Slew South Solar Array to Sun
10	Transition to On-orbit Mode

9.6.3 Experiment Operations

During the COLD-SAT mission, the TDRS network will provide uplink and downlink telemetry services as well as tracking support, with some backup downlink capability supplied by the GSTDN system. COLD-SAT will continuously record experiment and bus data throughout the mission. Data will be stored on board in bubble memory, and will be dumped once per orbit during a scheduled ten minute TDRSS coverage window. During this window, the previous orbit's data and real-time data will be downlinked and recorded for processing. Command uplink for the next orbital period of bus and experiment activity will also be performed during this window.

9.6.3.1 Experiment Control. Experiment control will be performed by generic, function specific software shells. Each experiment function (i. e. tank chill, no-vent fill, etc.) will be performed by a specific shell resident in SCE memory. Experiment shell identification, individual component activation, logic test limits, and instrumentation value limits for a particular experiment will be uplinked to spacecraft RAM as a control data set, along with execution time tags. Prior to

9.6.3.3 Integrated Experiment Plan. Class I and II experiments for the COLD-SAT mission have been combined to form an integrated experiment plan. This plan provides individual tank LH₂ quantity accounting, boiloff, and experiment losses, as well as cumulative elapsed time and total LH₂ remaining. Two versions of the integrated plan have been generated to determine the effects of additional time required for ground support shift scheduling. These plans are included in Appendix D.

The first version assumed non-stop experiment operation for 24 hours a day, seven days a week until all experiments defined in the ERD have been performed. This plan indicates that all defined experiments can be performed in 51 days with approximately 28 kg of LH₂ remaining. This plan does not include any additional time for anomaly resolution or modified experiment "repeats" that may occur.

The second version reflects the shift scheduling guidelines provided by the NASA/LeRC/CFTO as follows:

1. Two shifts per day, seven days per week for the first month;
2. Two shifts per day, five days per week for the next two months;
3. One shift per day, five days per week for the remainder of the mission.

The "shift scheduled" plan extends to 64 days in length, and as a result of the additional boiloff, all of the defined experiments cannot be completed. An effort to minimize the additional LH₂ loss was attempted by scheduling the eight hour shift breaks coincident with experiment operations that required minimal ground support. These operations include post-transfer thermodynamic conditioning, TVS experiments, prechill tank heating, and tank chill. Experiments that cannot be performed are listed in Table 9-5 by ERD experiment number, and are cross referenced to the appropriate tank.

The first incomplete experiment is encountered at 48 days into the mission. At that point there is approximately 80 kg of usable LH₂ onboard, but this is insufficient to perform a fill experiment in Tank 2 which requires 85 kg of LH₂. Similar conditions occur at 57 days into the mission for experiments in Tank 3. At this point 33 kg of usable LH₂ remains, with fill experiments in Tank 3 requiring 42 kg.

Table 9-5. Incomplete Experiments in the Shift-Scheduled Plan

	Tank 2	Tank 3
No Vent Fill	I-4.13	I-4.8
Vented Fill	II-9.10	II-9.6

At this point in the development of the COLD-SAT concept, the safety analyses have identified many of the potential accident areas which must be analyzed further. The spacecraft design and ground operations will be in accordance with Eastern Space and Missile Center Regulations (ESMCR 127-1) (Reference 10-1), Range Safety requirements, and Air Force regulations concerning Explosives Safety and Occupational Safety and Health. For payload (spacecraft) processing in Astrotech International Corporation facilities, compliance with their Safety Policy Manual (Reference 10-2) is required. Chapters 2-5 of ESMCR 127-1 identifies the spacecraft design and operational requirements that must be met to obtain range safety approval for launch. Reference 10-3 is a Preliminary Satellite System Safety Package prepared under this contract.

10.1 LAUNCH VEHICLE AND COLD-SAT GROUND SUPPORT

The Commercial Atlas I vehicle is baselined by GDSS as the Expendable Launch Vehicle (ELV) for COLD-SAT. The Commercial Launch Services (CLS) division of General Dynamics will provide a specific set of design and operations requirements that define spacecraft-peculiar Range Safety and spacecraft processing requirements. All of COLD-SAT fluid GSE requirements are met with currently developed hardware that is used for Centaur LH₂ fueling and inflight venting connections. The experiment tank ground/ascent vent is routed along the side of the payload fairing to allow for an interface with the existing Centaur ground/ascent venting system. At the time of fairing separation, the vent line to the experiment is detached by means of a vent line disconnect activated by fairing motion forces. The Centaur vent system is detached in the same manner. The existing launch pad umbilical tower will service the COLD-SAT experiment as well as the Centaur upper stage. A duplicate umbilical/retention system from Centaur GSE will be installed higher up the tower to perform required ground support for COLD-SAT. Umbilical disconnect and retraction is initiated at liftoff similar to the current Centaur system.

10.2 HAZARDS

10.2.1 On-Orbit Environment

The low-Earth-orbit environment includes hazards caused by micrometeoroids and man-made debris. To meet a reliability goal of 0.92 for Class I experiments, analysis indicates the need for shielding around the experiment to prevent tank and fluid line penetration and/or damage to the insulation. Therefore, the experiment primary structure surrounds the experiment module, and is a semi-monocoque design consisting of aluminum honeycomb with aluminum inner and outer skins and aluminum structural ring elements. This structure carries experiment module loads and provides the desired protection against micrometeoroids and debris.

10.2.2 Tanks

The experiment LH₂ tanks are designed and analyzed according to MIL-STD 1522A, The Safe Design and Analysis of Pressurized Missile Structures. The ultimate factor is 1.25 which comes from the MSFC Handbook 505. The tanks are designed for the pumping of LH₂ from Tank 1 to the other tanks dependent upon which experiment is being conducted. Gaseous helium and gaseous hydrogen pressurization tanks for experiment use are vendor items selected on availability, space qualification and a structural safety factor of 2.0. Pressurization tank maximum operating pressure is 27.6 MPa with the design pressure being 55.2 MPa.

10.2.3 Bus Subsystems

A preliminary identification of the major hazards, and the design features implemented to mitigate the probability of occurrence are listed in Table 10-1. These features spans the design, manufacture, test, and operational phases of the COLD-SAT program. Table 10-2 lists the procedures and design specification/drawing that will be used to assure all necessary safety considerations are addressed, and Table 10-3 list the major safety restrictions imposed by the COLD-SAT safety policies. These have been identified to a commensurate level with the system design maturity, and during subsequent design phases, more detailed issues will be analyzed to assure that all hazards are considered and evaluated to minimize their impact.

10.2.4 Ordnance Subsystems

All ordnance operations on the ETR are considered hazardous and are subject to stringent controls. These operations normally consist of transportation/shipment/mating, electrical connection, render safe, removal/demate, launch and disaster control. The COLD-SAT specific ordnance subsystems include liquid propellants defined by DOD for siting, storage and handling purposes, and the entire electroexplosive subsystem which includes the power source, firing circuits, control circuits, monitoring circuits, and initiation devices. The design of these subsystems shall be in accordance with ESMCR 127-1, paragraphs 3.13 and 5.13, and be covered by a Range Safety-approved operating procedure.

Table 10-1. Preliminary Hazard Analysis

MAJOR HAZARD	DESIGN FEATURES	MAJOR HAZARD	DESIGN FEATURES
PROPULSION (RCS)		PYROTECHNICS (EED'S)	
Propellant Tank/ Lines Rupture Release of toxic substances hazardous to personnel	<ul style="list-style-type: none"> • Design to guidelines and safety factors req'd by ESMCR 127-1, Par. 3.12.2 & 3.12.3. • Maintain environmental temp. control to prevent tank over pressure • Design with materials compatibility 	Premature/Inadvertent Operation of EED's Premature deployment of appendages causing injury to personnel and/or damage to equipment	<ul style="list-style-type: none"> • Select approved initiators eg. NSI-1 (NASA) meeting req'm'ts of ESMCR 127-1 • Design wiring/shielding per ESMCR 127-1 req'm'ts for ordnance • Provide single failure tolerance against inadvertent electrical actuation of EEDs. • Make provision for tethering of deployables after EEDs are installed. Remove tethers on pad before launch.
Propellant Loading GSE Rupture and/or leakage of propellant Release of toxic substances hazardous to personnel	<ul style="list-style-type: none"> • Design propellant loading and pressurizing GSE to detailed requirements of ESMCR 127-1, Par. 3.12 • Use gas aspirators instead of water aspirators per NASA KSC letter CP-PSO-146-88, June 7, 1988 	MECHANICAL GSE	
Leakage of Propellant through fill/drain valves and/or thrusters Toxic hazard to personnel	<ul style="list-style-type: none"> • Select qualified fill/drain valves with primary & secondary seals • Provide single failure tolerance against inadvertent thruster valve opening (electrical) • Provide two series flow control devices (mechanical barriers) below propellant tanks. • Procedurally load & pressurize propulsion system late in the ground operations sequence to minimize time hazard 	Failure of Ground Handling Equipment Causing injury or death to personnel and/or damage to equipment	<ul style="list-style-type: none"> • Design lifting and handling equipment to ESMCR 127-1 Par. 3.6.2. • Conduct required proof tests and NDI • Inspect for cracks or damage prior to each use
ELECTRICAL		TT&C	
Electrical Short or Overload Resulting in fire and/or damage to equipment, injury to personnel	<ul style="list-style-type: none"> • Select flight proven materials • Design to accepted derating criteria • Use nonflammable materials where possible • Use conservative space-use electrical design practices • Provide appropriate fusing and/or current limiting devices. 	RF Radiation Personnel hazard if RF level is above safe levels where personnel are work- ing. Applicable during ground operations or on-pad transmissions	<ul style="list-style-type: none"> • Determine by analysis at what distance from antenna aperture the RF energy reaches a safe level. • Place warning signs and barriers to prevent personnel from approaching the RF source closer than the defined safe distance. Provide appropriate warnings in RF test procedures.
Battery Burst/ Electrolyte Leakage.	<ul style="list-style-type: none"> • Design battery pressure vessels to appropriate safety factor over worst case pressure build-up. • Perform pressure vessel lot burst tests to demonstrate design burst • Perform pressure vessel cycling tests to verify "Safe Life". • Provide audible warning system in charging GSE to preclude over pressure. 	INTERFACES	
		Satellite/Experiment Mechanical stress concentrations at attach points resulting in pressure vessel failure Electrical-inadvertent command/control signals producing hazardous results in experiment.	<ul style="list-style-type: none"> • Design for adequate safety margin. • Design for avoidance of stress concentration at mounting points • Hazardous electrical interfaces are TBD.

Table 10-2. Procedures Which Control Hazards

DESIGN SPECIFICATIONS/DRAWINGS	PROCEDURES (GENERIC)
<ul style="list-style-type: none"> • Satellite System Spec • Propulsion Subsystem Spec • TT&C Subsystem Spec • Electrical Subsystem Spec • Satellite/Experiment Interface Requirements Document • Individual GSE Design Specs for <ol style="list-style-type: none"> 1) Handling Equipment 2) Lifting Equipment 3) Propellant loading and pressurizing equipment 4) Integrated system test complex (ISTC) 	<ul style="list-style-type: none"> • Launch Base Operations Procedure • Propulsion Subsystem Operations (MEOP) • Propellant Loading and Pressurization • Ordnance Installation and Checkout • TT&C Performance (RF) • Satellite Transportation & Handling • Battery Charge/Discharge Operations • Satellite/Experiment Interface Verification • GSE Individual Unit Validation Procedures

Table 10-3. Major Safety Restrictions Imposed By Safety Policies

Propulsion System And Ordnance System	System design and operations must be in accordance with ESMCR 127-1.
RF Transmission	Design and operations shall be in accordance with ESMCR 127-1, Paragraph 3.8.1.
Satellite/Experiment Interfaces	At least single failure tolerance shall be provided against inadvertent occurrence of any potentially catastrophic satellite-controlled experiment function.
Handling and lifting GSE and propulsion loading GSE	Must comply in design and operations with requirements of ESMCR 127-1

11
RELIABILITY

11.1 SPACECRAFT RELIABILITY

The entire COLD-SAT spacecraft must have a system reliability of at least 0.92, exclusive of the launch vehicle, for accomplishing the complete set of Class I experiments. No reliability requirements are specified for accomplishing the Class II experiments, but if the Class I's and Class II's are intermingled, thus lengthening the time and increasing the number of operations conducted prior to completion of the Class I's, the Class II's will impact reliability and possibly impact system design.

The systems of the spacecraft bus are generally the same as or similar to those used on some Earth-orbiting satellites. Much of the experiment module systems either contain unique components or use familiar components in a unique system configuration. Thus the experiment module has been allocated a lower reliability design goal than the spacecraft bus. The anticipated maximum on-orbit time required to accomplish the Class I experiments is six months. For this period, Table 11-1 gives allocated design goals and estimated reliabilities for the spacecraft bus, experiment module systems, and micrometeoroid/debris shield. The estimated overall reliability is 0.9506. The design philosophy for achieving these goals includes:

- Use of redundancy and other enhancements to reduce the number of single-point failure modes;
- Use of proven designs and design concepts to the extent possible, including previously qualified or flight-proven designs;
- Use of fail-safe and fault-tolerant designs;
- Use of redundant electronic assemblies with extensive cross-strapping;
- Use of redundancy for some electro-mechanical and mechanical components;
- Short circuit protection for all electronic systems;
- Minimization of component types;
- Parts derating to enhance reliability.

Table 11-1. COLD-SAT Reliability Goals for Class I Experiments

<u>Design Area</u>	<u>Allocations</u>	<u>Estimates (6 Months)</u>
Spacecraft Bus Module	0.975	0.9926
Experiment	0.954	0.9674
Micrometeoroid/ Debris Shield	0.990	0.990
Overall	0.920	0.9506

11.2 BUS MODULE RELIABILITY

The failure rates, modeling considerations, and redundancy implementations used in the reliability assessments for the bus subsystems are derived principally from current geosynchronous spacecraft programs including INSAT, GOES, SCS and INTELSAT V and INTELSAT VII. The appropriate adjustments in failure rates and duty cycles have been incorporated for low Earth orbit environmental considerations for items such as the batteries and solar array drive mechanisms.

Some of the key reliability features of the COLD-SAT bus subsystem design, in addition to those already mentioned, include specifically:

- Redundancy for momentum wheels, gyros, cable and rod cutters, etc ;
- Redundancy for all attitude control sensors and actuators using qualified and heritage or flight-proven designs;
- Redundant seats for thruster valves and a backup flow path for the helium pressure regulator;
- Current generation spacecraft control electronics design with full redundancy, frequent cross-strapping, increased operational flexibility for higher numerical reliability in the command, telemetry and attitude control processing functions than earlier spacecraft;
- Redundant squibs or pyrotechnic devices for all actuations (solar array deployments).

Most spacecraft bus failure effects in the conceptual design are isolated to single electronic units and will not disable or degrade the performance of the remainder of the spacecraft or redundant functional units. This approach to the COLD-SAT bus spacecraft design provides operational flexibility, fail-safe features, and the highest assurance of completing the COLD-SAT mission.

Table 11-2 provides a summary of the bus reliability results. The six month spacecraft bus reliability of 0.9926 exceeds the 0.9750 allocation assigned to the bus module.

Table 11-2. Spacecraft Bus Module Reliability Assessment Summary

Bus Subsystems	Ps(6 mo.)	Ps(1 yr)
TC&R Transponder	0.9984	0.9966
Spacecraft Controller Electronics	0.9997	0.9988
Electrical Power	0.9965	0.9920
ADCS	0.99997	0.9999
Propulsion	0.9981	0.9959
Structure	>0.9999999	>0.9999999
Solar Array Deployment	0.9999427	0.9999427
Total Bus	0.9926	0.9832
Bus Module Allocation	0.9750	

11.3 EXPERIMENT MODULE RELIABILITY

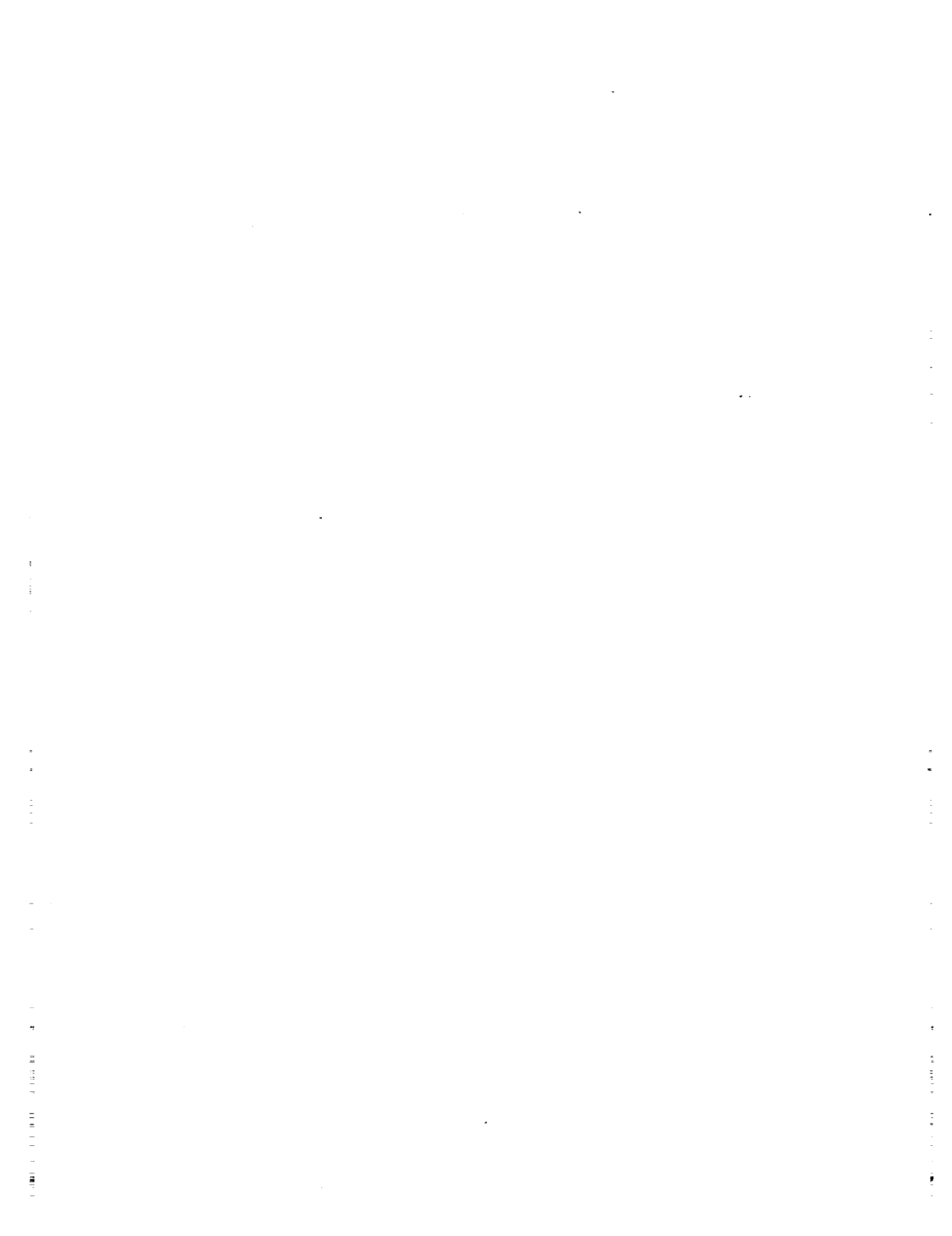
Specific experiment module components will be either active or dormant, depending on the experiment in process. Dormant failure rates have been assumed to be 10 percent of the active failure rate.

The equipment used for each experiment was identified, and was associated collectively as Tank 1, Tank 2 or Tank 3 equipment. A single-string design was defined for each group and its failure rate evaluated and coupled with the necessary operating time to define a minimum level reliability. The improvement factor thus needed to meet specified reliability requirements was defined, and redundancy features determined. The Tank 1 single-string failure rate was found to be lower than for the other two tanks, but it had much higher operating time, and thus set the pattern for redundancy configurations and helped establish where redundancy in the fluid system was most beneficial.

The active times were determined for each set of tank equipment, and the dormant times estimated as the remainder required to total six months. The overall reliability of each set of tank equipment was determined as the product of the active and dormant period reliabilities. The experiment module reliability for Class I experiments was then determined as the product of the three tank groups multiplied by the instrumentation reliability. Table 11-3 gives the estimated reliabilities, with the experiment module having a reliability of 0.9674.

Table 11-3. Experiment Module Reliability Assessment Summary

<u>Experiment Equipment Group</u>	<u>Ps (6 Months)</u>
Tank 1 Group	0.9883
Tank 2 Group	0.9895
Tank 3 Group	0.9939
Instrumentation	<u>0.9953</u>
Overall	0.9674



12.1 TECHNOLOGICAL RISKS

We have rated component technological risks based on technological maturity. We recognize that true risk also reflects complexity, dependency, failure probability, technical merit, and the consequences of failure based on cost, schedule and technical merit. In order to rate the technological maturity of each class of components they have been given a development category rating of A, B, C, or D according to the following definitions.

- A Those components which can use existing hardware or qualified designs.
- B Those components which require new designs, but for which existing and proven design techniques are available.
- C Those components which require new designs which are at or near the state-of-the-art.
- D Those components which require new designs which are beyond the state-of-the-art.

We have assigned a technical risk factor based on a 0.001 to 10 log scale. The rating of risk using a log scale allows risk to be evaluated on an order of magnitude basis. Items scored between 0.001 and 0.01 are low risk, and have either proven launch vehicle or spacecraft flight heritage, or are available as an off-the-shelf, high quality component. Items scored between 0.01 and 0.1 are low-to-medium-risk components which require a small amount of risk mitigation such as verifying minor package engineering modifications, or which are expected to satisfy qualification requirements based on similarity to components that are qualified to equivalent or more stringent criteria. Items rated between 0.1 to 1 represent medium to high risk and require risk abatement by conducting tests. Risk factors between 1 to 10 are allocated to high risk items. High risk components require technology demonstration or concept validation, a significant amount of package engineering, development and optimization for spaceflight applications, and full qualification testing.

12.1.1 Experiment Module

Tables 12-1 and 12-2 show the technical risk factor for the experiment module mechanical and avionics categories, respectively. The technology development category is the same as discussed in Section 5.11. Note that the scoring system allows the possibility of an item in the technology development category to have a low risk factor or conversely an item in the category for existing qualified hardware to have a high risk factor. The technology development category and technical risk factor are independent and do not necessarily correlate. The components of greatest concern are the H₂ two-phase flowmeters and cryogenic LH₂ pump. A flowmeter alternative is discussed in Section 5.11. Our present design allows for both pressurized and pump-assisted transfer of LH₂.

12.1.2 Spacecraft Bus

The design of the spacecraft bus has concentrated on using existing flight-qualified components where ever possible (see Section 7.1.4). The technological risk and heritage of the bus hardware is given in Table 12-3. There are five bus components that have a significant risk: the spacecraft structure, the spacecraft control electronics (SCE), the hydrazine tanks, the magnetic torquers, and the battery charge converter (BCC). The new structure will be based on technologies used in existing Ford Aerospace spacecraft. The spacecraft control electronics is being developed as part of the INTELSAT VII program and will have its critical design review in March, 1990. However, its data concentrator unit (DCU) for the experiment support will be customized to meet COLD-SAT experiment instrumentation interface requirements. New hydrazine propellant tanks and propellant management devices based on existing technology will be needed. The magnetic torquers must be sized and tested to match the spacecraft and orbital environment where they will be used, but this will

Table 12-1. Development Categories and Technological Risk Factors for Experiment Module Mechanical Components

TECHNOLOGY DEVELOPMENT CATEGORY*	TECHNICAL RISK FACTOR**	DESCRIPTION	COMMENTS
B	0.8	ACCUMULATOR	DESIGNED AND BUILT IN-HOUSE TO MIL-STD-1522A
B	0.8	BOTTLE, GASEOUS HELIUM	DESIGNED TO MIL-STD-1522A
B	0.8	BOTTLE, GASEOUS HYDROGEN	DESIGNED TO MIL-STD-1522A
B	0.05	DIFFUSER	DESIGNED AND FABRICATED IN-HOUSE
B	1	DISCONNECT, SELF SEALING	EATON IS CANDIDATE (ALT. NON SELF SEALING PLUS VALVE)
B	0.9	EVAPORATOR	IN-HOUSE DESIGN AND FABRICATION
A	0.001	FILTER, CRYOGENIC	AVAILABLE OFF SHELF FROM MANY VENDORS
A	0.001	FILTER, HIGH PRESSURE GAS	AVAILABLE OFF SHELF FROM MANY VENDORS
A	0.09	HEATER, ACCUMULATOR	RAYCHEM, TAYCO ARE SOURCES
A	0.09	HEATER, TANK 1	RAYCHEM, TAYCO ARE SOURCES
A	0.09	HEATER, TANK 2 LAD	RAYCHEM, TAYCO ARE SOURCES
A	0.09	HEATER, TANK 2 WALL	RAYCHEM, TAYCO ARE SOURCES
A	0.09	HEATER, TANK 3 VENT	RAYCHEM, TAYCO ARE SOURCES
A	0.09	HEATER, TANK 3 WALL	RAYCHEM, TAYCO ARE SOURCES
A	0.09	HEATER, VENT SYSTEM	RAYCHEM, TAYCO ARE SOURCES
C	1	LAD, TANK 1	SYSTEM DEVELOPMENT REQUIRED
C	1	LAD, TANK 2	SYSTEM DEVELOPMENT REQUIRED
A	0.2	MULTIPLE LAYER INSULATION	SHELD AHL, NATIONAL METALIZING, APEX.MILLS, IN-HOUSE FIT
A	0.001	ORIFICE	VISCOJET
C	4	PUMP, CRYOGENIC	SUNSTRAND & ALLIED SIGNAL ARE CANDIDATES
B	0.5	REGULATOR, CRYOGENIC	VALCOR, CONSOLIDATED ARE CANDIDATES
B	0.02	REGULATOR, HIGH PRESSURE	HTL, VALCOR, CONSOLIDATED, PARKER
B	0.9	SUBCOOLER	IN-HOUSE DESIGN AND FABRICATION REQUIRED
B	0.8	TANK 1	DESIGNED AND FABRICATED IN-HOUSE TO MIL-STD-1522A
B	0.8	TANK 2	DESIGNED AND FABRICATED IN-HOUSE TO MIL-STD-1522A
B	0.2	TANK 3	DESIGNED AND FABRICATED IN-HOUSE TO MIL-STD-1522A
A	0.01	TRANSITION JOINT, EXPLOSION-WELDED, 2219 TO 304L	EXPLOSIVE FABRICATORS / FLOWN ON APOLLO
A	0.001	TUBING 1/2" MIL-T-8808A	OFF-SHELF SS 304L EXTRUSION TUBING
A	0.001	TUBING 1/4" MIL-T-8808A	OFF-SHELF SS 304L EXTRUSION TUBING
A	0.001	TUBING 3/8" MIL-T-8808A	OFF-SHELF SS 304L EXTRUSION TUBING
C	0.9	TVS, COMPACT	SUNSTRAND IS CANDIDATE
C	0.09	TVS, TANK 1	IN-HOUSE DEVELOPMENT REQUIRED
C	0.09	TVS, TANK 2	IN-HOUSE DEVELOPMENT REQUIRED
C	0.09	TVS, TANK 3	IN-HOUSE DEVELOPMENT REQUIRED
B	0.15	VALVE, CHECK, CRYOGENIC	CONSOLIDATED CONTROLS, HTL
B	1	VALVE, SHUTOFF, CRYOGENIC	PARKER, VALCOR, CONSOLIDATED CONTROL
B	0.3	VALVE, SHUTOFF, HIGH PRESSURE	PARKER, VALCOR, CONSOLIDATED CONTROL
A	0.05	VALVE, MANUAL	PARKER, CONSOLIDATED, VALCOR
B	0.2	VALVE, RELIEF	VALCOR IS CANDIDATE
C	0.2	VAPOR COOLED SHIELD	IN-HOUSE DEVELOPMENT REQUIRED

* SEE TEXT FOR DEFINITION

** .001 TO .01 LOW RISK: PREVIOUSLY FLOWN ON LAUNCH VEHICLE OR SPACECRAFT
 .01 TO .1 LOW-MEDIUM RISK: THIS RANGE WILL REQUIRE RELATIVELY LITTLE RISK MITIGATION
 .1 TO 1 MED-HIGH RISK: THIS RANGE WILL REQUIRE MITIGATION BY TEST OR TEST DATA
 1 TO 10 HIGH RISK: THIS RANGE WILL REQUIRE EXTENSIVE DESIGN DEVELOPMENT AND QUAL TESTING

Table 12-2. Development Categories and Technological Risk Factors for Experiment Module Avionics Components

TECHNOLOGY DEVELOPMENT CATEGORY*	TECHNICAL RISK FACTOR**	DESCRIPTION	PART NUMBER	COMMENTS
A	0.003	ACCELEROMETER, TRIAX	TEXTRON 11	FLOWN ON SHUTTLE, EXPLORER, USAF S73-5, SATURN, ETC
A	0.05	CONVERTER, DC/DC (10V)	TBD	SOURCE IS TBD-NOT CONSIDERED HIGH RISK
A	0.05	CONVERTER, DC/DC (28V)	TBD	SOURCE IS TBD-NOT CONSIDERED HIGH RISK
A	0.001	CURRENT SHUNT	TBD	OFF THE SHELF HIGH QUALITY RESISTOR
B	0.1	EXPERIMENT CONTROL UNIT (ECU)	TBD	IN-HOUSE DESIGN AND FAB USING QUALIFIED PIECE PARTS
A	0.05	INVERTER	TBD	SOURCE IS TBD
B	0.03	LIQUID/VAPOR DETECTOR	57-01004	TAYCO ENGINEERING
D	4	METER, FLOW	QUANTUM DYN	CURRENTLY IN TECHNOLOGY VERIFICATION
A	0.001	PRESS XDCR (0-30mV)	PA8224	GENERAL DYNAMICS-FLOWN ON CENTAUR
B	0.8	REMOTE TELEMETRY UNIT (RTU)	FAC	FAC DEVELOPED FOR INTELSTAT-7, DELTA QUAL REQD
A	0.001	TEMP XDCR, PROBE	55-01259	GENERAL DYNAMICS-FLOWN ON CENTAUR
A	0.001	TEMP XDCR, SURFACE	55-01284	GENERAL DYNAMICS-FLOWN ON CENTAUR
A	0.001	TEMP XDCR, ZERO-G	65-01006	GENERAL DYNAMICS-FLOWN ON CENTAUR

* SEE TEXT FOR DEFINITION

** SEE TABLE 12-1 FOR DEFINITIONS

Table 12-3. Spacecraft Bus Component Risk and Heritage Assessment

SUBSYSTEM/ITEM	DEVELOPMENT CATEGORY	TECHNICAL RISK FACTOR	Number	Degree of Modification	Heritage	Launch Date
STRUCTURE	B	0.5		NEW		
PROPULSION						
PRESSURANT TANK	A	0.001	1	EXISTING	EUROSTAR	
PROPELLANT TANKS	B	0.1	4	NEW		
THRUSTERS	A	0.001	24	EXISTING	INTELSAT V	12/6/80
HIGH PRESSURE LATCH VALVE	A	0.001	2	EXISTING	EURECA	8/1/91
LOW PRESSURE LATCH VALVE	A	0.001	8	EXISTING	INTELSAT V	12/6/80
SOLENOID VALVE	A	0.001	1	EXISTING	INTELSAT VII	12/1/92
FILTER	A	0.001	3	EXISTING	INTELSAT V	12/6/80
HIGH PRESSURE TRANSDUCER	A	0.001	1	EXISTING	INTELSAT V, INSAT	I-V, 12/80; INSAT, 8/83
LOW PRESSURE TRANSDUCER	A	0.001	5	EXISTING	INTELSAT V	12/6/80
FILL/ DRAIN/TEST PORT VALVE	A	0.001	10	EXISTING	INTELSAT V	12/6/80
PRESSURE REGULATOR	A	0.002	1	MINOR MODIFICATION	SCS, INSAT	SCS, 4/89; INSAT, 8/84
I, I & C						
SPACECRAFT CONTROL ELECTR.	B	0.8				
PROCESSOR	B	0.8	2	EXISTING	INTELSAT VII	12/1/92
DATA CONCENTRATOR UNIT	B	0.8	8	EXISTING	INTELSAT VII	12/1/92
COMMAND RECEIVER	A	0.002	2	EXISTING	COBE	10/1/89
TELEMETRY TRANSMITTER	A	0.002	2	EXISTING	COBE	10/1/89
DATA STORAGE UNIT	A	0.001	2	EXISTING	GINGA	2/5/87
DIPLEXER	A	0.001	1	EXISTING	GOES I-M	3/29/90
HIGH GAIN ANTENNA	B	0.1	1	NEW		
ANTENNA GIMBAL	B	0.1	1	NEW		
HIGH GAIN ANT. CONTROL ELECTR.	B	0.1	1	NEW		
HYBRID	A	0.001	1	EXISTING	GOES I-M	3/29/90
OMNI ANTENNA	A	0.001	1	EXISTING	DSCS III	10/30/82

Table 12-3. Spacecraft Bus Component Risk and Heritage Assessment (Cont.)

SUBSYSTEM/ITEM	DEVELOPMENT CATEGORY	TECHNICAL RISK FACTOR	Number	Degree of Modification	Heritage	Launch Date
ATTITUDE CONTROL						
REACTION WHEELS	A	0.002	4	MINOR MODIFICATION	INTELSAT V, IRAS	I-V, 12/80; IRAS 1/83
REACTION WHEEL ELECTRONICS	A	0.002	4	MINOR MODIFICATION	GOES I-M	3/29/90
CONICAL EARTH SENSOR	A	0.001	2	EXISTING	LANDSAT D	7/16/82
EARTH SENSOR ELECTRONICS	A	0.001	1	EXISTING	LANDSAT D	7/16/82
COARSE ANALOG SUN SENSOR	A	0.001	6	EXISTING	GOES I-M	3/29/90
CASS ELECTRONICS	A	0.001	1	EXISTING	GOES I-M	3/29/90
DIGITAL SUN SENSOR	A	0.001	2	EXISTING	GOES I-M	3/29/90
DIGITAL SUN SENSOR ELECTRONICS	A	0.001	1	EXISTING	GOES I-M	3/29/90
SOLAR ARRAY DRIVE ASSEMBLY	A	0.001	2	EXISTING	INTELSAT V	12/6/80
SOLAR ARRAY DRIVE ELECTRONICS	A	0.001	1	EXISTING	GOES I-M	3/29/90
DIGITAL INTEGRATING RATE ASS.	A	0.001	1	EXISTING	INTELSAT V, IRAS	I-V, 12/80; IRAS 1/83
DIRA INTERFACE UNIT	A	0.001	1	EXISTING	INTELSAT V, IRAS	I-V, 12/80; IRAS 1/83
VALVE DRIVER ASSEMBLY	A	0.001	2	EXISTING	INSAT	8/30/83
MAGNETIC TORQUER	A	0.06	3	MODIFIED	INTELSAT V	12/6/80
POWER SYSTEM ELECTRONICS						
SOLAR ARRAYS	A	0.003	2	MINOR MODIFICATION	SCS, GOES I-M	SCS-4/89; GOES 1-3/90
SEQUENTIAL SHUNT UNITS	A	0.002	4	MINOR MODIFICATION	INTELSAT V	12/6/80
NI-CD BATTERY	A	0.002	2	MODIFIED	INTELSAT V	12/6/80
BATTERY CHARGE CONTROLLER	C	1	2	NEW		
POWER CONTROL UNIT	A	0.005	1	MINOR MODIFICATION	INTELSAT V	12/6/80
THERMAL CONTROL						
HEATERS	A	0.001	TBD	EXISTING	Previous FAC Satellites	

also utilize existing technology. The BCC will be based on technology being developed at Ford Aerospace in support of the Space Station.

12.2 FACILITIES

Facilities needed to conduct the COLD-SAT program include those for engineering, manufacturing, testing, payload processing, launch and control of spacecraft operations. Section 9 (Operations) provides some information concerning facility features required for assembly, checkout and launch of COLD-SAT.

12.2.1 Test Facilities

Table 12-4 lists appropriate test facilities at General Dynamics Space Systems Division, Ford Aerospace Space Systems Division, Arnold Engineering Development Center (AEDC), Air Force Astronautics Laboratory (AFAL), NASA/LeRC and NASA/MSFC. Liquid nitrogen testing of many components would be done in GDSS's fluid Systems Integration Laboratory (SIL), and much of the hydrogen systems testing could be done at the GDSS Sycamore Canyon hazardous material test site. Hydrogen tanks could be tested at the LeRC K Site at their Plumbrook test facility. Vacuum chamber testing of the entire spacecraft can be done in the Ford Aerospace space simulation facility with LN₂ substituted for LH₂. Large chambers at AEDC and AFAL could accommodate hydrogen but would require some refurbishment. The chamber at MSFC could be used but could not accommodate the fully assembled spacecraft.

Table 12-4. Test Facilities

<u>SOURCE</u>	<u>FACILITY</u>
VENDORS	•COMPONENT TEST FACILITIES
GENERAL DYNAMICS	•CLIMATICS •SPACE SIMULATION •PNEUMATICS •MECHANICAL / ACCELERATION, PYRO-SHOCK, VIBRATION, MODAL ANALYSIS •ACOUSTICS •CRYOGENIC SYSTEMS (FLUID SIL) •HAZARDOUS MATERIAL TEST SITE (LIQUID HYDROGEN) •STRUCTURAL
FORD AEROSPACE	•EMC •VIBRATION •CLIMATIC •SPACE SIMULATION
NASA	•LeRC B-2 •LeRC K SITE (LIQUID HYDROGEN COMPATIBLE) •MSFC SPACE SIMULATION FACILITY (LIQUID HYDROGEN COMPATIBLE) •CCAFS COMPLEX 36
AEDC	•LARGE VACUUM CHAMBER (LIMITED LIQUID HYDROGEN COMPATABILITY, 10 M DIA., 20 M HIGH)
AFAL	•LARGE VACUUM CHAMBER (9 M DIA. SPHERE, LIQUID HYDROGEN COMPATABLE)

12.2.2 Spacecraft Processing and Checkout

Table 12-5 lists facilities for spacecraft processing and checkout. General Dynamics Commercial Launch Services Inc. primarily utilizes the facilities owned and operated by Astrotech Space Operations for spacecraft processing. Astrotech complies fully with all applicable federal, state, regional, and local statutes, ordinances, rules, and regulations relating to safety and environmental requirements. In the event that NASA chooses to use their own facilities for spacecraft processing, the facilities and their features are also listed.

12.3 TESTING

Test requirements will be established using the recommended guidelines of MIL-STD-1540B. A nearly complete experiment module shipset will be used for qualification purposes and will not be launched. This module will be useful for ground system simulations during the orbital phase of the mission.

Table 12-6 lists the required major tests and related major test facilities, and special test equipment for most phases of the COLD-SAT ground test program. The status of major facilities or special test equipment is identified using "E" for existing or "D" for to be developed. General Dynamics and Ford testing responsibilities are indicated, and the testing requirement reference given.

12.4 SCHEDULE

Figure 12-1 presents the Phase C/D master schedule. The SE&I activity will begin immediately after contract award, and GDSS will start the component and experiment module development while FAC begins the 39 month spacecraft bus and software development.

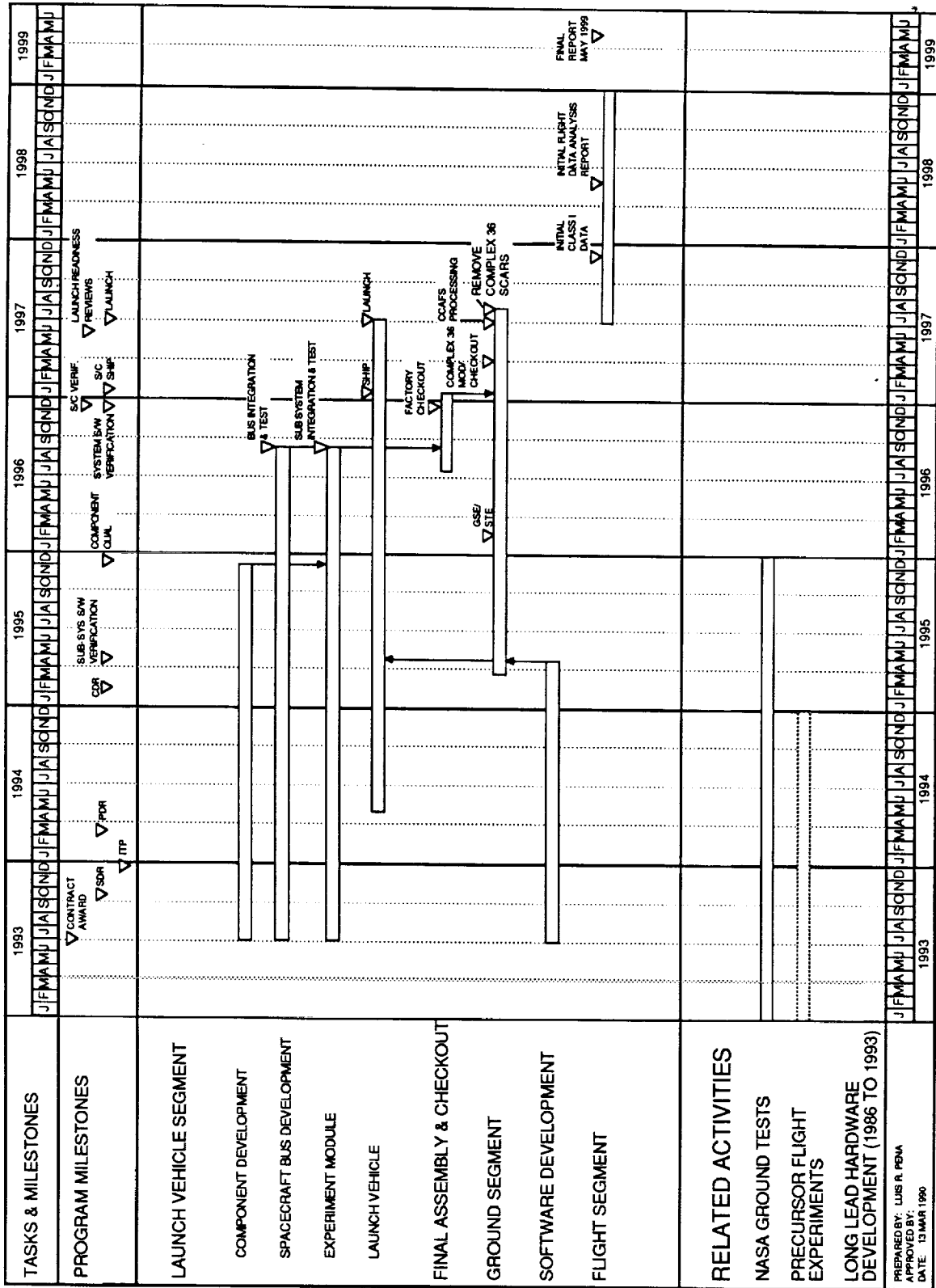
A systems design review is scheduled for three months after the contract start date. Six months after the contract award the integrated test plan will be released. A preliminary design review is scheduled for eight months after the contract award followed by the critical design review eleven months later.

Launch is scheduled for July 1997. The 42 month Atlas delivery time includes long lead procurement up to the launch date. The last GSE hardware would be delivered in March 1996 to facilitate the test of the integrated spacecraft. Some GSE would be delivered earlier to support the buildup of the experiment module and spacecraft bus. Bus and experiment integration will occur over a nine month period beginning in December 1995. The accepted spacecraft will be shipped to the launch site for launch preparations in parallel with the launch vehicle.

After the launch readiness review, final preparations would be made to support the launch. Immediately following the July launch all COLD-SAT scars to Launch Complex 36 would be removed. By eight months after the launch all initial Class I data would be available followed three months later by an initial data analysis report. The COLD-SAT Phase C/D activities end with the delivery of a final report in August 1999. The Phase C/D test schedule and launch vehicle schedule are presented in Appendix F.

Table 12-5. Spacecraft Processing and Checkout Facilities

<u>SPACECRAFT & LAUNCH FACILITIES</u>	<u>FEATURES</u>
PAYLOAD PROCESSING BUILDING (ASTROTECH BLDG. 1)	<ul style="list-style-type: none"> • AIRLOCK • THREE IDENTICAL AND ONE EXPANSION HIGH BAYS • TWO CONTROL ROOMS PER HIGH BAY • OFFICE COMPLEX AND SUPPORT AREAS • 100,000 CLEAN ROOMS • CRANES
SPACECRAFT CHECKOUT FACILITY (CCAFS BLDG. AE)	<ul style="list-style-type: none"> • HIGH AND LOW BAYS FOR SPACECRAFT CHECKOUT • MISSION DIRECTOR'S CENTER AND VIP OBSERVATION ROOM • TELEMETRY GROUND STATION AND RANGE COM LINK • CRANES
S/C PROCESSING & CHECKOUT (CCAFS BLDG. AM)	<ul style="list-style-type: none"> • GOOD ALTERNATE FACILITY • HIGH BAY WITH CRANE • CLEAN ROOM
S/C PROCESSING & CHECKOUT (CCAFS BLDG. AO)	<ul style="list-style-type: none"> • LARGEST HIGH BAY FLOOR AREA • 100,000 CLEAN ROOM • 100 LAMINAR FLOW CLEAN ROOM (SECOND FLOOR)
HAZARDOUS PROCESSING FACILITY (ASTROTECH BLDG. 2)	<ul style="list-style-type: none"> • AIRLOCK • SPACECRAFT PROCESSING HIGH BAY AND OPERATIONS ROOM • SPIN HIGH BAY AND CONTROL ROOM • PAM PROCESSING HIGHBAY AND CONTROL ROOM • EXPANSION HIGH BAY AND AIR LOCK • EXPLOSION-PROOF BAYS • SUPPORT AREAS
EXPLOSIVE SAFE AREA (CCAFS ESA 60A)	<ul style="list-style-type: none"> • ALTERNATE HAZARDOUS PROCESSING • STERILIZATION & ASSEMBLY BUILDING (5,660 SQUAREFT) • PROPELLANT LABORATORY (1,350 SQUARE FT) • INSTRUMENTATION LABORATORY • GROUND SUPPORT EQUIPMENT BUILDING (1,400 SQ FT) • 100,000 CVLASS CLEAN ROOMS • MEETS BLAST REQUIREMENTS
S/C ASSY AND ENCAPSULATION FACILITY No. 2 (KSC)	<ul style="list-style-type: none"> • ALTERNATE HAZARDOUS PROCESSING • HIGH BAY • TWO LOW BAYS • TEST CELL • TWO CONTROL ROOMS • LARGE SIZE
PAYLOAD STORAGE BUILDING (ASTROTECH BLDG. 3)	<ul style="list-style-type: none"> • THERMALLY-CONTROLLED ENVIRONMENT • SPACECRAFT STORAGE
WAREHOUSE STORAGE BUILDING (ASTROTECH BLDG. 4)	<ul style="list-style-type: none"> • NOT ENVIRONMENTALLY CONTROLLED



13
REFERENCES

- | REF.
NO. | REFERENCE |
|-------------|--|
| 2-1 | Schuster, J. R., "Cryogenic Fluid Management Technology, an Industry Perspective," <i>NASA/OAST In-space Technology Experiments Workshop Proceedings</i> , Volume II - Critical Technologies, Themes 1-4, December 1988. |
| 3-1 | Florschuetz, L. W., and Chao, B. T., "On the Mechanics of Vapor Bubble Collapse," <i>Trans. of ASME, J. of Heat and Mass Transfer</i> , May 1965, pp.209-220. |
| 3-2 | Prisnyakov, V. F., "Condensation of Vapor Bubbles in Liquid," <i>International Journal of Heat and Mass Transfer</i> , Vol. 14, 1971, pp.353-356. |
| 3-3 | Hewitt, H. C., and Parker, J. D., "Bubble Growth and Collapse in Liquid Nitrogen," <i>Trans. of ASME, J. of Heat Transfer</i> , Vol. 90, Series C, February 1968, pp.22-26. |
| 3-4 | Paynter, H. L., "Acquisition/Expulsion System for Earth Orbital System," NAS9-12182, Martin Marietta, June 1973. |
| 3-5 | "COLD-SAT Experiment Requirements Document," GDSS-CSAT-89-510, Contract NAS3-25062, General Dynamics Space Systems Division, San Diego, CA, March 6, 1989. |
| 3-6 | Masica, W. J. and Petrash, D. A., "Motion of Liquid-Vapor Interface in Response to an Imposed Acceleration," NASA TN D-3005, 1965. |
| 3-7 | Salzman, J. A. and Masica, W. J., "Experimental Investigation of Liquid-Propellant Reorientation," NASA TN D-3789, 1967. |
| 3-8 | Labus, T. L. and Masica, W. J., "Liquid Reorientation in Spheres by Means of Low-G Accelerations," NASA TM X-1659. |
| 3-9 | Sumner, I. E., "Liquid Propellant Reorientation of a Liquid in a Cylindrical Tank Due to Propulsive Settling in a Low- Gravity Environment," NASA TM-78969, July 1978. |
| 3-10 | Bowman, T. E. (Florida Institute of Technology), Unpublished notes, February 1979. |
| 3-11 | Sexton, R. E., "In Space Propellant Logistics," NAS8-27692, NAR-SD 72-SA-0053, June 1972. |
| 3-12 | Stark, J. A., "Low-G Fluid Transfer Technology Study," NASA CR-134911, May 1976. |
| 3-13 | Bereyni, S. G., "Vapor Ingestion Phenomenon in Hemispherically Bottomed Tanks in Normal Gravity and in Weightlessness," NASA/LeRC, TND 5704, April 1970. |
| 3-14 | Saterlee, H. M. and Chin, J. H., "LMSC Symposium on Fluid Mechanics and Heat Transfer Under Low-G Conditions," Palo Alto, CA., June 1965. |

REF.
NO.

REFERENCE

-
- 5-1 Anderson, J. and Eberhardt, R., "Cryogenic Storage System Development for Long Term Space Missions," AIAA / SAE / ASME 15th Joint Propulsion Conference, Las Vegas, Nevada, 1979.
- 5-2 Baljé, O. E., Turbomachines, John Wiley & Sons, New York, NY, 1981.
- 5-3 "Turbopump Systems for Liquid Rocket Engines," NASA SP-8107, August 1974.
- 5-4 Gluzek, F., et al, "Liquid Oxygen/Liquid Hydrogen Boost/Vane Pump for the Advanced Orbit Transfer Vehicle Auxiliary Propulsion System," NASA Report No. CR159648, September 1979.
- 5-5 Hemminger, J. A. and Ulbricht, T. E., "LOX/LH2 Vane Pump for Auxiliary Propulsion Systems," NASA Technical Memorandum prepared for 1985 JANNAF Propulsion Meeting.
- 5-6 Jasinski, T., Stacy, W. D., Honkonen, S. C. and Sixsmith, H., "A Generic Pump/Compressor Design for Circulation of Cryogenic Fluids," in R. W. Fast, ed., *Advances in Cryogenic Engineering*, Volume 31, Plenum Press, New York, NY, 1986.
- 5-7 Kreith, F., Principles of Heat Transfer, Harper & Row, Publishers, Inc., New York, NY, 1973.
- 5-8 Heat Exchanger Design Handbook, Hemisphere Publishing Corporation, Washington, D. C., 1983.
- 5-9 Rohsenow, W. M. and Choi, H., Heat, Mass and Momentum Transfer, Prentice-Hall, Inc., Englewood Cliffs, NJ, 1961.
- 6-1 Collier, J. G., Convective Boiling and Condensation, McGraw-Hill Book Company, New York, 1972.
- 6-2 Incropera, F. P. and DeWitt, D. P., Fundamentals of Heat Transfer, John Wiley and Sons, New York, 1981.
- 6-3 Kays, W. M. and Crawford, M. E., Convective Heat and Mass Transfer, McGraw-Hill Book Company, New York, 1980.
- 6-4 Honkonen, S. C., et al, "Analysis of Cryogenic Fluid Systems in Low-G," GDSS-ERR-89-406, General Dynamics Space Systems Division, 1989.
- 6-5 Aydelott, J. C., "Modeling of Space Vehicle Propellant Mixing," NASA TP-2107, Lewis Research Center, 1983.
- 6-6 McAdams W., Heat Transmission, McGraw-Hill Book Company, New York, 1954.
- 6-7 Heat Exchanger Design Handbook, Hemisphere Publishing Corporation, Washington, D.C., 1983.
- 6-8 Moore, R. W., et al, "Gas-Pressurized Transfer," *Advances In Cryogenic Engineering*, Vol. 5, 1959.

REF. NO.	REFERENCE
6-9	Epstein, M., "A Generalized Propellant Tank-Pressurization Analysis," <i>Advances In Cryogenic Engineering</i> , Vol. 10b, 1964.
6-10	Nein, M. E. and Thompson, J. F., "Experimental and Analytical Studies of Cryogenic Propellant Tank Pressurant Requirements," NASA TN D-3177, 1966.
6-11	Epstein, M., "Prediction of Liquid Hydrogen and Oxygen Pressurant Requirements," <i>Advances In Cryogenic Engineering</i> , Vol. 10, 1964.
6-12	Honkonen, S. C., et al, "Analysis of Cryogenic Fluid Systems in Low-G," GDSS-ERR-89-406, General Dynamics Space Systems Division, 1989.
6-13	England, J. E. and Keller, S. A., "Titan/Centaur Insulation System Calorimeter/Vacuum Performance Design Evaluation Testing," GDSS TM 890-88-1179, August 1988.
6-14	England, J. E., MacNeil, P. N. and Knoll, R. H., "Design, Development, and Test of Shuttle/Centaur G-Prime Cryogenic Tankage Thermal Protection Systems," NASA TM 89825, May 1987.
6-15	O'Neill, R. F. and Walter, M.D., "Vector Sweep User's Guide," GDSS-SP-85-011, December 1985.
6-16	Henniger, J. H., "Solar Absorptance and Thermal Emittance of Some Common Spacecraft Thermal Control Coatings," NASA-RP-1121, 1984.
6-17	Walters, T. W., "Aeroheating Analysis of Atlas/Centaur 14 ft. Payload Fairing Structure and Advanced Hardware, Addendum No. 1," TM 890-88-1132 Add. 1, 10 May 1988.
6-18	Bennett, F. O., "Propellant Management for Space-Based Systems," GDSS-ERR-85-504, December 1985.
6-19	Delil, A. A. M. and Heemskerk, J. F., "A Theoretical Investigation of Gas Conduction Effects on Multilayer Insulation Performance," NLR-TR-76018-U, September 1976.
6-20	Johnson, V. J. (ed), "A Compendium of the Properties of Materials At Low Temperatures (Phase 1)," NBS Cryogenics Laboratory, WADD TR 60-56, October 1960.
6-21	O'Neill, R. F. and Walter, M. D., "Thermal Analyzer Engineering Manual and User's Guide," GDSS-SP-85-012, December 15, 1985.
6-22	Kessler, D. J., "Orbital Debris Environment for Space Station," J8400021, 1984.
6-23	Kessler, D. J., "Predicting Debris," <i>Aerospace America</i> , June 1988, pp 22-24.
6-24	Vaughan, W. W., "Natural Environment Design Criteria for the Space Station Definition and Preliminary Design (First Revision)," NASA TM-86460, September 1984.
6-25	Cour-Palais, B. G., "Meteoroid Protection by Multiwall Structures," AIAA 69-372, AIAA Hypervelocity Impact Conference, Cincinnati, Ohio, April 30-May 2, 1969.

REF.
NO.

REFERENCE

-
- 6-26 Frost, V.C., "Meteoroid Damage Assessment," NASA SP-8042, May 1970.
- 6-27 "Buckling of Thin Walled Circular Cylinders," NASA SP-8007, Revised August 1968.
- 6-28 "Buckling of Thin Walled Truncated Cones," NASA SP-8019, September 1968.
- 6-29 "Atlas Mission Planner's Guide, "General Dynamics Commercial Launch Services Inc., Revision 1, March 1989.
- 6-30 "Aerospace Structural Metals Handbook," Formerly AFML-TR-68-115, Battelle Columbus Division, Columbus, OH.
- 6-31 "Structural Analysis Manual," General Dynamics Convair Division/Space Systems Division, 1988.
- 9-1 "COLD-SAT Experiment Requirements Document, Interim Draft," GDSS-CSAT-89-510, Contract NAS3-25062, General Dynamics Space Systems Division, March 1989.
- 10-1 "Range Safety," ESMCR 127-1.
- 10-2 "Safety Policy Manual," Astrotech International Corporation.
- 10-3 "Preliminary Satellite System Safety Package For Cryogenic On-Orbit Liquid Depot Storage, Acquisition and Transfer Satellite (COLD-SAT)," Contract NAS3-25062, General Dynamics Space Systems Division, July 1989.
- D-1 Incropera, F. P. and DeWitt, D. P., Fundamentals of Heat Transfer, John Wiley and Sons, New York, 1981.
- D-2 Tennekes, H. and Lumley, J. L., A First Course in Turbulence, The MIT Press, Cambridge, Massachusetts, 1983.
- D-3 Merino, F., et al, "Orbital Refill of Propulsion Vehicle Tankage," GDC-CRAD-80-001, General Dynamics Convair Division, 1980.
- D-4 White, F. M., Viscous Fluid Flow, McGraw-Hill Book Company, New York, 1974.
- D-5 Kays, W. M. and Crawford, M. E., Convective Heat and Mass Transfer, McGraw-Hill Book Company, New York, 1980.

APPENDIX A
EXPERIMENT MODULE ADDITIONAL DESIGN DETAILS



APPENDIX A
EXPERIMENT MODULE ADDITIONAL DESIGN DETAILS

A.1 SUMMARY OF EXPERIMENT MODULE GENERAL ARRANGEMENT STUDIES

Nine general arrangement studies were conducted of the experiment module using a fixed size for Tanks 1 and 3 coupled with geometry variations of Tank 2. Several locations for the tanks were considered. The prime objectives in all the cases were minimum weight, keeping the c.g. aft, gas storage flexibility, and overall feasibility. The sketches of the tank arrangements which were considered in the tradeoffs are shown in Figure A-1, including weights and c.g. locations. The quantity of gas storage bottles varies between the cases since the analysis was being conducted concurrently with the preparation of these studies.

In Case 1, Tank 3 is located forward and Tank 2 positioned aft inside the bus central cylinder. Gas storage is provided by seven bottles, of which three are located inside the bus central cylinder at the aft end and four positioned outboard on the conical section of the support structure. The fairing size for Tank 1 was estimated from the earlier, larger, Stage 2 tank design, and the fairing on Tank 2 was trimmed back to near the tops of the bulkheads. The outer structure includes micrometeoroid/debris shielding.

Case 2 is similar to Case 1 except the L/D for Tank 2 was further reduced, the fairings on Tank 1 trimmed back and Tank 1 moved further aft.

For Case 3, the supply Tank 1 was reconfigured and located aft inside the body structure of the bus, and Tanks 2 and 3 located forward. This change provided a favorable cg location but caused the bus central cylinder diameter to increase to the point where there was insufficient room for the bus equipment. Also, an additional structural adapter is required at the aft end to avoid developing a new size "V" band clamp system.

Estimates of the size and quantity of equipment required to be located under the insulation on Tank 2 dictated the fairing length increases shown in Case 4. The L/D for Tank 2 is larger and the gas storage bottles are located outside the bus central cylinder. Four of these gas bottles are located in the corners used for the support structure. No micrometeoroid/debris shielding is used.

In Case 5, Tank 3 and three gas storage bottles were installed inside the bus central cylinder and one additional bottle positioned at a corner inside the bus. Tank 2 is located forward and the outer structure is monocoque with no shielding. The combination of the gas bottles, Tank 3, and Tank 3 valve module located inside the bus central cylinder offered efficient packaging.

The general arrangement in Case 6 is the same as that shown for Case 1 except the station location of Tank 1 is moved forward slightly due to the longer fairings on Tank 2 and the outer structure is an open truss. Four gas bottles are used; three inside the bus central cylinder and one inside a corner of the bus.

Further definition of gas storage volumes and bottle designs warranted a revisit to Case 5 by generating two more cases (7 and 8) equipped with micrometeoroid/debris shielding. Detailed layouts were made which placed the three gas bottles, Tank 3, Tank 3 valve module, one junction module, and the avionics inside the bus central cylinder for Case 7.

For Case 8, the avionics were moved to the bus body panels due to considerations for cooling. Also, detailed equipment layouts were being completed which allowed further trimming of the forward fairings on Tanks 1 and 2.

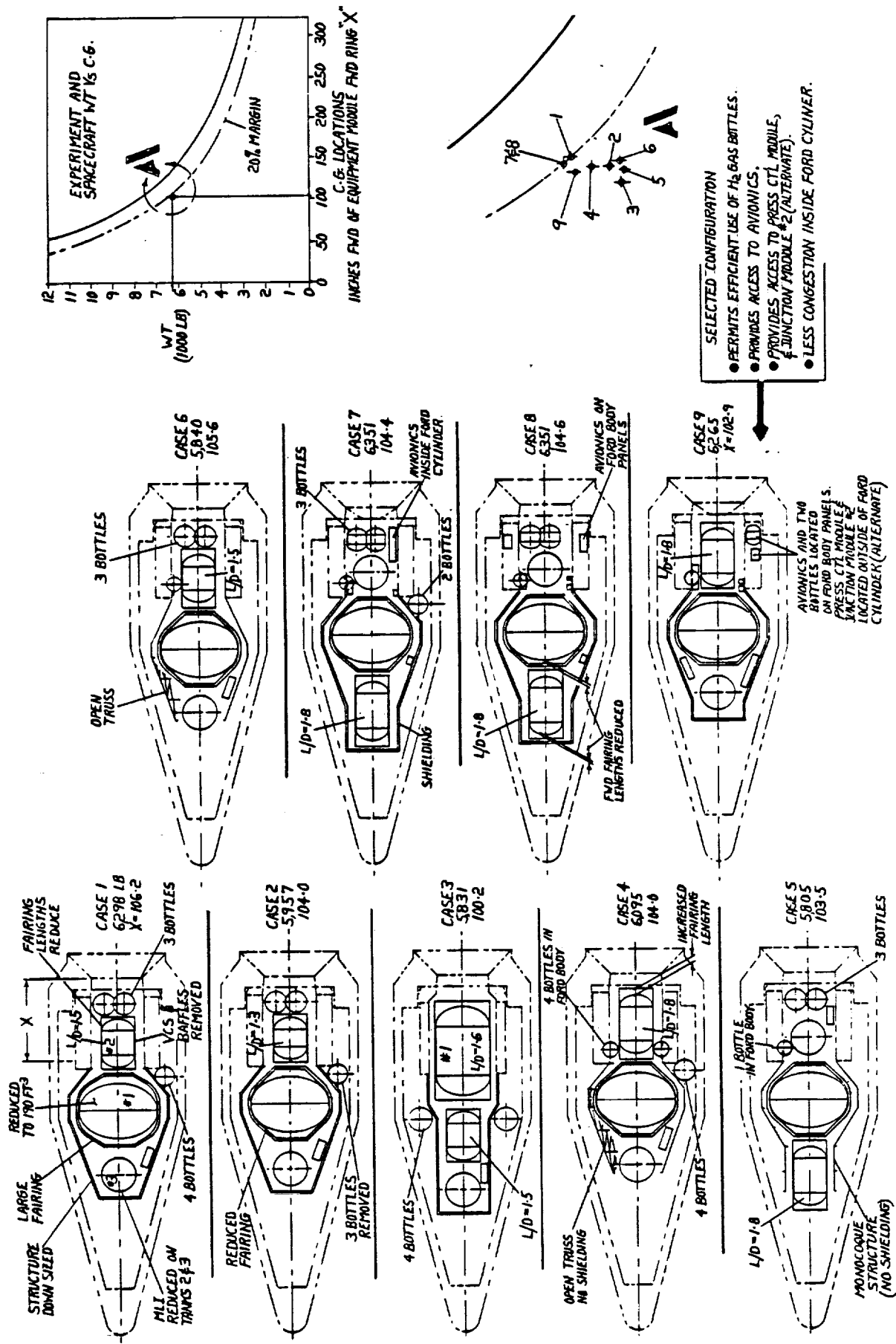


Figure A-1. Summary of General Arrangement Configurations

Further studies indicated that the hydrogen gas storage volume could be accommodated by two bottles located aft in the bus body structure as shown in the baseline Case 9. Tank 2 was therefore moved back into the bus central cylinder which permitted a length reduction in the outer structure. The advantages of Case 9 are listed in Figure A-1.

A.2 DETAILED MASS BREAKDOWN FOR TANKS 1,2 AND 3, AND THE OUTER STRUCTURE

Tables A-1 through A-5 present detailed mass breakdowns for the three tanks and the outer structure. In the table for Tank 1, for example, the categories are the basic shell, fairings, instrumentation, LAD, TVS/mixer, VCS, insulation, and miscellaneous. Similarly, for the outer structure the categories are aft conical section, aft cylindrical section, forward conical section, forward cylindrical section, and the forward cap.

The grand total mass for each tank assembly are the totals shown in Tables A-1, A-2 and A-3 plus masses for the systems located under the MLI and attached to the tanks. The basic shell masses are approximately 27 percent, 26 percent, and 19 percent of the grand totals for Tanks 1, 2, and 3, respectively.

For the all-aluminum outer structure, the inner skin carries the primary loads in the aft section and is approximately 50 percent of the aft section total mass. For the forward section, the inner skin gauge is determined by the micrometeoroid/debris protection requirements and is approximately 48 percent of the total forward section mass. For the composite/aluminum outer structure, where both skins react the loads, approximately 40 percent of the mass goes into these skins for the aft section.

A.3 TANK 3 ASSEMBLY, NOZZLE AND VENT DETAILS

A.3.1 Tank 3 Assembly

The horizontal arm of the cross structure has two flanged connections which permit placing the forward and horizontal pieces in the tank first, and then fastening them together with four bolts (Figure A-2). As many parts as possible are mounted on each structural piece and checked out on the bench before placing inside the tank.

The aft section of the structural cross and feed tubing are next placed into the tank, connected to the previous parts and checked out. The next step is to engage the access cover with the penetration fittings and the access opening ring. The assembly is then completed by welding all penetration interfaces and the access cover.

A.3.2 Tank 3 Internal Nozzle Details

Detail "D" and view "G-G" of Figure A-3 are views of the internal assembly at the center region of the tank. The structural support tubes (referred to earlier as the "cross structure") have two pairs of flanges to permit assembly and two fittings which distribute flow for spray fill (view E-E) and for pressurization. These fittings are machined integral with the flanges at one end and are butt-welded to the cross structure at the opposite end. The spray fill fittings feature three nozzles and the pressurization fitting is equipped with a screen-type diffuser. Both fittings have drilled flow passages. The cross structure is for support only and does not convey fluid.

The tubes which supply the radial spray, tangential spray and pressurization are supported from the cross structure with tube clamps as shown in views "G-G" and "F-F." Each tube has a mechanical

Table A-1. Tank 1 Mass Breakdown

COMPONENT	MASS (KG)
BASIC SHELL	
FORWARD BULKHEAD	50.0
AFT BULKHEAD	53.2
ACCESS OPENING RING	2.1
ACCESS OPENING DOOR	2.1
TANK SUPPORT FITTINGS	0.2
BULKHEAD PENETRATION FITTINGS FOR PLUMBING & ELECTRICAL	1.8
SUPPORT FITTINGS FOR MOUNTING SYSTEM MODULES ON FWD & AFT BULKHEADS	0.5

SUBTOTAL	109.9
FARINGS	
FORWARD FAIRING	11.3
AFT FAIRING	12.7
FORWARD FAIRING CAP	1.7
AFT FAIRING CAP	1.4
FWD FAIRING CAP RING	1.3
AFT FAIRING CAP RING	1.2
FAIRING CAP STIFFENERS	0.7
FAIRING MOUNTING RINGS	3.4
FAIRING SUPPORT FITTINGS	0.8
MISC. FASTENERS	0.5

SUBTOTAL	35.0
INSTRUMENTATION	
INSTRUMENTATION TREE MAST	0.5
INSTRUMENTATION TREE ARMS	0.9
INSTRUMENTATION TREE END FITTINGS	0.2
SENSORS	7.0
WIRING	3.6
ELECTRICAL PENETRATION RECEPTACLES	1.0

SUBTOTAL	13.2
LAD	
LAD CHANNELS	7.8
LAD SUPPORT FITTINGS	1.2
FLANGES, SEALS & "V" BANDS	0.5
MISC. FASTENERS	0.5

SUBTOTAL	10.0

Table A-1. Tank 1 Mass Breakdown (Cont.)

COMPONENT	MASS (KG)
TVS /MIXER	
TVS/MIXER ASSEMBLY	9.1
SUPPORT TRUSS	0.9
SUPPORT FITTINGS	0.1

SUBTOTAL	10.1
VCS	
VCS FORWARD BH'D	12.1
VCS AFT BH'D	11.2
FWD CAP	1.6
AFT CAP	1.4
TUBING	11.3
FWD & AFT CAPS	1.5
FWD CAP RING	0.5
AFT CAP RING	0.5
SUPPORT FITTINGS & MISC FASTENERS	1.0

SUBTOTAL	41.1
INSULATION	
MLI GORE BLANKETS	49.8
MLI CAP BLANKETS	4.1
FASTENERS, TAPE, ETC.	0.9
ELECTRICAL BONDING (GROUNDING)	0.5

SUBTOTAL	55.3
PURGE ENCLOSURE	
FWD RIGID SECTION	5.5
AFT SOFT SECTION	0.9
FWD STIFFENER RINGS	0.8
GIRTH FLANGES	3.2
FWD CAP STRUCTURE	3.3
AFT CAP STRUCTURE	3.2
AFT CAP SUPPORT STRUTS	0.9
FWD SECTIONS SUPPORT STRUTS	0.7
SUPPORT FITTINGS	0.2
GIRTH FLANGE FASTENERS	0.6
RIVETS, TAPE, CLIPS & STRUT BOOTS, SEALING COMPOUND	0.7
VENT VALVE SUPPORTS	0.9
VENT VALVE CLOSURES	0.7
TORSION SPRING ACTUATORS & PYRO PIN PULLERS	1.8
ELECTRICAL HARNESS	0.9

Table A-1. Tank 1 Mass Breakdown (Cont.)

COMPONENT	MASS (KG)
PURGE ENCLOSURE (CONT.)	
PRESSURE RELIEF VALVE	0.9
PURGE TUBING	0.9
PURGE DISCONNECTS	1.4

SUBTOTAL	27.5
OTHER	
TANK PRESSURIZATION DIFFUSER	0.9
TANK WALL TVS TUBING	4.5
TANK WALL HEATERS	2.3
TANK SUPPORT STRUTS WITH END FITTINGS	2.7
ENVIRONMENTAL MEMBRANE	0.9

SUBTOTAL	11.3

GRAND TOTAL	313.4

Table A-2. Tank 2 Mass Breakdown

COMPONENT	MASS (KG)
BASIC SHELL	
FWD BULKHEAD	4.0
AFT BULKHEAD	6.0
CYLINDRICAL SECTION	15.3
ACCESS OPENING RING	1.8
ACCESS OPENING DOOR	1.4
TANK SUPPORT FITTINGS	0.2
BULKHEAD PENETRATION FITTINGS (FOR PLUMBING & ELECTRICAL)	1.4

SUBTOTAL	30.1
FAIRINGS	
FWD FAIRING/CYLINDER	2.0
AFT FAIRING/CYLINDER	2.5
FWD & AFT CAPS	2.5
CAP RINGS	0.9
STIFFENERS	0.3
FAIRING MOUNTING RINGS	0.9
FAIRING SUPPORT FITTINGS	0.2
MISC. FASTENERS	0.5

SUBTOTAL	9.8
TANK WALL TVS & HEATERS	
TANK WALL TVS/CYLINDRICAL	2.2
TANK WALL TVS/BULKHEADS	1.0
TANK WALL HEATERS	1.8

SUBTOTAL	5.0
INSTRUMENTATION	
INSTRUMENTATION TREE ARMS	0.8
SENSORS	5.0
WIRING	2.3
ELECTRICAL PENETRATION RECEPTACLES	0.9

SUBTOTAL	9.0
FILL MANIFOLD	
FILL/SPRAY MANIFOLD	1.7
FWD SUPPORT FITTING	0.2
AFT FLEX JOINT	0.2

SUBTOTAL	2.1

Table A-2. Tank 2 Mass Breakdown (Cont.)

	MASS (KG)
LAD	
LAD CHANNELS	5.4
LAD VENT TUBES	0.9
LAD SUPPORT FITTINGS	0.8
FLANGES, SEALS & "V" BANDS	0.5
MISC FASTENERS	0.3

SUBTOTAL	7.9
INSULATION	
MLI SIDE WALL BLANKETS	14.0
MLI CAP BLANKETS	3.5
FASTENERS, TAPE, & CLOSE OUT BOOTS	0.7

SUBTOTAL	18.2
OTHER	
TANK SUPPORT STRUTS WITH END FITTINGS	1.4

GRAND TOTAL	83.5

Table A-3. Tank 3 Mass Breakdown

COMPONENT	MASS (KG)
BASIC SHELL	
FWD BULKHEAD	6.3
AFT BULKHEAD	5.5
ACCESS OPENING RING	2.2
ACCESS OPENING DOOR	1.5
TANK SUPPORT FITTINGS	0.2
BULKHEAD PENETRATION FITTINGS (FOR PLUMBING & ELECTRICAL)	0.4

SUBTOTAL	16.1
FAIRINGS	
SMALL AFT FAIRING	1.3
FAIRING SUPPORT FITTINGS	0.1
MISC. FASTENERS	0.1

SUBTOTAL	1.5
TANK WALL TVS & HEATERS	
TANK WALL TVS	1.5
TANK WALL HEATERS	0.8

SUBTOTAL	2.3
INSTRUMENTATION	
INSTRUMENTATION SENSOR	3.4
INTERNAL WIRING	0.9
ELECTRICAL PENETRATION RECEPTACLES	0.7

SUBTOTAL	5.0
INTERNAL ACCESSORIES	
INTERNAL SUPPORT TUBE	1.1
FILL BAFFLE	0.2
AFT SPRAY FITTING	0.1
INTERNAL CHECK VALVES	0.7
RADIAL SPRAY TUBES	0.2
TANGENTIAL SPRAY TUBES	0.4
PRESSURIZATION TUBE & DIFUSSER	0.1
TUBE CLIPS & SCREWS	0.2

SUBTOTAL	3.0

Table A-3. Tank 3 Mass Breakdown (Cont.)

COMPONENT	MASS (KG)
FAIRING	
INSULATION FAIRING	1.3
FAIRING SUPPORT FITTINGS	0.1

SUBTOTAL	1.4
MLI	
FWD CAP BLANKETS	0.9
AFT CAP BLANKETS	0.5
GORE BLANKETS	3.3

SUBTOTAL	4.7
OTHER	
TANK SUPPORT STRUTS INCLUDING END ATTACHMENTS	2.3

TOTAL TANK WEIGHT	36.3
LINES BETWEEN VALVE MODULE & TANK	
TUBES RUNNING FROM TANK TO VALVE MODULE	1.4
TUBE SUPPORT FAIRLEADS	0.5
MLI PREFORMED BOOT	0.2
MISC. FASTENERS	0.2
ELECTRICAL HARNESS	1.4

TOTAL	3.7

Table A-4. Aluminum Outer Structure Mass Breakdown

COMPONENT	WEIGHT (KG)
AFT CONICAL SECTION	
INTERFACE FITTINGS	4.3
INTERFACE BOLTS	1.0
AFT RING	4.2
HONEYCOMB	5.9
OUTER SKIN	5.6
INNER SKIN	43.6
ADHESIVE	3.3
ACCESS OPENING COVERS	4.5
UMBILICAL INTERFACE	2.3
KICK RING	8.5
OUTBOARD CLOSE OUT RINGS (OUTBOARD)	5.9
TANK SUPPORT FITTINGS	0.2
INTERMEDIATE RING	3.0
ACCESS OPENING INTERCOSTAL	0.7

SUBTOTAL	93.0
AFT CYLINDER SECTION	
ADHESIVE/CYLINDRICAL SECTION	2.4
HONEYCOMB	4.3
OUTER SKIN	4.1
INNER SKIN	31.3
FWD KICK RING	10.0
TANK SUPPORT FITTINGS	0.1

SUBTOTAL	52.2
AFT CONICAL & CYLINDRICAL SECTION FASTENERS	3.8
FORWARD CONICAL SECTION	
FWD CONICAL SECTION/AFT RING	5.0
OUTER SKIN	10.9
INNER SKIN	47.4
HONEYCOMB	12.4
ADHESIVE	6.4
INTERMEDIATE RINGS	7.1
ACCESS OPENINGS INTERCOSTALS	1.5
ACCESS OPENING DOOR FRAMES	1.9
FOWARD RING	4.4
TANK SUPPORT FITTINGS	0.1

SUBTOTAL	97.1

Table A-4. Aluminum Outer Structure Mass Breakdown (Cont.)

COMPONENT	WEIGHT (KG)
FORWARD CYLINDRICAL SECTION	
FWD CYLINDRICAL SECTION OUTER SKIN	1.9
INNER SKIN	8.6
HONEYCOMB	2.0
ADHESIVE	1.2
FWD RING	2.8

SUBTOTAL	16.5
FORWARD CAP	
FORWARD CAP PERIMETER RING	4.1
OUTER SKIN	1.3
INNER SKIN	5.9
HONEYCOMB	2.7
ADHESIVE	0.8
CORNER BUMPER	0.4

SUBTOTAL	15.2
FWD CONICAL & CAP SECTION FASTENERS	2.7
VENT	
FOWARD VENT PENETRATION FITTING	0.8
OUTBOARD BAFFLE INCLUDING SUPPORTS	1.6
INBOARD BAFFLE INCLUDING SUPPORTS	1.6

SUBTOTAL	4.0
GRAND TOTAL	284.5

Table A-5. Graphite/Epoxy Outer Structure Mass Breakdown

COMPONENT	WEIGHT (KG)
AFT CONICAL SECTION	
INTERFACE FITTINGS	4.3
INTERFACE BOLTS	1.0
AFT RING	4.2
SPLICE STRAP	1.2
AFT CORE FILL	4.4
HONEYCOMB	5.9
OUTER SKIN	8.1
INNER SKIN	20.3
ADHESIVE	3.3
FWD CORE FILL	4.0
ACCESS OPENING CORE FILL	0.8
ACCESS OPENING COVERS	1.5
UMBILICAL INTERFACE	2.3
KICK RING	8.5
OUTBOARD CLOSE OUT RINGS	5.9
TANK SUPPORT FITTINGS	0.2
SUBTOTAL	----- 75.9
AFT CYLINDRICAL SECTION	
CORE FILLS/FWD & AFT/AFT CYLINDER	9.3
HONEYCOMB	4.3
OUTER SKIN	5.8
INNER SKIN	14.6
ADHESIVE	2.4
FWD KICK RING	10.0
TANK SUPPORT FITTINGS	0.1
SUBTOTAL	----- 46.5
AFT CONICAL & CYLINDRICAL SECTION FASTENERS	2.7
FWD CONE, CYLINDER AND CAP SECTION SAME AS THAT SHOWN FOR THE ALL ALUMINUM DESIGN	135.4
GRAND TOTAL	260.5

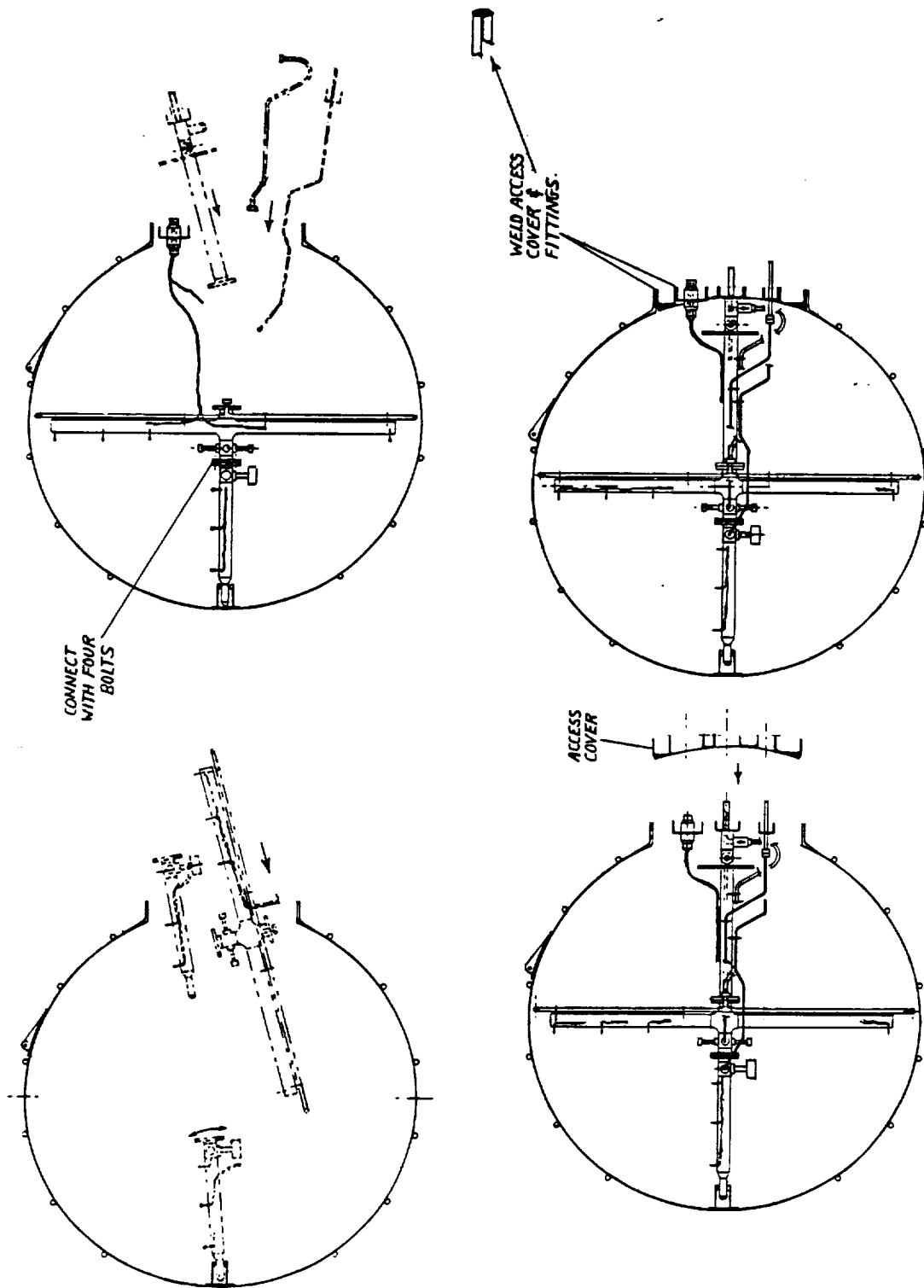


Figure A-2. Tank 3 Assembly

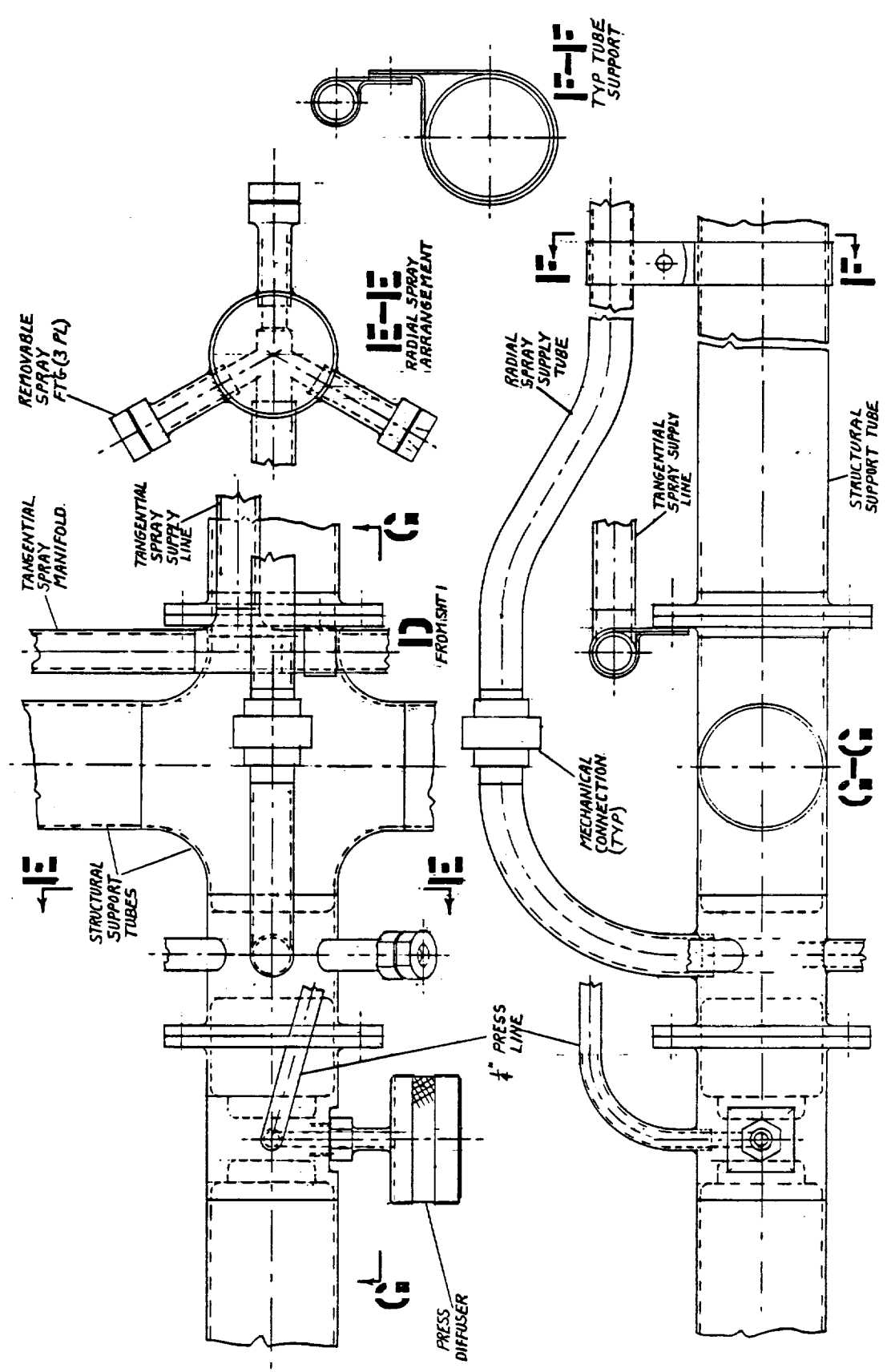


Figure A-3. Tank 3 Internal Nozzle Details

connection to permit assembly. The manifold for the tangential sprays is a straight tube section with a tee at the center. This tube is supported from the cross structure using tube clamps.

A.3.3 Tank 3 Vent Arrangement

The top of Tank 3 has one vent fitting which connects to three valves on the downstream end as shown in Figure A-4. This vent fitting is equipped with a CRES tube stub-up section which extends the end to a station location compatible for orbit arc welding when the valves and manifold are in place. The valves are manifolded together using 304L CRES tubes and fittings and are mounted on an aluminum alloy waffle plate using epoxy/fiberglass fairleads. The waffle plate has a hole for clearing the vent fitting stub-up and is attached to the tank with four fittings which are welded to the tank wall. The stub-up is connected to the valve manifold with a CRES flex hose section. The entire assembly is boxed in with an epoxy/fiberglass fairing and covered with two blanket layers of MLI. The edges of the MLI are trimmed to fit with the MLI blankets on the tank and secured at the corners with tape strips.

A.4 DETAILS OF THE FLUID COMPONENT MODULES

A.4.1 Tank 1 Pump Module

The layout in Figure A-5 presents the pump module configuration, along with a system schematic and a weight breakdown. This pump module is mounted off the aft bulkhead of Tank 1 and is located under the MLI. Two pumps and ten valves are interplumbed using 304L corrosion resistant steel (CRES) standard fittings and tubing connected by the orbit arc welding process. This welded assembly is mounted on an aluminum waffle panel using epoxy/fiberglass fairleads, saddles and CRES bands, similar to that described for the other modules, and the components are clamped in place rather than hard-mounted. This clamp-type mounting permits slippage at the saddles and fairleads during dimensional changes.

The envelope size indicated is not expected to increase when the instrumentation is added. For example the elbow fittings at the pump inlets and outlets can be special machined fittings which incorporate bosses for receiving pressure and temperature transducers. These bosses can be configured so that the transducers are seal-welded. During the seal welding, the transducers are chilled with a fixture.

A.4.2 Pressurization Control Module

The major components for the pressurization control module shown in Figure A-6 are two flowmeters, two pressure regulators, two valves, and two filters. The components are interplumbed using standard CRES fittings and tubing welded together with the orbit arc welding process. This welded assembly is clamped onto a waffle plate with epoxy/fiberglass fairleads, saddles and CRES bands. The entire assembly is enveloped with a fiberglass fairing which is covered with MLI.

The module is located aft near the pressurization storage bottles and is attached to outboard side of the bus central cylinder with bracketry bolted to the waffle panel. The MLI is locally cut out for clearing the brackets.

A.4.3 Tank 1 Evaporator Module

The major components for the evaporator module shown in Figure A-7 are two flowmeters, one accumulator, one evaporator, two pressure regulators, five valves, four relief valves and one pump.

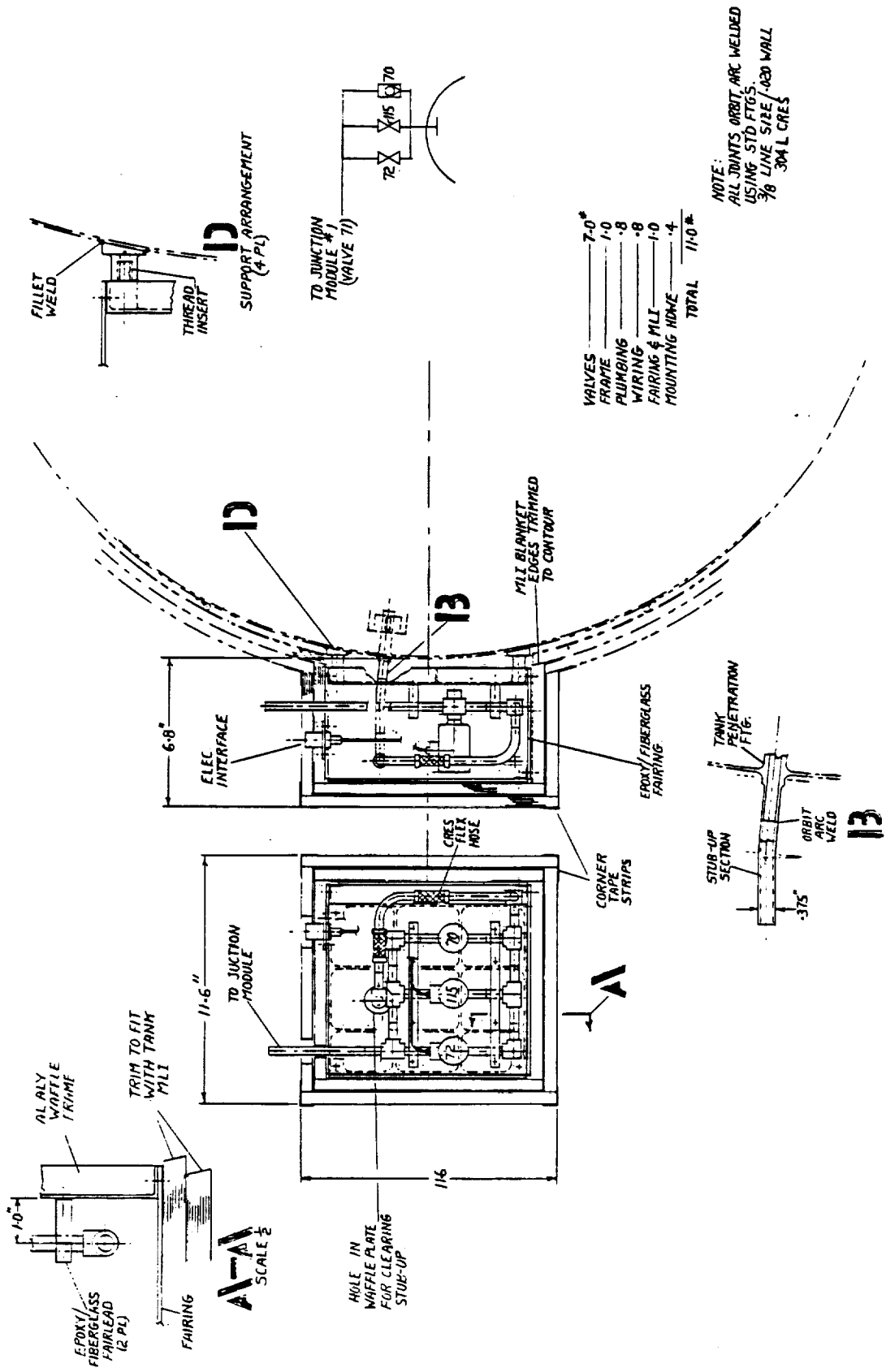


Figure A-4. Tank 3 Vent Arrangement

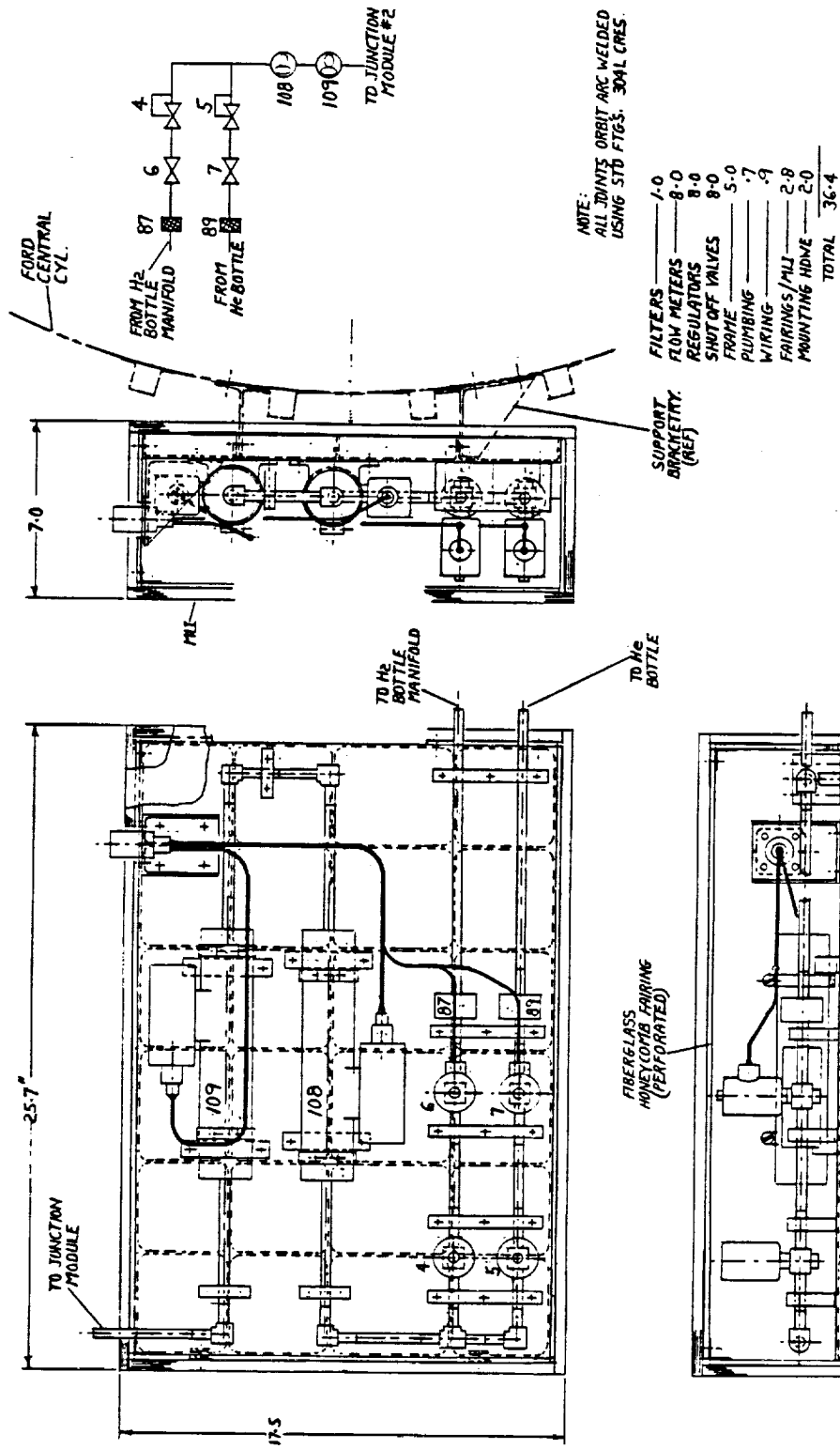


Figure A-6. Pressurization Control Module

The components are inter-plumbed with standard fittings and all connections are made with the orbit arc welding process. The plumbed assembly is clamped onto a waffle panel using epoxy/fiberglass fairleads, saddles and CRES bands. Shimming, as required, between panel, fairleads and saddles compensates for misalignments and avoids pre-stress conditions.

The assembly is covered with a preformed MLI envelope (not shown) prior to attaching to the tank bulkhead. For additional thermal isolation, an epoxy/fiberglass panel can be substituted for the waffle panel shown.

A.4.4 Junction Module

Referring to the vent and pressurization circuits on the system schematic, twelve valves and three flowmeters are interconnected to the three tanks, to the flight and ground vents, and to the pressure control module. These components are collected into one package (as shown in Figure A-8), interplumbed, and mounted on a waffle panel with epoxy/fiberglass fairleads and saddles. The entire package is boxed in with a fairing and covered with MLI. All tubes and fittings are 304L CRES connected with the orbit arc welding process. The complete module is supported with a system of links and struts from the outer structure.

A.5 EXPERIMENT MODULE ALTERNATIVE LIGHTWEIGHT STRUCTURE DESIGN USING GRAPHITE EPOXY

The general features shown in Figure A-9 are the same as that for the all-aluminum baseline design except that graphite/epoxy skins are used in the aft section. The loads are shared by both the inner and outer skins in the aft section only.

Referring to Figure A-10, the aft interface arrangement is basically the same as that for the all-aluminum design. The inner and outer skins are graphite/epoxy and the honeycomb core and ring is aluminum. Therefore, these two materials are separated by fiberglass scrim cloth to prevent corrosion (Details "D" and "C"). Aluminum foil is bonded to the outer skin to prevent exposure of the graphite epoxy to atomic oxygen (Detail "C"). Attachments between the "Z" ring, skins, strap and fittings are made with close fitting titanium blind fasteners.

The structural arrangement (Figure A-11) between the forward and aft cone frustrums and the aft short cylinder are the same as that for the all-aluminum design except for the foam-filled zones at each of the kick rings (Details "E" and "F") and the fiberglass scrim cloth additions for preventing corrosion.

A portion of the kick ring cross section shown in Figure A-11, Detail "F", forms a channel which must fit the I.D. and O.D. of the honeycomb sandwich cylinder. The tolerances are set up on both parts for a loose fit. Fastener pilot holes are drilled into the ring prior to assembly and after the two parts are engaged, epoxy is injected through the pilot holes which acts as a liquid shim. After the epoxy has hardened, the pilot holes are drilled out and the blind fasteners installed.

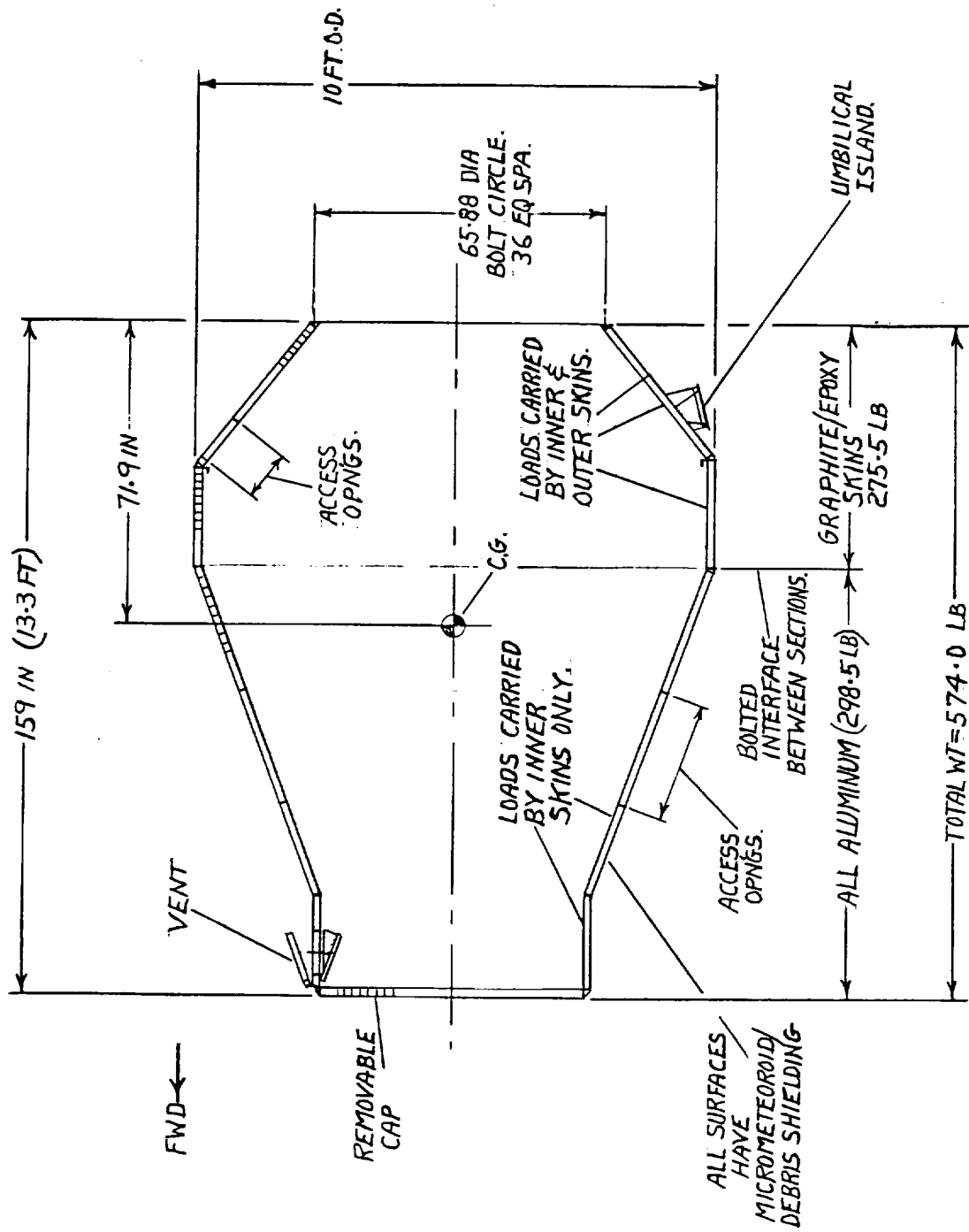


Figure A-9. Overall Features of the Graphite Epoxy and Aluminum Outer Structure

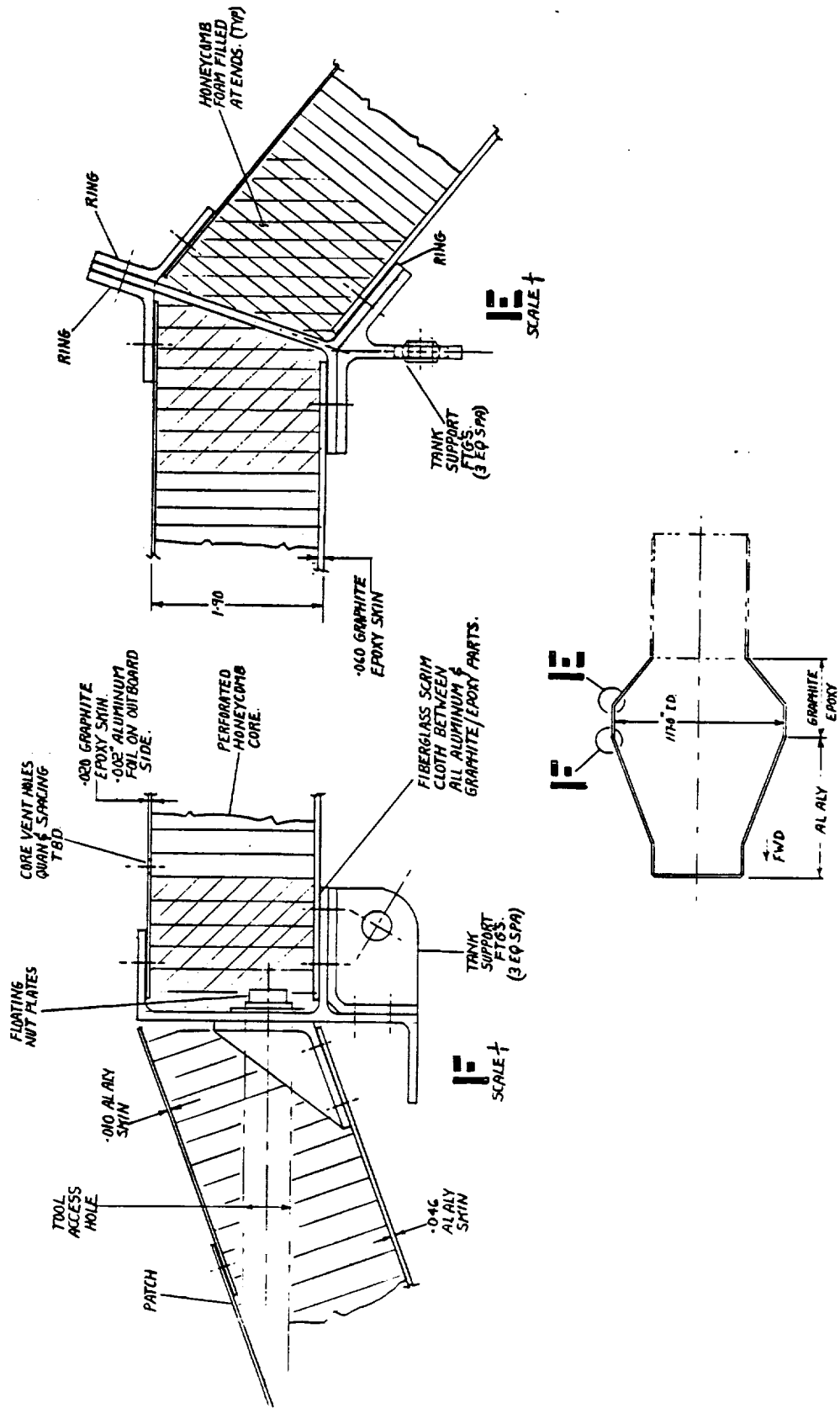


Figure A-11. Details of the Structural Joints of the Graphite/Epoxy Outer Structure

APPENDIX B
LIST OF EXPERIMENT MODULE
FLUID SYSTEM COMPONENTS

APPENDIX B
LIST OF EXPERIMENT MODULE FLUID SYSTEM COMPONENTS

Table B-1 lists the components that are identified by number in Figure 5-1 of the main body of this report.

Table B-1. Experiment Module Fluid System Components

ID*	TYPE	LINE SIZE (mm)	FUNCTION	TANK #
1	deleted component			
2	valve, relief	12.7	tank over-pressure relief - backup to #3	1
3	valve, shutoff, cryogenic	12.7	ground and flight tank vent control	1
4	regulator, high-pressure	9.5	reduce GH2 source pressure from 4000 to 50 psia	-
5	regulator, high-pressure	9.5	reduce helium source pressure from 4000 to 50 psia	-
6	valve, shutoff, high-pressure	9.5	bottle, hydrogen isolation	-
7	valve, shutoff, high-pressure	9.5	helium storage bottle isolation	-
8	valve, shutoff, cryogenic	9.5	tank vent control - backup to #10	2
9	deleted component			
10	valve, shutoff, cryogenic	9.5	tank vent control	2
11	valve, shutoff, cryogenic	6.4	TVS, compact supply control - backup to #27	1
12	valve, shutoff, cryogenic	9.5	tank pressurization control - backup to #13	1
13	valve, shutoff, cryogenic	9.5	tank pressurization control	1
14	valve, shutoff, cryogenic	9.5	tank pressurization control - backup to #13	1
15	valve, shutoff, cryogenic	6.4	tank pressurization control - backup to #16	2
16	valve, shutoff, cryogenic	6.4	tank pressurization control	2
17	valve, shutoff, cryogenic	6.4	tank pressurization control - backup to #16	2
18	valve, check	6.4	pressurization line backflow prevention	2
19	valve, check	9.5	pressurization line backflow prevention	1
20	deleted component			
21	valve, shutoff, cryogenic	6.4	passive TVS flow control (cyclically operated)	2
22	valve, shutoff, cryogenic	19	main inflow line isolation	2
23	valve, shutoff, cryogenic	19	radial nozzle isolation	2
24	valve, shutoff, cryogenic	9.5	transfer line vent control	2
25	valve, shutoff, cryogenic	6.4	passive TVS flow control (cyclically operated)	2
26	flowmeter, 2-phase	19	transfer mass flowrate feedback	2
27	valve, shutoff, cryogenic	6.4	TVS, compact supply control	1
28	valve, shutoff, cryogenic	6.4	TVS, compact supply control - backup to #27	1
29	orifice	6.4	TVS supply throttling	1
30	flowmeter, 2-phase	19	transfer mass flowrate feedback	1
31	valve, relief	19	transfer line over-pressure relief	1
32	valve, relief	12.7	fill/drain line over-pressure relief	-
33	valve, relief	9.5	evaporator over-pressure relief - backup to #38	-
34	valve, relief	12.7	fill/drain line over-pressure relief - backup to #32	-
35	valve, relief	9.5	evaporator over-pressure relief - backup to #38	-
36	valve, shutoff, cryogenic	19	ground fill/drain isolation - closed before disconnect for launch	1
37	disconnect, self-sealing	19	ground fill/drain interface - flight half of disconnect	1
38	valve, relief	9.5	evaporator over-pressure relief	-
39	valve, relief	9.5	evaporator over-pressure relief - backup to #38	-
40	valve, shutoff, cryogenic	6.4	passive TVS supply control - backup to #77	1
41	deleted component			
42	valve, relief	12.7	transfer line over-pressure relief	-
43	valve, relief	9.5	transfer line over-pressure relief	-
44	valve, shutoff, cryogenic	6.4	passive TVS supply control - backup to #77	1
45	valve, shutoff, cryogenic	12.7	transfer flow control - orificed	1
46	valve, shutoff, cryogenic	12.7	transfer flow control - orificed	1
47	valve, shutoff, cryogenic	12.7	transfer flow control - orificed	1
48	pump	6.4	evaporator supply for cold vapor pressurization	-
49	flowmeter, 2-phase	19	radial nozzle mass flowrate feedback - can be uni-directional	2
50	flowmeter, 2-phase	12.7	radial nozzle/main line mass flowrate feedback - bi-directional	3
51	valve, shutoff, cryogenic	6.4	tank pressurization control - backup to #60	2
52	filter, cryogenic	6.4	TVS supply contaminant filter - prevents blockage of throttling orifice #101	3
53	valve, shutoff, cryogenic	12.7	tangential nozzle isolation	3
54	valve, shutoff, cryogenic	9.5	transfer line vent	3
55	flowmeter, 2-phase	12.7	transfer mass flowrate feedback - can be uni-directional	3
56	valve, shutoff, cryogenic	12.7	main transfer line isolation	3

* From Figure 5-1.

Table B-1 (Cont.). Experiment Module Fluid System Components

ID*	TYPE		FUNCTION	TANK #
57	valve, shutoff, cryogenic	12.7	radial nozzle isolation	3
58	valve, shutoff, cryogenic	12.7	axial nozzle shutoff valve	3
59	valve, shutoff, cryogenic	6.4	passive TVS flow control (cyclically operated)	3
60	valve, shutoff, cryogenic	6.4	tank pressurization control	3
61	valve, shutoff, cryogenic	12.7	transfer flow control - orificed	1
62	valve, shutoff, cryogenic	12.7	transfer flow control - orificed	1
63	valve, shutoff, cryogenic	9.5	isolation of cold vapor regulator, high-pressure #41	1
64	accumulator	9.5	cold vapor pressurant flow capacitor	1
65	valve, shutoff, cryogenic	6.4	tank pressurization control - backup to #60	3
66	valve, shutoff, cryogenic	9.5	transfer line vent - backup to #54	3
67	valve, check	6.4	pressurization line backflow prevention	3
68	valve, shutoff, cryogenic	9.5	isolation of cold vapor regulator, high-pressure #20	1
69	deleted component			
70	deleted component			
71	valve, shutoff, cryogenic	9.5	tank vent control - backup to #115	3
72	valve, shutoff, cryogenic	9.5	tank vent control - backup to #115	3
73	evaporator	9.5	cold vapor pressurant evaporator - contains redundant heater element	-
74	diffuser	9.5	pressurization diffuser	1
75	diffuser	6.4	pressurization diffuser	2
76	diffuser	6.4	pressurization diffuser	3
77	valve, shutoff, cryogenic	6.4	passive TVS supply control	1
78	bottle, hydrogen		high-pressure GH2 storage for pressurization supply	
79	pump	19	fluid transfer - centrifugal, variable speed	-
80	pump	19	fluid transfer - centrifugal, variable speed	-
81	bottle, hydrogen		high-pressure GH2 storage for pressurization supply	
82	bottle, helium		high-pressure helium storage for pressurization supply	
83	valve, shutoff, cryogenic	12.7	flight vent back-pressure control - ~2 psia set point to prevent freezing	-
84	subcooler	12.7	subcool fluid during transfer	1
85	orifice	6.4	TVS supply throttling - backup to #96	1
86	valve, manual	9.5	high-pressure GH2 local isolation	-
87	filter, high-pressure	9.5	GH2 pressurization filter	-
88	valve, manual	9.5	high-pressure helium local isolation	-
89	filter, high-pressure	9.5	helium pressurization filter	-
90	valve, shutoff, cryogenic	12.7	flight vent back-pressure control - backup to #83	-
91	valve, check	12.7	axial nozzle backflow prevention	3
92	valve, check	12.7	radial nozzle backflow prevention	3
93	valve, check	12.7	tangential nozzle backflow prevention	3
94	valve, shutoff, cryogenic	9.5	transfer line vent control - backup to #24	2
95	orifice	9.5	subcooling heat exchanger flow throttling - viscojet assumed	1
96	orifice	6.4	passive TVS supply throttling	1
97	valve, shutoff, cryogenic	6.4	flight vent back-pressure control - backup to #83	2
98	orifice	6.4	passive TVS supply throttling	2
99	filter, cryogenic	6.4	TVS supply contaminant filter - prevents blockage of throttling orifice #98	2
100	TVS, compact	6.4	reduce tank pressure/temperature by venting gas	1
101	orifice	6.4	passive TVS supply throttling	3
102	valve, check	12.7	Centaur vent backflow prevention	-
103	valve, shutoff, cryogenic	19	axial nozzle isolation	2
104	valve, relief	9.5	valve, relief leakage isolation	-
105	flowmeter, 2-phase	12.7	flight vent flow feedback	-
106	valve, shutoff, cryogenic	12.7	ground and flight tank vent control - backup to #3	1
107	valve, shutoff, cryogenic	9.5	tank vent control - backup to #10	2
108	flowmeter, gas	9.5	pressurization gas mass flowrate feedback	-
109	flowmeter, gas	9.5	pressurization gas mass flowrate feedback - backup to #108	-
110	flowmeter, gas	9.5	cold vapor press gas mass flowrate feedback - backup to #112	-
111	flowmeter, gas	6.4	Tank #1 VCS vent flow feedback	1
112	flowmeter, gas	9.5	cold vapor pressurization gas mass flow feedback	-
113	orifice	6.4	TVS, compact supply throttling - backup to #29	1

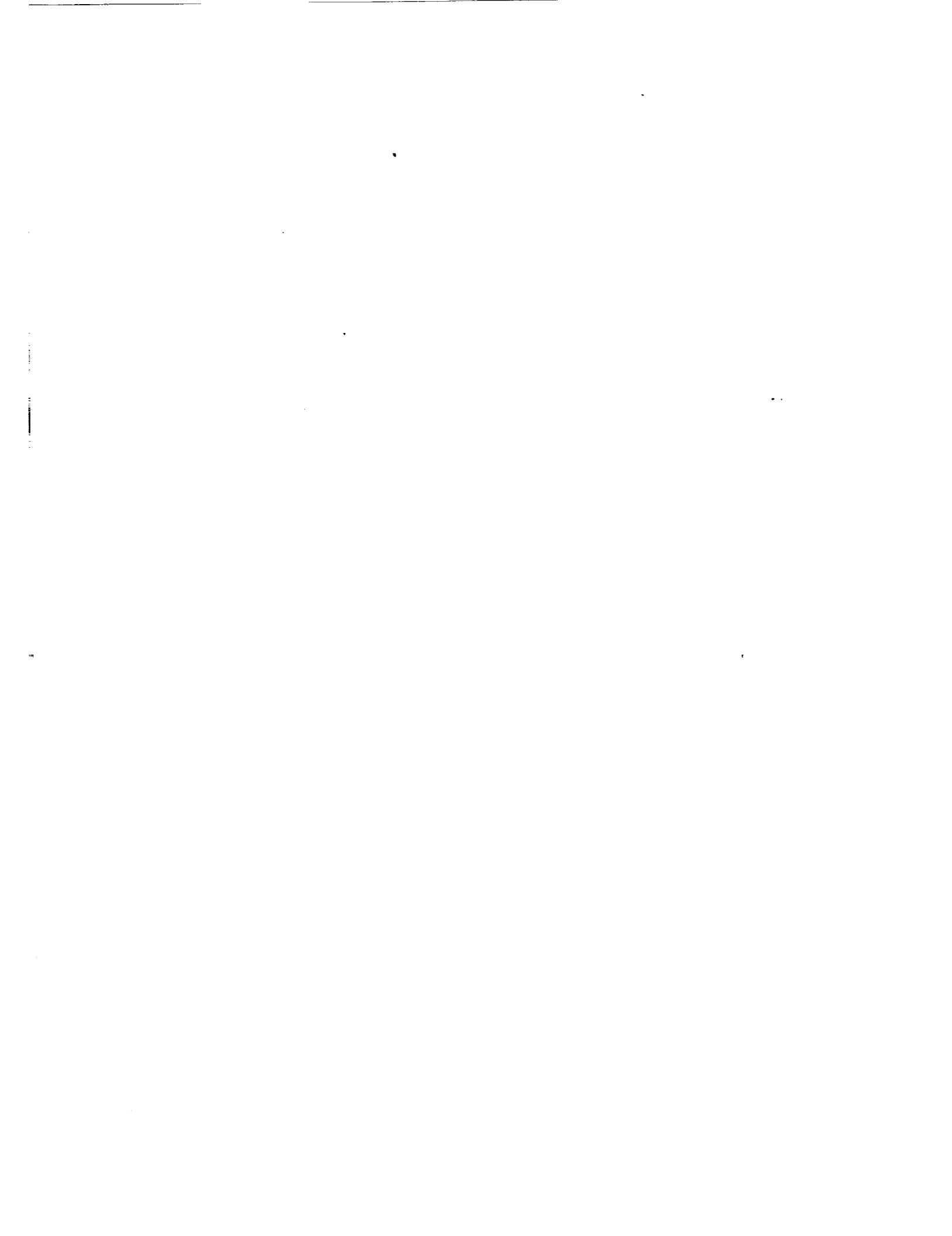
* From Figure 5-1.

Table B-1 (Cont.). Experiment Module Fluid System Components

ID*	TYPE		FUNCTION	TANK #
114	filter, cryogenic	6.4	TVS supply contaminant filter - prevents blockage of throttling orifice #113	1
115	valve, shutoff, cryogenic	9.5	tank vent control	3
116	valve, shutoff, cryogenic	19	transfer pump diversion	1
117	disconnect, self-sealing	12.7	Centaur vent interface - COLDSAT half of disconnect	-
118	disconnect, non-sealing	12.7	Centaur vent interface - Centaur half of disconnect	-
119	orifice	12.7	Centaur vent flow restriction	-
120	deleted component			
121	valve, shutoff, cryogenic	19	tank 2 to 3 pump diversion	1
122	flowmeter, gas	6.4	Tanks #2 & 3 VCS vent flow feedback	-
123	valve, shutoff, cryogenic	9.5	subcooler isolation	1
124	valve, shutoff, cryogenic	19	tank 2 to 3 pump diversion	-
125	valve, shutoff, cryogenic	9.5	subcooler isolation - backup to #123	-
126	valve, shutoff, cryogenic	19	transfer pump diversion	-
127	deleted component			
128	valve, shutoff, cryogenic	19	transfer pump diversion	-
129	valve, shutoff, cryogenic	19	transfer pump failure isolation	-
130	valve, shutoff, cryogenic	6.4	cold vapor pressurization pump isolation - backup to #131	-
131	valve, shutoff, cryogenic	6.4	cold vapor pressurization pump isolation	-
132	valve, shutoff, cryogenic	6.4	pressurization pump isolation valve	-
133	valve, shutoff, cryogenic	6.4	pressurization pump isolation valve	-
134	valve, shutoff, cryogenic	19	transfer pump diversion	1
135	valve, shutoff, cryogenic	19	transfer pump diversion	1
136	valve, shutoff, cryogenic	19	transfer pump diversion	1
137	valve, shutoff, cryogenic	12.7	transfer flow control - orificed	1
138	valve, shutoff, cryogenic	12.7	transfer flow control - orificed	1
139	valve, shutoff, cryogenic	12.7	transfer flow control - orificed	1
140	valve, shutoff, cryogenic	12.7	transfer flow control - orificed	1
141	valve, shutoff, cryogenic	12.7	transfer flow control - orificed	1
-	pump controller		transfer pump controller	-
-	pump controller		transfer pump controller	-
-	pump controller		cold vapor pressurization pump controller	-
-	pump controller		cold vapor pressurization pump controller	-

* From Figure 5-1.

APPENDIX C
INSTRUMENTATION AND CONTROL LISTS AND DIAGRAMS



APPENDIX C INSTRUMENTATION AND CONTROL LISTS AND DIAGRAMS

This appendix contains additional instrumentation and control information. Figures C-1 through C-8 present instrumentation electrical diagrams. Table C-1 lists experiment measurement requirements, and Table C-2 is a command list for the experiment module systems.

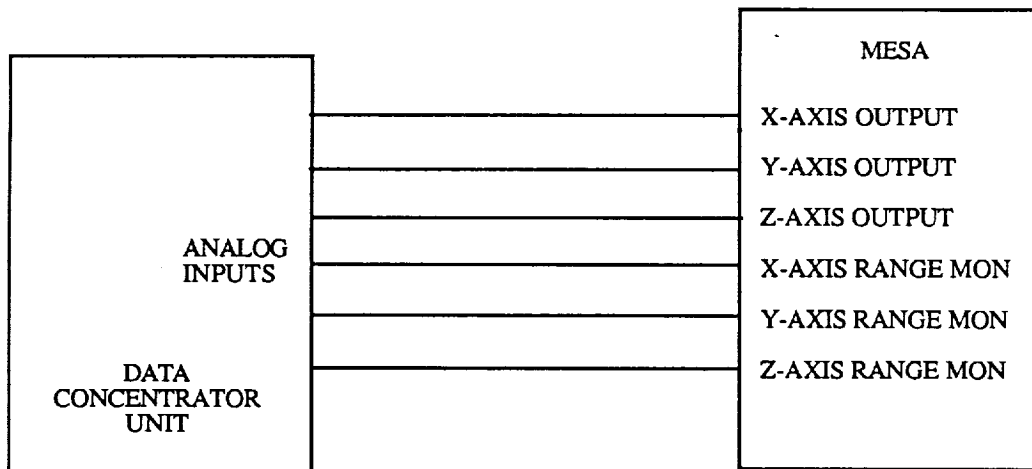


Figure C-1. Accelerometer Measurements

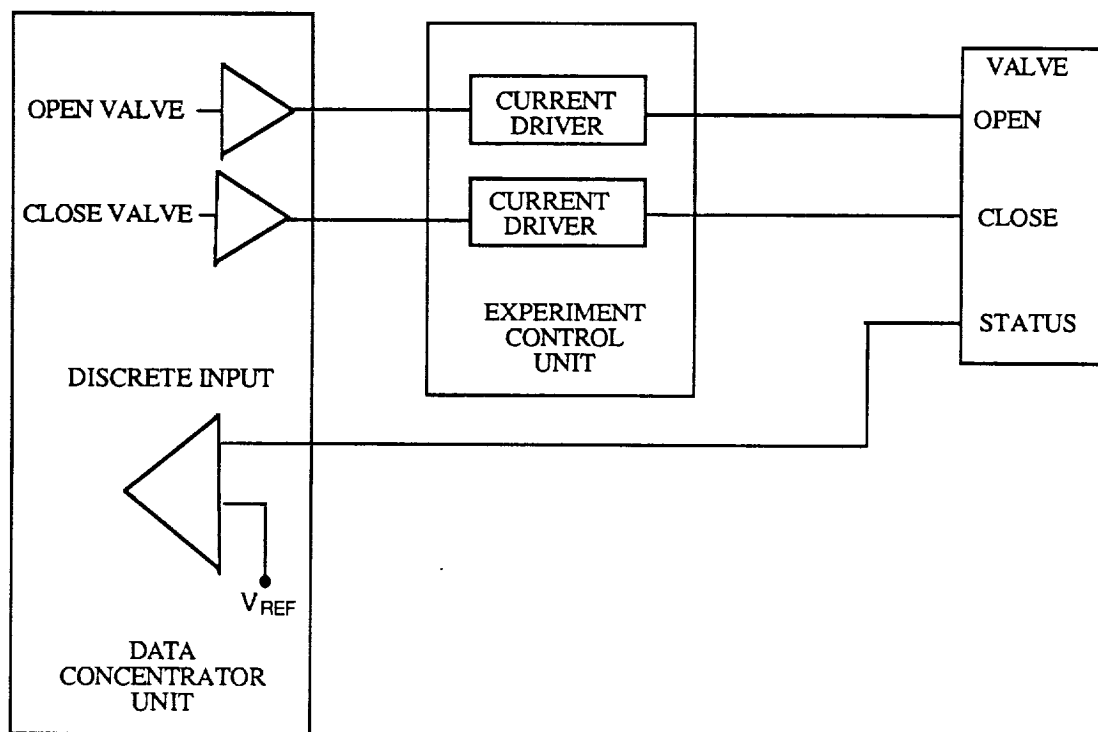


Figure C-2. Command Status Measurement

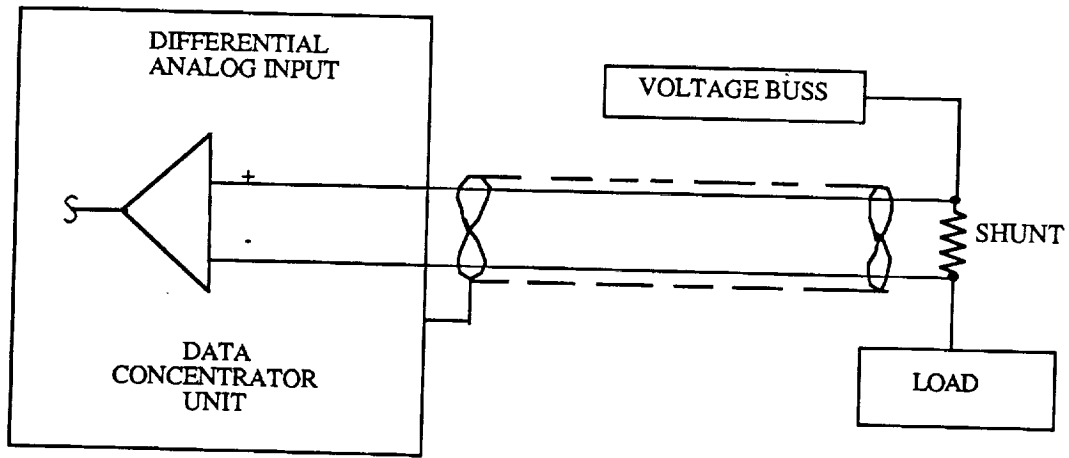


Figure C-3. Current Measurement

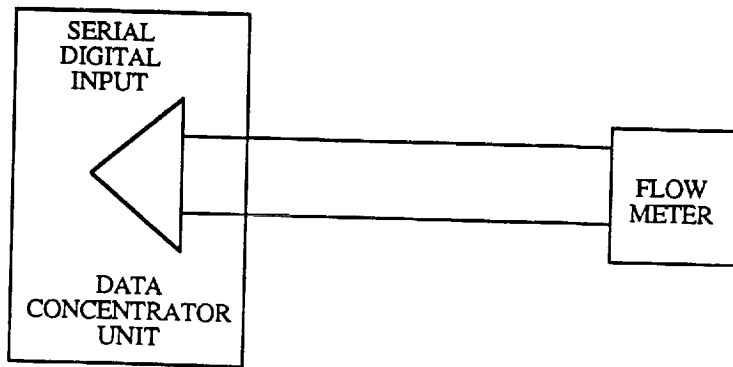


Figure C-4. Flow Measurements

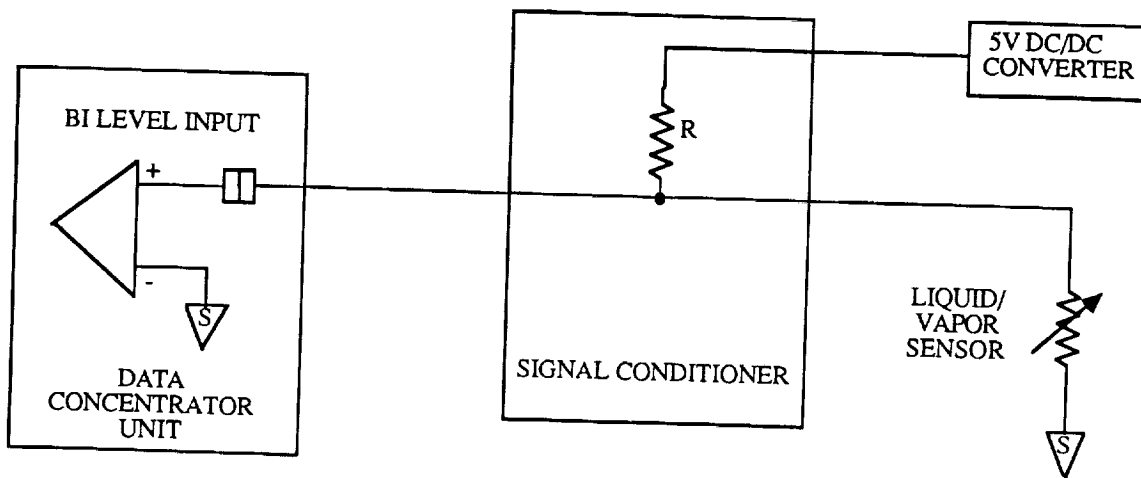


Figure C-5. Liquid vapor Sensor Measurement

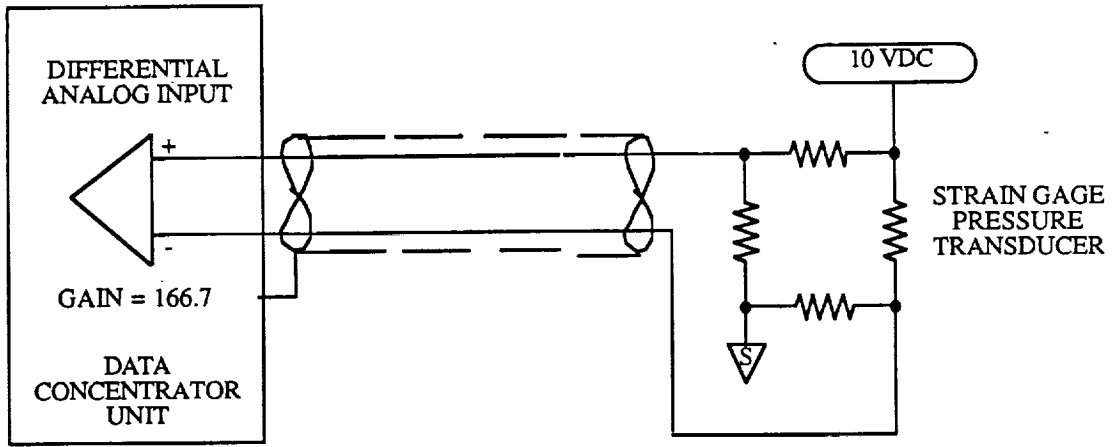


Figure C-6. Pressure Measurement

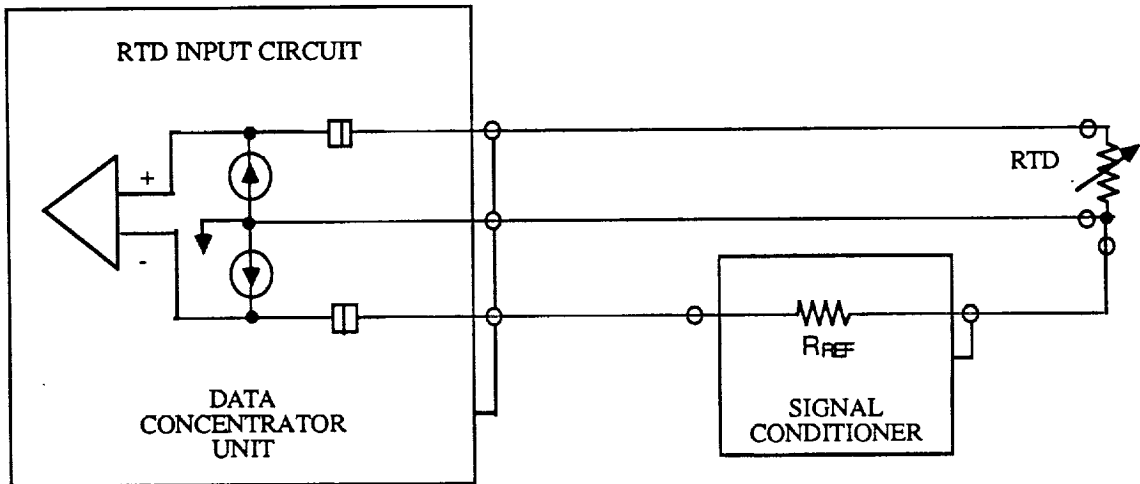


Figure C-7. Temperature Measurement

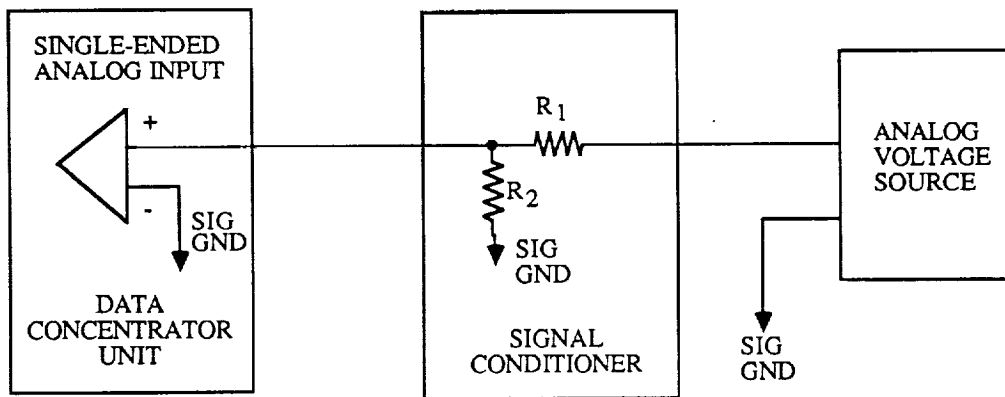


Figure C-8. Voltage Measurements

Table C-1. COLD-SAT Experiment Measurement Requirements

MEAS NO.	DESCRIPTION	MEAS RANGE		UNITS	SAMPLE PERIOD (SEC)
		LOW	HIGH		
E001C	UNREGULATED BUSS CURRENT	0	30	AMPS	1
E002C	28 V BUSS CURRENT	0	8	AMPS	1
E003C	INVERTER INPUT CURRENT	0	500	mA	1
E004C	5 V CONVERTER OUTPUT CURRENT	0	8	AMPS	1
E005C	10 V CONVERTER OUTPUT CURRENT	0	100	mA	1
E006C	VENT LINE HEATER CURRENT			AMPS	1
E007C	EVAPORATOR HEATER CURRENT			AMPS	1
E008C	TANK 3 LINE HEATER CURRENT			AMPS	1
E009C	TANK 1 HEATER CURRENT	0	1.5	AMPS	1
E010C	LAD HEATER CURRENT			AMPS	1
E011C	TANK 2 HEATER CURRENT	0	9	AMPS	1
E012C	TANK 3 HEATER CURRENT	0	3	AMPS	1
E013C	PRESSURIZATION PUMP CURRENT			AMPS	1
E014C	TRANSFER PUMP CURRENT			AMPS	1
E001V	UNREGULATED BUSS VOLTAGE	0	45	VDC	1
E002V	28 V BUSS VOLTAGE	0	35	VDC	1
E003V	5 V BUSS VOLTAGE	0	6	VDC	1
E004V	10 V BUSS VOLTAGE	0	12	VDC	1
X001A	X1-AXIS ACCELERATION	AUTO-RANGE	AUTO-RANGE	MICRO G	0.5
X002A	Y1-AXIS ACCELERATION	AUTO-RANGE	AUTO-RANGE	MICRO G	0.5
X003A	Z1-AXIS ACCELERATION	AUTO-RANGE	AUTO-RANGE	MICRO G	0.125
X004A	X2-AXIS ACCELERATION	AUTO-RANGE	AUTO-RANGE	MICRO G	0.5
X005A	Y2-AXIS ACCELERATION	AUTO-RANGE	AUTO-RANGE	MICRO G	0.5
X006A	Z2-AXIS ACCELERATION	AUTO-RANGE	AUTO-RANGE	MICRO G	0.125
X007A	X3-AXIS ACCELERATION	AUTO-RANGE	AUTO-RANGE	MICRO G	0.5
X008A	Y3-AXIS ACCELERATION	AUTO-RANGE	AUTO-RANGE	MICRO G	0.5
X009A	Z3-AXIS ACCELERATION	AUTO-RANGE	AUTO-RANGE	MICRO G	0.125
X010A	X1-AXIS ACCELERATION RANGE MONITOR	0	5	VDC	1
X011A	Y1-AXIS ACCELERATION RANGE MONITOR	0	5	VDC	1
X012A	Z1-AXIS ACCELERATION RANGE MONITOR	0	5	VDC	1

Table C-1. COLD-SAT Experiment Measurement Requirements (Cont.)

MEAS NO.	DESCRIPTION	MEAS RANGE		UNITS	SAMPLE PERIOD (SEC)
		LOW	HIGH		
X013A	X2-AXIS ACCELERATION RANGE MONITOR	0	5	VDC	1
X014A	Y2-AXIS ACCELERATION RANGE MONITOR	0	5	VDC	1
X015A	Z2-AXIS ACCELERATION RANGE MONITOR	0	5	VDC	1
X016A	X3-AXIS ACCELERATION RANGE MONITOR	0	5	VDC	1
X017A	Y3-AXIS ACCELERATION RANGE MONITOR	0	5	VDC	1
X018A	Z3-AXIS ACCELERATION RANGE MONITOR	0	5	VDC	1
X001D	VALVE 3 POSITION	CLOSED	OPEN	EVENT	1
X002D	VALVE 6 POSITION	CLOSED	OPEN	EVENT	1
X003D	VALVE 7 POSITION	CLOSED	OPEN	EVENT	1
X004D	VALVE 8 POSITION	CLOSED	OPEN	EVENT	1
X005D	VALVE 10 POSITION	CLOSED	OPEN	EVENT	1
X006D	VALVE 11 POSITION	CLOSED	OPEN	EVENT	1
X007D	VALVE 12 POSITION	CLOSED	OPEN	EVENT	1
X008D	VALVE 13 POSITION	CLOSED	OPEN	EVENT	1
X009D	VALVE 14 POSITION	CLOSED	OPEN	EVENT	1
X010D	VALVE 15 POSITION	CLOSED	OPEN	EVENT	1
X011D	VALVE 16 POSITION	CLOSED	OPEN	EVENT	1
X012D	VALVE 17 POSITION	CLOSED	OPEN	EVENT	1
X013D	VALVE 21 POSITION	CLOSED	OPEN	EVENT	1
X014D	VALVE 22 POSITION	CLOSED	OPEN	EVENT	1
X015D	VALVE 23 POSITION	CLOSED	OPEN	EVENT	1
X016D	VALVE 24 POSITION	CLOSED	OPEN	EVENT	1
X017D	VALVE 25 POSITION	CLOSED	OPEN	EVENT	1
X018D	VALVE 27 POSITION	CLOSED	OPEN	EVENT	1
X019D	VALVE 28 POSITION	CLOSED	OPEN	EVENT	1
X020D	VALVE 36 POSITION	CLOSED	OPEN	EVENT	1
X021D	VALVE 40 POSITION	CLOSED	OPEN	EVENT	1
X022D	VALVE 44 POSITION	CLOSED	OPEN	EVENT	1
X023D	VALVE 45 POSITION	CLOSED	OPEN	EVENT	1
X024D	VALVE 46 POSITION	CLOSED	OPEN	EVENT	1

Table C-1. COLD-SAT Experiment Measurement Requirements (Cont.)

MEAS NO.	DESCRIPTION	MEAS RANGE		UNITS	SAMPLE PERIOD (SEC)
		LOW	HIGH		
X025D	VALVE 47 POSITION	CLOSED	OPEN	EVENT	1
X026D	VALVE 51 POSITION	CLOSED	OPEN	EVENT	1
X027D	VALVE 53 POSITION	CLOSED	OPEN	EVENT	1
X028D	VALVE 54 POSITION	CLOSED	OPEN	EVENT	1
X029D	VALVE 56 POSITION	CLOSED	OPEN	EVENT	1
X030D	VALVE 57 POSITION	CLOSED	OPEN	EVENT	1
X031D	VALVE 58 POSITION	CLOSED	OPEN	EVENT	1
X032D	VALVE 59 POSITION	CLOSED	OPEN	EVENT	1
X033D	VALVE 60 POSITION	CLOSED	OPEN	EVENT	1
X034D	VALVE 61 POSITION	CLOSED	OPEN	EVENT	1
X035D	VALVE 62 POSITION	CLOSED	OPEN	EVENT	1
X036D	VALVE 63 POSITION	CLOSED	OPEN	EVENT	1
X037D	VALVE 65 POSITION	CLOSED	OPEN	EVENT	1
X038D	VALVE 66 POSITION	CLOSED	OPEN	EVENT	1
X039D	VALVE 68 POSITION	CLOSED	OPEN	EVENT	1
X040D	VALVE 71 POSITION	CLOSED	OPEN	EVENT	1
X041D	VALVE 72 POSITION	CLOSED	OPEN	EVENT	1
X042D	VALVE 77 POSITION	CLOSED	OPEN	EVENT	1
X043D	VALVE 90 POSITION	CLOSED	OPEN	EVENT	1
X044D	VALVE 94 POSITION	CLOSED	OPEN	EVENT	1
X045D	VALVE 103 POSITION	CLOSED	OPEN	EVENT	1
X046D	VALVE 106 POSITION	CLOSED	OPEN	EVENT	1
X047D	VALVE 107 POSITION	CLOSED	OPEN	EVENT	1
X048D	VALVE 115 POSITION	CLOSED	OPEN	EVENT	1
X049D	VALVE 116 POSITION	CLOSED	OPEN	EVENT	1
X050D	VALVE 121 POSITION	CLOSED	OPEN	EVENT	1
X051D	VALVE 123 POSITION	CLOSED	OPEN	EVENT	1
X052D	VALVE 124 POSITION	CLOSED	OPEN	EVENT	1
X053D	VALVE 125 POSITION	CLOSED	OPEN	EVENT	1
X054D	VALVE 126 POSITION	CLOSED	OPEN	EVENT	1

Table C-1. COLD-SAT Experiment Measurement Requirements (Cont.)

MEAS NO.	DESCRIPTION	MEAS RANGE		UNITS	SAMPLE PERIOD (SEC)
		LOW	HIGH		
X055D	VALVE 128 POSITION	CLOSED	OPEN	EVENT	1
X056D	VALVE 129 POSITION	CLOSED	OPEN	EVENT	1
X057D	VALVE 130 POSITION	CLOSED	OPEN	EVENT	1
X058D	VALVE 131 POSITION	CLOSED	OPEN	EVENT	1
X059D	VALVE 132 POSITION	CLOSED	OPEN	EVENT	1
X060D	VALVE 133 POSITION	CLOSED	OPEN	EVENT	1
X061D	VALVE 134 POSITION	CLOSED	OPEN	EVENT	1
X062D	VALVE 135 POSITION	CLOSED	OPEN	EVENT	1
X063D	VALVE 136 POSITION	CLOSED	OPEN	EVENT	1
X064D	VALVE 137 POSITION	CLOSED	OPEN	EVENT	1
X065D	VALVE 138 POSITION	CLOSED	OPEN	EVENT	1
X066D	VALVE 139 POSITION	CLOSED	OPEN	EVENT	1
X067D	VALVE 140 POSITION	CLOSED	OPEN	EVENT	1
X068D	VALVE 141 POSITION	CLOSED	OPEN	EVENT	1
X001F	TANK 1 FILL/ DRAIN FLOW (30)	0	400	lb/hr	0.5
X002F	TANK 2 FIL/DRAIN FLOW (26)	0	400	lb/hr	0.5
X003F	TANK 2 RADIAL SPRAY NOZZLE FLOW (49)	0	400	lb/hr	0.5
X004F	TANK 3 FILL/DRAIN FLOW (50)	0	400	lb/hr	0.5
X005F	TANK 3 SPRAY NOZZLE FLOW (55)	0	400	lb/hr	0.5
X006F	VENT LINE 1 FLOW (111)			lb/hr	0.5
X007F	VENT LINE 2 FLOW (122)			lb/hr	0.5
X008F	VENT LINE 4 FLOW (105)			lb/hr	0.5
X009F	COLD VAPOR PRESSURE 1 FLOW (110)	0	5	lb/hr	0.5
X010F	COLD VAPOR PRESSURE 2 FLOW (112)	0	5	lb/hr	0.5
X011F	STORED GAS PRESSURE 1 FLOW (108)	0	5	lb/hr	0.5
X012F	STORED GAS PRESSURE 2 FLOW (109)	0	5	lb/hr	0.5
X001P	TANK 1-1 PRESSURE	0	50	PSIA	1
X002P	TANK 1-2 PRESSURE	0	50	PSIA	1
X003P	TANK 1-3 PRESSURE	10	20	PSIA	1
X004P	TANK 1-4 PRESSURE	20	30	PSIA	1

Table C-1. COLD-SAT Experiment Measurement Requirements (Cont.)

MEAS NO.	DESCRIPTION	MEAS RANGE		UNITS	SAMPLE PERIOD (SEC)
		LOW	HIGH		
X005P	TANK 1 J-T VALVE 1 PRESSURE	0	20	PSIA	1
X006P	TANK 1 J-T VALVE 2 PRESSURE	0	20	PSIA	1
X007P	TANK 1 J-T VALVE 3 PRESSURE	0	20	PSIA	1
X008P	TANK 1 VENT LINE PRESSURE	0	20	PSIA	1
X009P	TANK 2-1 PRESSURE	0	50	PSIA	1
X010P	TANK 2-2 PRESSURE	0	50	PSIA	1
X011P	TANK 2-3 PRESSURE	10	20	PSIA	1
X012P	TANK 2-4 PRESSURE	20	30	PSIA	1
X013P	TANK 2 J-T VALVE PRESSURE	0	20	PSIA	1
X014P	TANK 2 VENT LINE PRESSURE	0	20	PSIA	1
X015P	TANK 3-1 PRESSURE	0	50	PSIA	1
X016P	TANK 3-2 PRESSURE	0	50	PSIA	1
X017P	TANK 3-3 PRESSURE	10	20	PSIA	1
X018P	TANK 3-4 PRESSURE	20	30	PSIA	1
X019P	TANK 3 J-T VALVE PRESSURE	0	20	PSIA	1
X020P	TANK 3 VENT LINE PRESSURE	0	20	PSIA	1
X021P	PRESSURIZATION LINE 1 PRESSURE	0	100	PSIA	1
X022P	PRESSURIZATION LINE 2 PRESSURE	0	100	PSIA	1
X023P	PRESSURIZATION LINE 3 PRESSURE	0	100	PSIA	1
X024P	PRESSURIZATION LINE 4 PRESSURE	0	100	PSIA	1
X025P	PRESSURIZATION LINE 5 PRESSURE	0	100	PSIA	1
X026P	PRESSURIZATION TANK 1 PRESSURE	0	4500	PSIA	1
X027P	PRESSURIZATION TANK 2 PRESSURE	0	4500	PSIA	1
X028P	PRESSURIZATION PUMP INLET PRESSURE	0	50	PSIA	1
X029P	PRESSURIZATION PUMP OUTLET PRESSURE	40	80	PSIA	1
X030P	TRANSFER PUMP OUTLET PRESSURE	0	50	PSIA	1
X031P	TRANSFER PUMP INLET PRESSURE	50	100	PSIA	1
X001S	TANK 1, INTERNAL, AXIAL-1, LIQUID/VAPOR STATE	LIQUID	VAPOR	EVENT	1
X002S	TANK 1, INTERNAL, AXIAL-2, LIQUID/VAPOR STATE	LIQUID	VAPOR	EVENT	1
X003S	TANK 1, INTERNAL, AXIAL-3, LIQUID/VAPOR STATE	LIQUID	VAPOR	EVENT	1

Table C-1. COLD-SAT Experiment Measurement Requirements (Cont.)

MEAS NO.	DESCRIPTION	MEAS RANGE		UNITS	SAMPLE PERIOD (SEC)
		LOW	HIGH		
X004S	TANK 1, INTERNAL, AXIAL-4, LIQUID/VAPOR STATE	LIQUID	VAPOR	EVENT	1
X005S	TANK 1, INTERNAL, AXIAL-5, LIQUID/VAPOR STATE	LIQUID	VAPOR	EVENT	1
X006S	TANK 1, INTERNAL, AXIAL-6, LIQUID/VAPOR STATE	LIQUID	VAPOR	EVENT	1
X007S	TANK 1, INTERNAL, AXIAL-7, LIQUID/VAPOR STATE	LIQUID	VAPOR	EVENT	1
X008S	TANK 1, INTERNAL, AXIAL-8, LIQUID/VAPOR STATE	LIQUID	VAPOR	EVENT	1
X009S	TANK 1, INTERNAL, RADIAL -1, LIQUID/VAPOR STATE	LIQUID	VAPOR	EVENT	1
X010S	TANK 1, INTERNAL, RADIAL -2, LIQUID/VAPOR STATE	LIQUID	VAPOR	EVENT	1
X011S	TANK 1, INTERNAL, RADIAL -3, LIQUID/VAPOR STATE	LIQUID	VAPOR	EVENT	1
X012S	TANK 1, INTERNAL, RADIAL -4, LIQUID/VAPOR STATE	LIQUID	VAPOR	EVENT	1
X013S	TANK 1, INTERNAL, RADIAL -5, LIQUID/VAPOR STATE	LIQUID	VAPOR	EVENT	1
X014S	TANK 1, INTERNAL, RADIAL -6, LIQUID/VAPOR STATE	LIQUID	VAPOR	EVENT	1
X015S	TANK 1, INTERNAL, RADIAL -7, LIQUID/VAPOR STATE	LIQUID	VAPOR	EVENT	1
X016S	TANK 1, INTERNAL, RADIAL -8, LIQUID/VAPOR STATE	LIQUID	VAPOR	EVENT	1
X017S	TANK 1, INTERNAL, RADIAL -9, LIQUID/VAPOR STATE	LIQUID	VAPOR	EVENT	1
X018S	TANK 1, INTERNAL, RADIAL-10, LIQUID/VAPOR STATE	LIQUID	VAPOR	EVENT	1
X019S	TANK 1, INTERNAL, RADIAL-11, LIQUID/VAPOR STATE	LIQUID	VAPOR	EVENT	1
X020S	TANK 1, INTERNAL, RADIAL-12, LIQUID/VAPOR STATE	LIQUID	VAPOR	EVENT	1
X021S	TANK 1, INTERNAL, RADIAL-13, LIQUID/VAPOR STATE	LIQUID	VAPOR	EVENT	1
X022S	TANK 1, INTERNAL, RADIAL-14, LIQUID/VAPOR STATE	LIQUID	VAPOR	EVENT	1
X023S	TANK 1, INTERNAL, RADIAL-15, LIQUID/VAPOR STATE	LIQUID	VAPOR	EVENT	1
X024S	TANK 1, INTERNAL, RADIAL-16, LIQUID/VAPOR STATE	LIQUID	VAPOR	EVENT	1
X025S	TANK 1, INTERNAL, RADIAL-17, LIQUID/VAPOR STATE	LIQUID	VAPOR	EVENT	1
X026S	TANK 1, INTERNAL, RADIAL-18, LIQUID/VAPOR STATE	LIQUID	VAPOR	EVENT	1
X027S	TANK 1, INTERNAL, RADIAL-19, LIQUID/VAPOR STATE	LIQUID	VAPOR	EVENT	1
X028S	TANK 1, INTERNAL, RADIAL-20, LIQUID/VAPOR STATE	LIQUID	VAPOR	EVENT	1
X029S	TANK 1, INTERNAL, RADIAL-21, LIQUID/VAPOR STATE	LIQUID	VAPOR	EVENT	1
X030S	TANK 1, INTERNAL, RADIAL-22, LIQUID/VAPOR STATE	LIQUID	VAPOR	EVENT	1
X031S	TANK 1, INTERNAL, RADIAL-23, LIQUID/VAPOR STATE	LIQUID	VAPOR	EVENT	1
X032S	TANK 1, INTERNAL, RADIAL-24, LIQUID/VAPOR STATE	LIQUID	VAPOR	EVENT	1
X033S	TANK 1 FILL/DRAIN LIQUID/VAPOR STATE	LIQUID	VAPOR	EVENT	1

Table C-1. COLD-SAT Experiment Measurement Requirements (Cont.)

MEAS NO.	DESCRIPTION	MEAS RANGE		UNITS	SAMPLE PERIOD (SEC)
		LOW	HIGH		
X034S	TANK 2, INTERNAL, AXIAL-1, LIQUID/VAPOR STATE	LIQUID	VAPOR	EVENT	1
X035S	TANK 2, INTERNAL, AXIAL-2, LIQUID/VAPOR STATE	LIQUID	VAPOR	EVENT	1
X036S	TANK 2, INTERNAL, AXIAL-3, LIQUID/VAPOR STATE	LIQUID	VAPOR	EVENT	1
X037S	TANK 2, INTERNAL, AXIAL-4, LIQUID/VAPOR STATE	LIQUID	VAPOR	EVENT	1
X038S	TANK 2, INTERNAL, AXIAL-5, LIQUID/VAPOR STATE	LIQUID	VAPOR	EVENT	1
X039S	TANK 2, INTERNAL, AXIAL-6, LIQUID/VAPOR STATE	LIQUID	VAPOR	EVENT	1
X040S	TANK 2, INTERNAL, AXIAL-7, LIQUID/VAPOR STATE	LIQUID	VAPOR	EVENT	1
X041S	TANK 2, INTERNAL, AXIAL-8, LIQUID/VAPOR STATE	LIQUID	VAPOR	EVENT	1
X042S	TANK 2, INTERNAL, RADIAL-1, LIQUID/VAPOR STATE	LIQUID	VAPOR	EVENT	1
X043S	TANK 2, INTERNAL, RADIAL-2, LIQUID/VAPOR STATE	LIQUID	VAPOR	EVENT	1
X044S	TANK 2, INTERNAL, RADIAL-3, LIQUID/VAPOR STATE	LIQUID	VAPOR	EVENT	1
X045S	TANK 2, INTERNAL, RADIAL-4, LIQUID/VAPOR STATE	LIQUID	VAPOR	EVENT	1
X046S	TANK 2, INTERNAL, RADIAL-5, LIQUID/VAPOR STATE	LIQUID	VAPOR	EVENT	1
X047S	TANK 2, INTERNAL, RADIAL-6, LIQUID/VAPOR STATE	LIQUID	VAPOR	EVENT	1
X048S	TANK 2, INTERNAL, RADIAL-7, LIQUID/VAPOR STATE	LIQUID	VAPOR	EVENT	1
X049S	TANK 2, INTERNAL, RADIAL-8, LIQUID/VAPOR STATE	LIQUID	VAPOR	EVENT	1
X050S	TANK 2, INTERNAL, RADIAL-9, LIQUID/VAPOR STATE	LIQUID	VAPOR	EVENT	1
X051S	TANK 2, INTERNAL, RADIAL-10, LIQUID/VAPOR STATE	LIQUID	VAPOR	EVENT	1
X052S	TANK 2, INTERNAL, RADIAL-11, LIQUID/VAPOR STATE	LIQUID	VAPOR	EVENT	1
X053S	TANK 2, INTERNAL, RADIAL-12, LIQUID/VAPOR STATE	LIQUID	VAPOR	EVENT	1
X054S	TANK 2, INTERNAL, RADIAL-13, LIQUID/VAPOR STATE	LIQUID	VAPOR	EVENT	1
X055S	TANK 2, INTERNAL, RADIAL-14, LIQUID/VAPOR STATE	LIQUID	VAPOR	EVENT	1
X056S	TANK 2, INTERNAL, RADIAL-15, LIQUID/VAPOR STATE	LIQUID	VAPOR	EVENT	1
X057S	TANK 2, INTERNAL, RADIAL-16, LIQUID/VAPOR STATE	LIQUID	VAPOR	EVENT	1
X058S	TANK 2, FILL/DRAIN, LIQUID/VAPOR STATE	LIQUID	VAPOR	EVENT	1
X059S	TANK 3, INTERNAL, AXIAL-1, LIQUID/VAPOR STATE	LIQUID	VAPOR	EVENT	1
X060S	TANK 3, INTERNAL, AXIAL-2, LIQUID/VAPOR STATE	LIQUID	VAPOR	EVENT	1
X061S	TANK 3, INTERNAL, AXIAL-3, LIQUID/VAPOR STATE	LIQUID	VAPOR	EVENT	1
X062S	TANK 3, INTERNAL, AXIAL-4, LIQUID/VAPOR STATE	LIQUID	VAPOR	EVENT	1
X063S	TANK 3, INTERNAL, AXIAL-5, LIQUID/VAPOR STATE	LIQUID	VAPOR	EVENT	1

Table C-1. COLD-SAT Experiment Measurement Requirements (Cont.)

MEAS NO.	DESCRIPTION	MEAS RANGE		UNITS	SAMPLE PERIOD (SEC)
		LOW	HIGH		
X064S	TANK 3,INTERNAL, AXIAL-6, LIQUID/VAPOR STATE	LIQUID	VAPOR	EVENT	1
X065S	TANK 3,INTERNAL, AXIAL-7, LIQUID/VAPOR STATE	LIQUID	VAPOR	EVENT	1
X066S	TANK 3,INTERNAL, AXIAL-8, LIQUID/VAPOR STATE	LIQUID	VAPOR	EVENT	1
X067S	TANK 3,INTERNAL, RADIAL-1, LIQUID/VAPOR STATE	LIQUID	VAPOR	EVENT	1
X068S	TANK 3,INTERNAL, RADIAL-2, LIQUID/VAPOR STATE	LIQUID	VAPOR	EVENT	1
X069S	TANK 3,INTERNAL, RADIAL-3, LIQUID/VAPOR STATE	LIQUID	VAPOR	EVENT	1
X070S	TANK 3,INTERNAL, RADIAL-4, LIQUID/VAPOR STATE	LIQUID	VAPOR	EVENT	1
X071S	TANK 3,INTERNAL, RADIAL-5, LIQUID/VAPOR STATE	LIQUID	VAPOR	EVENT	1
X072S	TANK 3,INTERNAL, RADIAL-6, LIQUID/VAPOR STATE	LIQUID	VAPOR	EVENT	1
X073S	TANK 3,INTERNAL, RADIAL-7, LIQUID/VAPOR STATE	LIQUID	VAPOR	EVENT	1
X074S	TANK 3,INTERNAL, RADIAL-8, LIQUID/VAPOR STATE	LIQUID	VAPOR	EVENT	1
X075S	TANK 3,INTERNAL, RADIAL-9, LIQUID/VAPOR STATE	LIQUID	VAPOR	EVENT	1
X076S	TANK 3,INTERNAL, RADIAL-10, LIQUID/VAPOR STATE	LIQUID	VAPOR	EVENT	1
X077S	TANK 3,INTERNAL, RADIAL-11, LIQUID/VAPOR STATE	LIQUID	VAPOR	EVENT	1
X078S	TANK 3,INTERNAL, RADIAL-12, LIQUID/VAPOR STATE	LIQUID	VAPOR	EVENT	1
X079S	TANK 3,INTERNAL, RADIAL-13, LIQUID/VAPOR STATE	LIQUID	VAPOR	EVENT	1
X080S	TANK 3,INTERNAL, RADIAL-14, LIQUID/VAPOR STATE	LIQUID	VAPOR	EVENT	1
X081S	TANK 3,INTERNAL, RADIAL-15, LIQUID/VAPOR STATE	LIQUID	VAPOR	EVENT	1
X082S	TANK 3,INTERNAL, RADIAL-16, LIQUID/VAPOR STATE	LIQUID	VAPOR	EVENT	1
X083S	TANK 3, FILL/DRAIN, LIQUID/VAPOR STATE	LIQUID	VAPOR	EVENT	1
X084S	TANK 3, VENT LINE, LIQUID/VAPOR STATE	LIQUID	VAPOR	EVENT	1
X001T	TANK 1, INTERNAL,AXIAL-1, TEMP	25	50	DEGR	10
X002T	TANK 1, INTERNAL,AXIAL-2, TEMP	25	50	DEGR	10
X003T	TANK 1, INTERNAL,AXIAL-3, TEMP	25	50	DEGR	10
X004T	TANK 1, INTERNAL,AXIAL-4, TEMP	25	50	DEGR	10
X005T	TANK 1, INTERNAL,AXIAL-5, TEMP	25	50	DEGR	10
X006T	TANK 1, INTERNAL,AXIAL-6, TEMP	25	50	DEGR	10
X007T	TANK 1, INTERNAL,AXIAL-7, TEMP	25	50	DEGR	10
X008T	TANK 1, INTERNAL,AXIAL-8, TEMP	25	50	DEGR	10
X009T	TANK 1, INTERNAL, RADIAL, L1-1 TEMP	25	50	DEGR	10

Table C-1. COLD-SAT Experiment Measurement Requirements (Cont.)

MEAS NO.	DESCRIPTION	MEAS RANGE		UNITS	SAMPLE PERIOD (SEC)
		LOW	HIGH		
X010T	TANK 1, INTERNAL, RADIAL, L1-2 TEMP	25	50	DEGR	10
X011T	TANK 1, INTERNAL, RADIAL, L1-3 TEMP	25	50	DEGR	10
X012T	TANK 1, INTERNAL, RADIAL, L1-4 TEMP	25	50	DEGR	10
X013T	TANK 1, INTERNAL, RADIAL, L1-5 TEMP	25	50	DEGR	10
X014T	TANK 1, INTERNAL, RADIAL, L1-6 TEMP	25	50	DEGR	10
X015T	TANK 1, INTERNAL, RADIAL, L1-7 TEMP	25	50	DEGR	10
X016T	TANK 1, INTERNAL, RADIAL, L1-8 TEMP	25	50	DEGR	10
X017T	TANK 1, INTERNAL, RADIAL, L2-1 TEMP	25	50	DEGR	10
X018T	TANK 1, INTERNAL, RADIAL, L2-2 TEMP	25	50	DEGR	10
X019T	TANK 1, INTERNAL, RADIAL, L2-3 TEMP	25	50	DEGR	10
X020T	TANK 1, INTERNAL, RADIAL, L2-4 TEMP	25	50	DEGR	10
X021T	TANK 1, INTERNAL, RADIAL, L2-5 TEMP	25	50	DEGR	10
X022T	TANK 1, INTERNAL, RADIAL, L2-6 TEMP	25	50	DEGR	10
X023T	TANK 1, INTERNAL, RADIAL, L2-7 TEMP	25	50	DEGR	10
X024T	TANK 1, INTERNAL, RADIAL, L2-8 TEMP	25	50	DEGR	10
X025T	TANK 1, INTERNAL, RADIAL, L3-1 TEMP	25	50	DEGR	10
X026T	TANK 1, INTERNAL, RADIAL, L3-2 TEMP	25	50	DEGR	10
X027T	TANK 1, INTERNAL, RADIAL, L3-3 TEMP	25	50	DEGR	10
X028T	TANK 1, INTERNAL, RADIAL, L3-4 TEMP	25	50	DEGR	10
X029T	TANK 1, INTERNAL, RADIAL, L3-5 TEMP	25	50	DEGR	10
X030T	TANK 1, INTERNAL, RADIAL, L3-6 TEMP	25	50	DEGR	10
X031T	TANK 1, INTERNAL, RADIAL, L3-7 TEMP	25	50	DEGR	10
X032T	TANK 1, INTERNAL, RADIAL, L3-8 TEMP	25	50	DEGR	10
X033T	TANK 1, INTERNAL, RADIAL, L4-1 TEMP	25	50	DEGR	10
X034T	TANK 1, INTERNAL, RADIAL, L4-2 TEMP	25	50	DEGR	10
X035T	TANK 1, INTERNAL, RADIAL, L4-3 TEMP	25	50	DEGR	10
X036T	TANK 1, INTERNAL, RADIAL, L4-4 TEMP	25	50	DEGR	10
X037T	TANK 1, INTERNAL, RADIAL, L4-5 TEMP	25	50	DEGR	10
X038T	TANK 1, INTERNAL, RADIAL, L4-6 TEMP	25	50	DEGR	10
X039T	TANK 1, INTERNAL, RADIAL, L4-7 TEMP	25	50	DEGR	10

Table C-1. COLD-SAT Experiment Measurement Requirements (Cont.)

MEAS NO.	DESCRIPTION	MEAS RANGE		UNITS	SAMPLE PERIOD (SEC)
		LOW	HIGH		
X040T	TANK 1, INTERNAL, RADIAL, L4-8 TEMP	25	50	DEGR	10
X041T	TANK 1, INTERNAL, LAD/TVS- 1 TEMP	25	50	DEGR	60
X042T	TANK 1, INTERNAL, LAD/TVS- 2 TEMP	25	50	DEGR	60
X043T	TANK 1, INTERNAL, LAD/TVS- 3 TEMP	25	50	DEGR	60
X044T	TANK 1, INTERNAL, LAD/TVS- 4 TEMP	25	50	DEGR	60
X045T	TANK 1, INTERNAL, LAD/TVS- 5 TEMP	25	50	DEGR	60
X046T	TANK 1, INTERNAL, LAD/TVS- 6 TEMP	25	50	DEGR	60
X047T	TANK 1, INTERNAL, LAD/TVS- 7 TEMP	25	50	DEGR	60
X048T	TANK 1, INTERNAL, LAD/TVS- 8 TEMP	25	50	DEGR	60
X049T	TANK 1, INTERNAL, LAD/TVS- 9 TEMP	25	50	DEGR	60
X050T	TANK 1, INTERNAL, LAD/TVS- 10 TEMP	25	50	DEGR	60
X051T	TANK1, INT COMPACT TVS HEX-1, TEMP	25	50	DEGR	1
X052T	TANK1, INT COMPACT TVS HEX-2, TEMP	25	50	DEGR	1
X053T	TANK1, INT COMPACT TVS HEX-3, TEMP	25	50	DEGR	1
X054T	TANK1, INT COMPACT TVS HEX-4, TEMP	25	50	DEGR	1
X055T	TANK1, INT COMPACT TVS HEX-5, TEMP	25	50	DEGR	1
X056T	TANK1, INT COMPACT TVS HEX-6, TEMP	25	50	DEGR	1
X057T	TANK1, INT COMPACT TVS HEX-7, TEMP	25	50	DEGR	1
X058T	TANK1, INT COMPACT TVS HEX-8, TEMP	25	50	DEGR	1
X059T	TANK1, INT COMPACT TVS HEX-9, TEMP	25	50	DEGR	1
X060T	TANK1, INT COMPACT TVS HEX-10, TEMP	25	50	DEGR	1
X061T	TANK 1, INT WALL MOUNTED TVS-1, TEMP	25	530	DEGR	10
X062T	TANK 1, INT WALL MOUNTED TVS-2, TEMP	25	530	DEGR	10
X063T	TANK 1, INT WALL MOUNTED TVS-3, TEMP	25	530	DEGR	10
X064T	TANK 1, INT WALL MOUNTED TVS-4, TEMP	25	530	DEGR	10
X065T	TANK 1, INT WALL MOUNTED TVS-5, TEMP	25	530	DEGR	10
X066T	TANK 1, INT WALL MOUNTED TVS-6, TEMP	25	530	DEGR	10
X067T	TANK 1, INT WALL MOUNTED TVS-7, TEMP	25	530	DEGR	10
X068T	TANK 1, INT WALL MOUNTED TVS-8, TEMP	25	530	DEGR	10
X069T	TANK 1, INT WALL MOUNTED TVS-9, TEMP	25	530	DEGR	10

Table C-1. COLD-SAT Experiment Measurement Requirements (Cont.)

MEAS NO.	DESCRIPTION	MEAS RANGE		UNITS	SAMPLE PERIOD (SEC)
		LOW	HIGH		
X070T	TANK 1, INT WALL MOUNTED TVS-10, TEMP	25	530	DEGR	10
X071T	TANK 1, EXTERNAL TVS-1 TEMP	25	400	DEGR	10
X072T	TANK 1, EXTERNAL TVS-2 TEMP	25	400	DEGR	10
X073T	TANK 1, EXTERNAL TVS-3 TEMP	25	400	DEGR	10
X074T	TANK 1, EXTERNAL TVS-4 TEMP	25	400	DEGR	10
X075T	TANK 1, INTERNAL WALL-1, TEMP	25	50	DEGR	10
X076T	TANK 1, INTERNAL WALL-2, TEMP	25	50	DEGR	10
X077T	TANK 1, INTERNAL WALL-3, TEMP	25	50	DEGR	10
X078T	TANK 1, INTERNAL WALL-4, TEMP	25	50	DEGR	10
X079T	TANK 1, INTERNAL WALL-5, TEMP	25	50	DEGR	10
X080T	TANK 1, INTERNAL WALL-6, TEMP	25	50	DEGR	10
X081T	TANK 1, INTERNAL WALL-7, TEMP	25	50	DEGR	10
X082T	TANK 1, INTERNAL WALL-8, TEMP	25	50	DEGR	10
X083T	TANK 1, INTERNAL WALL-9, TEMP	25	50	DEGR	10
X084T	TANK 1, INTERNAL WALL-10, TEMP	25	50	DEGR	10
X085T	TANK 1, VCS-1 TEMP	25	400	DEGR	60
X086T	TANK 1, VCS-2 TEMP	25	400	DEGR	60
X087T	TANK 1, VCS-3 TEMP	25	400	DEGR	60
X088T	TANK 1, VCS-4 TEMP	25	400	DEGR	60
X089T	TANK 1, VCS-5 TEMP	25	400	DEGR	60
X090T	TANK 1, VCS-6 TEMP	25	400	DEGR	60
X091T	TANK 1, VCS-7 TEMP	25	400	DEGR	60
X092T	TANK 1, VCS-8 TEMP	25	400	DEGR	60
X093T	TANK 1, VCS-9 TEMP	25	400	DEGR	60
X094T	TANK 1, VCS-10 TEMP	25	400	DEGR	60
X095T	TANK 1, VCS-11 TEMP	25	400	DEGR	60
X096T	TANK 1, VCS-12 TEMP	25	400	DEGR	60
X097T	TANK 1, VCS-13 TEMP	25	400	DEGR	60
X098T	TANK 1, VCS-14 TEMP	25	400	DEGR	60
X099T	TANK 1, VCS-15 TEMP	25	400	DEGR	60

Table C-1. COLD-SAT Experiment Measurement Requirements (Cont.)

MEAS NO.	DESCRIPTION	MEAS RANGE		UNITS	SAMPLE PERIOD (SEC)
		LOW	HIGH		
X100T	TANK 1, VCS-16 TEMP	25	400	DEGR	60
X101T	TANK 1, MLI-1, PROFILE TEMP	25	530	DEGR	60
X102T	TANK 1, MLI-2, PROFILE TEMP	25	530	DEGR	60
X103T	TANK 1, MLI-3, PROFILE TEMP	25	530	DEGR	60
X104T	TANK 1, MLI-4, PROFILE TEMP	25	530	DEGR	60
X105T	TANK 1, MLI-5, PROFILE TEMP	25	530	DEGR	60
X106T	TANK 1, MLI-6, PROFILE TEMP	25	530	DEGR	60
X107T	TANK 1, MLI-7, PROFILE TEMP	25	530	DEGR	60
X108T	TANK 1, MLI-8, PROFILE TEMP	25	530	DEGR	60
X109T	TANK 1, MLI-9, PROFILE TEMP	25	530	DEGR	60
X110T	TANK 1, MLI-10, PROFILE TEMP	25	530	DEGR	60
X111T	TANK 1, MLI-11, PROFILE TEMP	25	530	DEGR	60
X112T	TANK 1, MLI-12, PROFILE TEMP	25	530	DEGR	60
X113T	TANK 1, MLI-13, PROFILE TEMP	25	530	DEGR	60
X114T	TANK 1, MLI-14, PROFILE TEMP	25	530	DEGR	60
X115T	TANK 1, MLI-15, PROFILE TEMP	25	530	DEGR	60
X116T	TANK 1, MLI-16, PROFILE TEMP	25	530	DEGR	60
X117T	TANK 1, MLI- 1, EXT TEMP	430	530	DEGR	300
X118T	TANK 1, MLI- 2, EXT TEMP	430	530	DEGR	300
X119T	TANK 1, MLI- 3, EXT TEMP	430	530	DEGR	300
X120T	TANK 1, SUBCOOLER-1 TEMP	25	50	DEGR	1
X121T	TANK 1, SUBCOOLER-2 TEMP	25	50	DEGR	1
X122T	TANK 1, SUBCOOLER-3 TEMP	25	50	DEGR	1
X123T	TANK 1, SUBCOOLER-4 TEMP	25	50	DEGR	1
X124T	TANK 1, SUBCOOLER-5 TEMP	25	50	DEGR	1
X125T	TANK 1, SUBCOOLER-6 TEMP	25	50	DEGR	1
X126T	TANK 1, SUBCOOLER-7 TEMP	25	50	DEGR	1
X127T	TANK 1, SUBCOOLER-8 TEMP	25	50	DEGR	1
X128T	TANK 1, SUBCOOLER-9 TEMP	25	50	DEGR	1
X129T	TANK 1, SUBCOOLER-10 TEMP	25	50	DEGR	1

Table C-1. COLD-SAT Experiment Measurement Requirements (Cont.)

MEAS NO.	DESCRIPTION	MEAS RANGE		UNITS	SAMPLE PERIOD (SEC)
		LOW	HIGH		
X130T	TANK 1, STRUT-1 TEMP	25	530	DEGR	300
X131T	TANK 1, STRUT-2 TEMP	25	530	DEGR	300
X132T	TANK 1, STRUT-3 TEMP	25	530	DEGR	300
X133T	TANK 1, STRUT-4 TEMP	25	530	DEGR	300
X134T	TANK 1, STRUT-5 TEMP	25	530	DEGR	300
X135T	TANK 1, STRUT-6 TEMP	25	530	DEGR	300
X136T	TANK 1, FLUID LINE-1 TEMP	25	530	DEGR	10
X137T	TANK 1, FLUID LINE-2 TEMP	25	530	DEGR	10
X138T	TANK 1, FLUID LINE-3 TEMP	25	530	DEGR	10
X139T	TANK 1, FLUID LINE-4 TEMP	25	530	DEGR	10
X140T	TANK 1, FLUID LINE-5 TEMP	25	530	DEGR	10
X141T	TANK 1, FLUID LINE-6 TEMP	25	530	DEGR	10
X142T	TANK 1, CABLE-1 TEMP	25	530	DEGR	300
X143T	TANK 1, CABLE-2 TEMP	25	530	DEGR	300
X144T	TANK 1, CABLE-3 TEMP	25	530	DEGR	300
X145T	TANK 1, CABLE-4 TEMP	25	530	DEGR	300
X146T	TANK 2, LIQUID INLET TEMP	25	50	DEGR	1
X147T	TANK 2, INTERNAL, AXIAL-1 TEMP	25	530	DEGR	10
X148T	TANK 2, INTERNAL, AXIAL-2 TEMP	25	530	DEGR	10
X149T	TANK 2, INTERNAL, AXIAL-3 TEMP	25	530	DEGR	10
X150T	TANK 2, INTERNAL, AXIAL-4 TEMP	25	530	DEGR	10
X151T	TANK 2, INTERNAL, AXIAL-5 TEMP	25	530	DEGR	10
X152T	TANK 2, INTERNAL, AXIAL-6 TEMP	25	530	DEGR	10
X153T	TANK 2, INTERNAL, AXIAL-7 TEMP	25	530	DEGR	10
X154T	TANK 2, INTERNAL, AXIAL-8 TEMP	25	530	DEGR	10
X155T	TANK 2, INTERNAL, WALL-1 TEMP	25	530	DEGR	60
X156T	TANK 2, INTERNAL, WALL-2 TEMP	25	530	DEGR	60
X157T	TANK 2, INTERNAL, WALL-3 TEMP	25	530	DEGR	60
X158T	TANK 2, INTERNAL, WALL-4 TEMP	25	530	DEGR	60
X159T	TANK 2, INTERNAL, WALL-5 TEMP	25	530	DEGR	60

Table C-1. COLD-SAT Experiment Measurement Requirements (Cont.)

MEAS NO.	DESCRIPTION	MEAS RANGE		UNITS	SAMPLE PERIOD (SEC)
		LOW	HIGH		
X160T	TANK 2, INTERNAL, WALL-6 TEMP	25	530	DEGR	60
X161T	TANK 2, INTERNAL, WALL-7 TEMP	25	530	DEGR	60
X162T	TANK 2, INTERNAL, WALL-8 TEMP	25	530	DEGR	60
X163T	TANK 2, INTERNAL, WALL-9 TEMP	25	530	DEGR	60
X164T	TANK 2, INTERNAL, WALL-10 TEMP	25	530	DEGR	60
X165T	TANK 2, INTERNAL, WALL-11 TEMP	25	530	DEGR	60
X166T	TANK 2, INTERNAL, WALL-12 TEMP	25	530	DEGR	60
X167T	TANK 2, INTERNAL, WALL-13 TEMP	25	530	DEGR	60
X168T	TANK 2, INTERNAL, WALL-14 TEMP	25	530	DEGR	60
X169T	TANK 2, INTERNAL, LAD/TVS-1 TEMP	25	530	DEGR	60
X170T	TANK 2, INTERNAL, LAD/TVS-2 TEMP	25	530	DEGR	60
X171T	TANK 2, INTERNAL, LAD/TVS-3 TEMP	25	530	DEGR	60
X172T	TANK 2, INTERNAL, LAD/TVS-4 TEMP	25	530	DEGR	60
X173T	TANK 2, INTERNAL, LAD/TVS-5 TEMP	25	530	DEGR	60
X174T	TANK 2, INTERNAL, LAD/TVS-6 TEMP	25	530	DEGR	60
X175T	TANK 2, INTERNAL, LAD/TVS-7 TEMP	25	530	DEGR	60
X176T	TANK 2, INTERNAL, LAD/TVS-8 TEMP	25	530	DEGR	60
X177T	TANK 2,INTERNAL, BAFFLE-1 TEMP	25	530	DEGR	60
X178T	TANK 2,INTERNAL, BAFFLE-2 TEMP	25	530	DEGR	60
X179T	TANK 2,INTERNAL, BAFFLE-3 TEMP	25	530	DEGR	60
X180T	TANK 2,INTERNAL, BAFFLE-4 TEMP	25	530	DEGR	60
X181T	TANK 2, WALL MOUNTED TVS-1 TEMP	25	50	DEGR	10
X182T	TANK 2, WALL MOUNTED TVS-2 TEMP	25	50	DEGR	10
X183T	TANK 2, WALL MOUNTED TVS-3 TEMP	25	50	DEGR	10
X184T	TANK 2, WALL MOUNTED TVS-4 TEMP	25	50	DEGR	10
X185T	TANK 2, WALL MOUNTED TVS-5 TEMP	25	50	DEGR	10
X186T	TANK 2, WALL MOUNTED TVS-6 TEMP	25	50	DEGR	10
X187T	TANK 2, WALL MOUNTED TVS-7 TEMP	25	50	DEGR	10
X188T	TANK 2, WALL MOUNTED TVS-8 TEMP	25	50	DEGR	10
X189T	TANK 2, WALL MOUNTED TVS-9 TEMP	25	50	DEGR	10

Table C-1. COLD-SAT Experiment Measurement Requirements (Cont.)

MEAS NO.	DESCRIPTION	MEAS RANGE		UNITS	SAMPLE PERIOD (SEC)
		LOW	HIGH		
X190T	TANK 2, WALL MOUNTED TVS-10 TEMP	25	50	DEGR	10
X191T	TANK 2, MLI PROFILE-1 TEMP	25	400	DEGR	60
X192T	TANK 2, MLI PROFILE-2 TEMP	25	400	DEGR	60
X193T	TANK 2, MLI PROFILE-3 TEMP	25	400	DEGR	60
X194T	TANK 2, MLI PROFILE-4 TEMP	25	400	DEGR	60
X195T	TANK 2, MLI PROFILE-5 TEMP	25	400	DEGR	60
X196T	TANK 2, MLI PROFILE-6 TEMP	25	400	DEGR	60
X197T	TANK 2, MLI PROFILE-7 TEMP	25	400	DEGR	60
X198T	TANK 2, MLI PROFILE-8 TEMP	25	400	DEGR	60
X199T	TANK 2, MLI PROFILE-9 TEMP	25	400	DEGR	60
X200T	TANK 2, MLI PROFILE-10 TEMP	25	400	DEGR	60
X201T	TANK 2, MLI-1 EXTERIOR TEMP	400	530	DEGR	60
X202T	TANK 2, MLI-2 EXTERIOR TEMP	400	530	DEGR	60
X203T	TANK 2, MLI-3 EXTERIOR TEMP	400	530	DEGR	60
X204T	TANK 2, MLI-4 EXTERIOR TEMP	400	530	DEGR	60
X205T	TANK 2, MLI-5 EXTERIOR TEMP	400	530	DEGR	60
X206T	TANK 2, MLI-6 EXTERIOR TEMP	400	530	DEGR	60
X207T	TANK 2, MLI-7 EXTERIOR TEMP	400	530	DEGR	60
X208T	TANK 2, MLI-8 EXTERIOR TEMP	400	530	DEGR	60
X209T	TANK 2, STRUT-1 TEMP	25	530	DEGR	300
X210T	TANK 2, STRUT-2 TEMP	25	530	DEGR	300
X211T	TANK 2, STRUT-3 TEMP	25	530	DEGR	300
X212T	TANK 2, STRUT-4 TEMP	25	530	DEGR	300
X213T	TANK 2, STRUT-5 TEMP	25	530	DEGR	300
X214T	TANK 2, STRUT-6 TEMP	25	530	DEGR	300
X215T	TANK 2, FLUID LINE-1 TEMP	25	530	DEGR	10
X216T	TANK 2, FLUID LINE-2 TEMP	25	530	DEGR	10
X217T	TANK 2, FLUID LINE-3 TEMP	25	530	DEGR	10
X218T	TANK 2, FLUID LINE-4 TEMP	25	530	DEGR	10
X219T	TANK 2, FLUID LINE-5 TEMP	25	530	DEGR	10

Table C-1. COLD-SAT Experiment Measurement Requirements (Cont.)

MEAS NO.	DESCRIPTION	MEAS RANGE		UNITS	SAMPLE PERIOD (SEC)
		LOW	HIGH		
X220T	TANK 2, FLUID LINE-6 TEMP	25	530	DEGR	10
X221T	TANK 2, CABLE-1 TEMP	25	530	DEGR	300
X222T	TANK 2, CABLE-2 TEMP	25	530	DEGR	300
X223T	TANK 2, CABLE-3 TEMP	25	530	DEGR	300
X224T	TANK 2, CABLE-4 TEMP	25	530	DEGR	300
X225T	TANK 3, LIQUID INLET TEMP	25	50	DEGR	1
X226T	TANK 3,INTERNAL, WALL-1 TEMP	25	530	DEGR	60
X227T	TANK 3,INTERNAL, WALL-2 TEMP	25	530	DEGR	60
X228T	TANK 3,INTERNAL, WALL-3 TEMP	25	530	DEGR	60
X229T	TANK 3,INTERNAL, WALL-4 TEMP	25	530	DEGR	60
X230T	TANK 3,INTERNAL, WALL-5 TEMP	25	530	DEGR	60
X231T	TANK 3,INTERNAL, WALL-6 TEMP	25	530	DEGR	60
X232T	TANK 3,INTERNAL, WALL-7 TEMP	25	530	DEGR	60
X233T	TANK 3,INTERNAL, WALL-8 TEMP	25	530	DEGR	60
X234T	TANK 3,INTERNAL, AXIAL-1 TEMP	25	530	DEGR	10
X235T	TANK 3,INTERNAL, AXIAL-2 TEMP	25	530	DEGR	10
X236T	TANK 3,INTERNAL, AXIAL-3 TEMP	25	530	DEGR	10
X237T	TANK 3,INTERNAL, AXIAL-4 TEMP	25	530	DEGR	10
X238T	TANK 3,INTERNAL, AXIAL-5 TEMP	25	530	DEGR	10
X239T	TANK 3,INTERNAL, AXIAL-6 TEMP	25	530	DEGR	10
X240T	TANK 3,INTERNAL, AXIAL-7 TEMP	25	530	DEGR	10
X241T	TANK 3,INTERNAL, AXIAL-8 TEMP	25	530	DEGR	10
X242T	TANK 3, MLI EXT-1 TEMP	400	530	DEGR	60
X243T	TANK 3, MLI EXT-2 TEMP	400	530	DEGR	60
X244T	TANK 3, MLI EXT-3 TEMP	400	530	DEGR	60
X245T	TANK 3, MLI EXT-4 TEMP	400	530	DEGR	60
X246T	TANK 3, MLI EXT-5 TEMP	400	530	DEGR	60
X247T	TANK 3, MLI EXT-6 TEMP	400	530	DEGR	60
X248T	TANK 3, MLI EXT-7 TEMP	400	530	DEGR	60
X249T	TANK 3, MLI EXT-8 TEMP	400	530	DEGR	60

Table C-1. COLD-SAT Experiment Measurement Requirements (Cont.)

MEAS NO.	DESCRIPTION	MEAS RANGE		UNITS	SAMPLE PERIOD (SEC)
		LOW	HIGH		
X250T	TANK 3, MLI PROFILE-1 TEMP	25	530	DEGR	60
X251T	TANK 3, MLI PROFILE-2 TEMP	25	530	DEGR	60
X252T	TANK 3, MLI PROFILE-3 TEMP	25	530	DEGR	60
X253T	TANK 3, MLI PROFILE-4 TEMP	25	530	DEGR	60
X254T	TANK 3, MLI PROFILE-5 TEMP	25	530	DEGR	60
X255T	TANK 3, MLI PROFILE-6 TEMP	25	530	DEGR	60
X256T	TANK 3, MLI PROFILE-7 TEMP	25	530	DEGR	60
X257T	TANK 3, MLI PROFILE-8 TEMP	25	530	DEGR	60
X258T	TANK 3, MLI PROFILE-9 TEMP	25	530	DEGR	60
X259T	TANK 3, MLI PROFILE-10 TEMP	25	530	DEGR	60
X260T	TANK 3, MLI PROFILE-11 TEMP	25	530	DEGR	60
X261T	TANK 3, MLI PROFILE-12 TEMP	25	530	DEGR	60
X262T	TANK 3, MLI PROFILE-13 TEMP	25	530	DEGR	60
X263T	TANK 3, MLI PROFILE-14 TEMP	25	530	DEGR	60
X264T	TANK 3, MLI PROFILE-15 TEMP	25	530	DEGR	60
X265T	TANK 3, STRUT-1 TEMP	25	530	DEGR	300
X266T	TANK 3, STRUT-2 TEMP	25	530	DEGR	300
X267T	TANK 3, STRUT-3 TEMP	25	530	DEGR	300
X268T	TANK 3, STRUT-4 TEMP	25	530	DEGR	300
X269T	TANK 3, STRUT-5 TEMP	25	530	DEGR	300
X270T	TANK 3, STRUT-6 TEMP	25	530	DEGR	300
X271T	TANK 3,FLUID LINE-1 TEMP	25	530	DEGR	10
X272T	TANK 3,FLUID LINE-2 TEMP	25	530	DEGR	10
X273T	TANK 3,FLUID LINE-3 TEMP	25	530	DEGR	10
X274T	TANK 3,FLUID LINE-4 TEMP	25	530	DEGR	10
X275T	TANK 3,FLUID LINE-5 TEMP	25	530	DEGR	10
X276T	TANK 3,FLUID LINE-6 TEMP	25	530	DEGR	10
X277T	TANK 3, CABLE-1 TEMP	25	530	DEGR	300
X278T	TANK 3, CABLE-2 TEMP	25	530	DEGR	300
X279T	TANK 3, CABLE-3 TEMP	25	530	DEGR	300

Table C-1. COLD-SAT Experiment Measurement Requirements (Cont.)

MEAS NO.	DESCRIPTION	MEAS RANGE		UNITS	SAMPLE PERIOD (SEC)
		LOW	HIGH		
X280T	TANK 3, CABLE-4 TEMP	25	530	DEGR	300
X281T	EVAPORATOR-1 TEMP	25	400	DEGR	10
X282T	EVAPORATOR-2 TEMP	25	400	DEGR	10
X283T	LIQUID LINE 1 TEMP	25	530	DEGR	10
X284T	LIQUID LINE 2 TEMP	25	530	DEGR	10
X285T	LIQUID LINE 3 TEMP	25	530	DEGR	10
X286T	LIQUID LINE 4 TEMP	25	530	DEGR	10
X287T	LIQUID LINE 5 TEMP	25	530	DEGR	10
X288T	LIQUID LINE 6 TEMP	25	530	DEGR	10
X289T	LIQUID LINE 7 TEMP	25	530	DEGR	10
X290T	LIQUID LINE 8 TEMP	25	530	DEGR	10
X291T	LIQUID LINE 9 TEMP	25	530	DEGR	10
X292T	LIQUID LINE 10 TEMP	25	530	DEGR	10
X293T	LIQUID LINE 11 TEMP	25	530	DEGR	10
X294T	LIQUID LINE 12 TEMP	25	530	DEGR	10
X295T	LIQUID LINE 13 TEMP	25	530	DEGR	10
X296T	LIQUID LINE 14 TEMP	25	530	DEGR	10
X297T	LIQUID LINE 15 TEMP	25	530	DEGR	10
X298T	LIQUID LINE 16 TEMP	25	530	DEGR	10
X299T	LIQUID LINE 17 TEMP	25	530	DEGR	10
X300T	LIQUID LINE 18 TEMP	25	530	DEGR	10
X301T	LIQUID LINE 19 TEMP	25	530	DEGR	10
X302T	LIQUID LINE 20 TEMP	25	530	DEGR	10
X303T	LIQUID LINE 21 TEMP	25	530	DEGR	10
X304T	LIQUID LINE 22 TEMP	25	530	DEGR	10
X305T	LIQUID LINE 23 TEMP	25	530	DEGR	10
X306T	LIQUID LINE 24 TEMP	25	530	DEGR	10
X307T	PRESSURIZATION LINE 1 WALL TEMP	25	530	DEGR	1
X308T	PRESSURIZATION LINE 2 WALL TEMP	25	530	DEGR	1
X309T	PRESSURIZATION LINE 3 WALL TEMP	25	530	DEGR	1

Table C-1. COLD-SAT Experiment Measurement Requirements (Cont.)

MEAS NO.	DESCRIPTION	MEAS RANGE		UNITS	SAMPLE PERIOD (SEC)
		LOW	HIGH		
X310T	PRESSURIZATION LINE 4 WALL TEMP	25	530	DEGR	1
X311T	PRESSURIZATION LINE-1 FLUID TEMP	25	530	DEGR	1
X312T	PRESSURIZATION LINE-2 FLUID TEMP	25	530	DEGR	1
X313T	PRESSURIZATION LINE-3 FLUID TEMP	25	530	DEGR	1
X314T	PRESSURIZATION LINE-4 FLUID TEMP	25	530	DEGR	1
X315T	VENT OUTLET-1 TEMP	25	530	DEGR	10
X316T	VENT OUTLET-2 TEMP	25	530	DEGR	10
X317T	VENT OUTLET-3 TEMP	25	530	DEGR	10
X318T	GAS STORAGE BOTTLE 1 TEMP	300	580	DEGR	300
X319T	GAS STORAGE BOTTLE 2 TEMP	300	580	DEGR	300
X320T	GAS STORAGE BOTTLE 3 TEMP	300	580	DEGR	300
X321T	EXPERIMENT COMPARTMENT AMBIENT TEMP	360	660	DEGR	10
X322T	DCU BASE TEMP	360	660	DEGR	10
X323T	ACCELEROMETER BASE TEMP	550	560	DEGR	10
X324T	PRESSURIZATION PUMP INLET TEMP	25	50	DEGR	60
X325T	PRESSURIZATION PUMP OUTLET TEMP	25	50	DEGR	60
X326T	TRANSFER PUMP INLET TEMP	25	50	DEGR	60
X327T	TRANSFER PUMP OUTLET TEMP	25	50	DEGR	60

Table C-2. COLD-SAT Experiment Commands

CMD NO	DESCRIPTION
1	VALVE 3 ON
2	VALVE 3 OFF
3	VALVE 6 ON
4	VALVE 6 OFF
5	VALVE 7 ON
6	VALVE 7 OFF
7	VALVE 8 ON
8	VALVE 8 OFF
9	VALVE 10 ON
10	VALVE 10 OFF
11	VALVE 11 ON
12	VALVE 11 OFF
13	VALVE 12 ON
14	VALVE 12 OFF
15	VALVE 13 ON
16	VALVE 13 OFF
17	VALVE 14 ON
18	VALVE 14 OFF
19	VALVE 15 ON
20	VALVE 15 OFF
21	VALVE 16 ON
22	VALVE 16 OFF
23	VALVE 17 ON
24	VALVE 17 OFF
25	VALVE 21 ON
26	VALVE 21 OFF
27	VALVE 22 ON
28	VALVE 22 OFF
29	VALVE 23 ON
30	VALVE 23 OFF
31	VALVE 24 ON
32	VALVE 24 OFF
33	VALVE 25 ON
34	VALVE 25 OFF
35	VALVE 27 ON
36	VALVE 27 OFF
37	VALVE 28 ON
38	VALVE 28 OFF
39	VALVE 36 ON
40	VALVE 36 OFF
41	VALVE 40 ON
42	VALVE 40 OFF
43	VALVE 44 ON
44	VALVE 44 OFF
45	VALVE 45 ON

Table C-2. COLD-SAT Experiment Commands (Cont.)

CMD NO	DESCRIPTION
46	VALVE 45 OFF
47	VALVE 46 ON
48	VALVE 46 OFF
49	VALVE 47 ON
50	VALVE 47 OFF
51	VALVE 51 ON
52	VALVE 51 OFF
53	VALVE 53 ON
54	VALVE 53 OFF
55	VALVE 54 ON
56	VALVE 54 OFF
57	VALVE 56 ON
58	VALVE 56 OFF
59	VALVE 57 ON
60	VALVE 57 OFF
61	VALVE 58 ON
62	VALVE 58 OFF
63	VALVE 59 ON
64	VALVE 59 OFF
65	VALVE 60 ON
66	VALVE 60 OFF
67	VALVE 61 ON
68	VALVE 61 OFF
69	VALVE 62 ON
70	VALVE 62 OFF
71	VALVE 63 ON
72	VALVE 63 OFF
73	VALVE 65 ON
74	VALVE 65 OFF
75	VALVE 66 ON
76	VALVE 66 OFF
77	VALVE 68 ON
78	VALVE 68 OFF
79	VALVE 71 ON
80	VALVE 71 OFF
81	VALVE 72 ON
82	VALVE 72 OFF
83	VALVE 77 ON
84	VALVE 77 OFF
85	VALVE 90 ON
86	VALVE 90 OFF
87	VALVE 94 ON
88	VALVE 94 OFF
89	VALVE 103 ON
90	VALVE 103 OFF

Table C-2. COLD-SAT Experiment Commands (Cont.)

CMD NO	DESCRIPTION
91	VALVE 106 ON
92	VALVE 106 OFF
93	VALVE 107 ON
94	VALVE 107 OFF
95	VALVE 115 ON
96	VALVE 115 OFF
97	VALVE 116 ON
98	VALVE 116 OFF
99	VALVE 121 ON
100	VALVE 121 OFF
101	VALVE 123 ON
102	VALVE 123 OFF
103	VALVE 124 ON
104	VALVE 124 OFF
105	VALVE 125 ON
106	VALVE 125 OFF
107	VALVE 126 ON
108	VALVE 126 OFF
109	VALVE 128 ON
110	VALVE 128 OFF
111	VALVE 129 ON
112	VALVE 129 OFF
113	VALVE 130 ON
114	VALVE 130 OFF
115	VALVE 131 ON
116	VALVE 131 OFF
117	VALVE 132 ON
118	VALVE 132 OFF
119	VALVE 133 ON
120	VALVE 133 OFF
121	VALVE 134 ON
122	VALVE 134 OFF
123	VALVE 135 ON
124	VALVE 135 OFF
125	VALVE 136 ON
126	VALVE 136 OFF
127	VALVE 137 ON
128	VALVE 137 OFF
129	VALVE 138 ON
130	VALVE 138 OFF
131	VALVE 139 ON
132	VALVE 139 OFF
133	VALVE 140 ON
134	VALVE 140 OFF
135	VALVE 141 ON

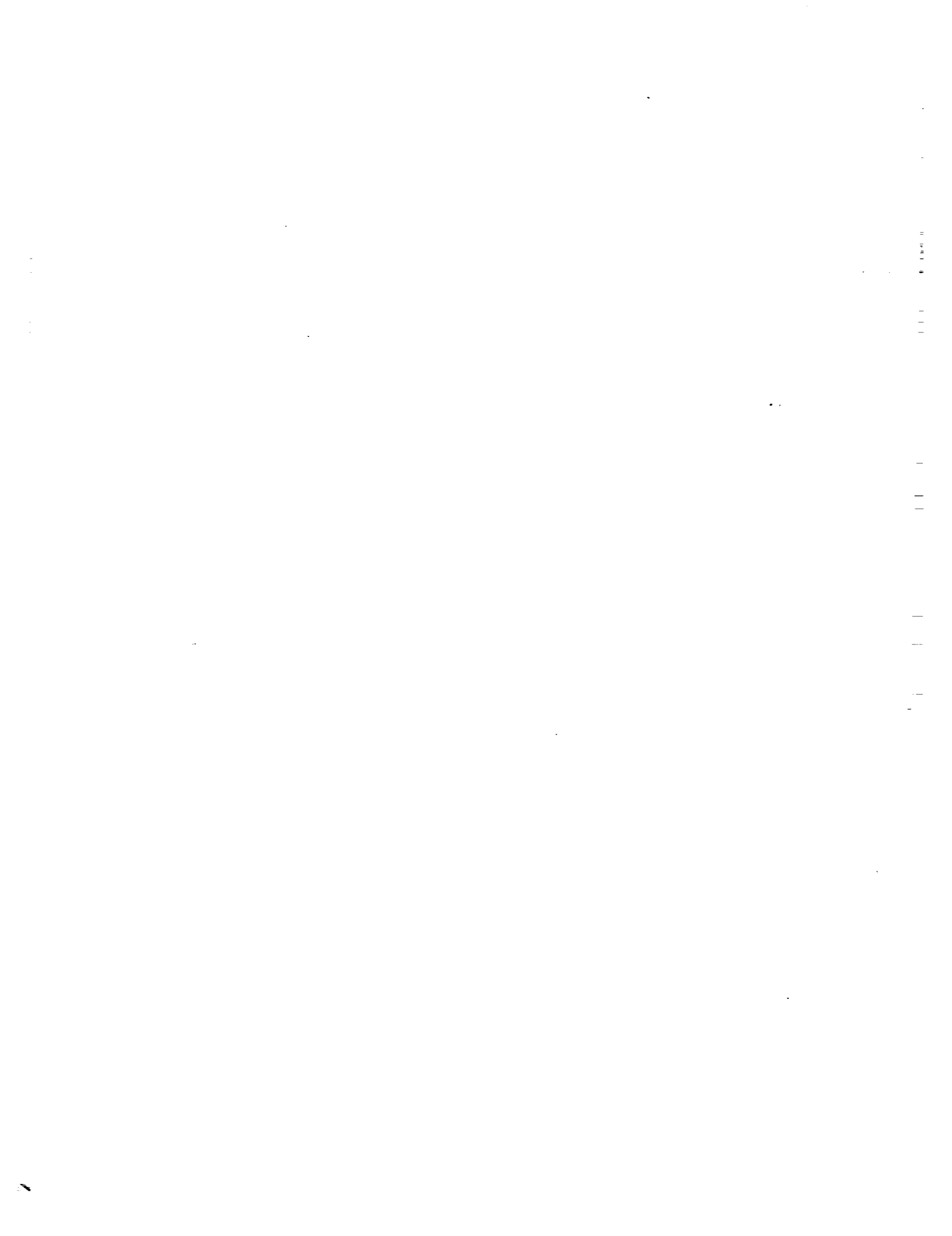
Table C-2. COLD-SAT Experiment Commands (Cont.)

CMD NO	DESCRIPTION
136	VALVE 141 OFF
137	DCU A POWER ON
138	DCU A POWER OFF
139	DCU B POWER ON
140	DCU B POWER OFF
141	28 V CONVERTER A POWER ON
142	28 V CONVERTER A POWER OFF
143	28 V CONVERTER B POWER ON
144	28 V CONVERTER B POWER OFF
145	10 V CONVERTER A POWER ON
146	10 V CONVERTER A POWER OFF
147	10 V CONVERTER B POWER ON
148	10 V CONVERTER B POWER OFF
149	5 V CONVERTER A POWER ON
150	5 V CONVERTER A POWER OFF
151	5 V CONVERTER B POWER ON
152	5 V CONVERTER B POWER OFF
153	INVERTER A POWER ON
154	INVERTER A POWER OFF
155	INVERTER B POWER ON
156	INVERTER B POWER OFF
157	ACCUMULATOR HTR 1 POWER ON
158	ACCUMULATOR HTR 1 POWER OFF
159	ACCUMULATOR HTR 2 POWER ON
160	ACCUMULATOR HTR 2 POWER OFF
161	VENT LINE HTR POWER ON
162	VENT LINE HTR POWER OFF
163	HEATER POWER ON
164	HEATER POWER OFF
165	HEATER POWER ON
166	HEATER POWER OFF
167	HEATER POWER ON
168	HEATER POWER OFF
169	HEATER POWER ON
170	HEATER POWER OFF
171	TANK 1 HTR POWER ON
172	TANK 1 HTR POWER OFF
173	LAD HTR POWER ON
174	LAD HTR POWER OFF
175	TANK 2 HTR POWER ON
176	TANK 2 HTR POWER OFF
177	TANK 3 HTR POWER ON
178	TANK 3 HTR POWER OFF
179	FLOW METER 26 POWER ON
180	FLOW METER 26 POWER OFF

Table C-2. COLD-SAT Experiment Commands (Cont.)

CMD NO	DESCRIPTION
181	FLOW METER 30 POWER ON
182	FLOW METER 30 POWER OFF
183	FLOW METER 50 POWER ON
184	FLOW METER 50 POWER OFF
185	FLOW METER 55 POWER ON
186	FLOW METER 55 POWER OFF
187	FLOW METER 105 POWER ON
188	FLOW METER 105 POWER OFF
189	FLOW METER 108 POWER ON
190	FLOW METER 108 POWER OFF
191	FLOW METER 109 POWER ON
192	FLOW METER 109 POWER OFF
193	FLOW METER 110 POWER ON
194	FLOW METER 110 POWER OFF
195	FLOW METER 111 POWER ON
196	FLOW METER 111 POWER OFF
197	FLOW METER 112 POWER ON
198	FLOW METER 112 POWER OFF
199	FLOW METER 122 POWER ON
200	FLOW METER 122 POWER OFF
201	PUMP 1 POWER ON
202	PUMP 1 POWER OFF
203	PUMP 2 POWER ON
204	PUMP 2 POWER OFF
205	PUMP 3 POWER ON
206	PUMP 3 POWER OFF
207	ACCELEROMETER A POWER ON
208	ACCELEROMETER A POWER OFF
209	ACCELEROMETER B POWER ON
210	ACCELEROMETER B POWER OFF
211	ACCELEROMETER C POWER ON
212	ACCELEROMETER C POWER OFF

APPENDIX D
TANK FLUID MOTION AND HEAT TRANSFER CONSIDERATIONS



APPENDIX D
TANK FLUID MOTION AND HEAT TRANSFER CONSIDERATIONS

D.1 BACKGROUND ACCELERATION DISTRIBUTION

Buoyancy-driven fluid motion in the tank is dependent on the magnitude and direction of the acceleration vector. The acceleration vector is composed primarily of two components, axial and radial. Accelerations perpendicular to the orbit plane will be small.

The component of acceleration directed along the spacecraft axis is due primarily to atmospheric drag and the centripetal acceleration caused by spacecraft pitching:

$$\text{Axial Acceleration} = -\omega^2 x - \text{drag} \quad (\text{D-1})$$

where x is the axial distance from the center of gravity of the spacecraft. The axial acceleration and the axial distance are assumed positive in the direction of spacecraft motion. The spacecraft is in a circular orbit, 1300 km from the Earth. The orbit period is 111.5 minutes, which corresponds to a pitch rate of $\omega = 9.4 \times 10^{-4}$ rad/s. The magnitude of the atmospheric drag is $g/g_0 = 0.02 \times 10^{-7}$, and was estimated using a ballistic coefficient equal to 50 kg/m². The magnitude of the centripetal acceleration is as much as two orders of magnitude greater than the atmospheric drag.

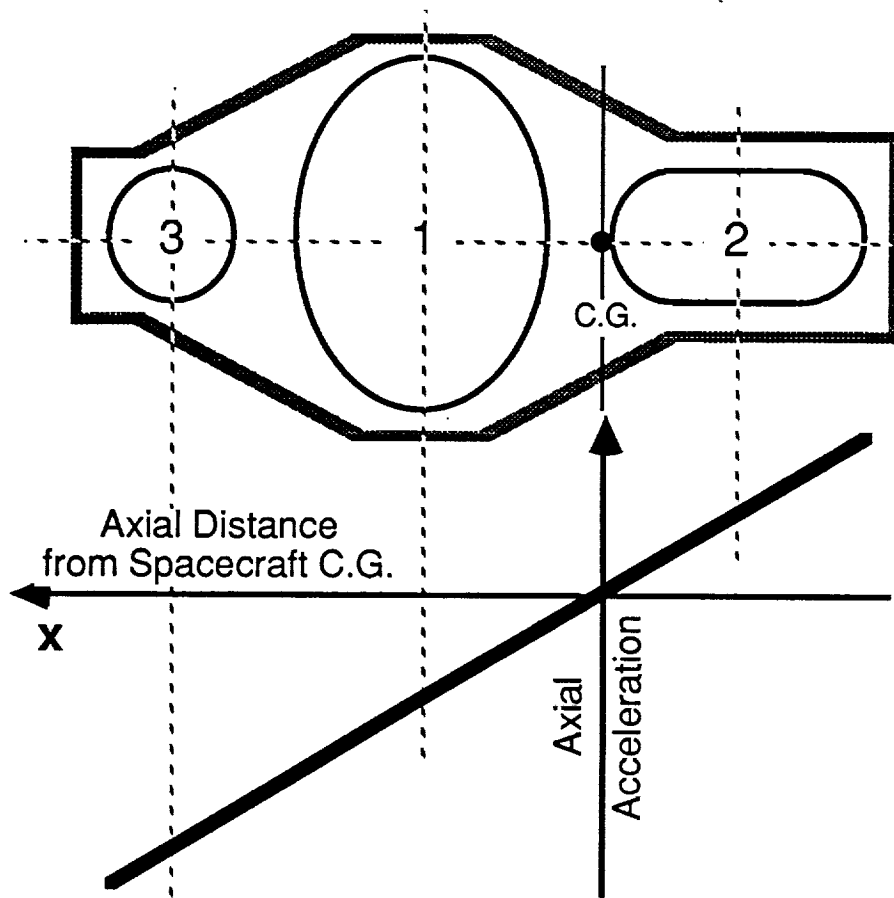
The axial acceleration is zero at the center-of-gravity of the spacecraft, and it varies linearly along the spacecraft axis as shown in Figure D-1. The largest axial acceleration, $g/g_0 = 3.5 \times 10^{-7}$, occurs at the front of Tank 3. The smallest axial acceleration, $g/g_0 = -0.06 \times 10^{-7}$, occurs at the front of Tank 2. The axial acceleration is most uniform in Tank 3, where the variation is 32 percent. The variation is greatest in Tank 2, i.e., 188 percent.

The radial acceleration component is the difference between the centripetal acceleration of the orbiting spacecraft and the Earth's gravitational attraction:

$$\text{Radial Acceleration} = \omega^2 R - \frac{G M_{\text{Earth}}}{R^2} \approx 3 r \omega^2 \quad (\text{D-2})$$

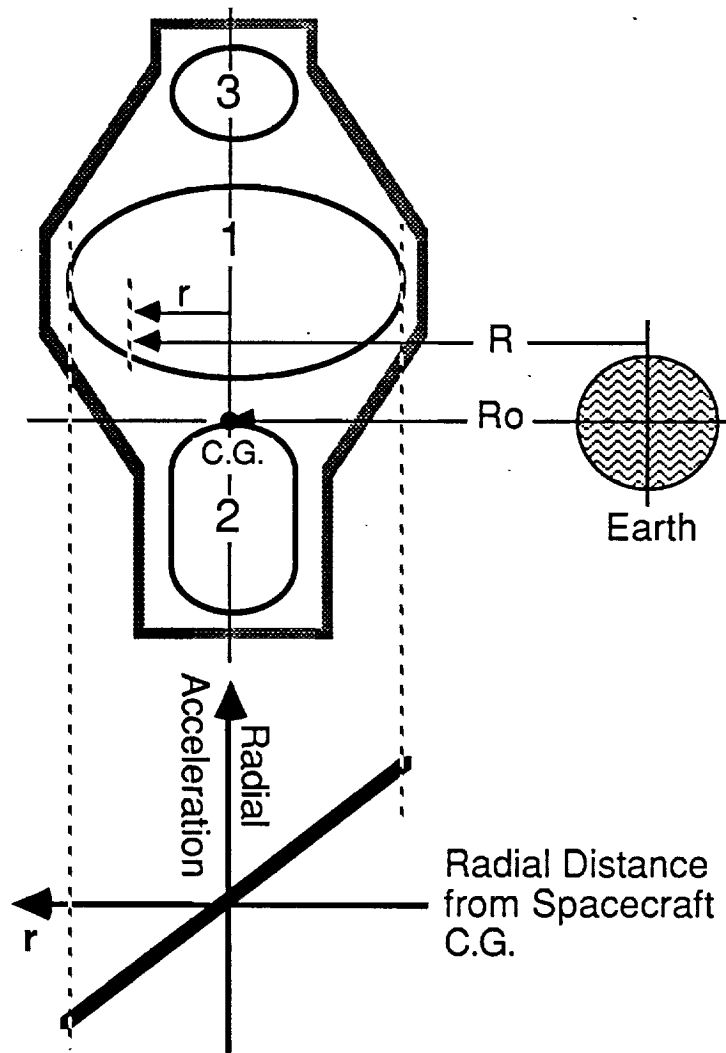
where R is the radial distance from the center of the Earth, r is the radial distance from the spacecraft axis, M_{Earth} is the mass of the Earth, and G is the universal gravitational constant. The linear approximation for the radial acceleration distribution on the spacecraft is valid when R is much greater than r , as is the case here. As shown in Figure D-2, the centripetal acceleration and Earth's gravitational attraction are in balance along the axis of the spacecraft, so the net radial acceleration is zero. In the outer regions of the tank, where the former is greater than the latter, the net radial acceleration is positive, i.e., directed away from Earth. In the inner regions of the tank, the Earth's attraction is greater than the centripetal acceleration and the net radial acceleration is negative, i.e., directed toward the Earth. The largest radial acceleration, $g/g_0 = 3.26 \times 10^{-7}$, occurs at the inner and outer edges of the supply tank. The diameters of the receiver tanks are nearly the same, consequently the maximum radial acceleration is also nearly the same in these tanks, $g/g_0 \sim 1.4 \times 10^{-7}$.

The magnitude and direction of the acceleration vector varies spatially within the three tanks, as shown in Figure D-3. The acceleration level varies the most in Tank 2, where the minimum is $g/g_0 = 0.06 \times 10^{-7}$ and the maximum is less than $g/g_0 = 2.19 \times 10^{-7}$. The acceleration level is most uniform in Tank 3, where the minimum is $g/g_0 = 2.54 \times 10^{-7}$ and the maximum is less 3.78×10^{-7} . The acceleration levels and directions will vary as the C.G. moves due to liquid transfers between tanks. Spacecraft accelerations due to disturbances and ACS activity will also be superimposed on the



Axial Acceleration x 10+7 G's at different tank locations			
	Tank 1	Tank 2	Tank 3
Front	-1.92	0.06	-3.50
Center	-1.15	0.88	-3.02
Back	-0.37	1.71	-2.54
Variation	135%	188%	32%

Figure D-1. Background Axial Acceleration Distribution



Radial Acceleration x $10+7$ G's at different tank locations			
	Tank 1	Tank 2	Tank 3
Outer	-3.26	-1.37	-1.44
Center	0	0	0
Inner	3.26	1.37	1.44

Figure D-2. Background Radial Acceleration Distribution

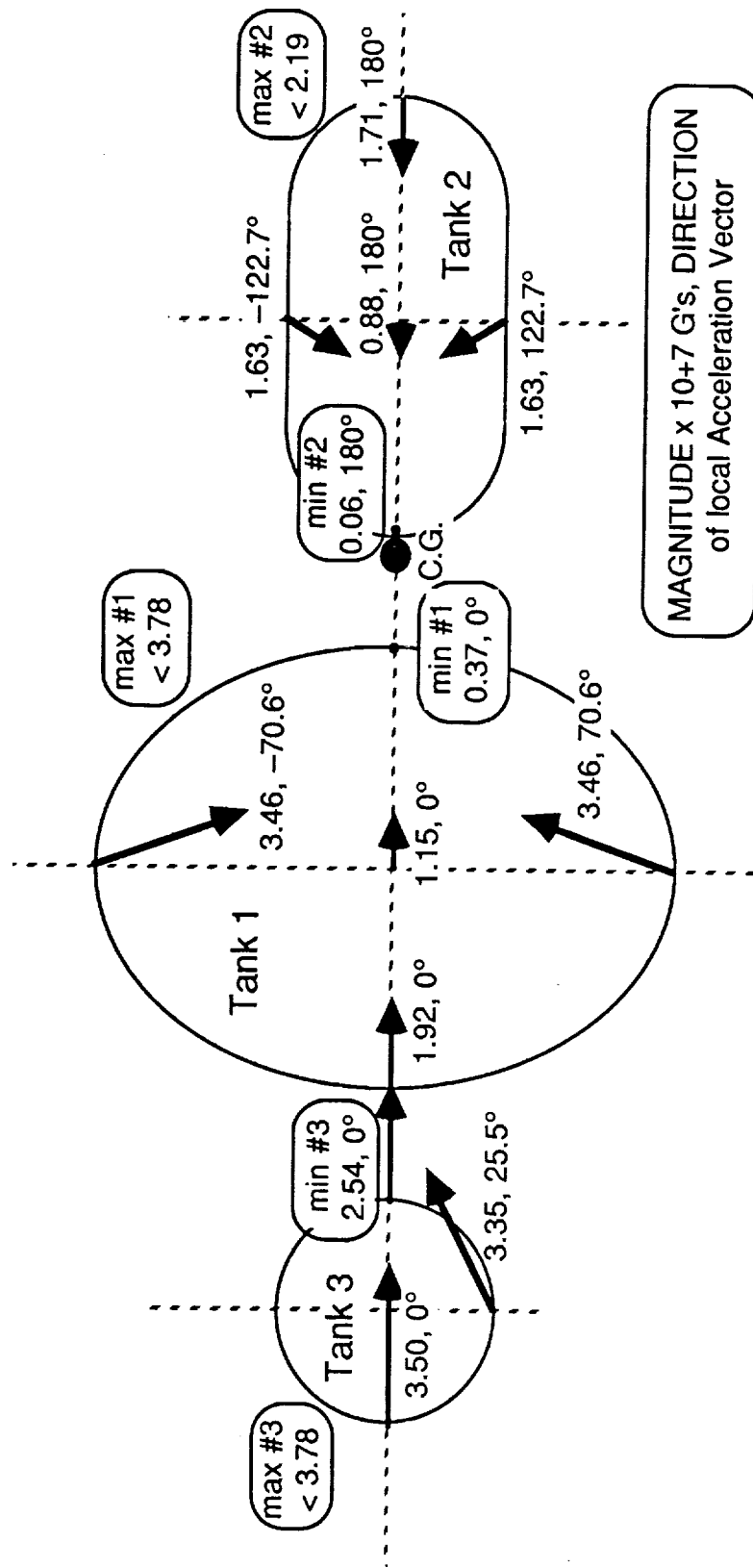


Figure D-3. Magnitude and Direction of Background Acceleration Vector

acceleration levels discussed in this section. These acceleration levels are too low to significantly affect the liquid orientation within the tank, which will be dominated by surface tension. However, buoyancy-induced fluid motion will be affected by the magnitude and direction of the acceleration vector.

D.2 CHILLDOWN MODEL IMPROVEMENTS

The GDNVF program can be used to predict the time necessary to chilldown a tank prior to a no-vent fill. The chilldown consists of a series of charge, hold, and vent cycles. The heat transfer regime changes during the charge-hold-vent cycle, as shown in Figure D-4. The actual magnitude of the heat transfer coefficient will depend on fluid properties, which change during the charge-hold-vent cycle. Forced convection occurs during the short charge phase (typically about 10 seconds). About 90 percent of the total chilldown time is due to the hold phase (typically about 1000 seconds). A free convection correlation has been used to model the heat transfer during the hold phase. The actual heat transfer coefficient is expected to be higher because of fluid motion persistence and possibly because of the lower heat transfer limit due to conduction. Models that more accurately predict the heat transfer during the hold phase have been implemented in the GDNVF program in order to decrease the predicted chilldown time.

D.2.1 Conduction Heat Transfer Limit

The free convection correlation (Reference D-1) used in GDNVF predicts that the Nusselt number, and therefore the heat transfer coefficient, decrease to zero as the acceleration level decreases to zero:

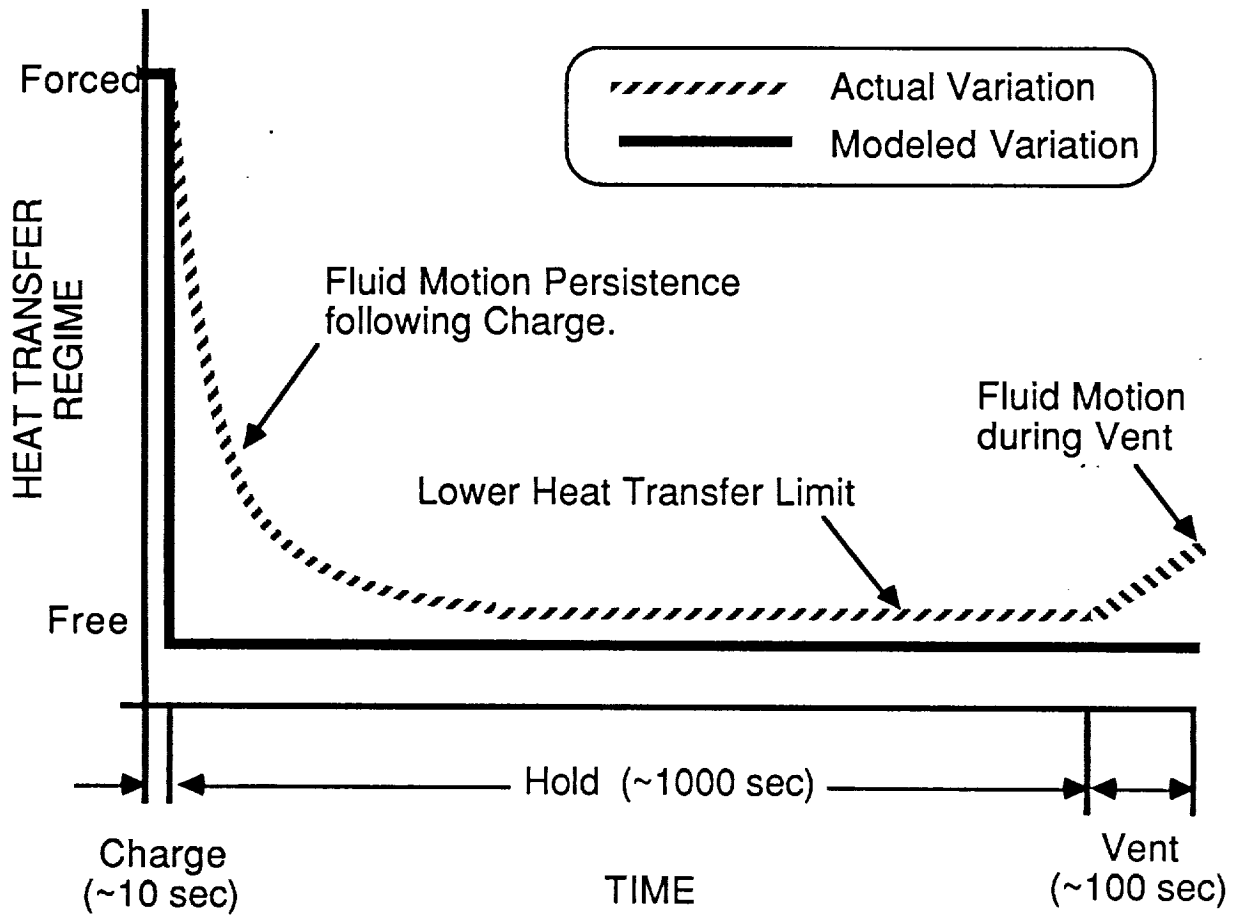
$$\text{Nu} = c_1 (\text{Gr Pr})^{c_2} \quad (\text{D-3})$$

where Nu and Gr are based on the tank diameter. For laminar free convection, the constants c_1 and c_2 have values of 0.555 and 0.25, respectively. Figure D-5 shows the variation of Nu for a range of acceleration levels. "Typical" conditions during the hold phase in Tank 3 have been used to evaluate fluid properties and wall-to-bulk fluid temperature differences. These results are strongly dependent on these conditions. For the given example, the predicted Nusselt number has a value of 2 for the background acceleration level expected on COLD-SAT, $g/g_0 = 10^{-7}$. As discussed below, this Nusselt number is unrealistically low.

The physical lower limit for heat transfer is pure conduction. The Nusselt number for pure conduction heat transfer will be constant, i.e., it does not depend on the flow field or the acceleration level. The heat transfer coefficient will depend only on the thermal conductivity and the relevant conduction length scale:

$$\text{Nu} = h \delta / k = \text{constant} \quad (\text{D-4})$$

The conduction length scale is initially short when temperature gradients are confined near the wall. It will increase with time, but is always expected to be less than the tank radius. For a single node ullage model, as used in GDNVF, half the tank radius represents a good, upper limit for the conduction length scale. For this case the lower conduction heat transfer limit results in a Nusselt number (based on tank diameter) of 4. For micro-g acceleration levels, the free convection correlation used in the GDNVF program often under-predicts the heat transfer coefficient, as shown in Figure D-5. This causes the predicted chilldown times to be unrealistically long. The conduction heat transfer model discussed here is expected to be a conservative lower limit for the actual heat transfer in the tank.



As the Temperature and Pressure change, the Fluid Properties will vary causing changes in the magnitude of the Heat Transfer Coefficient.

Figure D-4. Heat Transfer Regimes During the Charge-Hold-Vent Cycle

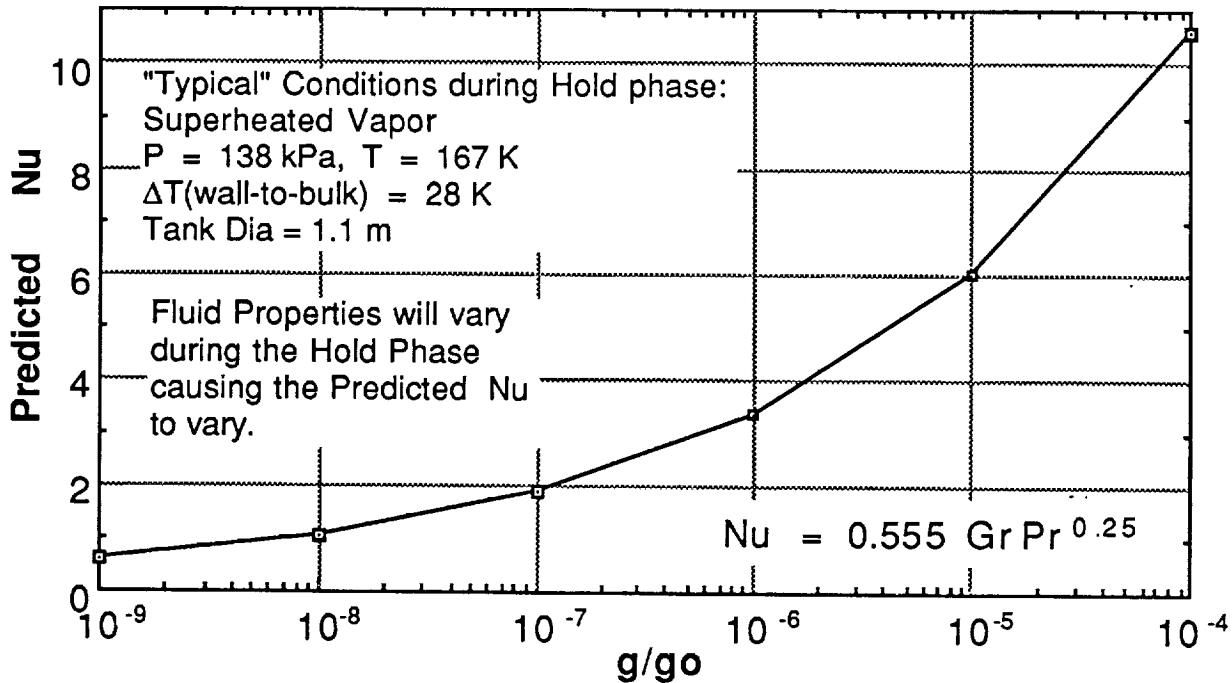


Figure D-5. Free Convection Heat Transfer Predicted Using Empirical Correlation

D.2.2 Large Turbulent Eddy Decay Model

Fluid motion persistence after the charge phase will also enhance the heat transfer coefficient during the hold phase, relative to pure free convection. The nozzle configuration will determine the characteristics of the fluid motion in the tank and the heat transfer, so the computer model should reflect this. Three different nozzle configurations will be tested on COLD-SAT; tangential, axial, and radial, as shown schematically in Figure D-6. Tangential nozzles will generate a tangential mean flow pattern that is expected to be the most "organized" and persistent of the three. Tangential flow analyses are discussed in Appendix D.3. Radial nozzles are expected to generate the least "organized" flow field that will probably be the least persistent. A conservative fluid motion persistence model was developed and implemented into the GDNVF program to account for the enhanced heat transfer, relative to pure free convection, immediately following the charge phase.

D.2.2.1 Model Assumptions. No "organized" fluid motion exists in the tank, i.e., the time-averaged fluid velocity at all locations in the tank is assumed to be zero. However, fluctuating velocities due to turbulence are non-zero. Turbulence decays with time. In the absence of a mean shear layer, turbulence production is small (Reference D-2). This is a conservative assumption, since it would be very difficult to generate a flow field where the mean velocity at all locations is zero. Mean shear layers in the tank will decrease the decay rate of turbulence and increase the duration of fluid motion persistence.

"Large" eddies are assumed to convect all the energy from the tank wall. Convection by "small" eddies will be neglected. This assumption is conservative. Large eddies are considered to be the same order-of-magnitude as the tank size. Small eddies ride on top of the large eddies, but do not transfer energy any appreciable distance due to their size.

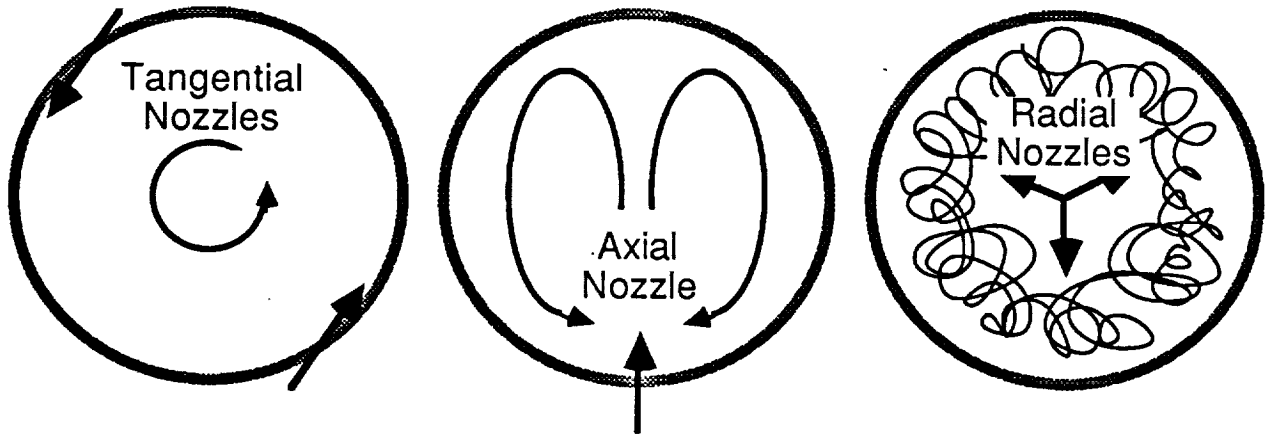


Figure D-6. Effect of Nozzle Configuration on Flow Pattern in Tank

Large eddies lose a negligible fraction of their kinetic energy by direct viscous dissipation. They break-up and transfer their energy to smaller and smaller eddies, until the eddy size becomes so small that their kinetic energy is dissipated by viscosity. The transfer of energy from “large” eddies to “small” eddies proceeds at a rate dictated by the inviscid inertial behavior of the eddies. This rate is independent of viscosity. The rate of decay of “small” eddies is dependent on viscosity. The viscous dissipation rate is much lower than the inviscid dissipation rate assumed for the large eddies, consequently this assumption is also conservative.

D.2.2.2 Fluctuating Velocity Decay. The kinetic energy per unit mass of the large eddies is $u^2/2$, where u is the magnitude of the fluctuating velocity. Assuming the large eddies lose all of their kinetic energy within one “turn-over” time ($\pi D_{\text{eddy}} / u$), the dissipation rate for the kinetic energy of the large eddies can be expressed as:

$$\epsilon = \frac{d\left(\frac{1}{2} u^2\right)}{dt} \approx \frac{\Delta\left(\frac{1}{2} u^2\right)}{\Delta t} \approx K \frac{\left(-\frac{1}{2} u^2\right)}{\left(\frac{\pi D_{\text{eddy}}}{u}\right)} \approx \frac{-K u^3}{6 D_{\text{eddy}}} \quad (\text{D-5})$$

where D_{eddy} is the diameter of the large eddies and K is an empirical constant that whose order-of-magnitude is unity. This expression can be rearranged and integrated:

$$\int_{u_0}^u \frac{1}{u^2} du = -\frac{K}{6} \int_0^t \frac{1}{D_{\text{eddy}}} dt \quad (\text{D-6})$$

where u_0 is the initial fluctuating velocity at time, t , equal to zero. To integrate this expression, the eddy diameter will be assumed constant and equal to the tank size, L_{tank} . The eddy size will actually decrease with time, however, most of the heat will be convected from the wall by “large” eddies whose size is on the order of the tank size. The following equation expresses the decay of the fluctuating velocity associated with large turbulent eddies with time:

$$\frac{u}{u_0} = \frac{1}{1 + \left(\frac{K u_0}{6 L_{\text{tank}}}\right) t} \quad (\text{D-7})$$

D.2.2.3 Convection Coefficient Decay. The GDNVF program requires an expression for the heat transfer coefficient. The decay of the heat transfer coefficient will be assumed to be related to the decay of the fluctuating velocity. The forced convection heat transfer coefficient used in the GDNVF program during the charge phase is given below (Reference D-3):

$$\frac{h_o L}{k} = 0.163 \left(\frac{\rho u_o L}{\mu} \right)^{3/4} Pr^{1/3} \quad (D-8)$$

where h_o is the wall convection coefficient while the nozzles are on, u_o is the entering fluid velocity, and L is the length scale that equals the quotient of the tank volume and the jet nozzle area. This is an empirical correlation obtained from tank fluid mixing data. When the nozzles are turned off, the convection coefficient (h) will decrease as the fluid velocity (u) in the tank decreases:

$$\frac{h}{h_o} = \left(\frac{u}{u_o} \right)^{3/4} \quad (D-9)$$

Inserting the expression for the fluid velocity decay results in the following expression for the decay of the convection coefficient with time:

$$\frac{h}{h_o} = \left[\frac{1}{1 + \left(\frac{K u_o}{6 L_{\text{tank}}} \right) t} \right]^{3/4} \quad (D-10)$$

The tank size has been used as a representative length scale for the large eddies. This is an upper limit, the actual length scale of the large eddies will be smaller. However, the entering fluid velocity is used to represent the velocity scale of the large eddies at the instant the nozzles are turned off. This is also an upper limit, the actual fluctuating velocity will be less, even while the nozzles are on. The above two effects may cancel, so the value of the ratio u_o/L_{tank} used in the model may be reasonable.

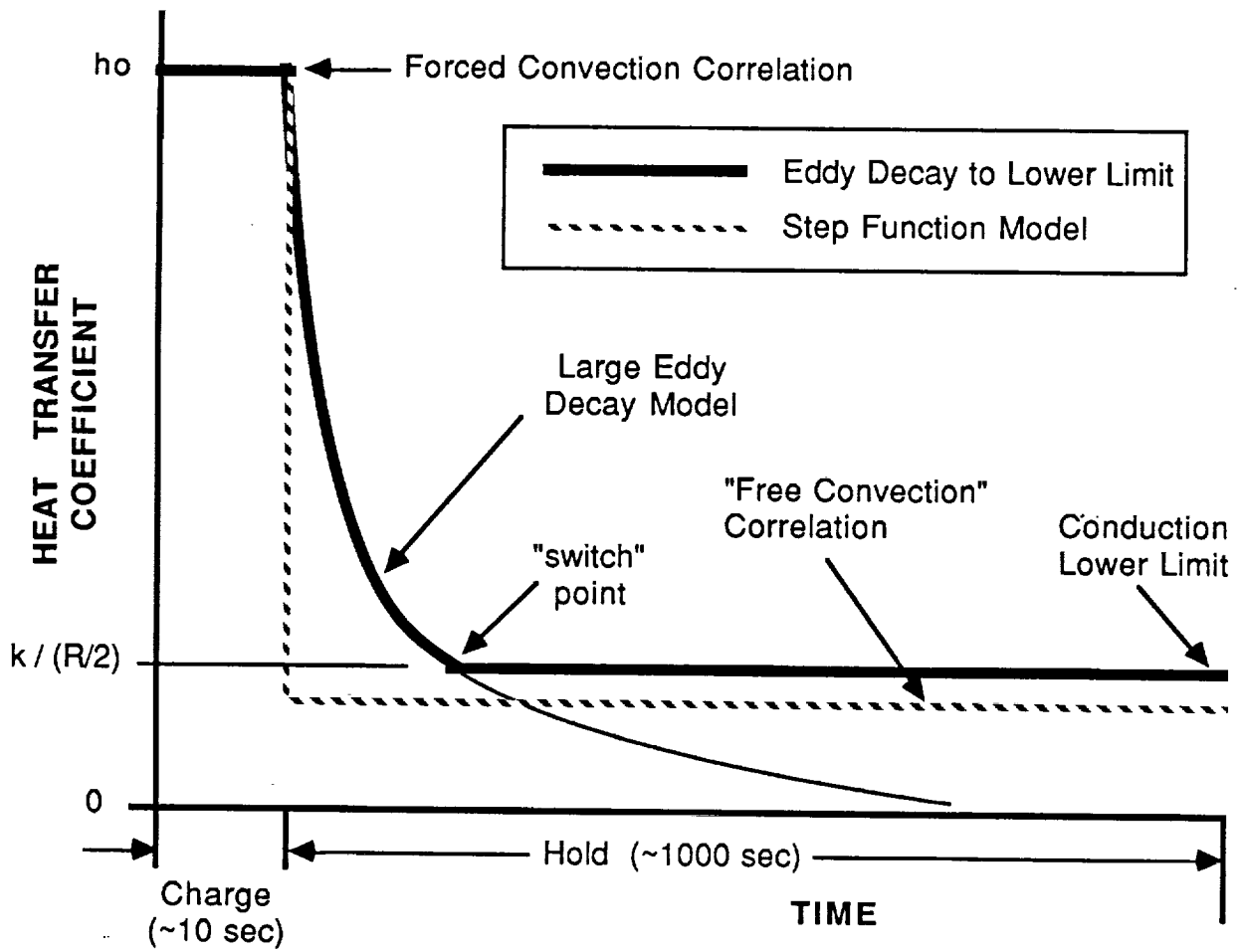
As previously discussed, many conservative assumptions were used in the development of this model. As shown in Table D-1, this model predicts a rapid decay of the heat transfer coefficient with time. The actual duration of the fluid motion persistence may be longer.

Table D-1. Decay of the Heat Transfer Coefficient Associated with Large Turbulent Eddies

$\frac{t u_o}{L_{\text{tank}}}$	0.1	0.3	1	2	3	5	10	20	30	100	300	1000	3000
$\frac{h}{h_o}$ (%)	99	96	89	81	74	63	48	33	26	12	5.2	2.1	0.94

D.2.3 Tank Chillover Results

The model improvements implemented into the GDNVF program are shown schematically in Figure D-7. Previously the heat transfer coefficient was stepped down from pure forced convection during the charge phase to pure free convection during the hold phase, as calculated using empirical correlations. The current large eddy decay model accounts for fluid motion persistence following the charge phase, and predicts a more gradual decay in the heat transfer coefficient. This model



The relative magnitudes of the conduction lower limit and the "free convection" correlation is dependent on the acceleration level.

Variations in the fluid properties will cause variations in the magnitude of the heat transfer coefficient.

Figure D-7. Model Improvements Implemented Into GDNVF

artificially predicts that the heat transfer coefficient decays to zero as the fluid velocity decays to zero. During the hold phase, the program uses the largest of the following three estimates for the heat transfer coefficient; large eddy decay model, free convection correlation, or conduction heat transfer limit.

The large eddy decay model is dependent on an empirical constant, K , which is expected to have a value near unity. The sensitivity of the chilldown time to the value of this constant is shown in Figure D-8. If K is large, the heat transfer coefficient is stepped-down from the forced convection value to the lower heat transfer limit, i.e., instantaneous decay. For the conditions shown in Figure D-8, the predicted chilldown time is 9 hours. The chilldown time decreases by about 25 percent, to 6.8 hours, when the empirical constant K equals the recommended value of unity. The chilldown time is most sensitive to K values less than unity. However, K values less than unity result in shorter chilldown times and are therefore less conservative. A value of K equal to zero represents the case of no decay, i.e., the heat transfer coefficient remains at the forced convection value.

The effect of the acceleration level on the chilldown time is shown in Figure D-9. The step-function decay to "free convection" represents the former model in the GDNVF program. This model predicts longer chilldown times than the current large eddy decay model to the lower heat transfer limit. Also shown is a result for a step-function decay to the lower heat transfer limit, which lies between the two other models. The hold phase accounts for about 90 percent of the chilldown time, consequently, the conduction lower limit model results in substantial reductions in the predicted chilldown times at low acceleration levels, where the "free convection" correlation under-predicts the actual heat transfer coefficient. At high acceleration levels the conduction lower limit model will not be implemented because the heat transfer coefficient calculated using the free convection correlation will be greater. The effect of fluid motion persistence decreases as the acceleration level increases because the difference between the forced convection coefficient and the free convection coefficient decreases.

D.3 TANGENTIAL FLOW.

Fluid motion persistence during the hold phase following a charge phase is dependent on the nozzle configuration. The large turbulent eddy decay model described in Section D.2 represents a worst case analysis that is probably most applicable to injection from a number of radial nozzles. The flow pattern from a set of tangential nozzles is expected to be more "organized", and therefore persist longer. The following tangential flow analysis is applicable to a long cylindrical tank with a circular cross-section. The following summary represents an up-date of on-going research.

D.3.1 Velocity Profile Following a Charge

Before the decay of a tangential flow can be analyzed, the initial velocity profile must be determined. The velocity profile following injection from tangential flow nozzles located on the tank wall is unknown, however, some characteristics are known. At the tank wall the fluid velocity must be zero, i.e., "no-slip". At the tank centerline the angular velocity must be finite, therefore the tangential velocity must be zero. This boundary condition is equivalent to no-shear at the centerline, i.e., fluid near the centerline spins as a solid disk. Since the charge phase is short, the angular momentum and kinetic energy of the entering fluid will be conserved as the liquid droplets rapidly evaporate and the resulting vapor fills the tank to equalize pressure. These four conditions are written in mathematical form below:

$$u = 0 \quad \text{at} \quad r = r_0, \text{ no-slip at the wall.} \quad (\text{D-11})$$

$$u = 0 \quad \text{at} \quad r = 0, \text{ no-shear at the centerline or finite angular velocity at centerline.} \quad (\text{D-12})$$

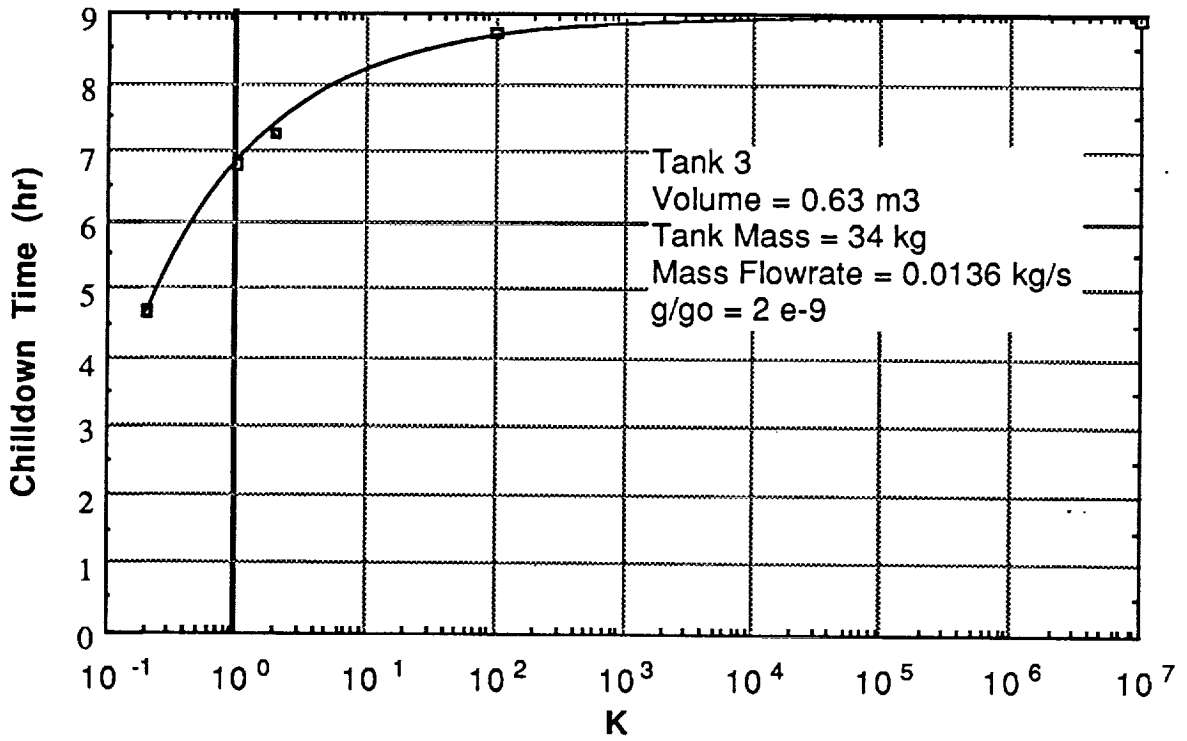


Figure D-8. Chiddown Time Sensivity to Model Constant

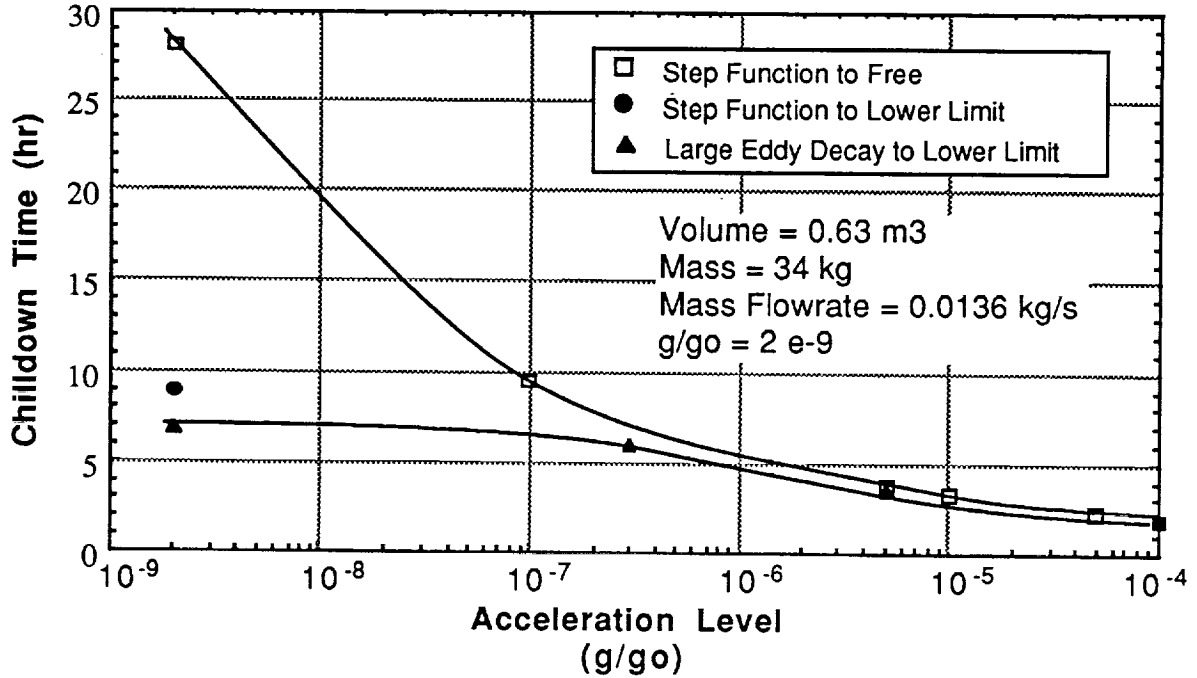


Figure D-9. Acceleration Level Effects on the Chiddown Time

$$M_{\text{fluid}} u_o r_o = \int_0^{r_o} u r \, dm \quad \text{or} \quad \frac{r_o^3 u_o}{2} = \int_0^{r_o} u r^2 \, dr, \quad \text{conserve angular momentum.} \quad (\text{D-13})$$

$$M_{\text{fluid}} u_o^2 = \int_0^{r_o} u^2 \, dm \quad \text{or} \quad \frac{r_o^2 u_o^2}{2} = \int_0^{r_o} u^2 r \, dr, \quad \text{conserve kinetic energy.} \quad (\text{D-14})$$

where u is the tangential velocity, u_o is the entering fluid velocity, r is the radial distance from the center of the tank, r_o is the tank radius, and M_{fluid} is the total fluid mass injected into the initially evacuated tank. The mathematical form of the velocity profile will be assumed to be a polynomial. A considerable amount of algebra leads to the following tangential velocity profile:

$$\frac{u}{u_o} = 6.53 \left(\frac{r}{r_o}\right) - 7.58 \left(\frac{r}{r_o}\right)^3 + 1.06 \left(\frac{r}{r_o}\right)^5 \quad (\text{D-15})$$

The angular velocity profile can be calculated from the tangential velocity profile, $\omega = u/r$:

$$\frac{\omega}{\omega_o} = 6.53 - 7.58 \left(\frac{r}{r_o}\right)^2 + 1.06 \left(\frac{r}{r_o}\right)^4 \quad (\text{D-16})$$

These profiles are plotted in Figure D-10. The maximum angular velocity occurs at the tank axis because the fluid spins faster as the radial position decreases. The low angular velocity gradient near the tank axis implies the fluid in this region spins as a solid disk, i.e., no-shear. The tangential velocity is zero at the wall and the centerline. The maximum tangential velocity occurs about half-way between the wall and the centerline.

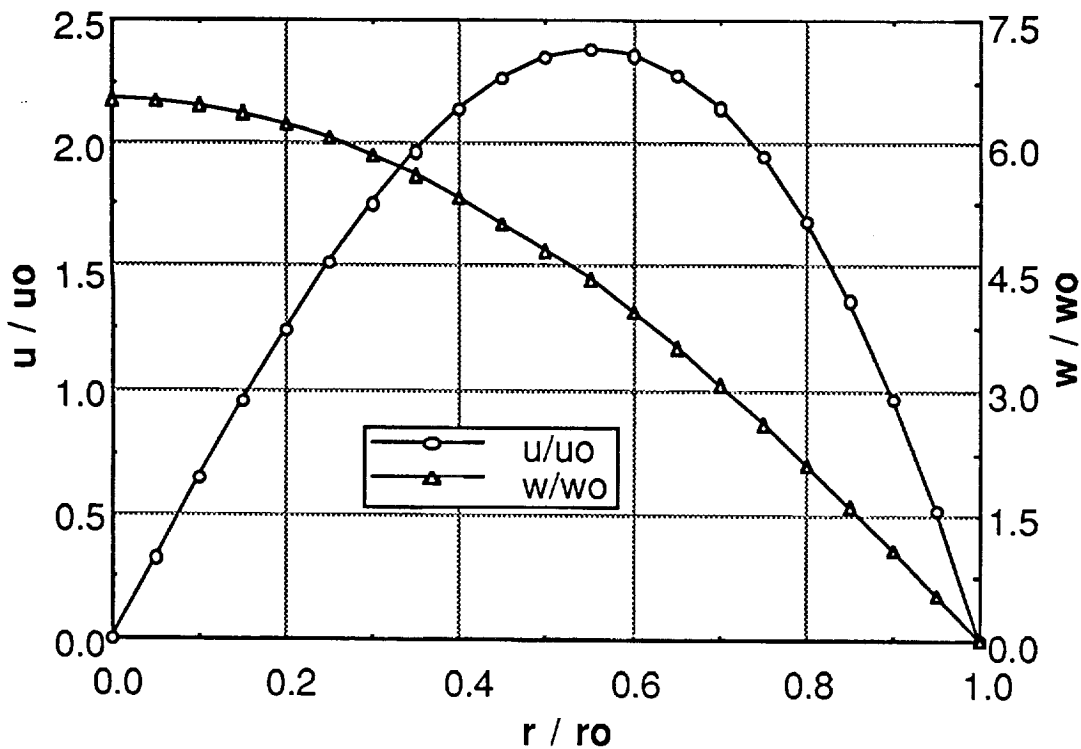


Figure D-10. Initial Velocity Profiles

5

D.3.2 Decay of Laminar Tangential Flow

The angular momentum equation governing a decaying tangential flow can be derived from a force balance on a fluid ring. Fluid properties are assumed to be constant:

$$\frac{\partial \omega}{\partial t} = \nu \left[\frac{\partial^2 \omega}{\partial r^2} + \frac{3}{r} \left(\frac{\partial \omega}{\partial r} \right) \right] \quad (D-17)$$

where ν is the kinematic viscosity and t is the time. Using the following dimensionless groups,

$$W = \frac{\omega}{\omega_0}, \quad T = \frac{t \nu}{r_0^2}, \quad R = \frac{r}{r_0}, \quad U = \frac{u}{u_0} \quad (D-18)$$

the governing angular momentum equation and boundary conditions can be non-dimensionalized:

$$\frac{\partial W}{\partial T} = \frac{\partial^2 W}{\partial R^2} + \frac{3}{R} \left(\frac{\partial W}{\partial R} \right) \quad (D-19)$$

$$\frac{\partial W}{\partial R} (R=0) = 0, \quad \text{No-shear on the tank centerline.}$$

$$W(R=1) = 0, \quad \text{No-slip at the tank wall.}$$

$$W(T=0) = 6.53 - 7.58 R^2 + 1.06 R^4, \quad \text{Initial velocity profile.}$$

where $\omega_0 = u_0 / r_0$. The dimensionless forms of the governing partial differential equation and boundary conditions are solved using the method of lines with cubic Hermite polynomials. This algorithm is a standard routine in the IMSL library.

The decay of the tangential and angular velocity profiles are shown in Figures D-11 and D-12 respectively. Fluid motion has nearly stopped by $T=1$. This corresponds to 5.5 hours for superheated vapor at 172 kPa, 111 K in a 0.104 meter diameter tank. These are "typical" conditions during the hold in Tank 2. Fluid property variations, which will occur during the hold phase, are not taken into account in this analysis.

Currently only the momentum equation has been solved. To obtain heat transfer results, a solution to the energy equation is required. Approximate heat transfer results can be obtained using the Reynolds analogy (Reference D-4):

$$St = \frac{Nu}{Re Pr} \approx \frac{C_f}{2} \quad \text{or} \quad Nu \approx \frac{D \tau_{wall} Pr}{u_{peak} \mu} = \frac{D^2 Pr}{2 u_{peak}} \left(\frac{\partial \omega}{\partial r} \right)_{wall} \quad (D-20)$$

The tank diameter, $D = 2r_0$, is used for the length scale in the Nusselt number and Reynolds number. The peak tangential velocity at a given time is used as the velocity scale in the Reynolds number. In cylindrical coordinates, the wall shear stress is related to the angular velocity gradient, $\tau_{wall} = \mu r_0 (\partial \omega / \partial r)$. The Reynolds analogy assumes a similarity exists between the near wall gradients in temperature and velocity. The diffusivities for heat and momentum must be nearly equal. For laminar flows, the Reynolds analogy is valid for fluids having a Prandtl number near unity. For

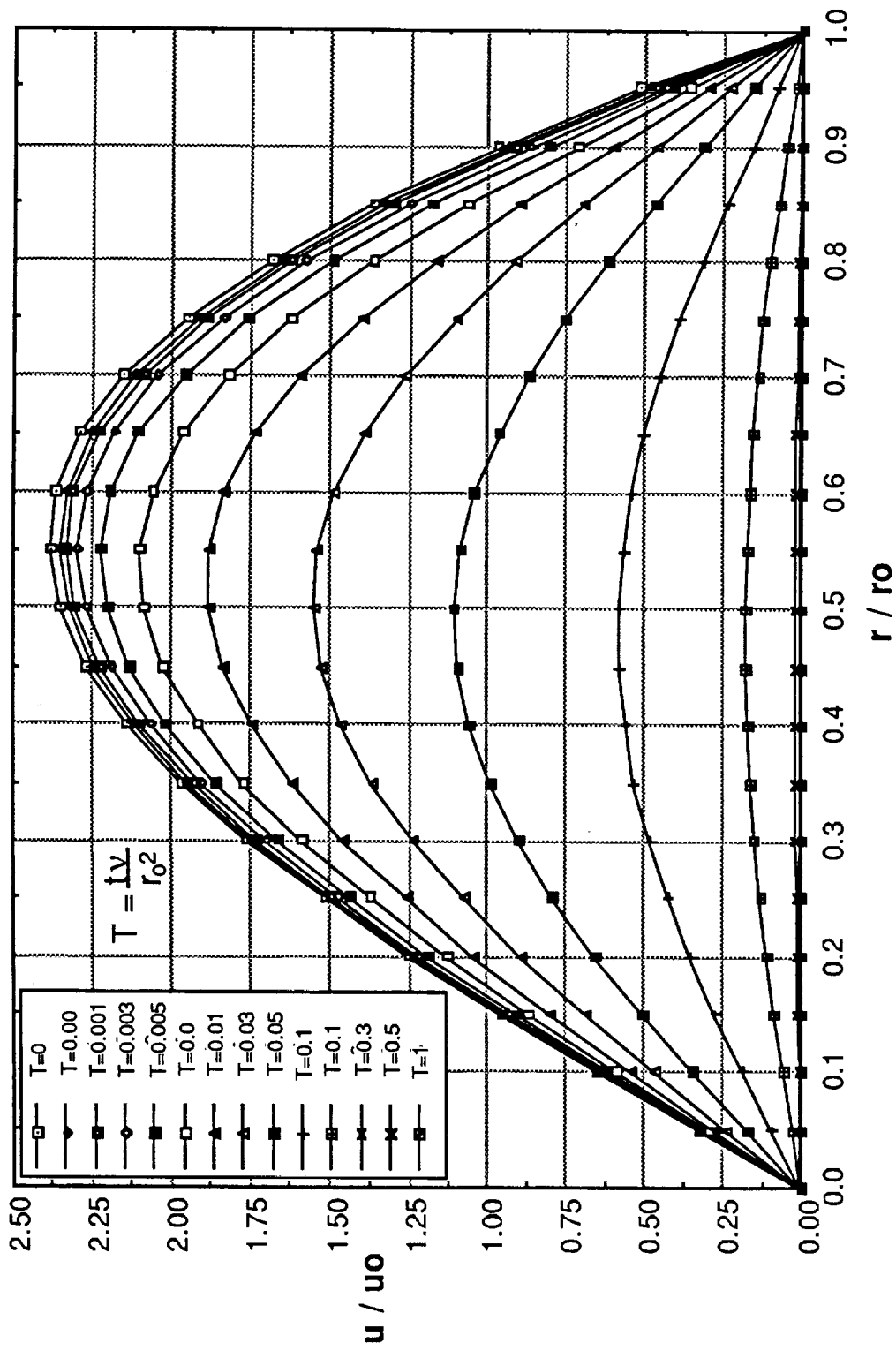


Figure D-11. Laminar Flow, Tangential Velocity Decay

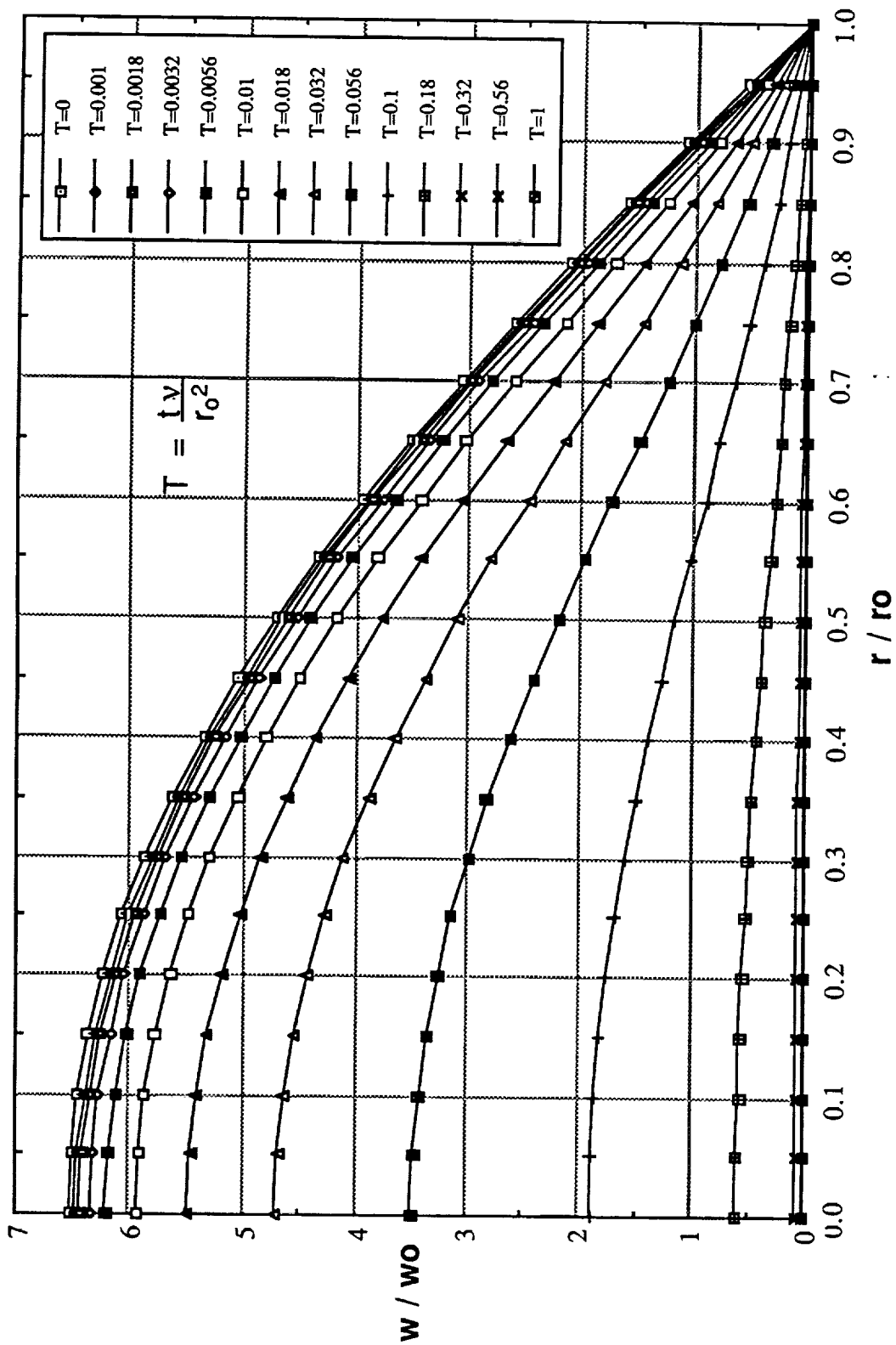


Figure D-12. Laminar Flow, Angular Velocity Decay

turbulent flows, where the “eddy” diffusivities are much greater than molecular diffusivities, the Reynolds analogy is valid for flows with a “turbulent” Prandtl number near unity. For most turbulent and laminar gas flows the Reynolds analogy is a good approximation.

Using the Reynolds analogy, the decay of the Nusselt number was determined from the decaying velocity profile. As shown in Figure D-13, the variation in Nu is small for a laminar, decaying, tangential flow. It is initially slightly greater than 6, and decreases to a constant value of 4. This value is approximately the same as for fully-developed laminar flow through a circular pipe (Reference D-5). For a pipe with constant wall temperature the Nusselt number has a value of 3.66. For a pipe with uniform heat flux the Nusselt number is 4.36. A constant value for Nu, i.e., independent of the flow field, implies molecular conduction is the dominant heat transfer mechanism. Heat must conduct through the fluid which is moving tangentially. Tangential velocities do not convect heat away from the wall. Radial velocities, i.e., flow towards or away from the wall, are required to enhance the heat transfer coefficient relative to pure conduction.

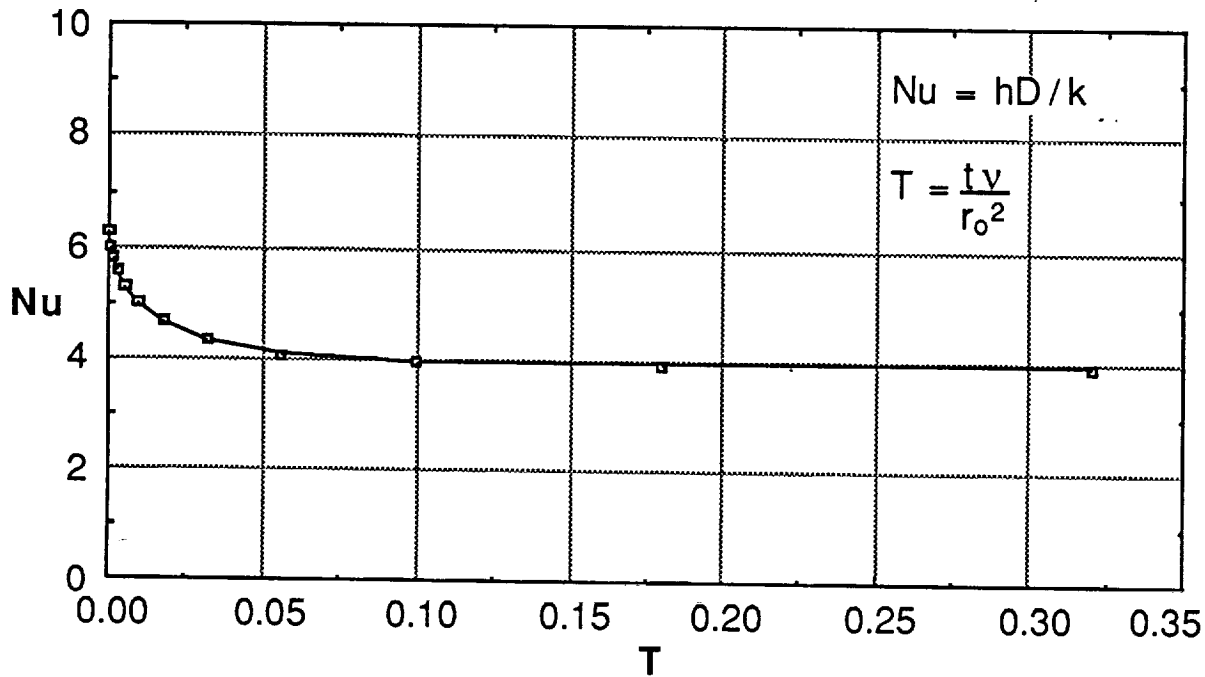


Figure D-13. Laminar Flow, Convection Coefficient Decay

D.3.3 Decay of Turbulent Tangential Flow

A turbulent tangential flow will have a non-zero, fluctuating, radial velocity component, even when the mean radial velocity component is small. As a result, the diffusivities for both momentum and energy are enhanced relative to molecular diffusivities. The “turbulent” heat flux is typically much larger than the conducted heat flux. Turbulent flows are also much more dissipative than laminar flows.

The magnitude of the Reynolds number, immediately following the charge phase, will indicate whether the flow is laminar or turbulent at the start of the hold phase:

$$Re = u_0 \rho D / \mu = 2.3 \times 10^5 \quad (D-21)$$

where u_0 is the the entering fluid velocity. A conservatively low value of 3.05 m/s has been assumed. D is the tank diameter, which has a value of 0.104 meters for Tank 2. Superheated vapor

properties have been evaluated at a “typical” condition during the hold phase: 172 kPa, 111 K. This Reynolds number is defined in a manner similar to a pipe Reynolds number where turbulent flow is expected for $Re > 2300$. This Reynolds number is based on the thickness of the flow, not the length of the flow. For a flat plate boundary layer, turbulent flow is expected when the Reynolds number, based on the momentum thickness, is greater than 200 (Reference D-5). The momentum thickness is typically one-tenth the boundary layer thickness. Consequently, a flat plate boundary layer will transition to turbulent when the Reynolds number, based on the thickness of the boundary layer, becomes greater than 2000. The Reynolds number for flow immediately following the charge phase is roughly two-orders of magnitude greater than the transition Reynolds number, therefore turbulent flow is expected during the hold phase.

The governing angular momentum equation described above is valid only for laminar flows, i.e., flows with no fluctuating velocity components. To take into account the “turbulent” diffusivity, the widely used “eddy” diffusivity concept will be used (Reference D-5). The kinematic viscosity will be replaced with an “effective” viscosity which is the sum of the molecular viscosity and a “turbulent” viscosity:

$$\nu_{\text{eff}} = \nu + \nu_{\text{turb}} \quad (\text{D-22})$$

ν is a property of the fluid, while ν_{turb} is a property of the flow. For turbulent flows the turbulent viscosity is typically 10 to 100 times greater than the molecular viscosity due to the enhanced diffusivity caused by turbulent eddies. Using the eddy diffusivity concept, the dimensionless form of the governing angular momentum equation becomes:

$$\frac{\partial W}{\partial T} = \left(\frac{\nu_{\text{turb}}}{\nu} + 1 \right) \left[\frac{\partial^2 W}{\partial R^2} + \frac{3}{R} \left(\frac{\partial W}{\partial R} \right) \right] \quad (\text{D-23})$$

The dimensionless groups are the same as those defined earlier in this section. A simple mixing length model will be used to calculate the turbulent viscosity (Reference D-5):

$$\frac{\nu_{\text{turb}}}{\nu} = \left(\frac{\omega_0 r_0^2}{\nu} \right) R L^2 \left(\frac{\partial \omega}{\partial R} \right) \quad (\text{D-24})$$

For turbulent flows an additional dimensionless parameter ($\omega_0 r_0^2 / \nu$), i.e., the initial Reynolds number, is required to describe the flow field. L is the mixing length, normalized by the tank radius. The mixing length equals the smaller of the two expressions given in Equation D-25 (Reference D-5).

$$L = \kappa \left(\frac{y}{r_0} \right) \left[1 - \exp \left(\frac{-y \sqrt{\tau_{\text{wall}} / \rho}}{A^+} \right) \right] \quad \text{or} \quad L = \frac{\lambda}{r_0} \quad (\text{D-25})$$

The first expression is a mixing length model for the inner region of the turbulent boundary layer that includes a damping function to better model the viscous sublayer near the wall. The second expression is a simple mixing length model for the outer region. For a turbulent boundary layer, velocity and temperature gradients are confined near the wall, consequently the inner region model is more important than the outer region model. The quantity y is the distance from the wall and τ_{wall} is the wall shear stress. The parameters κ , A^+ , and λ are dimensionless model constants that for a “standard” turbulent boundary layer have values of 0.41, 26, and 0.085, respectively.

The decay of the tangential and angular velocity profiles are shown in Figures D-14 and D-15, respectively. These results are valid for an initial Reynolds number equal to $\omega_0 r_0^2 / \nu = 100,000$. The turbulent tangential flow decays more rapidly than the laminar tangential flow discussed earlier. Fluid motion has nearly stopped by $T=0.1$. This corresponds to 0.55 hours for superheated vapor at 172 kPa, 111 K in a 0.104 meter diameter tank. These are "typical" conditions during the hold phase in Tank 2. Fluid property variations, which will occur during the hold phase, are not taken into account in this analysis. Figure D-16 shows a comparison of the angular velocity profiles in the region near the wall. In the turbulent case, velocity gradients are much steeper near the wall.

The decay of the turbulent heat transfer coefficient was approximated using the Reynolds analogy. A comparison of the laminar and turbulent results are shown in Figure D-17. Both start with the same initial velocity profile, consequently, the Nusselt number has an initial value of ~ 6 for both cases. For the turbulent case the Nusselt number rapidly increases to a maximum of 30, then gradually decreases and approaches the laminar flow results, i.e., $Nu \sim 4$. It is physically unlikely that the actual Nusselt number increases after the charge is terminated. This anomalous behavior is a result of using an inappropriate initial velocity profile. For the turbulent case, the initial profile should be "turbulent", i.e., steep gradients should be confined near the wall and shallow velocity gradients should exist near the center of the tank. Additional work is required in this area. Since time is plotted on a log-scale, the initial Nu variation appears "stretched-out". The profile changes quickly to a more "turbulent" configuration. The maximum Nusselt number is reached at $T \sim 10^{-4}$. This corresponds to only 2 seconds for "typical" conditions during a hold (172 kPa, 111 K). The Nusselt number for the turbulent case takes more than 6 minutes to converge to the laminar flow values.

The heat transfer results for decaying laminar and turbulent tangential flows are compared to results for decaying large turbulent eddies in Figure D-18. The large turbulent eddy model was modified to include a smooth transition to the conduction limit. To obtain a valid comparison, the large turbulent eddy results were also normalized by the maximum value of the convection coefficient predicted using the turbulent tangential flow model. For most of the time, the heat transfer coefficients for the two turbulent cases are greater than for the laminar flow case. All three cases converge to the same value, which represents the pure conduction limit. The turbulent tangential flow persists almost ten times longer than the turbulent eddy flow field, which contains no mean flow component.

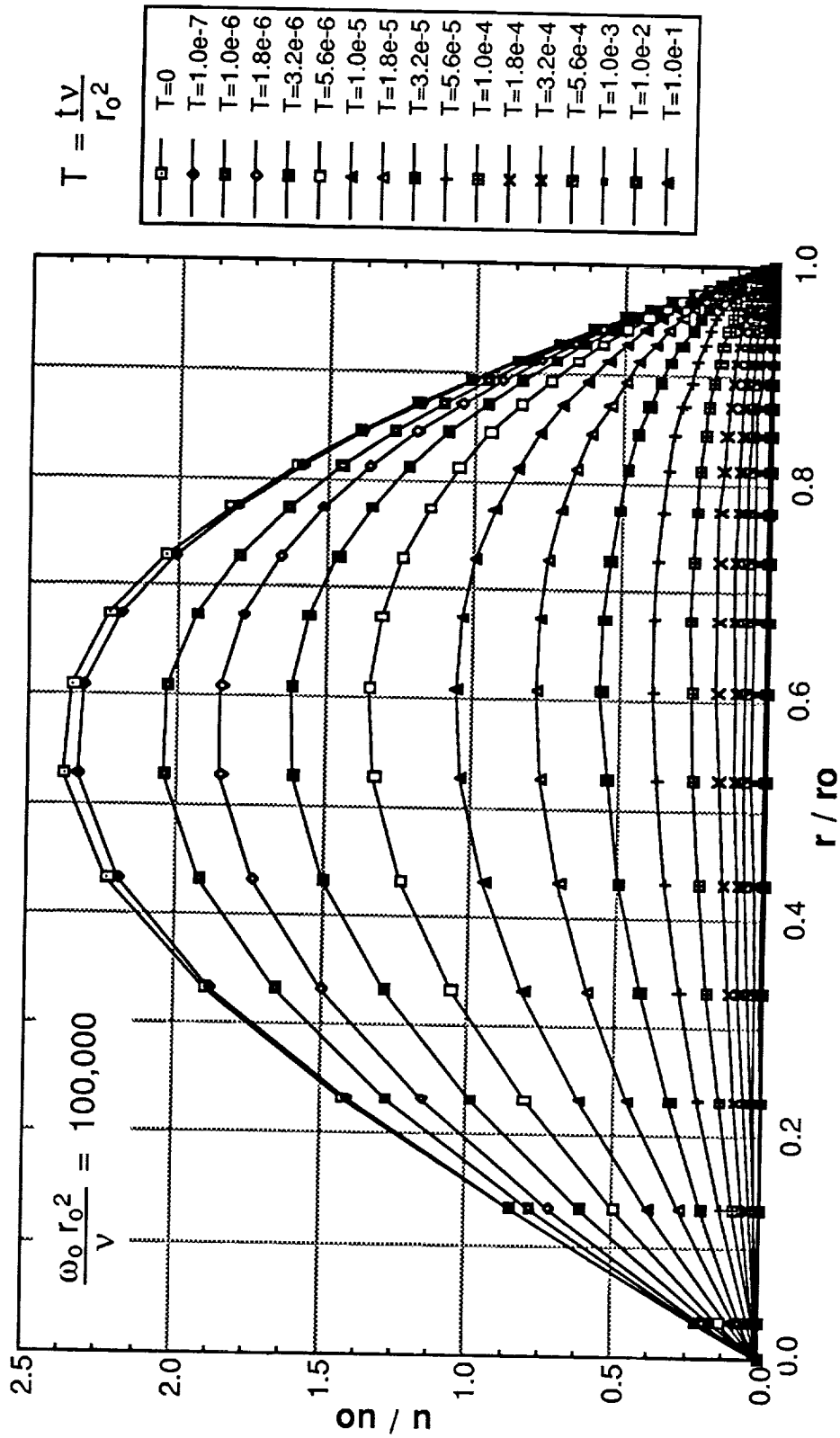


Figure D-14. Turbulent Flow, Tangential Velocity Decay

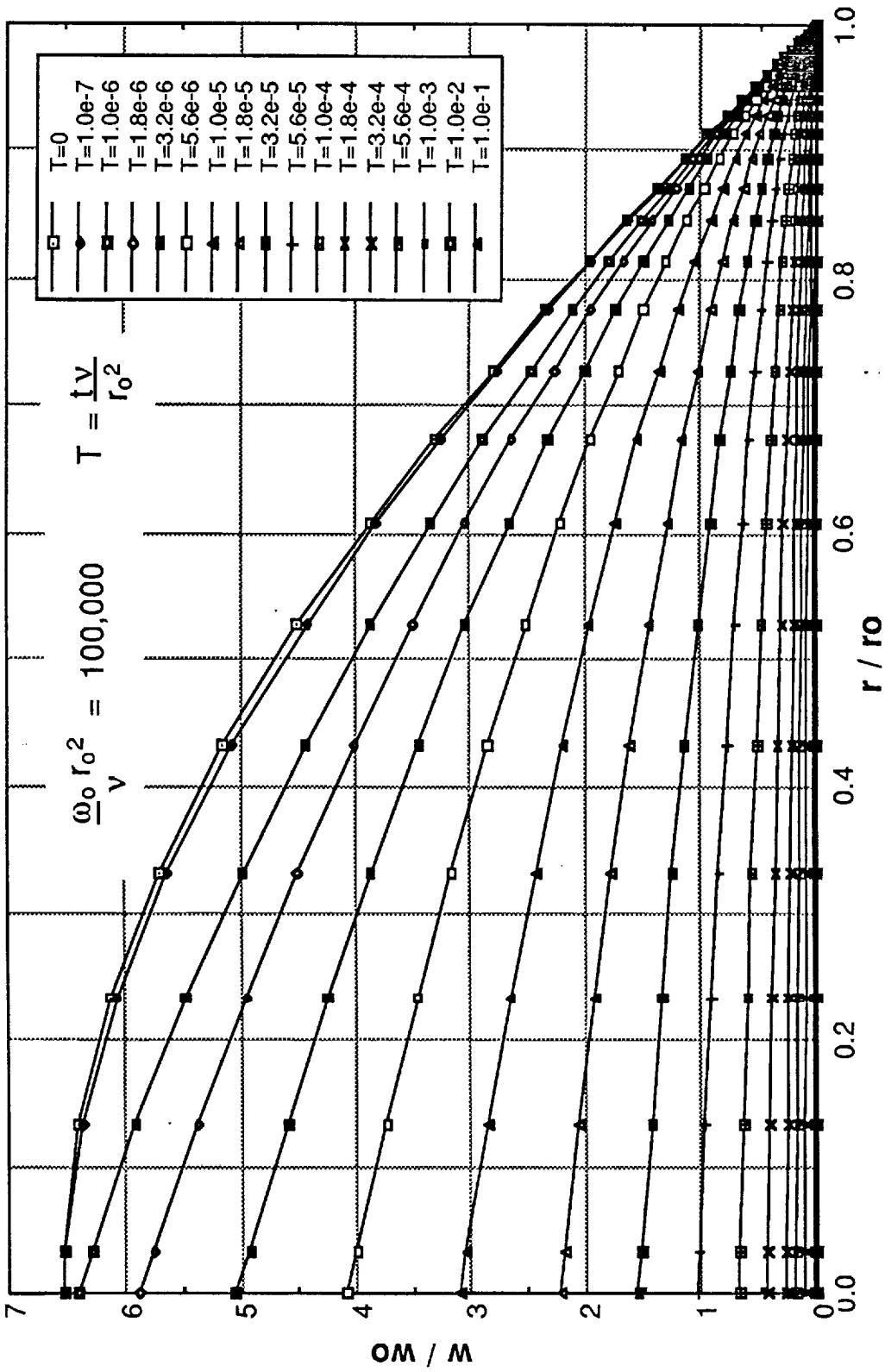
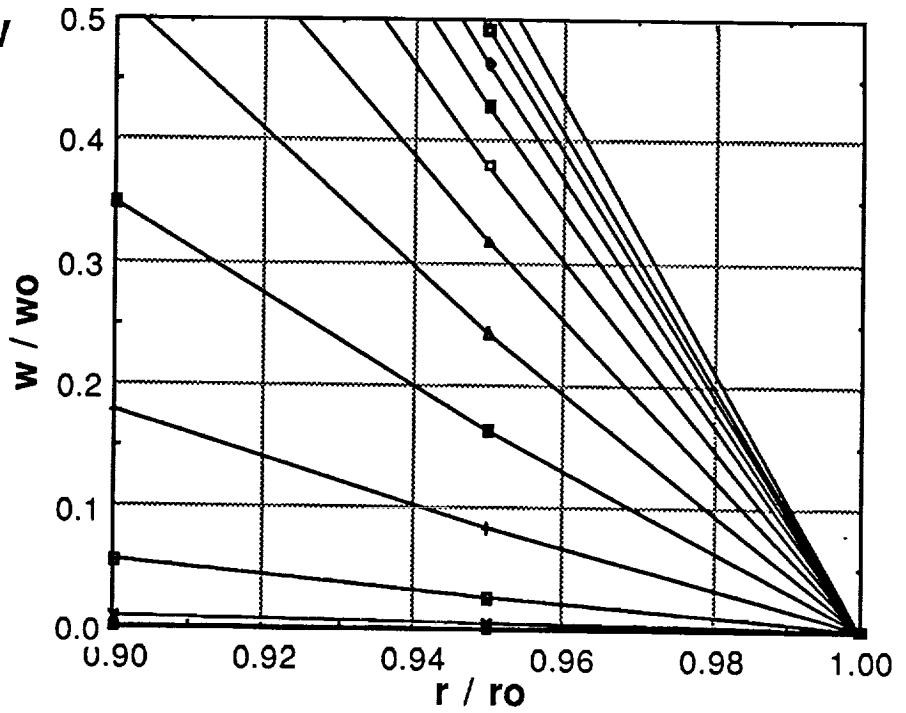
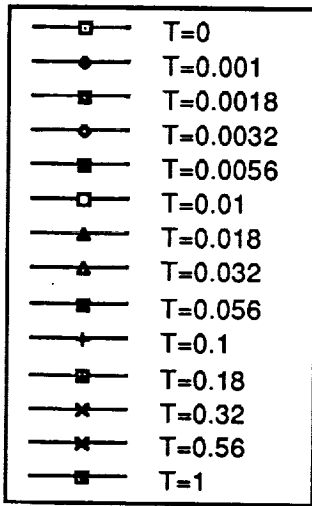


Figure D-15. Turbulent Flow, Angular Velocity Decay

LAMINAR FLOW



TURBULENT FLOW

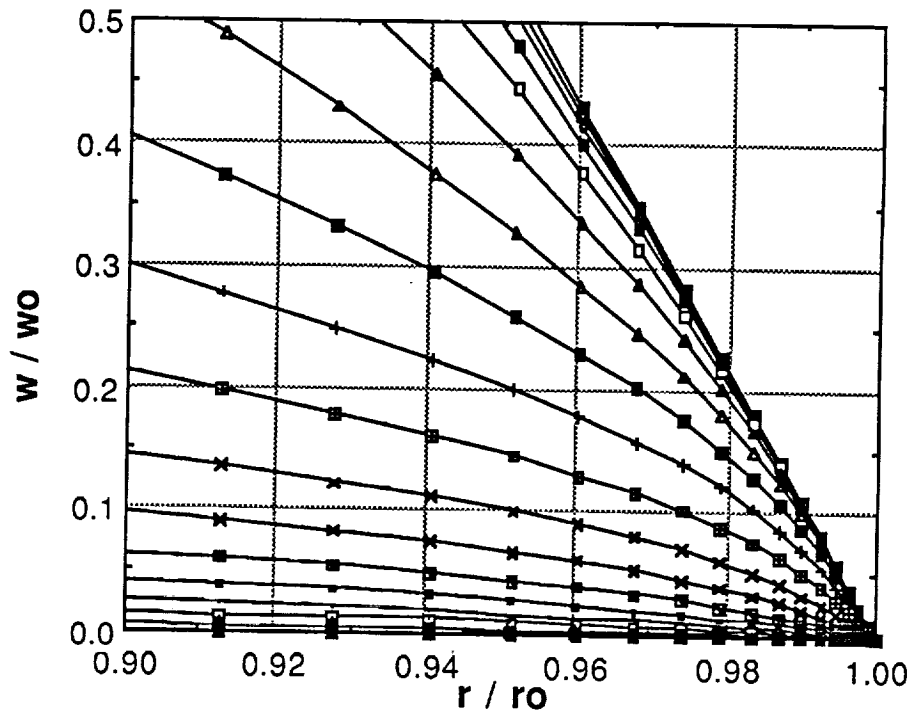
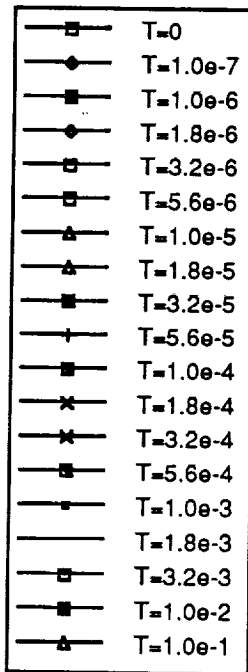


Figure D-16. Comparison of Laminar and Turbulent Near-Wall Velocity Profiles

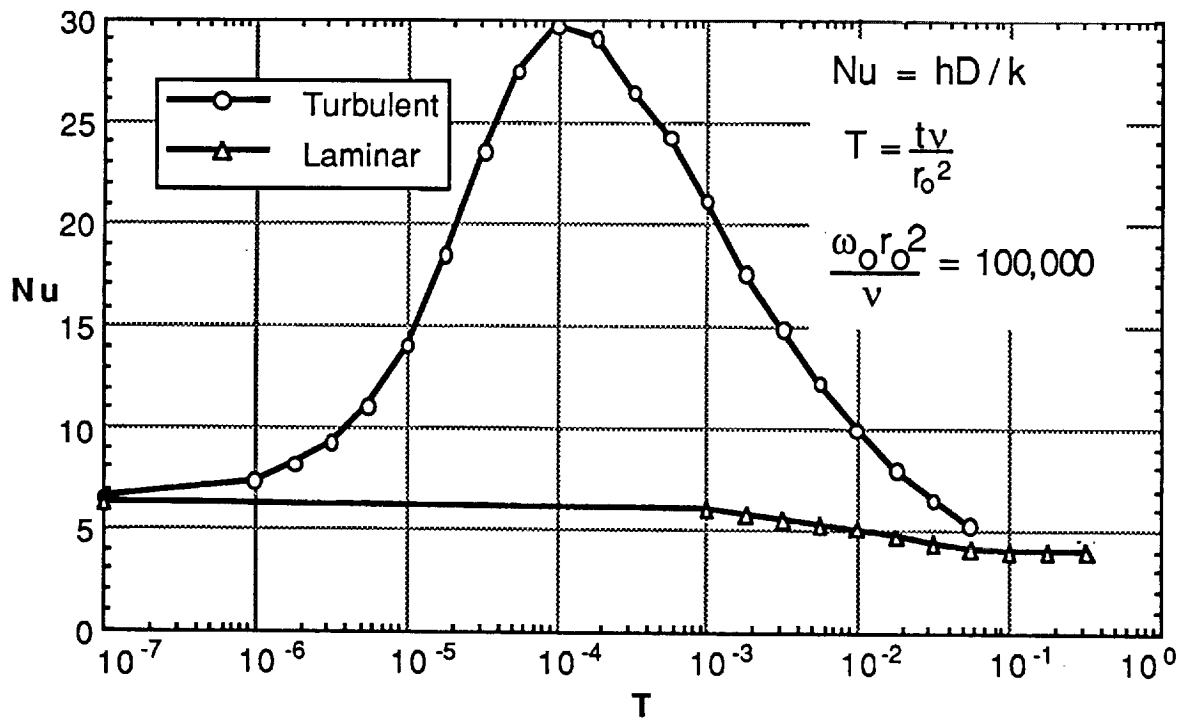


Figure D-17. Comparison of Nusselt Number Decay for Laminar and Turbulent Tangential Flow Cases

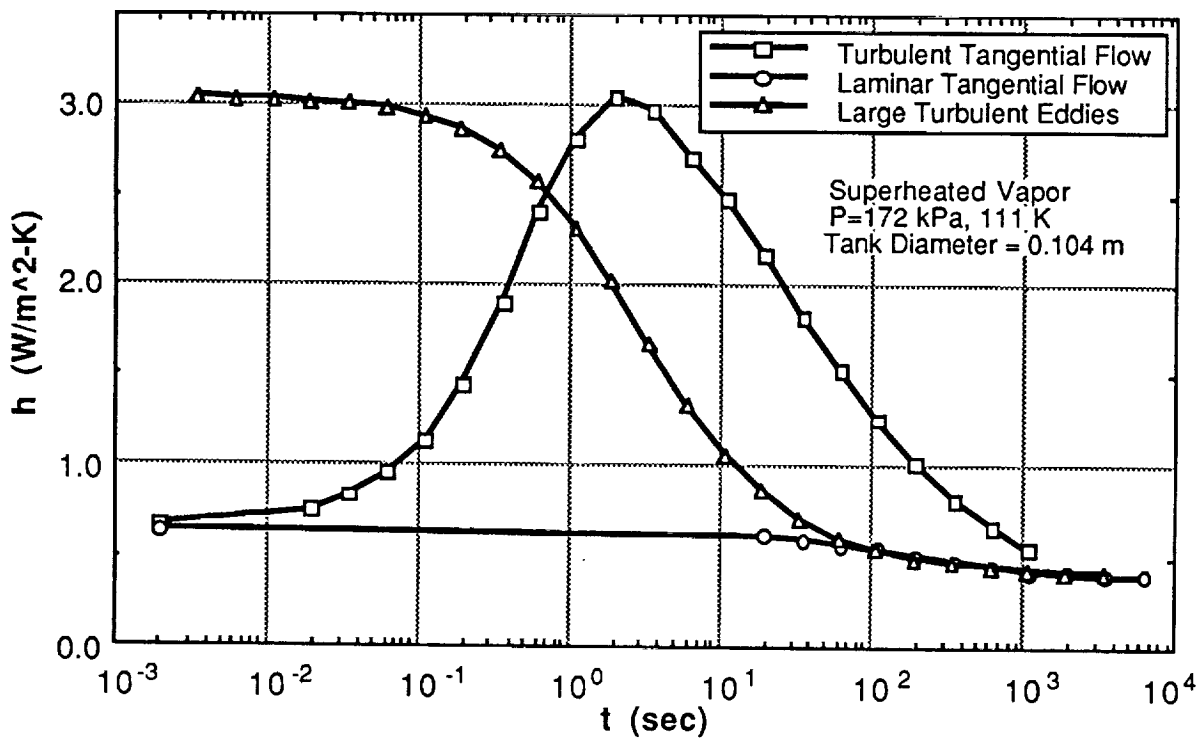


Figure D-18. Comparison of Heat Transfer Results

APPENDIX E
DETAILED EXPERIMENT SEQUENCES

APPENDIX E
DETAILED EXPERIMENT SEQUENCES

This appendix contains two lists of the sequenced tests that are performed in order to carry out the Class I and Class II experiments. Table E-1 lists the experiments as if they were performed one after the other, such as might be done if the Spacecraft Operations and Control Center (SOCC) was continually fully staffed. Table E-2 lists the experiments as if they were performed according to the staffing plan provided by NASA.

Table E-1. Experiment Sequence Based on Continual Staffing of SOCC

Seq No.	Orien./g Lvl. (10 ⁶)	Test Numbers	Event Description	Time Reqd. (Hrs)	Elapsed Time (Hrs)	DAYS	FINAL TANK VOLUME			H2 MASS BALANCE			
							T1 kg	T2 kg	T3 kg	PARAS LOSS	TEST LOSS	BAL kg	
4			Launch	0.0	0.0	0.0	365	0	0	0	0.0	0.0	364.5
5	I-1.1		Pressure Control	72.0	72.0	3.0	361	0	0	0	3.3	0.0	361.2
6	I-1 @95%		Thermal strat, mixer & TVS T1	114.0	186.0	7.8	343	0	0	0	18.6	0.0	342.6
7			Ht T3 {16}		186.0	7.8	343	0	0	0	0.0	0.0	342.6
8	II-7		[Line Chill]	1.0	187.0	7.8	341	0	0	0	0.0	1.2	341.4
9	I-3.5		Chill Tank 3	6.0	193.0	8.0	337	0	0	0	0.3	4.0	337.2
10	-/100		No Vent Fill Tank 3	0.5	193.5	8.1	295	0	0	42	9.5	0.0	337.2
11			Condition Tank 3	3.4	196.9	8.2	295	0	0	40	9.2	1.7	335.5
12	II-5		[Liq Outflow], Xfer T3 to T1	0.5	197.4	8.2	331	0	0	4	10	0.0	335.5
13	+/50	II-9.1	Vented Fill	0.5	198.4	8.3	331	0	0	43	9.8	0.0	334.8
14	+/1	II-5	[Liq Outflow], Xfer T3 to T1	2.0	200.4	8.4	331	0	0	4	8	0.0	334.8
15			[Dump Tank 3]	16.0	216.4	9.0	330	0	0	0	0.7	0.0	331.2
16			Ht T3 {16}	1.0	217.4	9.1	329	0	0	0	0.0	1.2	329.3
17	II-7		[Line Chill]	6.2	223.6	9.3	325	0	0	0	0.3	4.0	325.0
18	I-3.6		Chill Tank 3	1.7	225.3	9.4	283	0	0	42	9.5	0.0	325.0
19	-/100	I-4.3	No Vent Fill Tank 3	3.4	228.7	9.5	283	0	0	40	9.2	1.7	323.3
20			Condition Tank 3	0.5	229.2	9.6	319	0	0	4	10	0.0	323.3
21	II-5		[Liq Outflow], Xfer T3 to T1	1.7	230.9	9.6	279	0	0	43	9.8	0.0	322.6
22	+/50	II-9.2	Vented Fill	0.5	231.4	9.6	319	0	0	4	8	0.0	322.6
23	II-5		[Liq Outflow], Xfer T3 to T1	2.0	233.4	9.7	319	0	0	0	0.1	3.5	319.0
24			[Dump Tank 3]	16.0	249.4	10.4	318	0	0	0	0.7	0.0	318.3
25			Ht T3 {16}	1.0	250.4	10.4	317	0	0	0	0.0	1.2	317.1
26	II-7		[Line Chill]	6.0	256.4	10.7	313	0	0	0	0.0	4.0	312.8
27	I-3.3		Chill Tank 3	1.7	258.1	10.8	271	0	0	42	9.5	0.0	312.8
28	I-4.4		No Vent Fill Tank 3	3.4	261.5	10.9	271	0	0	40	9.2	1.7	311.1
29			Condition Tank 3	0.3	261.8	10.9	307	0	0	4	10	0.0	311.1
30	II-5		[Liq Outflow], Xfer T3 to T1	0.5	262.3	10.9	267	0	0	43	9.8	0.0	310.4
31	+/100	II-9.3	Vented Fill	0.5	262.8	11.0	307	0	0	4	8	0.0	310.4
32	II-5		[Liq Outflow], Xfer T3 to T1	2.0	264.8	11.0	307	0	0	0	0.1	3.5	306.8
33	II-10		[Dump Tank 3]	1.0	265.8	11.1	305	0	0	0	0.0	1.6	305.2
34	II-7		[Line Chill]	17.9	283.7	11.8	291	0	0	0	0.8	12.0	291.5
35	1-3.12		Chill Tank 2	1.1	284.8	11.9	207	55	85	9.5	0.0	0.0	291.5
36	-/100	1-4.12	No Vent Fill Tank 2	8.0	292.8	12.2	206	55	78	8.8	0.0	0.0	291.5
37			Cond T2	0.5	293.3	12.2	206	55	78	8.8	0.0	0.0	284.6
38	II-4		Tank Press	4.0	297.3	12.4	282	75	3	3	0.0	0.0	284.5
39	II-6		LAD Performance	1.0	298.3	12.4	282	75	0	0	0.0	2.7	281.8
40	II-10		Dump T2	1.0	299.3	12.5	264	70	18	20	0.0	0.0	281.8
41	1-5.7		LAD Fill Tank 2	1.0	300.3	12.5	196	52	85	9.5	0.0	0.0	280.9
42	+/50	II-9.7	Vented Fill	0.2	300.5	12.5	196	52	85	9.5	0.0	0.0	280.9
43	II-4		Tank Press										

Table E-1. Experiment Sequence Based on Continual Staffing of SOCC (Cont.)

Seq No.	Orien./g Lvl. (10*6)	Test Numbers	Event Description	Time Req'd. (Hrs)	Elapsed Time (Hrs)	DAYS	FINAL TANK VOLUME			H2 MASS BALANCE			
							T1 kg	T2 kg	T3 kg	PARAS LOSS	TEST LOSS	BAL kg	
44		[II-6]	LAD Performance	0.5	301.0	12.5	278	74	3	0	0.0	0.0	280.9
45		[II-10]	Dump T2	1.0	302.0	12.6	278	74	0	0	0.0	2.7	278.2
46		[II-7]	Ht T2 {22}	22.0	324.0	13.5	277	74	0	0	1.0	0.0	277.2
47		[II-7]	[Line Chill]	1.0	325.0	13.5	276	74	0	0	0.0	1.6	275.5
48		1-3-13	Chill Tank 2, Heat T3	18.9	343.9	14.3	262	70	0	0	0.9	12.0	261.8
49		1-4-11	No Vent Fill Tank 2	3.5	347.4	14.5	177	47	85	95	0.0	0.0	261.8
50			Cond T2	8.0	355.4	14.8	177	47	78	88	0.0	0.0	254.9
51		[II-4]	Tank Press	0.5	355.9	14.8	177	47	78	88	0.0	0.0	254.8
52		[II-6]	LAD Performance	4.0	359.9	15.0	252	67	3	0	0.0	0.0	254.8
53		[II-10]	Dump T2	1.0	360.9	15.0	252	67	0	0	0.0	2.7	252.1
54		1-5-6	LAD Fill Tank 2	1.0	361.9	15.1	234	63	18	20	0.0	0.0	252.1
55		[II-9.8]	Vented Fill	3.5	365.4	15.2	164	44	87	98	0.0	0.9	251.2
56		[II-4]	Tank Press	0.2	365.6	15.2	164	44	87	98	0.0	0.0	251.1
57			Xfer T2 to T1	0.5	366.1	15.3	242	65	9	0	0.0	0.0	251.1
58		[II-10]	Dump T2	1.0	367.1	15.3	242	65	0	0	0.0	8.9	242.2
59		I-1 (@ 65%)	Thermal strat, mixer & TVS T1	264.0	631.1	26.3	217	58	0	0	25.2	0.0	217.0
60		[II-7]	[Line Chill]	1.0	632.1	26.3	216	58	0	0	0.0	1.2	215.8
61		1-3-10	Chill Tank 2	17.9	650.0	27.1	202	54	0	0	0.8	12.0	202.1
62		1-4-14	No Vent Fill Tank 2	3.4	653.4	27.2	117	31	85	95	0.0	0.0	202.1
63			Cond T2	8.0	661.4	27.6	117	31	78	88	0.0	0.0	195.2
64		[II-4]	Tank Press	0.5	661.9	27.6	117	31	78	88	0.0	0.0	195.2
65		[II-6]	LAD Performance	4.0	665.9	27.7	193	51	3	0	0.0	0.0	195.2
66		[II-10]	Dump T2	1.0	666.9	27.8	192	51	0	0	0.0	2.7	192.5
67		1-5-3	LAD Fill Tank 2	1.0	667.9	27.8	175	47	18	20	0.0	0.0	192.5
68		[II-9.9]	Vented Fill	1.0	668.9	27.9	104	28	87	98	0.0	0.9	191.6
69		[II-4]	Tank Press	0.2	669.1	27.9	104	28	87	98	0.0	0.0	191.5
70			Xfer T2 to T1	0.5	669.6	27.9	125	33	67	75	0.0	0.0	191.5
71		I-1 (@ 75%)	Thermal strat & TVS T2	93.0	762.6	31.8	120	32	65	73	0.0	0.0	185.2
72		[II-4]	Line Chill/Tank Press	0.2	762.8	31.8	120	32	63	71	0.0	1.6	183.5
73			Xfer T2 to T1	0.5	763.3	31.8	175	47	9	10	0.0	0.0	183.5
74		[II-10]	Dump T2, Vent Line	1.0	764.3	31.8	175	47	0	0	0.0	9.2	174.6
75		[II-7]	[Line Chill]	1.0	765.3	31.9	173	46	0	0	0.0	1.2	173.4
76		I-3-7	Chill Tank 3	2.0	767.3	32.0	170	45	0	0	0.1	3.5	169.8
77		I-4-5	No Vent Fill Tank 3	1.7	769.0	32.0	128	34	0	0	0.0	0.0	169.8
78			Condition Tank 3	3.4	772.4	32.2	128	34	0	0	1.7	0.0	168.1
79		[II-5]	[Liq Outflow], Xfer T3 to T1	0.3	772.7	32.2	165	44	0	0	0.0	0.0	168.1
80		[II-10]	[Dump Tank 3]	2.0	774.7	32.3	164	44	0	0	0.0	3.5	164.5
81		[II-9.4]	Vented Fill	0.5	775.2	32.3	121	32	0	0	0.1	0.0	163.8
82		[II-5]	[Liq Outflow], Xfer T3 to T1	0.3	775.5	32.3	160	43	0	0	0.0	0.0	163.8
83		[II-10]	[Dump Tank 3]	2.0	777.5	32.4	160	43	0	0	0.1	3.5	160.2

Table E-1. Experiment Sequence Based on Continual Staffing of SOCC (Cont.)

Seq No.	Orien./g Lvl. (10 ⁶)	Test Numbers	Event Description	Time Reqd. (Hrs)	Elapsed Time (Hrs)	DAYS			FINAL TANK VOLUME						H2 MASS BALANCE				
						T1	T2	T3	T1	T2	T3	kg	%	kg	%	kg	%	PARAS LOSS	TEST LOSS
84	20/100	I-1 (@ 40%)	Thermal strat. mixer & TVS T1	104.0	881.5	36.7			140	37	0	0	0	0	0	0	19.8	0.0	140.4
85		I-3.8	Chill Tank 3	2.3	883.8	36.8			137	37	0	0	0	0	0	0	0.1	3.5	136.8
86		I-4.9	No Vent Fill Tank 3	1.7	885.5	36.9			95	25	0	0	42	9.5	0.0	0.0	0.0	136.8	
87			Condition Tank 3	3.4	888.9	37.0			95	25	0	0	40	9.2	1.7	0.0	0.0	135.1	
88		[II-5]	[Liq Outflow], Xfer T 3 to T2	0.3	889.2	37.1			132	35	0	4	8	0.0	0.0	0.0	0.0	135.1	
89	+100	[II-9.5]	Vented Fill	0.8	890.0	37.1			91	24	0	43	9.8	0.0	0.0	0.0	0.0	134.4	
90		[II-5]	[Liq Outflow], Xfer T 3 to T2	0.3	890.3	37.1			131	35	0	4	8	0.0	0.0	0.0	0.0	134.4	
91		[II-10]	[Dump Tank 3]	2.0	892.3	37.2			131	35	0	0	0	0	0.1	3.5	130.8		
92		[II-7]	[Line Chill]	1.0	893.3	37.2			129	34	0	0	0	0	0.0	1.6	129.2		
93		1-3.11	Chill Tank 2, Heat T3	18.9	912.2	38.0			115	31	0	0	0	0	0.9	12.0	115.4		
94		1-4.15	No Vent Fill Tank 2	3.4	915.6	38.2			31	8	85	9.5	0	0	0.0	0.0	115.4		
95			Cond T2	8.0	923.6	38.5			30	8	78	8.8	0	0	6.9	0.0	108.5		
96		[II-4]	Tank Press	0.2	923.8	38.5			30	8	78	8.8	0	0	0.0	0.0	108.5		
97		I-5.8	LAD Fill T1	0.5	924.3	38.5			106	28	3	3	0	0	0.0	0.0	108.5		
98		[II-10]	Dump T2	1.0	925.3	38.6			106	28	0	0	0	0	0.0	2.7	105.8		
99		1-5.4	LAD Fill Tank 2	1.0	926.3	38.6			43	12	62	7.0	0	0	0.0	0.0	105.8		
100	+100	1-4.13	No Vent Fill Tank 2	0.8	927.1	38.6			21	6	85	9.5	0	0	0.0	0.0	105.8		
101		1-5.8, 9	LAD Fill T1	2.5	929.6	38.7			83	22	22	2.5	0	0	0.0	0.0	105.8		
102	100	I-1 (@ 10/25)	Thermal strat & TVS T1, T2	48.0	977.6	40.7			77	20	18	2.0	0	0	10.8	0.0	95.0		
103	+100	[II-9.10]	Vented Fill	3.5	981.1	40.9			7	2	87	9.8	0	0	0.0	0.9	94.0		
104		[II-7]	[Line Chill]	1.0	982.1	40.9			7	2	86	9.7	0	0	0.0	1.2	92.8		
105		I-3.1	Chill Tank 3	5.5	987.6	41.2			2	1	86	9.7	0	0	0.4	4.0	88.4		
106		I-4.10	No Vent Fill Tank 3	0.5	988.1	41.2			2	1	44	5.0	42	9.5	0.0	0.0	88.4		
107			Condition Tank 3	6.8	994.9	41.5			2	1	44	4.9	39	8.8	3.5	0.0	84.9		
108		[II-5]	[Liq Outflow], Xfer T 3 to T2	0.3	995.2	41.5			2	1	61	6.8	22	5.0	0.0	0.0	84.9		
109		I-4.7	No Vent Fill Tank 3	1.3	996.5	41.5			2	1	41	4.6	42	9.5	0.1	0.0	84.8		
110			Condition Tank 3	3.0	999.5	41.6			2	0	41	4.6	41	9.2	1.6	0.0	83.3		
111		[II-5]	[Liq Outflow], Xfer T 3 to T2	0.3	999.8	41.7			2	0	77	8.6	4	1.0	0.0	0.0	83.2		
112		[II-10]	[Dump Tank 3]	2.0	1,001.8	41.7			2	0	77	8.6	0	0	0.1	4.4	78.7		
113		[II-7]	[Line Chill]	1.0	1,002.8	41.8			2	0	76	8.5	0	0	0.0	1.2	77.5		
114	+100	I-3.2	Chill Tank 3	7.7	1,010.5	42.1			1	0	72	8.1	0	0	0.3	3.6	73.6		
115		I-4.6	No Vent Fill Tank 3	0.8	1,011.3	42.1			1	0	30	3.4	42	9.5	0.0	0.0	73.5		
116			Condition Tank 3	6.8	1,018.1	42.4			1	0	30	3.4	39	8.8	3.5	0.0	70.0		
117		[II-5]	[Liq Outflow], Xfer T 3 to T2	0.3	1,018.4	42.4			1	0	65	7.3	4	8	0.0	0.0	70.0		
118		[II-10]	[Dump Tank 3]	2.0	1,020.4	42.5			1	0	65	7.3	0	0	0.1	3.5	66.3		
119			Ht T 3	16.0	1,036.4	43.2			0	0	65	7.3	0	0	1.1	0.0	65.2		
120		[II-7]	[Line Chill]	1.0	1,037.4	43.2			0	0	64	7.2	0	0	0.0	1.2	64.0		
121	+50	I-3.4	Chill Tank 3	6.2	1,043.6	43.5			0	0	60	6.7	0	0	0.3	4.0	59.7		
122	-100	I-4.2	No Vent Fill Tank 3	0.8	1,044.4	43.5			0	0	18	2.0	42	9.5	0.0	0.0	59.9		
123			Condition Tank 3	6.8	1,051.2	43.8			0	0	18	2.0	39	8.8	3.2	0.0	56.6		

Table E-1. Experiment Sequence Based on Continual Staffing of SOCC (Cont.)

Seq No.	Orien./g Lvl. (10 ⁶)	Test Numbers	Event Description	Time Reqd. (Hrs)	Elapsed Time (Hrs)	DAYS	FINAL TANK VOLUME			H2 MASS BALANCE				
							T1 kg	T2 kg	T3 kg	PARAS LOSS	TEST LOSS	BAL kg		
124		[II-5]	[Liq Outflow], Xfer T3 to T2	0.3	1,051.5	43.8	0	53	4	8	0.0	0.0	56.6	
125		I-5.1, [II-10]	LAD Fill T2, [Dump Tank 3]	2.0	1,053.5	43.9	0	53	0	0	0.0	3.5	53.1	
126			Ht T3	16.0	1,069.5	44.6	0	53	0	0	0.4	0.0	52.7	
127		I-3.9	Chill Tank 3	6.9	1,076.4	44.9	0	49	0	0	0.3	4.0	48.7	
128		I-4.8	No Vent Fill Tank 3	0.8	1,077.2	44.9	0	7	8	95	0.0	0.0	48.7	
129			Transfer T3 to T2	0.5	1,077.7	44.9	0	45	4	8	0.0	0.0	48.7	
130	+100	[II-6][II-9.6]	LAD Perf/Vented Fill	1.7	1,079.4	45.0	0	5	5	43	98	0.0	0.7	48.0
131			Transfer T3 to T2	0.5	1,079.9	45.0	0	15	17	33	75	0.0	0.0	48.0
132		I-1 (@ 75%)	Thermal strat & TVS T3	40.0	1,119.9	46.7	0	14	16	31	71	2.8	0.0	45.2
133	100	I-1 (@ 75%)	Thermal strat & TVS T3	40.0	1,159.9	48.3	0	13	15	29	66	2.8	0.0	42.4
134		I-5.5	LAD Fill T2	0.5	1,160.4	48.4	0	31	35	11	25	0.0	0.0	42.4
135	100	I-1 (@ 25%)	Thermal strat & TVS T3	41.2	1,201.6	50.1	0	30	34	9	20	3.1	0.0	39.3
136		[II-10]	Dump T3	2.0	1,203.6	50.2	0	30	34	0	0	0.0	8.9	30.3
137		[II-6]	LAD Performance	4.0	1,207.6	50.3	0	3	3	63	63	0.0	0.0	30.3
138		[II-10]	Dump T2	1.0	1,208.6	50.4	0	0	0	28	63	0.0	2.7	27.6
139		I-5.2	LAD Fill T2	0.5	1,209.1	50.4	0	24	27	4	8	0.0	0.0	27.6

Table E-2. Experiment Sequence Based on NASA Plan for Staffing of SOCC

Seq No.	Orien./g Lvl. (10*6)	Test Numbers	Event Description	Time Reqd. (Hrs)	Elapsed Time (Hrs)	DAYS	FINAL TANK VOLUME			H2 MASS BALANCE			
							T1 kg	T2 kg	T3 kg	PARAS LOSS	TEST LOSS	BAL kg	
4			Launch	0.0	0.0		365	0	0	0	0.0	0.0	364.5
5		I-1.1	Pressure Control	72.0	72.0	3.0	361	0	0	0	3.3	0.0	361.2
6		I-1 (@95%)	Thermal strat. mixer & TVS T1	114.0	186.0	7.8	343	0	0	0	18.6	0.0	342.6
7			Ht T 3 {16}		186.0	7.8	343	0	0	0	0.0	0.0	342.6
8			No Op, Shift Break	6.0	192.0	8.0	342	0	0	0	0.3	0.0	342.4
9		[II-7]	[Line Chill]	1.0	193.0	8.0	341	0	0	0	0.0	1.2	341.2
10		I-3.5	Chill Tank 3	6.0	199.0	8.3	337	0	0	0	0.3	4.0	336.9
11		I-4.1	No Vent Fill Tank 3	0.5	199.5	8.3	295	0	0	42	0.0	0.0	336.9
12			Condition Tank 3	3.4	202.9	8.5	295	0	0	40	1.7	0.0	335.2
13		[II-5]	[Liq Outflow], Xfer T 3 to T1	0.5	203.4	8.5	331	0	4	10	0.0	0.0	335.2
14		+/50 [II-9.1]	Vented Fill	0.5	203.9	8.5	291	0	43	9.8	0.0	0.7	334.5
15		+1 [II-5]	[Liq Outflow], Xfer T 3 to T1	0.5	204.4	8.5	331	0	4	8	0.0	0.0	334.5
16		[II-10]	[Dump Tank 3]	2.0	206.4	8.6	331	0	0	0	0.1	3.5	330.9
17			Ht T 3 {16}	16.0	222.4	9.3	330	0	0	0	0.7	0.0	330.2
18		[II-7]	[Line Chill]	1.0	223.4	9.3	329	0	0	0	0.0	1.2	329.0
19		I-3.6	Chill Tank 3	6.2	229.6	9.6	325	0	0	0	0.3	4.0	324.7
20		-/100 I-4.3	No Vent Fill Tank 3	1.7	231.3	9.6	283	0	42	9.5	0.0	0.0	324.7
21			Condition Tank 3	3.4	234.7	9.8	283	0	40	9.2	1.7	0.0	323.0
22			No Op, Shift Break	5.3	240.0	10.0	282	0	40	9.1	0.3	0.0	322.7
23		[II-5]	[Liq Outflow], Xfer T 3 to T1	0.5	240.5	10.0	318	0	4	10	0.0	0.0	322.7
24		+/50 [II-9.2]	Vented Fill	1.7	242.2	10.1	279	0	43	9.8	0.0	0.7	322.0
25		[II-5]	[Liq Outflow], Xfer T 3 to T1	0.5	242.7	10.1	318	0	4	8	0.0	0.0	322.0
26		[II-10]	[Dump Tank 3]	2.0	244.7	10.2	318	0	0	0	0.1	3.5	318.4
27			Ht T 3 {16}	16.0	260.7	10.9	318	0	0	0	0.7	0.0	317.7
28			No Op, Shift Break	3.3	264.0	11.0	318	0	0	0	0.1	0.0	317.5
29		[II-7]	[Line Chill]	1.0	265.0	11.0	316	0	0	0	0.0	1.2	316.3
30		I-3.3	Chill Tank 3	6.0	271.0	11.3	312	0	0	0	0.3	4.0	312.1
31		I-4.4	No Vent Fill Tank 3	1.7	272.7	11.4	270	0	42	9.5	0.0	0.0	312.1
32			Condition Tank 3	3.4	276.1	11.5	270	0	40	9.2	1.7	0.0	310.4
33		[II-5]	[Liq Outflow], Xfer T 3 to T1	0.3	276.4	11.5	306	0	4	10	0.0	0.0	310.4
34		+/100 [II-9.3]	Vented Fill	0.5	276.9	11.5	266	0	43	9.8	0.0	0.7	309.7
35		[II-5]	[Liq Outflow], Xfer T 3 to T1	0.5	277.4	11.6	306	0	4	8	0.0	0.0	309.7
36		[II-10]	[Dump Tank 3]	2.0	279.4	11.6	306	0	0	0	0.1	3.5	306.1
37			No Op, Shift Break	13.7	293.1	12.2	305	0	0	0	0.6	0.0	305.4
38		[II-7]	[Line Chill]	1.0	294.1	12.3	304	0	0	0	0.0	1.6	303.8
39		1-3.12	Chill Tank 2	17.9	312.0	13.0	290	0	0	0	0.8	12.0	290.1
40		-/100 1-4.12	No Vent Fill Tank 2	1.1	313.1	13.0	205	0	0	0	0.0	0.0	290.1
41			Cond T2	8.0	321.1	13.4	205	0	0	0	6.9	0.0	283.2
42		[II-4]	Tank Press	0.5	321.6	13.4	205	0	0	0	0.0	0.0	283.2
43		[II-6]	LAD Performance	4.0	325.6	13.6	280	0	0	0	0.0	0.0	283.2

Table E-2. Experiment Sequence Based on NASA Plan for Staffing of SOCC (Cont.)

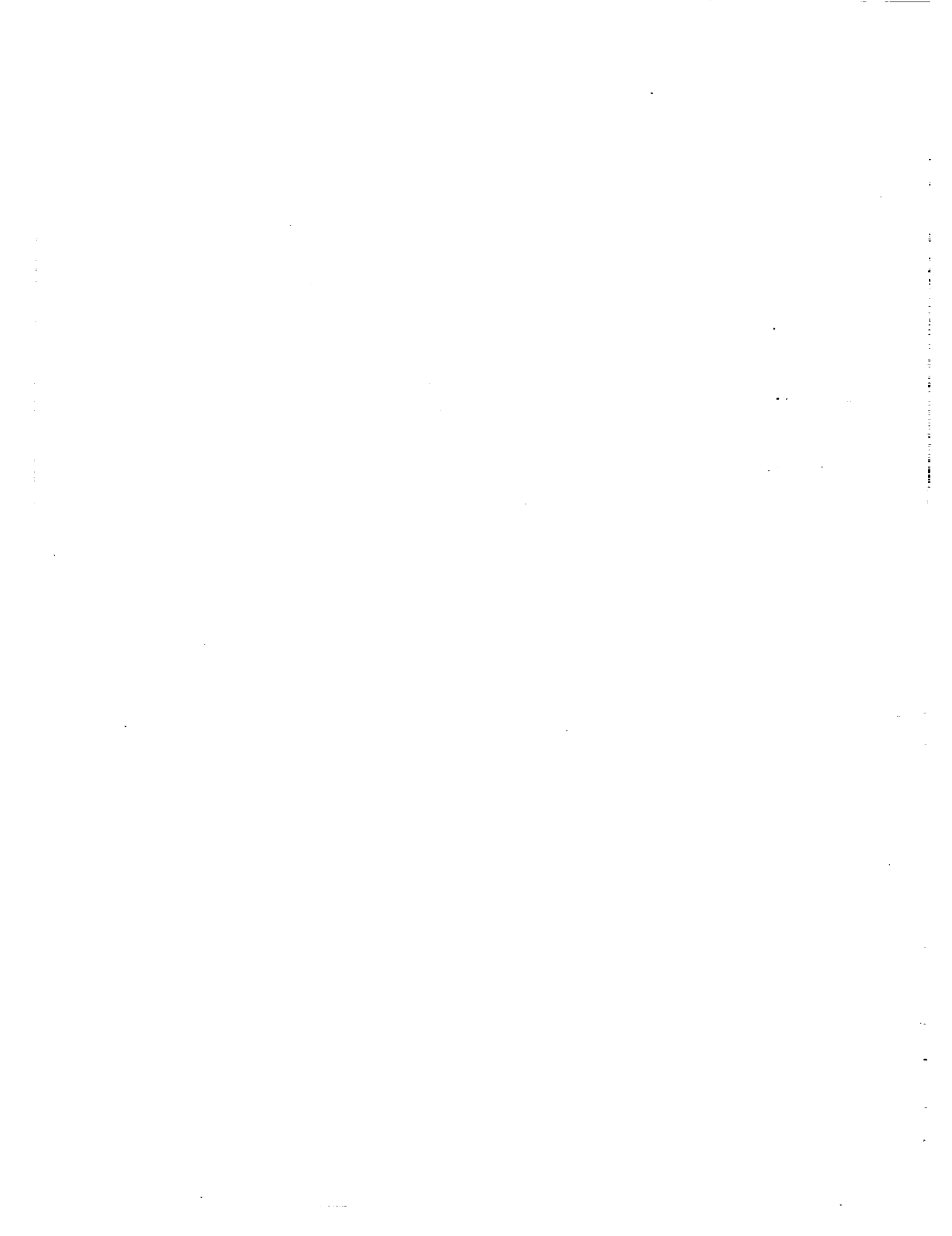
Seq No.	Orien./g Lvl. (10 ⁶)	Test Numbers	Event Description	Time Req'd. (Hrs)	Elapsed Time (Hrs)	DAYS	T1			T2			T3			H2 MASS BALANCE	
							kg	%	kg	%	kg	%	PARAS LOSS	TEST LOSS	BAL		
44		[II-10]	Dump T2	1.0	326.6	13.6	280	75	0	0	0	0	0	0	0.0	2.7	280.4
45		1-5.7	LAD Fill Tank 2	1.0	327.6	13.7	263	70	18	20	0	0	0	0	0.0	0.0	280.4
46	+/50	[II-9.7]	Vented Fill	1.0	328.6	13.7	195	52	85	95	0	0	0	0	0.0	0.9	279.5
47			No Op, Shift Break	7.4	336.0	14.0	194	52	85	95	0	0	0	0	0.5	0.0	279.0
48		[II-4]	Tank Press	0.2	336.2	14.0	194	52	85	95	0	0	0	0	0.0	0.0	279.0
49		[II-6]	LAD Performance	0.5	336.7	14.0	276	74	3	3	0	0	0	0	0.0	0.0	279.0
50		[II-10]	Dump T2	1.0	337.7	14.1	276	74	0	0	0	0	0	0	0.0	2.7	276.3
51			Ht T2 {22}	22.0	359.7	15.0	275	74	0	0	0	0	0	0	1.0	0.0	275.3
52		[II-7]	[Line Chill]	1.0	360.7	15.0	274	73	0	0	0	0	0	0	0.0	1.6	273.7
53		1-3.13	Chill Tank 2, Heat T3	18.9	379.6	15.8	260	69	0	0	0	0	0	0	0.9	12.0	259.9
54			No Op, Shift Break	4.4	384.0	16.0	260	69	0	0	0	0	0	0	0.2	0.0	259.7
55	-/100	1-4.11	No Vent Fill Tank 2	3.5	387.5	16.1	175	47	85	95	0	0	0	0	0.0	0.0	259.7
56			Cond T2	8.0	395.5	16.5	175	47	78	88	0	0	0	0	6.9	0.0	252.8
57		[II-4]	Tank Press	0.5	396.0	16.5	175	47	78	88	0	0	0	0	0.0	0.0	252.7
58		[II-6]	LAD Performance	4.0	400.0	16.7	250	67	3	3	0	0	0	0	0.0	0.0	252.7
59		[II-10]	Dump T2	1.0	401.0	16.7	250	67	0	0	0	0	0	0	0.0	2.7	250.0
60			No Op, Shift Break	7.0	408.0	17.0	250	67	0	0	0	0	0	0	0.3	0.0	249.7
61		1-5.6	LAD Fill Tank 2	1.0	409.0	17.0	232	62	18	20	0	0	0	0.0	0.0	249.7	
62	+/50	[II-9.8]	Vented Fill	3.5	412.5	17.2	161	43	87	98	0	0	0	0	0.0	0.9	248.8
63		[II-4]	Tank Press	0.2	412.7	17.2	161	43	87	98	0	0	0	0	0.0	0.0	248.7
64			Xfer T2 to T1	0.5	413.2	17.2	240	64	9	10	0	0	0	0	0.0	0.0	248.7
65		[II-10]	Dump T2	1.0	414.2	17.3	240	64	0	0	0	0	0	0	0.0	8.9	239.8
66		I-1 (@ 65%)	Thermal strat, mixer & TVS T1	264.0	678.2	28.3	215	57	0	0	0	0	0	0	25.2	0.0	214.6
67		[II-7]	[Line Chill]	1.0	679.2	28.3	213	57	0	0	0	0	0	0	0.0	1.2	213.4
68		1-3.10	Chill Tank 2	17.9	697.1	29.0	200	53	0	0	0	0	0	0	0.8	12.0	199.7
69		1-4.14	No Vent Fill Tank 2	3.4	700.5	29.2	115	31	85	95	0	0	0	0	0.0	0.0	199.7
70			Cond T2	8.0	708.5	29.5	115	31	78	88	0	0	0	0	6.9	0.0	192.8
71			No Op, Shift Break + weekend	59.5	768.0	32.0	112	30	77	86	0	0	0	0	4.1	0.0	188.7
72		[II-4]	Tank Press	0.5	768.5	32.0	112	30	77	86	0	0	0	0	0.0	0.0	188.7
73		[II-6]	LAD Performance	4.0	772.5	32.2	186	50	3	3	0	0	0	0	0.0	0.0	188.7
74		[II-10]	Dump T2	1.0	773.5	32.2	186	50	0	0	0	0	0	0	0.0	2.7	186.0
75		1-5.3	LAD Fill Tank 2	1.0	774.5	32.3	168	45	18	20	0	0	0	0	0.0	0.0	186.0
76	+/100	[II-9.9]	Vented Fill	1.0	775.5	32.3	98	26	87	98	0	0	0	0	0.0	0.9	185.1
77		[II-4]	Tank Press	0.2	775.7	32.3	98	26	87	98	0	0	0	0	0.0	0.0	185.1
78			Xfer T2 to T1	0.5	776.2	32.3	118	32	67	75	0	0	0	0	0.0	0.0	185.1
79	20	I-1 (@ 75%)	Thermal strat & TVS T2	93.0	869.2	36.2	114	30	65	73	0	0	0	0	6.4	0.0	178.7
80		[II-4]	Line Chill/Tank Press	0.2	869.4	36.2	114	30	63	71	0	0	0	0	0.0	1.6	177.1
81			Xfer T2 to T1	0.5	869.9	36.2	168	45	9	10	0	0	0	0	0.0	0.0	177.1
82		[II-10]	Dump T2, Vent Line	1.0	870.9	36.3	168	45	0	0	0	0	0	0	0.0	9.2	168.1
83		[II-7]	[Line Chill]	1.0	871.9	36.3	167	45	0	0	0	0	0	0	0.0	1.2	166.9

Table E-2. Experiment Sequence Based on NASA Plan for Staffing of SOCC (Cont.)

Seq No.	Orien./g Lvl. (10 ⁶)	Test Numbers	Event Description	Time Req'd. (Hrs)	Elapsed Time		T1 kg	FINAL TANK VOLUME			H2 MASS BALANCE			
					Time (Hrs)	Time (Days)		T2 kg	T3 kg	%	PARAS LOSS	TEST LOSS	BAL kg	
84		I-3.7	Chill Tank 3	2.0	873.9	36.4	163	0	0	0	0	0.1	3.5	163.3
85	+100	I-4.5	No Vent Fill Tank 3	1.7	875.6	36.5	121	0	0	42	95	0.0	0.0	163.3
86			Condition Tank 3	3.4	879.0	36.6	121	0	0	40	92	1.7	0.0	161.6
87		II-5	No Op, Shift Break + weekend	57.0	936.0	39.0	119	0	0	39	89	3.6	0.0	158.0
88		II-10	[Liq Outflow], Xfer T3 to T1	0.3	936.3	39.0	154	0	0	4	8	0.0	0.0	158.0
89		II-10	[Dump Tank 3]	2.0	938.3	39.1	154	0	0	0	0	0.1	3.5	154.4
90	+100	II-9.4	Vented Fill	0.5	938.8	39.1	110	0	0	43	98	0.0	0.7	153.7
91		II-5	[Liq Outflow], Xfer T3 to T1	0.3	939.1	39.1	150	0	0	4	8	0.0	0.0	153.7
92		II-10	[Dump Tank 3]	2.0	941.1	39.2	150	0	0	0	0	0.1	3.5	150.1
93	20/100	I-1 (@ 40%)	Thermal strat, mixer & TVS T1	104.0	1,045.1	43.5	130	0	0	0	0	19.8	0.0	130.3
94			No Op, Shift Break + weekend	58.9	1,104.0	46.0	128	0	0	0	0	2.7	0.0	127.6
95	I-3.8		Chill Tank 3	2.3	1,106.3	46.1	127	0	0	0	0	0.1	3.5	126.7
96	I-4.9		No Vent Fill Tank 3	1.7	1,108.0	46.2	85	23	0	42	95	0.0	0.0	126.7
97			Condition Tank 3	3.4	1,111.4	46.3	85	23	0	40	92	1.7	0.0	125.0
98		II-5	[Liq Outflow], Xfer T3 to T2	0.3	1,111.7	46.3	121	32	0	4	8	0.0	0.0	125.0
99	+100	II-9.5	Vented Fill	0.8	1,112.5	46.4	81	22	0	43	98	0.0	0.7	124.3
100		II-5	[Liq Outflow], Xfer T3 to T2	0.3	1,112.8	46.4	121	32	0	4	8	0.0	0.0	124.3
101		II-10	[Dump Tank 3]	2.0	1,114.8	46.5	121	32	0	0	0	0.1	3.5	120.7
102		II-7	[Line Chill]	1.0	1,115.8	46.5	119	32	0	0	0	0.0	1.6	119.1
103	1-3.11		Chill Tank 2, Heat T3	18.9	1,134.7	47.3	105	28	0	0	0	0.9	12.0	105.3
104	1-4.15		No Vent Fill Tank 2	3.4	1,138.1	47.4	21	5	85	95	0	0.0	0.0	105.3
105			Cond T2	8.0	1,146.1	47.8	20	5	78	88	0	6.9	0.0	98.4
106			No Op, Shift Break	5.9	1,152.0	48.0	20	5	78	87	0	0.4	0.0	98.0
107	II-4		Tank Press	0.2	1,152.2	48.0	20	5	78	87	0	0.0	0.0	98.0
108	I-5.8		LAD Fill T1	0.5	1,152.7	48.0	95	25	3	3	0	0.0	0.0	98.0
109	II-10		Dump T2	1.0	1,153.7	48.1	95	25	0	0	0	0.0	0.0	98.0
110	1-5.4		LAD Fill Tank 2	1.0	1,154.7	48.1	33	9	62	70	0	0.0	2.7	95.3
111	+100	1-4.13	No Vent Fill Tank 2	0.8	1,155.5	48.1	11	3	85	95	0	0.0	0.0	95.3
112		1-5.8, 9	LAD Fill T1	2.5	1,158.0	48.3	73	19	22	25	0	0.0	0.0	95.3
113	100	I-1 (@ 10/25)	Thermal strat & TVS T1, T2	48.0	1,206.0	50.3	66	18	18	21	0	10.8	0.0	84.5
114	+100	II-9.10	Vented Fill	3.5	1,209.5	50.4	11	3	73	82	0	0.0	0.9	84.5
115		II-7	[Line Chill]	1.0	1,210.5	50.4	11	3	72	81	0	0.0	1.2	83.2
116	I-3.1		Chill Tank 3	5.5	1,216.0	50.7	7	2	72	81	0	0.4	4.0	78.9
117	I-4.10		No Vent Fill Tank 3	0.5	1,216.5	50.7	7	2	30	34	42	95	0.0	78.9
118			(Condition Tank 3)		1,216.5	50.7	7	2	30	34	42	95	0.0	78.9
119			No Op, Shift Break + weekend	55.5	1,272.0	53.0	4	1	29	32	41	93	4.8	74.1
120		II-5	[Liq Outflow], Xfer T3 to T2	0.3	1,272.3	53.0	4	1	48	53	22	50	0.0	74.1
121	I-4.7		No Vent Fill Tank 3	1.3	1,273.6	53.1	4	1	28	31	42	95	0.1	74.0
122			Condition Tank 3	3.0	1,276.6	53.2	4	1	28	31	41	92	1.6	72.4
123		II-5	[Liq Outflow], Xfer T3 to T2	0.3	1,276.9	53.2	4	1	64	72	4	10	0.0	72.4

Table E-2. Experiment Sequence Based on NASA Plan for Staffing of SOCC (Cont.)

Seq No.	Orien./g Lvl. (10 ⁶)	Test Numbers	Event Description	Time Reqd. (Hrs)	Elapsed Time (Hrs)	DAYS	T1			T2			T3			H2 MASS BALANCE	
							kg	%	kg	%	kg	%	LOSS	TEST	LOSS	BAL	
124		[II-10]	[Dump Tank 3]	2.0	1,278.9	53.3	4	1	64	72	0	0	0.1	4.4	67.9		
125		[II-7]	[Line Chill]	1.0	1,279.9	53.3	4	1	63	70	0	0	0.0	1.2	66.7		
126	+100	I-3.2	Chill Tank 3	7.7	1,287.6	53.7	4	1	59	66	0	0	0.3	3.6	62.7		
127		I-4.6	No Vent Fill Tank 3	0.8	1,288.4	53.7	4	1	17	19	42	95	0.0	0.0	62.7		
128			Condition Tank 3	6.8	1,295.2	54.0	3	1	17	19	39	88	3.5	0.0	59.1		
129		[II-5]	[Liq Outflow], Xfer T 3 to T2	0.3	1,295.5	54.0	3	1	52	59	4	8	0.0	0.0	59.1		
130		[II-10]	[Dump Tank 3]	2.0	1,297.5	54.1	3	1	52	59	0	0	0.1	3.5	55.5		
131			Ht T 3	16.0	1,313.5	54.7	3	1	52	58	0	0	1.1	0.0	54.4		
132			No Op, Shift Break	5.9	1,319.4	55.0	2	1	52	58	0	0	0.4	0.0	54.0		
133		[II-7]	[Line Chill]	1.0	1,320.4	55.0	2	1	51	57	0	0	0.0	1.2	53.2		
134	+50	I-3.4	Chill Tank 3	6.2	1,326.6	55.3	2	1	47	52	0	0	0.3	4.0	48.9		
135	-100	I-4.2	No Vent Fill Tank 3	0.8	1,327.4	55.3	2	1	5	5	42	95	0.0	0.0	48.8		
136			Condition Tank 3	6.8	1,334.2	55.6	2	0	5	5	39	88	3.5	0.0	45.3		
137		[II-5]	[Liq Outflow], Xfer T 3 to T2	0.3	1,334.5	55.6	2	0	40	45	4	8	0.0	0.0	45.3		
138		I-5.1, [II-10]	LAD Fill T2, [Dump Tank 3]	2.0	1,336.5	55.7	2	0	40	45	0	0	0.1	3.5	41.6		
139			Ht T 3	16.0	1,352.5	56.4	1	0	39	44	0	0	1.1	0.0	40.5		
140		I-3.9	Chill Tank 3	6.9	1,359.4	56.6	1	0	35	40	0	0	0.3	4.0	36.2		
141		I-4.8	No Vent Fill Tank 3	0.8	1,360.2	56.7	1	0	-6	-7	42	95	0.0	0.0	36.2		
142			Transfer T3 to T2	0.5	1,360.7	56.7	1	0	32	36	4	8	0.0	0.0	36.1		
143	+100	[II-6][I-9.6]	LAD Perf/Vented Fill	1.7	1,362.4	56.8	1	0	-8	-9	43	98	0.1	0.7	35.4		
144			Transfer T3 to T2	0.5	1,362.9	56.8	1	0	2	2	33	75	0.0	0.0	35.4		
145		I-1 (@ 75%)	Thermal strat & TVS T3	40.0	1,402.9	58.5	0	0	1	1	31	71	3.4	0.0	32.0		
146	100	I-1 (@ 75%)	Thermal strat & TVS T3	40.0	1,442.9	60.1	0	0	0	0	29	66	2.8	0.0	29.1		
147			No Op, Shift Break + weekend	45.1	1,488.0	62.0	0	0	0	0	27	61	2.2	0.0	27.0		
148		I-5.5	LAD Fill T2	0.5	1,488.5	62.0	0	0	16	18	11	25	0.0	0.0	27.0		
149	100	I-1 (@ 25%)	Thermal strat & TVS T3	41.2	1,529.7	63.7	0	0	15	17	9	20	3.1	0.0	23.9		
150			No Op, Shift Break	6.3	1,536.0	64.0	0	0	15	17	9	19	0.5	0.0	23.4		
151		[II-10]	Dump T3	2.0	1,538.0	64.1	0	0	15	17	0	0	0.0	8.9	14.8		
152		[II-6]	LAD Performance	4.0	1,542.0	64.3	0	0	3	3	12	28	0.0	0.0	14.8		
153		[II-10]	Dump T2	1.0	1,543.0	64.3	0	0	0	0	12	27	0.0	2.7	12.1		
154		I-5.2	LAD Fill T2	0.5	1,543.5	64.3	0	0	9	10	4	8	0.0	0.0	12.1		



APPENDIX F
ADDITIONAL SCHEDULE INFORMATION



APPENDIX F ADDITIONAL SCHEDULE INFORMATION

F.1 TEST SCHEDULE

Figure F-1 presents the Phase C/D test schedule. Some long lead components (valves, flowmeters, etc.) will require development before the start of Phase C/D in order to permit component selection without jeopardizing the COLD-SAT schedule. The test program schedule relates major tests to overall program activities. Design development starts at the contract award date. After tanks are individually qualified, additional development testing will be done to ensure the thermodynamic vent systems (TVSs), vapor-cooled shield (VCS), and liquid acquisition devices (LADs) are operating as expected. These systems are expected to be confirmed in ground test to support the completion of the design development phase. The spacecraft bus and experiment module will be tested in parallel to support integrated spacecraft acceptance tests. The integrated, tested spacecraft will be shipped to the launch site for payload processing, vehicle stacking, integrated launch vehicle testing, and final checkout before launch.

F.2 LAUNCH VEHICLE SCHEDULE

Figure F-2 presents the launch vehicle schedule. The Atlas I is well defined and provides a mature, reliable system to place the COLD-SAT spacecraft into the desired orbit. The vehicle configuration identified for deployment of COLD-SAT will be flown and proven on several missions before launch vehicle contract award according to this conservative schedule. The schedule for integration, production of the Atlas I system and launch of COLD-SAT in July 1997 is realistic. It provides 36 months of integration effort prior to shipment, and another six months for shipment and launch preparations at Cape Canaveral Air Force Station. It is important to plan and implement COLD-SAT deployment with a comfortable, low-risk schedule to assure a smooth deployment for timely flight data return.

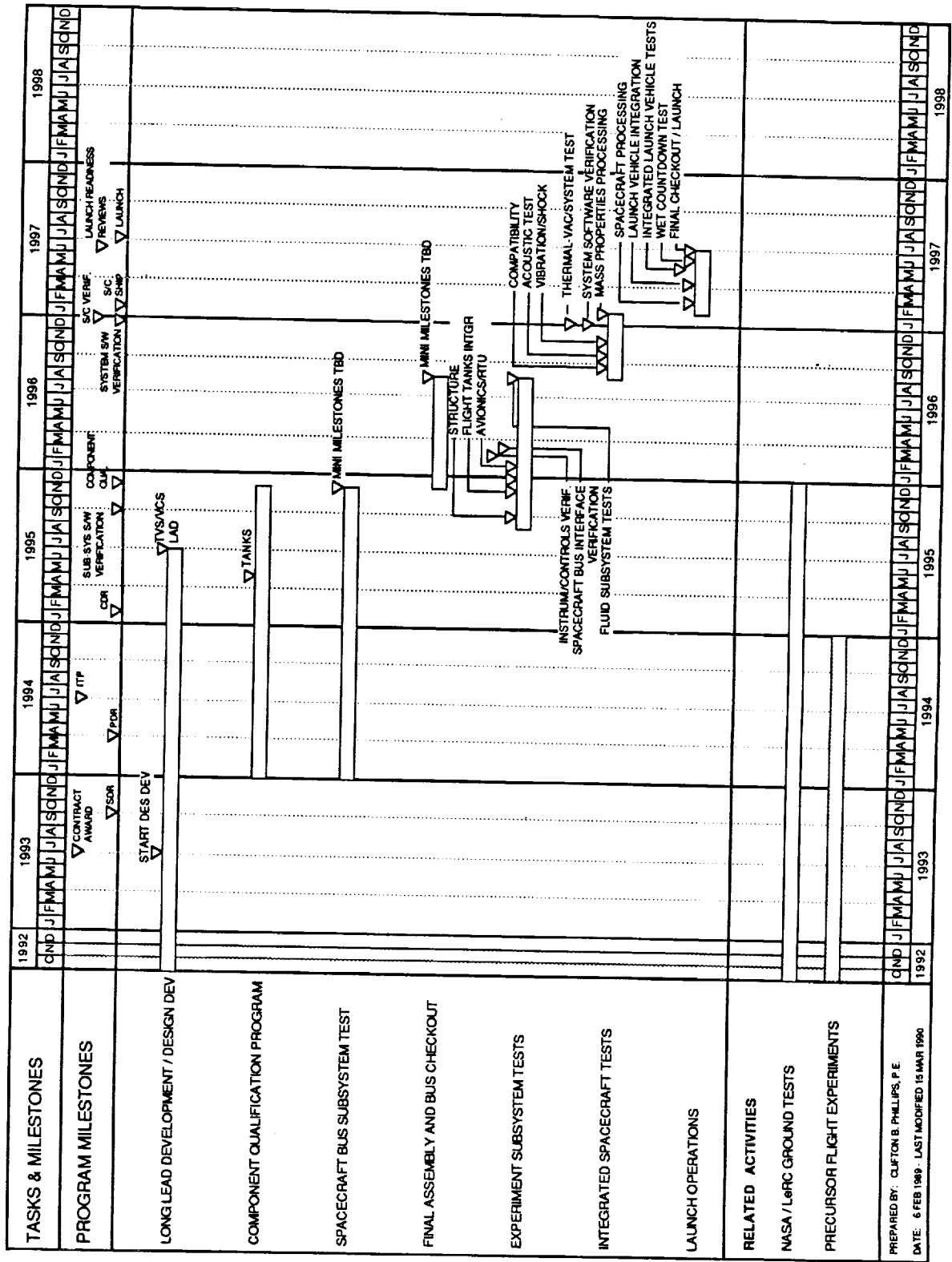


Figure F-1. COLD-SAT Phase C/D Test Schedule

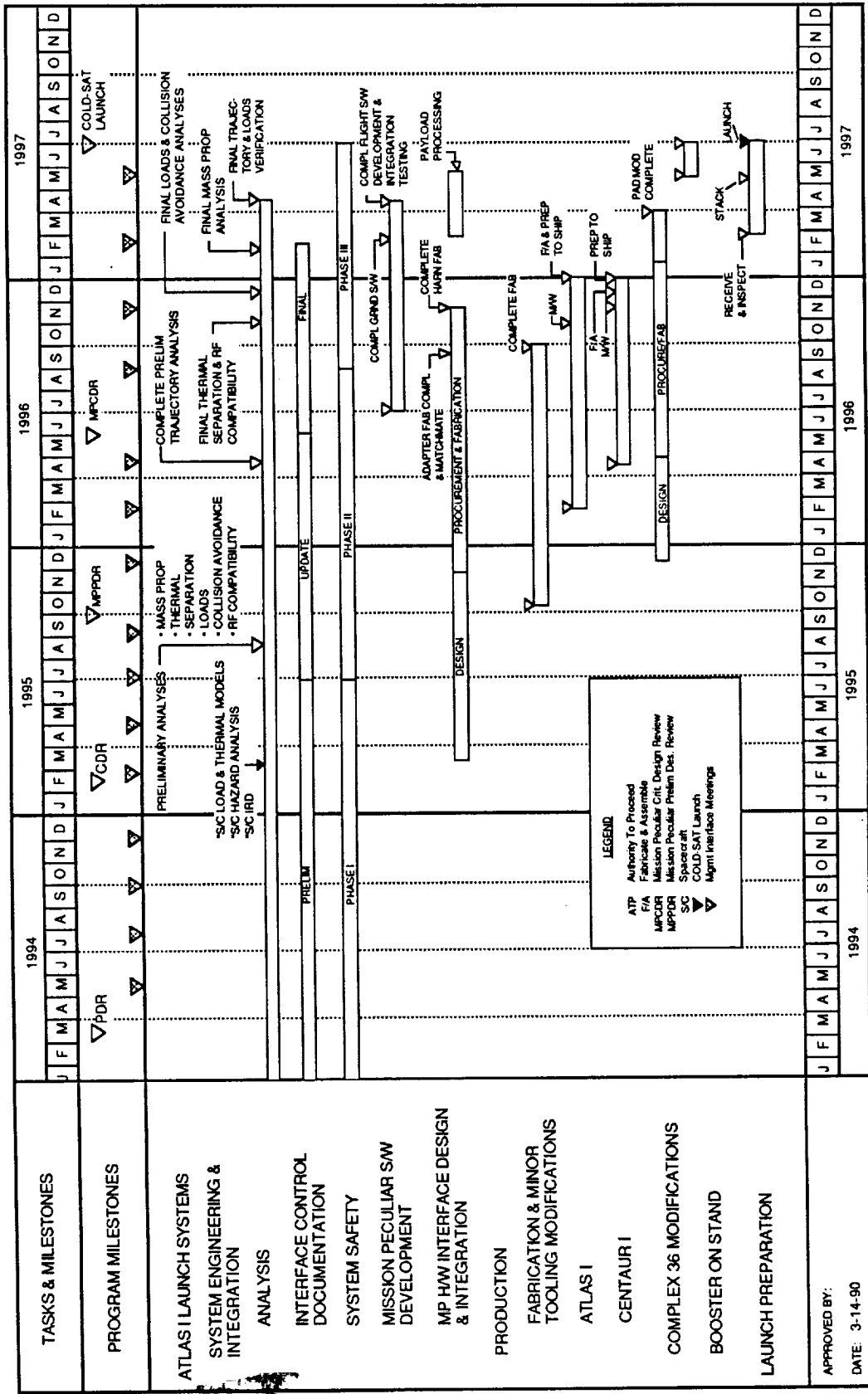


Figure F-2. Launch Vehicle Schedule

1. Report No. NASA CR-185249		2. Government Accession No.		3. Recipient's Catalog No.	
4. Title and Subtitle Cryogenic On-Orbit Liquid Depot Storage, Acquisition, and Transfer Satellite (COLD-SAT) Feasibility Study Final Report				5. Report Date July 1990	
				6. Performing Organization Code	
7. Author(s) John R. Schuster, Edwin J. Russ, Joseph P. Wachter, et. al.				8. Performing Organization Report No.	
				10. Work Unit No.	
9. Performing Organization Name and Address General Dynamics Space Systems Division P.O. Box 85990 San Diego, California 92138				11. Contract or Grant No. NAS3-25062	
				13. Type of Report and Period Covered Contract Report, March 1988 through February 1990	
12. Sponsoring Agency Name and Address National Aeronautics and Space Administration Lewis Research Center Cleveland, Ohio 44135				14. Sponsoring Agency Code	
				15. Supplementary Notes	
16. Abstract The Cryogenic On-Orbit Liquid Depot Storage, Acquisition, and Transfer Satellite (COLD-SAT) will perform subcritical liquid hydrogen handling experiments under low gravity conditions to provide engineering data for future space transportation missions. Comprising the four Class I "enabling" experiments are tank pressure control, tank chilldown, tank no-vent fill, and liquid acquisition device fill/refill. The nine Class II "enhancing" experiments are tanker thermal performance, pressurization, low-gravity settling and outflow, liquid acquisition device performance, transfer line chilldown, outflow subcooling, low-gravity vented fill, fluid dumping, and advanced instrumentation. Consisting of an experiment module mated to a spacecraft bus, COLD-SAT will be placed in an initial 1300 km circular orbit by an Atlas commercial launch vehicle, and will perform experiments in a semi-autonomous mode for a period of up to six months. The three-axis-controlled spacecraft bus provides electric power, control and data management, communications, and attitude control along with propulsive acceleration levels ranging from 10^{-6} g to 10^{-4} g. It is desired to understand the effects that low acceleration levels might have on the heat and mass transfer processes involved in some of the experiments. The experiment module contains the three liquid hydrogen tanks, valves, pressurization and pumping equipment, and instrumentation. Within the highly insulated tanks are specialized fluid management equipment that might be used in future space transportation systems. At launch all the liquid hydrogen for the experiments is contained in the largest tank, which has helium-purged insulation to prevent cryo-pumping of air on the launch pad. The tank is loaded by the hydrogen tanking system used for the Centaur upper stage of the Atlas. After reaching orbit the two smaller tanks become receivers for fluid transfers, and when tanked, become the vessels for performing many of the experiments.					
17. Key Words (Suggested by Author(s)) COLD-SAT, orbital experiments, low gravity, cryogenic, propellant management, liquid hydrogen, pressure control, venting, liquid acquisition, liquid transfer, space transportation, orbital depot			18. Distribution Statement Unclassified - [REDACTED] Subject Category 20		
19. Security Classif. (of this report) Unclassified		20. Security Classif. (of this page) Unclassified		21. No of pages 430	22. Price* A06